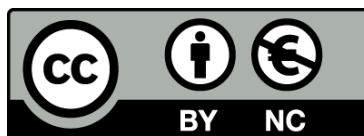




UNIVERSITAT_{DE}
BARCELONA

Exploring the regulation and function of TIGAR in cancer cells

Helga Simon Molas



Aquesta tesi doctoral està subjecta a la llicència **Reconeixement- NoComercial 4.0. Espanya de Creative Commons.**

Esta tesis doctoral está sujeta a la licencia **Reconocimiento - NoComercial 4.0. España de Creative Commons.**

This doctoral thesis is licensed under the **Creative Commons Attribution-NonCommercial 4.0. Spain License.**



UNIVERSITAT^{DE}
BARCELONA

Faculty of Medicine and Health Sciences
Department of Physiological Sciences

Doctoral Programme in Biomedicine

Exploring the regulation and function of TIGAR in cancer cells

This Doctoral Thesis is presented by Helga Simon Molas
to achieve the Doctoral Degree by the University of Barcelona.

Author:

Helga Simon Molas

Directors:

Dr. Ramon Bartrons Bach

Dr. Anna Manzano Cuesta

L'Hospitalet de Llobregat, 2019

Tu pots dir "la meva barca"
però les veles sempre són del vent.

ANTONINA CANYELLES

AGRAÏMENTS

Sabia que escriuria aquests agraïments en un balcó a plena llum del sol. No és casualitat, com tampoc ho és tancar aquesta etapa. Segurament, els materials i mètodes d'una tesi doctoral no són el que hi ha escrit al final d'aquest llibre, sinó el que escrivim aquí. Sense la calidesa de tantes portes i finestres obertes –o que s'han deixat obrir– aquest tesi no hauria estat així.

Gràcies, primer de tot, al meu pare i a la meva mare per respondre als inacabables perquès d'una nena amb pèls de punxa, per plantar una caravana al mig del món i dir-nos 'vinga, sortiu' i per recolzar les decisions o qüestionar-les la mida justa per fer-nos dubtar i canviar sense haver-ho de reconèixer massa. I gràcies, Judit, per fer de germana gran quan cal, hi ha coses que les he après de veure't triar a tu, i espero que segueixis sent la petita d'aquesta manera sempre. Visca el suc de tomàquet de Glasgow.

I si aquests són els meus tres buffers 10X principals que portava preparats d'abans de l'etapa científica, ara venen els protocols indispensables. Gràcies, Ramon, per preguntar-me un dia de l'estiu del 2012 si preferia fer les pràctiques sobre el gen PFKFB3 (que es regulava per mil coses i tenia un paper clau en càncer) o sobre un gen nou, TIGAR, que més o menys se sabia què feia, però no estava clar del tot. El meu agraïment cap a tu es resumeix en una paraula: llibertat. Gràcies per tenir sempre la porta del despatx oberta, una resposta científica preparada i un argument humanístic per defensar-la. Anna, ho diem en broma però no podria ser més veritat: ets la meva mare científica i és molt difícil explicar per què. El més fàcil seria dir que de tu he après com funciona tot a Bellvitge i gairebé totes les tècniques d'aquesta tesi (no hauria aconseguit ni una sola lligació sense la teva ajuda), però seria massa simplista. Sense la vitalitat i bondat que irradies la meva idea de tesi no seria la mateixa, i no crec que tingui mai més cap directora ni director tan humà com tu. Gràcies una vegada més, i sé que no serà l'última. A tots dos, Ramon i Anna, us agraeixo moltíssim que féssiu fàcil compaginar la ciència i la poesia durant aquell any boig. La cita que encapçala aquesta tesi penja en un racó del lab, i tampoc és casualitat.

Però no, aquesta tesi no s'ha fet només entre tres. Justo al entrar al lab, primeríssima mesa com no podia ser de otra manera: Esther Adanero. Gracias, Esther, por hacer el trabajo más distendido y no enfadarte cuando sí, algo rompíamos... Y gracias (y por extensión también a Alfonso) por hacer más fácil esa mudanza que nos montamos en medio de unos meses de trabajo de locos. Seguim cap a dins del lab, i cap al sud del país. Ana, d'aquest estiu no passa que vinc a Tarragona. Ser companyes de lab va ser genial: ens vam ajudar en transfeccions, en relleus de Mojitada i també a suportar l'avorriment extrem en algunes xerrades del congrés de València. Gràcies per seguir preguntant com ens va, ets un exemple de 'currante' total. I, a l'altra banda de la paret, en companyia del LAS3000: l'Àurea! Sempre va bé que la part PFKFB3 de la família es miri la part TIGAR i ajudi a veure una mica de llum entremig dels núvols. Gràcies pel teu esperit engrescador (segur que en Pere Renom ho corrobora!), per animar-nos amb el projecte dels limfos, i per ajudar-me a formar part de la família SCB. Esther Castaño, baixar una planta i rebre ajuda en l'anàlisi de les PCR o de la citometria no podria ser més fàcil. Moltes gràcies per oferir-te sempre a donar un cop de mà i revisar les qüestions més tècniques dels treballs, has estat una part del grup molt important tot i no compartir parets. Ara els agraïments de grup internacionals. Cap a Mèxic: muchísimas gracias Miguel por hacer los primeros westerns y las primeras extracciones de RNA conmigo,

sé que andabas liado esos meses así que te lo agradezco mucho. I cap a Londres: moltes gràcies, Laura, per ajudar-me al començament quan en Pere i jo érem els babies del lab, i per extensió també a l'Andy, pels vostres consells "que no s'assequi la membrana!". Finalment, gràcies a tots els estudiants de batxillerat, grau i màster que heu format part del grup intermitentment, tant a aquells que heu participat directament en alguns dels experiments d'aquesta tesi, com als qui amb les vostres ganes d'aprendre ens feu sentir útils. He de mencionar especialment la Clàudia i la Irene, per la 'currada' que va fer amb el projecte dels limfos i el promotor de TIGAR; la Paula, per les estones compartides; la Carla, per obrir els horitzons de TIGAR al cervell; i en Mikel, por dejar clarísimo que un médico y un promotor se pueden entender maravillosamente.

I tornem als CCiT: moltíssimes gràcies, Bea i Benja, per resoldre dubtes tècnics que sovint us devien semblar dignes de nens de parvulari. Crec que sou les persones de Bellvitge que més cops deveu posar cara de pòquer davant les fatalitats dels nostres experiments. Gràcies, Benja, per meravellar-te amb mi del marcatge dels controls negatius i no dir-me que em limités al western. Sempre em quedarà el DAPI.

A la resta de les Ciències Fisiològiques, els d'aquí i els qui esteu escampats pel món. Moltes gràcies Cris, sense els teus ChIPs encara dubtaria de si Nrf2 i TIGAR tenen alguna cosa a veure o no... I gràcies també Francesc per descobrir-me l'ECR Browser i pels teus consells de biologia molecular. Al 4175 he d'agrair un bon grapat d'anticossos, minuts de centrifuga, algun mil·lilitre de FBS inactivat i el rescat més barat de la història: em va costar només un paquet de Voll Damm, i ara ja ens en podem riure. Moltíssimes gràcies per això últim, Dani i Ismael. A la Sonia, perquè ets l'única persona que ha aconseguit fer-me entrar a una classe d'spinning (tot i que no la vaig acabar) i vam riure una bona estona, i per animar-me sempre amb els drames de la tesi. A la Petra, pels teus consells sobre diferents tècniques metabòliques (i ho dic en català), i també a en Jose Carlos per explicar-me com anava aquesta gran idea del GeoProfiles, gràcies. A tota la resta de companys de *tupper*, Carol, Jose, Ana Maria, Pau, Juan, Marc, Norma, Arturo, Chus, Joan i Leo, per fer l'estona de la saleta més entretinguda. Hem estat estrets, però ben avinguts! Gràcies també a aquells que porteu la paella pel mànec amb el tema de l'EPIF. A tothom amb qui he compartit Mojitadas, gràcies també perquè almenys trobem un dia a l'any per fer pinya (colada). Gracias, Edu, por tus consejos con las inmunos, nos acordamos de ti en cada puré. A l'equip Cervezas (habrá que retomar el schedule, no?) i molt especialment al Baile Bellvitge, amb la Natalia, la Betta i la Tai, perquè sempre tindreu una casa a Barcelona, i és bonic tenir cases (o sofàs, és igual!) arreu del món. I a la Cris Moncunill, per la oportunitat que em vas donar de començar a tastar el món de la comunicació científica, ara quan veig un pot de Dentican em fa il·lusió i tot!

A aquelles persones que fan que la feina al lab sigui més fàcil i agradable, gràcies Josep Maria per gestionar les compres i tornar-nos religiosament fins l'últim cèntim de la llet en pols; gracias también, Montse, por tu implicación en el Departamento desde el primer día y por preguntarme siempre cómo lo llevaba desde la poyata de al lado; y muchas gracias Carmen por eso de 'pisa, pisa aunque esté mojado que no quiero que te caigas', sort en tenim de tu!

Passadís enllà, agrair al laboratori de Nefrologia la seva col·laboració en aquesta tesi, molt especialment a la Núria, a en Pere i a l'Anna Vidal. Sense vosaltres el treball en limfos no hauria estat possible. Anna,

ets una de les persones més implicades que conec. Gràcies per deixar-me compartir amb vosaltres l'ABP i per posar-m'ho sempre fàcil, va ser molt enriquidor. Parlant de docència, gràcies també a la Susana, t'hauré de deixar aquests agraïments a la bústia dos portals més enllà: gràcies per ser la meva primera mestra de pràctiques.

A aquells amb qui hem col·laborat al llarg d'aquesta tesi, gràcies. Al laboratori d'en Joan Gil amb els MLPA, al de l'Oscar Yanes perquè la metabolòmica ha estat una contribució enorme, a l'Annie Rodolose, a qui no conec personalment però em va demostrar que ciència és compartir el que sabem, al Santi per estar sempre disposat a parlar de capes d'electrons, i a en Biel, que tot i que no sé si és legal incloure un membre del tribunal als agraïments, t'agraïxo molt l'interès i l'ajuda per entendre què tenen a veure PGAM i TIGAR.

També a aquells laboratoris que m'han acollit quan no funcionaven els nostres aparells... Als grups d'en Jose Luis Rosa, en Ricardo Pérez, en Joan Blasi i la Mireia Martín, gràcies per la vostra amabilitat.

Per acabar el recorregut pel passadís, faré dues parades. Gràcies, Anna Plana, per compartir nervis i dubtes aquests últims mesos, ens en sortirem! I muchas gracias, Ana Méndez, por ser un ejemplo de rigor. En los ratos compartidos en vuestro despacho he visto que, aunque ser IP en Bellvitge pueda ser más difícil que en otras partes, la clave es no claudicar nunca. I l'última parada al departament veí: Fàrmaco! Gràcies, Víctor, per deixar clar que pel passadís de la 4a planta hi circulen persones, que fem ciència i altres coses. Gràcies també Marc pels viatges de Camins Infinitos, qui ens ho anava a dir!

Vull agrair també a la meva comissió de seguiment, Cristina Muñoz, Maria Soley i Pablo García-Roves, els vostres consells. M'ha servit molt el seguiment que heu fet i gràcies a vosaltres he pogut redirigir alguns dels experiments d'aquesta tesi i repensar coses.

Creuant la Gran Via, no em volia oblidar d'en Joan i la Gemma de la Unitat de Comunicació Científica de l'IDIBELL. A tots dos, per donar-me l'oportunitat d'explicar la nostra feina a la societat amb aquest 'De professió, científic' i molt especialment a en Joan pel pont cap a l'SCB, l'Horiginal i Sitges. Gràcies.

I ara ve el paràgraf dedicat als mesos d'abril a juliol del 2016, que tampoc podia deixar passar. Thank you, Karen Vousden, for opening the doors of your lab to me, working in the nest of TIGAR was wonderful. I would like to thank the whole lab, but especially Julianna, Fabio, Bob, Mylene, Eric, Flore and Andreas for your help with the protocols and for making the stay easy. Julianna, I still keep the paper tag that you gave me with a present for changing the media for you. I am so glad we met each other, Ana and I wait for you in Barcelona! Ana, thank you for becoming an enthusiast of Catalonia, I knew you'd like it! If the defense of this thesis is acceptable, I am sure our conversations will have a lot to do! And, finally, thank you Sam for making me part of your family. I know I have a room in Glasgow, and you know that Ivy has an auntie in Barcelona.

M'agradaria deixar constància també d'aquells que heu fet possible que aquesta tesi hagi durat quatre anys, malgrat la beca era només de tres perquè no us puc estar més agraïda. Vull agrair molt sincerament a l'SCB la confiança que heu dipositat en mi. Vaig començar aquest camí de la comunicació científica una mica a ulls clucs, però m'heu fet sentir com a casa i m'heu permès veure que compaginar recerca i

divulgació és de les coses més enriquidores que hi ha. Gràcies especialment a en Raül i la Marina, per dir que sí sabent que no havia fet mai un *twit*, i a tot el comitè directiu en general. Vull agrair també a la UCC+i de la UB que confiéssiu en mi durant aquell mes, va ser curt però va ser una gran oportunitat.

I ara sí, enfilem la recta *last but not least* total. A totes les Cabres, no us anomeno una per una perquè la part científica de la tesi ha de començar en algun moment, però moltes gràcies per les tremperes, les rutes, les fotos per sempre amb cavalls de plàstic, la poesia, els sopars a Gràcia, ... Un lumí sempre serà un refugi. Per relació directa entre aquesta tesi i el vostre temps, gràcies especialment a la Jove, per ser-hi durant tot el camí: al poblet, a Sants quan només teníem el temps just d'un birra, o el primer dia de sol post-dipòsit a Plaça Osca. I a la Clara i l'Alberich, gràcies per haver-me ajudat a fer créixer, encara amb el cap a les pipetes i arribant sempre tard, aquest *A la vora* tan nostre.

A la Finca, perquè vaig venir a viure a Barcelona amb la teoria que tenint Sant Just tan a prop no faria amics a la ciutat, i m'heu tirat la teoria per terra. Visca les estones de desconexió tan necessàries d'aquests últims anys.

A l'Elena, l'Helena, l'Amèlia i l'Alexandra, perquè si vam sobreviure a tres canvis de nom de carrera, tot el que vingui després és pan comido. Aquí, a Madrid i a Berlín. Gràcies pels ànims que només els amics del mateix ram saben donar.

I, sempre amb alegria (amb o sense drap a la mà), moltíssimes gràcies a l'Helena i la Roser perquè una vegada una casa ho va canviar tot. Sé que sempre tindrem una finestra turquesa des d'on mirar el concert de les estrelles, tranquil·lament.

Al Jose, per dosificar-me el nerviosisme i per ser calma. Et queda un mes de lidiar amb aquesta endimoniada, però a Canet veurem sortir el sol. Fas la vida bonica. Bonica, i punt. Gràcies.

Finalment, a la resta de tiets i tietes, cosins i cosines i a la meva àvia. Gràcies per les llargues sobretaules, per ser-hi sempre i per molts més ous de Pasqua i cavalcades o succedanis que ens agraden tant o més. Gràcies també per preguntar per la tesi i haver fet un esforç per entendre de què va això de la vida científica. I també dir, i no sé si agraïment és la paraula, que alguns dies d'aquesta tesi han estat un homenatge als qui han marxat, d'una manera o una altra. Gràcies també a la família d'en Jose, per cuidar-nos i omplir-nos el rebost, que sempre fa la tesi més fàcil. I, finalment, vull reservar un espai concret a la Gisela, perquè sé que hi serem sempre; a la Nati, per saber escoltar i sempre tenir una paraula senzilla; a l'Adrià i l'Oriol, perquè va ser la primera idea de doctor tangible que vaig tenir; i al meu avi, perquè per ell al balcó neixen flors a cada instant.

This work was supported by Instituto de Salud Carlos III – FIS PI13/0096 and PI17/00412 and Fondo Europeo de Desarrollo Regional (FEDER) *Una manera de hacer Europa*.

With the support of *Secretaria d'Universitats i Recerca del Departament d'Economia i Coneixement de la Generalitat de Catalunya*.



TABLE OF CONTENTS

FIGURE AND TABLE LEGENDS	IV
ABBREVIATIONS	1
INTRODUCTION	5
CANCER: ONE NAME, MULTIPLE FACTS.....	7
1. General considerations on cancer metabolism: catabolism for anabolism	9
2. Glycolytic metabolism	11
2.1. Obtaining the carbons: the glycolytic phenotype.....	11
2.2. Using the carbons: key glycolytic enzymes.....	15
2.2.1. Capturing glucose through phosphorylation by HK.....	15
2.2.2. PFK-1 and the Fru-6-P/Fru-1,6-P ₂ substrate cycle	15
2.2.3. PFK-2/FBPase-2: the importance of Fru-2,6-P ₂	17
2.2.4. TIGAR.....	23
2.2.5. From Fru-1,6-P ₂ to PEP: the forgotten enzymes	30
2.2.6. Pyruvate kinase: the last step of glycolysis	30
3. Diversion of carbons: metabolic pathways branching from glycolysis	31
3.1. Hexosamine-phosphate pathway	31
3.2. Pentose phosphate pathway.....	31
3.3. Serine and glycine synthesis pathway and one-carbon metabolism.....	32
3.4. Lipid synthesis	33
4. The fate of pyruvate carbons: lactate or acetyl-CoA?	34
5. Mitochondrial metabolism in brief: should we still call the TCA cycle a “cycle”?	35
6. Oncogenic orchestrators of cancer cell metabolism: special attention to oxidative stress	38
6.1. Pi3K/mTORC.....	40
6.2. HIF-1 α	41
6.3. c-Myc	41
6.4. p53	42
6.5. Oxidative stress and antioxidant defenses.....	44
6.5.1. Reactive oxygen species.....	44
6.5.2. A focus on Nrf2.....	44
6.6. Tumour microenvironment.....	49
HYPOTHESIS AND AIMS	51

RESULTS CHAPTER I

TIGAR AND GLYCOLYSIS INHIBITION: IS THAT REDUNDANT?	55
CONTEXT	57
1. Crosstalk between TIGAR and PFKFB3	59
1.1. Characterization of TIGAR induction in response to <i>PFKFB3</i> inhibition	59
1.2. Phenotypical consequences of inhibiting <i>PFKFB3</i> and <i>TIGAR</i>	65
2. TIGAR modulation in response to other glycolytic inhibitors	73
2.1. Response to the PFK-2 inhibitor 3PO	73
2.2. Response to glucose deprivation	76
3. TIGAR contribution to cell survival under metabolic stress	77
4. Discussion	85

RESULTS CHAPTER II

ROLE OF TIGAR IN THE METABOLISM OF CANCER CELLS: IS IT ALL ABOUT FRU-2,6-P ₂ ?	89
CONTEXT	91
1. <i>In silico</i> study of TIGAR protein sequence and structure	92
2. Metabolic determinations by spectrophotometry	97
3. Metabolomic and fluxomic analyses by LC-MS/MS	99
3.1. Metabolomic abundance analyses	100
3.2. Fluxomic analyses	104
4. Determination of redox potential	108
5. Analysis of genes involved in glucose metabolism	109
6. Study of key proteins involved in the metabolism of glucose and glutamine	111
7. Discussion	113

RESULTS CHAPTER III

CONTROL OF <i>TIGAR</i> EXPRESSION BY <i>Nrf2</i>	117
CONTEXT	119
1. <i>In silico</i> study of the human <i>TIGAR</i> promoter	120
2. Regulation of <i>TIGAR</i> expression by <i>Nrf2</i> chemical inducers in HeLa cells	124
3. Regulation of <i>TIGAR</i> by <i>NFE2L2</i> expression in HeLa cells	127
4. <i>TIGAR</i> and <i>Nrf2</i> in NSCLC	129
4.1. A model with pathological relevance: NSCLC	129
4.2. <i>TIGAR</i> regulation by <i>Nrf2</i> in NSCLC	133
4.2.1. Characterisation of the A549, H460 and H1299 cell lines	133
4.2.2. Effects of <i>Nrf2</i> modulation on the expression of <i>TIGAR</i> in NSCLC cell lines	136
5. Cloning and functional characterisation of the human <i>TIGAR</i> promoter	143
5.1. Cloning of regulatory AREs located at <i>TIGAR</i> promoter	143
5.2. Functional assays of <i>TIGAR</i> promoter activation by <i>Nrf2</i>	146

6. Nrf2 as a transcriptional regulator of mouse <i>Tigar</i>	150
6.1. Modulation of <i>Tigar</i> gene expression by Nrf2 in IDGs	150
6.2. <i>In silico</i> study of the promoter of mouse <i>Tigar</i> gene	152
6.3. Binding of Nrf2 to the promoter of mouse <i>Tigar</i> gene	154
7. Discussion	156
RESULTS CHAPTER IV	
LOOKING AT TIGAR IN RESPONSE TO OXIDATIVE STRESS: LOCATION ALSO MATTERS.....	159
CONTEXT	161
1. Screening of primary antibodies for <i>Tigar</i> immunofluorescence in mouse cells	162
2. Subcellular localisation of TIGAR under oxidative stress	163
2.1. TIGAR location in unstressed conditions	163
2.2. TIGAR location under oxidative stress	166
3. Contribution of TIGAR to cell survival in stress conditions	173
4. Discussion	174
GENERAL DISCUSSION	177
CONCLUSIONS	187
MATERIALS AND METHODS	191
REFERENCES	237
ANNEX. PUBLICATIONS	251

FIGURE AND TABLE LEGENDS

FIGURE LEGENDS

INTRODUCTION

Figure 1. The hallmarks of cancer.....	8
Figure 2. Main differences in the fuels and metabolic pathways used by quiescent and proliferative cells.....	9
Figure 3. Oxidative metabolism in quiescent and proliferative cells.....	11
Figure 4. Molecular basis of ¹⁸ F-2-deoxy-glucose positron emission tomography (PET).....	12
Figure 5. Main metabolic pathways altered in cancer cells.....	14
Figure 6. Regulation of the Fru-6-P/Fru-1,6-P ₂ substrate cycle.....	16
Figure 7. PFK-2/FBPase-2 structure.....	17
Figure 8. Domain organization and phosphorylated residues of PFK-2/FBPase-2 isoenzymes.....	19
Figure 9. Schematic representation of human <i>TIGAR</i> gene.....	23
Figure 10. <i>TP53</i> and <i>TIGAR</i> alterations and expression.....	25
Figure 11. Structure of human <i>TIGAR</i>	26
Figure 12: <i>TIGAR</i> mRNA and protein levels across tissues.....	27
Figure 13: <i>TIGAR</i> mRNA and protein levels in several types of cancer.....	28
Figure 14: Kaplan Meier curves of <i>TIGAR</i> expression in liver cancer.....	29
Figure 15. Electron transport chain and oxidative phosphorylation.....	37
Figure 16. Oncogenic orchestrators of cancer metabolism.....	39
Figure 17. p53 role as a pro-survival or an apoptosis enhancer gene.....	43
Figure 18. Mechanisms of Nrf2 activation in quiescent and proliferative cells.....	45
Figure 19. The KEAP1/Nrf2 system.....	47
Figure 20. Contribution of Nrf2 to cellular metabolism.....	48
Figure 21. Metabolic coupling between cancer cells and cancer-associated fibroblasts.....	49

RESULTS CHAPTER I

Figure 22. <i>TIGAR</i> and <i>PFKFB3</i> genetic alterations in human cancers.....	58
Figure 23. Crosstalk between <i>PFKFB3</i> and <i>TIGAR</i>	60
Figure 24. Analysis of the Akt signalling pathway after <i>PFKFB3</i> and/or <i>TIGAR</i> inhibition.....	61
Figure 25. Analysis of p53 in response to <i>PFKFB3</i> and <i>TIGAR</i> inhibition.....	63
Figure 26. Analysis of Nrf2 in response to <i>PFKFB3</i> inhibition.....	64
Figure 27. Time course of reactive oxygen species in <i>PFKFB3</i> -inhibited cells.....	65
Figure 28. Reactive oxygen species analysis in <i>PFKFB3</i> and <i>TIGAR</i> -inhibited cells.....	66
Figure 29. Effect of <i>PFKFB3</i> and <i>TIGAR</i> silencing on P-H2AX (S139) foci formation.....	67
Figure 30. Effect of <i>PFKFB3</i> and <i>TIGAR</i> silencing on autophagy.....	68
Figure 31. Effect of <i>PFKFB3</i> and <i>TIGAR</i> silencing on mitochondrial reduction capacity.....	69
Figure 32. Effect of <i>PFKFB3</i> and <i>TIGAR</i> silencing on cellular viability.....	70

Figure 33. RT-MLPA analysis of apoptotic-related genes after <i>PFKFB3</i> or <i>TIGAR</i> inhibition	71
Figure 34. Analysis of the effects of 3PO treatment at 24 h.	73
Figure 35. Analysis of the effects of 3PO and glucose deprivation treatments at 72 h.	75
Figure 36. Bright field images of HeLa cells overexpressing <i>TIGAR</i>	77
Figure 37. Bright field images of HeLa cells with inhibited <i>TIGAR</i> or <i>PFKFB3</i>	77
Figure 38. Extracellular glucose and lactate analysis after <i>TIGAR</i> and <i>PFKFB3</i> modulation	79
Figure 39. Bright field images of HeLa cells with <i>TIGAR</i> overexpression in the presence of stress stimuli	80
Figure 40. Bright field images of HeLa cells with <i>TIGAR</i> inhibition in the presence of stress stimuli.....	81
Figure 41. Analysis of the effects of <i>TIGAR</i> modulation in the presence of stress stimuli	83
Figure 42. Extracellular glucose and lactate analysis after <i>TIGAR</i> modulation in stress conditions.	84

RESULTS CHAPTER II

Figure 43. Multiple Sequence Alignment of TIGAR with other histidine phosphatases.....	95
Figure 44. BLAST local alignments of TIGAR with PGAM B and FBPase-2	94
Figure 45. EMBOSS Needle global alignments of TIGAR with PGAM B and FBPase-2.....	95
Figure 46. Pairwise structural alignment of TIGAR with PGAM B, FBPase-2 and PFKFB3.....	96
Figure 47. Confirmation of the modulation of <i>TIGAR</i> and <i>PFKFB3</i> by western blot.....	97
Figure 48. Fru-2,6-P ₂ concentration in <i>TIGAR</i> overexpressing and <i>TIGAR</i> or <i>PFKFB3</i> -inhibited cells.....	97
Figure 49. 3-PG, 2-PG, PEP and Pyr concentration in <i>TIGAR</i> overexpressing and <i>TIGAR</i> -inhibited cells.....	98
Figure 50. Analysis of metabolites abundance in <i>TIGAR</i> overexpressing cells.....	101
Figure 51. Analysis of metabolites abundance in <i>TIGAR</i> -inhibited cells.....	103
Figure 52. Fluxomic analyses of cytosolic metabolites in <i>TIGAR</i> overexpressing and <i>TIGAR</i> -inhibited cells	105
Figure 53. Fluxomics analyses of mitochondrial metabolites in <i>TIGAR</i> -inhibited cells.....	107
Figure 54. Analysis of NAD ⁺ /NADH and NADP ⁺ /NADPH ratios after <i>TIGAR</i> modulation.....	108
Figure 55. RT-qPCR analysis of metabolic genes in <i>TIGAR</i> overexpressing cells	109
Figure 56. RT-qPCR analysis of metabolic genes in <i>TIGAR</i> or <i>PFKFB3</i> -inhibited cells	110
Figure 57. Western blot analysis of metabolic enzymes in <i>TIGAR</i> overexpressing cells	111
Figure 58. Western blot analysis of metabolic enzymes in <i>TIGAR</i> or <i>PFKFB3</i> -inhibited cells	112

RESULTS CHAPTER III

Figure 59. Study of human <i>TIGAR</i> promoter and first intron with ECR Browser	122
Figure 60. Regulation of Nrf2 and TIGAR by tBHQ	125
Figure 61. Analysis of Sulforaphane and DMF effects on <i>NFE2L2</i> , <i>NQO1</i> and <i>TIGAR</i> expression.	126
Figure 62. TIGAR modulation by Nrf2 inhibition in HeLa cells.....	127
Figure 63. Effect of tBHQ in Nrf2-inhibited cells.....	128
Figure 64. TIGAR modulation by Nrf2 overexpression in HeLa cells	128
Figure 65. Frequency of genetic alterations in <i>NFE2L2</i> and <i>KEAP1</i> in human cancer.....	129
Figure 66. Frequency of genetic alterations in the Nrf2 pathway, <i>TIGAR</i> , <i>PIK3CA</i> and <i>TP53</i> in NSCLC	131
Figure 67: Molecular mechanisms driving Nrf2 overactivation in ADC and SQCC.....	132

Figure 68: Basal protein levels in A549, H460 and H1299 cell lines.....	133
Figure 69: Immunofluorescence analysis of Nrf2 basal levels in A549, H460 and H1299 cell lines.....	134
Figure 70: Immunofluorescence analysis of p53 basal levels in A549, H460 and H1299 cell lines.....	135
Figure 71. Modulation of <i>TIGAR</i> mRNA levels by Nrf2 inhibition in A549 cells.....	137
Figure 72. Modulation of TIGAR protein levels by Nrf2 inhibition in A549 cells.....	138
Figure 73. TIGAR modulation by Nrf2 inhibition in H460 cells.....	139
Figure 74. TIGAR modulation by Nrf2 inhibition in H1299 cells.....	139
Figure 75: <i>CDKN1A</i> expression in A549, H460 and H1299 in response to Nrf2 inhibition.....	140
Figure 76: Immunofluorescence analysis of p53 in response to Nrf2 inhibition in A549 cells.....	141
Figure 77. TIGAR modulation by Nrf2 overexpression in ADC cells.....	142
Figure 78. Primers designed for the amplification of TIGAR promoter and first intron.....	144
Figure 79. Cloning workflow for the obtention of TIGAR promoter constructs.....	145
Figure 80. TIGAR modulation by several transcription factors.....	147
Figure 81. Luciferase assays of AREs in TIGAR promoter.....	149
Figure 82. Analysis of <i>Tigar</i> expression under Nrf2 modulation in mouse IDGs.....	151
Figure 83. Study of mouse <i>Tigar</i> promoter and first intron with ECR Browser.....	155
Figure 84. Nrf2 binding to AREs in mouse <i>Tigar</i>	154
Figure 85. Specific binding of Nrf2 to ARE 1 in mouse <i>Tigar</i> promoter.....	155

RESULTS CHAPTER IV

Figure 86. Evaluation of the specificity of antibodies for the detection of mouse <i>Tigar</i>	162
Figure 87. Generation of PDAC cell lines stably expressing flagged-TIGAR-GFP (f-TIG-GFP) fused protein.....	163
Figure 88. TIGAR and Tom20 colocalisation in iCT cells.....	164
Figure 89. TIGAR and Tom20 colocalisation in iKO cells.....	165
Figure 90. Localisation of TIGAR under oxidative stress in iCT cells.....	167
Figure 91. Localisation of TIGAR under oxidative stress in iKO cells.....	168
Figure 92. Y-tubulin distribution under oxidative stress.....	169
Figure 93. ROS-dependent effect of the phenotype induced by H ₂ O ₂ in iCT cells.....	170
Figure 94. ROS-dependent effect of the phenotype induced by H ₂ O ₂ in iKO cells.....	171
Figure 95. Tigar localisation under oxidative stress in PDAC cells.....	172
Figure 96. Evaluation of TIGAR contribution to the proliferation of PDAC cells.....	173

MATERIALS AND METHODS

Figure M-1. Western blot analysis of cellular extracts obtained with Subcellular Fractioning Buffers I and II.....	200
Figure M-2. Schematic representation of a humid chamber for immunofluorescence	207
Figure M-3. RT-qPCR with TaqMan Assays	211
Figure M-4. Annexin/PI staining to measure cell death.....	213
Figure M-5. Reactions involved in the Fru-2,6-P ₂ assay.....	216
Figure M-6. Reactions involved in the assay for the determination of Pyr, PEP, 2PG and 3PG.	220
Figure M-7. Basis of the NAD(P)/NAD(P)H assays.....	222
Figure M-8. Location of BACs RP11-177D20 and RP11-74J21 in human chromosome 12.....	224
Figure M-9. TOPO TA cloning system	225
Figure M-10. Map of pCR-2.1-TOPO vector	226
Figure M-11. Map of pGL3 Basic	227
Figure M-12. Map of pGL3 Promoter	227
Figure M-13. Restriction enzyme strategies performed	230
Figure M-14. Basis of the T4 DNA ligase reaction.....	229
Figure M-15. Map of pBABE-puro vector.....	232
Figure M-16. InFusion cloning.....	233
Figure M-17. Processes involved in the transduction of eukaryotic cells.....	234

TABLE LEGENDS

INTRODUCTION

Table I. Properties of the human PFK-2/FBPase-2 isoenzymes	18
------------------------------------------------------------------	----

RESULTS CHAPTER II

Table II. Summary of the main metabolic alterations induced by TIGAR and PFKFB3 modulation	113
--------------------------------------------------------------------------------------------------	-----

RESULTS CHAPTER III

Table III: Identification of Nrf2 targets by microarray analysis.....	136
-----------------------------------------------------------------------	-----

Table IV. Study of <i>TP53</i> modulation in a microarray analysis of Nrf2-inhibited cells	140
--------------------------------------------------------------------------------------------------	-----

Table V. Experiments performed by Dr. Ventura's Lab in IDGs in which <i>Tigar</i> expression has been analysed	150
----------------------------------------------------------------------------------------------------------------------	-----

RESULTS CHAPTER IV

Table VI. Primary antibodies used for the detection of mouse <i>Tigar</i>	162
---------------------------------------------------------------------------------	-----

MATERIALS AND METHODS

Table M-I. Cell lines used in this thesis and origin.....	195
-----------------------------------------------------------	-----

Table M-II. Small interfering RNAs (siRNAs) used in this thesis	198
-----------------------------------------------------------------------	-----

Table M-III. Overexpression plasmids used in this thesis.....	198
---------------------------------------------------------------	-----

Table M-IV. Protease and phosphatase inhibitors used for RIPA buffer	199
----------------------------------------------------------------------------	-----

Table M-V. Protease and phosphatase inhibitors used for subcellular fractioning	200
---------------------------------------------------------------------------------------	-----

Table M-VI. Compatibility between protein assays and lysis buffers.....	202
-------------------------------------------------------------------------	-----

Table M-VII. Recipe for two electrophoresis gels.....	203
-------------------------------------------------------	-----

Table M-VIII. Primary antibodies used for western blot	205
--------------------------------------------------------------	-----

Table M-IX. Secondary antibodies used for western blot.....	205
-------------------------------------------------------------	-----

Table M-X. Primary antibodies used for immunofluorescence.....	208
----------------------------------------------------------------	-----

Table M-XI. Secondary antibodies used for immunofluorescence	208
--------------------------------------------------------------------	-----

Table M-XII. Nuclear markers used for immunofluorescence.....	208
---------------------------------------------------------------	-----

Table M-XIII. TaqMan Assays (Thermo Fisher Scientific) used in this thesis	212
----------------------------------------------------------------------------------	-----

Table M-XIV. Reactive species detected by DCFDA and CellROX Green.....	212
------------------------------------------------------------------------	-----

Table M-XV. Preparation of a standard curve of Fru-2,6-P ₂	219
-----------------------------------------------------------------------------	-----

Table M-XVI. Primers used for the obtention of fragments D, J, 8 and 15.....	225
------------------------------------------------------------------------------	-----

Table M-XVII. LB and LB-Agar recipes.....	231
-------------------------------------------	-----

ABBREVIATIONS

2,3-BPG	2,3-bisphosphoglycerate	FAS	Fatty acid synthase
2-PG	2-phosphoglycerate	FBPase1	Fructose 1,6-bisphosphatase
3-PG	3-phosphoglycerate	FBS	Foetal bovine serum
3PHP	3-phosphohydroxypyruvate	FDG-PET	¹⁸ F-2-deoxy-D-glucose positron emission tomography
3PO	3-(3-pyridinyl)-1-(4-pyridinyl)-2 propen-1-one	Fru-1,6-P₂	Fructose-1,6-bisphosphate
3PS	3-phosphoserine	Fru-2,6-P₂	Fructose-2,6-bisphosphate
6PGD	6-phosphogluconate dehydrogenase	Fru-6-P	Fructose-6-phosphate
ACD	Adenocarcinoma	G3P	Glyceraldehyde-3-phosphate
Acetyl-CoA	Acetyl coenzyme A	G6PD	Glucose-6-phosphate dehydrogenase
ACL	ATP citrate lyase	GAPDH	Glyceraldehyde-P-dehydrogenase
Act-D	Actinomycin-D	GFP	Green fluorescent protein
ALDO	Aldolase	GLS1/2	Glutaminase 1 and 2
ALT1	Alanine transaminase 1	Glu	Glutamate
AMPKα	AMP-activated protein kinase α	Glu-6-P	Glucose-6-phosphate
ARE	Antioxidant response element	Glut1/3	Glucose transporter 1 and 3
ATF4	Activating transcription factor 4	GPI	Glucose phosphate isomerase
ATM	Ataxia telangiectasia-mutated	GPX	Glutathione peroxidase
BACs	Bacterial artificial chromosomes	GR	Glutathione reductase
BHA	Butylated hydroxyanisole	GSSG	Oxidized glutathione
CAFs	Cancer-associated fibroblasts	GST	Glutathione S-transferases
CAV1	Caveolin 1	H₂O₂	Hydrogen peroxide
ChIP	Chromatin immunoprecipitation	HDM2	Ubiquitin ligase double minute 2 homolog
ConA	Concanavalin A	HIF-1α	Hypoxia inducible factor 1 α
COX	Cytochrome c oxidase	HK-I/II	Hexokinase I and II
CRE	cAMP Response Elements	IDG-SW3	Immortomouse/Dmp1-GFP-SW3 cells
CREB1	cAMP Response Element-Binding Protein 1	iPFK-2	Inducible PFK-2
CS	Citrate synthase (CS)	KEAP1	Kelch-like ECH-associated protein 1
DCFDA	Dichlorofluorescein diacetate	LC3	Microtubule-associated protein 1 light chain 3
DMF	Dimethyl fumarate	LC-MS/MS	Liquid chromatography with mass spectrometry
DNP-MRSI	Dynamic nuclear polarization-enhanced magnetic resonance spectroscopic imaging	LDHA/B	Lactate dehydrogenase A and B
ECR	Evolutionary Conserved Regions	LKB1	Tumour suppressor liver kinase B1
ENO	Enolase	IPFK-2	Liver PFK-2
ER	Endoplasmic reticulum	LPS	Lipopolysaccharide
FACS	Fluorescence-activated cell sorter		

MCT4	Monocarboxylate transporter 4	PGME	Erythrocyte bisphosphoglycerate mutase
ME	Malic enzyme	PHA	Phytohemagglutinin
Methyl-THF	5,10-methylene-tetrahydrofolate	PHGDH	Phosphoglycerate dehydrogenase
MK2	MAPK-activated protein kinase 2	Pi	Inorganic phosphate
MTHFD1/2	Methylene-tetrahydrofolate dehydrogenase 1 and 2	PI	Propidium Iodide
mTORC1	Mechanistic target of rapamycin complex 1	PI3K	Phosphatidylinositol 3-kinase
MTT	3-(4,5-dimethylthiazol-2-yl)-2,5-diphenyltetrazolium bromide	PK	Pyruvate Kinase
NAC	N-acetyl-cysteine	PKA-C	Protein kinase A, B (Akt) and C
NADH	Nicotinamide adenine dinucleotide	PP-1	Protein phosphatase 1
NADPH	Nicotinamide adenine dinucleotide phosphate	PP2A	Protein phosphatase 2A
NFκB	Nuclear Factor kappa B	PPI-PFK	Pyrophosphate phosphofructokinase
Noco	Nocodazole	PPP	Pentose phosphate pathway
Nrf2	Nuclear factor (erythroid-derived 2)-like 2	PPARγ	Peroxisome proliferator-activated receptor gamma
NSCLC	Non-small cell lung cancer	Pyr	Pyruvate
OAA	Oxaloacetate	Rb	Retinoblastoma protein
OXPHOS	Oxidative phosphorylation	R5P	Ribose-5-phosphate
PC	Pyruvate carboxylase	RSK	Ribosomal S6 kinase
PCR	Polymerase chain reaction	ROS	Reactive oxygen species
PDAC	Pancreatic ductal adenocarcinoma	RTK	Receptor tyrosine kinases
PDH	Pyruvate dehydrogenase	RT-MLPA	Reverse transcriptase multiplex ligation-dependent probe amplification
PDK1	Pyruvate dehydrogenase kinase	RT-qPCR	Real-time quantitative PCR
PEP	Phosphoenolpyruvate	SCO2	Synthesis of cytochrome c oxidase 2
PFA	Paraformaldehyde	SDH	Succinate dehydrogenase
PFK-1	6-phosphofructo-1-kinase	SFN	Sulforaphane
PFK-158	(E)-1-(4-Pyridinyl)-3-[7-(trifluoromethyl)-2-quinoliny]-2-propen-1-one	SHMT1/2	Hydroxyl methyltransferase 1
PFK-2/FBPase-2	6-phosphofructo-2-kinase/fructose-2,6-bisphosphatase	siRNA	Small-interfering RNA
PFKFB1-4	6-Phosphofructo-2-Kinase/Fructose-2,6-Biphosphatase 1-4	SP1	Specificity Protein 1
PFK-L	Liver PFK-1	SQCC	Squamous cell carcinoma
PFK-M	Muscle PFK-1	tBHP	Tert-butyl-hydroperoxide
PFK-P	platelet PFK-1	tBHQ	Tert-butyl-hydroquinone
PGAM	Phosphoglycerate mutase	TCA	Tricarboxylic acid
PGK	Phosphoglycerate kinase	TCGA	The cancer genome atlas
		TGF-β1	Transforming growth factor beta 1
		THF	Tetrahydrofolate
		TIGAR	TP53-induced glycolysis and apoptosis regulator

TME	Tumour microenvironment
TOM20	Translocase of outer mitochondrial membrane 20
TPI	Triose-phosphate isomerase
TRX	Thioredoxin
TSC2	Tuberous sclerosis 2
TSS	Transcription start site
uPFK-2	Ubiquitous PFK-2
αKG	Alpha-ketoglutarate

INTRODUCTION



CANCER: ONE NAME, MULTIPLE FACTS

The study of a specific alteration in cancer cells usually arises from the finding that a particular molecule, being it a gene, a protein, a metabolite, a secondary messenger or any other player, is different in cancer patients compared to the healthy population. Far from the existence of a common signature of cancer alterations, the reality is that each patient's tumour is characterized by hundreds of different molecular traits, which can contribute to the development of the tumour. Any of these traits can be at the basis for the initiation of a research project. Although this scenario of variability is from where our researches arise, still a general effort to find common signatures among tumours is made. Given the difficulty of studying the causes and consequences of the particular alterations found within each patient's tumour, the most common strategy is to analyse genes or pathways that are altered in a group of patients. The classification of tumours into groups, which are referred to as tumour types or tumour subtypes -if a more precise classification is performed- is useful but, at the same time, we should always have in mind that these groups are somehow artefacts that clinicians and researchers have invented to make the study of millions of different ecosystems, which are the tumours, simpler.

Some years ago, Hanahan and Weinberg summarized a total of six features, then modified to ten, that were constantly observed in tumours. This organizing principle for rationalizing the complexities of neoplastic disease contributed to define a common draw of what a tumour is but, more importantly, helped to better understand and integrate different approaches to address cancer treatment (1,2). Altered metabolism is a common feature in most tumours and, because of that, it is considered as one of the hallmarks of cancer. The other signatures shared by most tumours are sustained proliferative signalling, evasion of growth suppressors, resistance to cell death, capacity of replicative immortality, induction of angiogenesis, activation of invasion and metastasis, and evasion of the immune system. Besides, two enabling characteristics -as the authors named them- foster these hallmarks: genome instability, which creates the genetic diversity to allow these transformation events, and inflammation, which increases the effect of all these alterations by potentiating cell dysregulation (2). Moreover, these alterations are interconnected in a way that usually one contributes to another (**Figure 1**).

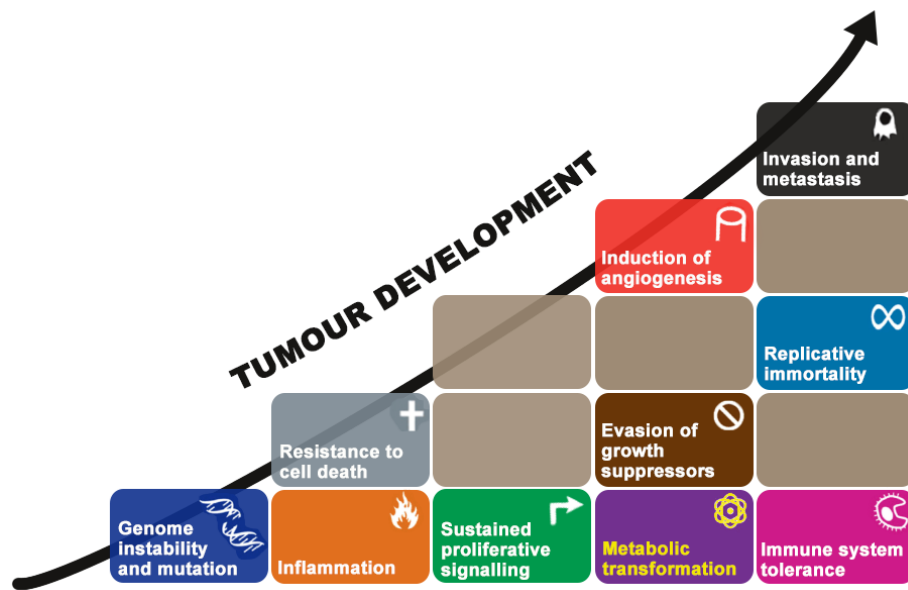


Figure 1. The hallmarks of cancer. The ten hallmarks described by Hanahan and Weinberg (1,2) are represented as key building blocks in the process of tumour development, which is represented as a stair. In this representation, related hallmarks are close to each other (e.g. sustained proliferative signalling triggers oncogenic metabolic pathways), and those alterations that are more important in the initiation of transformation are situated at the base. The beige building blocks represent specific alterations that are required in each cancer type and differentiate the oncogenic process in each patient.

In the complex landscape of tumour metabolism, this thesis is mainly focused in the study of a particular gene, the ***TP53-Induced Glycolysis and Apoptosis Regulator (TIGAR)*** (3). This gene, originally named as *c12orf5*, was discovered during a computer-based analysis of microarray data trying to find novel p53-regulated genes that are activated in response to ionizing radiation (4). TIGAR discovery occurred only nine years before the beginning of this thesis and the findings that are summarized in this work aim to enlarge the knowledge about this gene and the homonymous protein that it codifies, from the perspective of basic research. In this sense, we have not been focused on a single type of cancer, but different cell lines have been used in order to answer each question. The result of this are several pieces of information that have helped us to better understand the role of TIGAR in cancer cell metabolism. TIGAR was described as a fructose-2,6-bisphosphate (Fru-2,6-P₂) phosphatase (3). The study of enzymes regulating Fru-2,6-P₂ levels is important in the context of cancer research given that it is the main allosteric stimulator of 6-phosphofructo-1-kinase (PFK-1) and, thus, a key player in the metabolic transformation. To situate the scenario in which TIGAR acts, the main features of cancer cell metabolism are reviewed in this Introduction.

1. General considerations on cancer metabolism: catabolism for anabolism

Metabolic transformation cannot be defined as a list of altered metabolic pathways. Indeed, it is the result of overtaken regulatory mechanisms and compensation events that take place in cancer cells that drive the reorganization of the whole tumour metabolism. Cancer cells, in the same way as other proliferating cells, have not only to meet various energetic requirements, but also to satisfy the anabolic demands of macromolecular biosynthesis: nucleotides, lipids and proteins for proliferation and growth. These processes are accurately regulated in normal proliferating cells, whereas they are aberrantly driven in cancer (5) (**Figure 2**).

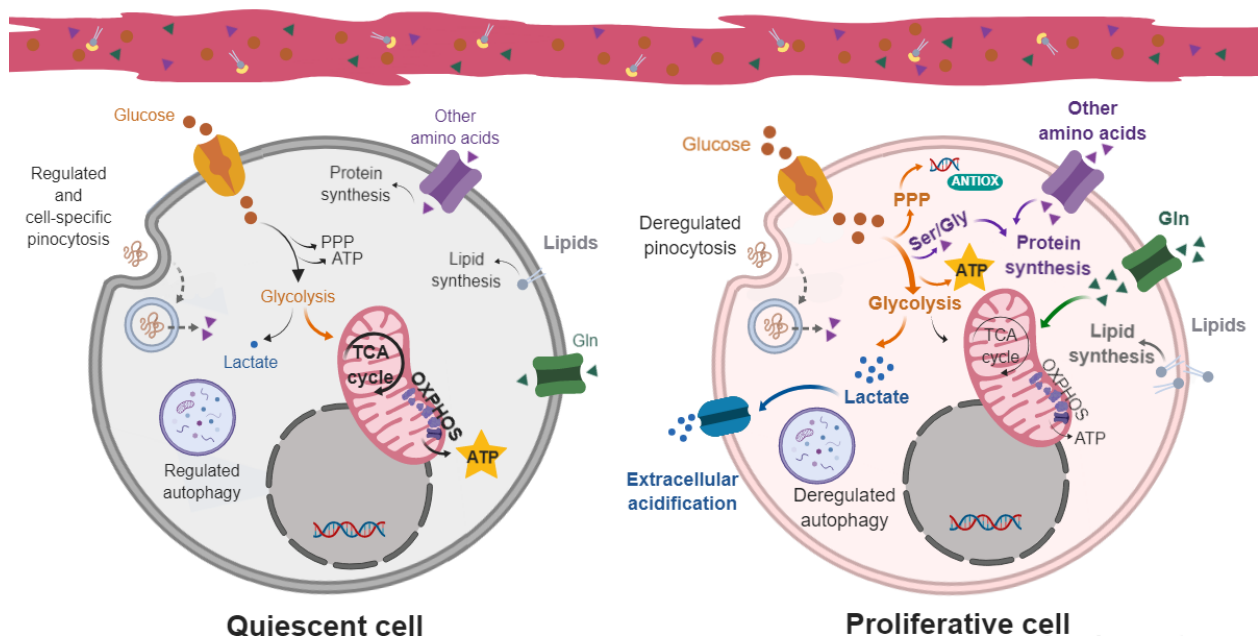


Figure 2. Main differences in the fuels and metabolic pathways used by quiescent and proliferative cells. Proliferative cells show increased uptake of all kinds of fuel, the most important of which are glucose (in orange) and glutamine (in green). The main source of ATP in these cells is glycolysis, whereas mitochondrial metabolism accomplishes this function in quiescent cells, with increased TCA cycle and OXPHOS. Enhanced glycolysis in proliferative cells increases lactate production (in blue), causing an acidification of extracellular media. Other pathways that are increased during proliferation are the pentose phosphate pathway (PPP), which generates nucleotides and NADPH, the serine and glycine synthesis pathway and other anabolic pathways for protein and lipid synthesis. In proliferative cells, pinocytosis and autophagy are sometimes deregulated to obtain additional nutrients. Image created with BioRender.

In general, cancer cells take up all kinds of fuel present in the tumour microenvironment to fulfil their needs, being glucose, lactate, glutamine, acetate and phospholipids the most important molecules (6). The processes for introducing these molecules into the cell vary depending on the nature of each compound: sugars and amino acids need to be internalized through transporters, whereas lipids can diffuse through the membrane and big cargo such as proteins can be introduced by pinocytosis (7).

Once inside the cell, the main metabolic pathways through which these molecules are oxidized are glycolysis, the pentose phosphate pathway, glutaminolysis and the tricarboxylic acid (TCA) cycle (**Figure 2**). It is important to note that amino acids, acetate and phospholipids are usually incorporated into anabolic pathways, instead of catabolic ones (6,8). In the case of amino acids, they are either used for protein synthesis or in the reactions that allow the conversion of one amino acid into another, catalysed by transaminases. Phospholipids and acetate, in their turn, are mainly used for the synthesis of fatty acids required for the generation of new cellular membranes. One example of the pro-tumoral benefits of increased fatty acid anabolism is prostate cancer, in which fatty acid synthase has been reported to exhibit copy-number gain (9). On the contrary, it is also true that some specific tumours also demonstrate dependency on fatty acids oxidation, as it is the case of a subtype of B cell lymphoma (10).

Apart from these key metabolic pathways, several reactions of amino acid synthesis such as the serine and glycine synthesis pathway, the *de novo* synthesis of lipids, purines and pyrimidines, and the generation of nicotinamide adenine dinucleotide phosphate (NADPH) and glutathione are also essential processes in the complex metabolic network that arises from central carbon metabolism in cells. Finally, oxidative phosphorylation (OXPHOS) is crucial for the coupling of ATP generation to the high number of NADH and FADH₂ molecules generated through oxidative pathways (**Figure 2**).

2. Glycolytic metabolism

Considering that this thesis is focused on the study of TIGAR, an enzyme described to inhibit glycolysis, the main enzymes of this pathway will be further discussed, with special attention to those involved in the metabolism of Fru-2,6-P₂.

2.1. Obtaining the carbons: the glycolytic phenotype

Glucose and glutamine are the most important fuels in cancer cells. Regarding the utilization of glucose, one of the most relevant features of cancer cells is the glycolytic phenotype, which consists in accelerated uptake and metabolization of glucose regardless of oxygen availability (Figure 3).

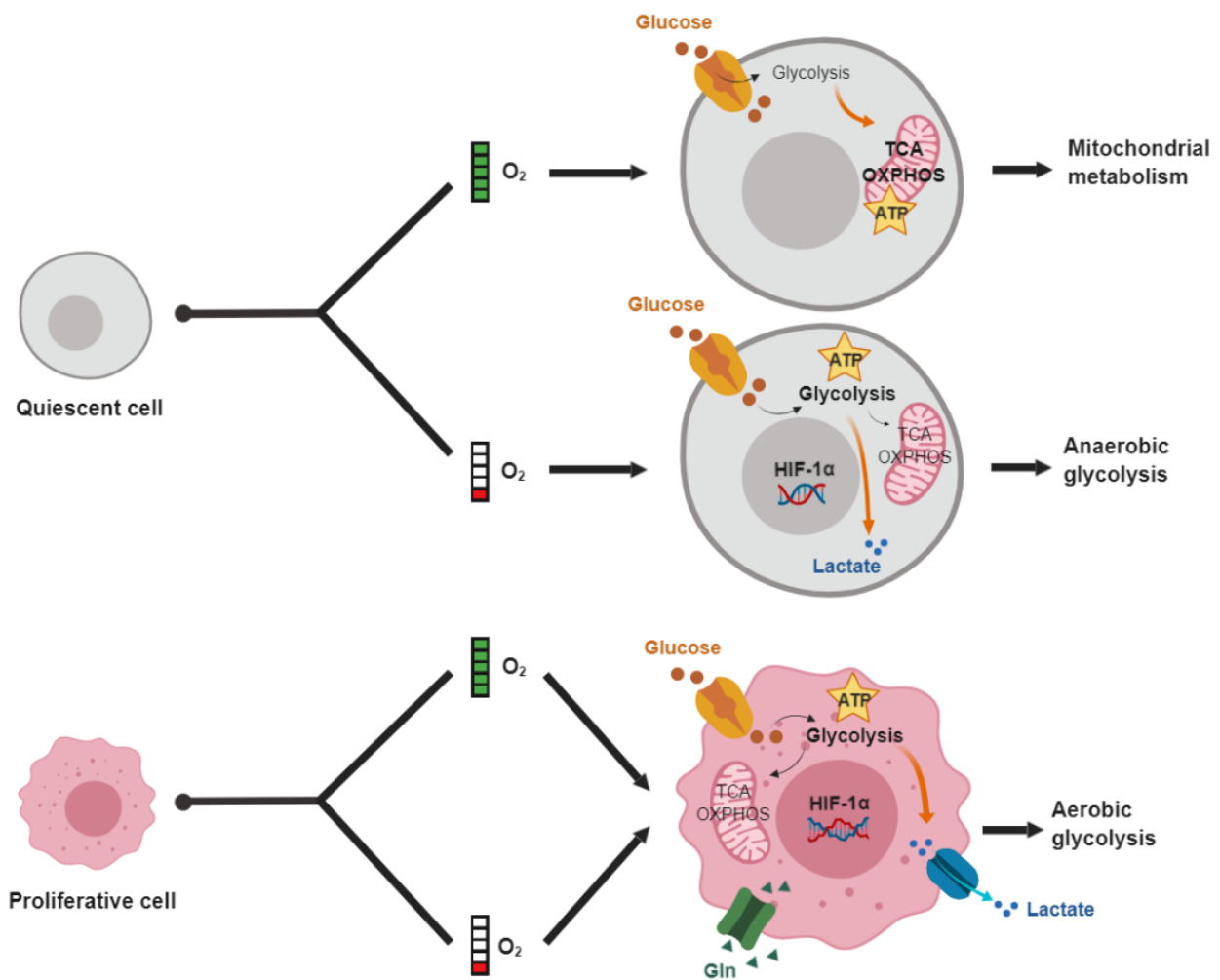


Figure 3. Oxidative metabolism in quiescent and proliferative cells. The main metabolic pathways that quiescent and proliferative cells display in conditions of high oxygen (green O₂ bar) or low oxygen (red O₂ bar) are illustrated. The main fuels used by these cells in each of the conditions are also depicted. Quiescent cells shift mitochondrial metabolism towards anaerobic glycolysis at low oxygen conditions, whereas proliferative cells are mainly glycolytic regardless of oxygen levels, in what is called aerobic glycolysis. Image created with BioRender.

Most non-proliferating differentiated cells metabolize glucose to pyruvate (Pyr) through glycolysis, and then completely oxidize most of the Pyr to CO₂ through the TCA cycle in the mitochondria (Figure 3). NADH and FADH₂ generated in the TCA cycle are oxidized in the mitochondrial electron transport chain, generating an electrochemical gradient of protons that is coupled to the production of ATP. The final acceptor of the electrons in this chain is oxygen. As a result, non-proliferative cells rely on oxygen availability for ATP production to maintain their integrity. In low oxygen conditions, the electron transport chain is impaired, and cells shift their metabolism towards glycolysis in what is known as anaerobic glycolysis (Figure 3). In contrast, proliferative cells display high glycolytic rates even in the presence of adequate oxygen levels, a process called aerobic glycolysis (Figure 3). This phenomenon was firstly evidenced by Otto Warburg in 1927 and, for this reason, it is also termed “the Warburg effect” (11). In the clinics, this hallmark has been exploited in ¹⁸F-2-deoxy-D-glucose positron emission tomography (FDG-PET), an imaging technique that is based on the detection of the radioactivity emitted by this analogue of glucose that is absorbed by proliferative tissues and cannot be further metabolised beyond hexokinase (HK) and thus accumulates (Figure 4).

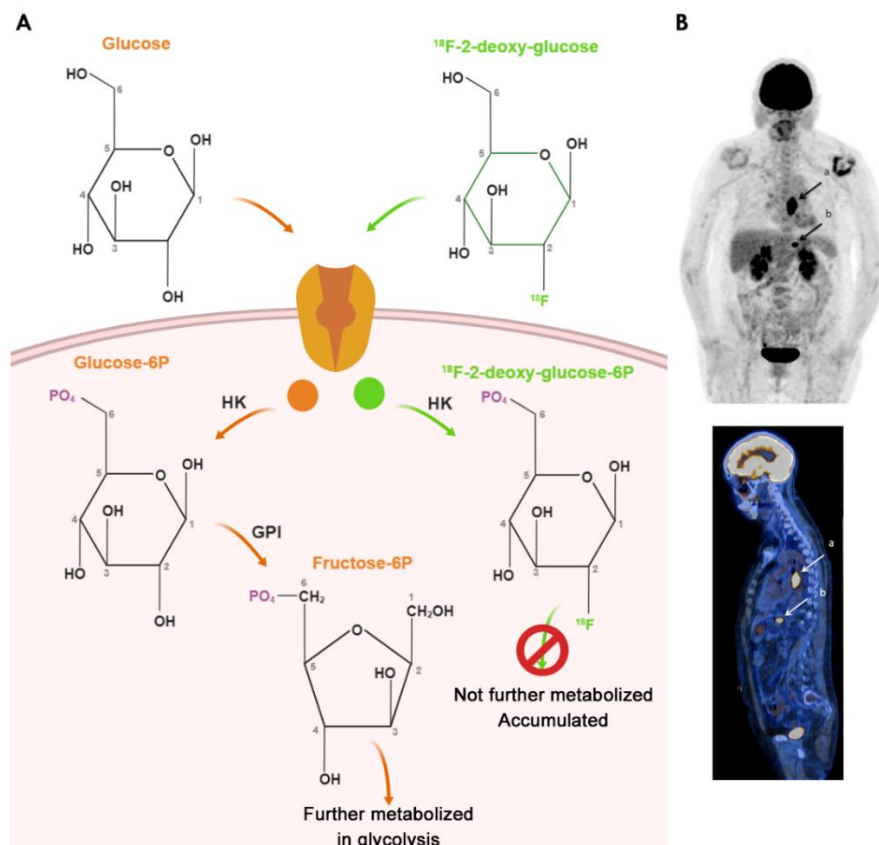


Figure 4. Molecular basis of ¹⁸F-2-deoxy-glucose positron emission tomography (PET). (A) Schematic representation of the metabolism of ¹⁸F-2-deoxy-glucose compared to glucose. Both glucose and ¹⁸F-2-deoxy-glucose can be phosphorylated by HK, but only Glu-6-P can be further metabolized by GPI to Fru-6-P given that ¹⁸F-2-deoxy-glucose-6-P has ¹⁸F substituting the hydroxyl group at C₂. (B) Initial staging of a woman with oesophageal squamous cell carcinoma of the middle third of the oesophagus. PET maximum intensity projection image (upper image) and sagittal fused positron emission tomography/computed tomography image (lower image) showing ¹⁸F-2-deoxy-glucose uptake in (a) the primary oesophageal tumour and (b) in a celiac lymph node. PET images from (12). Image created with BioRender.

PET represents a potent tool to detect precancerous and cancerous lesions and to track the evolution and response to oncological treatments. In the early 1990s, studies using FDG-PET showed that most tumours displayed increased glucose uptake in about an order of magnitude higher than that of normal tissue (13), which caused the resurgence of the study of bioenergetics in cancer. The increased glucose uptake largely depends on the rate of glucose phosphorylation by hexokinases and the upregulation of glucose transporters 1 and 3 (Glut1 and Glut3) (14). More than 90% of primary and metastatic tumours have high glucose uptake, which directly correlates with tumour aggressiveness (13,15). In the last years, a new technique based on the imaging of hyperpolarized ^{13}C -labelled substrates, which also takes advantage of the Warburg effect displayed by tumours, has been developed. The technique is known as dynamic nuclear polarization-enhanced ^{13}C magnetic resonance spectroscopic imaging (DNP-MRSI) and increases the sensitivity of magnetic resonance. Although PET is more sensitive, DNP-MRSI allows for the detection of ^{13}C -glucose products separated from glucose and, thus, can detect tumours located in those organs in which glucose and ^{18}F -2-deoxy-D-glucose accumulate, such as the bladder. Besides, imaging of injected ^{13}C -pyruvate can reveal brain tumours which are also difficult to detect by PET (16). The laboratory of Dr. Kevin Brindle (Cambridge) has been working on this field for years and has started a clinical trial using the imaging of hyperpolarized ^{13}C -pyruvate in patients receiving radiotherapy.

Far from the view of glycolysis as a metabolic pathway focused only on the generation of ATP – something that is true for the brain, red muscle, erythrocytes, sperm cells and renal medulla (17)– cancer cells take advantage of this pathway to increase the flux of glycolytic intermediates to key anabolic pathways. The diversion of glucose-6-phosphate (Glu-6-P) to oxidative pentose phosphate pathway (PPP), fructose-6-phosphate (Fru-6-P) to hexosamine-phosphate pathway and non-oxidative PPP, glyceraldehyde-3-phosphate (G3P) to non-oxidative PPP, 3-phosphoglycerate (3-PG) to *de novo* serine and glycine synthesis, and G3P to lipids synthesis are some examples of cataplerosis in glycolysis (**Figure 5**). These and other metabolic crossroads are discussed in Section 3 of this Introduction. **Figure 5** will be used throughout this Introduction to situate the different metabolic pathways commented.

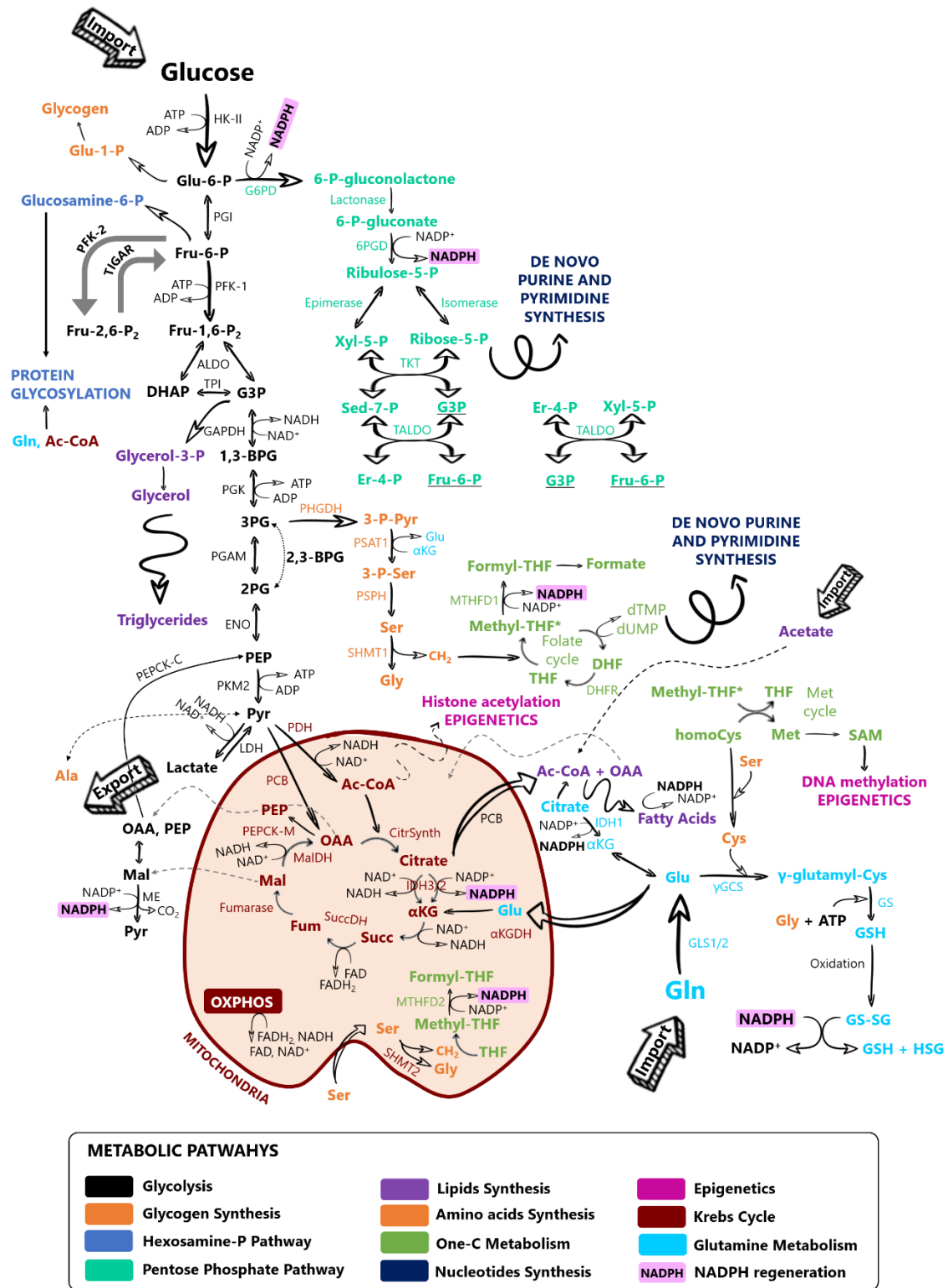


Figure 5. Main metabolic pathways altered in cancer cells. The most important metabolic reactions involved in the oxidation of glucose and glutamine in cancer cells are depicted. A colour code is used to indicate each metabolic pathway. Connections between central carbon metabolism and biosynthetic pathways are indicated.

2.2. Using the carbons: key glycolytic enzymes

Studies of glycolysis regulation in the 1960s, including thermodynamic assessments and measurements of intracellular metabolite concentrations, led to the identification of non-equilibrium reactions catalysed by HK, PFK-1, and pyruvate kinase (PK) (18). These reactions are the checkpoints for the control of glycolytic flux. HK and PFK-1 control the first steps of the pathway according to the availability of glucose and the energy state of the cell, and PK restricts the last step and, by doing so, is able to regulate the whole flux through the pathway.

2.2.1. Capturing glucose through phosphorylation by HK

HK catalyses the first reaction of glycolysis, converting glucose to the non-exportable Glu-6-P (**Figures 5, 6**). Of the four known HK isoenzymes (I, II, III, and IV), the type II and to a lesser extent the type I isozymes are overexpressed in rapidly growing, highly glycolytic tumours. The gene encoding *HK-II* was firstly described to be amplified in hepatoma cells, showing that increased gene copy number is one of the mechanisms involved in the aberrant expression of metabolic genes in cancer cells (19). Interestingly, already in 1955, it was described that the expression of glucose-6-phosphatase, an enzyme that dephosphorylates glucose in the liver in order to complete the last step of gluconeogenesis and allow the secretion of glucose to the blood, decreased progressively during carcinogenesis and was almost absent in the hepatomas (20). These data shows the commitment of transformed cells to utilize all the glucose available regardless of their previous metabolic condition.

2.2.2. PFK-1 and the Fru-6-P/Fru-1,6-P₂ substrate cycle

PFK-1 is a tetrameric protein, with three different genes encoding the muscle, liver and platelet (PFK-M, PFK-L and PFK-P, respectively) human isoenzymes. This enzyme catalyses the phosphorylation of Fru-6-P to fructose-1,6-bisphosphate (Fru-1,6-P₂) by ATP (**Figures 5, 6**). Tumours do not usually exhibit overexpression of PFK-1, although preference for the expression of the PFK-L isoenzyme has been observed in breast cancer (21). This first commitment step of Fru-6-P is highly regulated by the so-called Fru-6-P/Fru-1,6-P₂ substrate cycle, which involves the activity of two other enzymes that are mainly regulated by the availability of their substrates and products: fructose 1,6-bisphosphatase (FBPase1) and 6-phosphofructo-2-kinase/fructose-2,6-bisphosphatase (PFK-2/FBPase-2). FBPase1 catalyses the opposite reaction to PFK-1 and its loss is a common event in human cancers (22). Accordingly, FBPase1 activity suppresses cancer cell growth (23). The other key player in this substrate cycle is the homodimeric bifunctional enzyme PFK-2/FBPase-2, responsible for the synthesis and degradation of Fru-2,6-P₂ (**Figures 5, 6**).

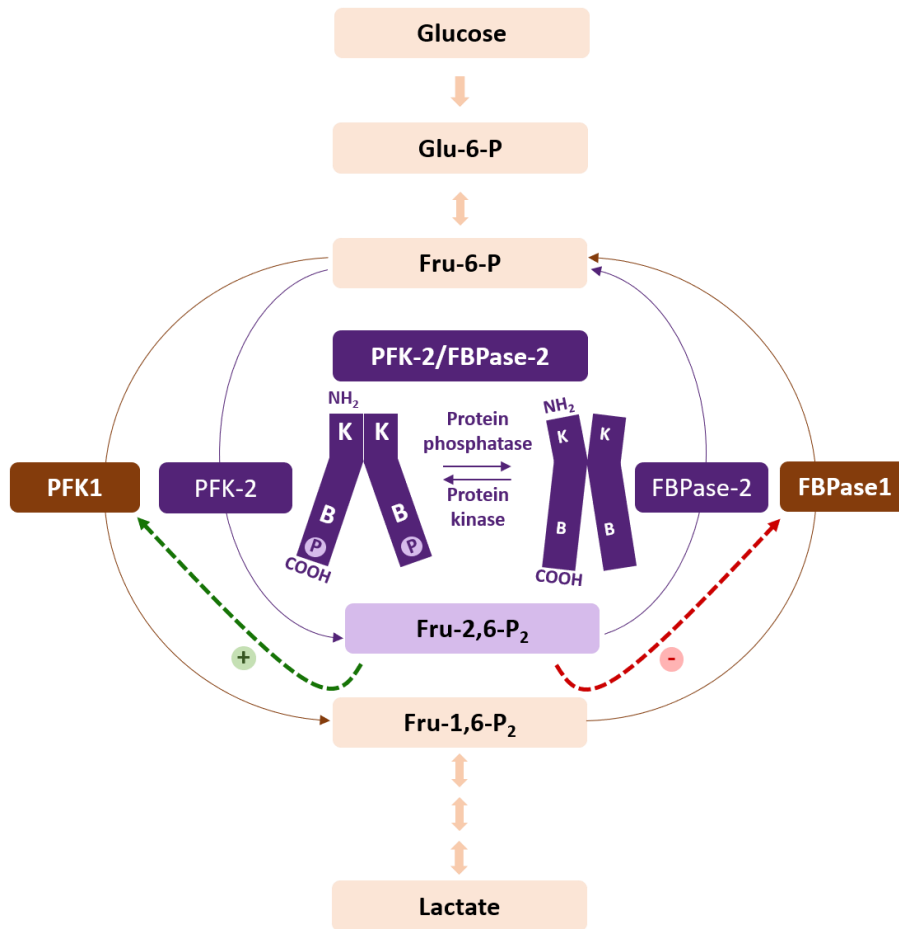


Figure 6. Regulation of the Fru-6-P/Fru-1,6-P₂ substrate cycle. Fru-2,6-P₂ is synthesized and degraded by PFK-2/FBPase-2, respectively. Increased levels of this metabolite allosterically activate PFK-1 and inhibit FBPase1, increasing the synthesis of Fru-1,6-P₂ and, thus, the glycolytic flux. Phosphorylation of PFKFB2 or PFKFB3 isoenzymes increases the kinase activity of the enzyme. The kinases and phosphatases responsible for this regulation vary according to the isoenzyme. PFKFB1 is not represented by this figure, as phosphorylation of this isoenzyme increases its bisphosphatase activity. Phosphorylation of PFKFB4 has not been described to date. Published in (24).

2.2.3. PFK-2/FBPase-2: the importance of Fru-2,6-P₂

Each of the monomers of PFK-2/FBPase-2 consists of two functional domains (25–27). The N-terminal domain is responsible for the kinase activity, which catalyses Fru-2,6-P₂ synthesis using Fru-6-P and ATP as substrates; whereas the C-terminal domain contains the bisphosphatase activity (26–28) and is responsible for the hydrolytic degradation of Fru-2,6-P₂ into Fru-6-P and inorganic phosphate (Pi) (**Figure 7**).

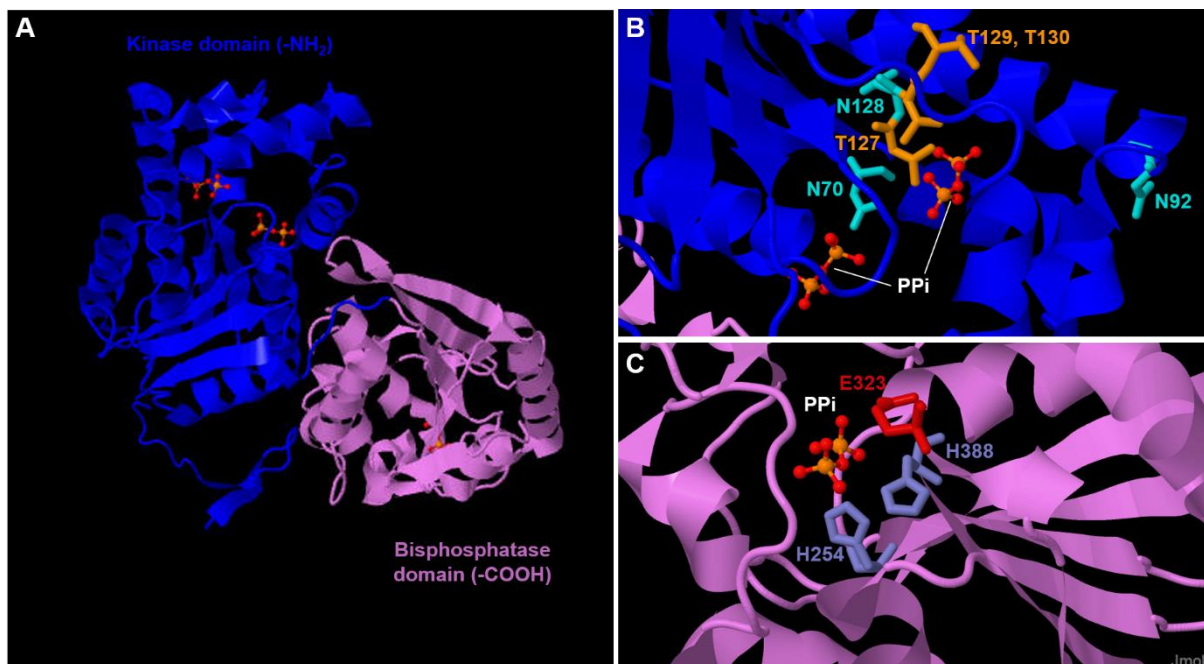


Figure 7. PFK-2/FBPase-2 structure. The structure of PFKFB3 was downloaded from Protein Data Band (Reference Number: 3QPU). **(A)** General view of the protein where the kinase and phosphatase domains have been coloured in blue and violet, respectively. PPI is represented in the ball-and-stick model. **(B)** Zoom into the kinase active site in which the residues important for Fru-6-P phosphorylation are represented in sticks coloured according to the type of amino acid (blue for asparagine, N; orange for threonine, T). The exact positions of the amino acids forming this active site have been obtained through a BLAST alignment of PFKFB3 with PFKFB1, in which N76, N97, N133, T132, T134 and T135 were described as key residues for the kinase activity (29). The residues shown in the image are the corresponding aligned residues in PFKFB3. PPI is represented in the ball-and-stick model. **(C)** Zoom into the phosphatase active site in which the residues important for Fru-2,6-P₂ dephosphorylation are represented in sticks coloured according to the type of amino acid (grey for histidine, H; red for glutamic acid, E). PPI is represented in the ball-and-stick model. Images were created with Jmol: an open-source Java viewer for chemical structures in 3D. <http://www.jmol.org/>.

The balance between the kinase and the bisphosphatase activities of PFK-2/FBPase-2 ultimately determines the concentration of Fru-2,6-P₂, which constitutes the most important mechanism for increased PFK-1 activity in tumours. Given that Fru-2,6-P₂ does not take part as an intermediary in any metabolic interconversion, and it is highly liable in the acid extracts used to measure phosphorylated metabolites in tissues, it escaped from discovery until 1980, when its levels were found significantly increased in hepatocytes in the presence of glucose and disappeared upon incubation with glucagon, displaying an elegant switching mechanism between glycolysis and gluconeogenesis (27,30). With the same atomic composition as the product of PFK-1, Fru-1,6-P₂, but different distribution of phosphates,

it allosterically activates PFK-1 by increasing its affinity for Fru-6-P (17) and releases it from ATP-mediated inhibition. Besides, Fru-2,6-P₂ acts synergistically with AMP in activating PFK-1 and inhibiting FBPase1 (25,26,30). Therefore, the discovery of Fru-2,6-P₂ constituted a landmark in the understanding of how liver carbohydrate metabolism is regulated. Nowadays, it is widely known that this metabolite plays a major role in controlling glycolysis in other tissues and in proliferating and transformed cells (24,25,27,31). Indeed, Fru-2,6-P₂ concentration is significantly higher in tumour cells than in normal cells (32,33).

PFK-2/FBPase-2 was firstly described in rats, where the liver and muscle isoenzymes were characterized (34). From then, other mammalian bifunctional isoenzymes have been identified, which are encoded by four genes (*PFKFB1-4*) (28) with different expression according to tissue and developmental stage (35) (**Table I**).

Gene	Chromosomal location	Kinase/phosphatase ratio	Isoenzymes	Regulation
<i>PFKFB1</i>	Xp11.21	2.5 (rat liver)	IPFK-2 (liver)	PKA
		1.2 (bovine liver)	mPFK-2 (muscle)	PP2A
		0.4 (rat muscle)	fPFK-2 (foetal)	
<i>PFKFB2</i>	1q32.1	1.8 (bovine heart)	hPFK-2 (heart)	AMPK, PKA, PKB, PKC, RSK Glucocorticoids, androgens, RNA LINC00092
<i>PFKFB3</i>	10p15.1	710 (human placenta)	uPFK-2 (ubiquitous)	AMPK, PKA, PKB, PKC, Smad, RSK, HIF-1 α , p38-MK2
		3.1 (bovine brain)	iPFK-2 (inducible)	Oestrogens, adenosine, LPS p53, S-glutathionylation, demethylation
<i>PFKFB4</i>	3p21.31	4.1 (rat testis)	tPFK-2 (testis)	HIF-1 α , P-PPAR γ
		0.9 (human testis)		

Table I. Properties of the human PFK-2/FBPase-2 isoenzymes. Information regarding their gene name, chromosomal location, isoenzymes, enzymatic activity and regulation is shown. Positive and negative regulators are written in green and red, respectively.

PFKFB1 is predominantly expressed in liver and muscle, and in some stages during foetal development, *PFKFB2* codes for the heart isoenzyme, *PFKFB3* was initially described in brain and now it is also known to be the main isoenzyme in placenta and proliferating cells and, finally, *PFKFB4* is preferentially expressed in testis and some other proliferative tissues. Importantly, tissue- and cell-specific isoenzymes are not totally exclusive, and several cells express more than one type of isoenzyme (36). *PFKFB2*, *PFKFB3* and *PFKFB4*, but not *PFKFB1*, have been found expressed in several types of cancer, being *PFKFB3* the most common isoenzyme found in these malignancies (36). As it can be appreciated in **Table I**, one gene can code for more than one isoform. However, *PFKFB1-4* are usually used to refer to the most-abundant isoforms IPFK-2, hPFK-2, uPFK-2 and tPFK-2, respectively. These different isoenzymes share highly

conserved catalytic core domains (85%) but greatly differ in their kinetic properties and responses to regulatory signals and tissue distribution. The differences are mostly due to the highly divergent N- and C-terminal regulatory domains (**Figure 8**). However, some sequence differences in residues surrounding the active sites in the catalytic domains also contribute to the kinetic differences (37).

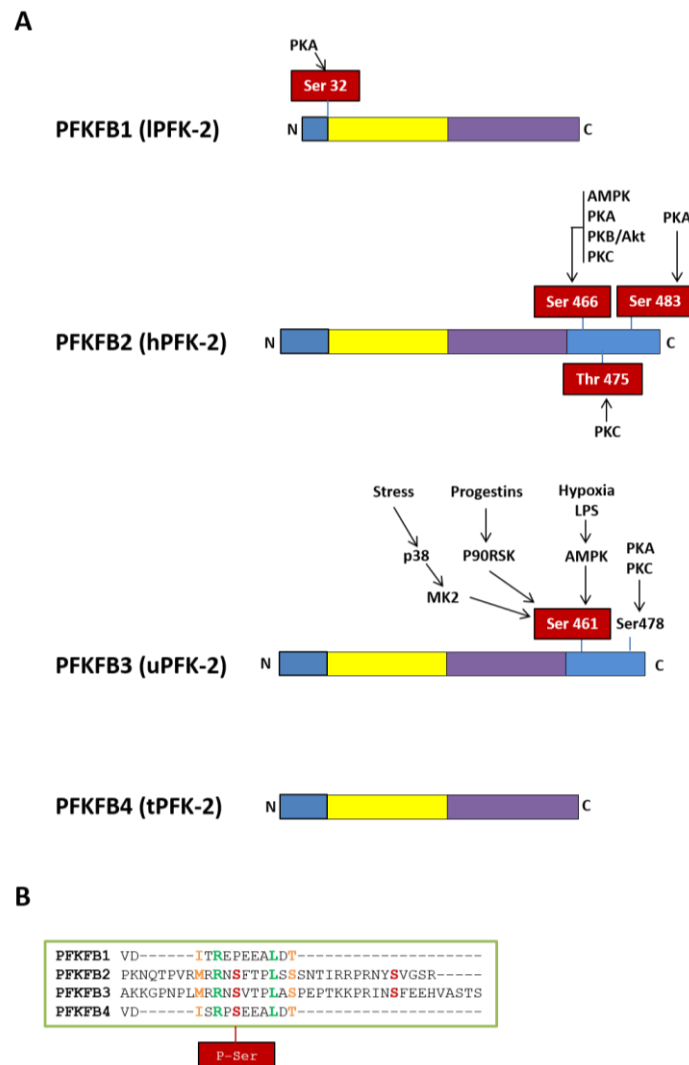


Figure 8. Domain organization and phosphorylated residues of PFK-2/FBPase-2 isoenzymes. (A) The N-terminal and C-terminal domains of PFK-2 are shown in yellow and purple, respectively. Regulatory regions with residues susceptible of phosphorylation by different protein kinases are shown in blue. The phosphorylated residues are highlighted in red boxes and the kinases described to phosphorylate each residue are indicated. **(B)** A common sequence for phosphorylation in serine residues is shared by PFKB2-4. Published in (24).

One of the clearest examples of the involvement of terminal regions in the regulation of PFK-2 isoenzymes is found in the proteins encoded by *PFKFB1* gene. Unlike muscle and foetal transcripts, the liver transcript (IPFK-2) contains an extra exon encoding the N-terminal end which contains the S32 residue, that can be phosphorylated by the cAMP-dependent protein kinase A (PKA) in response to glucagon and activates the bisphosphatase activity. The phosphorylation can be reversed by protein phosphatase 2A (PP2A), which increases the kinase activity of the liver isoenzyme. This regulation is

exclusive to the liver since it contributes to the switch from glycolysis to gluconeogenesis (25–27,30,38) upon glucagon signalling. On the contrary, phosphorylation events by different protein kinases are activating signals in isoenzymes PFKFB2 and PFKFB3 (**Table I, Figure 8**).

An important part of this thesis is addressed to describe the relationship between PFK-2 and, more specifically, PFKFB3, and TIGAR. Because of that, the most important features of PFK-2 isoenzymes expressed by cancer cells are reviewed in the following paragraphs.

PFKFB2 is expressed in cancer cells from different origins such as acute lymphoblastic leukemia, prostate, ovarian and gastric cancer, hepatocellular carcinoma, melanoma, osteosarcoma and glioma (28,39,40) and can undergo multisite phosphorylation, integrating signals from many pathways. Of special interest for this work is the finding that amino acids increase Fru-2,6-P₂ synthesis in rat cardiomyocytes and in the cancer cell lines MCF7 and HeLa through protein kinase B (PKB/Akt)-mediated phosphorylation of PFKFB2 (41).

The **PFKFB3** gene was cloned from a cDNA library of foetal brain and has been found expressed in all the tissues in which it has been studied (42–46). The variable C-terminal domain can undergo alternative splicing to produce six different isoforms (47). The two main isoforms are generated by alternative splicing of exon 15 and differ in their C-terminal sequences, the 4.553 bp mRNA variant, initially named as ubiquitous PFK-2 (uPFK-2) (46), and the 4.226 bp mRNA inducible PFK-2 (iPFK-2) variant, which was described to be overexpressed in response to hypoxia or during the S or DNA synthesis phase of the cell cycle. All the experiments included in this thesis are based on uPFK, which is the most abundant variant.

During years, research in Dr. Bartrons' Lab has focused on the study of molecules able to regulate PFKFB3. It has been described that hypoxia (48–50), progestin (43,51), oestrogens (52) and stress stimuli (41) induce **PFKFB3** through the interactions of hypoxia inducible factor 1 α (HIF-1 α), the progesterone receptor, the oestrogen receptor and the serum response factor, respectively, with the promoter of the gene. Besides, other stimuli have been described to activate PFKFB3, including insulin (33), pro-inflammatory molecules such as interleukin-6 (53,54), lipopolysaccharide (LPS) and adenosine (55). In parallel to the development of this thesis, the group has described that the transforming growth factor beta 1 (TGF- β 1) (56) and mitogenic lectins such as concanavalin A (ConA) and phytohemagglutinin (PHA) also increase **PFKFB3** expression (57,58). The publication describing the effect of PHA on **PFKFB3** expression in human lymphocytes can be found in the Annex at the end of this thesis.

The **PFKFB3** gene expresses the PFK-2/FBPase-2 isoenzyme with the highest kinase/bisphosphatase ratio (K/B = 710), favouring the net synthesis of Fru-2,6-P₂ and eliciting high concentrations of this metabolite in proliferating and tumour cells (59). Importantly, its kinase activity is even more exacerbated when the enzyme is phosphorylated. Different protein kinases can phosphorylate PFKFB3 by covalent modification

of its C-terminal domain and, among them, the phosphatidylinositol 3-kinase (PI3K)-Akt pathway is known to control PFKFB3 activity downstream of growth factors signalling (57,60,61). Moreover, overexpression of *PFKFB3* in HEK293 cells potentiates insulin-dependent phosphorylation of Akt and Akt substrates, evidencing a positive regulation loop between Akt and PFKFB3 (62). This is an example of how the hallmarks of cancer, previously introduced, are interconnected. During this thesis, the dependency on Akt for PFKFB3 activation during lymphocytes activation has been described in a publication previously mentioned (58).

PFKFB3 is constitutively overexpressed in different cancer cell lines and in several human leukemias and solid tumours including ovarian and thyroid carcinomas, colon adenocarcinoma, breast cancer, gastric and colon tumours, hepatocellular carcinoma, myeloproliferative neoplasms, glioblastoma and astrocytomas, and has been associated with lymph node metastasis and the TNM stage. PFKFB3 can also represent a biomarker and an anti-neoplastic target in gastric cancer. Besides, PFKFB3 is associated to lung fibrosis and the development of resistance to treatment in cases of chronic myeloid leukaemia and hepatocellular carcinoma. These studies have been reviewed by the group during the development of this thesis (36). A work from our group described for the first time the effects of *PFKFB3* inhibition in HeLa cancer cells, showing that PFKFB3-targeting small-interfering RNA (siRNA) decreases glycolysis, induces cell-cycle delay and inhibits anchorage-independent growth (63). This work was determinant for the initiation of some of the experiments performed during this thesis. Nowadays, several pharmacological inhibitors of PFKFB3 have been developed, being 3-(3-pyridinyl)-1-(4-pyridinyl)-2-propen-1-one (3PO) the first to be described (64). From 3PO, different synthetic derivatives have been generated and there is one third-generation molecule with potential clinical use on phase I clinical trial, (E)-1-(4-Pyridinyl)-3-[7-(trifluoromethyl)-2-quinolinyl]-2-propen-1-one (PFK-158), which exhibits increased potency and improved pharmacokinetic properties compared to previous PFKFB3 inhibitors (36,64,65). Recently, PFK158 has demonstrated to synergize with carboplatin to reduce the volume of highly metastatic paclitaxel-resistant mouse ovarian tumours (66). PFKFB3 is a clear example of how basic research is fundamental to the improvement of clinical therapies, as the gene was firstly described twenty years ago (43,44) and we currently have therapeutic molecules targeting it. At the same time, and beyond the potential clinical utility of these inhibitors, it is important to consider that these drugs constitute important tools in basic research. For example, our group has recently demonstrated that suppressing PFKFB3 activity with 3PO or siRNAs significantly eliminates the ability of T98G cells to form colonies, which is one of the hallmarks of transformation (56). Besides, 3PO has been used in several experiments presented in this thesis to study the relationship between PFKFB3 and TIGAR.

Although most of the evidences show that PFKFB3 silencing impairs the progression of cancer cells, it is known that reactive oxygen species (ROS) can induce a pro-survival response through S-glutathionylation or methylation of the enzyme, which decreases its metabolic activity and redirects the glycolytic flux to the PPP. In this way, PFKFB3 inhibition increases NADPH and helps cancer cells to face ROS (67,68). Similarly, activation of p53 in response to cell damage inhibits *PFKFB3* expression and increases the flux to the PPP in order to synthesize nucleotides out of ribose-5-phosphate (R5P) (69). These studies evidence that metabolic transformation in cancer not only pursues the obtaining of energy through glycolysis, but also the activation of several pathways branching from Glu-6-P that can contribute to cell survival.

PFKFB4 gene encodes a PFK-2/FBPase-2 isoenzyme that is expressed in the testis under the regulation of testosterone (70). Moreover, it has been demonstrated that *PFKFB4* mRNA and protein levels are regulated by hypoxia and glucose concentration in cancer cell lines from different organs such as the prostate, liver, colon, bladder, stomach, pancreas, lung and breast (24). One of the cancers in which PFKFB4 has been more studied is prostate cancer, where this gene is required to balance glycolytic activity and antioxidant capacity to maintain the redox balance. *PFKFB4* mRNA expression is increased in metastatic prostate cancer cells compared to primary tumours, and its inhibition increases Fru-2,6-P₂ concentration. This indicates that PFKFB4 mainly functions as a fructose-2,6-bisphosphatase in these particular cells (71). Because of its capacity to increase the PPP and decrease ROS levels, *PFKFB4* is considered a tumour promoter gene. However, its expression is compatible with high glycolytic flux, as it has been recently shown in mitogen-stimulated thymocytes, in which *PFKFB3* and *PFKFB4* expression are induced in parallel (57).

Through overexpression of one or more of the *PFKFB* genes, cancer cells maintain high levels of Fru-2,6-P₂ and, consequently, high PFK-1 activity and flux through glycolysis, in parallel with overexpression of genes that promote the flux through pathways branching from glycolysis.

2.2.4. TIGAR

As it has been previously stated, TIGAR was discovered during a computer-based analysis of microarray data trying to find novel p53-regulated genes in response to ionizing radiation (4).

The human *TIGAR* gene is located at 12p13.32 and consists of six exons spanning a genomic region of about 39 Kb coding for a unique mRNA transcript variant of 8.2 Kb with an 813 bp coding sequence (**Figure 9**).

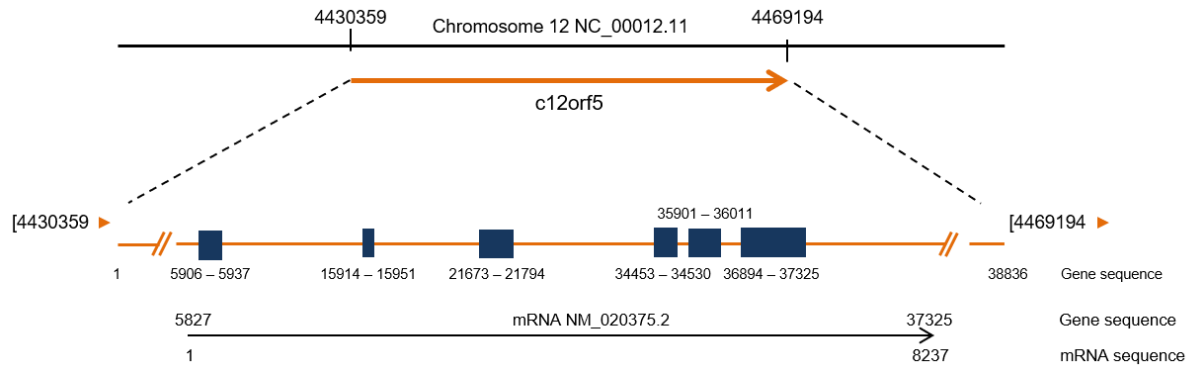


Figure 9. Schematic representation of human *TIGAR* gene. The location of *c12orf5* (*TIGAR*) in human chromosome 12 is indicated. The distribution of introns and exons of *TIGAR* gene is represented, as well as the resulting mRNA. The corresponding NCBI references for the genomic region (NC_00012.11) and mRNA (NM_020375.2) are indicated. Published in (72).

The group of Dr. Karen Vousden described the main features of this p53-induced gene in a paper in *Cell* in 2006, in which the group of Dr. Ramon Bartrons participated characterising the metabolic activity of *TIGAR* protein and showing that *TIGAR* exerts bisphosphatase activity on Fru-2,6-P₂, generating Fru-6-P (3). Given that Fru-2,6-P₂ is the most potent allosteric activator of PFK-1, *TIGAR* was described as an enzyme that inhibits glycolysis and potentiates the PPP. In fact, the capacity of *TIGAR* to increase the ratio NADPH/NADP⁺ and protect from hydrogen peroxide (H₂O₂)-induced apoptosis was confirmed to be dependent on the activity of glucose-6-phosphate dehydrogenase (G6PD) (3). However, two of the main findings of this first publication have been proved to be more complex than what they seemed to be.

In one hand, *TIGAR* phosphatase activity has been described to be not exclusive to Fru-2,6-P₂ and, indeed, other glycolytic intermediaries such as 2,3-bisphosphoglycerate (2,3-BPG), 2-phosphoglycerate (2-PG) and phosphoenolpyruvate (PEP) can be dephosphorylated by *TIGAR*, at least *in vitro* (73). More than 170 studies have been published from 2006 adding pieces of information about this gene. The most important data that has inspired the design of some of the hypothesis and experiments of this thesis are summarised in the following paragraphs.

On the other hand, *TIGAR* has been found overexpressed in different cancer cells and tumours in which *TP53* is either lost or mutated (24), evidencing the participation of other transcription factors in the control of *TIGAR* expression. As an example of this independency of *TIGAR* from *TP53*, the genetic alterations and expression of both genes have been analysed in glioma. Genetic data have been obtained from the TCGA-PanCancer whole genome analysis performed in this cancer type, which is available in the online platform cBioportal. *TIGAR* or *TP53* alterations were detected in 8% and 51% of patients, respectively (**Figure 10A**).

Interestingly, the most frequent alteration detected in *TIGAR* was amplification (represented in red), whereas *TP53* was mainly mutated, with either missense or truncating mutations (in green or dark grey, respectively). *TIGAR* and amplification and *TP53* mutation coexist within the same sample (**Figure 10A**). Regarding expression, no correlation was found between the mRNA levels of the two genes, evidencing that *TIGAR* can be overexpressed in tumours where *TP53* is poorly expressed and the other way around (**Figure 10B**). *TP53* mutations can have different phenotypical outcomes. As reviewed by Kasthuber and Lowe (74), wild type p53 controls apoptosis, antioxidant mechanisms, the DNA damage response and cell cycle. In cancer, several mutations have been described, some of them resulting in complete loss-of-function or in activation of specific functions which contribute to tumour survival such as antioxidant mechanisms, as it could be the case if *TIGAR*. Besides, gain-of-function mutations have also been described in *TP53*, which selectively increase some functions of the wild-type and give rise to new roles (**Figure 10C**). Selection-of-function and gain-of-function mutations of *TP53* can be pro-oncogenic and, in these cases, *TIGAR* and *TP53* can be overexpressed at the same time, contributing to tumour development.

Two p53 binding sites have been described in *TIGAR* gene, one upstream of the first exon, in *TIGAR* promoter, and the other one within the first intron. The intronic p53-binding site was described to be the functional one in human through chromatin immunoprecipitation (ChIP) experiments (3). Mouse *Tigar* is only weakly responsive to p53 and it contains also a promoter and an intronic p53 binding sites, being the promoter one the most effective. This suggests that the weaker p53 binding site in humans, which is the promoter one, is structurally and functionally conserved between mouse and human but the stronger intronic binding site in humans is not functional in the mouse (75).

Apart from p53, the Specificity Protein 1 (SP1) and the cAMP Response Element-Binding Protein 1 (CREB1) have more recently been described to transcriptionally regulate *TIGAR* (76,77).

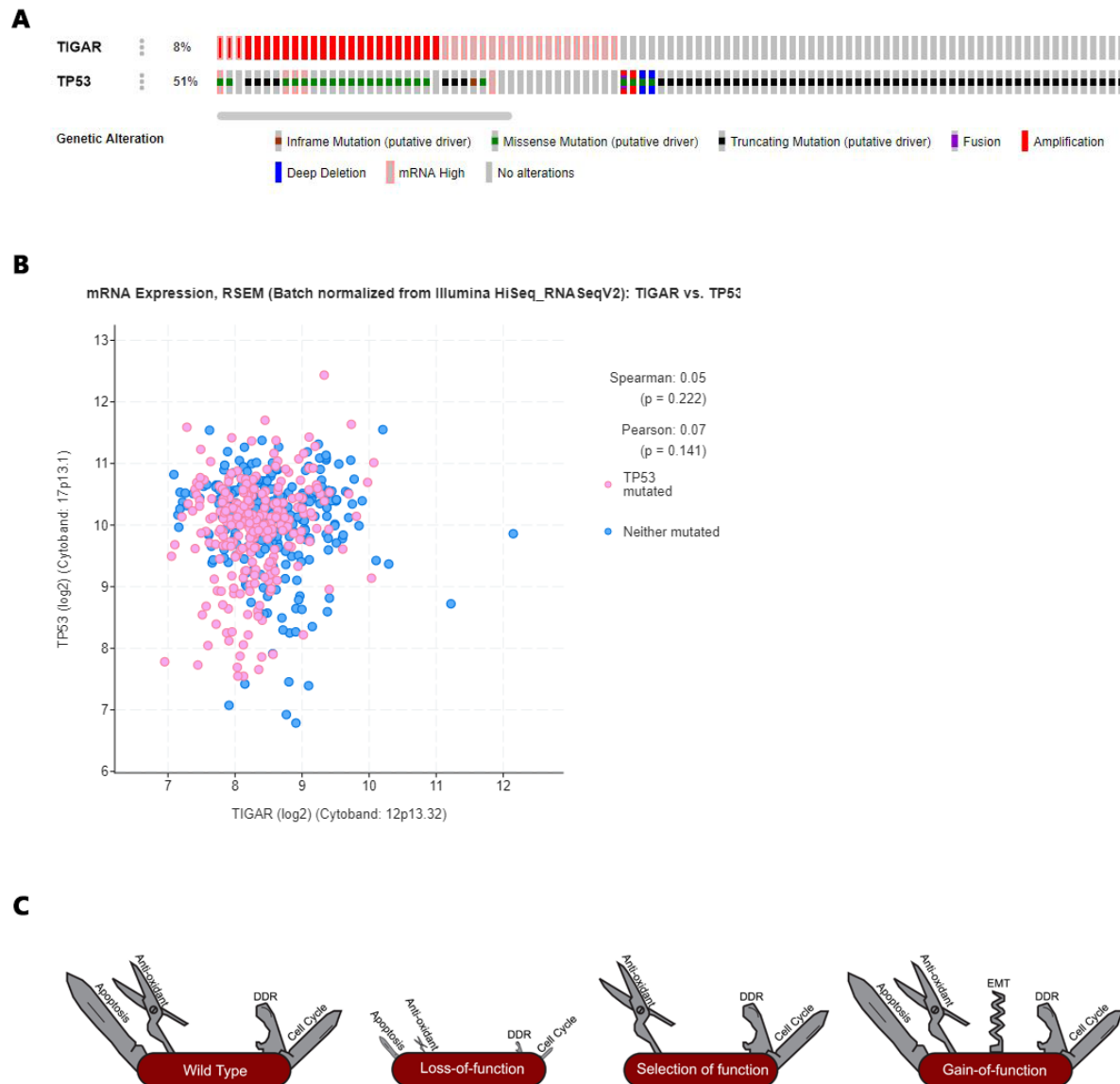


Figure 10. TP53 and TIGAR alterations and expression. (A-B) Data were obtained from TCGA-PanCancer study of gliomas, available in cBioPortal (178,179). **(A)** Patients are represented individually in columns. Percentage of alterations in either TIGAR or TP53 is calculated for all samples, and the type of alteration is represented by different colours. **(B)** Expression of TIGAR (X axis) and TP53 (Y axis) in glioma samples. **(C)** Schematic representation of divergent phenotypes of p53 mutations: (a) wild-type, (b) loss or partial loss of function, (c) selection of function, or (d) gain-of-function. Adapted from (74).

TIGAR can be induced by doxycycline (3), nutlin-3 (78), radiotherapy (4,79), hypoxia (80,81), extracellular glutamine, lactate (82), tumour necrosis factor α and radiotherapy mimetics (83). Moreover, during this thesis we have described that TIGAR is also induced by the Akt signalling pathway in response to the metabolic stress caused by PFKFB3 knockdown (84). These results are presented in Results Chapter I.

The human TIGAR protein is composed of 270 amino acids and has a molecular weight of 30 kDa. It contains a bisphosphatase active site in which two histidine residues, H11 and H198, and one glutamic acid, E89, are essential for its activity. This catalytic triad is characteristic of proteins of the histidine phosphatase superfamily (85). In TIGAR, H11 forms a transient phosphoenzyme during catalysis, H198 stabilizes the transition state and E89 is a H⁺ acceptor and donor (Figure 11). The functionality of these residues was described in *Danio rerio* (86) and it is conserved in human. These three residues are identical between TIGAR, FBPase-2 (3), erythrocyte 2,3-bisphosphoglycerate mutase (PGME) and phosphoglycerate mutases 1 and 2 (PGAM B and PGAM M, respectively). During this thesis, these similarities have been explored through sequence and structural comparisons, which are reported in Results Chapter II. The mutation of either H11 or H198 in human TIGAR abolishes its phosphatase activity on Fru-2,6-P₂. The mutation of an additional residue also conserved in histidine phosphatases, E102, together with H11 and H198 (known as triple mutant TIGAR) has similar consequences to the single mutation of H11 or H198 (3).

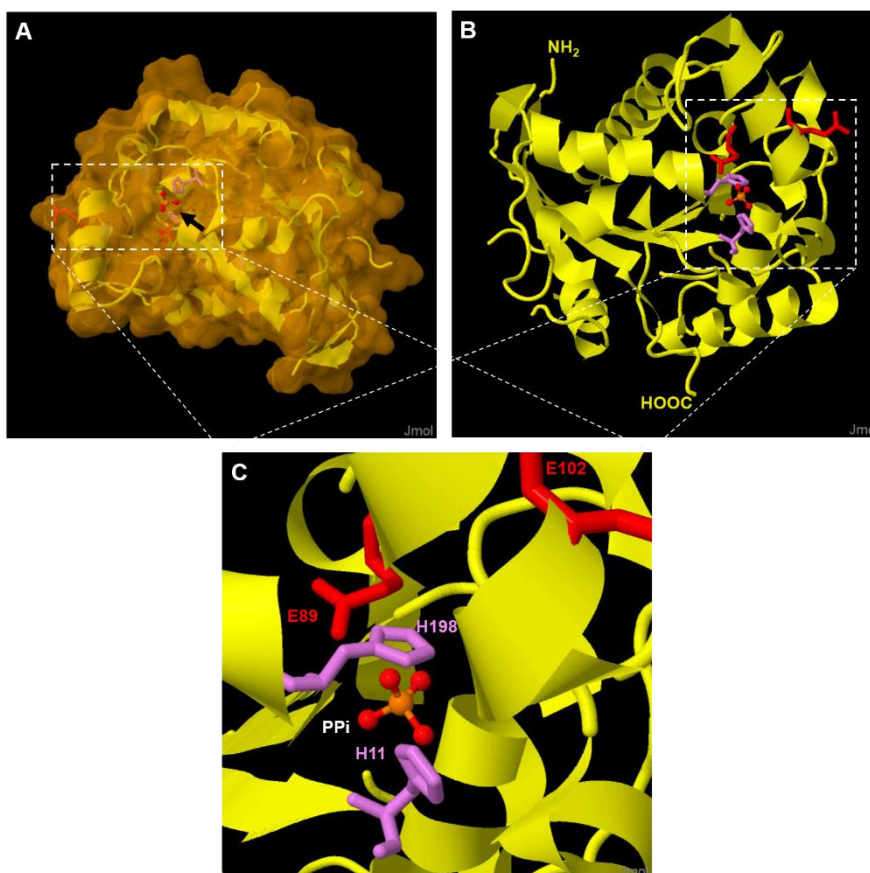


Figure 11. Structure of human TIGAR. The structure of human TIGAR has been downloaded from PDB (Reference Number: 3DCY) and is represented in yellow. The three residues of TIGAR active site plus an additional residue conserved in other histidine phosphatases are represented in sticks coloured according to the type of amino acid. H11 and H198 are coloured in purple and E89 and E102 are coloured in red. **(A)** Visualisation of TIGAR surface, where the access to the catalytic core is indicated by a black arrow and PPi can be appreciated inside. **(B)** Schematic representation of TIGAR with the most relevant residues coloured. **(C)** Zoom into the catalytic core. Images were created with Jmol: an open-source Java viewer for chemical structures in 3D. <http://www.jmol.org/>.

TIGAR is mainly localized in the cytoplasm, but it has been described to bind to HK-II in the outer mitochondrial membrane under hypoxic conditions (87) and the presence of TIGAR in the nucleus has been found to contribute to DNA damage repair (88).

In terms of expression, *TIGAR* mRNA levels have been detected in all the tissues that have been analysed to date. The tissues with the highest *TIGAR* expression, both in terms of mRNA and protein levels, are the lung, liver, gastrointestinal tract, kidney, urinary bladder and male tissues (Figure 12).

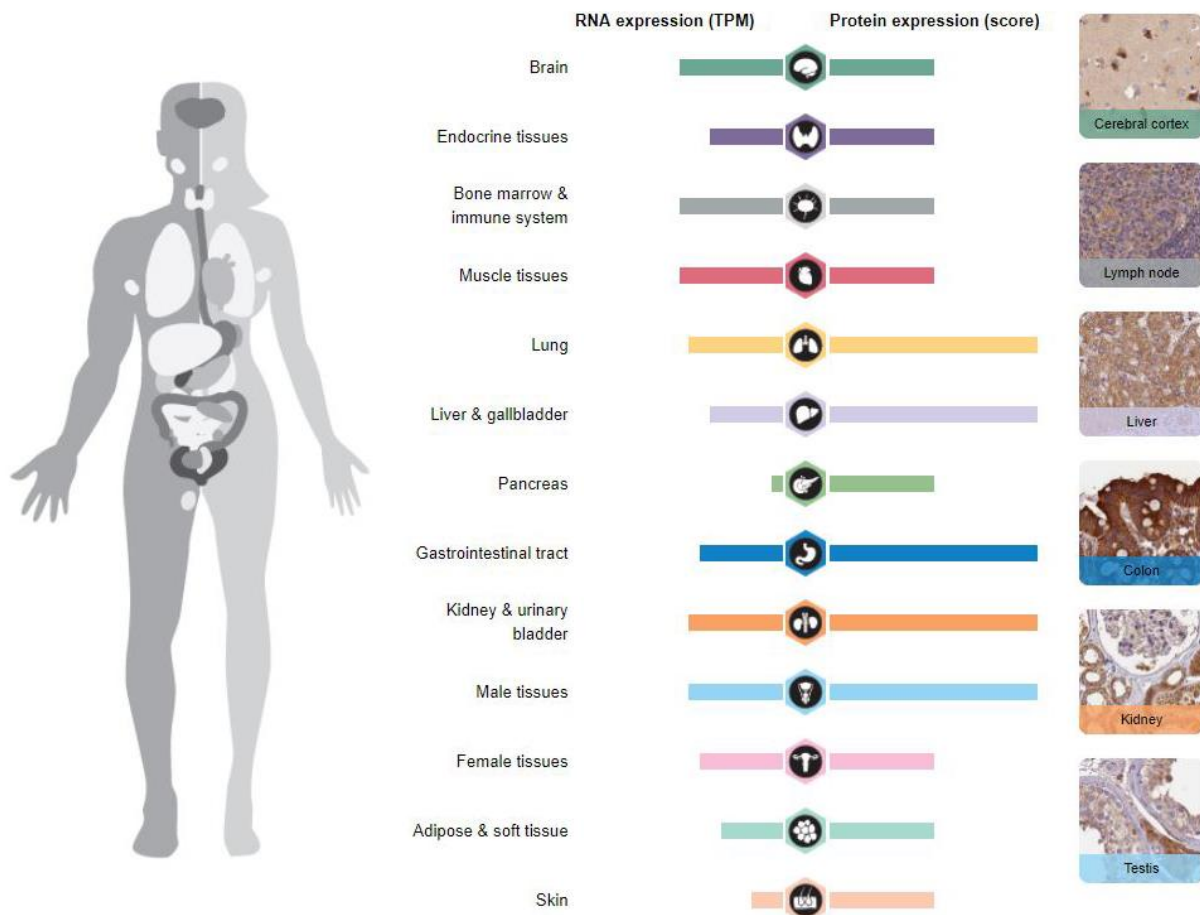


Figure 12: TIGAR mRNA and protein levels across tissues. Representation of TIGAR levels across the human body. Analysed tissues are divided into color-coded groups according to common functional features. Images of selected tissues at the right panel provide a visual summary of the protein expression profile. The grey human body highlights those tissues in which more expression has been detected, both in female and male. From the Human Protein Atlas (89) available from www.proteinatlas.org.

Mouse *Tigar* knock-out is viable and, indeed, it does not show any deficiency for normal growth or development. However, this model revealed the importance of *Tigar* in intestinal regeneration. *Tigar* deficiency impairs intestinal regeneration, which can be rescued by ROS scavengers and nucleosides, highlighting the antioxidant role of *Tigar* in mouse colon (90). On the other hand, *Tigar* suppression reduced tumour growth and improved survival in a mouse intestinal adenoma model, while elevated *Tigar* expression supported cancer progression (90). Thus, balanced levels of this protein seem to be

required for the physiological homeostasis of tissues, but *Tigar* overexpression can contribute to oncogenic transformation in those cells exposed to high ROS levels.

The types of human cancer with the highest expression of *TIGAR*, both in terms of mRNA and protein levels, are gliomas, head and neck tumours, stomach and colorectal cancer, testis cancer and melanoma (**Figure 13**).

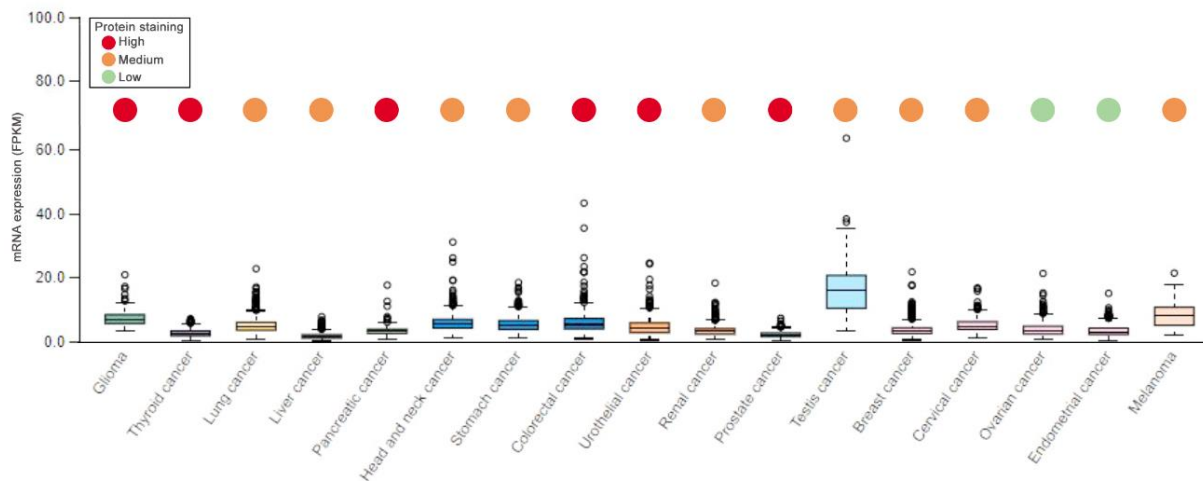


Figure 13: TIGAR mRNA and protein levels in several types of cancer. The graph shows RNA-seq data from The Cancer Genome Atlas (TCGA) expressed as fragments per kilobase million (FPKM). Analysed tissues are divided into color-coded groups according to common functional features. The evaluation of TIGAR protein levels with three different TIGAR-specific antibodies is represented by red, orange and green dots, according to high, medium or low TIGAR levels, respectively. The figure was adapted from the Human Protein Atlas (98) available from www.proteinatlas.org.

Mostly, TIGAR contribution to cancer is linked to its effects on the PPP. TIGAR downregulation inhibits the growth of several cancer cell lines (24) and increases the susceptibility to radiotherapy in p53 wild-type and mutated glioblastoma cell lines (79). In nasopharyngeal cancer, the potent anticancer treatment 1-(3-C-ethynyl-beta-d-ribo-pentofuranosyl)cytosine decreases TIGAR levels and depletes NADPH, a phenotype that is rescued by *TIGAR* overexpression (91). Moreover, in multiple myeloma cells inhibition of the C-terminal subunit of mucin 1 oncoprotein increases ROS levels and downregulates *TIGAR* expression, resulting in decreased NADPH and glutathione levels and promoting ROS-mediated apoptosis/necrosis (92). Nevertheless, high *TIGAR* expression in certain cancers such as hepatocarcinoma is linked to reduced progression-free survival, highlighting the importance of this gene in tumour development (**Figure 14**). Based on these observations, some studies have proposed TIGAR as an antitumoral target in cancer. This is what illustrates the study by Canaparo, *et al.*, in which a sonodynamic therapy tested in a neuroblastoma cell model decreased *TIGAR* expression and proliferation, possibly through increased ROS levels (93). Similarly, *TIGAR* abrogation increased radiation-induced cell death in glioblastoma-derived cell lines, in which the ataxia telangiectasia-mutated (ATM)-Nuclear Factor kappa B (NFkB)-TIGAR axis has been described to be involved in radio resistance (83).

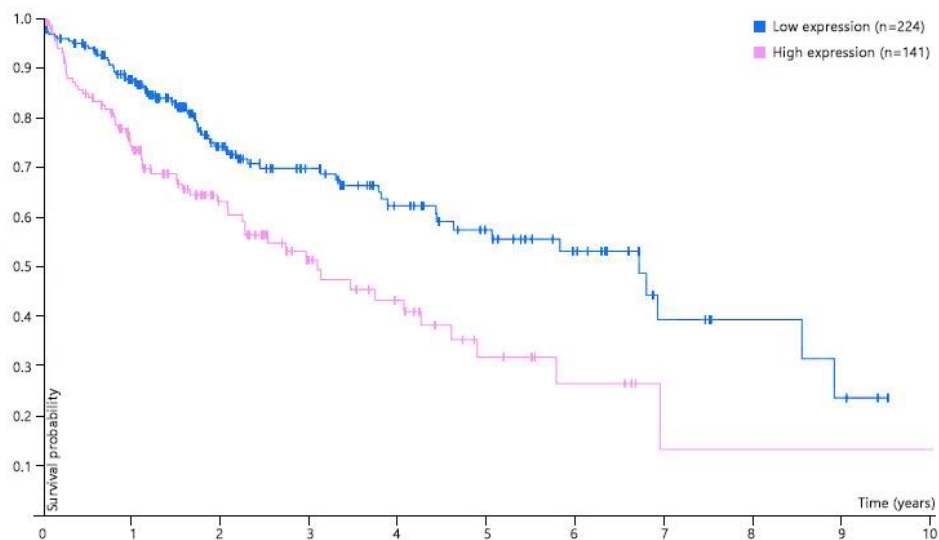


Figure 14: Kaplan Meier curves of *TIGAR* expression in liver cancer. The graph indicates the survival probability of patients with hepatocarcinoma depending on *TIGAR* expression. Patients were classified in two groups according to the expression of *TIGAR*. The prognosis of each group of patients was examined by Kaplan-Meier survival estimators, and the survival outcomes of the two groups were compared by log-rank tests. A log rank P value less than 0.001 indicates a prognostic gene. 5-year survival in the group of patients with high *TIGAR* expression was 32%, whereas in the group with low *TIGAR* expression it was 57% (log rank P value was 0.00032), indicating that *TIGAR* is an unfavourable prognostic marker in liver cancer. Source: The Human Protein Atlas (89) available at www.proteinatlas.org.

Besides its already mentioned role as an antioxidant, *TIGAR* has been described to inhibit autophagy (3). Moreover, some studies have related *TIGAR* with senescence, although the results in this field are controverted. Some experiments trying to analyse the contribution of *TIGAR* to senescence were performed during this thesis but have not been included given that no concluding results were obtained. Other roles for *TIGAR* in cancer have also been proposed, some of which involve the regulation of cell cycle. *TIGAR* was found to dephosphorylate the retinoblastoma protein (Rb) and stabilize the Rb-E2F1 complex, thus delaying entry into the S phase (94,95). This opens the possibility of other substrates for *TIGAR* phosphatase activity beyond glycolytic intermediates.

More specific information related to each of the features regarding *TIGAR* that have been addressed in this thesis (i.e. relationship with PFKFB3, enzymatic activity and transcriptional control) is provided at the beginning of each Results Chapter.

2.2.5. From Fru-1,6-P₂ to PEP: the forgotten enzymes

For years, the steps involved in the oxidation of Fru-1,6-P₂ to PEP were not considered as potential cancer drivers. These steps include the reactions catalysed by aldolase (ALDO), glyceraldehyde-P-dehydrogenase (GAPDH), triose-phosphate isomerase (TPI), phosphoglycerate kinase (PGK), phosphoglycerate mutase (PGAM) and enolase (ENO) (Figure 5). However, different studies from The Cancer Genome Atlas (TCGA) indicate that the genes encoding for these enzymes are as much altered as genes coding for known cancer drivers such as PFK-1 or PFK-2 in certain tumour subsets such as glioblastoma multiforme, suggesting that these genes could potentially be therapeutic targets in specific malignancies. Indeed, these enzymes are involved in the metabolism of 3PG, the first metabolite in the *de novo* serine and glycine synthesis pathway, which is increased in tumour cells as it will be further exposed in Section 3.3 of this Introduction.

2.2.6. Pyruvate kinase: the last step of glycolysis

To balance biosynthetic outputs of glycolysis with its role in providing pyruvate that supports TCA cycle activity, proliferating cells have evolved a novel mechanism to regulate the last step of glycolysis. This step is regulated by PK, an enzyme that converts PEP to the final product of glycolysis, pyruvate (Figure 5). Four different isoenzymes encoded by two different genes have been identified. Except for the liver, kidney and red blood cells, which express tissue-specific PK isoforms PKL and PKR, respectively, most tissues express the muscular form of PK (PKM). While PKM1 is more efficient at producing Pyr, the majority of proliferating cells and essentially all cancer cells express the PKM2 variant, which has a lower affinity for PEP (96). The decrease in the activity of PK is one of the reasons for considering glycolysis as a source of molecules for biosynthesis rather than an ATP producing pathway. Unlike PKM1, the activity of PKM2 activity is highly regulated and, indeed, growth-factor-dependent signal transduction inhibits PKM2, leading to accumulation of glycolytic intermediates until the cell has fulfilled its growing needs and can completely oxidize glucose to obtain ATP. In glycolysis, the net energetic production is only 2 ATP per molecule of glucose oxidized, something that looks ridiculous compared to the ATP yield of oxidative phosphorylation, which is 15 times higher (5). However, the fact that cancer cells produce low levels of ATP although maintaining a high glycolytic flux is what allows for the continuous operation of the pathway, given that ATP is an allosteric inhibitor of key enzymes such as PFK-1 and PK. Besides, ATP production through glycolysis is much faster than through oxidative phosphorylation (5).

3. Diversion of carbons: metabolic pathways branching from glycolysis

Glycolytic intermediates are involved in diverse biosynthetic reactions. Accordingly, the rate-limiting enzymes of pathways branching from glycolysis are frequently upregulated in tumours.

3.1. Hexosamine-phosphate pathway

The hexosamine-phosphate pathway, in which Fru-6-P is the first substrate, is particularly important for the glycosylation of proteins that are secreted or placed on the surface of cells (Figure 5). However, in cancer cells most of the glucose is either redirected to the synthesis of amino acids and nucleotides or converted to pyruvate and lactate. In oncogenic Kras-driven pancreatic ductal adenocarcinoma (PDAC), an important fraction of glucose is diverted towards the hexosamine-phosphate and the pentose phosphate pathways (97).

3.2. Pentose phosphate pathway

The PPP branches from glycolysis at the first committed step of glucose metabolism and consumes Glu-6-P as the primary substrate. The PPP is required for the synthesis of ribonucleotides and is a major source of NADPH. NADPH is essential for fatty acid synthesis and for the reduction of oxidized glutathione (GSSG) by glutathione reductase (GR), that splits GSSG into two molecules of GSH by the addition of two electrons and two protons obtained from NADPH. GSH is oxidized by ROS and for this reason a continuous supply of NADPH is required. Two phases or branches integrate the PPP: the oxidative branch and the non-oxidative branch. In the oxidative branch, NADPH is generated in the irreversible reactions catalysed by G6PD and 6-phosphogluconate dehydrogenase (6PGD). The final product of the oxidative branch is R5P, which serves as the primary substrate for purine and pyrimidine synthesis. The non-oxidative branch comprises a series of reversible reactions that recruit additional glycolytic intermediates, such as Fru-6-P and G3P and combine them with R5P, generating other phosphorylated metabolites that can be reintroduced into glycolysis (Figure 5) (98). Unlike canonical models, there is evidence that the synthesis of R5P is not restricted to the oxidative PPP. In Kras-driven PDAC, KrasG12D drives glycolytic intermediates into the non-oxidative PPP, thereby decoupling ribose biogenesis from NADP/NADPH-mediated redox control (97).

Recently, several neoplastic lesions involving enzymes from both the oxidative and non-oxidative branches have been shown to facilitate the flux of glucose into the PPP. Indeed, dependency of B cell malignancies on the PPP has been described, as these transformed B cells rely on the activity of the serine-threonine-PP2A, which dephosphorylates PFKFB2 and redirects glucose flux to the PPP, conferring antioxidant protection. Importantly, *TIGAR* overexpression mimics the activity of PP2A, confirming an equivalent role for these two phosphatases in these tumours (99).

Apart from the transcriptional upregulation of several enzymes of the PPP, an acute activation of the oxidative PPP has been described as a short-term response independent of transcription in skin cells

exposed to high levels of oxidative damage. In these cells, in which ROS-derived UV exposure result in DNA mutations that can eventually initiate a melanoma, oxidative stress triggers G6PD activity, increasing the pool of ribose-phosphates that return to glycolysis through the non-oxidative PPP and are redirected back to oxidative PPP due to ROS-mediated inhibition of GAPDH (100). This rerouting into the PPP maximizes NADPH production and is essential to prevent oxidative damage.

3.3. Serine and glycine synthesis pathway and one-carbon metabolism

Although the first clues about the overactivation of the *de novo* serine synthesis pathway in tumours date from 1980s (101), it became a forgotten field of study until very recently, when interest on the role of this pathway in tumorigenesis emerged again. Amplification of the gene encoding phosphoglycerate dehydrogenase (*PHGDH*) has been described in breast cancer (102) and melanoma (103). This enzyme is the responsible for the redirection of 3-PG from glycolysis to this anabolic pathway through an initial reaction in which 3-phosphohydroxypyruvate (3PHP) is formed at expenses of NAD⁺ reduction. Two irreversible reactions couple the transamination of 3-phosphohydroxypyruvate into 3-phosphoserine (3PS), with the conversion of Glu to α -ketoglutarate (α KG), catalysed by phosphoserine aminotransferase 1 (PSAT1). Finally, 3PS is converted into serine (104) (**Figure 5**). As metabolic flux studies revealed, some cancer cells utilize 50% of glucose-derived carbons in serine biosynthesis (103).

Serine is required for the synthesis of phospholipids (such as phosphatidylserine) and, more importantly, for the synthesis of other amino acids such as glycine and cysteine. One of the most important roles of serine is the transference of one-carbon units to the folate cycle, in the so-called **one-carbon metabolism** (**Figure 5**), which involves the synthesis of glycine. This reaction, catalysed by serine hydroxyl methyltransferase 1 (SHMT1) in the cytosol and SHMT2 in the mitochondria, transfers the carbon to a carrier molecule, tetrahydrofolate (THF), generating 5,10-methylene-THF (methyl-THF) and glycine. Then methyl-THF undergoes a series of oxidative-reductive transformations, creating a battery of one-carbon-THF species (105). Species derived from the THF cycle are utilized as substrates for the biosynthesis of purines, thymidine, and to produce S-adenosylmethionine in the methionine cycle, necessary for cellular methylation reactions including epigenetic regulation. One of the molecules in the methionine cycle is the precursor of cysteine, which together with glutamine and glycine is a key amino acid in the synthesis of glutathione. In addition, oxidation of one-carbon-THF by methylene-tetrahydrofolate dehydrogenases 1 and 2 (MTHFD1/2) is an important source of NADPH (105,106) (**Figure 5**).

Remarkably, dietary restriction of serine and glycine in genetically engineered mouse models of lymphoma and intestinal adenoma reduced tumour growth, an effect that was further improved by antagonizing the antioxidant response through *TIGAR* inhibition (107). The fact that tumours show

increased *de novo* serine and glycine synthesis pathway does not exclude their dependency on external supply of these amino acids. Because of that, most of culture media are supplemented with these and other amino acids. This dependency of cancer cell lines does not always reflect the reality of tumours, as some addictions are developed during cell culture.

3.4. Lipid synthesis

Cells require different types of lipids. In one hand, they need to synthesize phospholipids for cellular membranes, something that is required for cell division and, consequently, also for the progression of cancer. Besides, they also need to build triacylglycerides for energy storage in the body. Considering the composition of each of these two types of lipids, cells need acetyl-CoA for the synthesis of fatty acids that are the main components of the two types of lipids, and glycerol-3-P for the structure of triglycerides and to build the hydrophilic phosphate groups of phospholipids. Thus, the synthesis of lipids is linked to the diversion of G3P from glycolysis (**Figure 5**). Downstream of glycolysis, glucose-derived pyruvate that enters the TCA cycle contributes to the production of mitochondrial citrate, which can be exported again to the cytosol, split into oxaloacetate (OAA) and acetyl-CoA by ATP citrate lyase (ACL) and feed *de novo* fatty acid synthesis (5). Fatty acid synthase (FAS) is responsible for the synthesis of fatty acids out of malonyl-CoA and acetyl-CoA and requires NADPH (**Figure 5**). Both TCA and FAS are induced in tumour cells and their activity is required for proliferation to build the membranes of new cells (108). Indeed, inhibition of FAS downregulates the expression of the oncogene *p185^{HER2}* in *HER2* overexpressing breast cancer cell lines and FAS inhibitors synergize with the humanized antibody directed against *p185^{HER2}* trastuzumab, increasing cell death in these cells (109). The increased synthesis of NADPH by the PPP-promoter activity of TIGAR that has been described in certain cells (3) might not only contribute to ROS detoxification, but also to increase FAS activity.

4. The fate of pyruvate carbons: lactate or acetyl-CoA?

Pyruvate has two main fates: to be converted into lactate in the cytosol by lactate dehydrogenase (LDH) or to enter the mitochondria and generate acetyl coenzyme A (acetyl-CoA) by the action of pyruvate dehydrogenase (PDH) (**Figure 5**). The emerging evidence favours the hypothesis that glycolysis is utilized by proliferating cells as a versatile production line that generates metabolic intermediates for numerous biosynthetic processes. Any excessive glycolytic flux not utilized for biosynthesis is preferentially converted to lactate to help preserve a sufficient pool of NAD⁺ to sustain glycolysis and avoid flooding the mitochondria with a supply of NADH that would suppress the TCA cycle. Most tumours have aberrantly increased expression of *LDHA*, which codes for the LDH isoenzyme with the highest affinity for pyruvate, producing high levels of lactate (110). This, coupled with overexpression of the monocarboxylate transporter 4 (*MCT4*), which exports lactate to the extracellular media, results in the acidification of the tumour microenvironment (**Figure 5**). Although lactate excretion is not the only mechanism for the development of the acidic extracellular environment observed in solid tumours (111), it contributes to it and has been proposed as the reason and purpose of the Warburg effect. Lactate is involved in different hallmarks of carcinogenesis apart from metabolic reprogramming, including angiogenesis, immune escape, cell migration and metastasis (112). Remarkably, PKM2-expressing cells generate more glucose-derived lactate relative to cells expressing PKM1, regardless that PKM2 has less affinity for pyruvate as it has been mentioned before. An alternative glycolytic pathway has been proposed in rapidly proliferating cells in which the phosphate of PEP is transferred to the catalytic His¹¹ of human PGAM, producing pyruvate in the absence of PKM2 activity (113) (**Figure 5**). This might explain the high lactate production detected in many tumour cells in which PK activity is low. However, the enzyme responsible for this activity has not been identified yet, and indeed TIGAR has been proposed as a candidate to accomplish this function (73).

Another question that is difficult to answer is why the rate of lactate production is so high when most of the pyruvate could be oxidized to enhance ATP production in the mitochondria. One explanation proposed is that cells need high-flux mechanisms to eliminate the high levels of pyruvate produced by the overactivation of glycolysis. Pyruvate oxidation in mitochondria requires import into this organelle followed by activity of highly-regulated enzymes such as PDH. Thus, overexpression of *LDH* solves the problem, as it rapidly converts pyruvate into lactate, that can be easily secreted (114).

Finally, it should also be mentioned that pyruvate can be converted to alanine by alanine transaminase 1 (ALT1) in the cytoplasm, coupling this reaction with the deamination of glutamate (Glu) to α KG, which is another example of anaplerotic reactions from glycolytic intermediates (**Figure 5**).

5. Mitochondrial metabolism in brief: should we still call the TCA cycle a “cycle”?

Although it was originally proposed that tumours harboured mitochondrial alterations that forced cells to use glycolysis as the main source of energy (115,116), it is now known that mitochondrial respiration is functional in cancer cells and, indeed, it is the primary source of ATP in most tumours (5). However, glycolytic activity significantly affects the respiration capacity of tumour tissues being respiration and oxidative phosphorylation inhibited by glucose, a phenomenon that is known as the “Crabtree effect” in honour of who firstly described it (117).

As exposed at the beginning of this Introduction, tumour cells need rapid supply of energy to face stress situations such as oxygen or nutrient withdrawal, but what is even more important for their progression is to have an available pool of biomolecules comprising lipids, hexosamine sugars, amino acids and nucleotides to allow proper cell proliferation and growth. In this sense, the role of the TCA cycle is crucial given that it is a hub for biosynthesis. TCA cycle integrates the entrance of the two most important fuels in cancer cells: glucose and glutamine. Glucose-derived pyruvate enters the mitochondria where it can be oxidized to acetyl-CoA by PDH (**Figure 5**). To produce citrate, citrate synthase requires an available pool of mitochondrial OAA and acetyl-CoA to continue the cycle. In a simplified picture of mitochondrial metabolism, carbons from OAA and acetyl-CoA are exchanged through a series of reactions that we group by the name of TCA cycle, generating NADH, FADH₂ and CO₂. However, evidence indicates that these reactions are not that much coupled, especially in proliferating cells. Instead, exchange of metabolites occurs between the mitochondria and the cytosol. The most important “truncation” of the cycle is the transference of citrate to the cytosol to generate acetyl-CoA and contribute to *de novo* lipid synthesis. Besides, other intermediaries such as OAA and α KG supply intracellular pools of non-essential amino acids. This efflux of metabolites is referred to as ‘cataplerosis’ (114) and it is essential in proliferating cells to sustain biosynthesis, and also contributes to the regeneration of NADPH through the reaction catalysed by malic enzyme (ME) (**Figure 5**).

To meet the required levels of OAA for citrate synthase to work, cells must have an influx of intermediates to resupply the TCA cycle, which is called ‘anaplerosis’. There are two major sources of anaplerotic metabolites: pyruvate, which can be directly metabolized to OAA through pyruvate carboxylase (PCB), and amino acids, being glutamine (Gln) the most important. Gln is oxidized by glutaminases 1 and 2 (GLS1, GLS2) and converted into glutamate, which is further metabolised to α KG and introduced into the TCA cycle (**Figure 5**). The amino group from Gln is transferred to α -keto acids to form non-essential amino acids. During anaplerosis, α KG is metabolized through the TCA cycle reactions and produces OAA. However, an alternative is that glutamine-derived α KG is converted to malate and then to pyruvate through mitochondrial or cytoplasmic ME, generating NADPH (**Figure 5**) (114,118).

The branching of the TCA cycle is usually a consequence of deregulated metabolic fluxes, which increase or decrease some metabolites and force reactions work in a specific direction, without involving genetic alterations in the TCA cycle coding genes. However, there are also examples in which TCA cycle enzymes function as tumour suppressors and, thus, loss-of-function mutations in their coding genes are associated with cancer formation, as it is the case for succinate dehydrogenase (SDH). SDH deficiency commits cells to consume extracellular pyruvate and increases the synthesis of aspartate from glycolysis-derived carbons, through the intermediate formation of OAA by pyruvate carboxylase (119).

Apart from the catabolic and anabolic functions of the TCA cycle, these reactions are of major importance to produce NADH and FADH₂. These molecules, generated in the mitochondrial matrix, are oxidized to NAD⁺ and FAD by complexes I and II of the electron transport chain, respectively, located at the inner mitochondrial membrane. The tight relation between the TCA cycle and the electron transport chain is evident, given that complex II is indeed succinate dehydrogenase, an enzyme of the TCA cycle. The electrons of NADH and FADH₂ are transferred through coenzyme Q and complex III to complex IV, where they are conducted to the matrix. The final acceptor of the electrons transferred is oxygen, in a reaction catalysed by complex IV that generates water (**Figure 15**). The energy from electrons allows for the pumping of protons from NADH and FADH₂ to the intermembrane space, creating an electrochemical gradient between this compartment and the matrix. Protons, however, cannot diffuse through the membrane to compensate the gradient and are canalized through complex V (ATP synthase) to the mitochondrial matrix. ATP synthase couples the proton flux to the phosphorylation of ADP by Pi, producing ATP, in what is called OXPHOS. As it is exposed in Section 6.5 of this Introduction, when electron leakage occurs, oxygen radicals are generated.

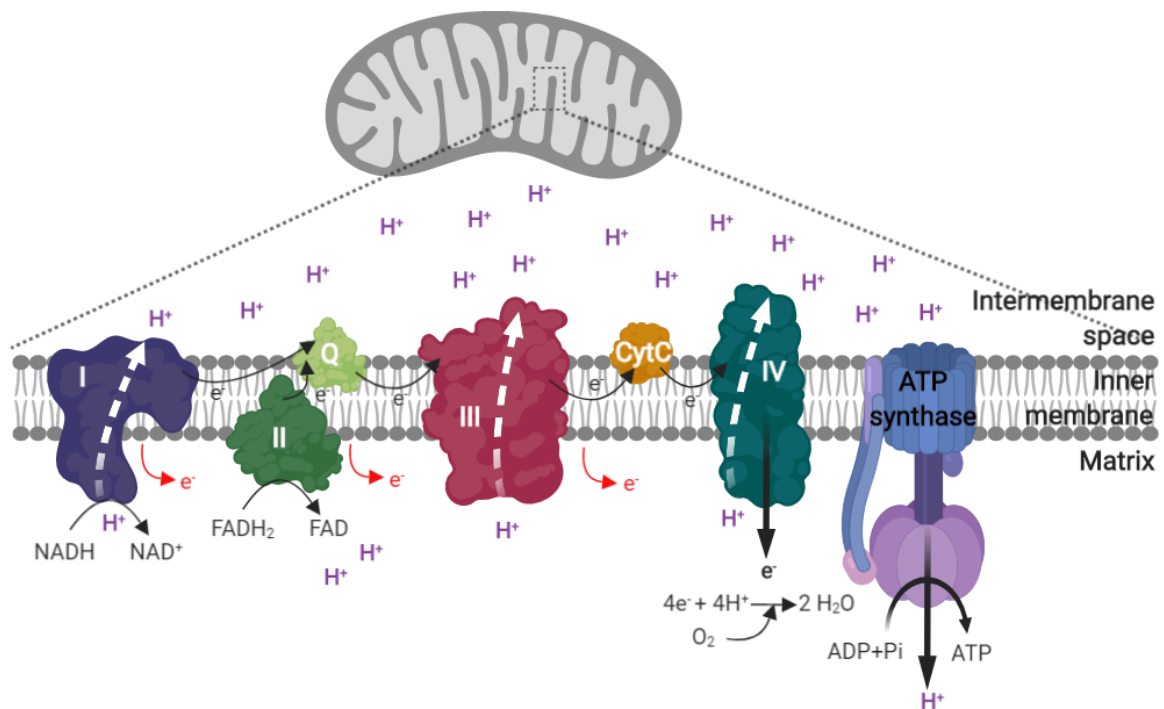


Figure 15. Electron transport chain and oxidative phosphorylation. The electron transport chain is a series of electron transporters embedded in the inner mitochondrial membrane that shuttles electrons from NADH and FADH₂ to molecular oxygen. In the process, protons are pumped from the mitochondrial matrix to the intermembrane space, and oxygen is reduced to form water. Proton electrochemical gradient is used to power the ATP synthase in what is called oxidative phosphorylation. The complexes involved are NADH-coenzyme Q oxidoreductase (complex I), succinate-dehydrogenase (complex II), electron transfer flavoprotein-Q oxidoreductase (Q), Q-cytochrome c oxidoreductase (complex III), cytochrome c oxidase (complex IV) and ATP synthase (complex V).

6. Oncogenic orchestrators of cancer cell metabolism: special attention to oxidative stress

Mammalian cells are not autonomous for initiating the alterations required for the deregulation of metabolism and the initiation of tumour development. Instead, they rely upon overactivated signalling cascades, which are usually triggered by growth factors and other external stimuli. It was originally proposed that oncogenes were responsible for the aberrant expression of metabolic enzymes. However, it is clear now that intracellular and extracellular factors by themselves can directly regulate metabolic proteins at the transcriptional, translational and post-translational levels.

The signalling pathways that modulate cellular metabolism under physiological conditions are highly conserved in tumour cells. However, one important difference between proliferating and non-proliferating cells is that the first ones possess alterations in several metabolic drivers which confer them the ability to avoid checkpoints. In this manner, metabolic pathways are not under control but, instead, they are subjected to the requirements of tumour cells growth. This derangement of the control mechanisms can be caused by cell-autonomous genetic factors that increase the expression of oncogenes and inactivate tumour suppressor genes, but also by non-genetic factors determined by the tumour microenvironment (TME) as it is the gradient of oxygenation, pH and nutrient availability, as well as growth factors and signalling molecules secreted by different cells in the TME, which importantly affect cancer cells (5,120).

In the following paragraphs the most important drivers involved in the regulation of PFKFB3 and TIGAR are commented (**Figure 16**).

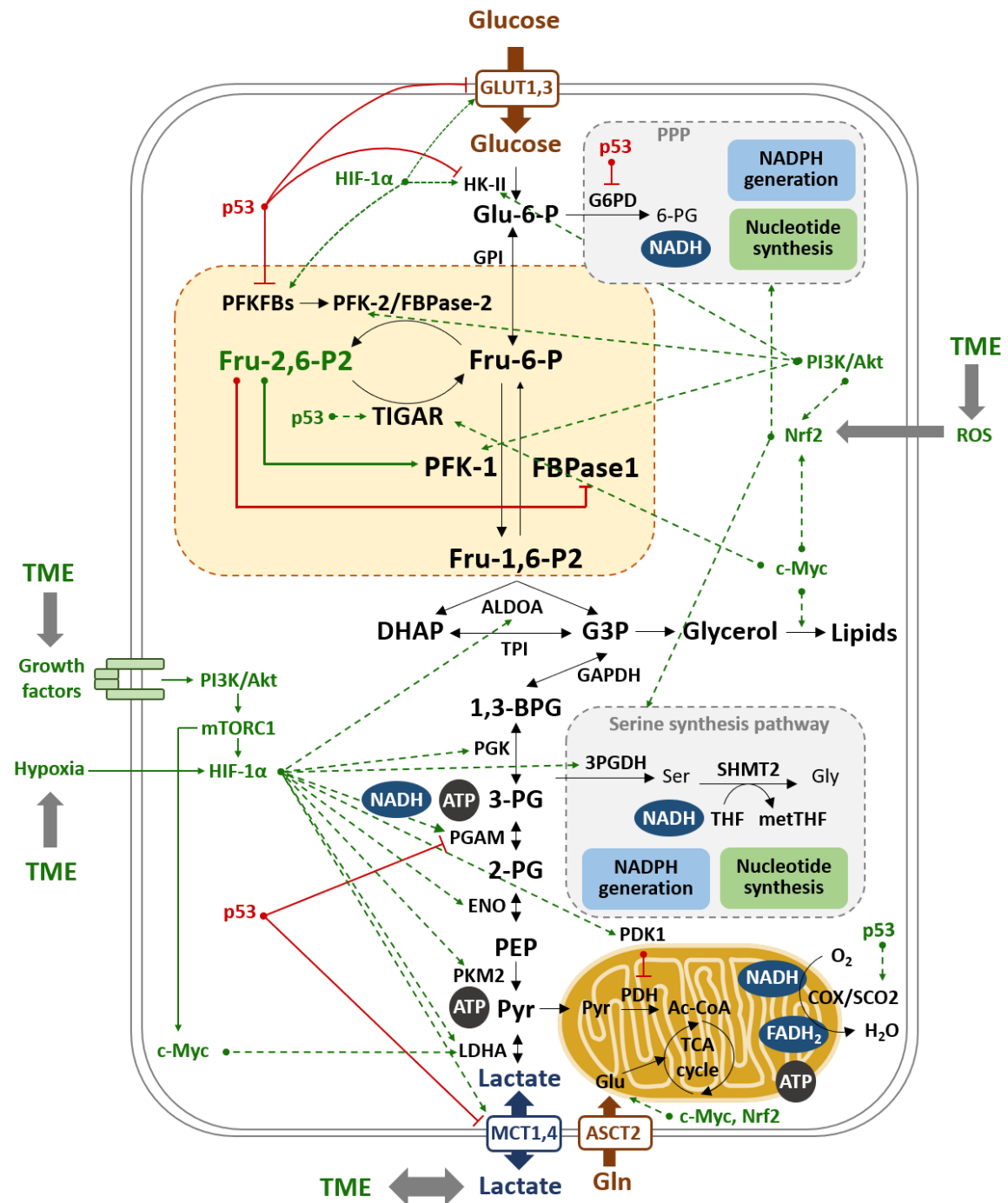


Figure 16. Oncogenic orchestrators of cancer metabolism. Schematic representation of the molecular mechanisms contributing to the Warburg effect that are more important for the regulation of PFKFB3 and TIGAR. Hypoxia and proliferating signals such as the PI3K/Akt pathway stabilize HIF-1 α , which transactivates most of the glycolytic genes, such as HK-II and PFKFBs and MCT lactate transporters. Excreted lactate, in turn, can modify the metabolism of other cells in the TME. On the contrary, the tumour suppressive role of p53 inhibits the glycolytic genes PFKFB3, PFKFB4, PGAM and the lactate transporter MCT1, and induces TIGAR, reducing the glycolytic flux and promoting the PPP. p53 stimulates respiration by inducing SCO2, a component of cytochrome c oxidase (COX) complex. Nrf2 is induced by ROS or proliferative signalling and triggers the expression of genes related with the PPP, the serine and glycine synthesis pathway and glutamine catabolism. c-Myc can induce Nrf2 and also contributes to lipid synthesis. Published in (24).

6.1. Pi3K/mTORC

Cells take up nutrients following the orders of ligand-initiated signal transduction and use them to maintain cell survival and growth. When cells receive a proliferating signal in a situation of low energy supply, the ATP levels required to activate the whole cellular machinery for proliferation are not sufficient and, in some cases, this leads to cell death. Considering this dependency on extracellular signals for cells to proliferate, something must be transgressed to initiate cellular transformation. Aberrant functioning of a signalling pathway which renders the cell autonomous for nutrient uptake is required for malignization. In the case of glucose uptake, overactivated receptor tyrosine kinases (RTK) initiate the overexpression of glucose transporters and their corresponding translocation to the cellular membrane (121). The insulin RTK can act through adaptor proteins to activate PI3K and produce phosphatidylinositol 3,4,5-triphosphate, which in turn brings to the membrane a serine threonine kinase, Akt, that activates the ability of cells to take up glucose. This is accomplished by enhancing the cellular ability to capture glucose through HK-dependent phosphorylation and by activating PFK-1 to commit the captured glucose to glycolysis (5). Akt-dependent activation of hexokinase, phosphofructokinase (5) and PFKFB3 (60,122) has been described (**Figure 16**).

Akt-mediated phosphorylation of one of the inhibitors of the mechanistic target of rapamycin (mTORC), the tuberous sclerosis 2 (TSC2; part of the TSC1-TSC2 complex) or the proline-rich Akt substrate of 40 kDa, activates mTOR. mTORC1 or mTORC2 complexes are formed depending on the proteins that bind to mTOR. mTORC1 is the better characterized and is modulated by different environmental cues, including growth factors (as transmitted via the PI3K/Akt pathway for example), energy status, amino acids, and oxygen levels (5). Although mTORC1 can regulate many cellular processes, it remains best known for elevating protein synthesis through direct phosphorylation of the translational regulators 4E-binding protein 1 and S6 kinase 1 (5), and also for inhibiting autophagy. Downstream of mTORC1 are different transcription factors from which are important to highlight for this thesis HIF-1 α and c-Myc, discussed further below (5) (**Figure 16**).

Antagonizing PI3K/Akt, the AMP-activated protein kinase α (AMPK α) responds to increased AMP/ATP ratio to repress mTOR. mTORC1 activity can be suppressed through either AMPK-mediated phosphorylation of the TSC1/2 complex, or the inhibitory phosphorylation of the mTORC1 scaffold protein regulatory-associated protein of mTOR (RAPTOR) (123).

6.2. HIF-1 α

Activation of PI3K results in an excess of glucose uptake, which is stored by metabolic tissues. The liver stores it by making glycogen first and then fatty acids, the muscle by synthesizing glycogen, and fat cells in the form of glucose-derived fat. In the case of tumours, however, cells do not have storage capacity for the extra glucose that they are instructed to take up, so the glycolysis-derived pyruvate needs to be metabolized through oxidative metabolism, increasing mitochondrial ROS. Cells deal with oxidative stress using various cell-intrinsic defence systems, as it will be reviewed further on this section. An alternative to oxidative metabolism is activating the cellular ability to secrete excess glucose-derived carbon back into the extracellular space as lactate, a reprogramming event that is dependent on HIF-1 α (121,124). Thus, the transcription factor HIF-1 α is responsible for the shift from oxidative metabolism to glycolytic metabolism through the transactivation of most glycolytic genes such as HK-II, PFKFBs, ALDOA, PGK, PGAM, ENO, PKM2, LDHA, as well as pyruvate dehydrogenase kinase (PDK1), which in turn inhibits PDH. Moreover, HIF-1 α activation increases the secretion of lactate through MCT4 and the vascularization of the tumour through upregulation of the vascular endothelial growth factor (27,48,121,124) (**Figure 16**).

As mentioned before, *PFKFB3* expression can be induced by HIF-1 α (40,49,125) (**Figure 16**). On the contrary, TIGAR levels are not controlled by hypoxia (90). However, TIGAR binds to HK-II in the mitochondria under low-oxygen conditions, independently of its phosphatase activity (87). This suggests that TIGAR might have other roles beyond its activity on Fru-2,6-P₂ during hypoxia.

6.3. c-Myc

The transcription factor c-Myc is a proto-oncogene activated by growth factors in non-proliferating cells. In tumour cells, it can be constitutively active due to gene amplification, single nucleotide polymorphisms, chromosomal translocation, or as a downstream effector of the mTORC1 pathway. c-Myc induces the expression of several genes involved in glycolysis, lactate production, glutamine metabolism, and the serine and glycine and fatty acid synthesis pathways (5,114) (**Figure 16**). In a mouse model of colon cancer induced by the loss of adenomatous polyposis coli gene, increased Wnt/ β -catenin signalling occurred in parallel to increased *c-Myc* and *Tigar* expression, and the deletion of *c-Myc* reduced *Tigar* mRNA, suggesting a link between these two genes. *Tigar* induction was not a direct response to Wnt/ β -catenin activity but to the activation of c-Myc, although the direct transcriptional control of *Tigar* by c-Myc has not been proved (126).

6.4. p53

The transcription factor p53, encoded by the *TP53* gene, is the most studied tumour suppressor gene, comprising pro-survival actions and pro-apoptotic effects (127) (**Figure 17**). The fine mechanisms dictating the specific p53 response are not fully understood and, although many players have been described, it is widely accepted that p53 action mostly depends on the cellular and genetic context.

In unstressed cells, p53 is rapidly degraded by the ubiquitin ligase double minute 2 homolog (HDM2), the homologous protein to the mouse Mdm2. In response to several kinds of stress, p53 is phosphorylated by several kinases, depending on the nature of the stress, and it is in these phosphorylated residues where the prolyl isomerase Pin1 binds, releasing p53 from HDM2 and stabilizing it (128). Currently, the mechanism underlying the preferential expression of p53 targets remains unknown. However, phosphorylation, acetylation or ubiquitination of specific residues of p53 have been proposed to differentially regulate the expression of pro-survival and pro-apoptotic genes (129) (**Figure 17**). p53 inhibits the expression of several glucose transporters and that of *PGAM*, which is consistent with its tumour suppressor role, but at the same time there are p53-response elements in the promoters of hexokinase and the same *PGAM*, suggesting that at least to some extent, context- or tissue-dependent differences determine the metabolic function of p53. Moreover, p53 activation can also contribute to cancer development (130). One example of this is the p53-driven induction of *TIGAR* expression. *TIGAR* was described as a p53-response gene that was induced by low levels of stress (4) (**Figures 16, 17**). Its bisphosphatase activity on Fru-2,6-P₂ attenuates glycolysis and increases NADPH levels, conferring resistance to ROS-induced apoptosis in a PPP-dependent manner (3). This helps cells to repair moderate levels of damage sustained under normal growth conditions or in response to mild stress. Regarding this, the capacity of p53 to modulate the PPP is not clear yet, as there are also evidences of p53 inhibition of G6PD (131).

With all, one should not forget that the p53 antioxidant capacity can also contribute to transformation and, consequently, the role of *TIGAR* as a tumour suppressor gene might be argued and, indeed, *TIGAR* might be considered a tumour promoter gene depending on the cellular context. The same happens with other pro-survival p53-target genes such as p21 (*CDKN1A*), which by arresting the cell cycle can give transformed cells the chance to repair mutations and avoid cell death (127).

Regarding the link between p53 and some key signalling routes, it is to consider that, although Akt/mTORC and p53 pathways antagonize to each other and AMPK and high AMP/ATP levels induce p53 activity, constitutive mTOR activation activates *TP53* translation, which results in apoptosis, something that could explain the low malignancy of some TCS negative tumours (132).

p53 has also an important role in OXPHOS, increasing the expression of the synthesis of cytochrome c oxidase 2 (*SCO2*) gene, which is required for the correct assembly of the COX complex in the mitochondrial electron transport chain, the major site of oxygen utilization in the eukaryotic cell.

Disruption of the *SCO2* gene in human cancer cells with wild-type *TP53* recapitulates the metabolic switch towards glycolysis that is exhibited by *TP53*-deficient cells (133). This link between p53 and mitochondrial metabolism provides a possible explanation for the Warburg effect occurring in cancer cells, most of which carry mutations in *TP53*.

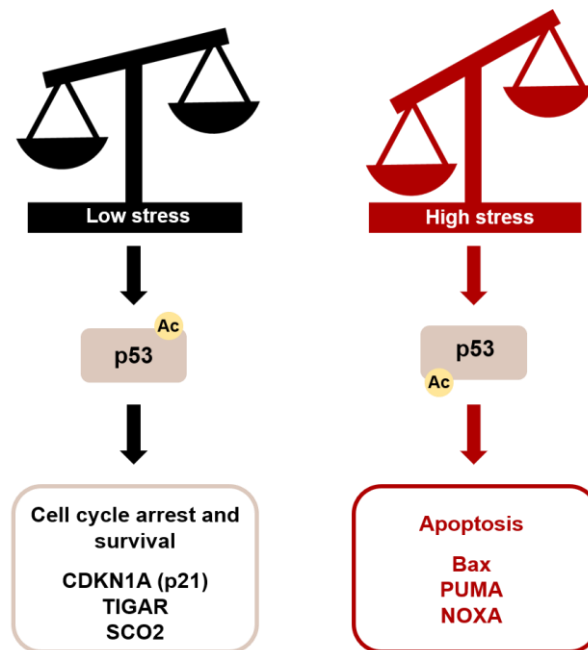


Figure 17. p53 role as a pro-survival or an apoptosis enhancer gene. Choice of response to p53 depends on many variables, including the extent of the stress. Low or repairable levels of stress or damage induce a pro-survival response of p53 involving control of glycolysis, cell cycle arrest and repair of genotoxic damage. More severe, irreparable or oncogenic stress leads to the activation of cell death or senescence. Examples of target genes that are transcriptionally activated by p53 in each context are provided. The preferential activation of target genes with different outcomes depends on post-translational modifications of p53 including acetylation, ubiquitination and phosphorylation.

6.5. Oxidative stress and antioxidant defenses

6.5.1. Reactive oxygen species

Oxidative stress is a common feature in tumour microenvironment. The term ROS includes the superoxide (O_2^-) and hydroxyl (HO^\cdot) free radicals as well as non-radical molecules such hydrogen peroxide (H_2O_2). These molecules are principally derived from the oxygen that is consumed in various metabolic reactions occurring mainly in mitochondria, peroxisomes and the endoplasmic reticulum (ER).

In mitochondria, the formation of unstable species is required for the transference of electrons between complexes but can lead to the direct transfer of electrons to oxygen in what is called 'electron leakage', as it has been mentioned before (**Figure 15**). O_2^- and H_2O_2 are formed when, instead of 4 e^- , only one or two e^- are transferred to O_2 , respectively. Mitochondria are considered the major source of ROS and several detoxifying enzymes are found in these organelles. Superoxide dismutase converts O_2^- to H_2O_2 , which in turn can be neutralized to water by catalase or converted into HO^\cdot through Fenton reactions.

Peroxisomes are involved in both the scavenging and the production of ROS through catalase-mediated decomposition of H_2O_2 and β -oxidation of long chain fatty acids and flavin oxidase activity, respectively. The ER constitutes an oxidizing environment that favours disulphide bond formation and protein folding and increases ROS levels through protein oxidation (134).

6.5.2. A focus on Nrf2

A crucial molecule involved in oxidative stress homeostasis is NADPH, which is the unique reducing agent that can be used by GR to regenerate GSH. Despite that NADH has a key role in the maintenance of the cellular redox balance required for the proper function of many reactions, it cannot substitute NADPH to regenerate GSH, as it was described many years ago (135). Thus, cells are extremely dependent on the reactions that produce NADPH. These reactions are catalysed by G6PD in the PPP, ME1 and ME2 located in the cytosolic and the mitochondrial compartment, respectively, and the folate cycle (**Figure 5**). GSH binds to oxidized molecules through glutathione S-transferase (GST), resulting in the reduction of the molecules. The neutralization of reactive oxygen and nitrogen species is particularly important given their genotoxic potential. In chronic inflammatory diseases such as rheumatoid arthritis and inflammatory bowel disease, these oxygen and nitrogen-derived species react to form peroxyxynitrite, a mutagenic agent. Hence, the accumulation of mutagenic agents that can interact with DNA, together with repeated tissue damage and regeneration of tissue, results in permanent genomic alterations such as point mutations, deletions, or rearrangements in proliferating cells (136). One of the most known mechanisms of ROS-induced DNA damage is the generation of nucleotide alterations as well as DNA

strand breaks. 8-hydroxylated guanine bases, for example, can pair with both adenine and cytosine bases and therefore can cause transversion mutations such as G:C to T:A. Interestingly, tumours under oxidative stress have been shown to exhibit up to 10-fold increase in 8-hydroxylated guanine levels compared to neighbouring normal cells (137).

To prevent all these phenomena, normal cells need potent antioxidant mechanisms. However, when these mechanisms are tailored to tumour cells, these malignant cells acquire the potential to survive even in oxidative environments and, thus, antioxidant proteins considered tumour suppressor genes start acting as tumour promoters.

The main inducible antioxidant programme within cells is regulated by **Nuclear factor (erythroid-derived 2)-like 2 (Nrf2)** (138). This transcription factor is encoded by the homologous gene **NFE2L2**, which is frequently overexpressed in cancer (**Figure 18**) and it needs to be differentiated from Nuclear respiratory factor 2 (NRF2), which has not been studied in this thesis.

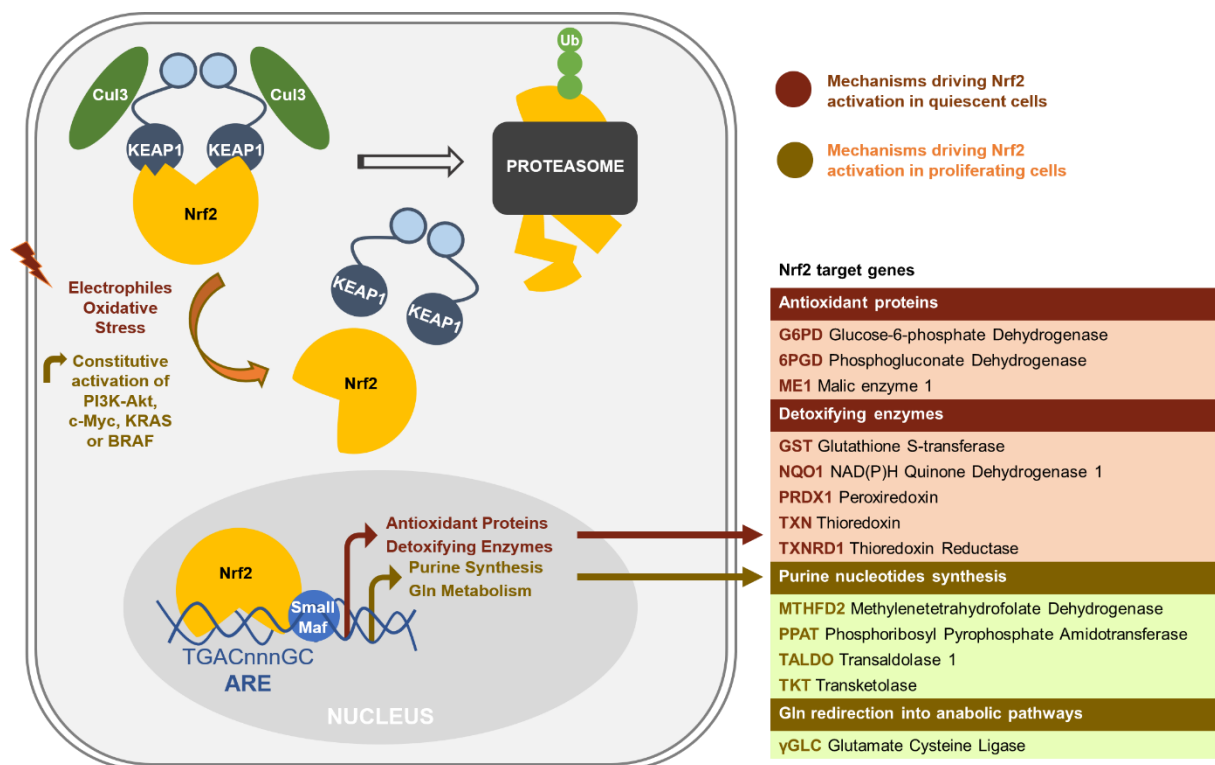


Figure 18. Mechanisms of Nrf2 activation in quiescent and proliferative cells. In quiescent cells (in brown), Nrf2 is activated by electrophiles or oxidant molecules that trigger its separation from KEAP1, allowing its translocation to the nucleus. In proliferative cells (in green) the active PI3K-Akt pathway increases the nuclear accumulation of Nrf2 and enables Nrf2 to promote metabolic activities that support cell proliferation in addition to enhancing cytoprotection. The functional expansion of Nrf2 reinforces the metabolic reprogramming triggered by proliferative signals.

Despite being essential for the maintenance of tissue integrity and preventing transformation, amplified Nrf2 activity contributes to tumour development by causing chemo- and radio-resistance, protecting from apoptosis, promoting invasiveness and angiogenesis and inhibiting senescence and autophagy (139). The pro-angiogenic role of Nrf2 is carried out through the transcriptional and post-transcriptional control of central regulators of endothelial activity, among which there is PFKFB3 (140). Under normal conditions, Nrf2 is subjected to a rapid turnover due to its binding to the ubiquitin ligase KEAP1, which triggers Nrf2 degradation through the proteasome (141). Upon exposure to electrophiles or ROS, the dissociation between the two proteins is induced and Nrf2 becomes active. In cancer cells, however, Nrf2 can be constitutively activated independently of ROS levels through the PI3K-Akt signalling pathway (142), c-Myc and KRAS and BRAF oncogenes (143).

The canonical pathway for Nrf2 activation is based on modifications in KEAP1 that trigger Nrf2 release. The “hinge and latch” model has been proposed to explain the binding between Nrf2 and KEAP1. Nrf2 binds to KEAP1 through the EDGE and the DLG motifs (nomenclature according to amino acid composition). The affinity of the DLG motif for KEAP1 is weaker than that of the EDGE motif, allowing for two conformations. The closed conformation implies the binding of Nrf2 to a KEAP1 dimer through EDGE and DLG motifs, whereas the opened conformation occurs when the DLG motif separates from KEAP1 and Nrf2 is bound to a single KEAP1 molecule through the EDGE motif. For this reason, the DLG motif is considered a “latch”. KEAP1 is highly rich in cysteine residues, which can be oxidized following exposure to electrophiles or ROS. Modifications in the redox status of these cysteines alter the conformational structure of KEAP1, especially when they are in the open conformation, and favour the dissociation from Nrf2, which can then translocate to the nucleus (141,144). Besides, the dissociation of Nrf2 from KEAP1 can also be promoted by non-electrophilic Nrf2 inducers which compete for the binding to KEAP1 (**Figure 19**).

On the other hand, post-translational modifications of Nrf2 can also induce its dissociation from KEAP1. The PI3K/Akt has also been shown to trigger Nrf2 activation, but the mechanisms involved remain still unknown (145). These KEAP1-independent pathways for Nrf2 activation are named as non-canonical pathways and are especially relevant in proliferating cells, in which Nrf2 can be constitutively activated independently of ROS levels (146).

When Nrf2 is liberated from KEAP1, it translocates to the nucleus due to the nuclear localisation signal located at the Neh1 domain and binds to antioxidant response elements (AREs) in the promoter of several pro-survival genes. AREs are typically sequences of 5'-TGAC/GnnnGC-3' (147), where n is any nucleotide, that function as a cis-regulatory element or enhancer in the promoter region of numerous genes involved in detoxification and anti-oxidation, such as NAD(P)H Quinone Dehydrogenase 1 (NQO1), GST, glutathione peroxidase (GPX), heme oxygenase 1 (HO-1) and thioredoxin 1 (Trx1) (141,142,144).

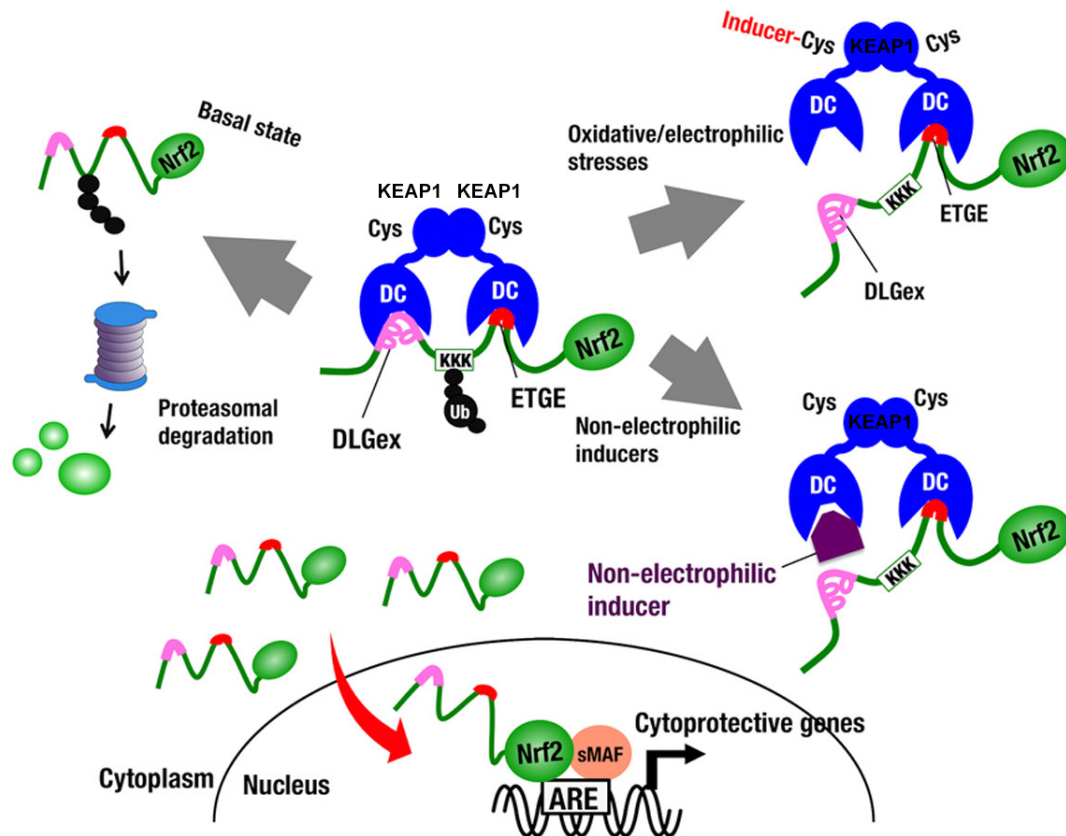


Figure 19. The KEAP1/Nrf2 system. In response to oxidative and electrophilic stresses, Nrf2 induces the expression of cytoprotective enzyme genes. Under unstressed conditions, Nrf2 is degraded in a KEAP1-dependent manner via the ubiquitin–proteasome pathway. KEAP1 homodimer binds to single Nrf2 molecules through DLG and ETGE motifs. Both motifs individually bind to a pocket in the double glycine repeat and C-terminal (DC) domain of KEAP1. Lysine (K) residues that reside between the two motifs are the targets of ubiquitination. Nrf2 inducers dissociate Nrf2 DLG motif from KEAP1 by modification of cysteine residues (Cys) of KEAP1 or by competing with Nrf2 to bind to KEAP1. Nrf2 is stabilized and *de novo* synthesized Nrf2 translocates into the nucleus, where it heterodimerizes with small Maf proteins (sMAf) and activates transcription through binding to antioxidant response elements (AREs) in the promoter of cytoprotective genes. Image from (144).

Recently, key metabolic genes, including G6PD, PGD, TKT and PEPCCK, have been described to be regulated by the ARE-Nrf2 system (142,148), broadening the scope of Nrf2 impact on cancer cell progression (Figure 20). Nrf2 role in the mitochondria is now being studied and some results point out that Nrf2 deficiency impairs the functioning of the electron transport chain and oxidative phosphorylation (149). Besides, activation of Nrf2 leads to enhanced consumption of glutamate for GSH synthesis, resulting in increased dependency of exogenous glutamine due to insufficient α KG to fulfil the TCA cycle (150) (Figure 20).

Apart from promoting NADPH and nucleotides synthesis through the PPP, Nrf2 has also been described to activate ME-1 and MTHFD2 (Figure 20) (142,151). In conclusion, Nrf2 constitutes an orchestrator of many different reactions that contribute to the control of redox homeostasis and has been described as a master regulator of all hallmarks of cancer, either by directly or indirectly promoting or blocking them (152).

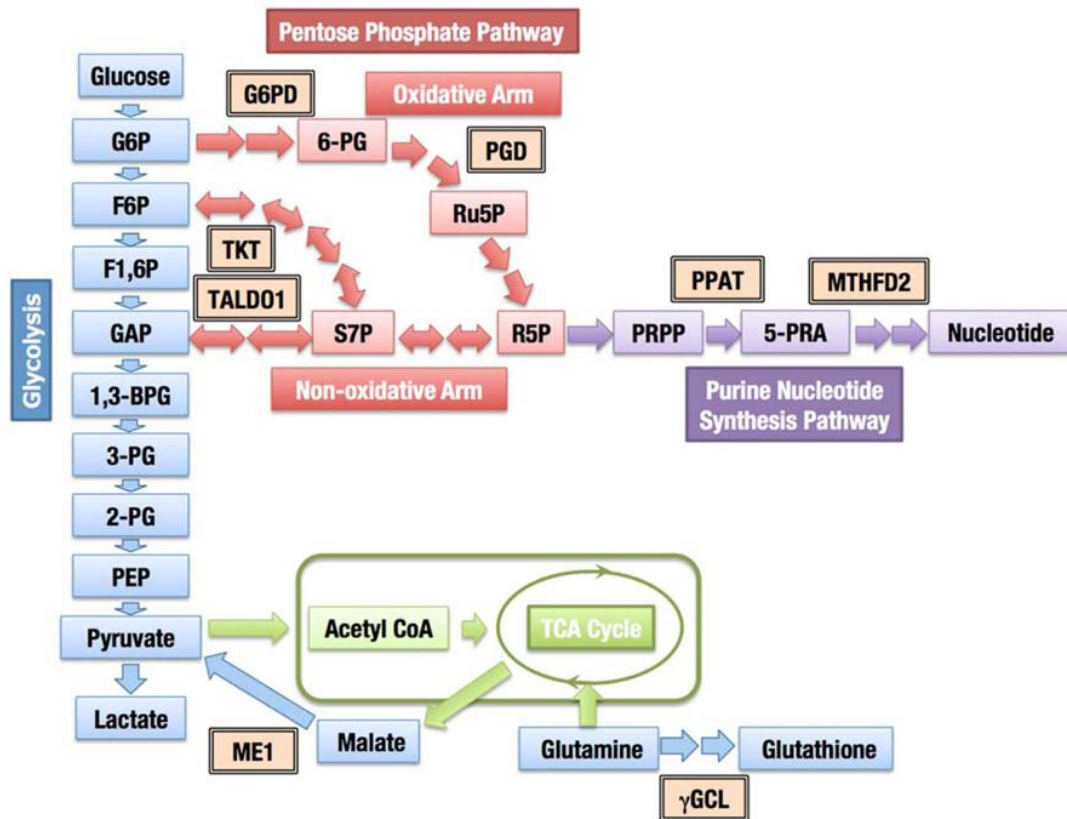


Figure 20. Contribution of Nrf2 to cellular metabolism. A schematic representation of glycolysis and pathways that use glycolytic intermediates to produce biomolecules is provided. The enzymes regulated through Nrf2 are indicated with double-framed boxes. Image from (145).

Finally, it is important to mention that crosstalk between Nrf2 and p53 has been described. p53-induced p21 can function to stabilize and enhance the activity of Nrf2, as an alternative mechanism of p53 to enhance the cellular antioxidant machinery (153,154).

6.6. Tumour microenvironment

The Warburg effect only partially explains tumour metabolism. In fact, it is now known that heterogeneity exists within tumours and that only some cells show increased glycolytic rate, while others predominantly use OXPHOS taking advantage of the metabolites produced by others, such as glycolysis-derived carbons and glutamine (120). In fact, what PET technique allows to visualize is the tumour mass, something that for years was interpreted as the signal of the glucose captured by tumour cells. It is now known that PET signal can come from tumour cells or from other types of cells within the tumour, such as cancer-associated fibroblasts (CAFs).

The “Reverse Warburg Effect” is the name of a novel theory of tumour metabolism based on a two-compartment model in which stromal cells are induced by cancer cells to undergo aerobic glycolysis (the classical Warburg effect) and then transfer back the products of glycolysis to tumour cells for their utilization in OXPHOS (155) (**Figure 21**).

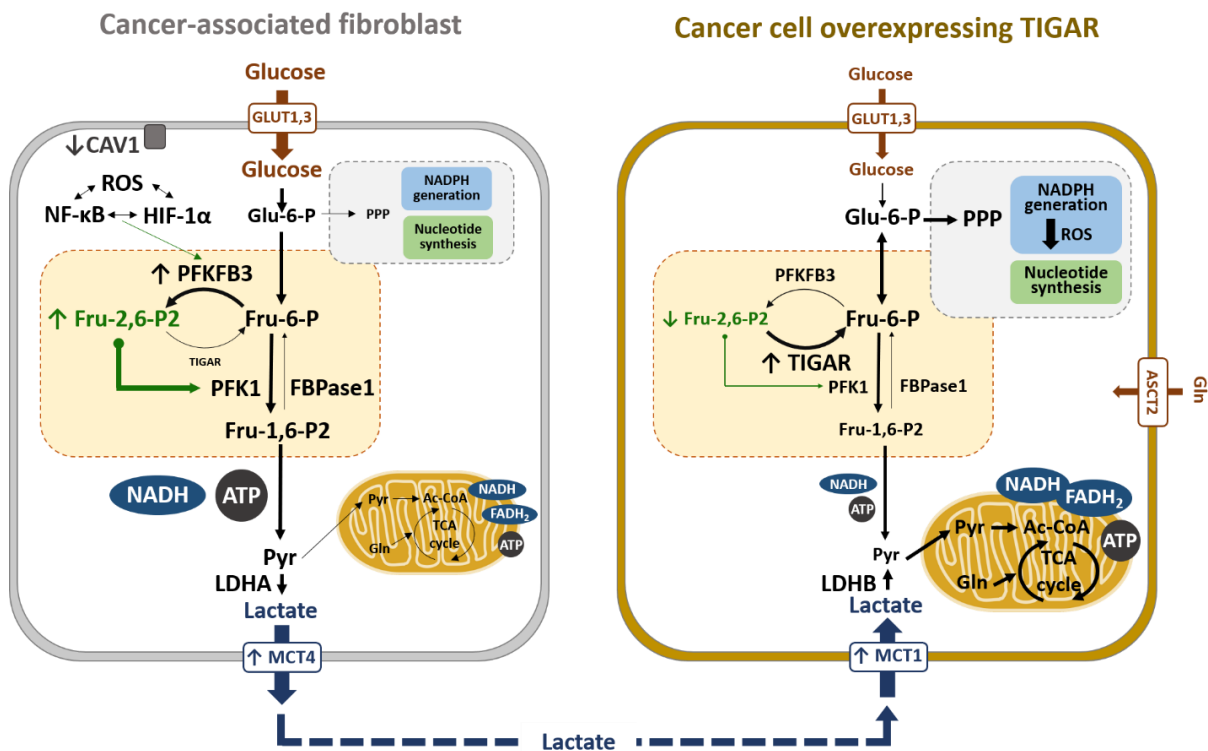


Figure 21. Metabolic coupling between cancer cells and cancer-associated fibroblasts. Lactate transport is crucial in the crossed-regulation of metabolism between cancer-associated fibroblasts and cancer cells. In the fibroblasts close to carcinoma cells, ROS produced by cancer cells, HIF-1 α , and NF- κ B induce glycolysis, downregulating CAV1 and upregulating MCT4, which results in increased lactate secretion in CAFs. Conversely, *TIGAR* overexpression in carcinoma cells alters their metabolic state, increasing the pentose phosphate pathway (PPP). Lactate released from CAFs is taken by cancer cells via MCT1 and converted to pyruvate, which can enter the TCA cycle. These cancer cells show high mitochondrial OXPHOS and low glycolysis, which is associated with high proliferation and low apoptosis rates, resulting in increased tumour growth.

The first evidences that trafficking occurred between cancer cells and surrounding cells appeared in colorectal cancer (156). The group of Ubaldo E Martinez-Outschoorn (MD in Thomas Jefferson University) has studied the Reverse Warburg Effect in breast cancer and has identified several players in this phenomenon. According to their studies, ROS produced by cancer cells induce HIF-1 α and NFkB-mediated reprogramming in CAFs, increasing glycolytic flux and lactate secretion through MCT4. HIF-1 α activation in CAFs triggers autophagy, which results in degradation of caveolin 1 (CAV1), the main component of caveolae, generating more ROS. On the other hand, overexpression of the lactate importer *MCT1* in cancer cells increases lactate-fuelled TCA cycle and OXPHOS in these cells (120,157) (**Figure 21**). Years before, inhibition of MCT1 in the SiHa human cervix squamous carcinoma cell line had already been shown to induce a shift from lactate-fuelled respiration to glycolysis, which rendered cells sensitive to glucose deprivation (158). Lactate, apart from participating in the crosstalk between cancer and CAFs, induces acidification of the extracellular media, which contributes both to tumour invasion and immune evasion (5,159).

In breast carcinoma cells, *TIGAR* overexpression has been described to induce the lactate importers MCT1 and MCT2, LDHB and GLS1. LDHB has high affinity for lactate, preferentially converting it to pyruvate. Oxygen consumption and ATP production are enhanced in *TIGAR* overexpressing cells in the presence of glutamine and lactate. When these cells are co-cultured with fibroblasts, a glycolytic phenotype consisting in increased HIF-1 α , PFKFB3 and LDHA is induced in the fibroblasts (**Figure 21**). Moreover, *TIGAR* overexpression in breast cancer cells favours tumour growth *in vivo*, as evidenced in three different xenograft models. Interestingly, the observation of increased expression of translocase of outer mitochondrial membrane 20 (*TOM20*) in *TIGAR* overexpressing carcinoma cells suggests other roles for this protein that might escape current knowledge (82).

Apart from the relationship between tumour cells and CAFs, the contribution of other cell types within the TME is crucial. In this sense, it is to mention the supply of fatty acids to tumour cells from tumour-associated adipocytes, as well as the involvement of endothelial cells in facilitating the exchange of all these metabolites and oxygen between cells (160). When vascularization is limited is when cellular vulnerabilities are evidenced, and cancer cells need to develop strategies for survival and growth that usually involve the exploitation of the metabolic activities of the surrounding cells.

HYPOTHESIS AND AIMS



TIGAR was described in 2006 as a p53 target gene coding for a protein with bisphosphatase activity on Fru-2,6-P₂. From then, several studies have confirmed that TIGAR is overexpressed in many tumour types, where it usually contributes to cell survival and to radio- and chemo-therapy resistance in some cases. However, p53 is mutated in more than 50% of human tumours, which makes it evident that other transcription factors are involved in the control of *TIGAR* expression. Nrf2 is the most important orchestrator of the antioxidant response in cancer cells and it has recently been described to control the expression of several metabolic genes involved in biosynthetic pathways, emerging as a good candidate for the p53-independent control of *TIGAR*.

On the other hand, Fru-2,6-P₂ is the most potent allosteric activator of PFK-1, a key enzyme for the maintenance of the glycolytic phenotype in tumour cells, which is one of the hallmarks of cancer. Thus, it looks difficult to understand how overexpression of *TIGAR*, the activity of which is meant to decrease Fru-2,6-P₂, fits with its role as a tumour-promoting gene. Even if TIGAR activity results in increased flux through the PPP, as it has been proposed, a balance between this enzyme and the protein responsible for the synthesis of Fru-2,6-P₂, PFK-2/FBPase-2, seems to be required to maintain high glycolytic flux.

The **hypothesis** of this thesis is that TIGAR contribution to the progression of cancer cells is beyond its phosphatase activity on Fru-2,6-P₂, and that the transcriptional control of *TIGAR* involves other factors rather than p53, one of which would be Nrf2.

In order to confirm this hypothesis, specific **objectives** were defined:

1. To determine the relationship between PFKFB3 and TIGAR and their contribution to tumour cell survival, making special attention to the role of TIGAR in situations of glycolytic impairment.
2. To elucidate the most important metabolic alterations induced by TIGAR overexpression and inhibition in cancer cells, trying to define which is the most relevant substrate of this enzyme.
3. To uncover whether the transcription factor Nrf2 is a modulator of *TIGAR* gene expression in cancer cells and determine the DNA response elements involved.
4. To analyse the subcellular distribution of TIGAR in response to oxidative stress with the aim of uncovering new mechanisms that contribute to the antioxidant function of this gene.

RESULTS CHAPTER I

TIGAR and glycolysis inhibition: is that redundant?



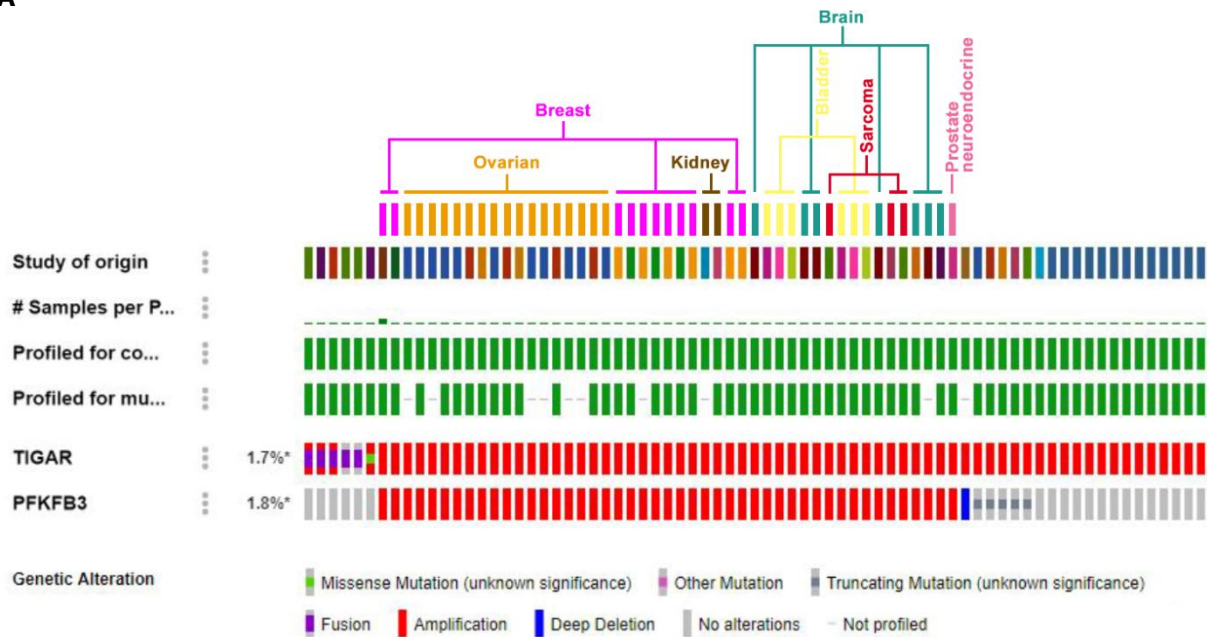
CONTEXT

The effects of inhibiting *PFKFB3* in HeLa cells were described by Dr. Bartrons' Lab in 2009. It was determined that *PFKFB3* inhibition decreased Fru-2,6-P₂, lactate and ATP concentration in cells and increased the flux of substrates into mitochondria. High resolution respirometry showed that *PFKFB3* inhibition increased the uncoupled respiration and had no effects on maximal respiration. In terms of phenotypical consequences, it was proved that *PFKFB3* inhibition compromised cell viability, anchorage-dependent and independent cell growth, cell viability and cell cycle progression (63,161).

Three years before, in collaboration with the group of Dr. Karen Vousden in *The Beatson Institute for Cancer Research* (Glasgow), our group showed that *TIGAR* inhibition by siRNA in U2OS cells increased Fru-2,6-P₂ concentration, and the overexpression of the enzyme decreased the concentration of this metabolite in these cells (3). Accordingly, in U2OS, *TIGAR* overexpression reduced glycolytic rate, which was determined by measuring the conversion of 5-³H-glucose to ³H-H₂O by enolase. Considering these findings and the similar results obtained overexpressing FBPase-2, *TIGAR* was described as a Fru-2,6-P₂ bisphosphatase and, consequently, as a glycolytic inhibitor (3). One of the main aims of this thesis was to determine whether the roles of *PFKFB3* and *TIGAR* were somehow related, in terms of metabolic activity and contribution to cell survival. Moreover, we considered important to clarify whether *TIGAR* acted only as a glycolytic inhibitor or could carry out other functions.

The analysis of all the studies available in cBioPortal revealed that *PFKFB3* and *TIGAR* genes are altered in 1,7% and 1,8% of all cancer patients, showing co-occurrence (**Figure 22**). This means that, although modification in the coding sequence of these genes is not very frequent, when one of the genes is altered, it is likely to find the other altered too. The most frequent alteration found in both *PFKFB3* and *TIGAR* is amplification, which shows that both genes contribute to cancer development (**Figure 22**). It is also important to note that many tumours display increased mRNA levels of these genes despite not carrying DNA alterations (24), something that needs to be considered to understand the importance of these genes in the control of cancer metabolism. mRNA expression was not reported in the analysis of cBioPortal data due to differences in the methodology for the determination of gene expression between studies.

Considering the role of *TIGAR* as a glycolytic inhibitor (3), which would situate it as a tumour suppressor gene due to its capacity to block the Warburg effect, it looks reasonable to study other roles for *TIGAR* that can explain its pro-oncogenic effector.

A**B**

A	B	Neither	A not B	B not A	Both	Log ₂ OR	p-Value	Tendency
TIGAR	PFKFB3	71501	878	949	67	2.523	<0.001	Co-occurrence

Figure 22. *TIGAR* and *PFKFB3* genetic alterations in human cancers. Data were obtained from cBioPortal (162,163) including all studies reported in the database, each of which has studied a specific type of cancer. **(A)** Patients are represented individually in columns. The overall percentage of alterations in either *TIGAR* or *PFKFB3* is indicated, and the type of alteration is represented by different colours. A more general classification has been performed according to tumour origin in the upper panel of the figure. **(B)** Table reporting the raw data for the mutual exclusivity/co-occurrence analysis performed by cBioPortal. The portal computes a set of simple statistics to identify patterns of mutual exclusivity or co-occurrence. For each pair of query genes (A and B), cBioPortal calculates an odds ratio (OR) that indicates the likelihood that the events in the two genes are mutually exclusive or co-occurrent across the selected cases:

$$OR = (N^{\circ} \text{ cases both genes altered} * N^{\circ} \text{ cases neither genes altered}) / (N^{\circ} \text{ cases A altered} * N^{\circ} \text{ cases B altered})$$

It then assigns each pair of genes to one category indicative of a tendency toward mutual exclusivity, co-occurrence or no association. To determine whether the identified relationship is significant for each gene pair, a Fisher's exact test is performed.

Previous experiments of the group had shown that the inhibition of *PFKFB3* in HeLa cells resulted in the induction of TIGAR protein levels (161). This interesting observation, which was completely unexpected, was a promising contribution to the characterisation of TIGAR. The work reflected in this first part of the thesis is focused on the characterization of TIGAR upregulation in response to *PFKFB3* suppression and other conditions that decrease glycolysis, and the phenotypical consequences of TIGAR induction and inhibition. The main aim of the results presented in this section was to elucidate the role of this gene in the survival of cancer cells, especially in scenarios of glycolytic blockage.

1. Crosstalk between TIGAR and PFKFB3

1.1. Characterization of TIGAR induction in response to *PFKFB3* inhibition

PFKFB3-targeting siRNA was transfected into HeLa cells at 75 nM, and *PFKFB3* and TIGAR were analysed by western blot at several time points, as shown in **Figure 23A**. *PFKFB3* was significantly inhibited in a time-dependent manner from 24 to 72 h. TIGAR protein levels were increased in parallel with *PFKFB3* downregulation, confirming the results previously obtained by the group. The highest induction was observed at 72 h after *PFKFB3*-targeting siRNA transfection (**Figure 23A,B**). To establish the contribution of *PFKFB3* and TIGAR in the response of HeLa cells to several parameters, we performed combined inhibition of these proteins by using combinations of 37,5 nM scrambled, *PFKFB3* or *TIGAR*-targeting siRNAs. Both proteins were significantly downregulated at 72 h when they were inhibited alone or in combination (**Figure 23C,D**). TIGAR was induced after 72 h of *PFKFB3*-targeting siRNA transfection by 1,5-fold compared to TIGAR levels in the scrambled condition. The analysis of *PFKFB3* and *TIGAR* expression by real-time quantitative polymerase chain reaction (RT-qPCR) at that time point revealed that *TIGAR* mRNA levels were significantly upregulated, while *PFKFB3* expression was significantly inhibited (**Figure 23E**), which was consistent with the results obtained at the protein level and suggested a transcriptional upregulation of TIGAR. As previous publications from the group showed, *PFKFB3* inhibition decreases Fru-2,6-P₂ concentration (63), something that has been also analysed and confirmed during this thesis. The metabolic effects of *PFKFB3* and TIGAR are further explored in Results Chapter II. However, it is important to mention here that the main question that arose from the observation that TIGAR was upregulated after *PFKFB3* inhibition was why cells responded to a blockage of glycolysis, such as *PFKFB3* inhibition, by upregulating TIGAR, an enzyme that would inhibit glycolysis as well. As summarized in **Figure 23F**, the logic answer would be that TIGAR enhanced the flux through the PPP and contributed to cell survival by providing NADPH and R5P in a situation of metabolic stress. To evaluate the validity of this hypothesis, we assessed the contribution of TIGAR to the viability of *PFKFB3*-inhibited cells. On the other hand, we aimed to describe the molecular mechanisms driving TIGAR induction in response to *PFKFB3* inhibition. This was important given that very few strategies, apart from transfection-based techniques, had been effective to modulate TIGAR protein levels until that moment. Thus, the finding of TIGAR upregulation in response to *PFKFB3* inhibition was relevant, and uncovering the pathways orchestrating it might help to describe new TIGAR modulators.

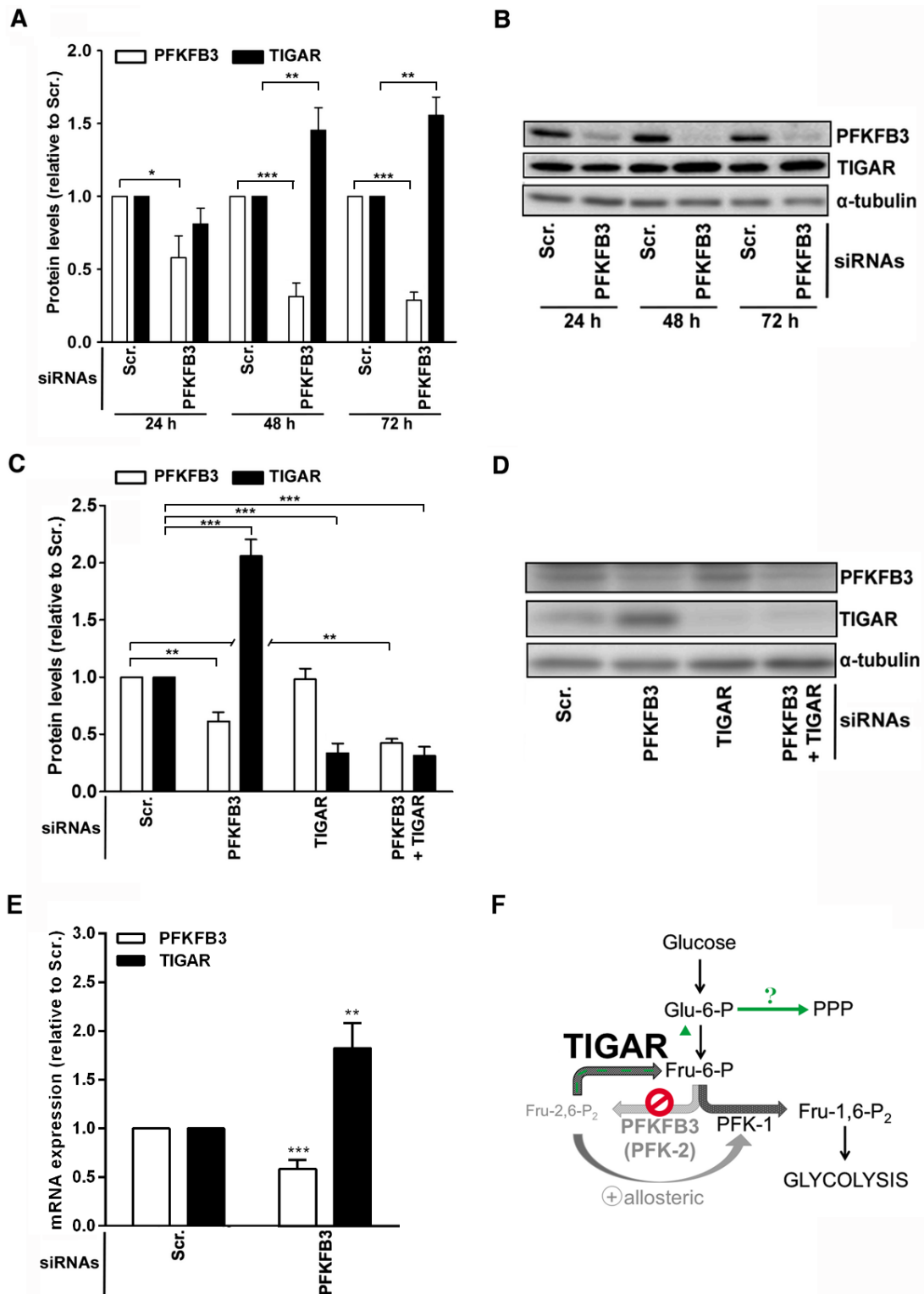


Figure 23. Crosstalk between *PFKFB3* and *TIGAR*. HeLa cells were transfected with 75 nM *PFKFB3* or *TIGAR*-targeting siRNAs and analysed at the indicated times. **(A)** Western blot analysis quantification of *PFKFB3* (white bars) and *TIGAR* (black bars) at 72 h post-siRNA transfection. **(B)** Western blot images of a representative experiment of the data reported in A. **(C)** Quantification of *PFKFB3* (white bars) and *TIGAR* (black bars) after 24 to 72 h of siRNA transfection. **(D)** Western blot images of a representative experiment of the data reported in C. **(E)** RT-qPCR analysis of *PFKFB3* (white bars) and *TIGAR* (black bars) after 72 h of siRNA transfection. **(F)** Schematic diagram of the metabolic consequences expected for *PFKFB3* inhibition and the subsequent *TIGAR* upregulation. All data are presented as the mean fold change relative to the scrambled siRNA (Scr.) of the corresponding time \pm SEM (A: n=3, C: n=5, E: n=7, *P < 0.05, **P < 0.01, ***P < 0.001).

As already discussed, it seemed unprovable that the upregulation of TIGAR after *PFKFB3* inhibition was consequence of a direct metabolic adaptation of cells. Thus, we focused on the analysis of several signalling pathways to determine if any of them could be mediating the crosstalk between the two enzymes. Preliminary results from Dr. Nieves Calvo pointed out that the signalling through the PI3K/Akt/mTORC2 cascade was increased in *PFKFB3*-inhibited cells (161). These results were confirmed (**Figure 24A,B**) and we determined also that *TIGAR* inhibition did not trigger the same pathway, confirming that Akt phosphorylation was present in the conditions of single *PFKFB3* inhibition and combined *PFKFB3* and *TIGAR* inhibition (**Figure 24C,D**).

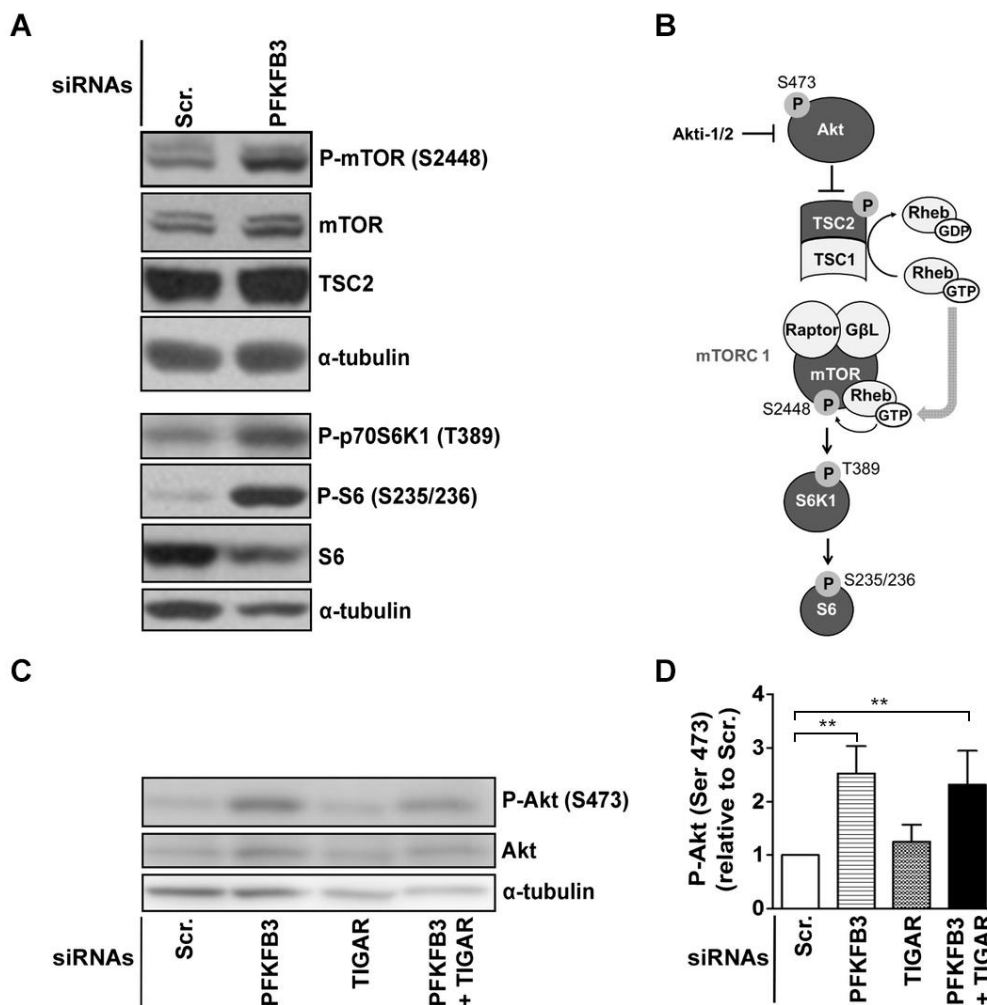


Figure 24. Analysis of the Akt signalling pathway after *PFKFB3* and/or *TIGAR* inhibition. HeLa cells were transfected with 75 nM *PFKFB3* or *TIGAR*-targeting siRNAs and protein was analysed by western blot at 72 h post-transfection. **(A)** Representative images of phosphorylated targets in the Akt signaling cascade. **(B)** Scheme of the Akt/mTORC signaling pathway. The proteins analysed by western blot are coloured in dark grey. **(C)** Western blot images showing Akt phosphorylation at S473 representative of the data reported in D. **(D)** Quantification of Akt phosphorylation, calculated as the ratio between phosphorylated Akt at S473 and total amounts of Akt. Data are presented as the mean fold change relative to the scrambled siRNA (Scr.) \pm SEM (D: n=4, **P < 0.01). ➤ *Continued on next page.*

Treatment of cells with the Akt inhibitor Akti-1/2 during the whole time of siRNA transfection resulted in the prevention of TIGAR induction in response to *PFKFB3* inhibition, showing that TIGAR increase is dependent on this signalling pathway (**Figure 24E,F**).

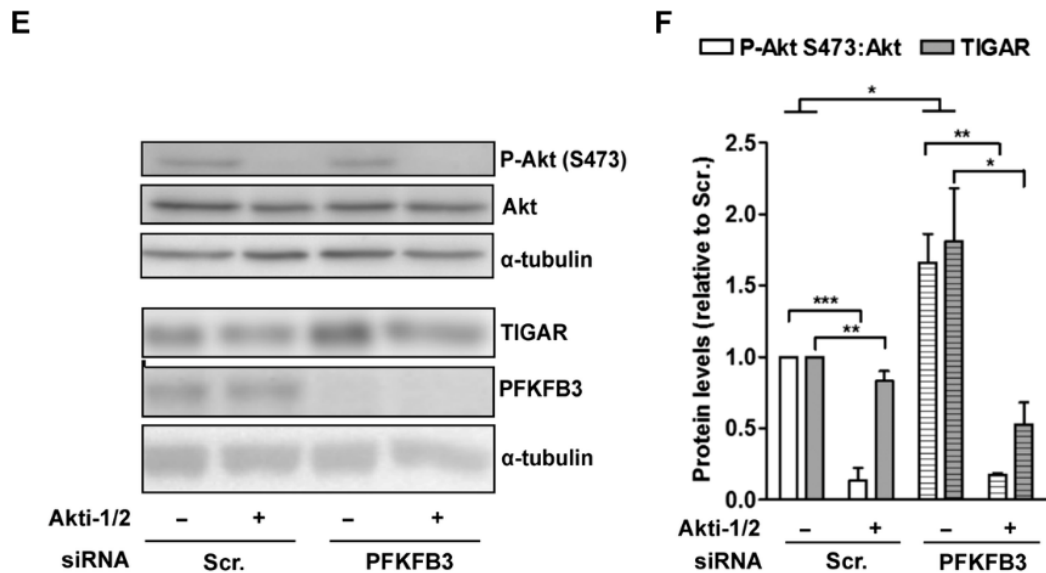


Figure 24. Analysis of the Akt signalling pathway after *PFKFB3* and/or *TIGAR* inhibition. *Continued.* (E) Western blot analysis of Akt phosphorylation at S473 and TIGAR after *PFKFB3*-targeting siRNA transfection, in the presence or absence of Akti-1/2, representative of three independent blots. (F) Quantification of Akti-1/2 effects in the mentioned proteins in three independent experiments. Data are presented as the mean fold change relative to scrambled siRNA (Scr.) ± SEM, and comparison between conditions is indicated by horizontal bars (F: n=3, *P < 0.05, **P < 0.01, ***P < 0.001).

With the aim of clarifying if p53 was involved in the upregulation of TIGAR in response to *PFKFB3* inhibition, we analysed *CDKN1A* expression, the gene that codes for p21, by RT-qPCR. HeLa cells express wild type *TP53*, but it is considered inactive given that these cells have the genome of the Human Papilloma Virus inserted in their own genome and encode for the E6 oncoprotein, which triggers ubiquitin-dependent p53 proteolysis (164). However, p53 reactivation has been reported in these cells (165), which made us think that this transcription factor might be involved in TIGAR upregulation in response to *PFKFB3* knockdown. Immunofluorescence detection of p53 revealed increased presence of this transcription factor in the nuclei of *PFKFB3*-inhibited cells and in cells where both *PFKFB3* and TIGAR were suppressed (**Figure 25A**). The total fluorescence per cell was quantified with ImageJ and it was evidenced that mean p53 levels were highly increased in *PFKFB3*-inhibited cells and in *PFKFB3* and TIGAR-inhibited cells (**Figure 25B**). p53 protein levels were also evaluated by western blot in *PFKFB3*-inhibited cells, and the results suggested increased levels of this transcription factor (**Figure 25C**). Additionally, the expression of *CDKN1A* (p21), a known p53 target, was slightly increased in *PFKFB3*-inhibited cells, although the difference was very small and not statistically significant (**Figure 25D**).

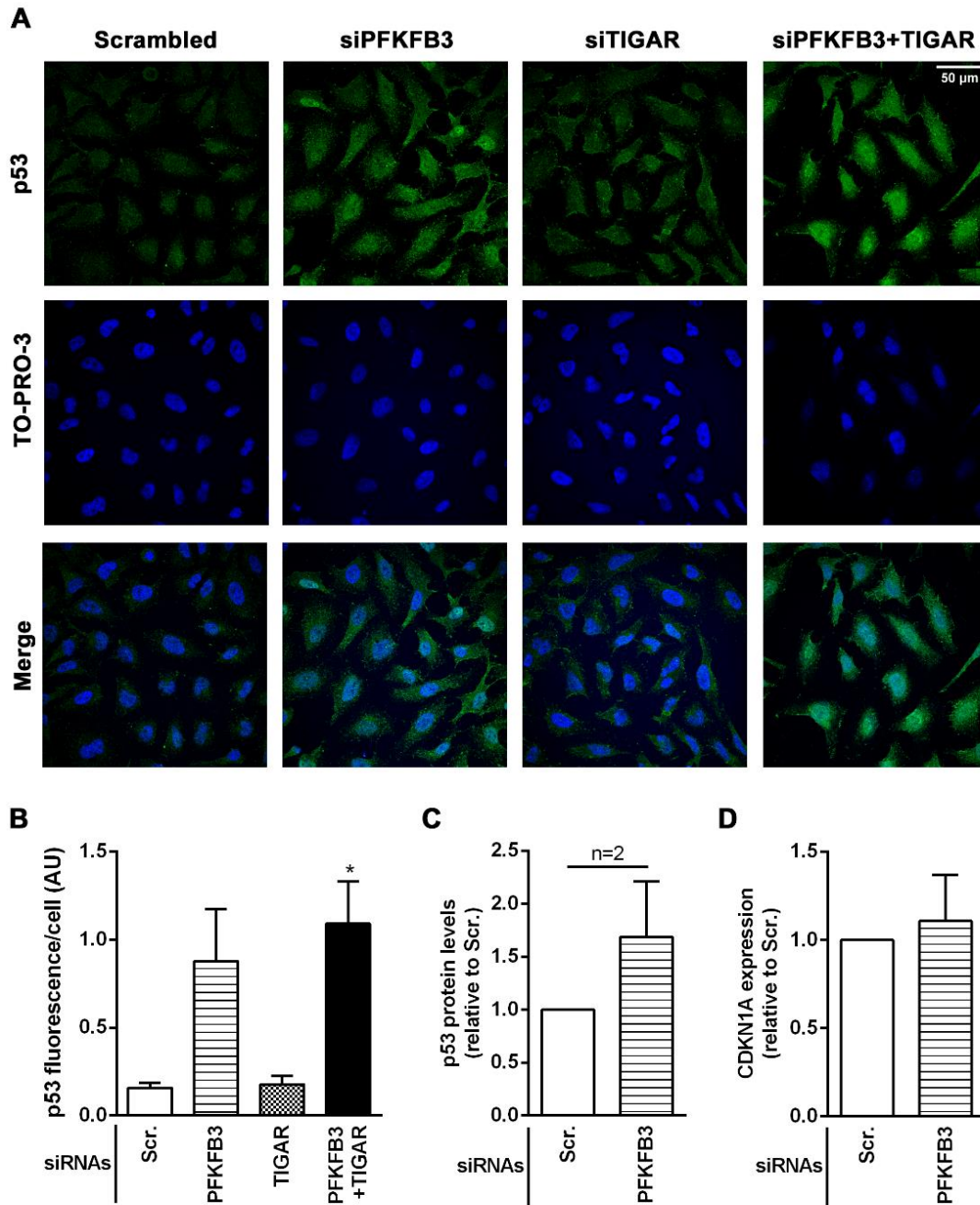


Figure 25. Analysis of p53 in response to *PFKFB3* and *TIGAR* inhibition. HeLa cells were transfected with 75 nM *PFKFB3* or *TIGAR*-targeting siRNAs and analysed at 72 h post-siRNA transfection. **(A)** Cells were fixed and immunofluorescence was performed with a primary antibody against total p53 and a secondary antibody conjugated with an Alexa488 fluorochrome (shown in green). Nuclei were stained with DAPI and are shown in blue. Images were acquired with Carl Zeiss LSM880 confocal microscope (Carl Zeiss). **(B)** Quantification of p53 fluorescence is expressed as mean fluorescence intensity per cell, calculated with FIJI (166) in at least 50 cells per condition. Comparisons were performed between each group and cells transfected with scrambled siRNA (* $P < 0.05$). **(C)** Western blot analysis of total p53 levels in *PFKFB3*-inhibited cells. Data are presented as the mean fold change in protein levels relative to scrambled siRNA (Scr.) \pm SEM **(D)** RT-qPCR analysis of *CDKN1A* (p21) expression in *PFKFB3*-inhibited cells. Data are presented as the mean fold change in expression relative to scrambled siRNA (Scr.) \pm SEM (B: n=3, C: n=2, D: n=4, * $P < 0.05$).

p53 was not the unique transcription factor enhanced by *PFKFB3* inhibition. Preliminary experiments with the Nrf2 transcription factor also showed increased levels of this protein by immunofluorescence (**Figure 26A**). The specificity of the staining was assessed by using Nrf2-inhibited cells in parallel and the quantification of total Nrf2 levels per cell confirmed increased staining of Nrf2 in *PFKFB3*-inhibited cells compared to control cells (**Figure 26B**). Moreover, western blot analysis also showed increased Nrf2 levels accompanied with significantly enhanced levels of the Nrf2 target G6PD (**Figure 26C,D**). These findings motivated one of the most important hypotheses of this thesis, which is the Nrf2-dependent modulation of *TIGAR*. Results Chapter III is fully dedicated to this topic.

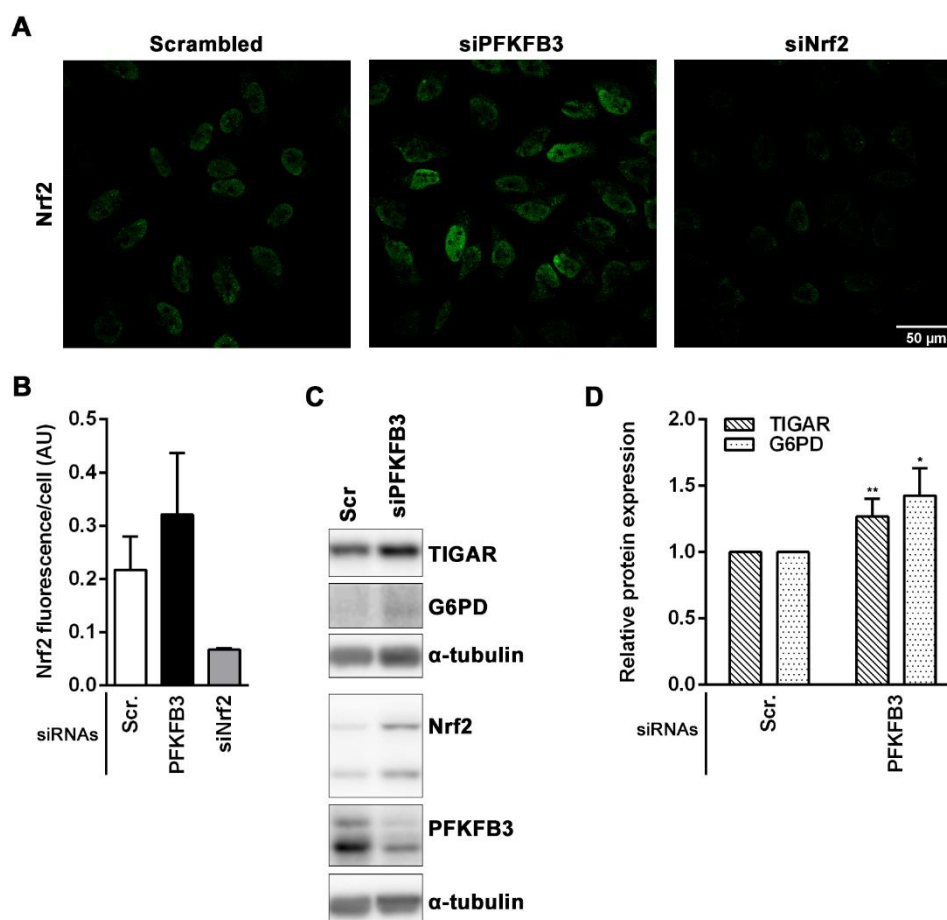


Figure 26. Analysis of Nrf2 in response to *PFKFB3* inhibition. HeLa cells were transfected with 75 nM *PFKFB3*-targeting siRNAs and analysed at 72 h post-siRNA transfection. **(A)** Cells were fixed and immunofluorescence was performed with a primary antibody against Nrf2 and a secondary antibody conjugated with an Alexa488 fluorochrome (shown in green). Nuclei were not properly stained in this immunofluorescence. Images were acquired with Carl Zeiss LSM880 confocal microscope (Carl Zeiss). **(B)** Quantification of Nrf2 fluorescence is expressed as mean fluorescence intensity per cell, calculated with FIJI (166) in at least 50 cells per condition. **(C)** Western blot analysis of TIGAR, Nrf2, Nrf2-target G6PD and *PFKFB3* in *PFKFB3*-inhibited cells. **(D)** RT-qPCR analysis of *TIGAR* and the Nrf2 target gene *G6PD* in *PFKFB3*-inhibited cells. Data are presented as the mean fold change in expression relative to scrambled siRNA (Scr.) \pm SEM (B: n=3, D: n=6).

1.2. Phenotypical consequences of inhibiting *PFKFB3* and *TIGAR*

Considering the established role of *TIGAR* as an enzyme contributing to oxidative stress detoxification in cells (79,167), we quantified ROS levels in HeLa cells after 72 h of *PFKFB3* and *TIGAR*-targeting siRNAs transfection. We used two different ROS detection probes, CellROX Green and 2',7'-dichlorofluorescein diacetate (DCFDA), the fluorescence of which was analysed by flow cytometry. The reactive species detected by each probe are detailed in the Materials and Methods Section.

A modest increase in ROS levels was evidenced in *PFKFB3*-inhibited cells (dotted bars) from 24 h after transfection compared to control cells (white bars). Tert-butyl-hydroperoxide (tBHP), a potent oxidant, was used as positive control (Figure 27).

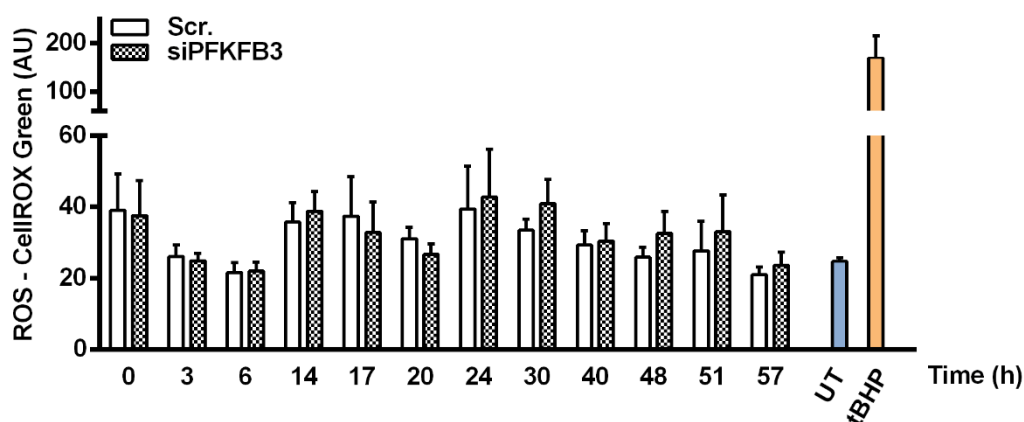


Figure 27. Time course of reactive oxygen species in *PFKFB3*-inhibited cells. HeLa cells were transfected with *PFKFB3*-targeting siRNA and ROS levels were determined with CellROX Green by flow cytometry after 72 h of transfection. ROS levels in untransfected cells (UT, blue bar) and tBHP-treated cells (orange bar) are reported. Mean fluorescence intensity in arbitrary units (AU) is shown (n=4).

The fluorescence emitted by CellROX Green was highly variable between experiments. With the aim of obtaining more robust results, we used a different probe, DCFDA. According to the results obtained with CellROX Green, DCFDA revealed increased oxidative stress after *PFKFB3* inhibition at 72 h post siRNA transfection. Surprisingly, *TIGAR* depletion did not affect ROS levels, but the combined inhibition of both proteins led to significantly increased oxidative stress compared to the scrambled condition (Figure 28A). This is illustrated by a shift in the fluorescence peak registered (Figure 28B). These results suggest that *PFKFB3* inhibition generates metabolic stress and renders cells more susceptible to alterations in antioxidant mechanisms such as *TIGAR*, which can be dispensable in unstressed conditions.

We performed several attempts to modulate ROS levels and study whether *TIGAR* induction in response to *PFKFB3* inhibition was mediated by ROS. However, no conclusive results were obtained. For that, two antioxidants were used: 1 μ M butylated hydroxyanisole (BHA) and 1,5 mM N-acetyl-cysteine (NAC).

As it can be observed in the ROS measurements with DCFDA, NAC was more potent at reducing the oxidative stress generated by *PFKFB3* depletion than BHA (Figure 28C,D). However, none of these molecules completely prevented the increase in ROS levels caused by *PFKFB3* suppression. Any of the molecules avoided the oxidative stress generated by the double inhibition of *PFKFB3* and *TIGAR* either. Albeit, when data were analysed independently and not relative to each Scrambled condition, a descent in oxidative stress was evidenced in all cells treated with antioxidants, proving the efficacy of these molecules. However, as it has been mentioned before, neither NAC nor BHA were potent enough to prevent the stress caused by *PFKFB3* and *TIGAR*-targeting siRNA transfections (Figure 28E). Accordingly, *TIGAR* induction was not prevented by the antioxidants (data not shown).

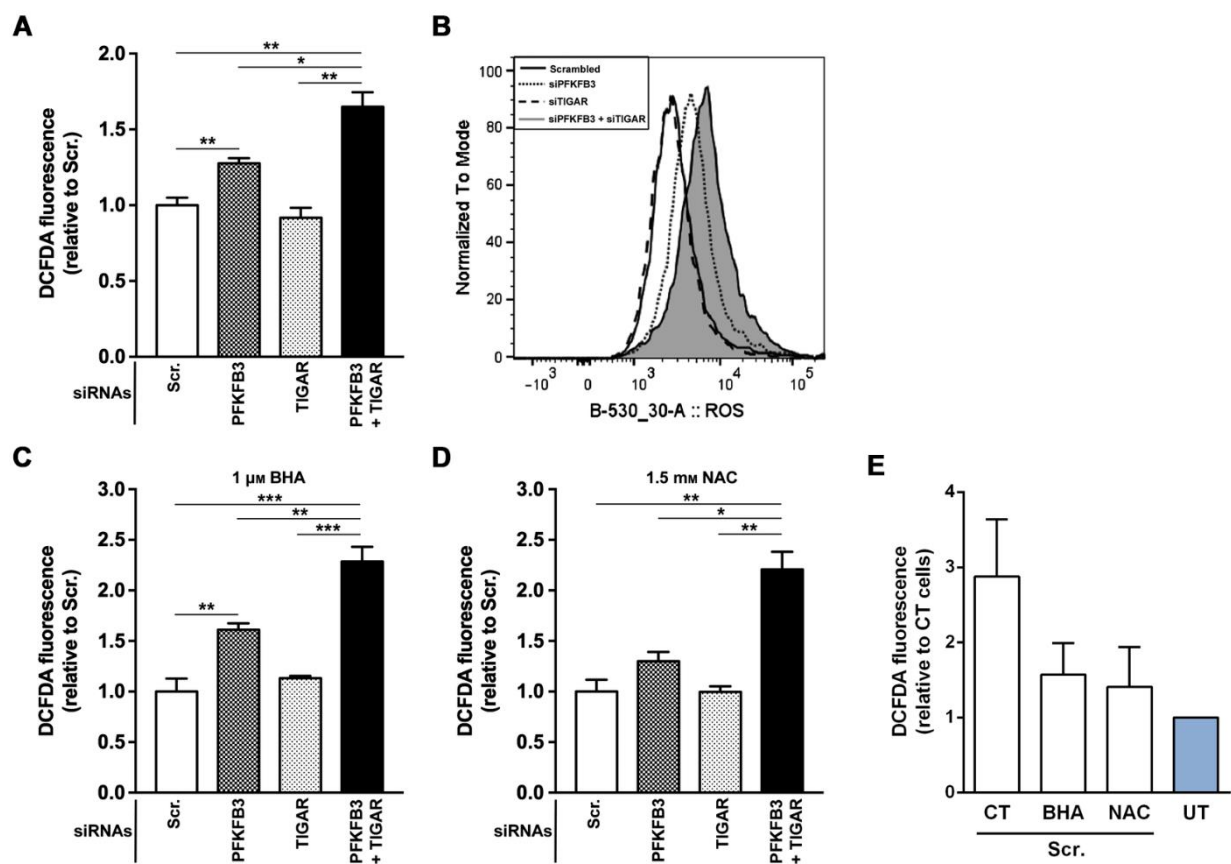


Figure 28. Reactive oxygen species analysis in *PFKFB3* and *TIGAR*-inhibited cells. HeLa cells were transfected with 75 nM *PFKFB3* or *TIGAR*-targeting siRNAs and analysed at 72 h post-siRNA transfection. **(A)** Quantification of DCFDA fluorescence normalized to HeLa cells transfected with the Scrambled siRNA (Scr.). **(B)** Raw data of DCFDA fluorescence peaks of a representative experiment. **(C and D)** Quantification of ROS levels after co-treatment with the antioxidant molecules **(C)** BHA and **(D)** NAC. DCFDA fluorescence was normalized to the ROS levels detected in HeLa cells transfected with the Scrambled siRNA (Scr.). **(E)** Analysis of ROS levels in cells transfected with the Scrambled siRNA (Scr.) in the presence or absence of BHA and NAC. DCFDA fluorescence was normalized to the ROS levels detected in untransfected cells (UT, blue bar) to determine the effects of antioxidant molecules at basal condition, which cannot not be appreciated in A-C. All data are presented as the mean fold change \pm SEM. Comparison between conditions is indicated by horizontal bars ($n=3$, * $P < 0.05$, ** $P < 0.01$, *** $P < 0.001$).

ROS can modify DNA bases causing genome instability, which can give place to DNA double strand breaks (168). One of the first alterations is the phosphorylation of histone γ -H2AX at Ser 139, which we used to quantify DNA damage in HeLa cells after the inhibition of *PFKFB3* and *TIGAR*. The results obtained showed that there were very few nuclei with P- γ -H2AX foci in the Scrambled condition, whereas the number of foci was significantly increased in single *PFKFB3* and *TIGAR*-targeted cells (Figure 29). In the case of *PFKFB3*-inhibited cells, these results are consistent with increased ROS levels found in these cells, as it has been shown in Figures 27-28. However, in the case of *TIGAR*-inhibited cells, we observed increased DNA damage with no changes in ROS levels. This could be explained either by a lack of sensibility of the DCFDA assay, or by the fact that DNA damage in these cells is independent of ROS.

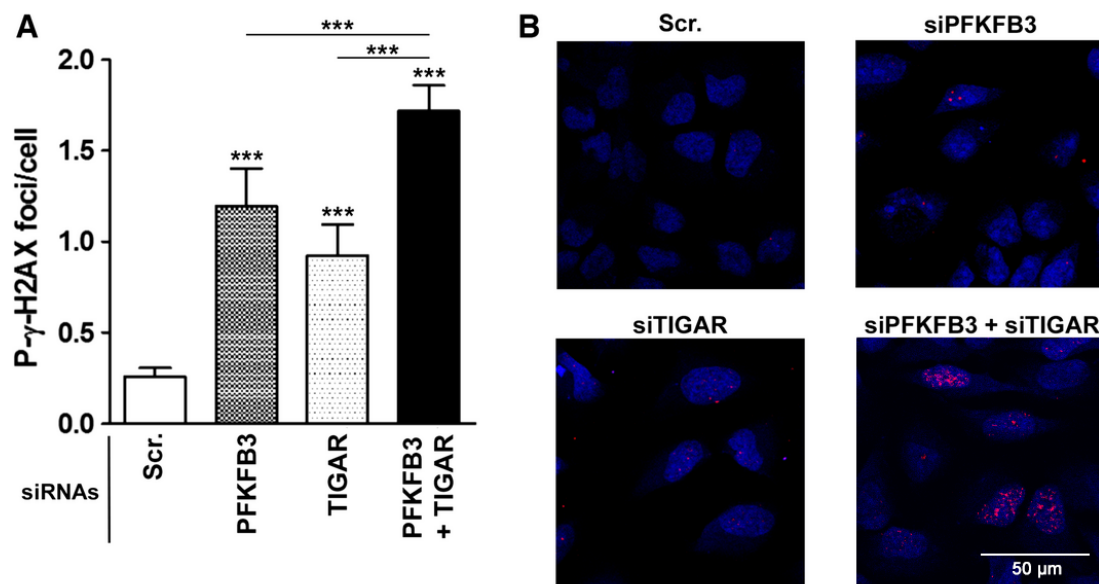


Figure 29. Effect of *PFKFB3* and *TIGAR* silencing on P-H2AX (S139) foci formation. HeLa cells were transfected with 75 nM *PFKFB3* or *TIGAR*-targeting siRNAs. At 72 h cells were fixed and immunofluorescence was performed using a P-H2AX (S139) specific antibody and a Cy3-conjugated secondary antibody (shown in red). Nuclei were stained with TO-PRO-3 and are shown in blue. **(A)** Quantification of the average number of foci per cell determined with FIJI from at least 150 cells counted from five randomly chosen fields of view in each condition. Data are presented as mean \pm SEM, and comparison between conditions is indicated by horizontal bars (** $P < 0.001$). **(B)** Images of a representative experiment with merged P-H2AX (S139) and nuclei channels.

Considering that several studies have related the expression of *TIGAR* and *PFKFB3* to autophagy, we wondered whether this process was affected by the inhibition of these two proteins in HeLa cells. As autophagy indicators, we analysed the cleavage of microtubule-associated protein 1 light chain 3 (LC3) with the ratio of its lipidated form (LC3-II) versus the unlipidated form (LC3-I) (Figure 30A,C), and the total amounts of p62 (Figure 30B,C). To assess whether we were properly detecting changes in the autophagic flux, we treated cells with chloroquine and rapamycin. Chloroquine increases the pH of the autophagosome, avoiding its fusion with the lysosome, and thus LC3-II, p62 and the other proteins contained in the autophagosome accumulate. On the other hand, rapamycin increases autophagy and lipidation of LC3 by inhibiting mTORC1. Although our results did not show significant differences in the levels of LC3 or p62 after *PFKFB3* or *TIGAR* inhibition, different distribution of LC3 forms was observed between *PFKFB3*- and *TIGAR*-silenced cells (Figure 30C), with the latter showing increased LC3-II, which could reflect increased autophagic flux, according to previous results (3,169,170). A growing amount of evidence in recent years argues for oxidative stress acting as the converging point of several stimuli triggering autophagy such as nutrient deprivation, viral infection or genotoxic stress (171). However, ROS levels were the same in *TIGAR*-silenced cells than in control cells in our experiments (Figure 28). Thus, either other mechanisms are involved in the modest increase in LC3 lipidation observed, or these changes in LC3 are not relevant and autophagy is not taking place in these cells.

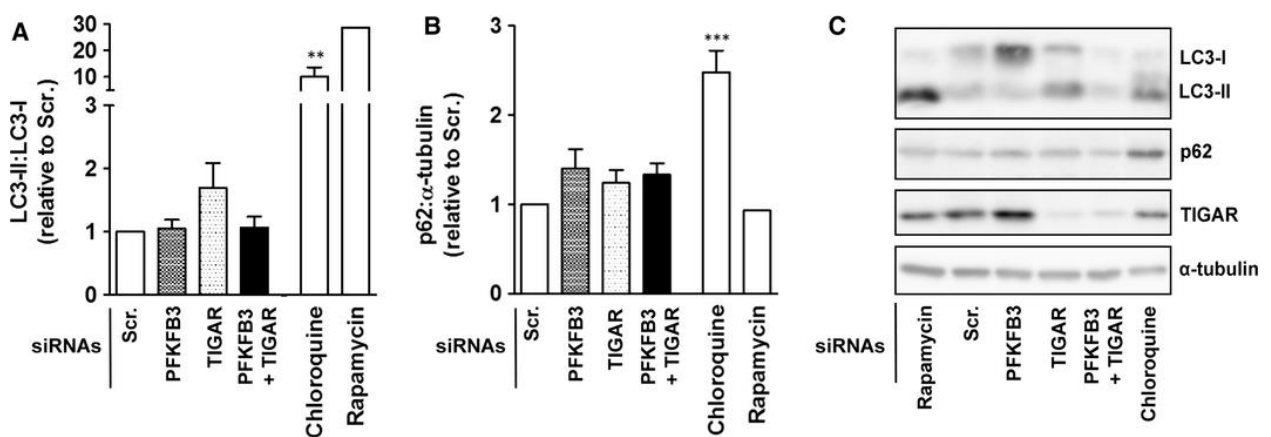


Figure 30. Effect of *PFKFB3* and *TIGAR* silencing on autophagy. HeLa cells were transfected with 75 nM *PFKFB3* or *TIGAR*-targeting siRNAs and analysed by western blot at 72 h post-transfection. Chloroquine and rapamycin were used as positive controls of LC3 lipidation. (A) Quantification of LC3-II and LC3-I protein levels. Data are expressed as the mean ratio LC3-II:LC3-I relative to scrambled siRNA (Scr.) \pm SEM (B) Quantification of mean p62 protein levels relative to Scr \pm SEM. (C) Western blot images of a representative experiment are shown. Protein levels were compared to those found in Scr. (n=4, **P < 0.01, ***P < 0.001).

A crucial question when studying the effects of the combined inhibition of *PFKFB3* and *TIGAR* was to determine if cell death was increased with this double-targeting approach. Based on the results of P-H2AX immunofluorescence, it looked reasonable to think that the conditions at which there was more DNA damage, which were *PFKFB3* silencing and the double inhibition, would show decreased cell viability. With this purpose, cell survival was assessed by two techniques: 3-(4,5-dimethylthiazol-2-yl)-2,5-diphenyltetrazolium bromide (MTT) assay and AnnexinV/Propidium Iodide (AnnexinV/PI) staining. Results from the MTT assay must be considered a measure of mitochondrial capacity, as the assay is based on the enzymatic reaction catalysed by NAD(P)H-dependent oxidoreductases, the activity of which is increased by NADH, which is produced in TCA cycle. Thus, the purple colour of formazan, the reduced form of MTT, is directly proportional to mitochondrial functioning. However, the readout of this analysis can be at the same time informative and confusing if MTT results are interpreted as a measure of cell viability. In our experimental conditions, the inhibition of *PFKFB3* did not affect MTT signal. However, *TIGAR* depletion significantly decreased MTT signal to 80%. Besides, the combined inhibition of *PFKFB3* and *TIGAR* decreased MTT signal to 60% (Figure 31).

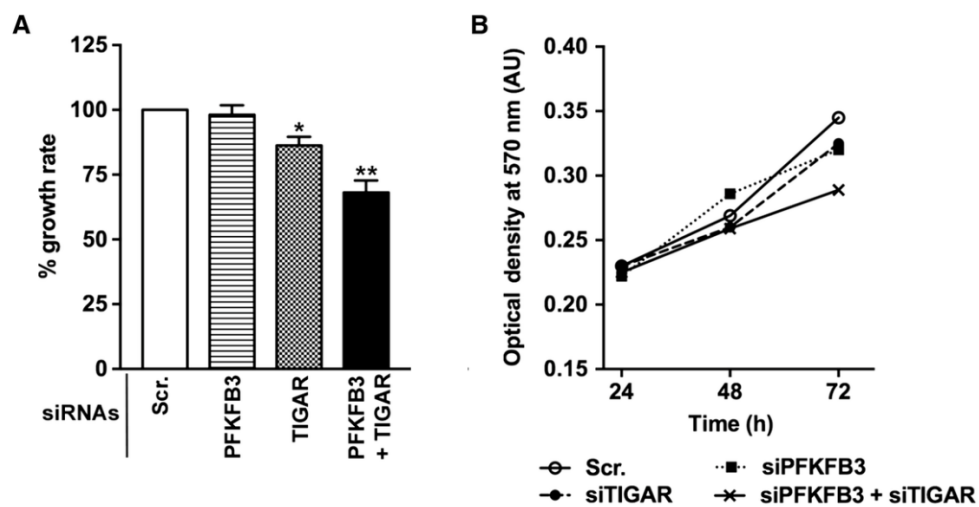


Figure 31. Effect of *PFKFB3* and *TIGAR* silencing on mitochondrial reduction capacity. MTT assay was performed 72 h after *PFKFB3* and/or *TIGAR*-targeting siRNA transfection. **(A)** Data are presented as the mean fold change in growth rate relative to the scrambled siRNA (Scr.) \pm SEM (n=3, *P < 0.05, **P < 0.01). **(B)** Raw data of a single experiment is shown (right panel).

The results from the MTT analysis must be interpreted in parallel with a measure of cell viability, as changes in cell number directly affect MTT signal. Flow cytometry analysis of cells stained with AnnexinV/PI after 72 h of siRNA transfection revealed that *PFKFB3* inhibition triggers early and late apoptosis as well as necrosis in HeLa cells (Figure 32). On the contrary, *TIGAR* inhibition alone did not affect cell viability, consistently with the results obtained in terms of ROS and DNA damage. However, when *TIGAR* was inhibited at the same time as *PFKFB3*, the effects were exacerbated, causing 15% decreased cell viability compared to *PFKFB3*-targeted cells, and leading to double number of apoptotic and necrotic cells (Figure 32).

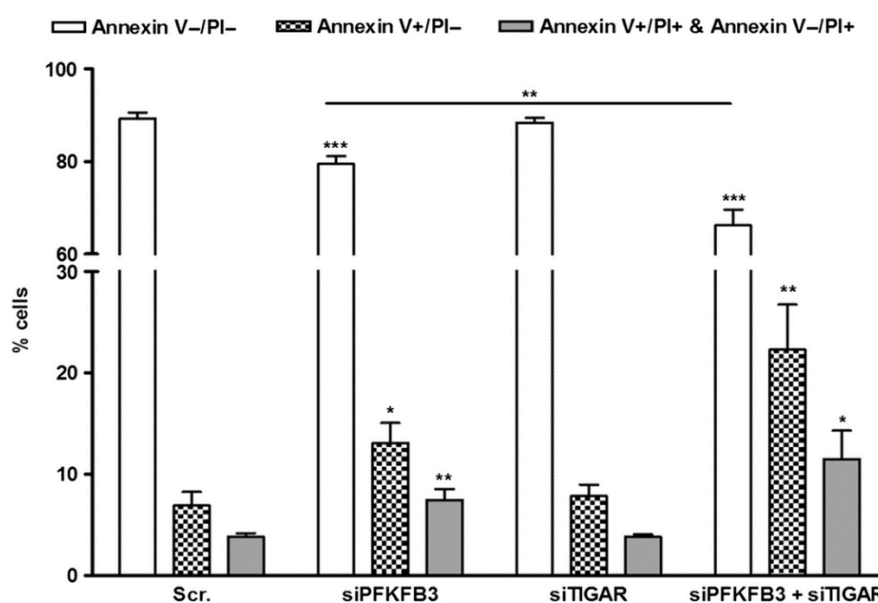
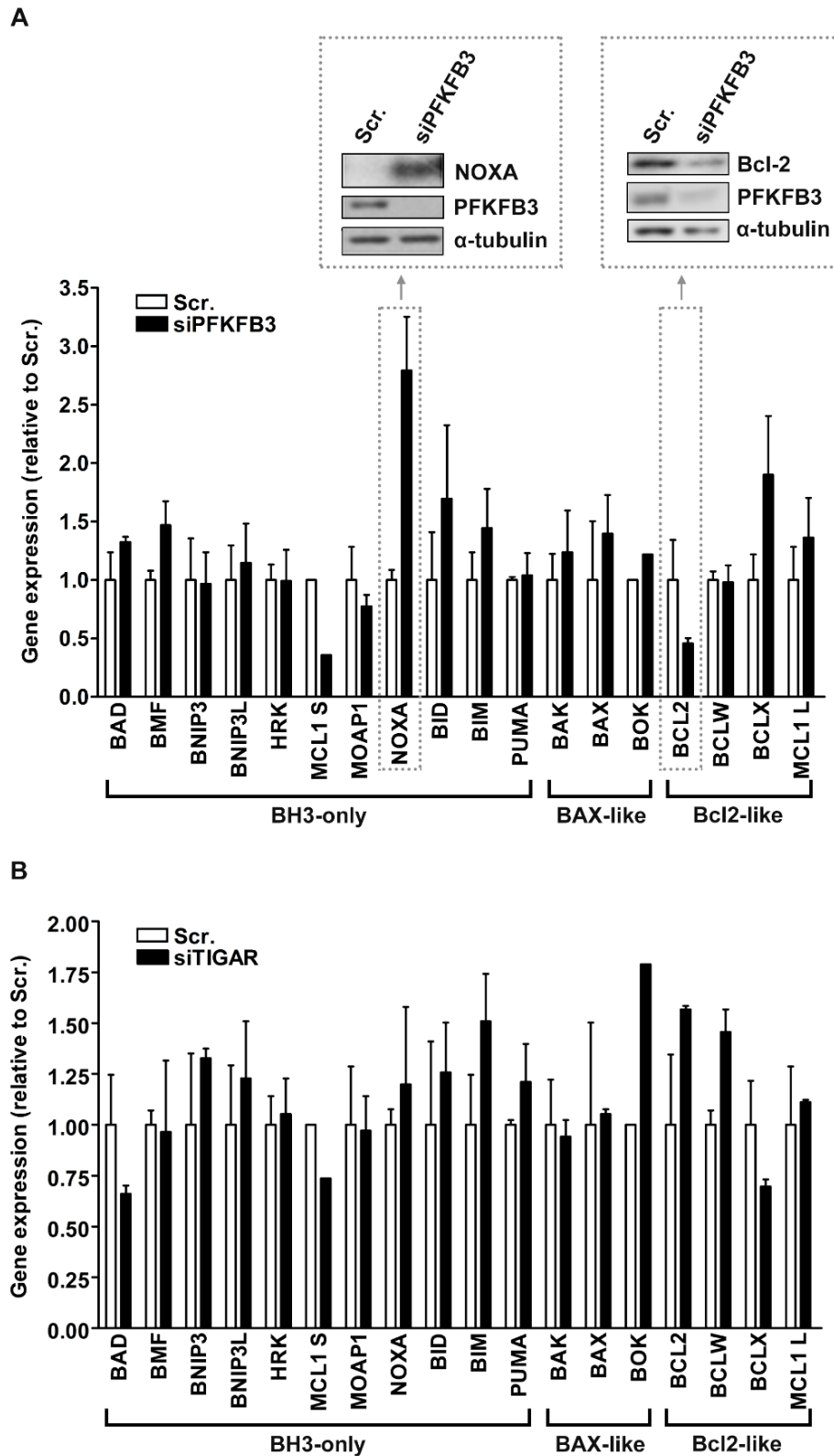


Figure 32. Effect of *PFKFB3* and *TIGAR* silencing on cellular viability. Annexin V-FITC/PI staining was performed 72 h after siRNA transfection. Populations of viable cells (AnnexinV-/PI-), early apoptotic cells (AnnexinV+/PI-) and late apoptotic or necrotic cells (AnnexinV+/PI+ and AnnexinV-/PI+) are shown. Data are presented as % of cells in each population \pm SEM and comparison between conditions is indicated by horizontal bars (n=6, *P < 0.05, **P < 0.01, ***P < 0.001).

In collaboration with the group of Dr. Joan Gil (Departament de Ciències Fisiològiques, Universitat de Barcelona), a reverse transcriptase multiplex ligation-dependent probe amplification (RT-MLPA) was performed to determine the expression of several apoptotic-related genes. The pro-apoptotic genes *NOXA*, *BIM* and *BID* were found overexpressed in *PFKFB3*-inhibited cells, whereas *BCL-2*, a pro-survival gene, was found decreased. Surprisingly, the expression of the proapoptotic splice variant *MCL1S* was found decreased and the expression of the antiapoptotic *BCLX* was found increased in these conditions (Figure 33A). In *TIGAR*-inhibited cells, a modest upregulation of *BIM*, *BOK* and *BCLW* and a slight downregulation of *MCL1L* were observed, but in general the expression profile was similar to control cells (Figure 33B). These results are in accordance with the Annexin V/PI assay (Figure 32) and corroborate that apoptosis is induced in *PFKFB3*-inhibited cells but not in *TIGAR*-inhibited cells.



Considering that *PFKFB3* has no effect in MTT signal but, instead, it decreases cell viability, it could be concluded that mitochondrial function is preserved in *PFKFB3*-inhibited cells although cell number is decreased. The explanation may be found in the analysis of the effects of *TIGAR* depletion. *TIGAR* inhibition decreases MTT signal but does not affect cell viability in HeLa cells, which indicates decreased mitochondrial activity, but it has no effect on cell viability. Thus, *TIGAR* induction in response to *PFKFB3* inhibition could be mediating an adaptive response from a glycolysis-focused metabolism towards a more oxidative phenotype, compensating the decrease in cell number with increased mitochondrial function. This is in accordance with previous data from the group showing that *PFKFB3* inhibition increases the uncoupled respiration (161).

2. TIGAR modulation in response to other glycolytic inhibitors

2.1. Response to the PFK-2 inhibitor 3PO

We have shown in the previous section that *TIGAR* mRNA and protein levels were increased after inhibition of *PFKFB3* expression. The next question was whether TIGAR induction was specific to the blockage of PFKFB3 or a common response to any kind of glycolytic blockage. With this purpose, we used a pharmacological inhibitor of PFKFB3, 3PO, which blocks the active site of PFK-2 (172). Based on previous publications using this inhibitor, we decided to treat HeLa cells with 10 μ M 3PO for 24 h. Western blot analyses did not reveal any significant modulation of TIGAR or PFKFB3 protein levels, although a slight increase in TIGAR and a slight decrease in PFKFB3 could be observed (**Figure 34A**). The analysis of the expression of these genes after 3PO treatment did not show any important changes in their mRNA levels (**Figure 34B**). To prove the efficacy of the inhibitor, Fru-2,6-P₂ concentration was measured and it was found decreased after 24 h of treatment (**Figure 34C**), in accordance with previous publications (64). When cells were observed at bright-field microscope, no apparent changes in cellular morphology or viability were detected after 3PO treatment (**Figure 34D**).

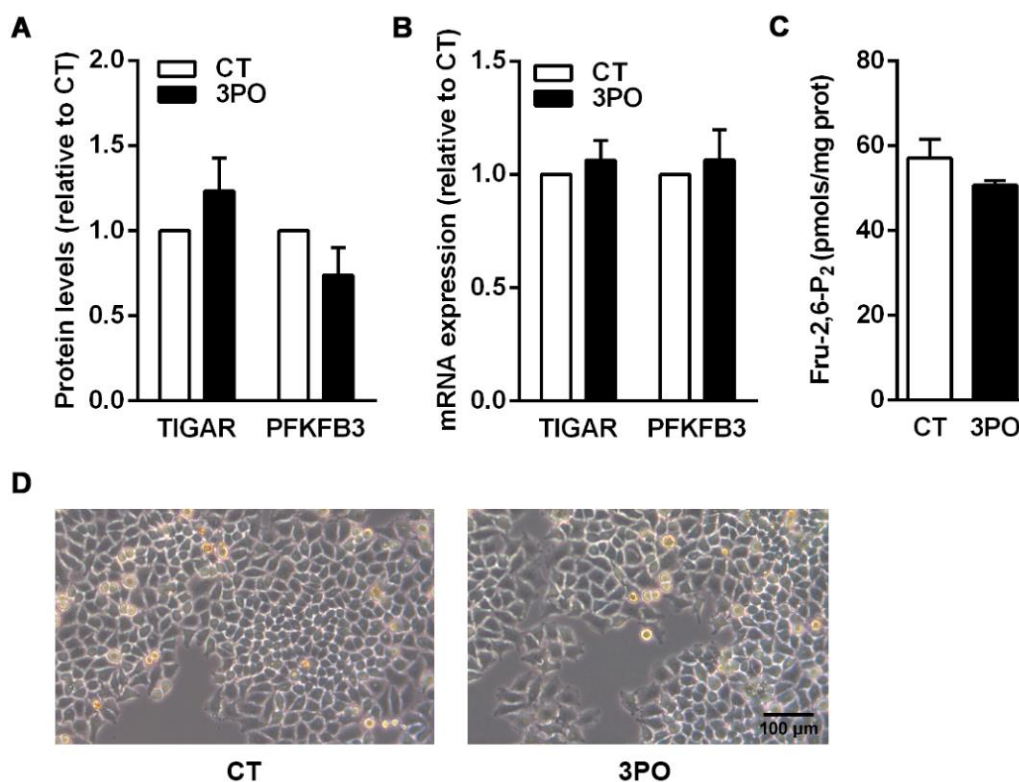


Figure 34. Analysis of the effects of 3PO treatment at 24 h. HeLa cells were treated with 10 μ M 3PO for 24 h and were subsequently analysed. **(A)** Western blot analysis quantification of PFKFB3 (white bars) and TIGAR (black bars). **(B)** RT-qPCR analysis of *PFKFB3* (white bars) and *TIGAR* (black bars) expression. **(C)** Determination of Fru-2,6-P₂ concentration. **(D)** Bright-field images of cells observed at 20X in a Leica microscope. Protein and mRNA data are represented as the mean fold change relative to the untreated cells (CT) whereas Fru-2,6-P₂ concentration is represented in absolute values \pm SEM (A: n=3, B: n=5, C: n=3).

Previous studies had shown that 3PO had a cytostatic effect in HeLa, reducing cellular viability to 75%, after 36 h of 10 μ M 3PO treatment (64). Considering these data, and given that we had detected a slight increase in TIGAR protein levels in HeLa cells after 24 h of 3PO treatment (**Figure 34**), we reconsidered the experimental conditions and the period of exposure to 3PO was increased to 72 h. This was also the time at which *PFKFB3*-targeting siRNA had its maximum effect on TIGAR protein levels, as it has been presented in the previous section (**Figure 23A**).

Western blot analysis of 3PO-treated cells for 72 h revealed significant induction of TIGAR and PFKFB3, according to the results published by(172). Interestingly, Akt and S6 phosphorylation levels were increased in parallel (**Figure 35A**). These results confirmed that TIGAR is induced in response to PFKFB3 blockage, either through a pharmacological or a transcriptional approach. Although experiments combining 3PO with Akti-1/2 would be required to confirm the signalling pathway responsible for TIGAR upregulation, the observation that Akt and S6 are phosphorylated after 3PO treatment suggests that the mechanism might be the same as in *PFKFB3*-silenced cells. As a preliminary analysis to determine if the PPP was increased in parallel to TIGAR, we checked the levels of TKT by western blot, which were found unaltered by 3PO treatment (**Figure 35A**).

RT-qPCR analysis of HeLa-treated cells revealed increased expression of *TIGAR* after 3PO treatment, with no modulation of *PFKFB3* mRNA levels (**Figure 35B**).

Fru-2,6-P₂ concentration was found significantly decreased by 10 μ M 3PO at 72 h (**Figure 35C**), confirming the efficacy of the inhibitor. However, the levels of extracellular lactate normalized to protein levels were not affected (**Figure 35D**), suggesting that the decrease in raw lactate concentration observed can be attributed to slightly increased cell death. 3PO-treated cells showed altered cellular shape, as it can be appreciated in the bright-field microscope images (**Figure 35E**). However, cellular viability measured by crystal violet assay was unaltered (**Figure 35F**), or at least we were not able to detect changes in viability with this method. In the first publication describing 3PO, viability was assessed by trypan blue assay (64), which is based on the capacity of live cells to exclude the dye through their intact cell membranes. It is possible that partially damaged cells, which would not be stained by trypan blue, are still attached to the plate and, thus, are stained with crystal violet, decreasing the sensitivity of the latter technique to detect cells prompted to death.

The observation that upregulation of TIGAR occurred both in response to PFKFB3 inhibition by siRNA and by 3PO suggested that TIGAR induction was caused by impaired PFKFB3 activity, and not as consequence of decreased PFKFB3 protein levels. Thus, we wondered whether other glycolytic inhibitors would have similar effects on *TIGAR* expression.

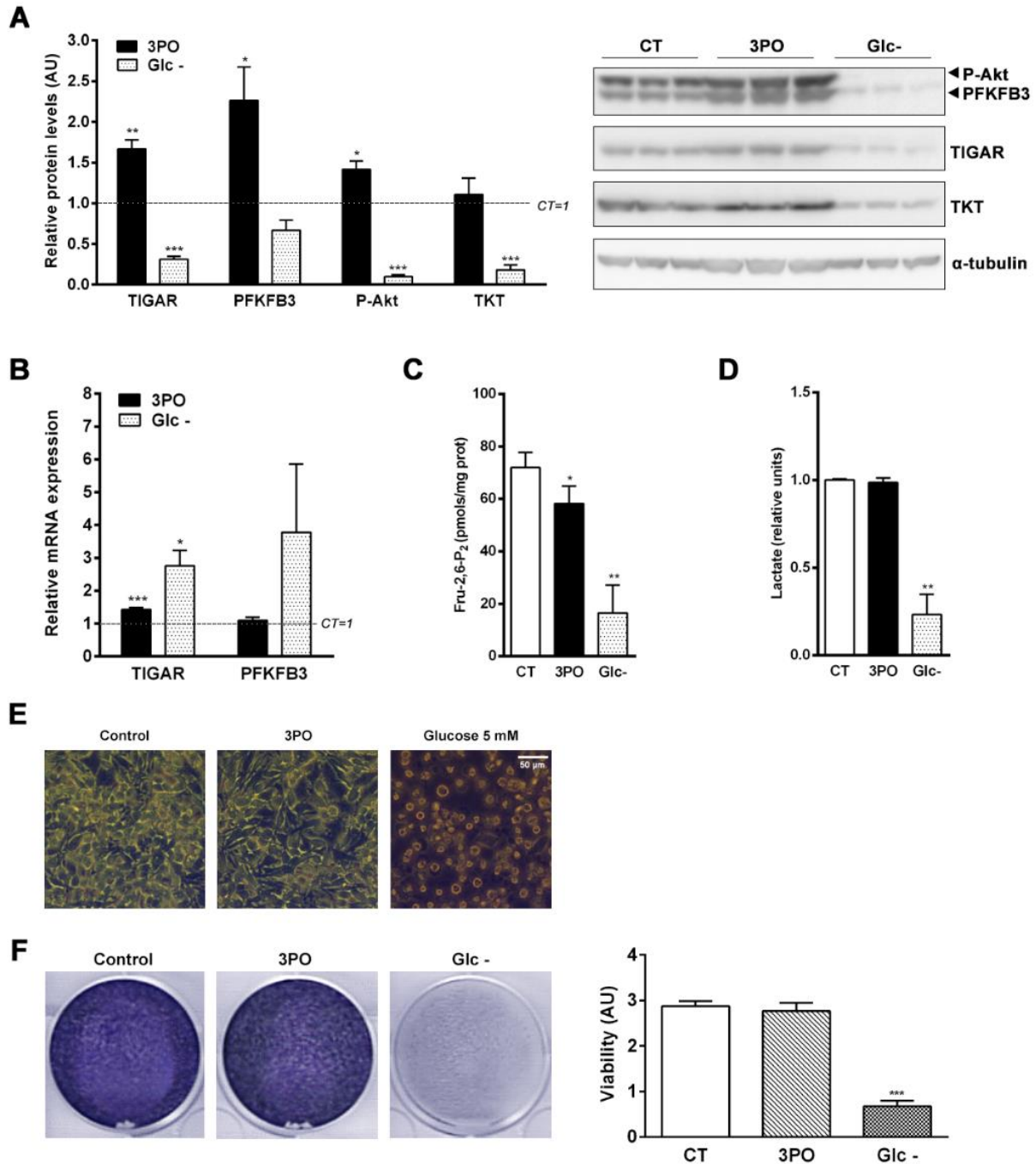


Figure 35. Analysis of the effects of 3PO and glucose deprivation treatments at 72 h. HeLa cells were treated with 10 μ M 3PO or 5mM glucose DMEM (Glc-) for 72 h and were subsequently analysed. **(A)** Western blot analysis of TIGAR, PFKFB3, P-Akt and TKT. Images from a representative experiment are shown. **(B)** RT-qPCR analysis of *PFKFB3* and *TIGAR* expression. **(C)** Determination of intracellular Fru-2,6-P₂ concentration. **(D)** Determination of extracellular lactate concentration. **(E)** Bright-field images of cells observed at 20X in a Leica microscope. **(F)** Determination of cell number by crystal violet (CV) assay. Representative stained plates are shown. Viability was quantified as arbitrary units (AU) of CV absorbance. Protein, mRNA and lactate data are represented as the mean fold change relative to the untreated cells (CT) whereas Fru-2,6-P₂ and crystal violet are represented in absolute values \pm SEM (A: n=3, B: n=4, C: n=6, D: n=4, F: n=1 with independent triplicates, *P < 0.05, **P < 0.01, ***P < 0.001).

2.2. Response to glucose deprivation

To fully answer the question of whether glycolytic blockage is the cause of *TIGAR* induction and not something exclusive to *PFKFB3* inhibition, we exposed cells to low glucose conditions (5 mM instead of 25 mM, which is the concentration used in complete media) for 72 h. In the western blot analysis, *TIGAR*, *PFKFB3*, P-Akt and P-S6 proteins, as well as the PPP enzyme TKT, were all found decreased, indicating that cells are not favouring growth or proliferation pathways and they are probably fated to death (**Figure 35A**).

Surprisingly, mRNA analysis revealed important overexpression of *TIGAR* and *PFKFB3* in cells maintained at low glucose conditions (**Figure 35B**). This might respond to a compensatory effect to increase the transcription of those genes that are being downregulated at the protein level, although we cannot dismiss the possibility that the low mRNA concentrations obtained from highly-damaged 5 mM glucose-treated samples altered the RT-qPCR analysis.

Fru-2,6-P₂ was significantly reduced by glucose deprivation, being the effect of this treatment much more pronounced than 3PO, as it was expected (**Figure 35C**). Accordingly, lactate extracellular concentration was significantly decreased (**Figure 35D**).

Glucose deprivation significantly compromised cell viability, as it is illustrated in the bright-field microscope images showing many dead cells floating in the media (**Figure 35E**). Staining in the crystal violet assay was significantly reduced to 30% compared to control cells (**Figure 35F**).

In the light of all the results presented so far, we cannot conclude that any intervention decreasing glycolysis triggers *TIGAR* expression, at least not at the protein level. Indeed, it seems that the inhibition of glycolysis needs to be sufficiently tuned to increase the expression of *TIGAR*, as it is the case of *PFKFB3* inhibition by siRNA and 3PO. This might occur in a context of transient nutrient deprivation in tumours, a stress that would trigger a pro-survival response in cancer cells in which it would be beneficial to increase glycolysis -through *PFKFB3* upregulation, for example- and anabolic pathways such as the PPP, in which *TIGAR* could have a role. However, when stress overcomes the capacity of cells to survive, processes focused on obtaining energy-producing molecules and ATP would be increased to avoid cell death and, if the stress was already too damaging, pro-apoptotic proteins might be activated to initiate programmed cell death.

3. TIGAR contribution to cell survival under metabolic stress

We have previously demonstrated that *TIGAR* overexpression confers protection against cell death when PFKFB3 is inhibited. Besides, *TIGAR* inhibition has been proved to increase the sensitivity of cells treated with H₂O₂ (3) and radiotherapy (79). However, *TIGAR* expression is not required for cell survival in unstressed conditions, and it is dispensable for normal growth and development (90). In our hands, no changes in the morphology or growth have been observed in *TIGAR* overexpressing HeLa cells compared to cells with basal TIGAR levels (Figure 36). However, a few dead cells could be detected in some experiments after 72 h of *TIGAR* inhibition (Figure 37), despite overall viability was not increased as it has been shown before (Figure 32). On the other hand, we had detected increased apoptosis in *PFKFB3*-inhibited cells (Figure 32), which was evident in subsequent experiments (Figure 37).

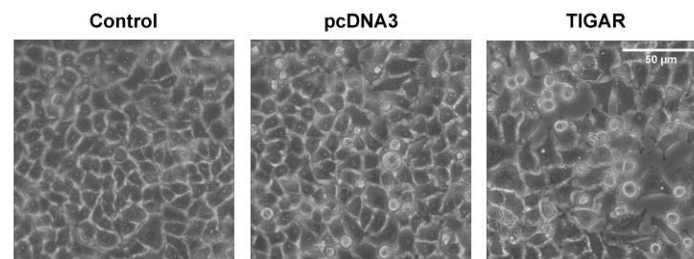


Figure 36. Bright field images of HeLa cells overexpressing *TIGAR*. HeLa cells were transfected with a pcDNA3 vector encoding human *TIGAR* gene. An empty pcDNA3 vector was used as control. Images were acquired at 24 h post-transfection with a Leica bright field microscope at 20X.

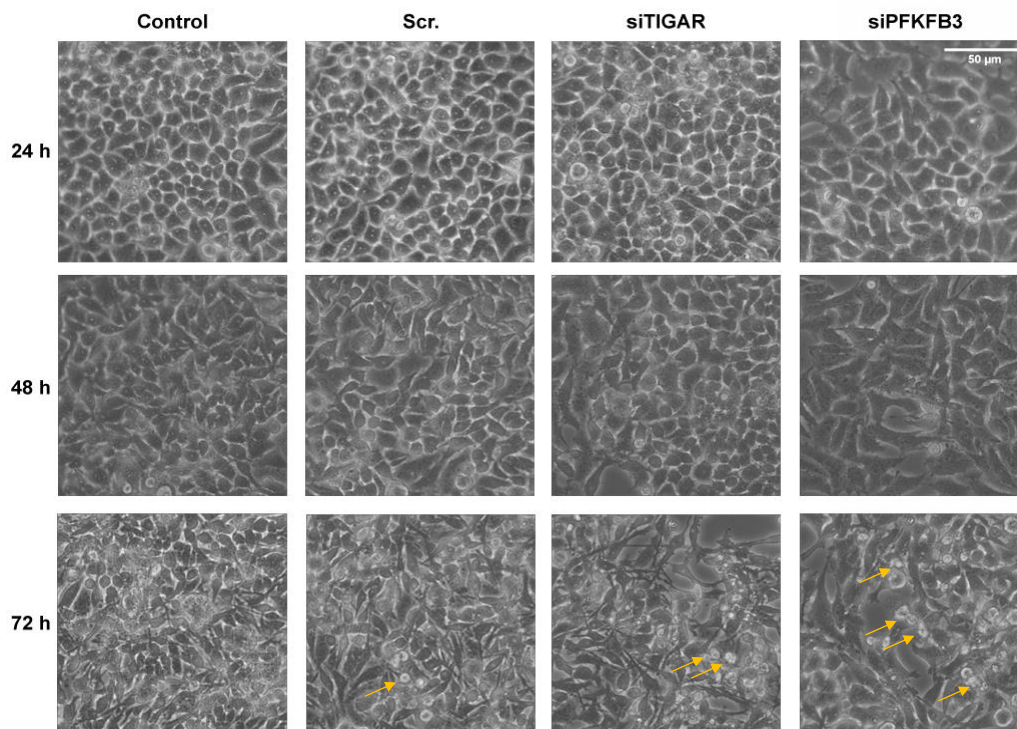


Figure 37. Bright field images of HeLa cells with inhibited *TIGAR* or *PFKFB3*. HeLa cells were transfected with *TIGAR* or *PFKFB3*-targeting siRNAs. Scrambled siRNA was used as control. Images were acquired at 72 h post-transfection with a Leica bright field microscope at 20X. Yellow arrows indicate apoptotic cells.

In the light of these results and considering that TIGAR was originally described as a Fru-2,6-P₂ phosphatase able to inhibit glycolysis and redirect the glucose flux towards the PPP, we aimed to determine the relationship between TIGAR effects on glycolysis. First, we determined glucose consumption in HeLa cells transfected with either a pcDNA3 vector expressing TIGAR or a TIGAR-targeting siRNA. We used PFKFB3-targeting siRNA as a control of the experiment, given that PFKFB3 inhibition has been shown to decrease glucose uptake (172). Overexpression of TIGAR and inhibition of both TIGAR and PFKFB3 were confirmed by western blot. The quantification of glucose in media was performed through an assay based on the reactions catalysed by glucose oxidase and peroxidase, which generate a brown product proportional to the amount of glucose oxidized. Glucose concentration was normalized to protein amount in each condition. Two types of analysis were performed, one with the media collected at the end of the experiment and a second analysis with cells incubated in fresh media for the last six hours. For this last experiment, media was removed at 24 h or 72 h after transfection, cells were washed twice with PBS and 1 mL of complete DMEM was added. The purpose of that was to investigate whether changes in TIGAR protein levels are sufficient to transform cells by altering their avidity for glucose.

The analysis of glucose concentration in the extracellular media at the end of the experiment, normalized by the protein levels in each condition, revealed significantly decreased glucose consumption in TIGAR-inhibited cells ($3,71 \pm 0,37$ mM) and PFKFB3-inhibited cells ($4,28 \pm 0,23$ mM) compared to cells transfected with the scrambled siRNA ($2,69 \pm 0,02$ mM) (**Figure 38A**). However, TIGAR overexpression did not alter glucose uptake.

On the other hand, the analysis of glucose concentration from HeLa cells incubated in fresh media for the last six hours of experiment revealed that only PFKFB3-inhibited cells displayed decreased glucose uptake (**Figure 38B**). Thus, it seems clear that transient inhibition of PFKFB3 is sufficient to alter the glycolytic metabolism of cells, which remain less efficient in capturing glucose than control cells in fresh media. On the contrary, TIGAR-inhibited cells do not maintain decreased glucose uptake when they are exposed again to high glucose media.

Extracellular lactate concentration was reduced in both TIGAR and PFKFB3-inhibited cells (**Figure 38C**), which is consistent with decreased glucose uptake in these conditions.

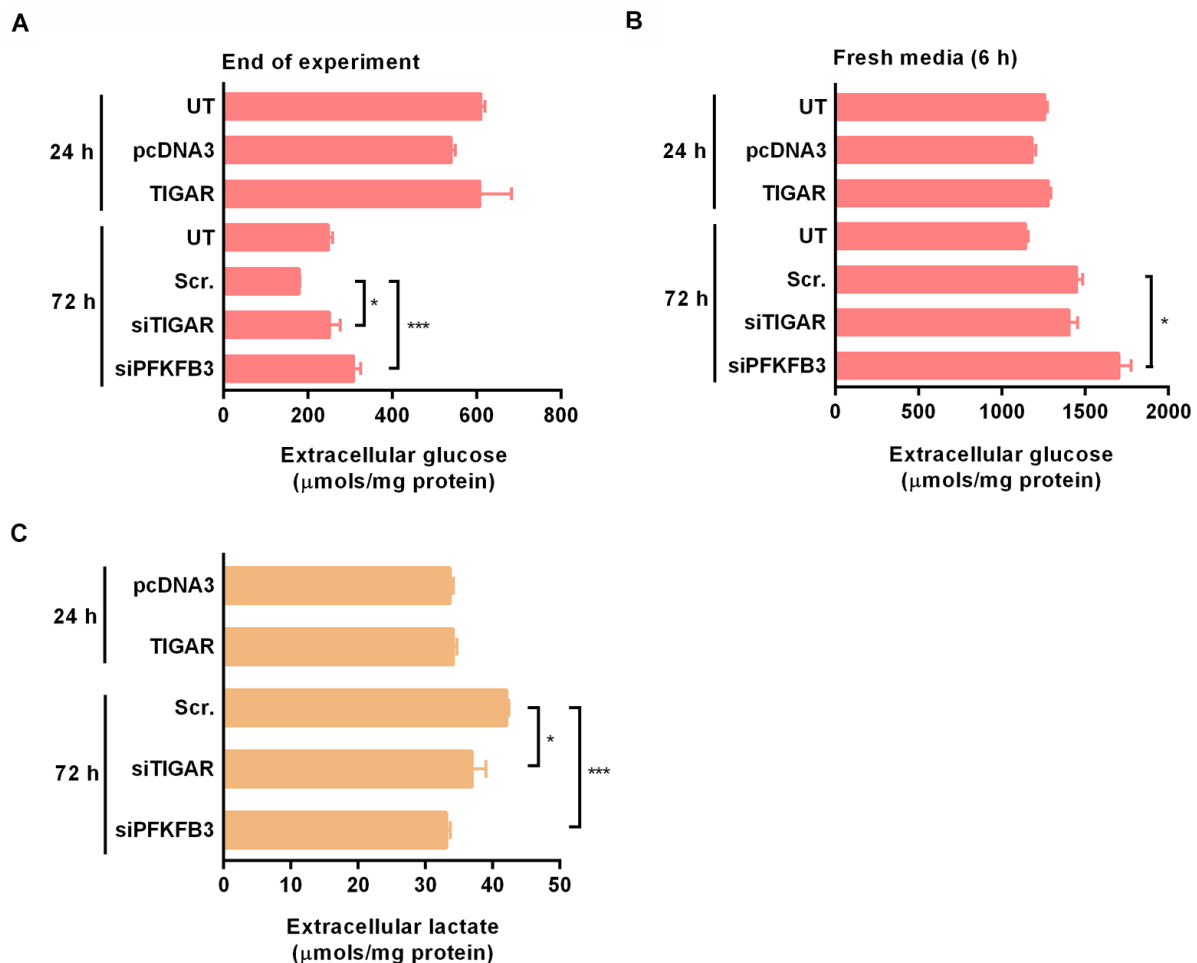


Figure 38. Extracellular glucose and lactate analysis after *TIGAR* and *PFKFB3* modulation. HeLa cells were transfected with either a pcDNA3 vector encoding human *TIGAR* gene (and the corresponding pcDNA3 empty vector control), or with *TIGAR* or *PFKFB3*-targeting siRNAs (and the corresponding scrambled siRNA as control) for 24 or 72 h, respectively. **(A-B)** Glucose concentration in media was determined and normalized to protein levels **(A)** at the end of each corresponding experiment (24 h for overexpression, 72 h for inhibition) or **(B)** after 6 h incubation in fresh media. **(C)** Concentration of lactate in the extracellular media was measured at the end of each corresponding experiment. Data are presented as $\mu\text{mols/mg protein} \pm \text{SEM}$ ($n=1$ with independent triplicates, * $P < 0.05$, ** $P < 0.01$, *** $P < 0.001$).

After observing that *TIGAR* inhibition has direct consequences on glucose oxidation, we aimed to determine which kind of stress does *TIGAR* confer resistance to. For that, we overexpressed and silenced *TIGAR* in HeLa cells in co-treatment with 5 mM glucose, 10 μM 3PO and H_2O_2 0,5 mM. These stimuli were chosen due to their capacity to block glycolysis, resembling *PFKFB3*-targeting siRNA, and to increase ROS. The stimuli were present from 4 h after plasmid or siRNA transfection until the end of the experiment.

The observation of cells at the microscope evidenced that there were no differences in cell viability between *TIGAR* overexpressing cells and control cells exposed to the stress stimuli (**Figure 39**). This is consistent with results previously shown in this thesis in which 3PO did not affect cell survival of HeLa cells after 24 h of treatment (**Figure 34D**).

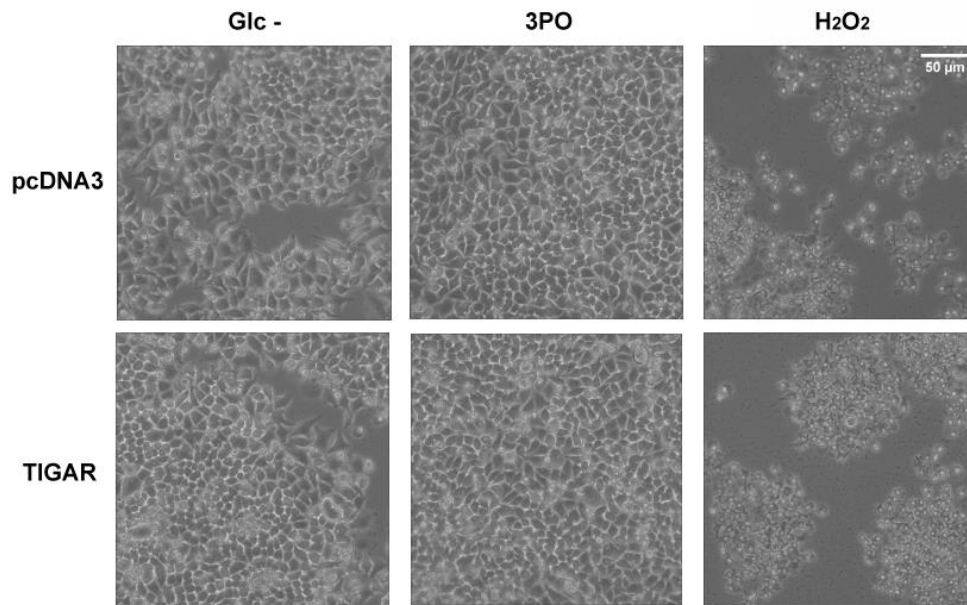


Figure 39. Bright field images of HeLa cells with *TIGAR* overexpression in the presence of stress stimuli. HeLa cells were transfected with a pcDNA3 encoding for human *TIGAR* or the corresponding pcDNA3 empty vector as control and co-treated with 5mM glucose DMEM (Glc-), 3PO or H₂O₂ (stress stimuli). Images were acquired at 27 h post-transfection with a Leica bright field microscope at 20X.

Interestingly, decreased number of cells was observed after treatment with glucose 5mM or 3PO in *TIGAR*-inhibited HeLa cells compared to control cells (**Figure 40**). Taking into account that inhibition experiments were performed at 72 h, this suggested that *TIGAR* inhibition affected the capacity of cells to overcome the stress produced by these glycolytic inhibitors in a time-dependent manner. H₂O₂ decreased the number of cells regardless of *TIGAR* levels (**Figures 39, 40**).

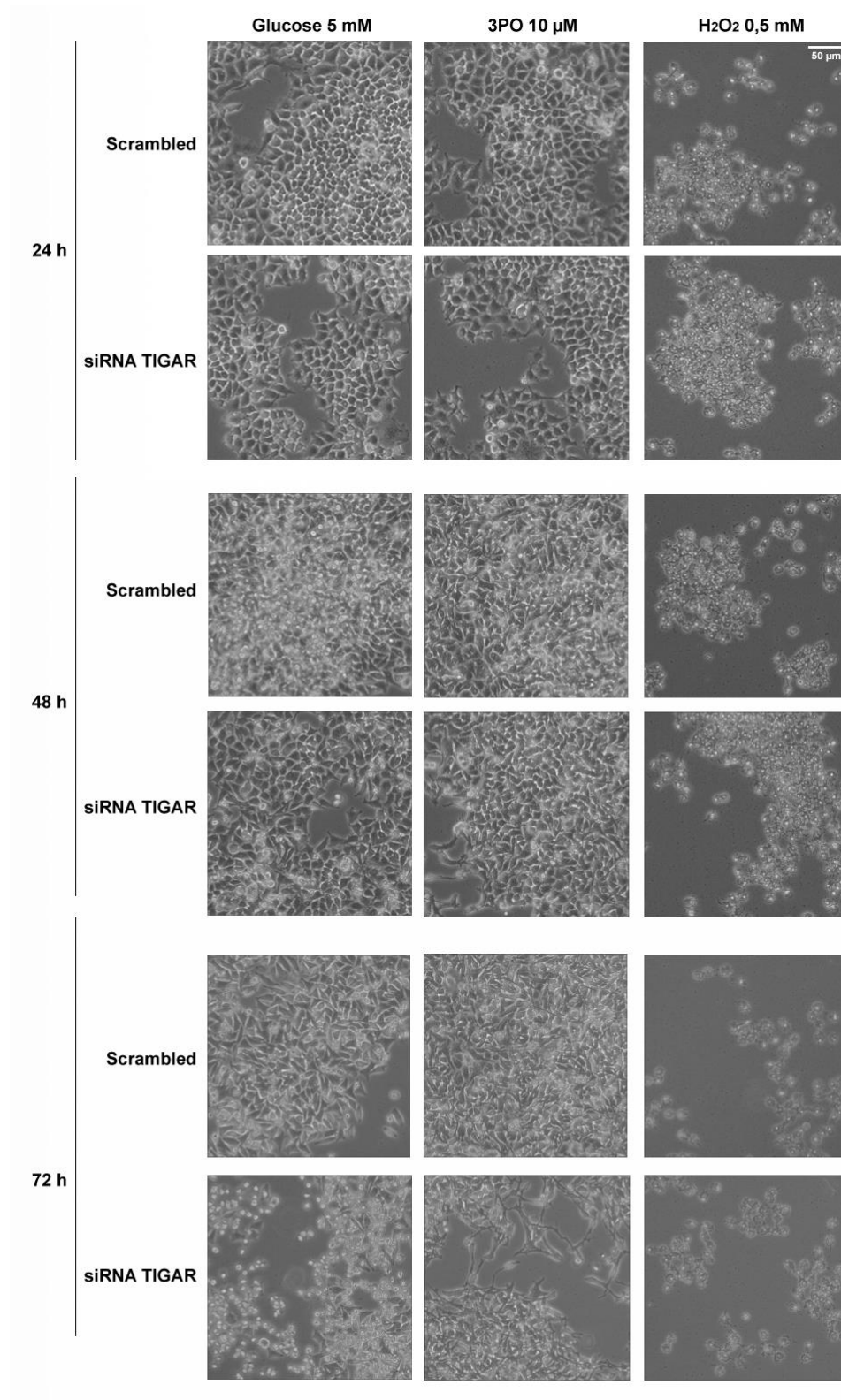


Figure 40. Bright field images of HeLa cells with *TIGAR* inhibition in the presence of stress stimuli. HeLa cells were transfected with a *TIGAR*-targeting siRNAs or the corresponding scrambled siRNA as control and co-treated with 5mM glucose DMEM (Glc⁻), 3PO or H₂O₂ (stress stimuli). Images were acquired at 72 h post-transfection with a Leica bright field microscope at 20X.

The effects of stress stimuli in combination with *TIGAR* overexpression or inhibition were confirmed by crystal violet assay. This assay corroborated that *TIGAR* overexpression did not affect the capacity of cells to grow in low glucose conditions or in the presence of 3PO (**Figure 41A**). However, a significant drop in cell survival was evidenced in *TIGAR*-silenced cells after glucose deprivation treatment. The same occurred in 3PO-treated cells, although the difference between *TIGAR*-inhibited cells and control cells was not statistically significant (**Figure 41B**). H₂O₂ significantly decreased cellular viability regardless of *TIGAR* levels (**Figure 41A,B**). An explanation for that would be that 0,5 mM H₂O₂ increased ROS-mediated cell death to such an extent that the potential antioxidant properties of *TIGAR* were overcome.

The metabolic adaptations of HeLa cells to the combination of *TIGAR* modulation with stress stimuli were also analysed at the protein level. *TIGAR* overexpression was confirmed by normalizing *TIGAR* protein levels to α -tubulin (**Figure 41C, lanes 6-9**). As it was expected, neither of the stress stimuli modulated *TIGAR* protein levels at 24 h. No changes in PFKFB3 were observed in cells transfected with pcDNA3 or pcDNA3-*TIGAR* in combination with stress stimuli. Akt and S6 were found phosphorylated in all conditions except for H₂O₂-treated cells (**Figure 41C**). Regarding *TIGAR* inhibition, the effect of *TIGAR*-targeting siRNA was confirmed by normalizing *TIGAR* protein levels to α -tubulin (**Figure 41D, lanes 6-9**). PFKFB3 was not altered by *TIGAR* inhibition, but its levels were decreased by glucose deprivation in both Scr. and *TIGAR*-transfected cells (**Figure 41D, lanes 3 and 7**). Akt and S6 were only phosphorylated in control and 3PO-treated cells, but not in cells maintained at 5 mM glucose, and *TIGAR* induction was only observed after 72 h of 3PO treatment (**Figure 41D**), confirming the results shown in **Figure 35**. It is interesting to note that glucose deprivation, which decreased PFKFB3 to a level comparable to PFKFB3-targeting siRNA but did not maintain P-Akt and P-S6 levels, did not result in *TIGAR* induction.

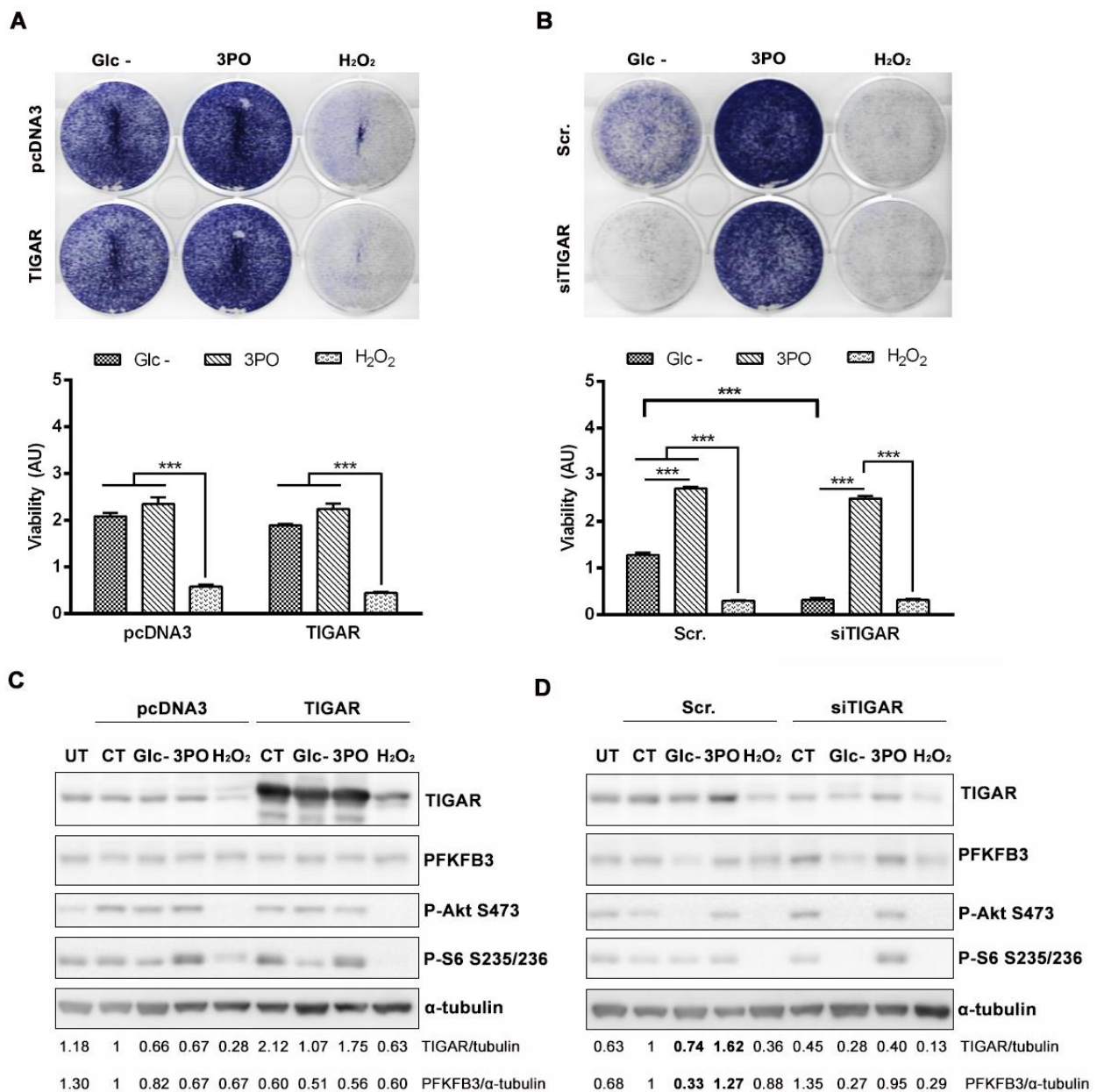


Figure 41. Analysis of the effects of *TIGAR* modulation in the presence of stress stimuli. HeLa cells with either *TIGAR* overexpression or inhibition were treated with 5mM glucose DMEM (Glc-), 3PO or H₂O₂ (stress stimuli). Viability and western blot analyses were performed at the indicated times. **(A and C)** HeLa cells were transfected with either a pcDNA3 vector encoding human *TIGAR* gene or the corresponding pcDNA3 empty vector for 24 in co-treatment with stress stimuli and **(A)** crystal violet assay and **(C)** western blot analysis were performed. **(B and D)** HeLa cells were transfected with either a *TIGAR*-targeting siRNA or the corresponding scrambled siRNA for 72 in co-treatment with stress stimuli and **(B)** crystal violet assay and **(D)** western blot analysis were performed. The normalization of *TIGAR* and PFKFB3 protein levels with α -tubulin is indicated below the western blot images. Data from crystal violet assays are presented as the mean absorbance in arbitrary units (AU) \pm SEM (n=1 with independent triplicates, ***P < 0.001).

The contribution of TIGAR to cell survival in response to glucose deprivation and 3PO was confirmed. In parallel, we aimed to determine whether *TIGAR* inhibition in combination with stress stimuli affected the uptake of glucose and lactate production. Glucose concentration was analysed at the end of the experiments (24 h for *TIGAR* overexpression and 72 h for *TIGAR* inhibition). As expected, *TIGAR* overexpressing cells and control cells showed the same capacity to uptake glucose in front of 5 mM glucose, 3PO and H₂O₂ (Figure 42A). The media from cells exposed to glucose deprivation showed less glucose concentration, this finding being totally expected and not informative (Figure 42A). 3PO did not affect glucose uptake nor at 24 or at 72 h (Figure 42A,B) and, on the contrary, glucose uptake was dramatically decreased in H₂O₂-treated cells both at 24 and 72 h (Figure 42A,B). Accordingly, lactate production was decreased in 5 mM glucose and H₂O₂-treated cells, with no differences between *TIGAR* overexpressing cells and control cells (Figure 42C). Lactate measurements in the experiments performed at 72 h revealed that 3PO decreased lactate export in both Scr. and *TIGAR* siRNA-transfected cells (Figure 42D), providing a potential explanation for the induction of TIGAR by 3PO at 72 h and not at 24 h post-treatment. Similar to overexpression experiments, 5mM glucose and H₂O₂ decreased lactate production regardless of TIGAR levels (Figure 42D).

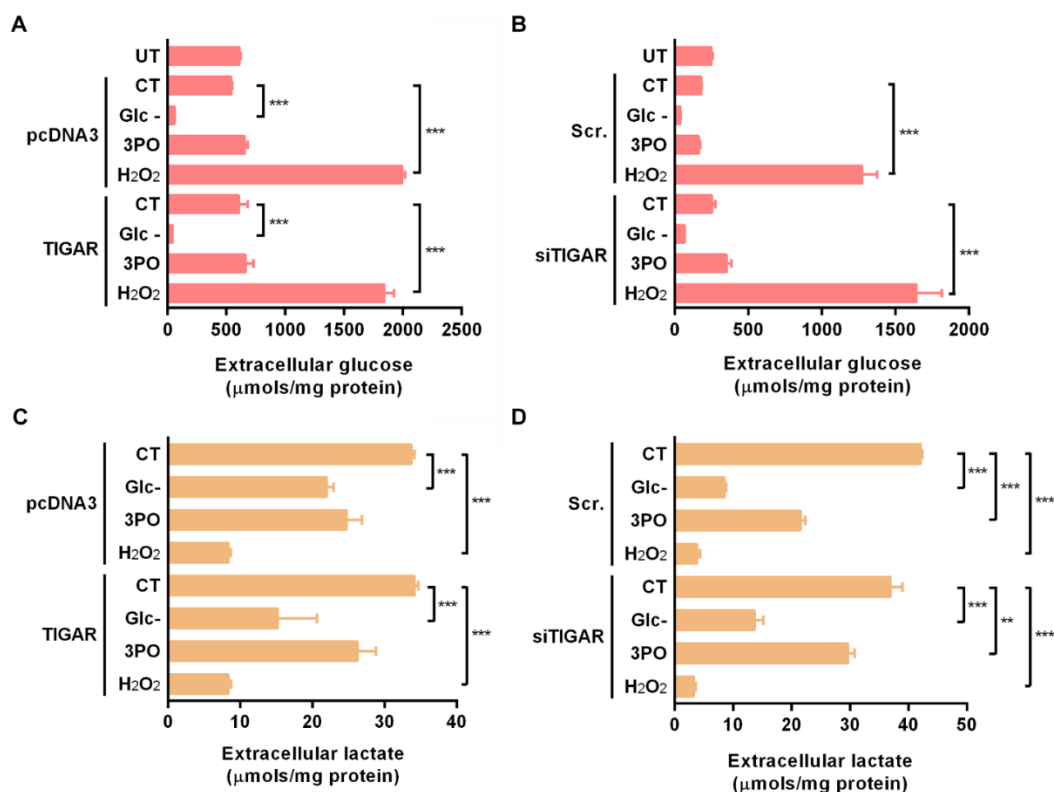


Figure 42. Extracellular glucose and lactate analysis after *TIGAR* modulation in stress conditions. HeLa cells transfected with either *TIGAR* overexpression plasmid or *TIGAR*-targeting siRNA were treated with 5mM glucose DMEM (Glc-), 3PO or H₂O₂ for 24 or 72 h, respectively. The concentration of (A, B) glucose and (C, D) lactate in the extracellular media were determined and normalized to protein levels. Data are presented as μmols/mg protein ± SEM (n=1 with independent triplicates, *P < 0.05, **P < 0.01, ***P < 0.001).

4. Discussion

The first results presented in this chapter showed that TIGAR is induced in response to the suppression of *PFKFB3* gene expression in an Akt-dependent manner. This was the first time that *TIGAR* expression was linked to the Akt signalling pathway and, thus, it constituted a new piece of information on the molecular mechanisms that control this enzyme in cancer cells. The functional relevance of TIGAR induction after PFKFB3 inhibition was found to be related to the survival of cancer cells. We were able to show that TIGAR protects from ROS-induced DNA damage, apoptosis and necrosis given that the combination of *PFKFB3* and *TIGAR* inhibition significantly exacerbated the damaging effects of PFKFB3 depletion alone. However, it remains unknown whether this protection depends on TIGAR enzymatic activity on Fructose-2,6-P₂, on other potential metabolic functions of this enzyme, or even on non-enzymatic functions of the protein, as it has been described for other enzymes (173). Deeper investigation on the metabolic functions of TIGAR is presented in Results Chapter II.

Further on this chapter, it has already been proved that 3PO, a pharmacological inhibitor of PFKFB3 which in fact is capable of inhibiting the kinase activity of the other PFKFB isoenzymes (57), is also able to induce TIGAR protein levels after 72 h, but not at 24 h. 3PO does not affect glucose uptake but it decreases lactate production to a greater extent than *PFKFB3*-targeting siRNA. After 72 h of 3PO treatment, cell death was slightly increased. On the contrary, HeLa cells maintained at 5 mM glucose conditions showed highly increased cell death and TIGAR was not induced in these cells. Importantly, Akt and S6 proteins were found phosphorylated in cells treated with 3PO while these phosphorylations were lost in 5 mM glucose-treated cells, suggesting the implication of Akt in TIGAR induction also in response to PFKFB3 enzymatic blockage, similarly to what we had described for the inhibition of *PFKFB3* gene expression. These results might point out that TIGAR upregulation is a compensatory response to imbalanced crosstalk with PFKFB3, more than a general response to glycolysis inhibition.

The finding that the Akt-mTORC1, a proliferative signalling pathway, was responsible for the link between PFKFB3 inhibition and TIGAR induction was initially surprising given that usually the AMPK- α pathway is the driver of the response to glycolytic impairment and decreased nutrient supply (174). Indeed, AMPK- α activation inhibits mTORC1, which is actually increased in *PFKFB3*-inhibited HeLa cells. The observation that only those conditions that increased P-Akt, i.e. PFKFB3 inhibition by siRNA and 3PO, were able to increase TIGAR protein levels regardless of their effect on glucose and lactate levels, suggested that TIGAR modulation is probably determined by a threshold in the stress levels. Possibly, those stimuli decreasing glycolysis to such an extent that downregulates proliferation pathways and increases cell death, are too much harming and do not modulate TIGAR levels. According to that, other studies have shown differential modulation of TIGAR depending on the doses of the DNA damaging agents applied. TIGAR is activated by moderate stress and contribute to ROS detoxification and DNA

repair. Nevertheless, when cells are exposed to high levels of stress, apoptosis-related pathways are prioritized and TIGAR is not induced (3,79).

A similar explanation could be applied to understand the low levels of TIGAR found in 0,5 mM H₂O₂-treated cells at both at 24 h and 72 h and the lack of differences between *TIGAR* overexpressing and *TIGAR*-inhibited cells in co-treatment with H₂O₂. The damage caused by 0,5 mM H₂O₂ could exceed TIGAR induction and trigger cell death in HeLa cells. However, *TIGAR* overexpression has been shown to protect against even higher H₂O₂ doses (0,5 mM to 10 mM) in U2OS and H1299 cells treated for 10 and 20 h, respectively (3). The differential response of HeLa cells U2OS or H1299 might be explained by either a more damaging effect due to increase time of exposure in HeLa, or to different tolerance of cell lines to ROS levels.

An important thing to discuss is the fact that the protective effect of TIGAR in front of ROS has not been directly attributed to an increase in *TIGAR* mRNA or protein levels (3,167). One possibility is that the high levels of TIGAR present at basal conditions allow for its antioxidant function independently of the upregulation of its protein levels. In this scenario, neither transcription nor translation would be required to confer protection against ROS. Another possibility might be the involvement of post-translational regulation mechanisms or changes in the subcellular location of TIGAR in response to ROS, something that is explored in Results Chapter IV.

The increased susceptibility to glycolytic impairment of *TIGAR*-inhibited cells contrasts with the mild effect of *TIGAR* inhibition in control cells. This is consistent with a recent study in which TIGAR knockdown has shown to enhance the ROS-mediated anticancer effect of the natural compound aescin, which is obtained from horse chestnut, by triggering apoptosis, although *TIGAR* inhibition alone did not impair cellular viability (175). Overall, it becomes clear that TIGAR carries on a tumour-promoter function in HeLa cells that becomes evident when cells are facing stress, but what is not that clear is whether this function can be attributed to the modulation of glycolysis. As it can be observed in our experiments, overexpression of *TIGAR* does not affect any of the parameters analysed, including glucose consumption, lactate production or viability, and *TIGAR* inhibition only slightly decreases lactate production and mitochondrial reduction capacity. *PFKFB3* inhibition, however, decreases glucose consumption, lactate production and cell survival, according to previous publications of the group (176). Therefore, it becomes evident that *PFKFB3* and TIGAR do not constitute opposed enzymatic entities in HeLa cells and indeed they seem to contribute to the growth of cancer cells by different mechanisms. *PFKFB3* effect is clearly related to its pro-glycolytic function, whether the contribution of TIGAR is probably beyond the role as a glycolytic inhibitor that was attributed to this enzyme (3), at least in HeLa cells. In this chapter, two metabolic parameters have been analysed, which are glucose consumption and lactate production. *TIGAR* overexpression did not alter neither of the parameters and, as it has been already mentioned,

TIGAR inhibition slightly decreased glucose uptake and lactate production. This is contradictory with the first publication about *TIGAR*, which showed that overexpression of the enzyme decreased glycolytic flux in U2OS and FL5.12 cell lines, as measured by the production of $^3\text{H-H}_2\text{O}$ from 5- ^3H -glucose by enolase (3). After years of research about *TIGAR* from this and other groups, the modulation of glycolysis by this enzyme seems to be dependent on the cellular model. The study of the metabolic function of *TIGAR* that has been performed during this thesis is reported in Results Chapter II.

RESULTS CHAPTER II

Role of TIGAR in the metabolism of cancer cells:

is it all about Fru-2,6-P₂?



CONTEXT

Many studies have been performed describing the involvement of TIGAR in certain types of cancer. All these publications are based on the first discovery in 2006 of TIGAR as a fructose-2,6-bisphosphatase enzyme, which decreases glycolytic rate by decreasing the positive allosteric activation that Fru-2,6-P₂ renders to PFK-1. This explanation, so far, seems to be contradictory with the fact that cancer cells have increased glycolytic rate. However, the contribution of TIGAR to the survival of cancer cells has been linked to its capacity to redirect glucose-6-phosphate to the PPP in a G6PD-dependent manner, at least in U2O2 (3). As it has been described in Results Chapter I of this thesis, *TIGAR* inhibition exacerbates the damaging effect of PFKFB3 blockage. Moreover, the capacity of TIGAR to increase the PPP is supported by the finding that *TIGAR* overexpression increases GSH/GSSG ratio, and *TIGAR* inhibition decreases this ratio (3). However, among the more than 170 publications that have studied TIGAR from different approaches and in different contexts, only nine, including (3), have directly evaluated the effects of TIGAR modulation on Fru-2,6-P₂ levels (73,80,82,84,86,177,178). Interestingly, Li and Jogl provided kinetic data revealing that the catalytic efficiency of TIGAR as a F26BPase is several orders of magnitude lower than that of the bifunctional liver enzyme PFK2/F26BPase (86). This gave rise to the study by Gerin *et al.* who considered that F26BP might not be the physiological substrate of TIGAR and re-evaluated the biochemical activity of the enzyme. Their findings showed that the Km of TIGAR for Fru-2,6-P₂ (1,25 mM) was higher than that for 2,3-BPG (0,142 mM), 2-PG (0,224 mM), 2-phosphoglycolate (0,79 mM) and PEP (0,90 mM) (73). In the same publication, *TIGAR* inhibition by shRNA efficiently increased 2,3BPG in all the human cell lines tested (HCT116, U2O2 and RKO) and TIGAR-KO mouse embryonic stem cells also showed significantly increased levels of 2,3BPG. However, Fru-2,6-P₂ concentration was increased in TIGAR-KO mouse embryonic stem cells, but not in human in HCT11 or RKO cell lines transfected with the shRNA. Only one of the shRNAs used was able to increase Fru-2,6-P₂ levels in the U2O2 cell line. Apart from this publication, no more contributions to elucidate the activity of TIGAR on other substrates have been made.

During this thesis, we have been interested in determining if the activity of TIGAR on Fru-2,6-P₂ is the most important role of this enzyme in all cancer cells, or if other roles of this enzyme should also be considered. The importance of this answer is not to determine the metabolite for which TIGAR has more avidity, but to clarify if it is correct to keep interpreting all the findings related to this enzyme with its capacity to modulate Fru-2,6-P₂ levels. With that purpose, we have used the HeLa cell line to perform our metabolic determinations in several conditions of TIGAR modulation.

1. *In silico* study of TIGAR protein sequence and structure

A multiple alignment using CLUSTALW was performed and the similarity between eight histidine phosphatases (TIGAR, PGME, PGAM B, PGAM M and PFKFB1-4) was analysed. Although it is widely assumed in the literature that TIGAR is similar to FBPase-2, we found that, indeed, it is at least equally similar to PGAM B than to FBPase-2. The findings leading to this conclusion are detailed below.

The residue that forms the phosphoenzyme in TIGAR, H11 (**Figure 43A, Zoom1**), together with E89 (**Figure 43A, Zoom2**), which acts as a H⁺ donor, are identical in the eight proteins. The residue E102 is identical in all of them except for PGME, where it is substituted for Q (**Figure 43A, Zoom2**). Regarding the third amino acid in the catalytic triad, H198, CLUSTALW did not show any H aligned in the other proteins. However, when shorter alignments were performed, specific H residues were completely aligned to H198 in all the other histidine phosphatases, according to (3). These residues are indicated in rectangles (**Figure 43A, Zoom3**). CLUSTALW generated a phylogenetic tree from the alignment which revealed that, indeed, TIGAR is closer to PGAMs than to PFKFBs (**Figure 43B**). This is consistent with the finding that 2,3-BPG, 2-PG and PEP are better substrates for TIGAR than Fru-2,6-P₂ (73).

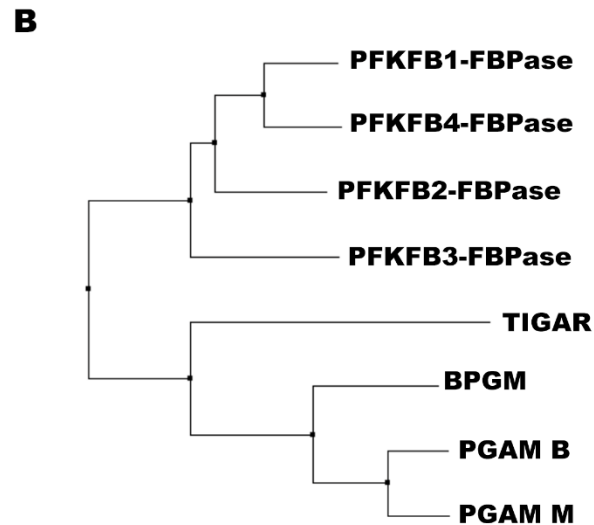
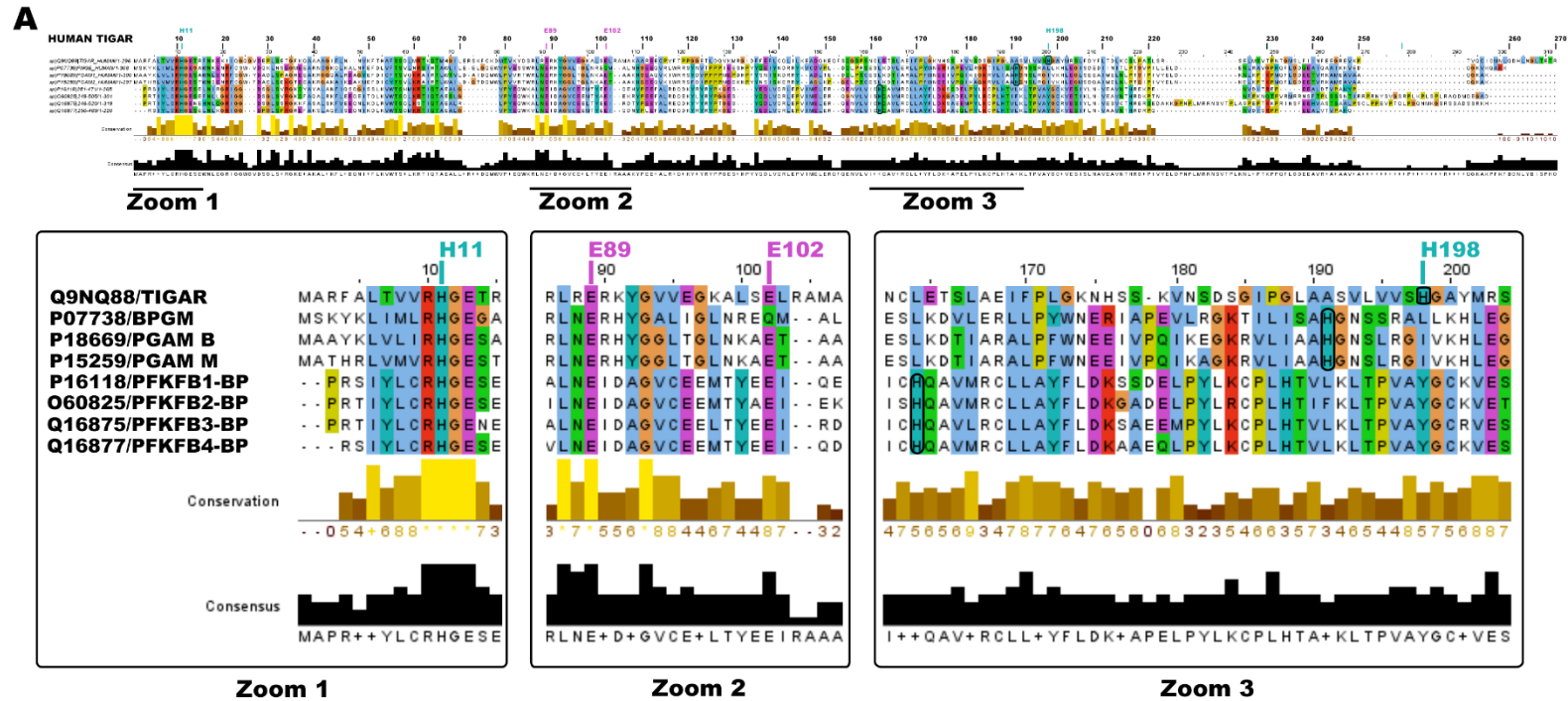


Figure 43. Multiple Sequence Alignment of TIGAR with other histidine phosphatases. TIGAR protein sequence (UniProt Entry Q9NQ88) was compared with erythrocyte bisphosphoglycerate mutase (BPGM, UniProt Entry P07738), phosphoglycerate mutases 1 and 2 (PGAM B, UniProt Entry P18669 and PGAM M, UniProt Entry P15259, respectively) and the bisphosphatase domain of PFKFB1-3 (P16118, O60825, Q16875, Q16877, respectively) through a multiple sequence alignment with Jalview (207) based on CLUSTALW (EMBL-EBI) (208). Multiple sequence alignments compare different sequences looking for conserved patterns that explain their functional relationship. **(A)** Alignment generated by Jalview with zoom to the most-relevant regions aligned. These regions contain the amino acids of TIGAR active site (H11, E89, E102 and H198). Amino acids are coloured according to their physicochemical properties according to Clustal colour scheme. **(B)** Phylogenetic tree generated by CLUSTALW alignment showing the evolution of the proteins compared according to their sequence similarities.

Furthermore, we checked the similarity between TIGAR and PGAM B, and TIGAR and the bisphosphatase domain of PFKFB3 by two different pairwise sequence alignment strategies: local alignment with BLAST, and global alignment with EMBOSS Needle. BLAST comparison, which analyses the similarity within blocks of aligned amino acids between two sequences, found three different blocks of aligned amino acids between PFKFB3 and TIGAR. In the case of PGAM, a long sequence of more than 100 amino acids together with a shorter sequence of less than ten amino acids were aligned (**Figure 44A**). The coverage of TIGAR sequence was slightly higher in the case of PGAM B, with more statistical power (**see Query cover in Figure 44B**), and the identity was slightly higher between TIGAR and the bisphosphatase domain of PFKFB3 (**see Identity in Figure 44B**). EMBOSS Needle global alignment, which analyses the similarity across the whole sequences, revealed an identity of 21,13% between TIGAR and PGAM B, and of 17,1% between TIGAR and the bisphosphatase domain of PFKFB3. Importantly, similarity was also higher between TIGAR and PGAM B (**Figure 45**). This supports the idea that, although there are more identical residues between TIGAR and the bisphosphatase domain of PFKFB3 within aligned clusters, the general protein sequence of TIGAR is more similar to that of PGAM. In the light of the results obtained *in silico*, all the *in vitro* experiments involving TIGAR inhibition and overexpression performed during this thesis have considered potential parallel functions of TIGAR on other phosphorylated substrates rather than Fru-2,6-P₂.

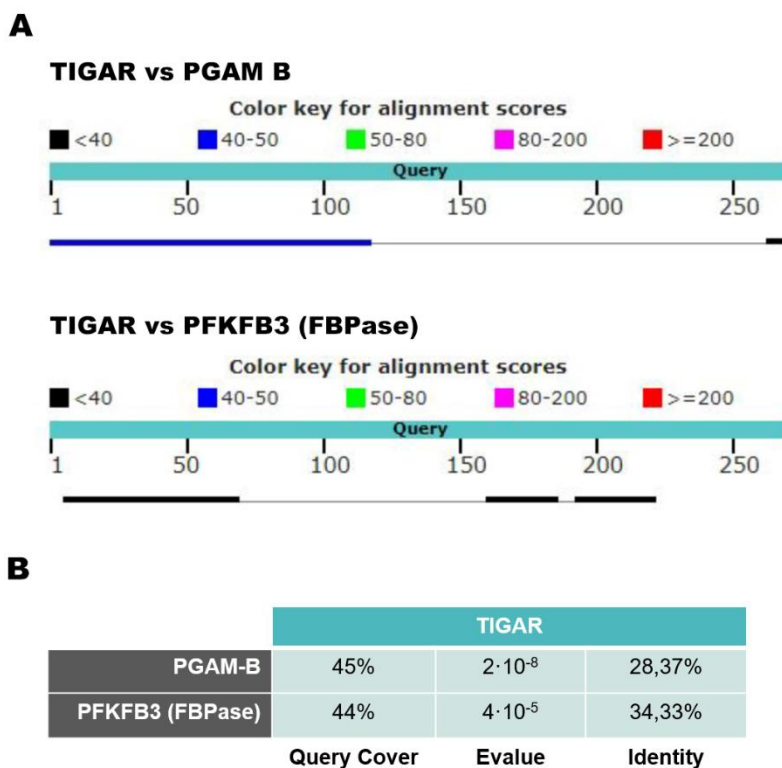


Figure 44. BLAST local alignments of TIGAR with PGAM B and FBPase-2. Basic local alignment search tool (BLAST) (209) was performed to compare TIGAR sequence with that of PGAM B and the bisphosphatase domain of PFKFB3. The protein matrix used to perform the alignment was Blocks of Amino Acid Substitution Matrix 62 (Blosum62). **(A)** Schematic representation of both alignments displayed by BLAST. The aligned regions are highlighted by the bold line. The colour of the line indicates the score of the alignment. **(B)** Summary table of the alignment: 'Query Cover' indicates the % of amino acids aligned from the total amino acids compared, 'E value' reflects the probability of the alignment to be found by chance and 'Identity' indicates the % of amino acids identical between the two sequences out of the amino acids aligned.

A**TIGAR vs PGAM B**

TIGAR	1	MARFALTVVRHGETRFNKEKIIQGQGVDEPLSETGFKQAAAAGIFLNMV-	49
PGAM	1	MAAYKLVLIIRHGESAWNLENRFSG-IYDADLSPAGHEEAKRGQALRDAG	49
TIGAR	50	-KFTAFSSDLMRTKQTMHGILERSKFCKD--MTVKYDSRLRERKYGVV	95
PGAM	50	YEFDICFTSVQKRAIRTLWTVLD----AIDQMWLPVVRTWRLNERHYGGL	95
TIGAR	96	EKGALSELRAMAKAAREECPVF----TPPGGETLDQVKMRGIDFFFLC	140
PGAM	96	TG--LNKAETAAKHGAEQVKIWRRSYDVPPPPMEPDH-----PFY----	133
TIGAR	141	QLILKEADQKEQFSQGSPS-NCLETSLAEIFPLGKNHSSKVNDSGIPGL	189
PGAM	134	SNISKDRRYADLTEDQLSPCESLKDITARALPFW-----NEEIVPQI	175
TIGAR	190	--AASVLVSHGAYMRS�FDYFLTDLKCSPATLSRSELSMVSPTMTGMSL	237
PGAM	176	KEGKRVLIAAHGMSLRGIVKHL-----EGLSEEAIMELNLPGTGIP-	215
TIGAR	238	FIINFEEGREVKPTVQICMNLQDHLNGLTETR-----	270
PGAM	216	--IVYELDKNLKPIKPMQFLGDEETVRKAMEAVAAQGKAKK	254

B**TIGAR vs PFKFB3 (FBPase)**

TIGAR	1	MARFALTVVRHGETRFNKEKIIQGQ-GVDEPLSETGFKQAAAAGIFL--N	47
PFKFB3	1	--PRTIYLCRHGENEHN----LQGRIGGDSGLSSRGKFFASALSKFVEEQ	44
TIGAR	48	NVKFTAFSSDLMRTKQTMHGILERSKFCKDMTVKYD--SRLRERKYGVV	95
PFKFB3	45	NLKDLRVMTSQLKSTIQT-----AEALRLPYEQWKALNEIDAGVC	84
TIGAR	96	EKGALSELR---AMAKAAREECP-VFTPPGGETLDQVKMRGIDFFFLCQ	141
PFKFB3	85	EELTYEEIRDTYPEEYALREQDKYYRYPTGESYQDLVQR-----LE	126
TIGAR	142	LILKEADQKEQFSQGSPSNCLTSLAEIFPLGKNHSSKVNDSGIPGLAA	191
PFKFB3	127	PVIMELERQE-----	136
TIGAR	192	SVLVVSHGAYMRS�FDYFLTD-----LKCSLPATLSRSELSMVSPTMTG	234
PFKFB3	137	NVLVICHQAVLRCLLAYFLDKSAEMPYLKCLHTVL---KLTPVAYGCR	183
TIGAR	235	MSLFIINFEEGREVKPTVQICMNLQDHLNGLTETR-----	270
PFKFB3	184	VESTYLN-----VESVC---THRRESEDAKKGPNLMRRNSVTP	219
TIGAR	271	-----	270
PFKFB3	220	LASPEPTKPRINSFEEHVASTSAALPSCLPPEVPTQLPGQNMKGSRSSA	269
TIGAR	271	-----	270
PFKFB3	270	DSSRKH	275

C

	TIGAR		
PGAM-B	21,3	37,1	19,9
PFKFB3 (FBPase)	17,1	26,7	46,9
	Identity (%)	Similarity (%)	Gaps (%)

Figure 45. EMBOSS Needle global alignments of TIGAR with PGAM B and FBPase-2. EMBOSS Needle global alignment (EMBL-EBI) (179) was performed to compare TIGAR sequence with that of **(A)** PGAM B and **(B)** the bisphosphatase domain of PFKFB3. The protein matrix used to perform the alignment was Blosum62. **(A, B)** Overall alignment using consensus alignment symbols: '.' for any small positive score, ':' for similarity scores more than 1.0, and '|' for an identity where both sequences have the same residue regardless of its score. **(C)** Summary table of the alignment: 'Identity' indicates the % of amino acids that are identical between the two sequences put of the total amino acids, 'Similarity' reflects the % of amino that, despite not being identical, are similar along the sequence, and 'Gaps' indicate the % of amino acids that are not totally different between the two sequences.

TIGAR, PFKFB3 and PGAM were also compared at the structural level by the PDB online tool for pairwise structural alignments, applying the flexible jFATCAT method (180). This algorithm detects aligned fragment pairs, superpositions of two continuous fragments in the two proteins to be compared, and allows flexibility with twists connecting different fragments, increasing the sensibility to detect common structures between proteins. The most important parameters to be compared in a pairwise structural analysis with jFATCAT are the number of twists needed to connect similar regions, the number of equivalent positions (Opt-equ) and the overall Root Mean Square Deviation (Opt-RMSD), which measures the difference between the predicted structure of a protein identical to the query structure and the observed structure. jFATCAT displays a visualization of the two proteins superposed in which similar structures are coloured, whereas non-aligned regions are painted in grey. According to the analyses performed, TIGAR is very similar to both PGAM B and the bisphosphatase domain of PFK-2, with any twists in neither of the two structure superpositions. However, Opt-equ and Opt-RMSD were higher between TIGAR and PGAM B than between TIGAR and FBPase-2, with a lower p-value, indicating that the identity and similarity between TIGAR and PGAM B is more statistically significant. As expected, similarity was not statistically significant when TIGAR was compared to the whole PFKFB3 structure (Figure 46).

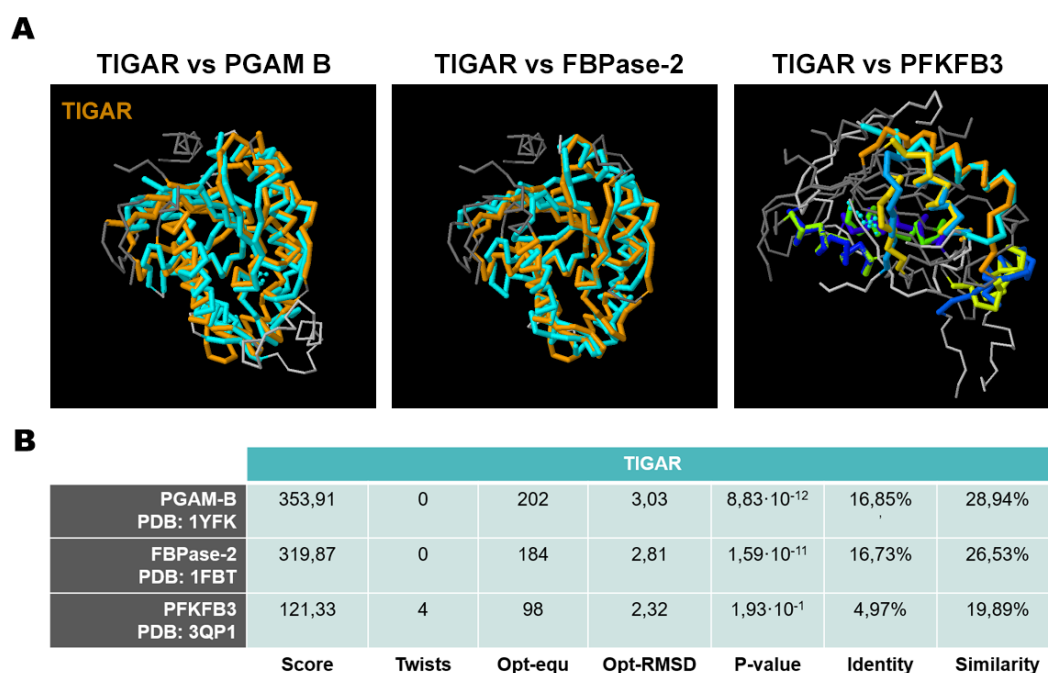


Figure 46. Pairwise structural alignment of TIGAR with PGAM B, FBPase-2 and PFKFB3. The structures of TIGAR (PDB: 3DCY), PGAM B (PDB: 1YFK), the rat bisphosphatase domain of PFK-2 (PDB: 1FBT) and human PFKFB3 (PDB: 3QP1) were compared with PDB pairwise structural alignment tool with the flexible jFATCAT method (199). **(A)** TIGAR is coloured in orange. Aligned structures are shown in blue colours and non-aligned regions are in grey. **(B)** Summary of the main parameters of the jFATCAT analysis, including overall score, number of twists, number of equivalent positions (Opt-equ), overall Root Mean Square Deviation (Opt-RMSD), p-value and percentages of identity and similarity. Images were created with Jmol: an open-source Java viewer for chemical structures in 3D. <http://www.jmol.org/>.

2. Metabolic determinations by spectrophotometry

For all the metabolic determinations included in this chapter, overexpression of *TIGAR* and inhibition of both *TIGAR* and *PFKFB3* were previously confirmed by western blot (**Figure 47**).

In order to clarify the functional relevance of *TIGAR* bisphosphatase activity, Fru-2,6-P₂ concentration was determined in HeLa cells after *TIGAR* inhibition and overexpression (**Figure 48**). The levels of this metabolite were also assayed in *PFKFB3*-inhibited cells, in which we had previously observed reduced Fru-2,6-P₂ concentration (63), as positive control samples in the assay. The quantification of Fru-2,6-P₂ is performed through the spectrophotometric analysis of NADH consumption in the latter of three reactions coupled to the phosphorylation of Fru-6-P to Fru-1,6-P₂ by potato pyrophosphate phosphofruktokinase (P_{Pi}-PFK), which is allosterically stimulated by Fru-2,6-P₂. The experimental procedures for the purification of P_{Pi}-PFK from potato and Fru-2,6-P₂ analysis are described in Materials and Methods section.

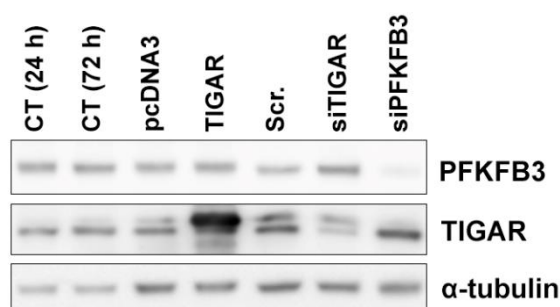


Figure 47. Confirmation of the modulation of *TIGAR* and *PFKFB3* by western blot. HeLa cells were transfected with either a pcDNA3 vector encoding human *TIGAR* gene (and the corresponding pcDNA3 empty vector control), or with *TIGAR* or *PFKFB3*-targeting siRNAs (and the corresponding scrambled siRNA) for 24 or 72 h, respectively. PFKFB3 and TIGAR were analysed by western blot and α -tubulin was used as endogenous control.

TIGAR overexpression caused a statistically significant decrease in Fru-2,6-P₂ concentration of 25% (**Figure 48A**). In *TIGAR*-inhibited cells, the concentration of this metabolite was slightly increased, despite the difference was not statistically significant (**Figure 48B**). These results support the idea that *TIGAR* exerts bisphosphatase activity on Fru-2,6-P₂, as it was initially described (3). Inhibition of *PFKFB3* effectively decreased Fru-2,6-P₂ concentration to 50 % (**Figure 48B**).

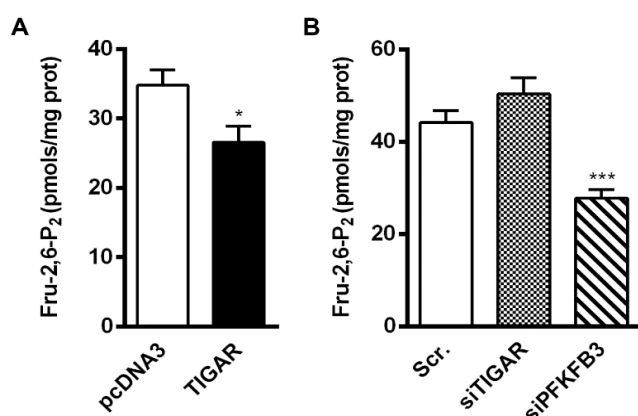


Figure 48. Fru-2,6-P₂ concentration in *TIGAR* overexpressing and *TIGAR* or *PFKFB3*-inhibited cells. (A) HeLa cells were transfected with either a pcDNA3 plasmid containing *TIGAR* human gene or the corresponding pcDNA3 empty vector and Fru-2,6-P₂ was determined after 24 h. (B) HeLa cells were transfected with 75 nM *PFKFB3* or *TIGAR*-targeting siRNAs or the corresponding scrambled siRNA and Fru-2,6-P₂ was determined after 72 h. Data are presented as pmols of Fru-2,6-P₂/mg protein \pm SEM (n=3 with independent triplicates, *P < 0.05, ***P < 0.001).

Considering the results obtained by Gerin, *et al.* (73), we determined the concentration of PEP, Pyr, 2-PG and 3-PG in HeLa cells after *TIGAR* overexpression and inhibition. *TIGAR* overexpression did not cause any significant change in the analysed metabolites (**Figure 49A**). On the other hand, *TIGAR* inhibition significantly increased pyruvate concentration (**Figure 49B**). These results did not seem to support the bisphosphatase of *TIGAR* on 2-PG or PEP proposed by Gerin, *et al.* (73) but suggested a role for *TIGAR* in the latter reactions of glycolysis, involving pyruvate. With the aim of widening the metabolic view of *TIGAR* effects further from the possibilities of spectrophotometer-based assays, we performed metabolomic and fluxomic studies the results of which can be found in the following pages.

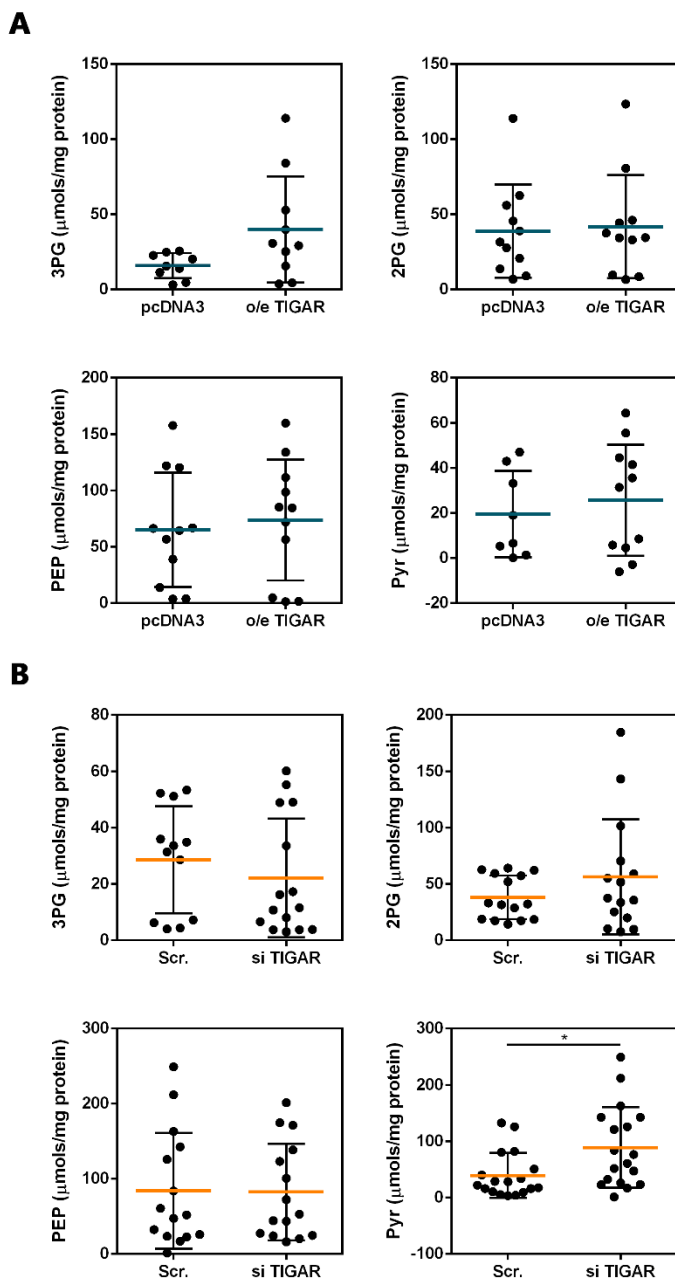


Figure 49. 3-PG, 2-PG, PEP and Pyr concentration in *TIGAR* overexpressing and *TIGAR*-inhibited cells. (A) HeLa cells were transfected with either a pcDNA3 plasmid containing *TIGAR* human gene or the corresponding pcDNA3 empty vector and the levels of the different metabolites were determined after 24 h. **(B)** HeLa cells were transfected with 75 nM *PFKFB3* or *TIGAR*-targeting siRNAs or the corresponding scrambled siRNA and the levels of the different metabolites were determined after 72 h. Data are presented as μmol of each metabolite/mg protein \pm SEM (A: n=4, B: n=6 with independent triplicates, *P < 0.05).

3. Metabolomic and fluxomic analyses by LC-MS/MS

In collaboration with Dr. Yanes Lab (Universitat Rovira i Virgili, Reus), twenty different metabolites were analysed through targeted liquid chromatography (LC) with mass spectrometry (MS) (LC-MS/MS) in HeLa cells after *TIGAR* overexpression or siRNA-mediated inhibition of *TIGAR* or *PFKFB3*. These twenty metabolites comprised intermediates of glycolysis and the TCA cycle, as well as some important metabolites of the PPP. Two types of analysis were performed, the first one consisting in the measurement of the abundance of each metabolite within each sample, and the second one consisting in the tracing of glucose flux within cells. For the first approach, abundance is equivalent to the amount of C12 corresponding to a given metabolite within the sample. For the flux analysis, cells were cultured for 6 h in media in which glucose was replaced by fully labelled ^{13}C -glucose at a concentration of 25 mM. In the analysis, the percentage of the different isotopologues for each metabolite was calculated. The term **isotopologue** refers to a molecule with at least one atom with a different number of neutrons than the parent molecule. That is, in our case, a metabolite with at least one atom of ^{13}C . Thus, isotopologues only differ in their isotopic composition and are metabolized through the same pathways. Isotopologues need to be differentiated from *isotopomers*, which have the same number of atoms of each isotope but in a different position. Isotopomers can be distinguished through nuclear magnetic resonance, which reports the information of the exact position of the isotope. However, LC-MS differentiates between isotopologues but not between the position of the isotopes.

In our case, since we are using fully-labelled ^{13}C -glucose, any metabolite generated from external glucose will be an isotopologue of the m+0 form of that metabolite, which does not contain any atom of ^{13}C . For example, three isotopologues will be detected for pyruvate, apart from the m+0 form: m+3, which contains three atoms of ^{13}C and corresponds to the pyruvate generated from the fully labelled ^{13}C -glucose through glycolysis, and m+1 and m+2, which correspond to the pyruvate that is not directly generated through glycolysis, but from the incorporation of a glycolytic intermediate into another pathway in which it is combined with a non-labelled molecule, as it might occur in the TCA cycle. Given that we are interested in understanding the effect of *TIGAR* in glycolytic metabolism, we will mainly focus on the analysis of abundance and the fluxes of isotopologues directly derived from glucose. However, all isotopologues were analysed for those metabolites involved in mitochondrial metabolism, given that glutamine is also an important source of carbons in cancer cells, which can be differentially used depending on the glycolytic capacity of cells.

3.1. Metabolomic abundance analyses

The effects of *TIGAR* overexpression were analysed at 24 h post-transfection and the differences were calculated compared to control cells overexpressing an empty pcDNA3 vector. The abundance of each metabolite was calculated relative to the abundance of an internal standard, $^{13}\text{C}_3$ -glycerol, which is not present in the biological sample and is added during the analysis at equal quantities in each sample.

We did not find any significant differences in the abundance of any of the twenty metabolites analysed in *TIGAR* overexpressing cells and control cells (**Figure 50**). However, there were some non-significant metabolic changes that might be interesting to confirm with more experiments. Intracellular glucose was modestly increased ① (**Figure 50**), whereas intracellular glutamine was slightly decreased ② (**Figure 50**). In the previous chapter, the analysis of extracellular glucose concentration did not reveal differences between *TIGAR* overexpressing cells and control cells (**Figure 38**). Therefore, more experiments should be performed to determine if metabolomics can reveal increased glucose concentration in *TIGAR* overexpressing cells which might go unnoticed in the enzymatic assays performed to measure glucose consumption due to lack of sensitivity.

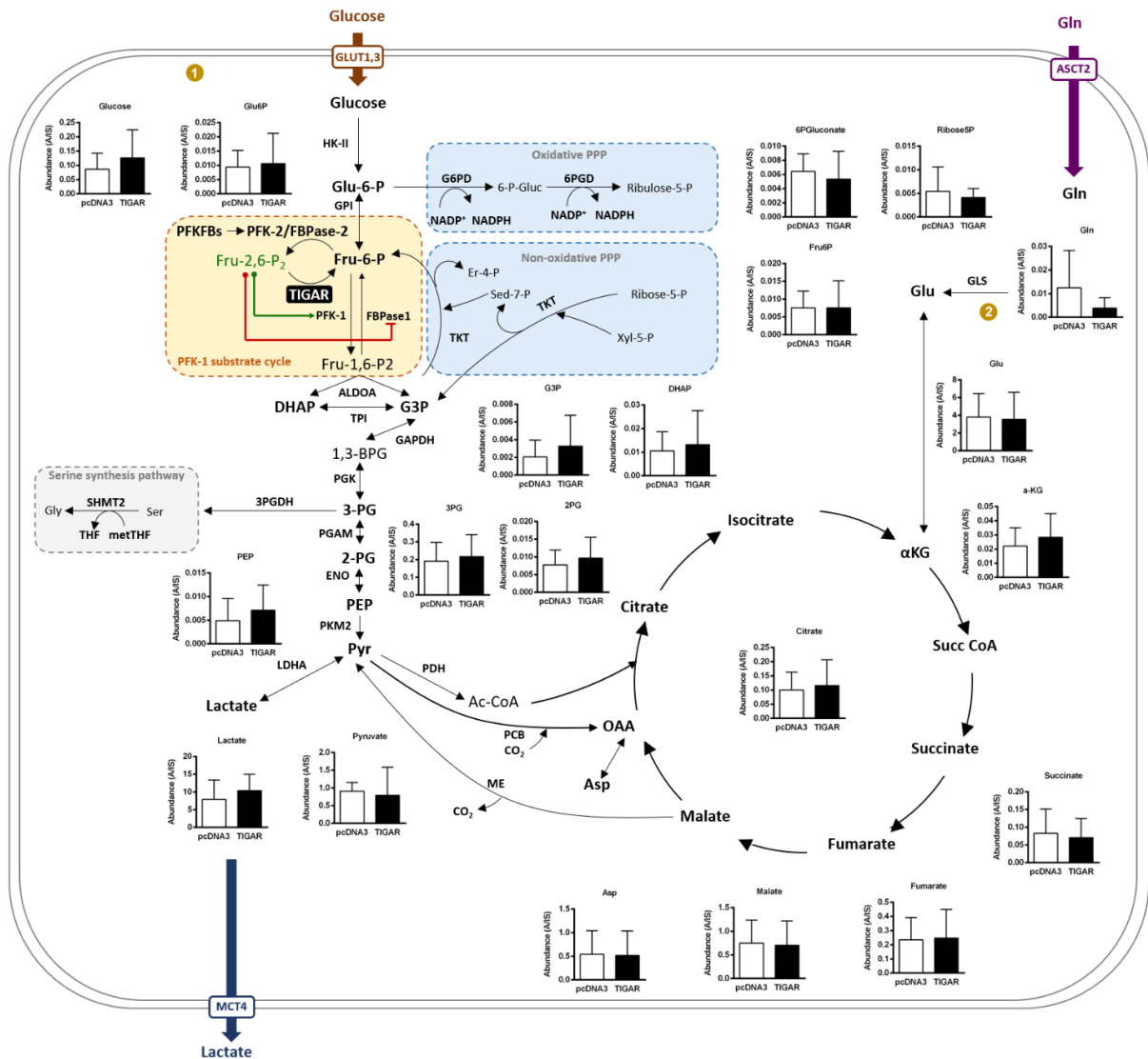


Figure 50. Analysis of metabolites abundance in *TIGAR* overexpressing cells. Schematic diagram of glycolysis, the first reactions of oxidative PPP and the TCA cycle showing metabolites abundance. HeLa cells were transfected with either a pcDNA3 plasmid containing *TIGAR* human gene or the corresponding pcDNA3 empty vector and samples were collected after 24 h for metabolomic analyses. Metabolites abundance is expressed relative to the abundance of the internal standard (IS) ¹³C₃-glycerol ± SD (n=2 with independent triplicates). Numbers in yellow refer to comments in the text.

TIGAR inhibition through siRNA did not render any statistically significant changes in the abundance of the studied metabolites either (Figure 51). However, some tendencies could be detected, which require more experiments to be confirmed. Oppositely to *TIGAR* overexpression, *TIGAR*-inhibited cells showed decreased intracellular glucose levels ❶, which is consistent with the analysis of extracellular glucose concentration presented in the previous chapter, which revealed decreased glucose consumption in *TIGAR*-inhibited cells (Figure 38). However, glycolytic intermediates such as G3P, DHAP, 3PG and PEP were increased ❷ (Figure 51) in parallel to increased pyruvate and lactate levels ❸ (Figure 51). These results are in accordance with previous literature that situates *TIGAR* as a glycolytic inhibitor (3). Contrarily to what would be expected from this literature, however, the PPP intermediates 6-phosphogluconate and ribose-5-P levels were raised in *TIGAR*-inhibited cells ❹ (Figure 51).

Some other non-significant changes could also be observed in those metabolites related to glutamine metabolism. Intracellular glutamine was found slightly increased in *TIGAR*-inhibited cells ❺ (Figure 51), as well as several metabolites produced during glutamine oxidation such as glutamate and α KG ❻ (Figure 51). These results, despite not being statistically significant, might suggest an effect of *TIGAR* inhibition in the TCA fuelling. Additionally, the TCA intermediates succinate and fumarate were also found increased in these cells ❼ (Figure 51). Although we have not performed an experiment with labelled glutamine and, thus, we cannot determine the fate of this amino acid within the cell, the results obtained suggest increased anaplerosis of glutamine in the TCA cycle in *TIGAR*-inhibited cells.

PFKFB3 inhibition did not affect the abundance of any of the metabolites analysed, except for Fru-6-P, glucose-6-P and 6-P-gluconate, which were increased ❹ (Figure 51). These results, although not being statistically significant, are in accordance with the fact that *PFKFB3* is the PFK-2 coding gene with the highest kinase/bisphosphatase ratio (36). *PFKFB3* inhibition decreases Fru-2,6-P₂, as it has been previously shown before and during this thesis and, consequently, PFK-1 is reduced. According to that, glycolysis and, consequently, lactate levels were expected to decrease in *PFKFB3*-inhibited cells. In metabolomic analyses, lactate levels were only slightly decreased after *PFKFB3* inhibition ❸ (Figure 51). These results are complemented by other determinations at the end of this chapter.

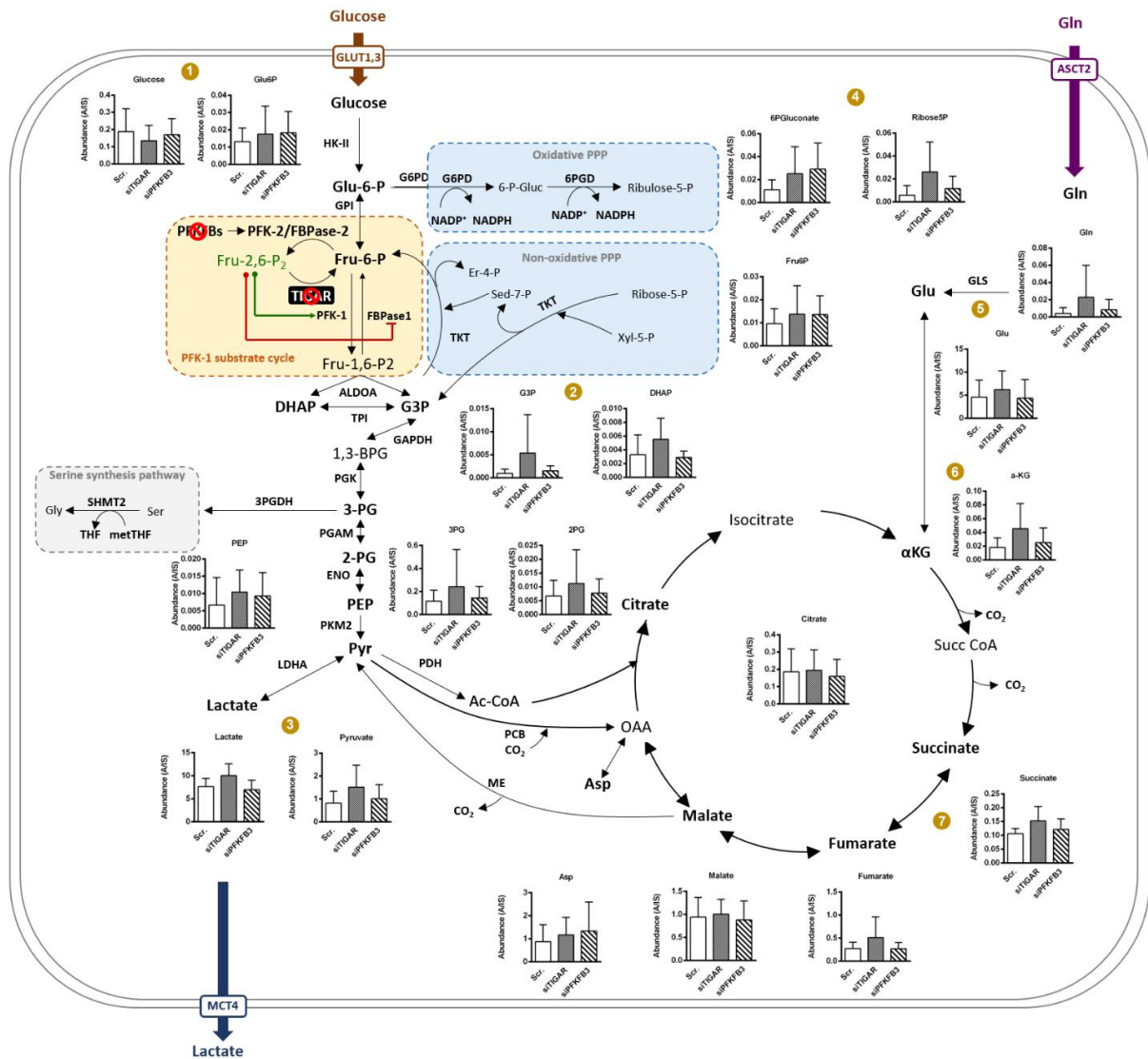


Figure 51. Analysis of metabolites abundance in TIGAR-inhibited cells. Schematic diagram of glycolysis, the first reactions of oxidative PPP and the TCA cycle showing metabolites abundance. HeLa cells were transfected with 75 nM PFKFB3 or TIGAR-targeting siRNAs or the corresponding scrambled siRNA and samples were collected after 72 h for metabolomic analyses. Metabolites abundance is expressed relative to the abundance of the internal standard (IS) ¹³C₃-glycerol ± SD (n=2 with independent triplicates). Numbers in yellow refer to comments in the text.

3.2. Fluxomic analyses

The analysis of metabolic fluxes complements the results obtained in terms of abundance and helps to understand whether the origin and fate of glycolytic metabolites is altered by TIGAR levels. For the analysis of flux through glycolysis, we focused on those isotopologues that reflect direct fluxes from ^{13}C -glucose. For this reason, the m+6 form is shown for six-carbon metabolic intermediates, whereas the m+3 form is shown for three-carbon intermediates. In the case of TCA cycle intermediates, all m+ forms are represented given that each of them reflects a different origin of the molecules and can inform about the contribution of glutamine and other substrates in mitochondrial anaplerosis (**Figure 52**).

The analysis of the flux through glycolysis in TIGAR-overexpressing cells did not reveal any differences compared to control cells (**Figure 52**), evidencing that the contribution of glucose to the formation of the studied metabolites is equal in these cells. These results reinforce those found in terms of abundance. TIGAR overexpression did not affect the isotopologue distribution of any of the mitochondrial metabolites analysed either (data not shown).

One of the most interesting metabolites to determine in the flux analysis were those related to the oxidative PPP. However, no changes were observed in glucose-6-phosphate, 6-phosphogluconate or ribose-5-phosphate in neither TIGAR overexpressing cells or TIGAR-inhibited cells **1** (**Figure 52**). These results do not support a strong effect of TIGAR on the redirection of glucose towards the PPP. However, it should be considered that our experiments were performed in the absence of damaging stimuli and, according to previous literature (79), the antioxidant function of TIGAR is especially relevant when cells are facing stress and might be irrelevant at basal conditions.

The only isotopologue significantly altered in TIGAR-inhibited cells was m+3 3PG, which was found increased **2** (**Figure 52**). This is in accordance with the absorbance analysis. The fact that m+3 isotopologue is increased means that 3PG is mainly produced from glucose. An alternative source of 3PG might be TCA-derived PEP obtained through the reaction catalysed by PCK-2.

PFKFB3 inhibition did not affect the isotopologue distribution of any of the cytosolic metabolites analysed (**Figure 52**).

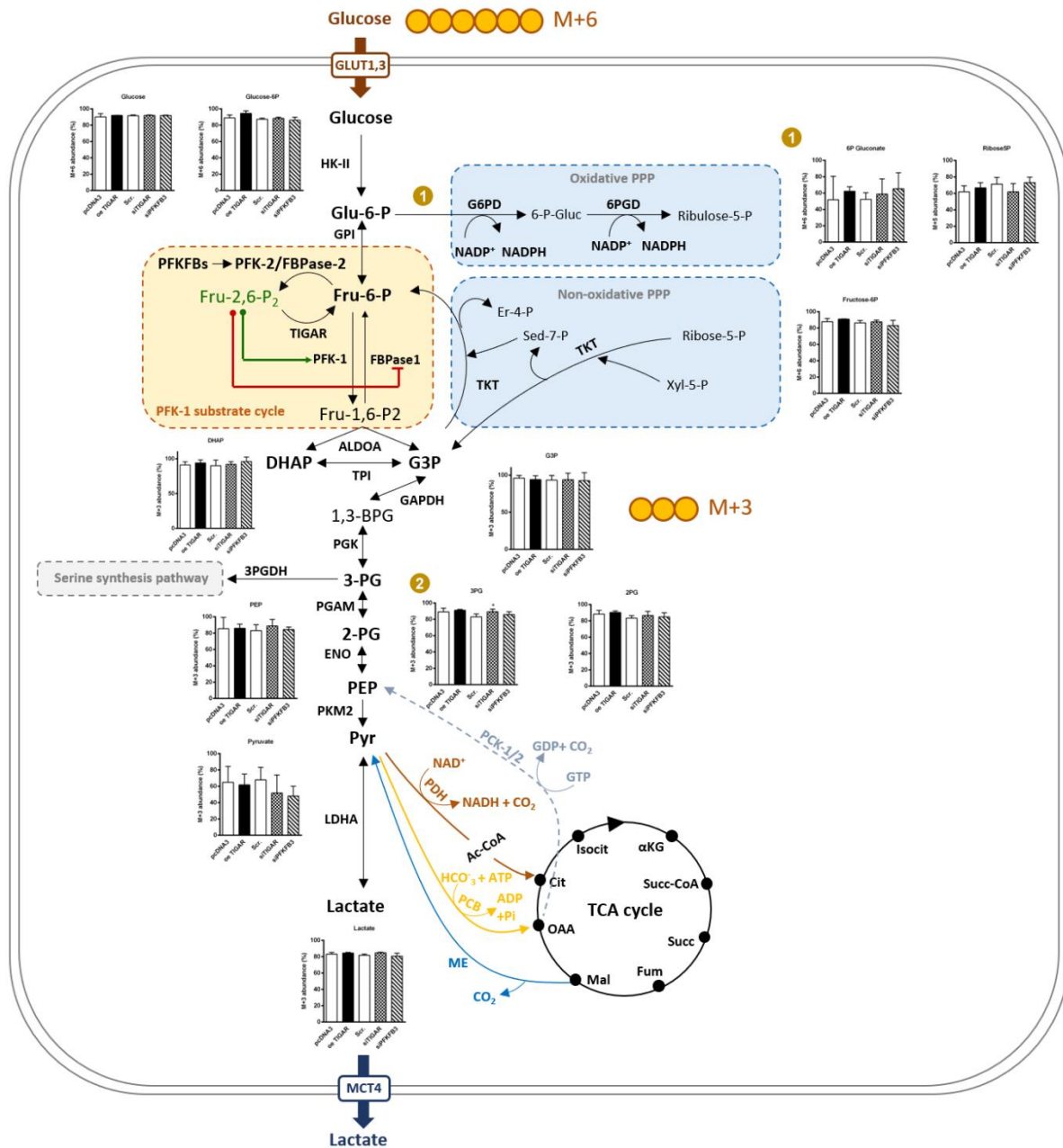


Figure 52. Fluxomic analyses of cytosolic metabolites in *TIGAR* overexpressing and *TIGAR*-inhibited cells. Schematic diagram of glycolysis and the first reactions of oxidative PPP showing the distribution of isotopologues from fully labelled ¹³C-glucose. HeLa cells transfected with either pcDNA-*TIGAR* or pcDNA3 vectors (in the case of overexpressing experiment), or *TIGAR*/*PFKFB3*/Scrambled siRNAs (in the case of silencing experiment) for 24 or 72 h, respectively. Cells were exposed to 25 mM fully labelled ¹³C-glucose in media containing 2 mM glutamine and 10% dialyzed FBS for 6 h and samples were collected for metabolomic analyses. Distribution of isotopologues for each metabolite is represented as m + x, where the m stands for natural mass of the metabolite and the x indicates the number of incorporated ¹³C carbons. Data are represented as the % of a given isotopologue (M+6 or M+3) among all isotopologues for a given metabolite ± SD (n=2 with independent triplicates, P < 0.05). Numbers in yellow refer to comments in the text.

Interestingly, *TIGAR* inhibition caused a shunt in the supply of carbons to the TCA cycle. ^{13}C -glucose flux analysis evidenced increased m+2 citrate ①, which is the product of citrate synthase (Figure 53). This enzyme combines a molecule of acetyl-CoA (2 carbons) with a molecule of OAA (4 carbons) and generates citrate (6 carbons). Thus, m+2 citrate contains two carbons from glucose-derived acetyl-CoA, reflecting the activity of pyruvate dehydrogenase (PDH). Additionally, m+3 aspartate (equivalent to m+3 OAA), m+3 malate and m+3 fumarate were found downregulated in *TIGAR*-inhibited cells ②, evidencing decreased activity of pyruvate carboxylase (PCB) (Figure 53). This enzyme combines a molecule of pyruvate (3 carbons) with HCO_3^- and generates OAA (4 carbons). Thus, m+3 isotopologues of TCA intermediates indicate the entrance of pyruvate to the TCA cycle through PCB.

Finally, m+0 forms of aspartate, malate and fumarate were found increased in *TIGAR*-inhibited cells ③, indicating that other substrates apart from glucose are fuelling the TCA cycle in these cells (Figure 53). This is consistent with the data from the abundance analysis, which suggested increased glutamine incorporation in the TCA cycle in *TIGAR*-inhibited cells (Figure 51).

PFKFB3 inhibition did not affect the isotopologue distribution of any of the mitochondrial metabolites analysed (data not shown).

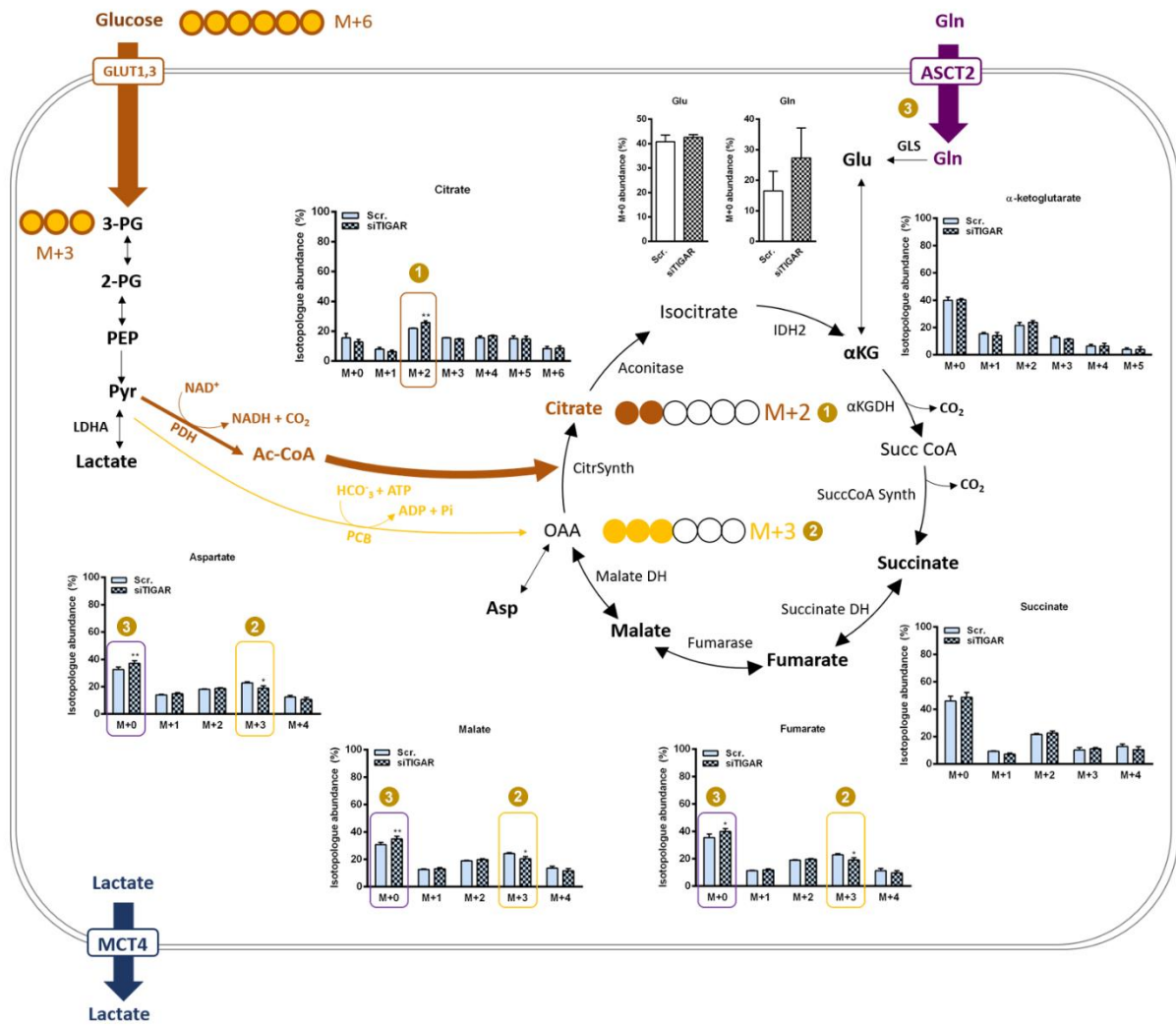


Figure 53. Fluxomics analyses of mitochondrial metabolites in *TIGAR*-inhibited cells. Schematic diagram of the TCA cycle and the main reactions providing metabolites to the TCA showing the distribution of isotopologues from fully labelled ^{13}C -glucose. This is an enlargement of the results presented in the previous figure. HeLa cells transfected with either pcDNA-*TIGAR* or pcDNA3 vectors (in the case of overexpressing experiment), or *TIGAR/PCFB3/Scrambled* siRNAs (in the case of silencing experiment) for 24 or 72 h, respectively. Then, cells were exposed to 25 mM fully labelled ^{13}C -glucose in a medium containing 2 mM glutamine and 10% dialyzed FBS for 6 h and samples were collected for metabolomic analyses. Distribution of isotopologues for each metabolite is represented as $M+x$, where M stands for natural mass of the metabolite and the x indicates the number of ^{13}C carbons incorporated. Data are represented as the % of a given isotopologue among all isotopologues for a given metabolite \pm SD ($n=2$ with independent triplicates, * $P < 0.05$, ** $P < 0.01$, *** $P < 0.001$). Numbers in yellow refer to comments in the text.

4. Determination of redox potential

Fluxomic analysis determined a preferential entrance of pyruvate to the TCA cycle through PDH rather than through PC in *TIGAR*-inhibited cells. This might be explained by increased NAD^+ in these cells, which would trigger the activity of dehydrogenases, in this particular case PDH, the activity of which is coupled to the generation of NADH. To confirm this, we analysed NAD^+ , NADH, NADP^+ and NADPH after 72 h of *TIGAR*-targeting siRNA transfection in HeLa cells. The ratio NAD^+/NADH was significantly increased in *TIGAR*-inhibited cells (Figure 54A), confirming our hypothesis. However, the ratio $\text{NADP}^+/\text{NADPH}$ was not significantly altered, although it was found slightly decreased after *TIGAR* inhibition (Figure 54B). We also determined the two redox ratios in *TIGAR* overexpressing cells. According to previous results, increased *TIGAR* levels did not cause any change in neither the NAD^+/NADH ratio (Figure 54C) or the $\text{NADP}^+/\text{NADPH}$ ratio (Figure 54D).

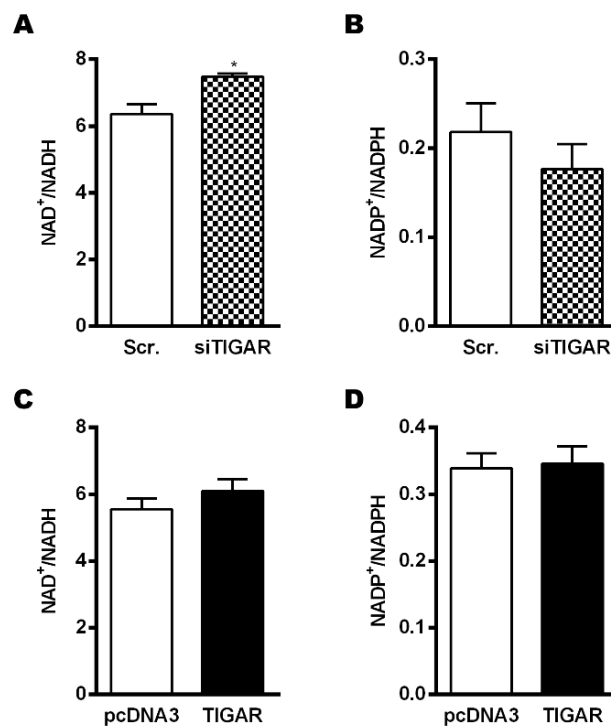


Figure 54. Analysis of NAD^+/NADH and $\text{NADP}^+/\text{NADPH}$ ratios after *TIGAR* modulation. HeLa cells transfected with either pcDNA-*TIGAR* or pcDNA3 vectors (in the case of overexpressing experiments), or *TIGAR*/PFKFB3/Scrambled siRNAs (in the case of silencing experiments) for 24 or 72 h, respectively. Determination of NAD^+ , NADH, NADP^+ and NADPH was performed with NAD/NADH-Glo™ and NADP/NADPH-Glo™ Assays (Promega). Data are presented as the mean of the ratios from triplicate samples for each condition \pm SEM. Student's t-test was used to analyse differences between groups (n=1 with independent triplicates, *P < 0.05).

5. Analysis of genes involved in glucose metabolism

In parallel to the metabolomic analyses, the expression of key genes involved in glucose metabolism and the pentose phosphate and serine synthesis pathways was determined by RT-qPCR in cells with increased (*TIGAR* overexpression) and decreased (siRNA-mediated inhibition) *TIGAR* protein levels.

HeLa cells with *TIGAR* overexpression did not show significant changes in any of the genes analysed (**Figure 55**).

A

Gene	<i>TIGAR</i> /pcDNA3 expression (difference between means \pm SEM)	p-value
TIGAR	748,9 \pm 266,6	0,0203
SLC1A2	1,127 \pm 0,1470	0,1877
HKII	1,145 \pm 0,08993	0,1579
G6PD	0,9661 \pm 0,09498	0,7335
TKT	0,9416 \pm 0,08189	0,5155
PHGDH	0,8578 \pm 0,1097	0,2427
LDHA	0,9470 \pm 0,1667	0,7614

B

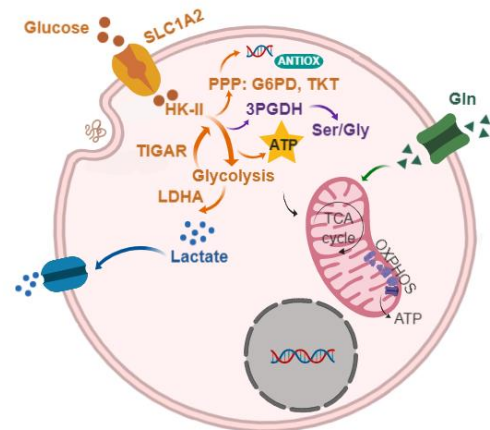


Figure 55. RT-qPCR analysis of metabolic genes in *TIGAR* overexpressing cells. (A) HeLa cells were transfected with either a pcDNA3 plasmid containing *TIGAR* human gene or the corresponding pcDNA3 empty vector (control cells) and samples were collected after 24 h for RNA extraction and RT-qPCR analysis. The table indicates the mean expression \pm SEM of each of the genes in *TIGAR* overexpressing cells relative to the expression in control cells. Expression in the control group was set to 1. The corresponding p-values are shown, and the statistically significant results are highlighted in bold ($P < 0.05$). Genes were analysed in four independent experiments except for *TIGAR* and *TKT*, which were analysed in three independent experiments. **(B)** Schematic diagram of glycolysis and the first reactions of oxidative PPP, the TCA cycle, serine and glycine synthesis pathway and glutamine catabolism. The genes analysed are written in bold capital letters.

TIGAR inhibition in HeLa cells significantly increased the expression of *TKT*, whereas the levels of the other genes analysed were not significantly affected. Interestingly, *SLC2A1* (GLUT1) mRNA levels were slightly increased in *TIGAR*-inhibited cells (**Figure 56A**).

Inhibition of *PFKFB3* also affected the expression of some key metabolic genes, causing a significant increase in *SLC1A2* (GLUT1), *HK-II* and *LDHA* expression (**Figure 56B**).

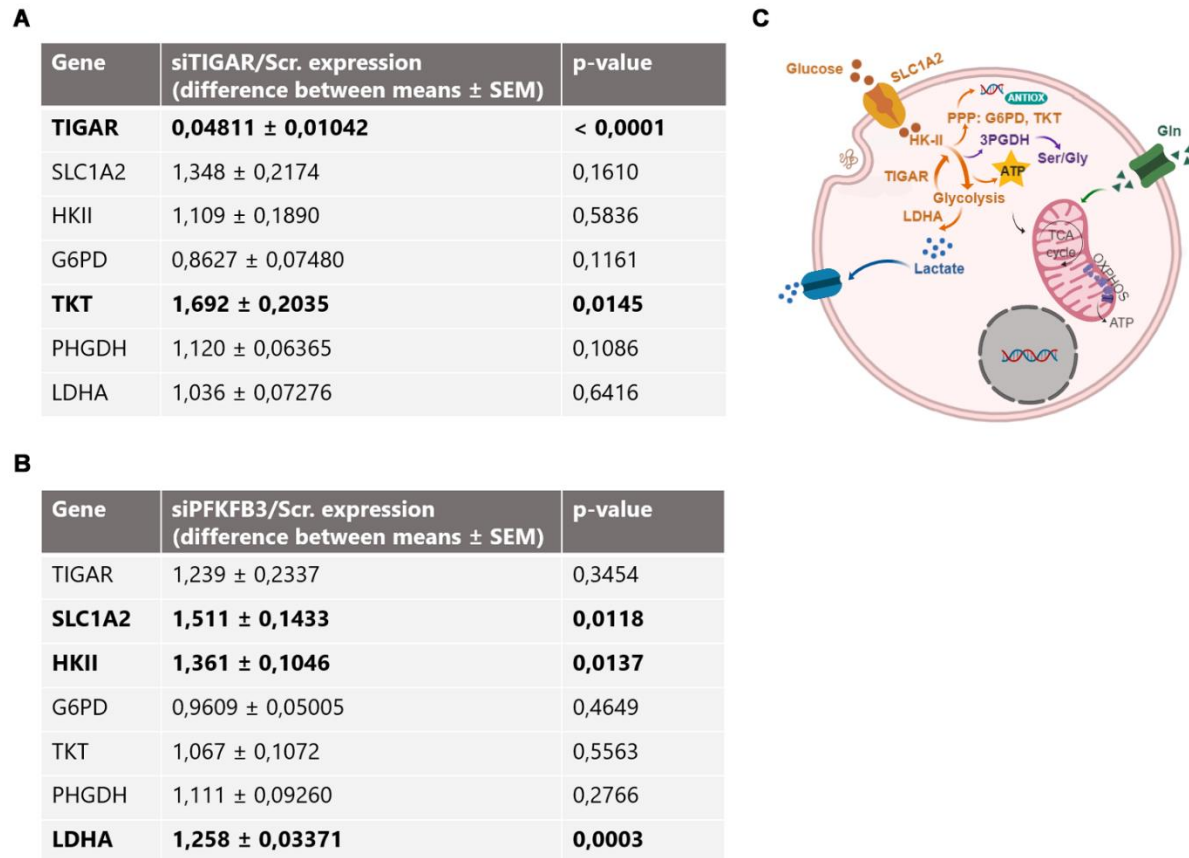


Figure 56. RT-qPCR analysis of metabolic genes in *TIGAR* or *PFKFB3*-inhibited cells. HeLa cells were transfected with either *TIGAR* or *PFKFB3*-targeting siRNAs or the corresponding scrambled siRNA (Scr., control cells) and samples were collected after 72 h for RNA extraction and RT-qPCR analysis. Each table indicates the mean expression \pm SEM of each of the genes in **(A)** *TIGAR* or **(B)** *PFKFB3*-inhibited cells relative to the expression in control cells. Expression in the control group was set to 1. The corresponding p-values are shown, and the statistically significant results are highlighted in bold ($P < 0.05$). Four independent experiments were analysed. **(C)** Schematic diagram of glycolysis and the first reactions of oxidative PPP, the TCA cycle, serine and glycine synthesis pathway and glutamine catabolism. The genes analysed are written in bold capital letters.

6. Study of key proteins involved in the metabolism of glucose and glutamine

To confirm the RT-qPCR results, we analysed the levels of several proteins involved in the metabolism of glucose and glutamine by western blot. The proteins analysed can be classified into three groups: proteins involved in glucose oxidation (HK-II, PFKFB3, TIGAR, TKT, PDH and PCB), lactate transporters (MCT1) and proteins linked to glutamine metabolism (GLS1).

HeLa cells overexpressing TIGAR showed significantly increased levels of the lactate importer MCT1, while the other enzymes, despite being all upregulated, did not show statistically significant changes compared to control cells (**Figure 57**). The highest increase was observed in PCB, but this enzyme was only analysed in two independent experiments and therefore this result is preliminary.

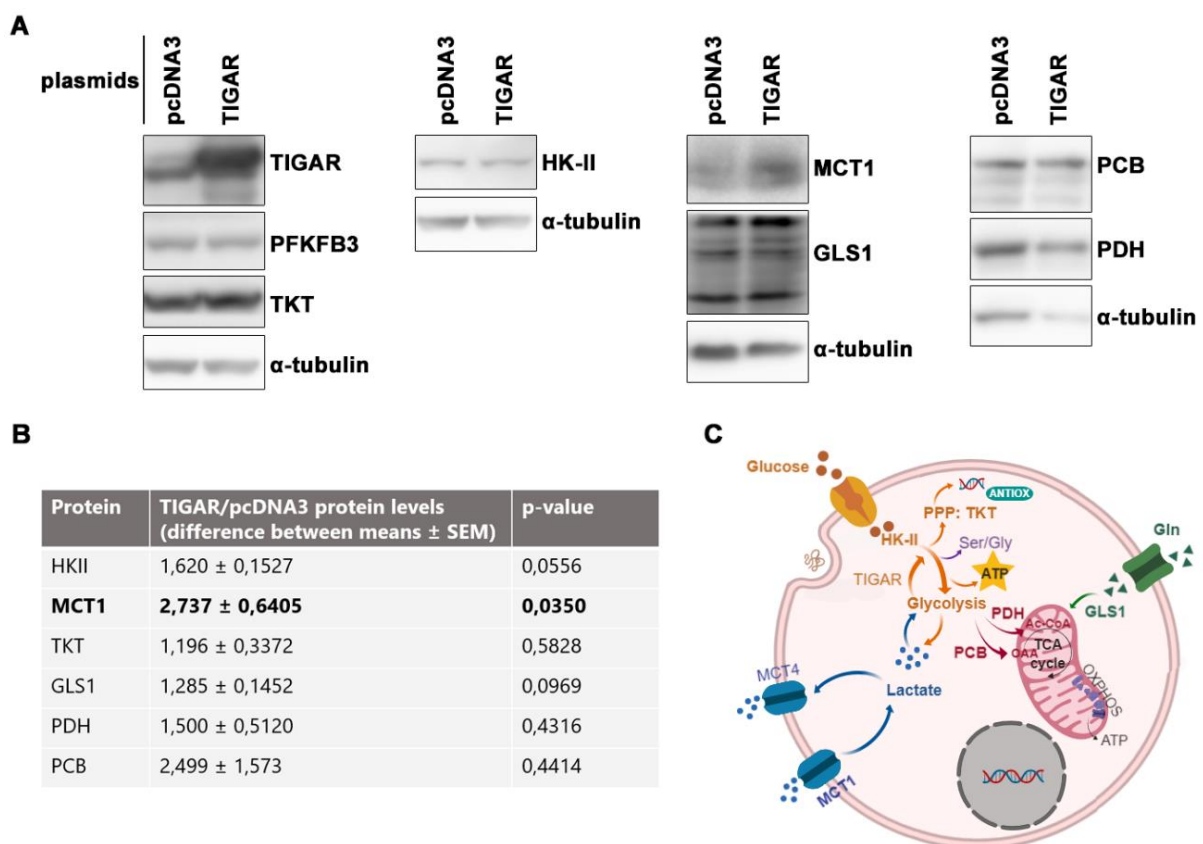


Figure 57. Western blot analysis of metabolic enzymes in TIGAR overexpressing cells. HeLa cells were transfected with either a pcDNA3 plasmid containing TIGAR human gene or the corresponding pcDNA3 empty vector (control cells) and samples were collected after 24 h for protein analysis. **(A)** Representative western blot images of each of the proteins analysed. **(B)** The table indicates the mean protein levels \pm SEM of each of the proteins in TIGAR overexpressing cells relative to the levels detected in control cells. Protein levels in the control group were set to 1. The corresponding p-values are shown, and the statistically significant results are highlighted in bold ($P < 0.05$). Proteins were analysed in four independent experiments except for PDH and PCB, which could be analysed in only two independent experiments. **(C)** Schematic diagram of glycolysis and the first reactions of oxidative PPP, the TCA cycle, serine and glycine synthesis pathway and glutamine catabolism. The genes analysed are written in bold capital letters.

Appositely to *TIGAR* overexpression, *TIGAR* inhibition resulted in a highly statistically significant decrease of PCB (**Figure 58A**). The other proteins analysed remained unaltered (**Figure 58A**), suggesting that the increased expression of *TKT* (**Figure 56A**) was not translated to increased levels of this protein. On the other hand, *PFKFB3*-inhibited cells did not show significant modulation of any of the enzymes analysed (**Figure 58B**), suggesting again that the increased expression of *HK-II* (**Figure 56B**) was not translated in increased levels of the protein.

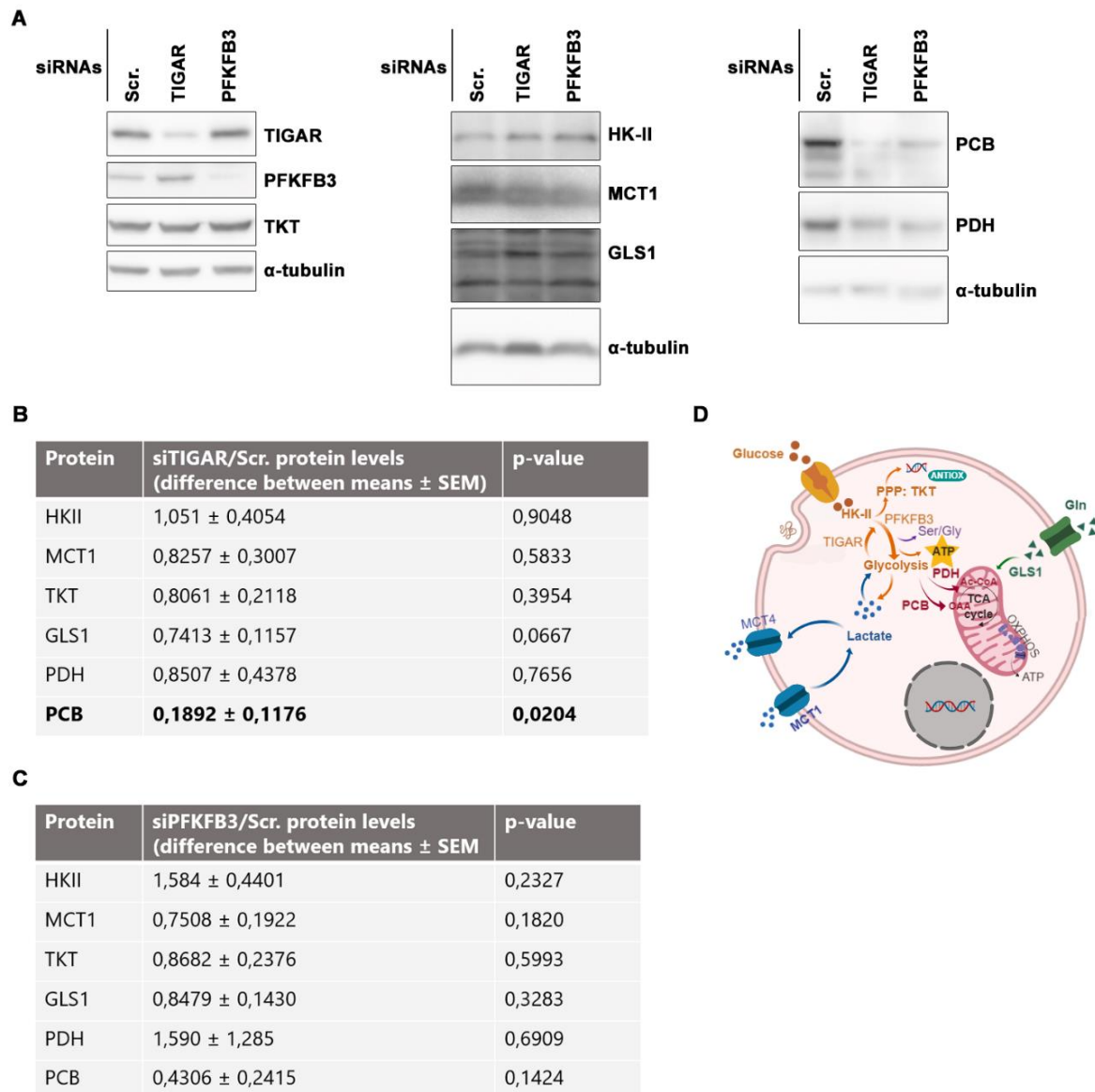


Figure 58. Western blot analysis of metabolic enzymes in *TIGAR* or *PFKFB3*-inhibited cells. HeLa cells were transfected with either *TIGAR* or *PFKFB3*-targeting siRNA or the corresponding scrambled siRNA (Scr., control cells) and samples were collected after 72 h for protein analysis. **(A)** Representative western blot images of each of the proteins analysed. **(B, C)** Tables indicate the mean protein levels \pm SEM of each of the proteins in **(B)** *TIGAR* or **(C)** *PFKFB3*-inhibited cells relative to the levels detected in control cells. Protein levels in the control group were set to 1. The corresponding p-values are shown, and the statistically significant results are highlighted in bold ($P < 0.05$). Proteins were analysed in four independent experiments except for PDH and PCB, which could be analysed in only two independent experiments. **(D)** Schematic diagram of glycolysis and the first reactions of oxidative PPP, the TCA cycle, serine and glycine synthesis pathway and glutamine catabolism. The genes analysed are written in bold capital letters.

7. Discussion

The main findings of this chapter are summarised in **Table II**, in an attempt to clarify the most important metabolic changes observed after TIGAR modulation. For the elaboration of the table, some of the non-statistically significant results that suggested important modulations of metabolites or genes have also been included.

	Metabolites abundance	Metabolic fluxes	Redox potential	Gene expression	Protein levels
↑ TIGAR	↓ Fru-2,6-P ₂	No important modulations.	No important modulations.	No important modulations.	↑ MCT1
	↑ Glucose (no sign.)				
	↓ Gln (no sign.)				
Partial glycolytic inhibition due to reduced Fru-2,6-P₂ concentration. Low intracellular Gln: decreased uptake or increased glutaminolysis. Increased lactate import.					
↓ TIGAR	↑ Extracellular glucose	↑ 3PG	↑ NAD ⁺ /NADH	↑ <i>TKT</i>	↓ PCB
	↑ Extracellular lactate	↑ M+2 citrate		↓ <i>G6PD</i>	
	↑ Fru-2,6-P ₂ (no sign.)	↓ M+3 Aspartate,			
	↓ Glucose (no sign.)	Malate, Fumarate			
	↑ Pyr	↑ M+0 Aspartate,			
	↑ Intracellular lactate (no sign.)	Malate, Fumarate			
	↑ Gln & Gln-derived metabolites (no sign.)	↑ M+0 Gln			
	Increased flux through glycolysis and glutaminolysis. Pyruvate enters the TCA cycle through PDH rather than through PCB.				
↓ PFKFB3	↓ Fru-2,6-P ₂	No important modulations.	No important modulations.	↑ <i>SLC2A1</i> , <i>HK-II</i> , <i>LDHA</i>	No important modulations.
	↑ Fru-6-P, Glu-6-P, 6PG (no sign.)				
	↓ Intracellular lactate (no sign.)				
Glycolytic inhibition due to decreased Fru-2,6-P₂ concentration.					

Table II. Summary of the main metabolic alterations induced by TIGAR and PFKFB3 modulation. The most relevant findings reported in this chapter, including the results that indicate an important contribution of TIGAR or PFKFB3 to the analysed parameter despite not being statistically significant, are described.

HeLa cells with high TIGAR levels showed significantly reduced Fru-2,6-P₂ concentration. TIGAR inhibition, however, had only a modest effect on the levels of this metabolite, which was found slightly increased. These results, together with previous findings indicating that TIGAR inhibition in HeLa cells does not always increase Fru-2,6-P₂ levels (84) show that, as well as the consequences of TIGAR upregulation can be interpreted due to its effect on Fru-2,6-P₂ levels, other players should also be considered when analysing the effects of TIGAR inhibition.

One of the most important observation in this chapter is that TIGAR overexpression in HeLa cells does not increase the abundance of PPP intermediates, as it was expected. However, M+6 isotopologues of these metabolites were found slightly increased in fluoxomic analyses, suggesting increased flux through

this pathway, which would be in accordance to what was originally described (3). However, $\text{NADP}^+/\text{NADPH}$ remained unaltered after *TIGAR* overexpression, questioning the role of *TIGAR* as a potent antioxidant enzyme in HeLa cells. Increased levels of MCT1 in *TIGAR* overexpressing cells, however, suggested alternative functions of *TIGAR* in the lower parts of glycolysis. Increased MCT1 indicates increased lactate import, which could account for the maintained lactate and pyruvate levels despite decreased in Fru-2,6-P₂. Previous publications have reported that oxidative cancer cells displaying *TIGAR* overexpression take advantage of cancer-associated fibroblasts, which mainly rely on glycolysis and produce lactate, by uptaking lactate from extracellular media and using it for TCA cycle anaplerosis (82). Our results are in accordance with these findings but, in this case, given that cells in our culture plates are all cancer cells, they might uptake lactate produced by themselves. Another possibility would be to consider the existence of different populations of HeLa cells within our plates, ones producing lactate and the others importing it.

Regarding *TIGAR* inhibition effects, the most evident consequence was the shift in the way that pyruvate enters the TCA cycle. Metabolites abundance analyses revealed decreased M+3 isotopologues of aspartate, malate and fumarate, and increased M+2 citrate. This indicates that in *TIGAR*-inhibited cells, pyruvate is oxidized into acetyl-CoA through PDH rather than to OAA through PCB. Accordingly, PCB protein levels were found decreased in *TIGAR*-inhibited cells. Consequently, alternative anaplerotic pathways must be required to supply OAA in *TIGAR*-inhibited cells. One possibility would be that increased glutamine and glutamine-derived metabolites, together with increased M+0 isotopologues of aspartate, malate and fumarate, accounted for OAA supply in these cells.

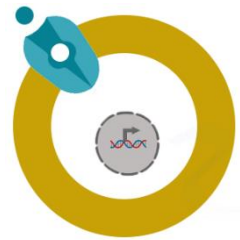
The fact that *TIGAR*-inhibited cells display more PDH than PCB activity is in accordance with the higher NAD^+/NADH ratio registered in these cells compared to cells with basal *TIGAR* expression, and would be compatible with previous studies indicating that *TIGAR* overexpression increases mitochondrial metabolism, which generates NADH in the TCA cycle (82). These results are also supported by the finding that *TIGAR*-inhibited cells showed decreased MTT signal, an assay that is based on the activity of NAD(P)H-dependent cellular oxidoreductases, as it has been shown in Results Chapter I.

In previous studies, *TIGAR* has been related to mitochondrial metabolism, with those cells overexpressing *TIGAR* being more oxidative than those with low *TIGAR* levels, which rely on glycolysis (82). In our experiments, the oxygen consumption has not been evaluated. However, increased NAD^+/NADH ratio and decreased MTT signal are indicators of decreased functioning of the Krebs cycle, which would be in accordance with previously published results (82). However, the molecular orchestrator of this shift remains uncovered, and whether the effects of *TIGAR* on mitochondrial metabolism depend on its phosphatase function is something that needs to be determined. Our spectrophotometrical analyses indicated that *TIGAR* inhibition increases pyruvate concentration without altering the levels of PEP, 2PG

or 3PG, which does not support the proposed activity of TIGAR as a PEP phosphatase independent of ATP production (73). On the other hand, the direct phosphatase activity of TIGAR on 2,3-BPG has not been evaluated given that this metabolite is not a substrate, but an intermediate, of the reactions assayed, and it could not be detected in metabolomic analyses either. Thus, the hypothesis of TIGAR as the phosphoglycolate-independent 2,3-BPG phosphatase previously described in the skeletal muscle of pig, rat and chicken (73,181) could not be tested in our experiments. However, the *in silico* sequence and structural comparisons performed during this thesis and also by other groups (73,86) show more similarity of TIGAR with other histidine phosphatases than with FBPase-2, which helps to understand the few metabolic effects of TIGAR modulation that can be directly attributed to Fru-2,6-P₂.

RESULTS CHAPTER III

Control of *TIGAR* expression by Nrf2



CONTEXT

Apart from p53 (3), two transcription factors have been described to bind to *TIGAR* promoter and modulate its expression, SP1 and CREB1 (77). Both studies were performed by the same group, who firstly described the induction of *TIGAR* promoter by SP1 (76) and then found a shorter construct which retained transcriptional activity despite lacking the SP1 binding site. This shorter construct was activated by the binding of CREB1 to CRE-binding (77). However, the physiological relevance of these findings still needs to be determined, especially considering that SP1 binds to the promoter of many different genes at basal conditions, and that no relationship has been established between cAMP, the main responsible for CREB activation, and *TIGAR*. Therefore, p53 is the unique transcription factor that has been described to link the already-known functions of *TIGAR* in cancer cell metabolism with its transcriptional control to date. More than 50% of tumours carry mutation in *TP53*, and indeed it is the gene most frequently altered in cancer (74). As it has been described in the Introduction section of this thesis, *TP53* mutations can have multiple outcomes, some of which result in loss-of-function of this tumour suppressor gene.

The independence of *TIGAR* expression from p53 levels in cancer cells has already been commented in the Introduction section. Previous studies of Dr. Ramon Bartrons' Lab showed that *TIGAR* inhibition decreased cellular viability in the *TP53*-wild type and null T98G and U87 glioblastoma cell lines, respectively. These effects occurred in parallel with increased ROS-mediated DNA damage, which was prevented by the antioxidant molecule BHA, indicating that *TIGAR* plays a protector antioxidant role in glioblastoma regardless of the presence of p53 (79). Thus, the identification of physiologically-relevant transcription mechanisms that explained how and under which stimuli is *TIGAR* overexpressed in cancer cells independently of *TP53* appeared as a crucial question to be addressed during this thesis.

Nrf2 transcription factor, encoded by the *NFE2L2* gene, is a master regulator of the antioxidant response in cells. It is activated by electrophiles and ROS, as well as by oncogenic proliferative pathways such as c-Myc and PI3K/Akt in cancer. After dissociation from KEAP1, Nrf2 translocates to the nucleus and binds to AREs in the promoter of target genes (144). Apart from detoxifying enzymes such as NQO1 or GST, which are classical Nrf2 targets, the PPP enzymes G6PD and TKT have recently been described as new metabolic targets of Nrf2 (142). Given the close relation between *TIGAR* and the PPP, we hypothesized that Nrf2 exerted transcriptional control on *TIGAR* gene. This hypothesis was also supported by the identification of several potential AREs in the promoter and first intron of *TIGAR* gene. The following pages summarize the main findings of this project.

1. *In silico* study of the human TIGAR promoter

With the purpose of studying the presence of AREs in the regulatory regions of human *TIGAR* gene, we performed an *in-silico* analysis from 8000 bp prior to the translation start codon (+1, ATG) to + 2000 bp, including part of the sequence of the first intron of TIGAR. The sequence studied covered 10.000 bp between the positions 4.423.165 to 4.433.160 bp of human chromosome 12, according to numbering of the Evolutionary Conserved Regions (ECR) Browser (182), which is slightly different from the numbering in the NCBI. This web page allows to study the conserved sequences among the genome of several species and it was very useful to identify which AREs in the human TIGAR promoter had more potential to be functional sites for Nrf2 binding.

Given that the automatic transcription factor prediction tools use different Nrf2 consensus binding motifs, the sequence corresponding to AREs, TGAC/GnnnGC (147), was manually tracked along the region of study. ECR Browser was used to determine the degree of conservation of the identified AREs across species. This tool provides a representation of the genomes in which horizontal red lines indicate the sequences that are conserved between the specie from which the input sequence is obtained, in this case humans, and the different species to which the sequence is compared, that are indicated in the right panel (**Figure 59**).

The first regulatory element of interest in the studied sequence was the p53 binding site 1 (BS1), located at -6.702 bp from the translation start codon (ATG, +1) (3) (**Figure 59**). p53 binding sites correspond to the sequences RRRCWWGYYY, where R is a purine (A/G), W is A/T and Y is a pyrimidine (T/C), and two of them have been identified in the human and mouse TIGAR promoters with different functional relevance. However, they are not conserved between these two species. p53 BS1 is conserved in *Pan troglodytes* and *Canis familiaris* and its functional relevance remains unknown given that the direct binding of p53 to this sequence has not been described to date. In this thesis the nomenclature for p53 binding sites has been maintained as in the publication where these regulatory elements were described, being p53 BS1 the furthest from the translation start codon (3). The AREs identified in this thesis have been named from the transcription start codon, being ARE 1 the closest to the coding sequence of TIGAR.

Seven potential AREs were originally identified along the studied sequence. However, only five of them (four in the promoter, AREs 1-4, and one in the first intron, ARE i1) were considered as potential Nrf2 binding sites according to their sequence and conservation. Two conditions were required for the inclusion of AREs in subsequent analyses: a) to be at least conserved in *Pan troglodytes*, the closest specie to humans, and b) to correspond to a TGAC/GnnnGC sequence, preferably to TGAC/GnnAGC, which has been reported as a common motif in the promoter of all Nrf2 target genes (183). TGACnnGC motifs are

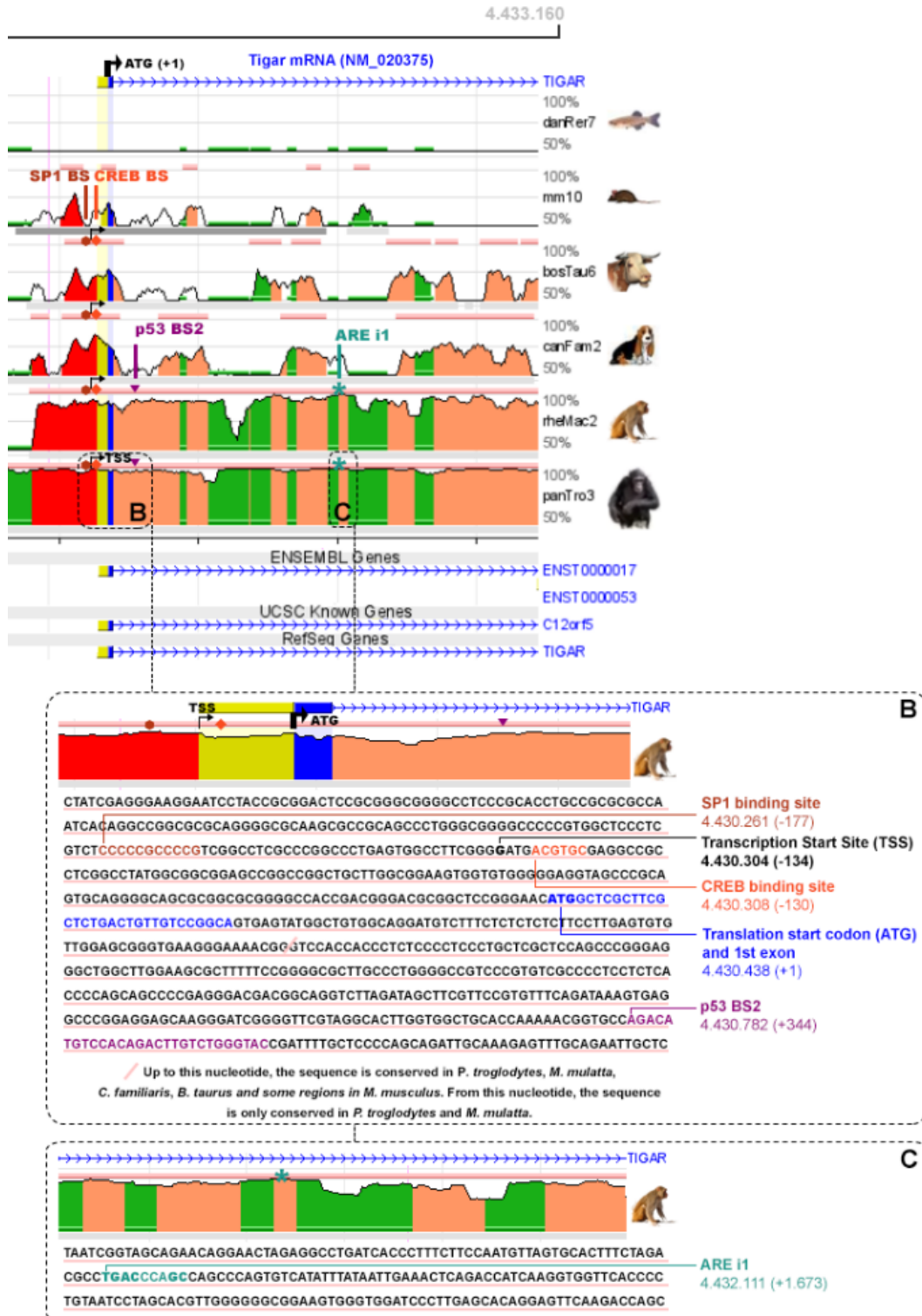
represented by the big blue asterisks, whereas small asterisks indicate TGAGnnnGC motifs. Besides, the conservation is indicated by horizontal red bars on the top of the sequence that corresponds to each specie.

ARE 4 is located at -6.103 bp and it is conserved in *Pan troglodytes*, whereas ARE 3 is located at -3.145 bp and it is conserved in *Rhesus macaque (Macaca mulatta)* and *Canis familiaris* (**Figure 59**). AREs 1 and 2 were identified at -1.500 and -1.107 bp, respectively, being ARE 2 conserved in *Pan troglodytes* and *Rhesus macaque* and ARE 1 only in *Pan troglodytes* (**Figure 59, Box A**). No AREs were detected close to the transcription start site (TSS), where the SP1 and CREB binding boxes are located (76,77): the SP1 response element is just before the TSS (-177 bp) whereas the CREB binding sequence is just after it (-130 bp). Both regulatory elements are conserved in *Canis familiaris*, *Bos taurus*, *Rhesus macaque* and *Pan troglodytes* (**Figure 59, Box B**), suggesting important roles for these transcription factors in the control of *TIGAR* expression.

The functional p53 binding site 2 (BS2) (3), is located in the first intron, at +344, and it is conserved in *Pan troglodytes* and *Rhesus macaque* (**Figure 59, Box B**). ARE i1 is located at +1.673 bp in the first intron and it is conserved in *Pan troglodytes* and *Rhesus macaque* (**Figure 59, Box C**) like the p53 BS2.



Figure 59. Study of human *TIGAR* promoter and first intron with ECR Browser. ECR Browser (available at <http://ecrbrowser.dcode.org>) (182) was used to analyse the sequence from 4.423.165 to 4.433.160 bp of human chromosome 12. The sequence was compared to the genome of *Pan troglodytes* (panTro3), *Rhesus macaque* (rheMac2), *Canis familiaris* (canFam2), *Bos taurus* (bosTau6), *Mus musculus* (mm10) and *Danio rerio* (danRer7). The image provided by ECR Browser has been modified to indicate the important elements for the study of antioxidant response elements (AREs) within *TIGAR* promoter and first intron. A legend is provided with all the details. Three additional boxes are used to zoom in **(A)** a region of *TIGAR* promoter in which two conserved AREs are found, **(B)** the region containing the minimal promoter with SP1, CREB and p53 binding sites and **(C)** the intronic region containing a conserved ARE. ➤ *Figure continued on next page.*



2. Regulation of *TIGAR* expression by Nrf2 chemical inducers in HeLa cells

With the aim of inducing Nrf2 in HeLa cells, we reviewed the Nrf2 activators available and found that several compounds, most of them derived from natural products and used as additives in food, have the capacity to induce the dissociation of Nrf2 from KEAP1. These compounds are usually electrophiles which interact with the cysteine residues of KEAP1 and induce a change on its conformation (141). Another strategy that can be used to induce Nrf2 is the treatment with oxidant molecules. In the first experiments of this thesis, and also in previous thesis of the group (184), we tried to modulate *TIGAR* levels by treating cells with H₂O₂ and tBHP with no conclusive results due to high inter- and intra-experimental variability of these molecules.

Tert-butyl-hydroquinone (tBHQ) is a specific Nrf2 inducer that interacts with KEAP1 cysteines, liberating Nrf2 and allowing its translocation to the nucleus (141,146). The treatment of HeLa cells with 50 μM tBHQ for 4 h resulted in increased translocation of Nrf2 to the nucleus (**Figure 60A**). Considering previous results which had reported the differential response of cancer cells to Nrf2 inducers depending on FBS concentration (185), HeLa cells were exposed to tBHQ at the conditions of 10% FBS (referred to as + *FBS*) and 0% FBS (referred to as - *FBS*). Immunofluorescence analysis revealed that Nrf2 translocated to the nucleus in response to tBHQ in a dose-dependent manner in the presence of FBS (**Figure 60B, upper panel**), whereas Nrf2 was exclusively cytoplasmatic in the absence of FBS, both in control and in tBHQ-treated cells (**Figure 60B, lower panel**). The western blot analysis of protein levels in tBHQ-treated cells showed that in complete medium tBHQ increased both *TIGAR* and *G6PD* protein levels, although *TIGAR* was only significantly increased by 50 μM tBHQ (**Figure 60C,D**). Nrf2 protein levels were not modified by tBHQ (**Figure 60D**). Interestingly, *G6PD* and *TIGAR* protein levels were equal in 50 μM tBHQ-treated cells and in control cells in serum-free conditions (**Figure 60D**). Analysis of *G6PD* and *TIGAR* expression should be performed to determine whether the slight increases observed at the protein levels are consequence of increased transcription of the genes. In parallel to the protein analysis, the antioxidant potential of tBHQ was assessed by measuring ROS levels by flow cytometry with the CellROX Green probe and a significant decrease in ROS was detected in 50 μM tBHQ-treated cells (**Figure 60E**), thus confirming that the Nrf2-orchestrated transcriptional program effectively decreased oxidative stress.

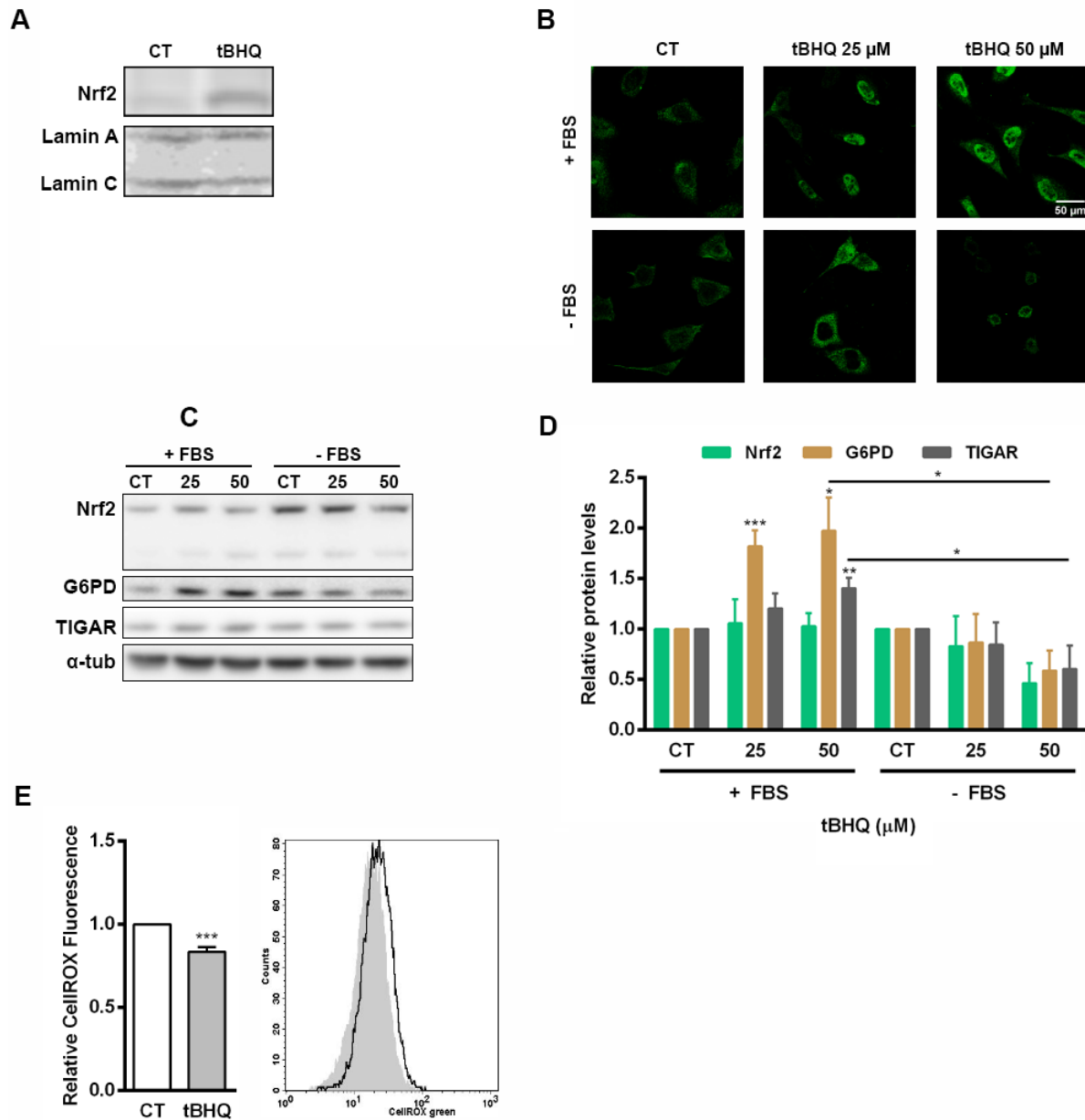


Figure 60. Regulation of Nrf2 and TIGAR by tBHQ. HeLa cells were treated with tBHQ at the indicated doses for 4 h in the presence or absence of 10% FBS. **(A)** Western blot analysis of nuclear fractions of HeLa cells treated with 50 μM tBHQ in the presence of 10% FBS. **(B)** Immunofluorescence analysis of Nrf2 in by Alexa488-conjugated secondary antibodies. Nuclear staining could not be detected in this experiment. **(C)** Representative images of western blot analysis of Nrf2, G6PD and TIGAR. α-tubulin was used as endogenous control. **(D)** Quantification of western blot analyses of cells treated at the mentioned conditions. **(E)** ROS quantification by CellROX Green in tBHQ-treated cells. Raw data of fluorescence peaks from a representative experiment is shown. Data are expressed relative to untreated cells (CT) ± SEM (D: n=4 in +FBS and n=3 in -FBS, E: n=3 with duplicates, *P < 0.05, **P < 0.01, ***P < 0.001).

To determine if the increase in TIGAR protein levels was exclusive to tBHQ or could be reproduced by other Nrf2 inducers, we treated HeLa cells with dimethyl fumarate (DMF) and sulforaphane (SFN), which are known to favour Nrf2 dissociation from KEAP1 (141,146). Cells were analysed at two different time points (4 and 24 h) by RT-qPCR and western blot. Western blot analysis of Nrf2 and TIGAR revealed significantly increased Nrf2 levels by 5 and 20 μ M SFN with no modulation of TIGAR protein levels (Figure 61A). At 24 h, results showed a similar modulation of these proteins (Figure 61D). In the same western blot analysis, no modulation of either Nrf2 or TIGAR protein levels was observed in cells treated with DMF at any of the times analysed (Figure 61A,D). In the RT-qPCR analysis, SFN was observed to cause a slight increase in the expression of the three genes at 4h after treatment (Figure 61B), which was exacerbated at 24 h (Figure 61E). 20 μ M DMF treatment increased the expression of *Nrf2*, *NQO1* and *TIGAR* both at 4h and 24 h (Figure 61C,F). Inhibition of transcription by Actinomycin-D (Act-D) prevented the induction of the three genes after DMF treatment (Figure 61C,F), confirming that the upregulation of *TIGAR* in response to the Nrf2 inducer DMF is transcription-dependent.

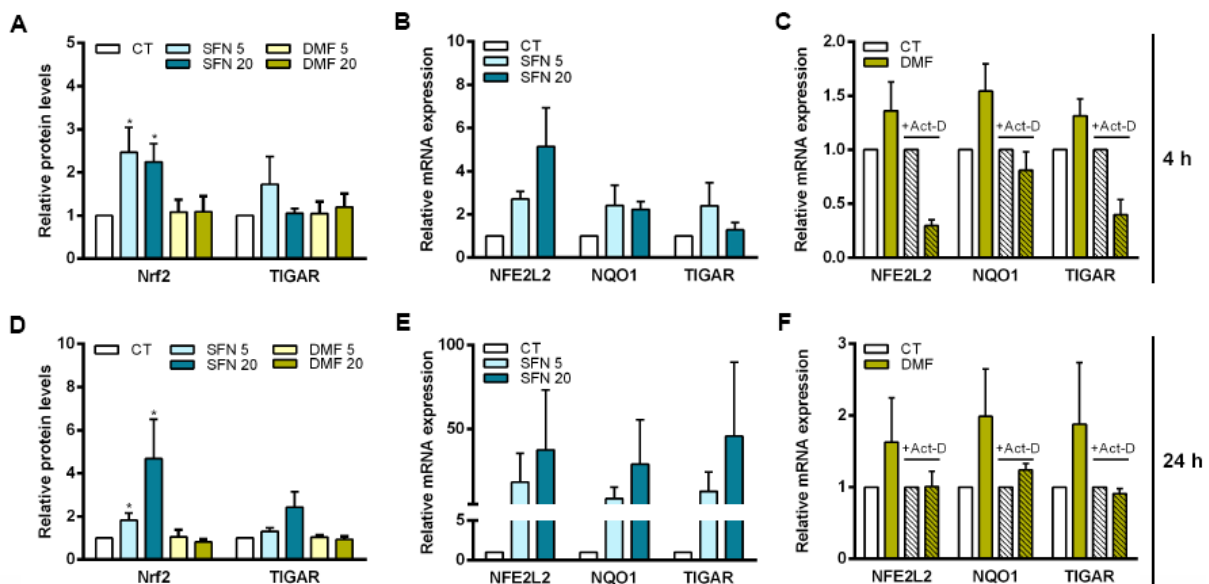


Figure 61. Analysis of Sulforaphane and DMF effects on *NFE2L2*, *NQO1* and *TIGAR* expression. HeLa cells were treated for 4 h (A-C) or 24 h (D-F) with the indicated doses of Sulforaphane (SFN) or Dimethyl fumarate (DMF). (A, D) Western blot analysis of Nrf2 and TIGAR in SFN and DMF-treated cells for (A) 4 and (D) 24 h. (B, E) RT-qPCR analysis of *NFE2L2* (Nrf2), *NQO1* and *TIGAR* in SFN-treated cells for (B) 4 and (E) 24 h. (C, F) HeLa cells were pre-treated with Actinomycin-D (Act-D) for 4 h and subsequently treated with DMF for (C) 4 and (F) 24 h. The expression of *NFE2L2* (Nrf2), *NQO1* and *TIGAR* was analysed by RT-qPCR. Data are presented as the mean fold change relative to untreated cells (CT) \pm SEM (n=3, *P < 0.05).

In summary, the results obtained with oxidant and antioxidant molecules pointed out a relation between Nrf2 and TIGAR, although several important questions remained unsolved. One of the most important issues was to determine if Nrf2 exerted a direct transcriptional control on *TIGAR* gene. Considering the presence of potential AREs in TIGAR promoter and the positive results obtained with DMF and SFN at the mRNA level, we proceeded to modulate Nrf2 through overexpression and siRNA experiments.

3. Regulation of TIGAR by *NFE2L2* expression in HeLa cells

The capacity of Nrf2 to control *TIGAR* mRNA levels was assessed by inhibition of the expression of the Nrf2 coding gene, *NFE2L2*, through siRNA as a first approach. Transfection of 100 nM *NFE2L2*-targeting siRNA on HeLa cells showed decreased expression of *NFE2L2*, *G6PD*, *NQO1* and *TIGAR* (Figure 62A). Accordingly, the protein levels of Nrf2, G6PD and TIGAR were significantly decreased by Nrf2 siRNA at 72 h post-transfection (Figure 62B,C). The gene in which the inhibition was more pronounced was *NFE2L2*, followed by the classical Nrf2 targets *NQO1* and *G6PD*, and *TIGAR*, the latter showing 40% decreased expression levels compared to control cells.

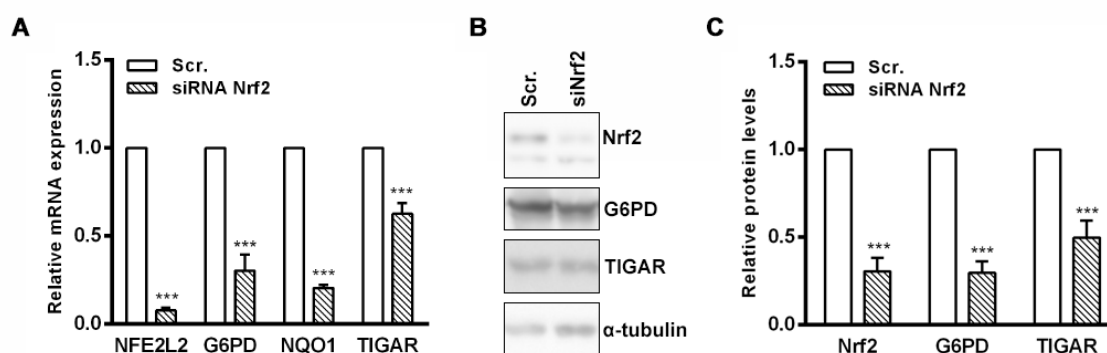


Figure 62. TIGAR modulation by Nrf2 inhibition in HeLa cells. HeLa cells were transfected with 100 nM *NFE2L2*-targeting siRNA and subsequently analysed after 72 h. **(A)** RT-qPCR analysis of *NFE2L2* (Nrf2), *G6PD*, *NQO1* and *TIGAR*. **(B)** Images representative of a western blot analysis of Nrf2, *G6PD* and *TIGAR*. **(C)** Quantification of independent western blot analyses. Data are presented as the mean fold change relative to the cells transfected with scrambled siRNA (Scr.) \pm SEM (A: each gene was analysed at least in 4 independent experiments, B: n=7, ***P < 0.001).

A single experiment with triplicates was performed by combining Nrf2 inhibition with tBHQ. Cells were transfected with *NFE2L2*-targeting siRNA and received a single dose of 50 μ M tBHQ 20 h after transfection. The expression of *NFE2L2*, *G6PD* and *TIGAR* was analysed at 24, 48 and 72 h after transfection (Figure 63). *NFE2L2*-targeting siRNA effectively decreased the expression of *NFE2L2*, *G6PD* and *TIGAR* compared to the scrambled siRNA, as it is indicated by red arrows (Figure 63). Treatment of tBHQ (yellow columns) did not affect the mRNA levels of any of the genes at basal conditions, but it counteracted the inhibitory effect of *NFE2L2*-targeting siRNA, as it is indicated by grey arrows. This effect was partial in the cases of *NFE2L2* and *G6PD*, as gene expression in transfected cells treated with tBHQ-treated cells never reaches the expression levels in scrambled cells, but it was more pronounced in the case of *TIGAR*, in which treatment of tBHQ completely prevented the decrease in mRNA levels caused by *NFE2L2*-targeting siRNA (Figure 63).

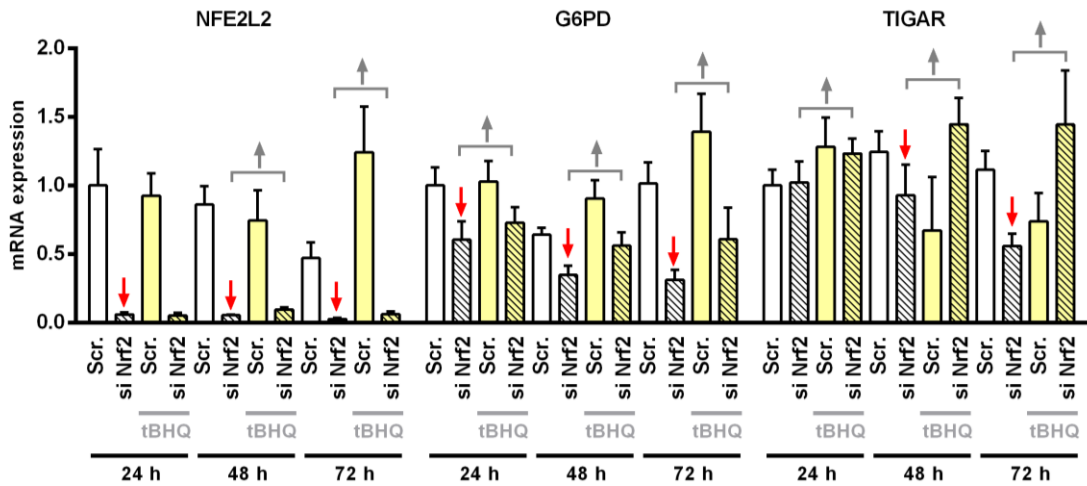


Figure 63. Effect of tBHQ in Nrf2-inhibited cells. HeLa cells were transfected with 100 nM *NFE2L2*-targeting siRNA for 24, 48 or 72 h and co-treated with tBHQ during the last 4 h. RT-qPCR analysis of *NFE2L2*, *G6PD* and *TIGAR* expression was performed. Data are expressed relative to Scrambled cells at 24 \pm SD of triplicates from a single experiment.

As a complementary strategy for the evaluation of the relation between Nrf2 and TIGAR in HeLa cells, the expression of *NFE2L2* was increased by transfecting cells with a pcDNA3 plasmid containing the Nrf2 coding sequence. *NFE2L2* overexpression significantly increased *NFE2L2*, *G6PD*, *NQO1* and *TIGAR* mRNA levels (Figure 64A). Western blot analysis confirmed Nrf2 upregulation and the resulting increases in the levels of TIGAR and G6PD (Figure 64B,C). It is important to note that increased Nrf2 protein levels were clearly evidenced in the western blot images (Figure 64B), whereas upregulation of G6PD and TIGAR were difficult to see in the blots and were not evidenced until quantification of western blot images was performed (Figure 64C). Overall, Nrf2 was proved to modulate the expression and protein levels of TIGAR in parallel with known Nrf2 targets such as G6PD and NQO1 in HeLa cells. These cells were used to characterise the direct binding of Nrf2 to *TIGAR* promoter, a set of *in silico* analyses and *in vitro* experiments that are deeply commented at the end of this chapter.

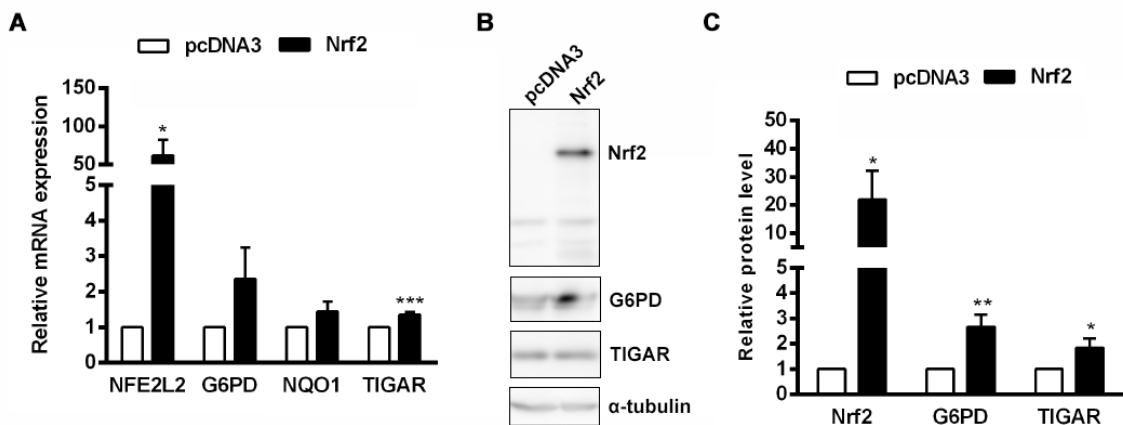


Figure 64. TIGAR modulation by Nrf2 overexpression in HeLa cells. HeLa cells were transfected with a pcDNA3 plasmid coding for *NFE2L2* gene (Nrf2) and subsequently analysed after 24 h. (A) RT-qPCR analysis of *NFE2L2*, *G6PD*, *NQO1* and *TIGAR*. (B) Representative western blot images of Nrf2, G6PD and TIGAR. (C) Quantification of independent western blot analyses. Data are presented as the mean fold change relative to scrambled (Scr.) siRNA-transfected cells \pm SEM (each gene was analysed at least in 4 independent experiments, *P < 0.05, **P < 0.01, ***P < 0.001).

4. TIGAR and Nrf2 in NSCLC

4.1. A model with pathological relevance: NSCLC

Nrf2 activation is specially important in those tumors presenting a highly oxidative environment, which is the case of the lung. In these tissues, stress response pathways must be tightly controlled to allow cells to tolerate high levels of ROS. Several mechanisms have been described in tumor cells which allow them to adapt to the increased stress signals. According to the data available in cBioportal, non-small cell lung cancer (NSCLC) is the second type of cancer in which Nrf2 coding gene, *NFE2L2*, is more altered (10% of the patients suffering from this type of cancer), only preceded by esophageal squamous cell carcinoma (Figure 65A). Lung cancer is also the second type of cancer in which *KEAP1* shows more alterations (15% of the patients), preceded by nerve sheath tumor (Figure 65B). The frequency of alterations in either *NFE2L2* or *KEAP1* in NSCLC patients is of 25%, which indicates that mutations in these genes are mutually exclusive (Figure 65C). In the light of these results, we decided to study TIGAR modulation by Nrf2 in lung cancer.

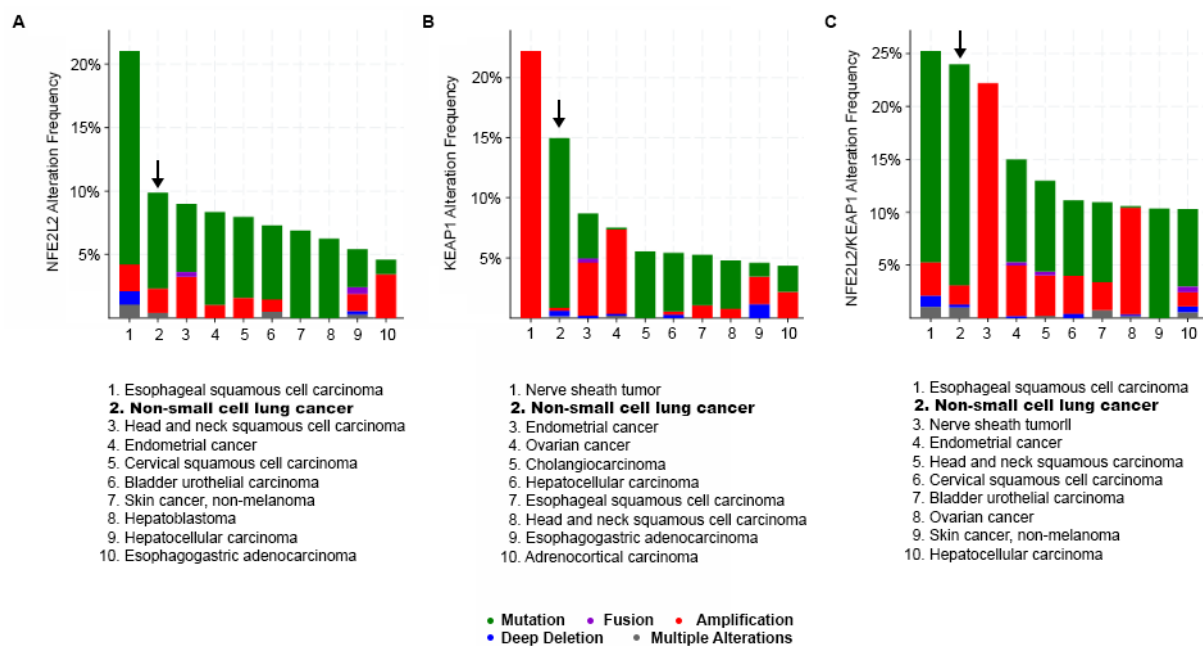


Figure 65. Frequency of genetic alterations in *NFE2L2* and *KEAP1* in human cancer. Graphs corresponding to the ten types of cancer with more alterations in (A) *NFE2L2* (Nrf2), (B) *KEAP1* or (C) *NFE2L2* and *KEAP1*. cBioPortal (162,163) was used to determine the frequency of genetic alterations detected in *NFE2L2* (Nrf2) and *KEAP1* in different human cancers. All Pan-Cancer/The Cancer Genome Atlas (TCGA) studies were included in the analysis. For those cancer types in which a Pan-Cancer/TCGA study was not available, at least one study from another project was included. Graphs show the percentage of patients with alterations of a given gene in each type of cancer.

Alterations in the KEAP1/Nrf2 pathway have been described to contribute to the pathogenesis of NSCLC and are being explored as potential therapeutic targets (186). TCGA Research Network has made a great contribution to the understanding of the molecular alterations of tumors from different origins by genetically profiling them and determining genetic signatures associated to each malignancy. NSCLC is a heterogeneous group of diseases among which adenocarcinoma (ADC) is the most common, followed by lung squamous cell carcinoma (SQCC). The analysis of ADC and SQCC data available in TCGA through cBioportal revealed that alterations in the *NFE2L2/KEAP1/CUL3* pathway were detected in 19,2% of ADC patients (**Figure 66A**) and 30% of SQCC patients (**Figure 66B**). Alterations in these genes showed mutual exclusivity (**Figure 66A,B**) given that alterations in more than one of these genes were rarely found in patients. These two types of cancer presented different distribution of alterations in the pathway, being KEAP1 the most altered in ADC (**Figure 66A**), whereas in SQCC the most altered gene was *NFE2L2* (**Figure 66B**). Besides, the status of PIK3CA and *TP53*, important drivers of NSCLC, was also analysed. Amplification of PIK3CA and mutations in *TP53* were more frequent in SQCC than in ADC patients (**Figures 8A,B**).

Important information can also be obtained from the analysis of the nature of alterations found in each gene. Missense mutations or deletions in *KEAP1* were frequent in ADC (**Figure 66A**), whereas *NFE2L2* amplification was the most frequent alteration in SQCC (**Figure 66B**). Regarding TIGAR, it was found more altered in SQCC than in ADC, being amplification the most common event in the 4% of SQCC patients with alterations in this gene (**Figure 66B**). Overall, these data indicated that the Nrf2 signalling pathway is increased in both NSCLC subtypes, but the mechanisms involved are different. A summary of the alterations that lead to Nrf2 constitutive activation in these tumours is provided in **Figure 67**.

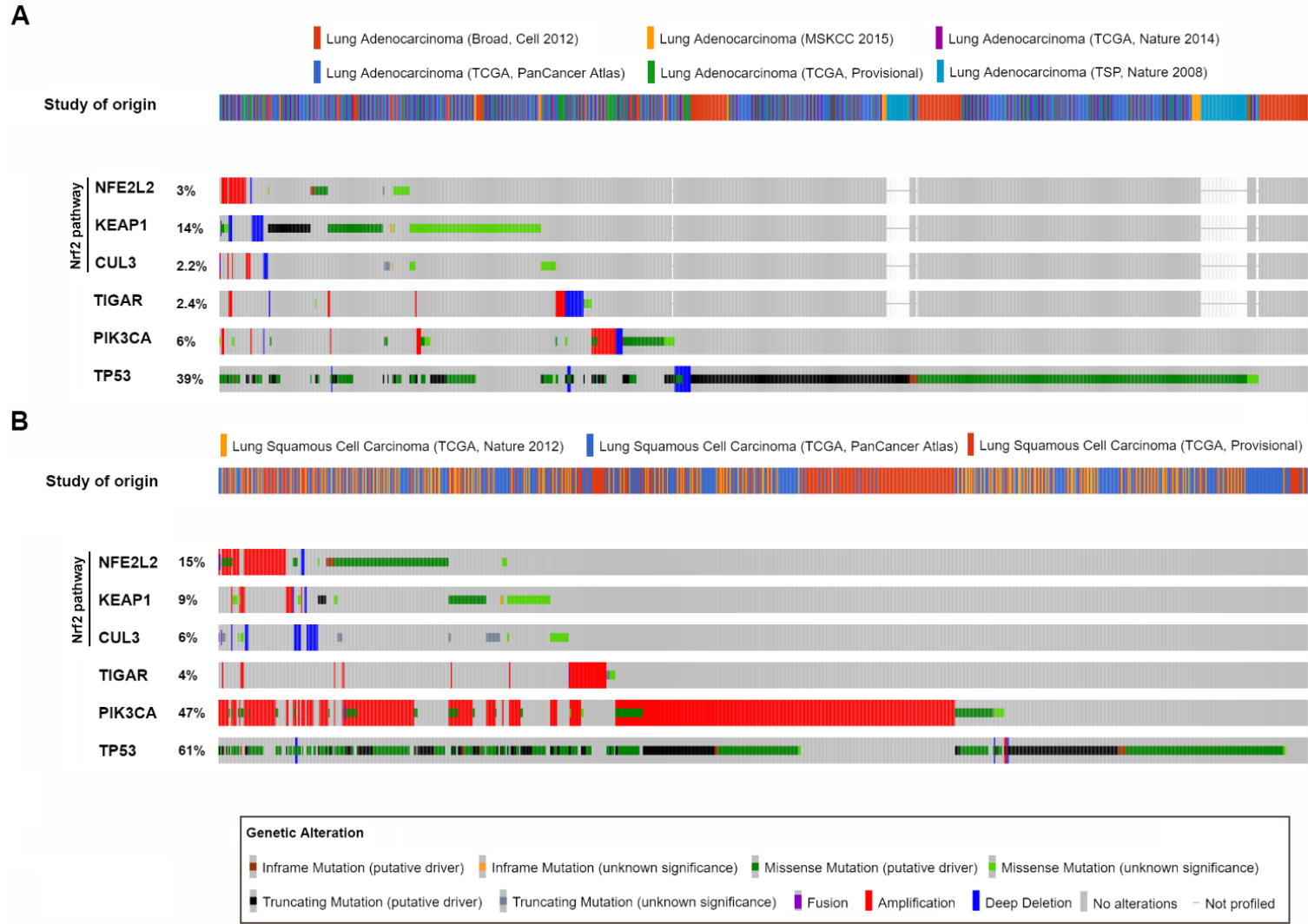


Figure 66. Frequency of genetic alterations in the Nrf2 pathway, TIGAR, PIK3CA and TP53 in NSCLC. cBioPortal (162,163) was used to determine the genetic alterations in (A) ADC and (B) SQCC each of these genes from all Pan-Cancer studies (TCGA). For those cancer types in which a Pan-Cancer study was not available, at least one study from another project was included. A legend is provided to identify each type of genetic alterations. This analysis does not include mRNA expression data.

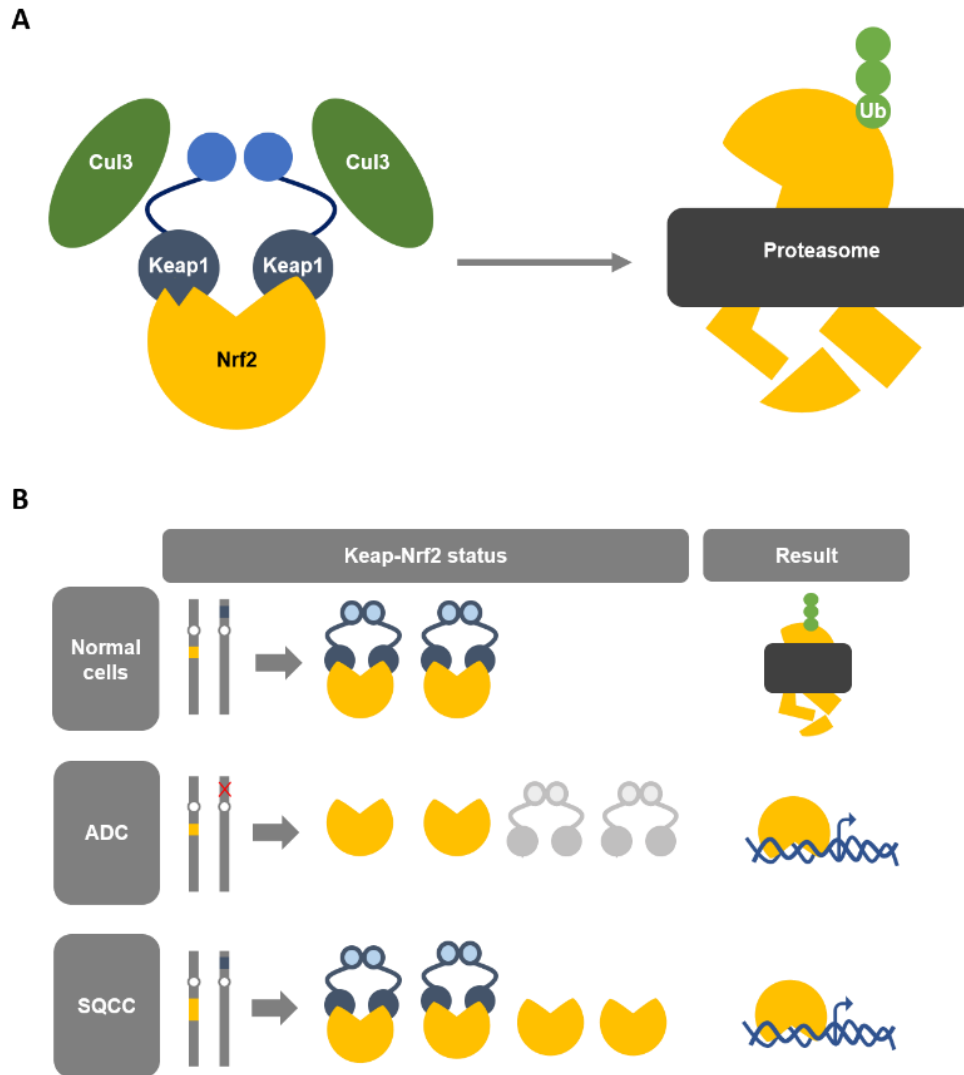


Figure 67: Molecular mechanisms driving Nrf2 overactivation in ADC and SQCC. (A) General mechanism for Nrf2 degradation in normal cells: KEAP1 binding to Nrf2 allows the ubiquitination of Nrf2 by Cul3 ubiquitin ligase and subsequent degradation in the proteasome. **(B)** Representation of the disbalance between Nrf2 and KEAP1 in lung adenocarcinoma (ADC) and lung squamous cell carcinoma (SQCC). In ADC, loss of *KEAP1* increases Nrf2 activity, whereas in SQCC increased Nrf2 activity is driven by *NFE2L2* overexpression.

4.2. TIGAR regulation by Nrf2 in NSCLC

4.2.1. Characterisation of the A549, H460 and H1299 cell lines

Three NSCLC cell lines with different genetic background were used for the experiments: A549, H460 and H1299. A549 and H460 are both ADC cell lines, whereas H1299 is a SQCC cell line (**Figure 68**). Nrf2 basal levels are higher in A549 than in H460, where they are almost undetectable by western blot. In the SQCC H1299 cell line, Nrf2 levels are similar to those in H460. Proteasomal inhibition by MG-132 treatment resulted in the accumulation of Nrf2 protein in all of them (**Figure 68A**). On the other hand, KEAP1 levels are undetectable in ADC cell lines, whereas this protein is present at basal conditions in H1299 (**Figure 68A**). Proteasomal inhibition results in increased KEAP1 levels in ADC cells, suggesting that in normal conditions this protein is rapidly degraded and cannot retain Nrf2 in the cytoplasm as it does in SQCC cells, in which MG132 does not affect KEAP1 levels. The differences in Nrf2 and KEAP1 basal levels are in accordance with the analysis from TCGA studies (**Figures 66,67**).

Regarding p53, western blot also confirmed the lack of *TP53* expression in H1299 and revealed increased levels of this protein after proteasomal inhibition in ADC cell lines. It can be appreciated that high levels of TIGAR are present at basal levels in all cell lines regardless of p53 levels, with no alterations observed after treatment with MG132, suggesting that TIGAR is not degraded through the proteasome (**Figure 68**).

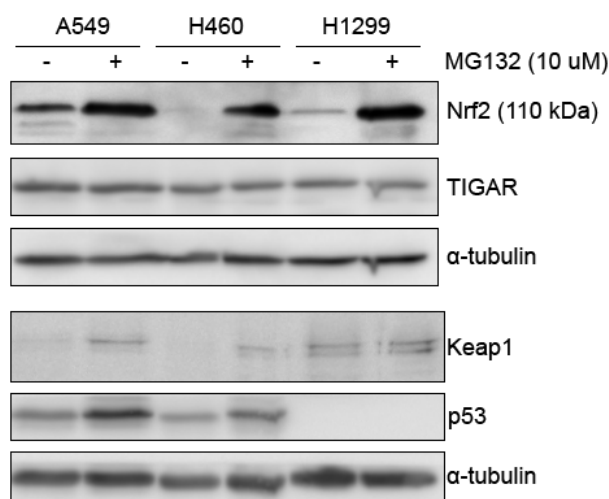


Figure 68: Basal protein levels in A549, H460 and H1299 cell lines. A549, H460 and H1299 cells were treated with the proteasome inhibitor MG-132 and analysed by western blot after 24 h. Western blot analysis of Nrf2, TIGAR, KEAP1 and p53 is shown. α-tubulin was used as endogenous control.

To determine the location of Nrf2 and p53 protein levels in these cells we performed immunofluorescence against these two proteins. Nrf2 was mainly localised in the nuclei of A549 cells and H460 cells, with a slight presence also in the cytoplasm of these cells. In H1299 cells, Nrf2 was uniformly distributed between nucleus and cytoplasm (**Figure 69**). It is relevant to note that, although Nrf2 protein levels were difficult to detect by western blot in H460 and H1299 cells, this protein was easily detected by immunofluorescence, confirming its presence in these cells and suggesting that different epitopes might be involved in the recognition of the protein by the polyclonal antibody used, which was the same in both techniques.

p53 was detected in the nucleus of A549 and H460 cells with no presence in the cytoplasm, and it was not detected in H1299 cells (**Figure 70**), consistent with western blot results (**Figure 68**).

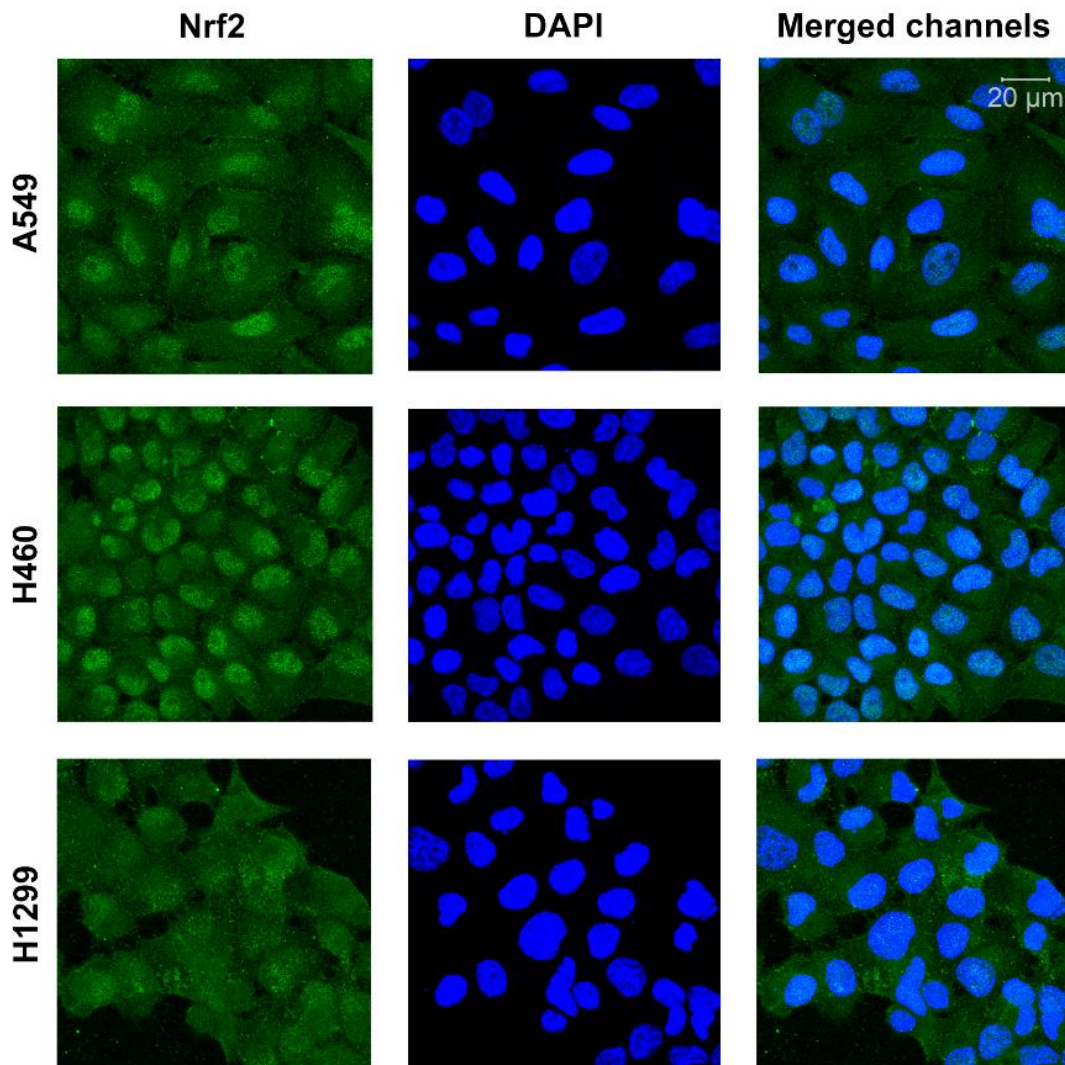


Figure 69: Immunofluorescence analysis of Nrf2 basal levels in A549, H460 and H1299 cell lines. Control A549, H460 and H1299 cells were fixed and immunofluorescence was performed. Nuclei were stained with DAPI (shown in blue). Nrf2 was immunodetected with a specific primary antibody and an anti-rabbit Alexa488-conjugated secondary antibody (shown in green).

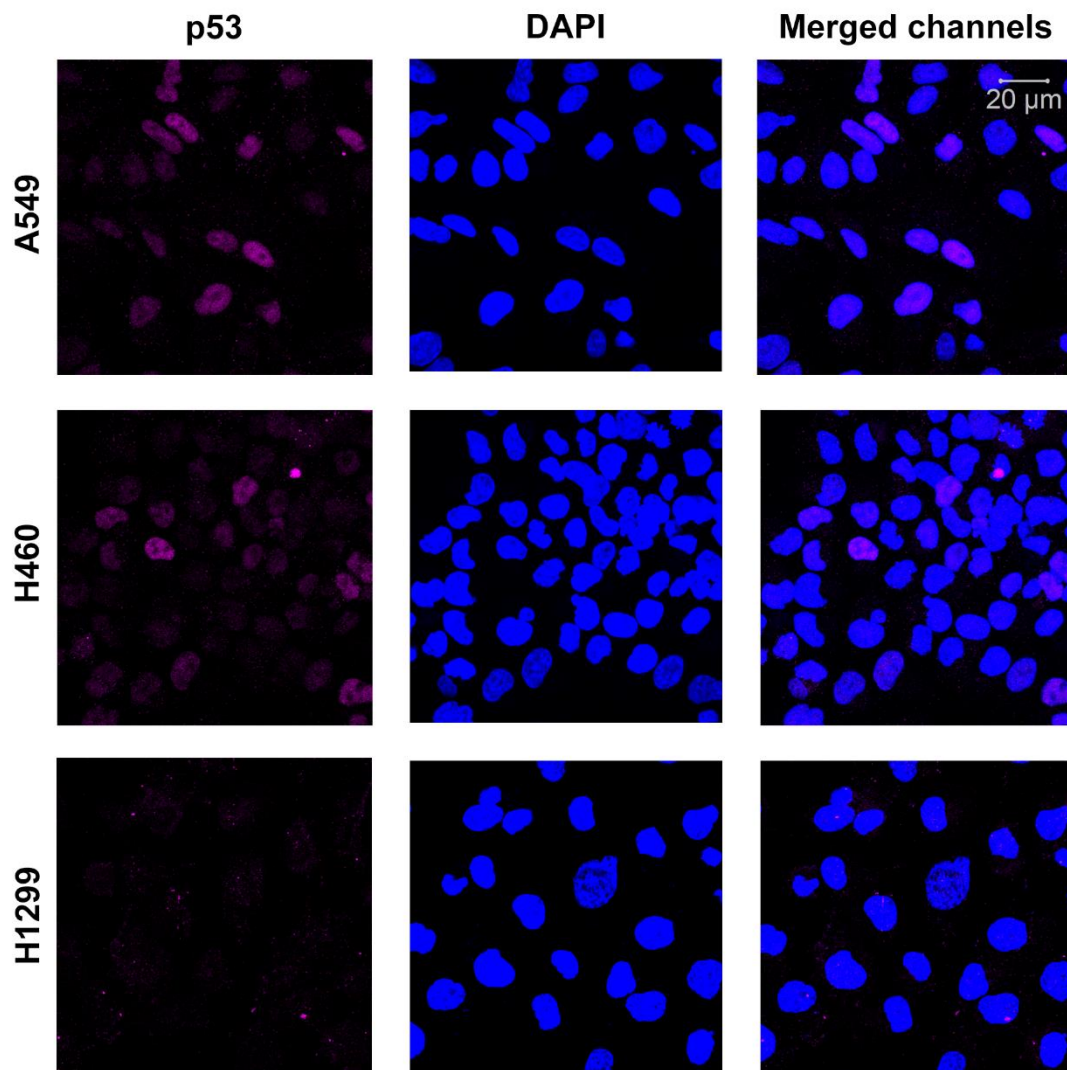


Figure 70: Immunofluorescence analysis of p53 basal levels in A549, H460 and H1299 cell lines. Control A549, H460 and H1299 cells were fixed and immunofluorescence was performed. Nuclei were stained with DAPI (shown in blue). p53 was immunodetected with a specific primary antibody and an anti-mouse Alexa488-conjugated secondary antibody (shown in magenta).

4.2.2. Effects of Nrf2 modulation on the expression of TIGAR in NSCLC cell lines

The low *KEAP1* expression in A549 and H460 cells makes them good models to study the effects of Nrf2 inhibition (142,187). A previous study analysed the effect of *NFE2L2* inhibition through three different siRNA in A549 cells with the aim of finding new Nrf2 target genes. The data from this study is available in Geoprofiles (accession number GSE28230) (142). In the publication in which this array was published, TIGAR was mentioned during the design of the study although there were any data informing about the effect of *NFE2L2* siRNAs on the expression of this gene. With the help of Dr. Annie Rodolosse (Institute for Research in Biomedicine, Barcelona), we reanalysed the data from the array and found that *TIGAR* mRNA levels were inhibited by one of the *NFE2L2*-targeting siRNAs used in that work, more specifically by HSS107130 siRNA, after 24 h of transfection. However, the other two siRNAs used did not decrease *TIGAR* expression, and one of them, HSS107128, even slightly increased the expression of the gene (Table III).

Gene	HSS107128	HSS107129	HSS107130
<i>NFE2L2 (Nrf2)</i>	18,75	25,69	15,86
<i>G6PD</i>	25,11	28,78	29,12
<i>HO-1</i>	18,74	18,17	16,07
<i>NQO1</i>	7,48	18,56	9,92
<i>TIGAR</i>	113,75	103,46	72,34

Table III: Identification of Nrf2 targets by microarray analysis. Re-analysis of data from the Geoprofiles array GSE28230 published by (142). A549 cells were transfected with three different *NFE2L2*-targeting siRNAs (HSS107128, HSS107129 and HSS107130) for 24 h and the expression of different genes was evaluated in a microarray. mRNA expression is presented as the percentage relative to cells transfected with scrambled siRNA. A reduction of at least 33% in the mRNA levels of a given gene in response to the three *NFE2L2*-targeting siRNAs was required for the gene to be considered an Nrf2 target. Genes meeting these conditions are shown in red. Grey colour indicates no modulation.

Two transfection procedures were performed to determine if TIGAR was controlled by the Nrf2 transcription factor: inhibition of *NFE2L2* expression through siRNA and overexpression of the gene with a pcDNA3 plasmid containing the whole *NFE2L2* coding sequence. Experiments were initiated with the A549 cell line to confirm the results obtained in the microarray analysis (Table III) and determine the effects of *NFE2L2*-targeting through siRNA on TIGAR protein levels. For all the experiments, the HSS107130 siRNA was used. More information regarding its target sequence can be found in Materials and Methods.

A time-course experiment with two siRNA concentrations was performed to analyse if *NFE2L2* silencing had a progressive effect on the expression of *NFE2L2* and Nrf2 target genes, and to determine an optimal end point for future experiments. Both 50 and 100 nM *NFE2L2*-targeting siRNA resulted in a significant decrease in *NFE2L2* mRNA levels at 24 and 48 h, which was maintained at 72 h. Accordingly, the expression of *G6PD* and *NQO1* were decreased by both doses of Nrf2 siRNA at all the times analysed. However, *TIGAR* mRNA levels were not decreased, and even a slight increase could be observed after *NFE2L2* inhibition, which statistically significant at 48 h and was maintained at 72 h (Figure 71). This effect was in accordance with the results obtained in the analysis of the Geoprofiles array (Table III) and seemed to indicate that Nrf2 exerted different control of *G6PD*, *NQO1* and *TIGAR* mRNA levels in A549 cells.

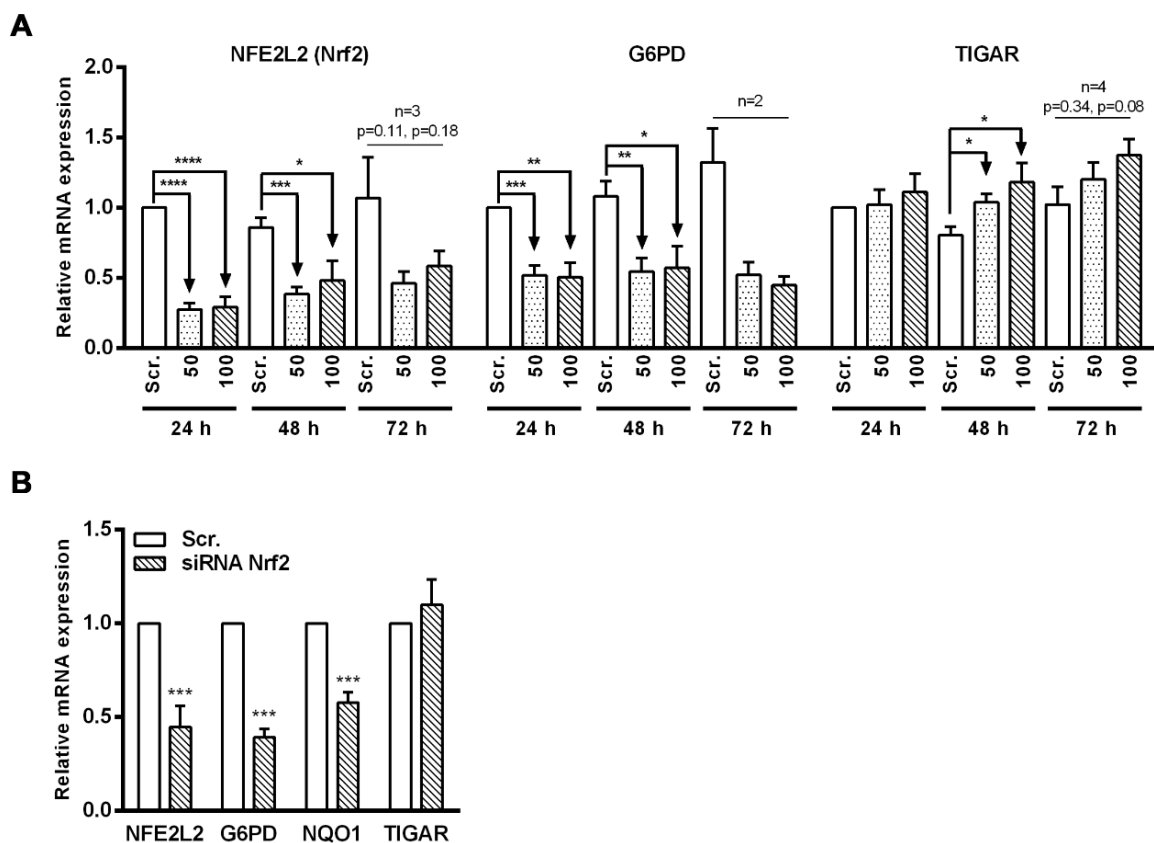


Figure 71. Modulation of *TIGAR* mRNA levels by Nrf2 inhibition in A549 cells. A549 cells were transfected with a *NFE2L2*-targeting siRNA and subsequently analysed at the indicated times. **(A)** RT-qPCR analysis *NFE2L2* (Nrf2), *G6PD* and *TIGAR* levels in A549 cells transfected with 50 and 100 nM *NFE2L2*-targeting siRNA for 24, 48 or 72 h. **(B)** RT-qPCR analysis *NFE2L2* (Nrf2), *G6PD*, *NQO1* and *TIGAR* in additional experiments performed at 72 h. Data are presented as the mean fold change relative to cells transfected with a scrambled siRNA (Scr.) \pm SEM (A: each gene was analysed at least in 3 independent experiments, B: each gene was analysed at least in 5 independent experiments, *P < 0.05, **P < 0.01, ***P < 0.001).

To better clarify the effect of Nrf2 inhibition on TIGAR we proceeded to analyse protein levels by western blot. Time-course analysis of protein levels revealed that Nrf2, HO-1 and TIGAR were significantly dropped from 24 h post-transfection to 72 h, when the levels were reduced by 50% compared to control cells (**Figure 72A-C**). In an analysis at 72 h with more samples, the levels of other proteins apart from the ones already mentioned above were determined. Nrf2, TIGAR, HO-1, G6PD and PCK-2 were all significantly downregulated at 72 h (**Figure 72D**).

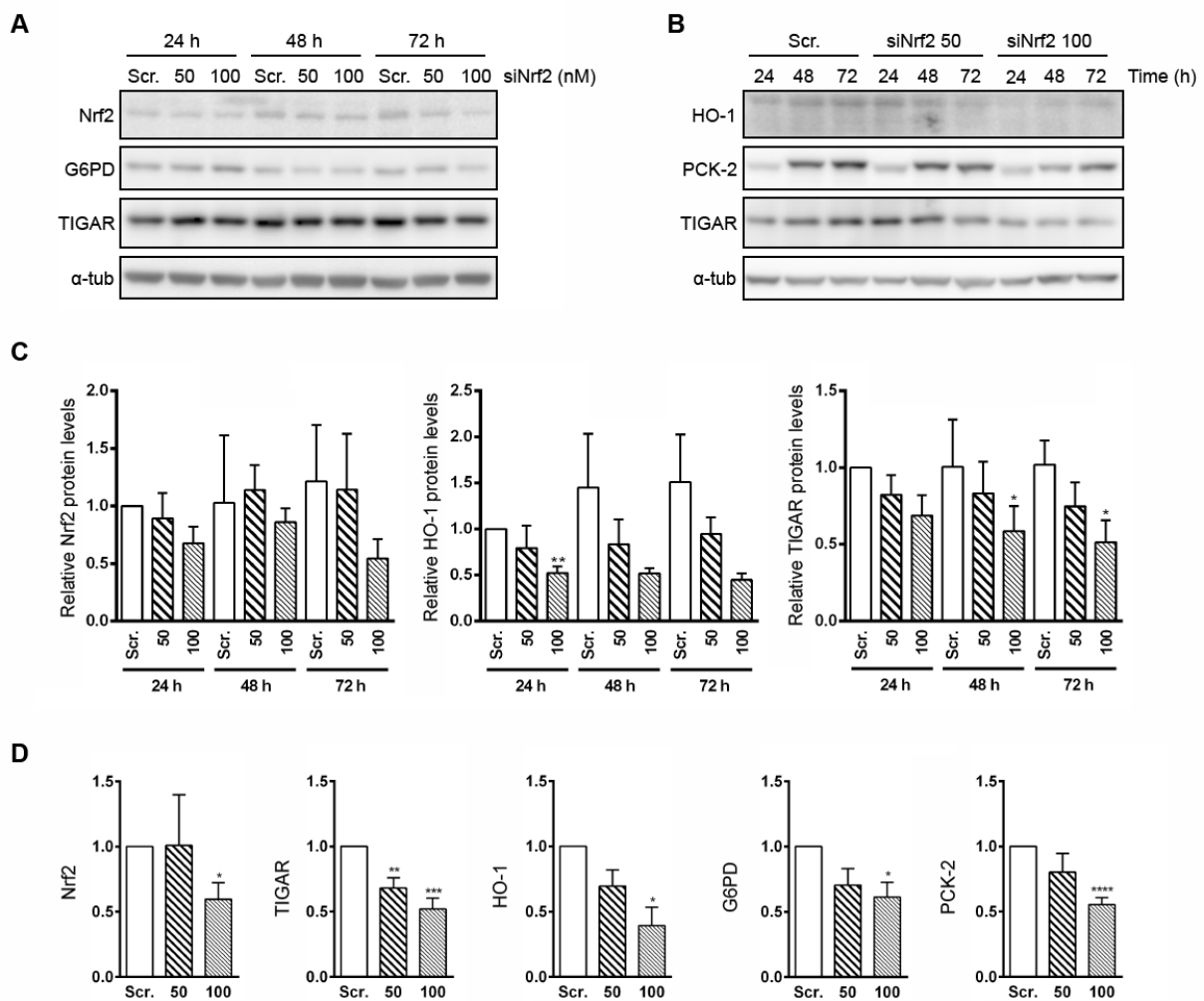


Figure 72. Modulation of TIGAR protein levels by Nrf2 inhibition in A549 cells. A549 cells were transfected with a *NFE2L2*-targeting siRNA and subsequently analysed at the indicated times. **(A)** Representative images of western blot analysis of Nrf2, G6PD and TIGAR after transfection with 50 or 100 nM *NFE2L2*-targeting siRNA at 24, 48 and 72 h. α -tubulin was used as endogenous control. **(B)** Representative images of western blot analysis of HO-1, PCK-2 and TIGAR. **(C)** Quantification of independent western blot analyses at the conditions mentioned in A and B. **(D)** Quantification of additional western blot analyses after 72 h of siRNA transfection. The levels of different proteins are shown. All data are presented as the mean fold change relative to cells transfected with scrambled siRNA (Scr.) \pm SEM (C: Nrf2 n=3, TIGAR n=5, HO-1 n=3, D: Nrf2 n=3, TIGAR n=7, HO-1 n=3, G6PD n=3, PCK-2 n=5, *P < 0.05, **P < 0.01, ***P < 0.001).

To determine the relevance of these findings, we performed the same experiments in another ADC cell line, H460. The inhibition of Nrf2 was proved by western blot (Figure 73A,B) but, surprisingly, neither G6PD nor TIGAR protein levels were found downregulated in the protein analysis (Figure 73A,B). The quantification of mRNA levels, however, revealed that the expression of *G6PD*, *NQO1* and *TIGAR*, as well as *NFE2L2* itself, was decreased by *NFE2L2*-targeting siRNA (Figure 73C), showing that Nrf2 suppression attenuated the expression of these genes without altering their protein levels. This response was just the opposite to what occurred in A549 cells.

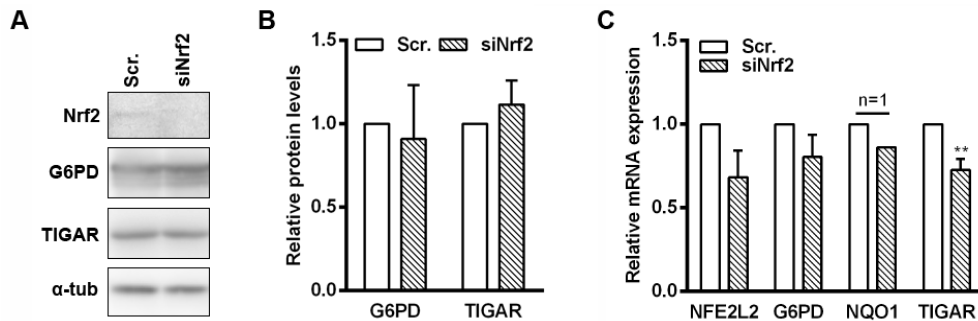


Figure 73. TIGAR modulation by Nrf2 inhibition in H460 cells. H460 cells were transfected with 100 nM *NFE2L2*-targeting siRNA and subsequently analysed after 72 h. **(A)** Western blot analysis of Nrf2, G6PD and TIGAR. **(B)** Quantification of independent western blot analyses. **(C)** RT-qPCR analysis of *NFE2L2* (Nrf2), *G6PD*, *NQO1* and *TIGAR*. Data are presented as the mean fold change relative to the cells transfected with scrambled siRNA (Scr.) \pm SEM (B: at least n=3, C: n=4, **P < 0.01).

Given that Nrf2 and p53 have shown to affect the expression of each other in previous studies (188), we transfected the SQCC H1299 cell line, which lacks *TP53*, with the *NFE2L2*-targeting siRNA. The aim of this experiment was to avoid interference of p53 in the regulation of *TIGAR* mRNA and protein levels in those cells in which Nrf2 was being suppressed. Western blot analyses of Nrf2-inhibited H1299 cells showed significant downregulation of G6PD protein levels with no changes in TIGAR levels (Figure 74A,B). On the other hand, RT-qPCR revealed decreased *NFE2L2* and *NQO1* expression, although *G6PD* mRNA levels were not modified and, surprisingly, *TIGAR* expression was significantly increased after Nrf2 elimination (Figure 74C).

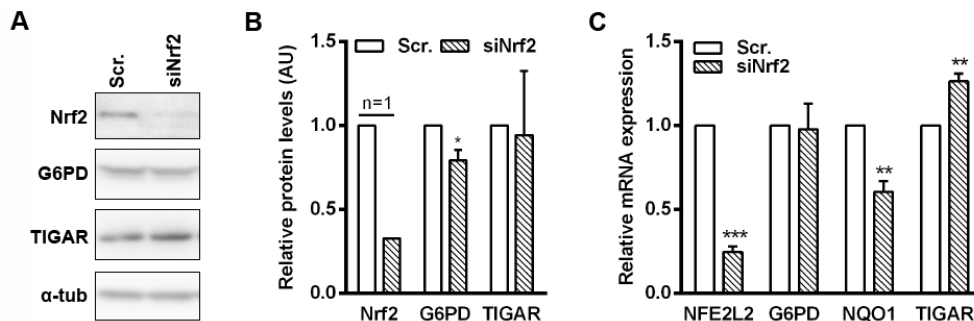


Figure 74. TIGAR modulation by Nrf2 inhibition in H1299 cells. H1299 cells were transfected with 100 nM *NFE2L2*-targeting siRNA and subsequently analysed after 72 h. **(A)** Western blot analysis of Nrf2, G6PD and TIGAR. **(B)** Quantification of independent western blot analyses. **(C)** RT-qPCR analysis of *NFE2L2* (Nrf2), *G6PD*, *NQO1* and *TIGAR*. Data are presented as the mean fold change relative to the cells transfected with scrambled siRNA (Scr.) \pm SEM (B: at least n=3, C: n=4, *P < 0.05, **P < 0.01, ***P < 0.001).

These results demonstrated that Nrf2 target genes can be independently regulated, as it is evidenced by the differential regulation of *G6PD* and *NQO1*. Furthermore, the increase in *TIGAR* mRNA levels in H1299 cells after Nrf2 suppression questioned our hypothesis of a compensatory effect driven by p53 when Nrf2 was eliminated. Thus, other mechanisms beyond Nrf2 and p53 must be controlling *TIGAR* expression in these cells. Nevertheless, the potential implication of p53 in the response of Nrf2-depleted A549 and H460 needed to be checked. One of the clues that led us to analyse p53 in our experiments was derived from the analysis of the Geoprofiles array GSE28230. Data indicated that the levels of *CDKN1A* (p21), a known p53 target gene, were found upregulated by the three *NFE2L2*-targeting siRNAs in A549 (Table IV), suggesting a potential role for p53 in the response to Nrf2 inhibition of these cells.

Gene	HSS107128	HSS107129	HSS107130
<i>TP53</i>	88,16	113,84	41,12
<i>CDKN1A</i> (p21)	208,74	168,53	143,66
<i>NOXA</i>	129,08	92,90	87,52

Table IV. Study of *TP53* modulation in a microarray analysis of Nrf2-inhibited cells. Re-analysis of data from the Geoprofiles array GSE28230 published by (142). A549 cells were transfected with three different *NFE2L2*-targeting siRNAs (HSS107128, HSS107129 and HSS107130) for 24 h and the expression of different genes was evaluated in a microarray. mRNA expression is presented as the percentage relative to cells transfected with scrambled siRNA. A reduction of at least 33% in the mRNA levels of a given gene in response to the three *NFE2L2*-targeting siRNAs was required for the gene to be considered an Nrf2 target (shown in red). During the re-analysis of this array, we established a second cutoff: an increase of at least 50% in mRNA expression was required to consider a gene overexpressed (shown in blue). Grey indicates no modulation.

We proceeded to analyse the expression of *CDKN1A* by RT-qPCR in our samples and found differences between cell lines. In A549, Nrf2 inhibition resulted in a slight increase in *CDKN1A* expression, whereas in H460 the mRNA levels of this gene were slightly decreased. Surprisingly, *CDKN1A* expression was significantly upregulated in H1299 after Nrf2 inhibition (Figure 75).

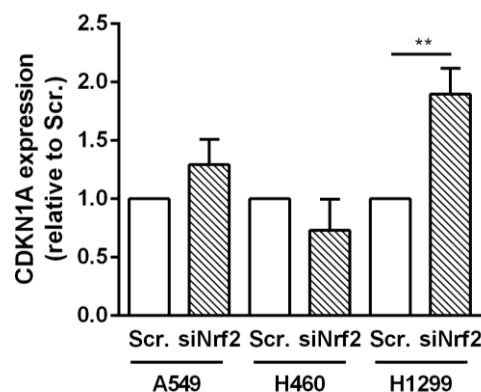


Figure 75: *CDKN1A* expression in A549, H460 and H1299 in response to Nrf2 inhibition. A549, H460 and H1299 cells were transfected with 100 nM *NFE2L2*-targeting siRNA and *CDKN1A* (p21) expression was determined by RT-qPCR after 72 h of siRNA transfection. Data are presented as the mean fold change relative to the cells transfected with scrambled siRNA (Scr.) \pm SEM (A549 n=7, H460 n=4, H1299 n=5, **P < 0.01).

However, immunodetection of p53 in Nrf2-inhibited A549 cells suggested decreased presence of this transcription factor in the nucleus (**Figure 76**), which would not support a potential activation of p53-dependent transcription of genes such as *CDKN1A* or *TIGAR*.

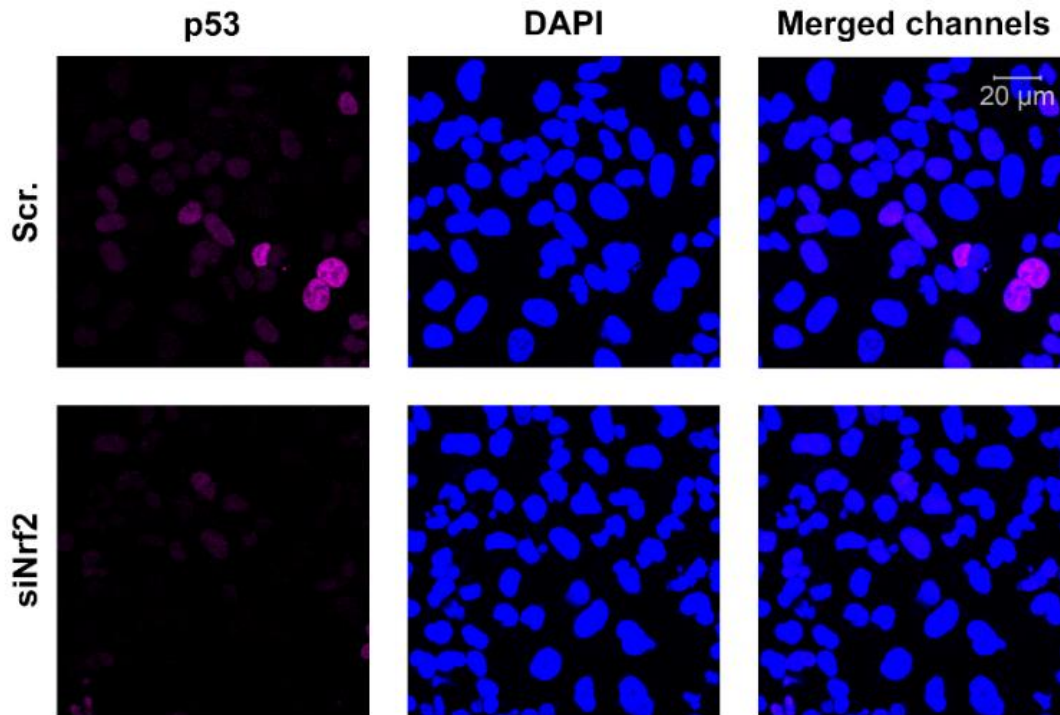


Figure 76: Immunofluorescence analysis of p53 in response to Nrf2 inhibition in A549 cells. A549 cells were transfected with 100 nM *NFE2L2*-targeting siRNA and after 72 h cells were fixed. p53 was detected with a specific primary antibody and an anti-mouse Alexa488-conjugated secondary antibody (shown in magenta). Nuclei were stained with DAPI (shown in blue).

In one hand, the fact that Nrf2 inhibition decreases *TIGAR* mRNA levels in H460 but not in A549 might be explained by a p53-driven compensatory effect in the latter cell line, which would be supported by increased *CDKN1A* expression. However, the finding that *CDKN1A* is upregulated in H1299 opens the possibility of the participation of other transcriptional regulators in the adaptation of ADC cells to Nrf2 depletion.

Given the variety of results obtained with Nrf2 siRNA in ADC cell lines, we wondered whether these cell lines would respond similarly to increased *NFE2L2* expression. Unfortunately, the levels of *NQO1*, *G6PD* and *TIGAR* were unaltered after *NFE2L2* overexpression both in A549 and H460 cells (Figure 77). This lack of response might be explained by high Nrf2 activity at basal conditions in these cells.

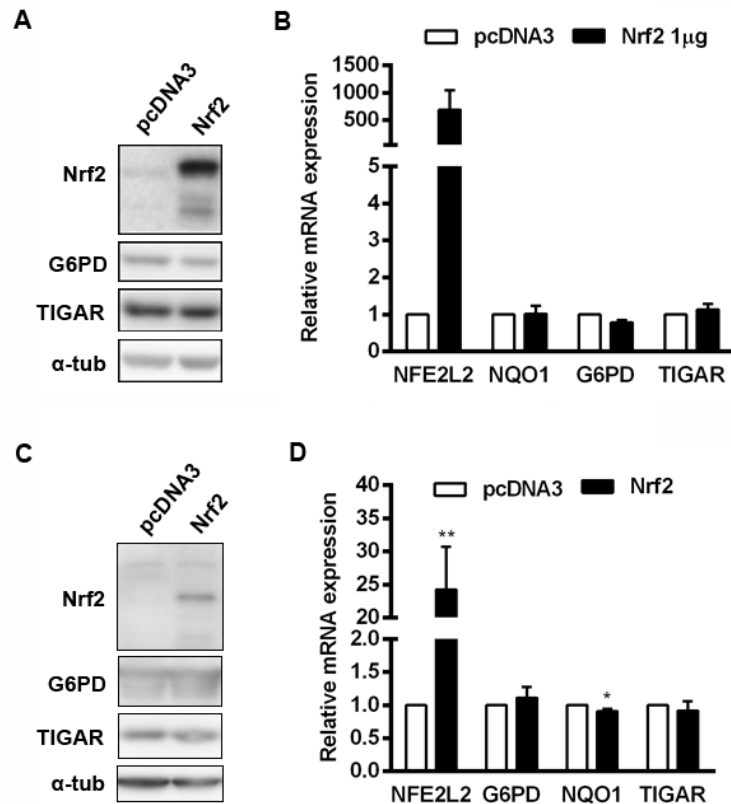


Figure 77. TIGAR modulation by Nrf2 overexpression in ADC cells. (A, B) A549 and (C, D) H460 cells were transfected with a pcDNA3 plasmid coding for *NFE2L2* (Nrf2) gene and subsequently analysed after 24 h. (A, C) Representative images of western blot analysis of Nrf2, G6PD and TIGAR. (B, D) RT-qPCR analysis of *NFE2L2* (Nrf2), *G6PD*, *NQO1* and *TIGAR*. Data are presented as the mean fold change relative to the cells transfected with a scrambled siRNA (Scr.) \pm SEM (B: n=3, D: n=5, *P < 0.05, **P < 0.01).

Despite the pathological interest of studying Nrf2 and TIGAR in NSCLC, the results with these cell lines were not concluding and we decided to continue the characterization of the binding of Nrf2 to TIGAR promoter in the model where we had obtained positive results in terms of expression, HeLa cells.

5. Cloning and functional characterisation of the human TIGAR promoter

5.1. Cloning of regulatory AREs located at TIGAR promoter

In the light of the *in-silico* analysis of the human TIGAR promoter, we decided to clone the three AREs closer to TIGAR translation start site, which are ARE 1, ARE 2 and ARE 3, plus the intronic are ARE i1. Several primers for the amplification of specific fragments by PCR were designed, as shown in **Figure 78**. PCR was performed from two bacterial artificial chromosomes (BACs) of human chromosome 12 provided by the Children's Hospital Oakland Research Institute (BAC numbers RP11-177D20 and RP11-74J21). Several constructions were obtained by PCR and cloned into TOPO TA vector. This cloning procedure is based on the recombination of 3'-A overhangs from PCR products with the TOPO vector, which has T-overhangs bound to topoisomerase I. A schematic representation of how this system works is provided in the Materials and Methods section. TOPO TA vectors include several restriction enzyme sites in their multicloning site that facilitate the subcloning of PCR fragments into the vectors of interest, which in our case were pGL3 Basic and pGL3 Promoter luciferase reporter vectors. **Figure 79** summarizes the cloning workflow performed for the obtention of the pGL3 constructs. Despite that several PCR fragments were obtained, only four constructs were finally cloned into luciferase reporter vectors due to difficulties in either the TOPO cloning of PCR constructs or the subsequent digestion and subcloning into pGL3 vectors. The four constructs obtained were named D, J, 8 and 15, according to the labelling of the bacterial colonies of origin (**Figure 79**). Constructs D and J contain ARE 1 and ARE 2 or only ARE 2, respectively, whereas constructs 15 and 8 contain ARE 1 and ARE 2 or only ARE 2, respectively, plus the TSS of TIGAR. The TSS comprises CREB1 and SP1 binding sites, which conform the minimal promoter of TIGAR. For this reason, constructs D and J were subcloned into pGL3 Promoter Vector, which has SV40 promoter, whereas constructs 8 and 15 were subcloned into pGL3 Basic Vector, which does not contain a promoter and, thus, requires the activation of TIGAR promoter to be expressed. In order to avoid alterations in the reading frame of the luciferase gene, constructs D and J were obtained with primer Reverse 2 and include the TSS but not the translation start codon (**Figures 78, 79**).

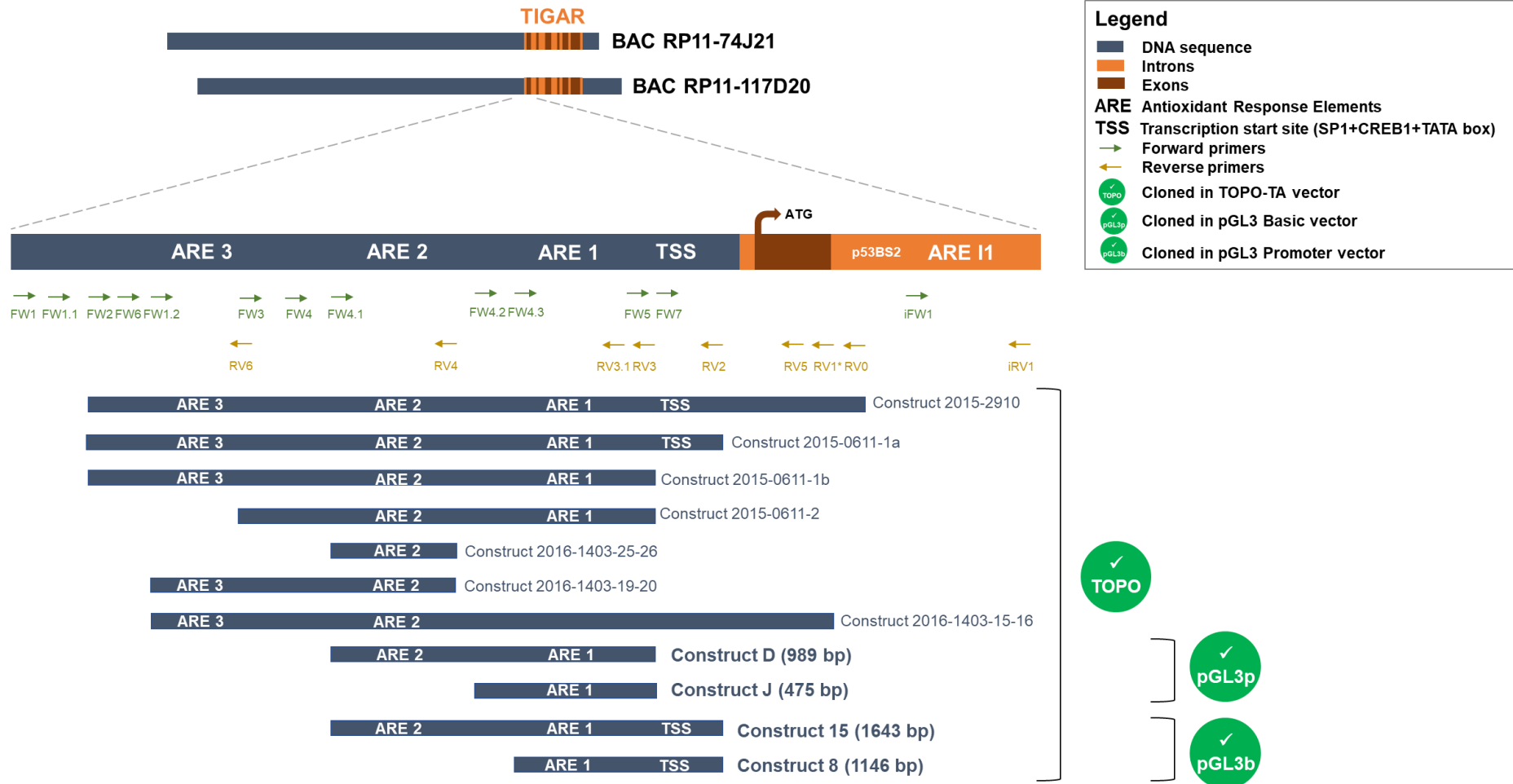


Figure 78. Primers designed for the amplification of TIGAR promoter and first intron. PCR were performed from two BACs of chromosome 12 using forward (FW) and reverse (RV) primers specific to the fragments of interest. The region of TIGAR promoter studied is shown in blue with AREs 1-3 and the transcription start site (TSS). The intronic region studied is shown in orange and contains ARE I1, p53 binding site 2 and the translation start codon, shown in brown. At the end of the process, several constructs had been cloned in TOPO vectors, whereas only four constructs (D, J, 15 and 8) were cloned in pGL3 vectors.

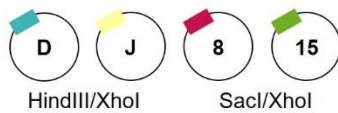
BAC RP11-74J21, BAC RP11-117D20

PCR: fragments of interest

TOPO TA cloning

- Digestion
- 5' vector dephosphorylation
- Ligation

pGL3 Basic cloning



- Digestion
- 5' vector dephosphorylation
- Ligation

pGL3 Promoter cloning

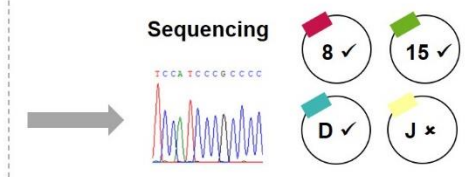
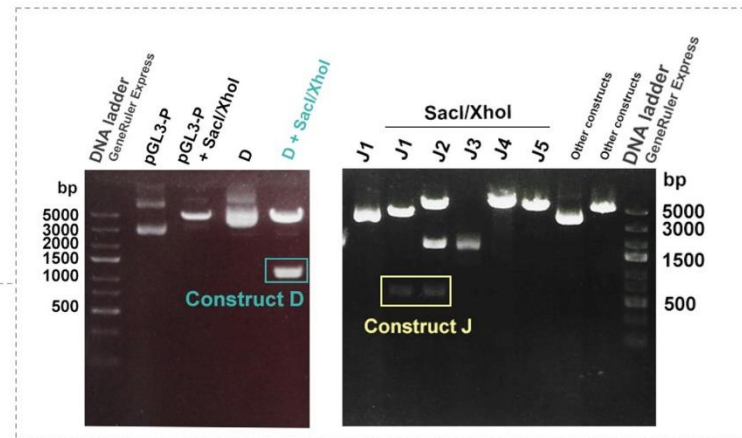
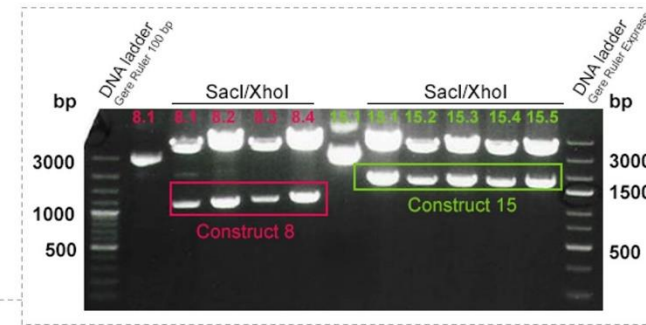
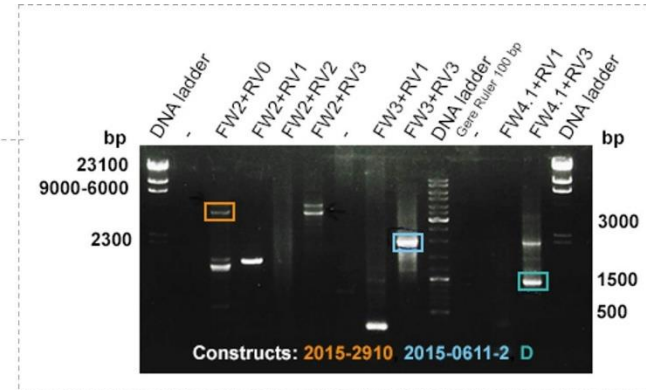
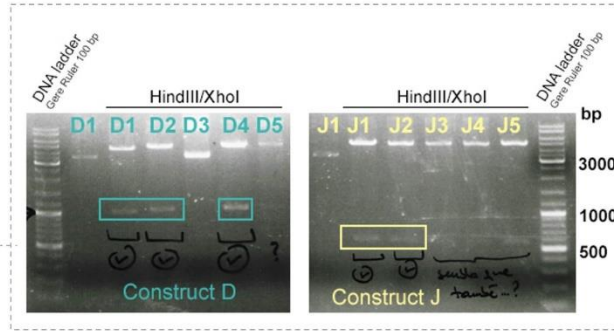
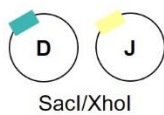


Figure 79. Cloning workflow for the obtention of TIGAR promoter constructs. A summary of the main steps in the cloning process is provided, including images from agarose gels representative of each of the steps. All constructs were firstly cloned with the TOPO-TA system and then subcloned in pGL3 basic vectors. Constructs D and J, which lack the minimal promoter of TIGAR, were subcloned in pGL3 promoter vectors. Sequencing was performed to confirm the constructions.

5.2. Functional assays of TIGAR promoter activation by Nrf2

In Sections 2 and 3 of this chapter it has been shown that the Nrf2 activator DMF, as well as overexpression of *NFE2L2*, increase *TIGAR* mRNA levels (Figures 61, 64). To clarify whether Nrf2 binds to the ARE sites that were identified in *TIGAR* promoter, the analysis of which is detailed in Section 1 of this chapter, we performed luciferase assays with the pGL3 vectors obtained (Figures 78, 79).

In order to have positive controls of induction of *TIGAR* transcription, the plasmids pcDNA3-flag p53, CMV-Sp1, pFETCH_CREB1 and pRK-ATF4 were acquired from Addgene in order to overexpress p53, Sp1, CREB1 and ATF4, respectively. HeLa cells were transfected with these plasmids in parallel to the transfection of pcDNA3-flag Nrf2 and cellular extracts were collected after 24 h for mRNA and protein analyses. All the plasmids effectively upregulated the levels of the corresponding proteins except for CREB1, the levels of which remained unaltered (Figure 80A). Interestingly, *TIGAR* protein levels were not modified by any of the overexpression plasmids. However, RT-qPCR analysis revealed upregulation of the mRNA levels of *TIGAR* by p53, SP1 and Nrf2 overexpressing plasmids (Figure 80B). As expected, CREB1 did not affect *TIGAR* expression (Figure 80B). p53 was the factor which yielded the most potent induction of *TIGAR* expression, triplicating *TIGAR* mRNA levels, followed by Nrf2 and SP1, which almost doubled *TIGAR* mRNA levels. These results are in accordance with the publications that have shown direct binding of p53, SP1 and CREB1 to *TIGAR* promoter (3,76,77). The fact that *TIGAR* protein levels are not increased by neither SP1, p53 or Nrf2 is consistent with previous findings reported in this chapter, where *NFE2L2* overexpression in HeLa induced an important increase in *TIGAR* mRNA levels but had only a slight effect on *TIGAR* protein (Figure 64). This suggests that, although several transcription factors are involved in the regulation of *TIGAR* expression, a robust regulation of *TIGAR* protein levels usually prevails over transcriptional control.

During the *in-silico* analysis of *TIGAR* promoter we realized that the Activating transcription factor 4 (ATF4) could also be involved in the regulation of *TIGAR* expression. ATF4, likewise CREB1, binds to cAMP Response Elements (CRE) and could therefore control *TIGAR* expression through the already-described CREB1 binding element. Even more interesting was the finding that ATF4 can bind to AREs and, indeed, it has been shown to interact with Nrf2 and control the expression of genes such as *HO-1* (189). Thus, we incorporated ATF4 to our experiments. The results showed that ATF4 overexpression increased *TIGAR* expression to a similar extent to p53 (Figure 80B). Similar to the other transcription factors transfected, *TIGAR* protein levels were not affected by ATF4 overexpression (Figure 80A).

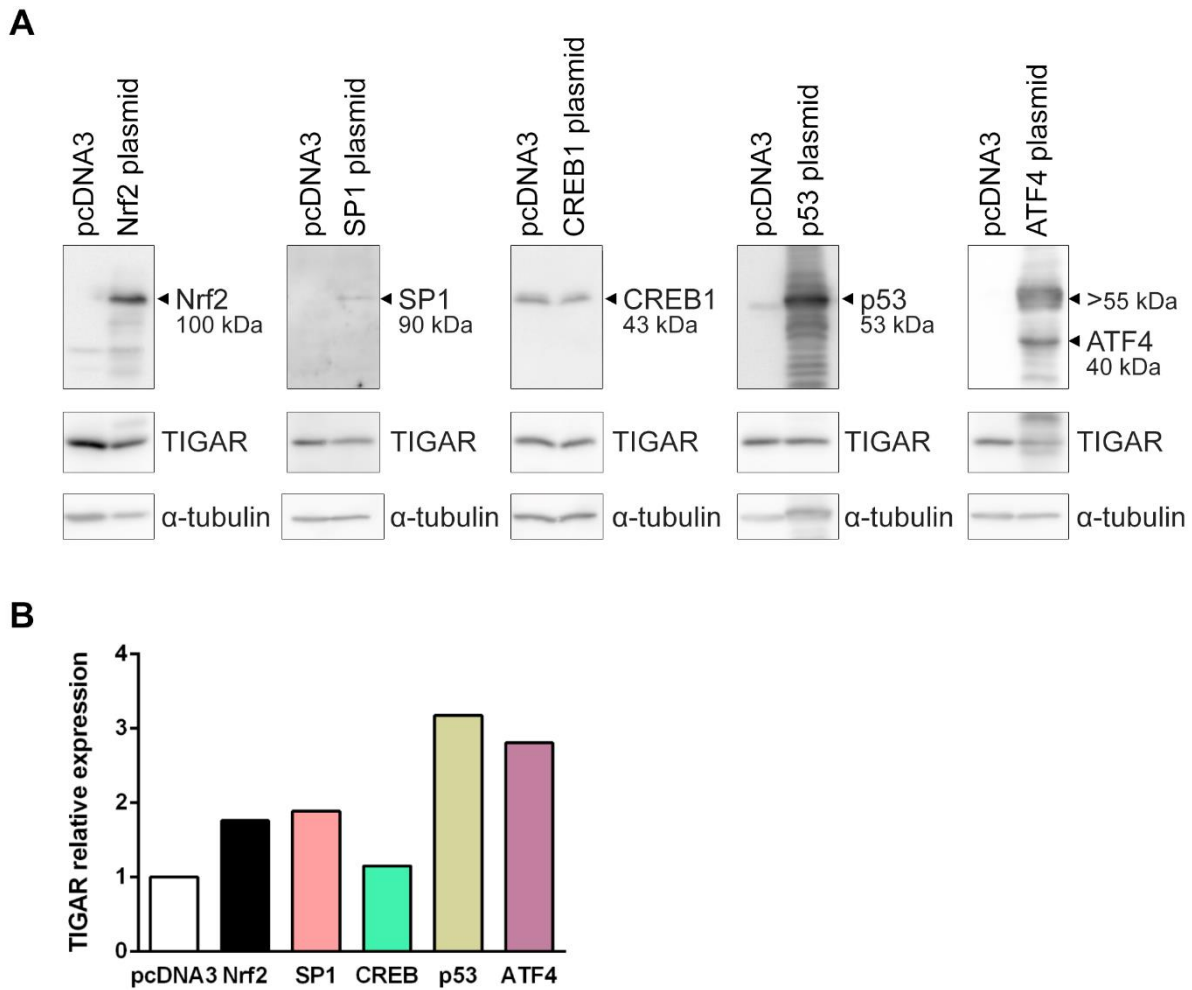


Figure 80. TIGAR modulation by several transcription factors. HeLa cells were transfected with Nrf2, SP1, CREB1, p53 or ATF4 overexpressing plasmids and protein and mRNA were determined after 24 h. **(A)** Western blot analysis of Nrf2, SP1, CREB1, p53, ATF4 and TIGAR protein levels. **(B)** RT-qPCR analysis of *TIGAR* mRNA levels. The results from a single experiment are shown.

Among the transcription factors that resulted in *TIGAR* mRNA upregulation, we decided to use SP1 to perform luciferase experiments. P53 was not suitable as a positive control given that the pGL3 constructs generated during this thesis do not include any of the p53 binding sites.

Some of the experiments regarding the functional characterization of *TIGAR* promoter are still being carried out, and therefore the results presented in this last section are preliminary. To date, two different luciferase experiments have been performed, one with constructs 8 and 15, which include the TSS, and another experiment with construct D, which does not contain the TSS (**Figure 81A**). Unfortunately, we have not obtained construct J in pGL3 promoter vector yet.

Constructions 8 and 15 (ARE1+TSS and ARE1+ARE2+TSS, respectively) were transfected into HeLa cells together with a β -galactosidase expression plasmid for the normalization of the luciferase results and the corresponding transcription factor Nrf2, SP1 or an empty pcDNA3 vector. A single experiment with independent triplicates has been performed to date, in which we could not detect β -galactosidase activity, and thus luciferase activity could not be normalized. When luciferase raw data were analysed, we could appreciate that luciferase activity was increased by constructions 8 and 15. However, this activity was independent of Nrf2 activation (**Figure 81B**). The single transfection of constructions 8 and 15 caused a high increase in the luciferase activity, suggesting that the presence of the sequences contained in these constructs strongly induces the expression of the pGL3 basic vector. Importantly, overexpression of SP1, which was carried out in parallel to Nrf2 experiments as a positive control, did not increase luciferase activity in any of the constructs either, suggesting an overall failure of the assay (**Figure 81B**). The high activity reported in empty pcDNA3-transfected cells could be explained by the presence of the TSS in both constructs, something that has been reported in other studies (76,77). However, an induction should be observed after overexpression of SP1, as others have shown (76). One explanation could be that luciferase activity is too high to appreciate any modulation by the SP1 or Nrf2.

As an alternative approach, luciferase assays with construct D have been performed. HeLa cells were transfected with a different β -galactosidase vector and the corresponding pGL3 promoter vector with construct D or the empty pGL3 promoter vector, together with Nrf2 overexpression plasmid or the corresponding pcDNA3 vector. The results showed that *NFE2L2* overexpression increased luciferase activity only in construct D, and not in the pGL3 empty vector, evidencing that either ARE1 and/or ARE2 are responsible for the binding of Nrf2 to the promoter of *TIGAR* (**Figure 81C**). It is to mention that in this experiment, β -galactosidase activity was detected but it was found to be induced by Nrf2 transfection and, thus, we could not normalize luciferase activity to these reads. Indeed, when the promoter of β -galactosidase expression plasmid was analysed, we found an ARE. As an alternative normalization system, we quantified protein levels in the lysates used for the determination of luciferase activity.

In conclusion, we have been able to show that the AREs present in construct D are potentially the binding sites for Nrf2. However, we need to obtain constructs with only one of the AREs to determine which one is the main responsible for Nrf2 control of *TIGAR* promoter. We are currently working on enzymatic digestions of construct D to eliminate one of the AREs and then religate the vector to obtain again functional luciferase reporter constructs.

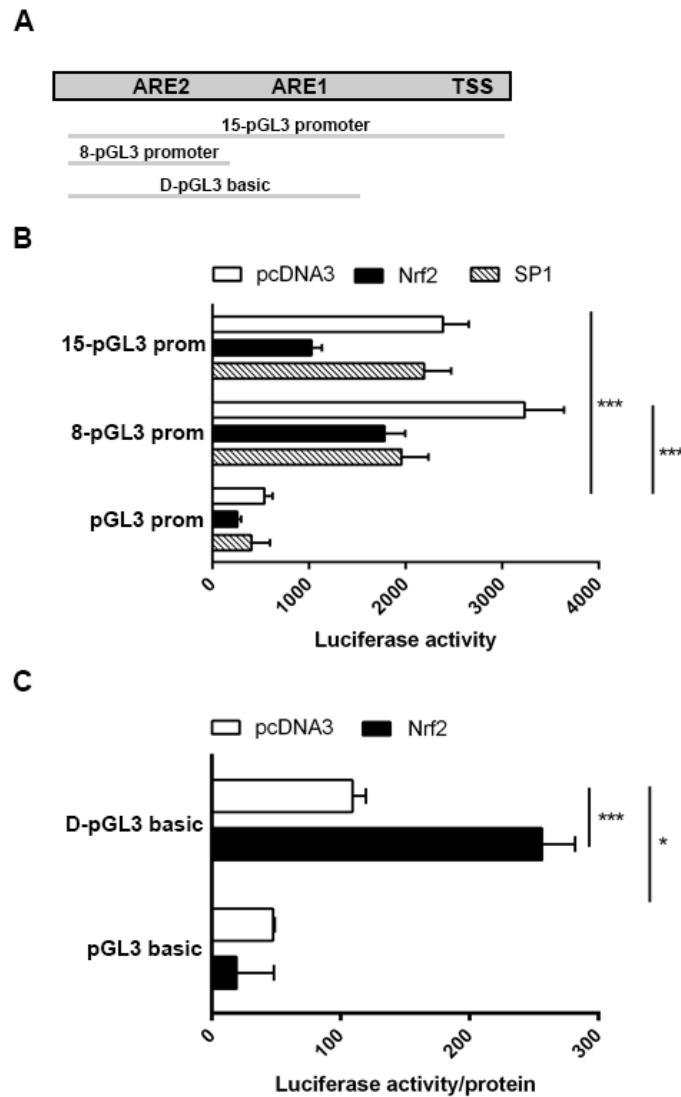


Figure 81. Luciferase assays of AREs in TIGAR promoter. HeLa cells were transfected with pGL3 luciferase reporter vectors containing constructs 8, 15 or D and luciferase activity was determined after the overexpression of Nrf2. **(A)** Schematic representation of the pGL3 constructs transfected: constructs 8 and 15 were cloned in pGL3 basic vectors and contain the TSS with the SP1 binding site, whereas construct D was cloned in pGL3 promoter vector and does not contain the TSS. **(B)** Luciferase activity from constructs 8, 15 and empty pGL3 basic vector in cells transfected with either Nrf2, SP1 or a pcDNA3 empty vector as control. Luciferase activity is reported as raw data from a single experiment with independent triplicates, mean \pm SD (** P < 0.001). **(C)** Luciferase activity from constructs D and empty pGL3 promoter vector in cells transfected with either Nrf2 or a pcDNA3 empty vector as control. Data are represented as the mean luciferase activity normalized to protein levels from one single experiment in each assay with independent triplicates \pm SD (* P < 0.05, ** P < 0.01, *** P < 0.001).

6. Nrf2 as a transcriptional regulator of mouse *Tigar*

6.1. Modulation of *Tigar* gene expression by Nrf2 in IDGs

In collaboration with Cristina Sánchez and Dr. Francesc Ventura (Departament de Ciències Fisiològiques, Universitat de Barcelona) we have been able to evaluate the expression of *Tigar* in different models of bone differentiation in mice. The group leadered by Dr. Ventura has years of experience in the differentiation process of osteoblasts to osteocytes. At the time when the experiments presented in this thesis were performed, Dr. Ventura's Lab was investigating whether Nrf2 could modulate the expression of genes involved in the differentiation of bone cells. For this, they were using Immortomouse/Dmp1-GFP-SW3 cells (IDG-SW3, referred to as IDGs), which replicate the process of osteoblast to osteocyte transition, and we had access to samples from several experiments, which are summarized in **Table V**. Besides, we could also evaluate the expression of *Tigar* in primary mouse osteoblasts. However, these results have not been included due to the lack of experiments in this model model.

Cells	Experiment
IDGs	Nrf2 overexpression with pMSCV-Nrf2-flag, cultured for 5 days. Control population: pMSCV-GFP-infected IDGs.
Differentiated IDGs	Treatment with 5 and 20 μ M DMF for 48 h. Control population: untreated IDGs.
Nrf2-CRISPR IDGs and the corresponding Nrf2 ^{+/+} control IDGs	Treatment with 5 and 20 μ M DMF for 48 h. Control population: untreated Nrf2 ^{+/+} IDGs.
Nrf2-CRISPR IDGs and the corresponding Nrf2 ^{+/+} control IDGs	Nrf2 overexpression with pMSCV-Nrf2-flag, cultured for 5 days. Control population: pMSCV-GFP-infected Nrf2 ^{+/+} IDGs.

Table V. Experiments performed by Dr. Ventura's Lab in IDGs in which *Tigar* expression has been analysed.

IDGs were infected with a murine stem cells virus (pMSCV) vector expressing human Nrf2 or the corresponding control vector expressing the green fluorescent protein (GFP). Nrf2 overexpression significantly induced the mRNA levels of *Tigar* in parallel to known Nrf2 target genes, such as *Trx1* and *Nqo1* (**Figure 82A**). As a complementary approach, IDGs were treated with DMF. This molecule had been previously tested in HeLa, where we showed that it induced *Nrf2* and *Tigar* expression, as previously reported in this chapter. 48 h treatment of IDGs with DMF significantly increased the expression of *Tigar* and that of the Nrf2 target genes *Trx1*, *Nqo1* and *G6pd* (**Figure 82B**).

In an attempt to confirm that the expression changes observed in Nrf2 target genes and *Tigar* relied on the activation of Nrf2, an Nrf2-CRISPRed IDG cell line was generated by Dr. Ventura's group. These cells showed decreased levels of *Nrf2*, *Nqo1*, *G6pd* and *Tigar* at basal conditions (**Figure 82C**, white bars) compared to Nrf2^{+/+} IDG cells (**Figure 82C**, grey dotted line), which were set as control. The function of endogenous mouse Nrf2 was evaluated by treating Nrf2-CRISPRed IDGs with DMF. The Nrf2 inducer was not able to enhance the expression of neither *Trx1*, *Nqo1*, *G6pd* or *Tigar* in Nrf2-CRISPRed IDGs

(Figure 82C, yellow bars), evidencing that endogenous *Nrf2* had been successfully eliminated by the CRISPR technology. The re-expression of heterologous human *Nrf2* in *Nrf2*-CRISPRed IDGs resulted in increased expression of all *Nrf2* target genes, including *Tigar* (Figure 82C, black bars). As expected, the combination of heterologous expression of human *Nrf2* and DMF treatment (Figure 82C, striped bars) increased the expression of *Nrf2* target genes to the same extent that *Nrf2* overexpression alone, confirming that the murine *Nrf2* is not functional in these cells.

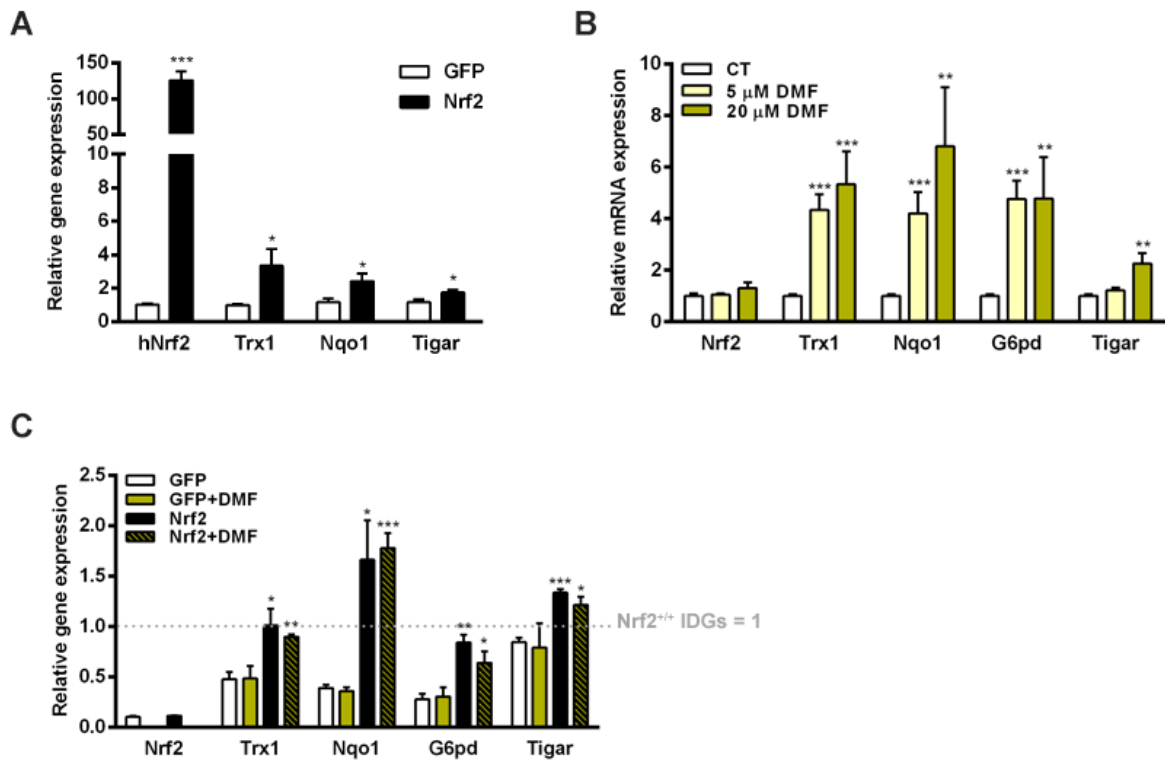


Figure 82. Analysis of *Tigar* expression under *Nrf2* modulation in mouse IDGs. (A) IDGs were infected with pMSCV-*Nrf2*-flag or pMSCV-GFP as control and gene expression was determined after 5 days of culture by RT-qPCR. (B) IDGs were treated with DMF at the indicated doses for 48 h and gene expression was determined after 5 days of culture by RT-qPCR. (C) *Nrf2*-CRISPRed IDGs were infected with pMSCV-*Nrf2*-flag or pMSCV-GFP as control and subsequently treated with DMF with 20 μ M DMF for 48 h. Gene expression was normalized to that of *Gapdh* and is expressed relative to untreated IDG cells with normal *Nrf2* expression (*Nrf2*^{+/+}). Mean expression \pm SEM is represented (n=4, *P < 0.05, **P < 0.01, and ***P < 0.001).

6.2. *In silico* study of the promoter of mouse *Tigar* gene

Considering that the expression of *Tigar* was significantly increased by Nrf2 overexpression and activation by DMF in mouse cells, we decided to analyse the binding of Nrf2 to *Tigar* promoter. For this, we performed an *in silico* study of 12 Kbp covering the promoter and first intron of mouse *Tigar* looking for sequences corresponding to the Nrf2 binding motif TGAC/GnnnGC (147). We identified five potential AREs, three of them in the promoter and the other two in the first intron of *Tigar*, close to the p53 binding site 2 (BS2) (**Figure 83**).

Eight different regions are conserved between mouse and human along the 12 Kbp of the mouse genome that were analysed, the majority of which are also conserved in *Pan troglodytes* (**Figure 83**). We only identified one potential ARE within the conserved regions between human and mouse, which was located at -5.762 bp from the translation start codon (ATG, +1) (**Figure 83, Box A**). AREs 2 and 3 were located in regions that were not conserved in neither *Pan troglodytes*, *Bos taurus* or *Homo sapiens* and, thus, were not further studied. ARE 4 is located between two of the fragments that are conserved in human, and thus it was not considered either. It is true that some regions that are not conserved between mouse and these species have shown to control mouse *Tigar* expression. This is the case of the p53 binding site 1 (BS1) (75). In our analysis, we excluded the AREs that were not conserved at least in human to try to look for common regulatory mechanisms between these two species.

Interestingly, the search for intronic AREs revealed that ARE i1, which is located at +273 bp, is included in the p53 BS2, which is partially conserved between mouse and human (**Figure 83, Box B**).



Figure 83. Study of mouse *Tigar* promoter and first intron with ECR Browser. ECR Browser (available at <http://ecrbrowser.dcode.org>) (182) was used to analyse the sequence between 127.104.600 to 127.116.500 of mouse chromosome 6. The sequence was compared with the genome of *Pan troglodytes* (panTro3), *Homo sapiens* (hg19) and *Bos taurus* (bosTau6). The image provided by ECR Browser has been modified to indicate the important elements for the study of antioxidant response elements (AREs) within *Tigar* promoter and first intron. A legend is provided with all the details. Two additional boxes are used to zoom in (A) a region of *Tigar* promoter containing a potential ARE and in (B) the region close to *Tigar* minimal promoter and first intron.

6.3. Binding of Nrf2 to the promoter of mouse *Tigar* gene

To finally determine the direct binding of Nrf2 to the potential AREs described in *Tigar* gene, several ChIP experiments were performed in collaboration with Cristina Sánchez, from Dr. Ventura's Lab. ARE 1 and ARE i1 were interrogated. These AREs were chosen for functional characterization given that ARE1 is conserved between human and mouse and ARE5 is within p53 BS2.

Primary osteoblasts were treated with DMF at 5 μ M for 24 h and, after performing the ChIP with a primary antibody specific to Nrf2, RT-qPCR was performed to determine the presence of the regions with the potential AREs in the immunoprecipitated DNA fractions bound to Nrf2. Specific primers for the amplification of the sequences surrounding each of these AREs were used and a schematic representation is provided in **Figure 84**. Results showed that the sequence corresponding to the ARE 1, located in *Tigar* promoter, was enriched in the fractions precipitated with the anti-Nrf2 antibody, confirming the binding of this transcription factor to *Tigar* promoter (**Figure 84A**). However, a non-significant increase was observed for the sequence corresponding to intronic ARE i1 (**Figure 84B**). Neither of the increases observed for the AREs were observed in the immunoprecipitates obtained with an antibody against the IgGs, showing the specificity of Nrf2 for this ARE (**Figure 84A,B**).

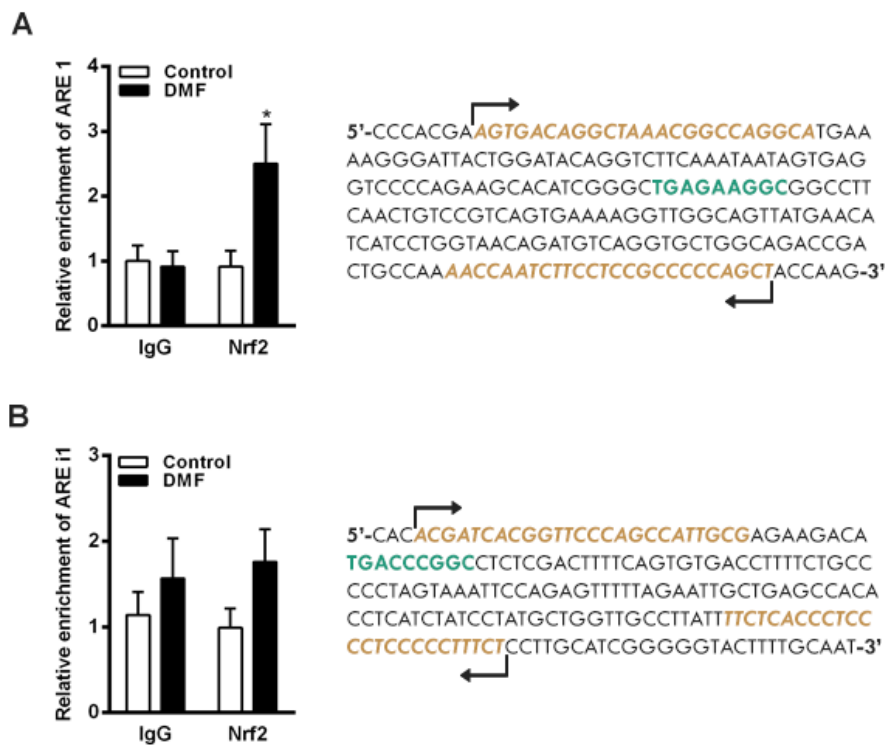


Figure 84. Nrf2 binding to AREs in mouse *Tigar*. Osteoblasts were treated with 5 μ M DMF for 24 h and genomic DNA was obtained. Chromatin immunoprecipitation was performed using a specific Nrf2 antibody and IgGs were used as control. Two AREs were interrogated, **(A)** one located in *Tigar* promoter (ARE 1) and **(B)** one located in the first intron of *Tigar* (ARE i1). The primers used for the amplification of the sequences surrounding the AREs in the immunoprecipitated fractions are shown in the right panel of the figure, written in orange. The sequences corresponding to AREs are written in green. Results were normalized to input chromatin and plotted relative to the enrichment of the IgG fraction in untreated IDG cells. Data are presented as mean enrichment \pm SEM (n=3 with duplicates, *P < 0.05).

As a complementary approach, a ChIP experiment was performed in control and Nrf2-CRISPRed IDG cells to confirm the specificity of Nrf2 to bind to the ARE located in *Tigar* promoter. This sequence was enriched in the DNA immunoprecipitated with an anti-Nrf2 antibody when Nrf2 was overexpressed in Nrf2^{+/+} IDGs (**Figure 85A**), but not in the Nrf2 CRISPRed IDG2 (**Figure 85B**). Although more experiments should be performed to evaluate the statistical power of this observation, these results seem to indicate that the binding of Nrf2 to ARE 1 in mouse *Tigar* promoter is specific.

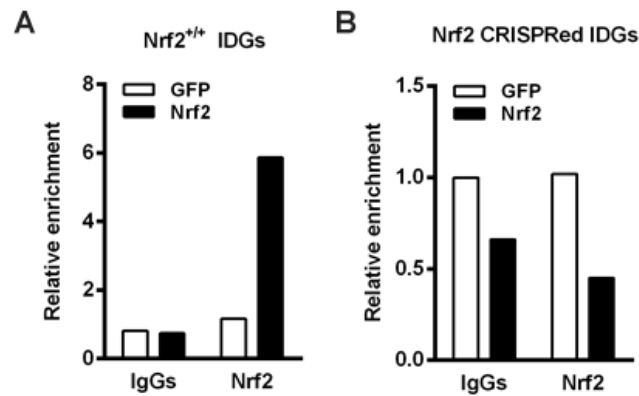


Figure 85. Specific binding of Nrf2 to ARE 1 in mouse *Tigar* promoter. Nrf2^{+/+} and Nrf2-CRISPRed IDGs were infected with pMSCV-Nrf2-flag or pMSCV-GFP as control and genomic DNA was obtained after 5 days of culture. Chromatin immunoprecipitation was performed using a specific Nrf2 antibody and IgGs were used as control. The enrichment of the sequence corresponding to ARE 1 in the Nrf2 and IgGs-immunoprecipitated fractions was assessed by RT-qPCR with specific primers in **(A)** Nrf2^{+/+} and **(B)** Nrf2-CRISPRed IDGs. Results were normalized to input chromatin and plotted relative to the enrichment of the IgG fraction in each cell type. Data from a single experiment are presented.

7. Discussion

In this chapter, we have analysed the contribution of Nrf2 in the transcriptional regulation of *TIGAR*. We have found that Nrf2 induction by DMF increases *TIGAR* mRNA levels in a transcription-dependent manner in HeLa, although this is not translated to an increase in TIGAR protein levels. When Nrf2 was overexpressed in these same cells, results were more reproducible and we could observe enhanced mRNA and protein levels of TIGAR. Accordingly, the inhibition of Nrf2 through siRNA reduced *TIGAR* expression and protein levels in HeLa cells. The direct binding of Nrf2 to *TIGAR* promoter will be assayed in forthcoming experiments by luciferase assays and ChIP. However, it is important to consider that, beyond *TIGAR* transcriptional control, highly conserved mechanisms seem to control the levels of *TIGAR* similarly to what occurs for housekeeping genes. This would explain why the overexpression of SP1 and p53, transcription factors that are known to bind to *TIGAR* promoter and induce its expression, increased *TIGAR* mRNA but not protein levels in HeLa cells. In other studies, TIGAR protein levels have been found increased after p53 induction in a p53 doxycycline-inducible SAOS-2 cell line and also after doxycycline treatment of U2OS cells (3), suggesting that the control of TIGAR protein levels by p53 might be cell-dependent.

HeLa cells are a good model for the discovery of molecular mechanisms common in cancer. However, given the clinical importance of the Keap-Nrf2 axis in NSCLC, where it is one of the mechanisms driving therapy resistance (186), we aimed to determine a potential contribution of TIGAR in the malignant phenotype of these tumours. For that, we inhibited Nrf2 levels in two ADC cell lines, A549 and H460, and one SQCC cell line, H1299. The results generated a lot of controversy given that none of the cell lines responded in the same way to Nrf2 inhibition. In A549, Nrf2 suppression reduced TIGAR protein levels but enhanced the expression of this gene. On the contrary, in H460 cells Nrf2 inhibition reduced *TIGAR* mRNA levels but did not affect its protein levels. Finally, Nrf2 inhibition in H1299 cells resulted in increased *TIGAR* expression with no changes at the protein level. Considering the cross-talk that has been described between Nrf2 and p53 (188), we evaluated *TP53* induction in those cells that showed increased *TIGAR* mRNA levels after Nrf2 inhibition: A549 and H1299, which lack *TP53*. To our surprise, mRNA levels of *CDKN1A* (p21) were increased in both A549 and H1299, showing that p53-alternative mechanisms were active and could explain *TIGAR* induction. However, these mechanisms remain unknown. To try to overcome the compensatory events after Nrf2 inhibition, we overexpressed Nrf2 in ADC cell lines, which did not cause any changes in *TIGAR* mRNA or protein levels.

The results obtained in NSCLC point out that there is a link between Nrf2 and TIGAR in these cancer cell types, although this connection is more clear in HeLa cells. In general, it seems that TIGAR protein levels are highly protected from variation by some unknown mechanism and that when they are decreased, as it is the case of A549, transcriptional mechanisms are induced to enhance *TIGAR* mRNA expression and

restore proteins levels. It is important to keep in mind, however, that metabolic events are carried out by enzymes and, thus, the most relevant changes are those at the protein level. Considering that, we should include *TIGAR* to the list of genes that need to be considered as Nrf2 targets, at least in ADC cells with high basal levels of Nrf2, as it is the case of A549. These cells have been previously used to describe novel Nrf2 target genes, such as G6PD, PGD, TKT and PEPCK, in a study in which *TIGAR* was evaluated only at the mRNA level and was not found significantly affected (142). Although the results of this thesis show that Nrf2 does not regulate *TIGAR* in all types of cells, *TIGAR* modulation should be considered when designing strategies of Nrf2 inhibition in ADC. *TIGAR* expression has been related to resistance to radiotherapy (79). Thus, if Nrf2 inhibition lead to decreased *TIGAR* levels in cancer-treated patients, that would draw an scenario of higher possibilities for therapy response. However, if the upregulation of *TIGAR* mRNA levels that we have observed *in vitro* after Nrf2 inhibition was reproduced in these tumours, the effects of therapies blocking Nrf2 for long periods should be evaluated to confirm that a refractory response based on increased *TIGAR* protein levels is not taking place. The findings reported in this thesis indicate that Nrf2 inhibition in certain kinds of tumours might be a double-edged sword depending on the alternative antioxidant mechanisms triggered by cells, one of which could be *TIGAR*.

This chapter begun with the identification and analysis of conservation of AREs in *TIGAR* promoter. Among the several AREs identified, three of them were more likely to be functional response elements due to their degree of conservation between species and the proximity to *TIGAR* TSS, and thus were selected to be cloned. We have been able to clone two of these AREs, the ones located in *TIGAR* promoter, in pGL3 luciferase reporter vector, the functional study of which has indicated that Nrf2 can bind to either one of two of these AREs. This has been described by overexpressing Nrf2 in HeLa cells and measuring the luciferase activity of the construct named 'D', which includes both ARE 1 and ARE 2. The next experiments in this project will be addressed to the obtention of each of the AREs in a pGL3 promoter vector for their independent functional characterisations. Once we confirm which ARE is responsible for Nrf2 binding to *TIGAR* promoter, we will perform chromatin immunoprecipitation assays in human cells to characterise the direct binding between Nrf2 and *TIGAR*, as we have performed in mouse cells thanks to the collaboration with the group of Dr. Francesc Ventura.

RESULTS CHAPTER IV

**Looking at TIGAR in response to oxidative stress:
location also matters**



CONTEXT

In the previous chapters of this thesis we have provided data to discuss the antioxidant function of TIGAR. In the first chapter, it has been shown that PFKFB3 inhibition induces *TIGAR* expression in parallel to increased ROS levels. In the second, spectrophotometric determinations and metabolomic analyses showed that, although TIGAR can dephosphorylate Fru-2,6-P₂, this effect does not result in increased flux through the PPP, neither in increased NADPH production. However, in the third chapter we have described a close relationship between the PPP-promoter Nrf2 and TIGAR in HeLa cells, being Nrf2 capable of inducing the activity of *TIGAR* promoter. All these results support the generalized idea of the involvement of TIGAR in the antioxidant response of cancer cells. Nevertheless, this relationship is not as simple as it is discussed in many publications. Indeed, one of the main questions is how TIGAR protects from ROS-induced cell death. As it has been previously commented along this thesis, the capacity of TIGAR to reduce apoptosis in response to H₂O₂ was proven in U2OS and H1299 cell lines (3). However, very few studies, performed in very specific models, have shown increased TIGAR protein levels after treatment with oxidant molecules (190). In fact, TIGAR levels are hardly altered in response to treatments and even the overexpression of transcription factors that increase *TIGAR* mRNA levels has failed to upregulate TIGAR protein, as it has been shown in the Results Chapter III. In this scenario, the involvement of transcriptional-independent mechanisms being responsible for the protective effects of TIGAR in front of ROS looks reasonable.

Subcellular location can be as important as protein amount for those proteins with a specific function in a certain organelle or intracellular space. Different metabolic enzymes, including HK, PFKFB3, PGAM and others, have been found in the nucleus, some of them carrying out the same function as in the cytoplasm and some others with a different or even unknown role. The term 'moonlighting proteins' refers to proteins that perform multiple autonomous and often unrelated functions, increasing functional options for the cell without increasing the number of genes that need to be replicated and transcribed (173). The group of Dr. Karen Vousden showed that TIGAR colocalizes with HK-II in the outer mitochondrial membrane under hypoxic conditions, an interaction that is determinant for cells to overcome the lack of oxygen. Interestingly, the capacity of TIGAR to increase HK-II activity under hypoxia is independent of TIGAR bisphosphatase activity on Fru-2,6-P₂ (87). Moreover, genotoxic drugs as well as hypoxia have been described to trigger TIGAR translocation to the nucleus, where it regulates the phosphorylation of ATM, a key protein in the DNA damage response (88).

During the thesis I had the opportunity to join the lab of Dr. Karen Vousden at the Beatson Institute for Cancer Research (UK), where I studied the subcellular localisation of mouse Tigar in response to oxidative stress. The most important findings of this project are summarised in the following pages.

1. Screening of primary antibodies for *Tigar* immunofluorescence in mouse cells

Considering that TIGAR localisation had been previously studied in human cells, the first thing to do was to determine if the same antibodies were suitable for immunofluorescence in mouse cells. With this purpose, several primary antibodies were tested in wild type *Tigar* (WT *Tigar*) and *Tigar*^{-/-} (*Tigar* KO) mouse PDAC cells by immunofluorescence (Table VI).

Catalogue number	Species of origin	Company
sc-74577	Mouse monoclonal	Santa Cruz Biotechnology
sc-67273	Rabbit polyclonal	Santa Cruz Biotechnology
AB10545	Rabbit polyclonal	Abcam
Homemade	Rabbit polyclonal	Vousden's Lab

Table VI. Primary antibodies used for the detection of mouse *Tigar*.

Rabbit polyclonal sc-67273 offered the highest signal-to-noise ratio, being hardly detected in *Tigar* KO cells, indicating its specificity. On the contrary, sc-74577 and the homemade rabbit polyclonal antibody had very low signal in WT *Tigar* cells, and AB10545 was highly unspecific. With the sc-67273 antibody, we determined that *Tigar* was uniformly distributed along the cytoplasm and the nucleus of PDAC cells at basal conditions (**Figure 86**).

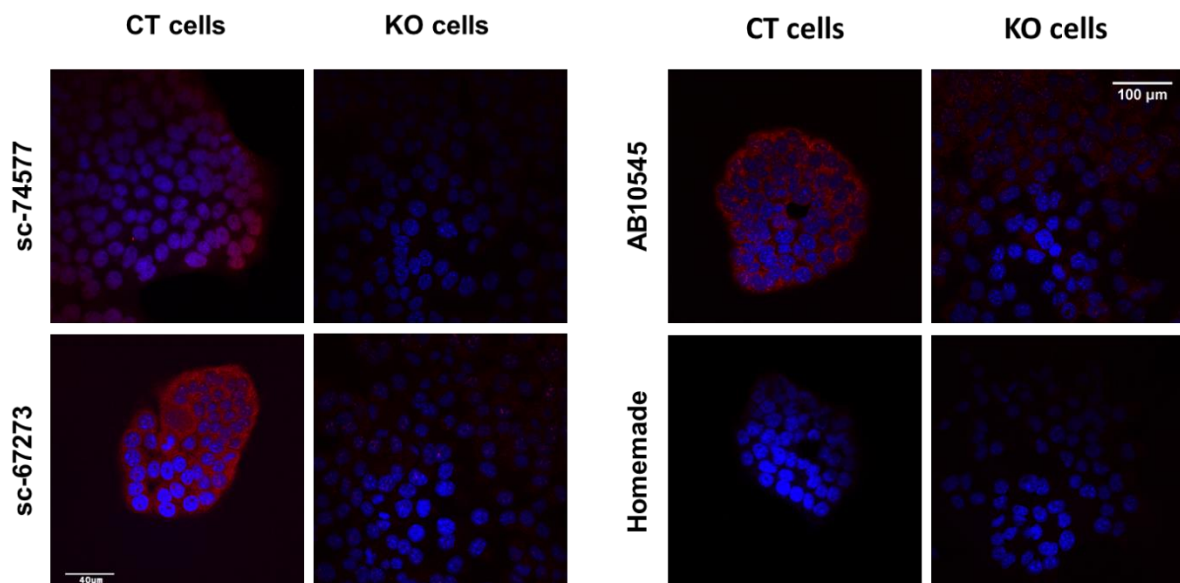


Figure 86. Evaluation of the specificity of antibodies for the detection of mouse *Tigar*. Immunofluorescence of *Tigar* was performed using three commercial antibodies (sc-74577, sc-67273 and AB10545) and one homemade antibody in WT *Tigar* (CT cells) and *Tigar*^{-/-} (KO cells). Anti-mouse and anti-rabbit Alexa 594-conjugated secondary antibodies were used (red) and nuclei were stained with DAPI (blue).

NOTE! The possibility to work with *Tigar* KO cells was very useful to select the best antibody for the detection of mouse and human TIGAR, which share 73% identity. sc-67273 antibody was used in all the subsequent experiments performed during this thesis and the antibody that was being used in the lab (LifeSpan BioSciences), which had shown high unspecificity in immunofluorescence experiments of TIGAR-inhibited cells through siRNA, was restricted to western blot.

2. Subcellular localisation of TIGAR under oxidative stress

2.1. TIGAR location in unstressed conditions

In order to determine the localisation of human TIGAR under oxidative stress, we generated a viral vector for the stable expression of human TIGAR fused with flag tag and EGFP (f-TIG-GFP). WT *Tigar* and *Tigar* KO PDAC cell lines were infected with this vector. Compared to immunofluorescence of endogenous TIGAR, which indeed would detect the mouse protein, this system allowed for an easy way to visualize TIGAR by confocal microscopy, along with the capacity to rescue Tigar function in *Tigar* KO PDAC cells. This was of interest to study the contribution of this gene in the response of PDAC cells to oxidative stress. Details on the cloning procedure and the infection of both WT *Tigar* (iCT) and *Tigar* KO (iKO) PDAC cells with viral particles can be found in the Materials and Methods section. A summary of the workflow is provided in **Figure 87A**, and a schematic representation of the DNA sequence and protein structure of the f-TIG-GFP construct can be consulted in **Figure 87B**. The expression of recombinant f-TIGAR-GFP by both cell types was confirmed by western blot, as shown in **Figure 87C**.

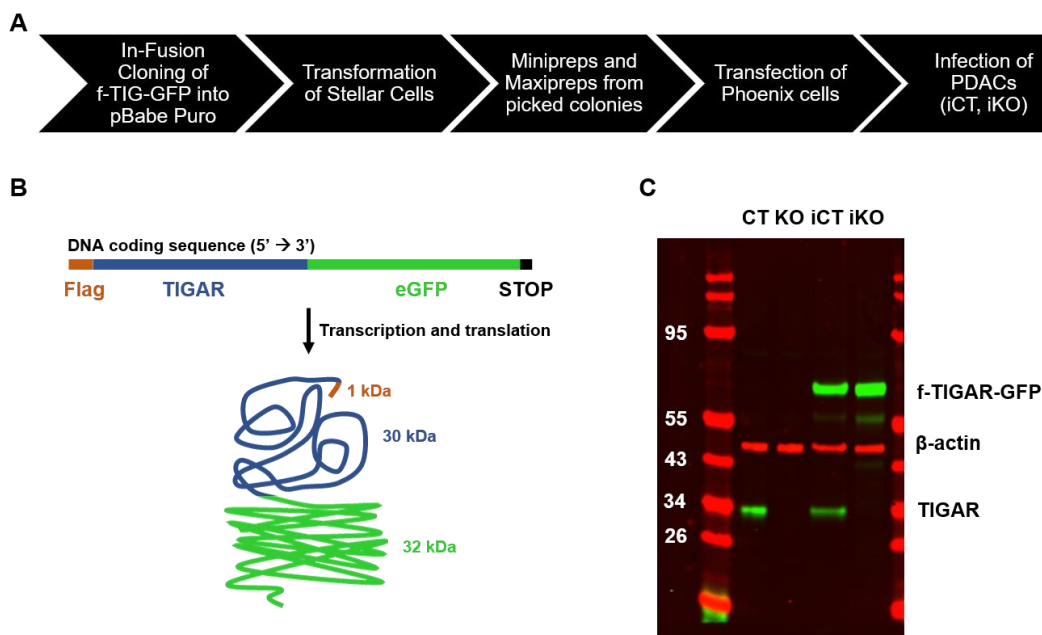


Figure 87. Generation of PDAC cell lines stably expressing flagged-TIGAR-GFP (f-TIG-GFP) fused protein. WT *Tigar* (CT) and *Tigar*^{-/-} (KO) PDAC cells were infected with a construct expressing f-TIG-GFP. **(A)** Workflow of the process: from cloning the DNA of interest to the infection of PDAC cells. **(B)** Schematic representation of the DNA sequence and protein structure of the f-TIG-GFP construct: flag is highlighted in orange, TIGAR in blue and EGFP in green. **(C)** Western blot analysis of TIGAR and β -actin in the parental cells (first two lanes, WT and KO) and the infected cells (third and fourth columns, iWT and iKO). Immunofluorescent secondary antibodies were used.

Considering previous literature describing the presence of TIGAR in the mitochondria of human cells (87), we wanted to determine if it was located in these organelles at basal conditions in PDAC cells. Immunofluorescence against Tom20, a member of the translocase of the outer membrane of the mitochondria, was performed in iCT and iKO PDAC cells using an Alexa 594-conjugated secondary antibody. The results showed that there was a small percentage of TIGAR colocalizing with Tom20 in both cell lines (**Figures 88, 89**, yellowish areas), suggesting that TIGAR can be located at the outer mitochondrial membrane at basal conditions. This was more evident in iKO cells, possibly because the fluorescence of f-TIG-GFP was also higher in these cells (**Figure 89**). However, the main signal emitted by the f-TIG-GFP recombinant protein was cytoplasmic, suggesting that the main function of TIGAR at basal conditions relies on its cytosolic location (**Figures 88, 89**).

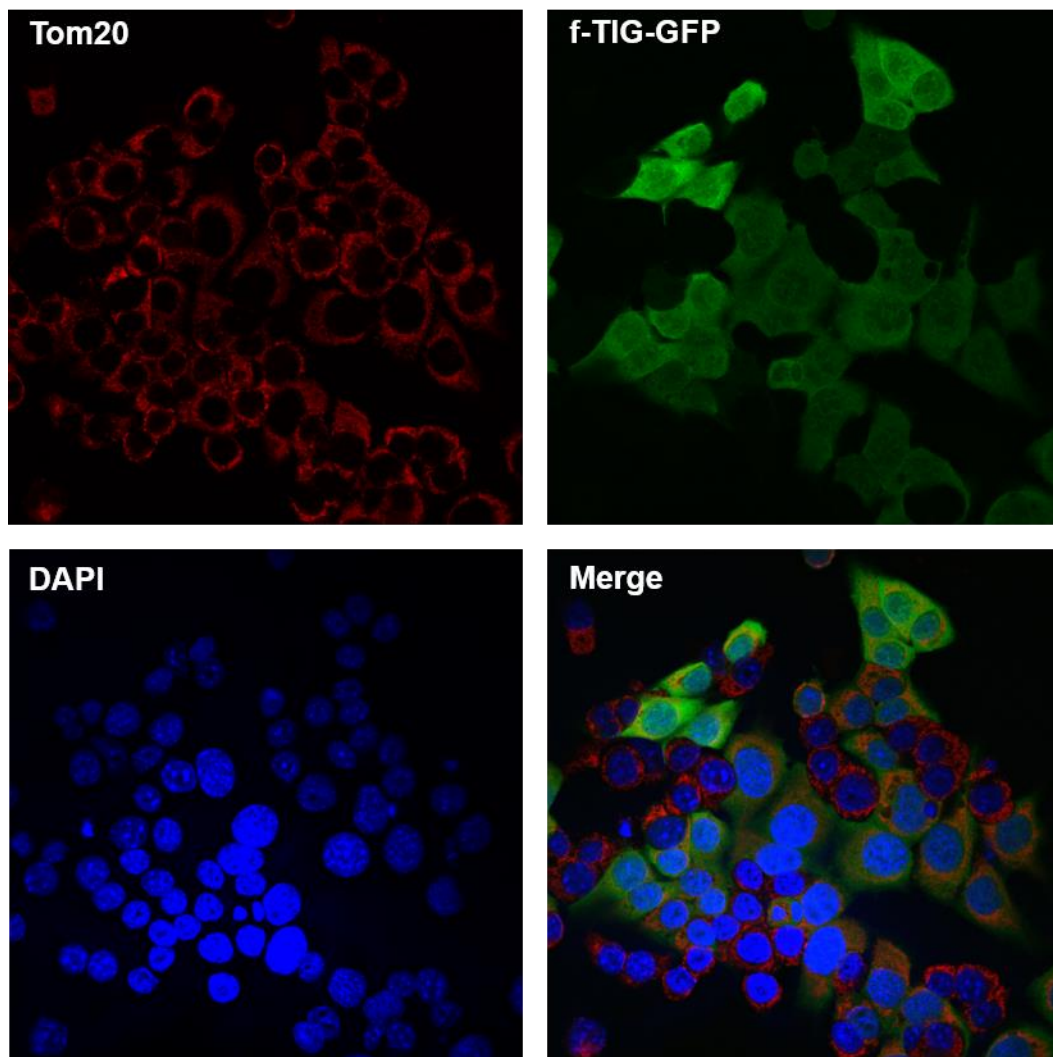


Figure 88. TIGAR and Tom20 colocalisation in iCT cells. Immunodetection of TIGAR and Tom20 was performed in WT *Tigar* PDAC cells infected with flag-TIGAR-GFP (f-TIG-GFP) using a Tom20 specific antibody and an Alexa 594-conjugated secondary antibody (shown in red). Nuclei were stained with DAPI (blue). Colocalisation between TIGAR and Tom20 can be observed in the Merge channel (yellowish areas).

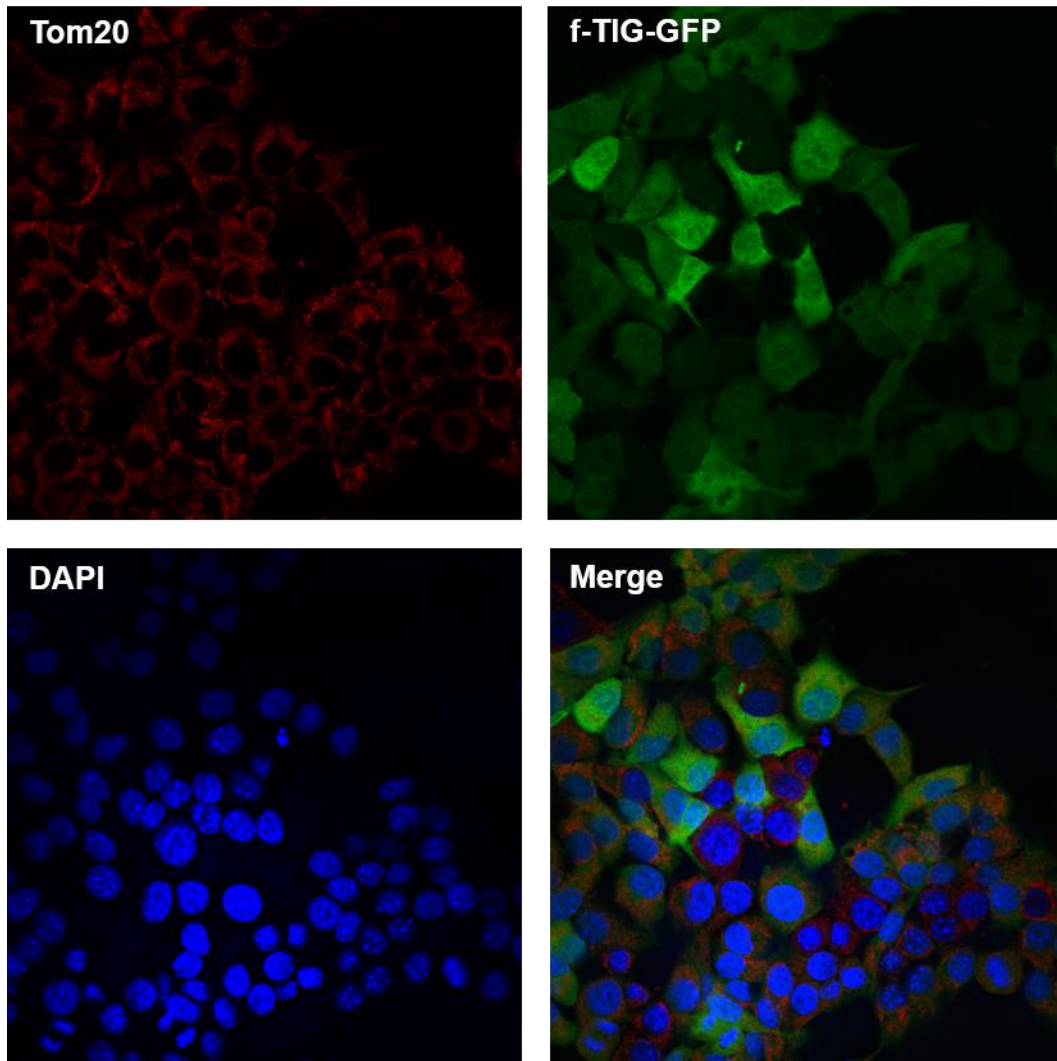


Figure 89. TIGAR and Tom20 colocalisation in iKO cells. Immunodetection of TIGAR and Tom20 was performed in *Tigar* KO PDAC cells infected with flag-TIGAR-GFP (f-TIG-GFP) (iKO cells) using a Tom20 specific antibody and an Alexa 594-conjugated secondary antibody (shown in red). Nuclei were stained with DAPI (blue). Colocalisation between TIGAR and Tom20 can be observed in the Merge channel (yellowish areas).

2.2. TIGAR location under oxidative stress

PDAC cells infected with f-TIG-GFP (iCT and iKO) were treated with 0,5 mM H₂O₂ for 24 h and subsequently analysed by immunofluorescence. The localisation of f-TIG-GFP was analysed in parallel to γ -tubulin, which was detected with an Alexa 594-conjugated secondary antibody. γ -tubulin is a key protein for the nucleation and anchoring of microtubules from the microtubule organizing centre, in animals called the centrosome, which is composed by two centrioles. Multiple components of the DNA damage response pathway are linked to the centrosome and genotoxic stress strongly affects its organization (191). Given that oxidative stress can induce DNA damage and TIGAR had been described to be involved in the DNA damage response (88), we found interesting to immunodetect γ -tubulin in our experiments.

Untreated iCT and iKO cells showed diffuse signal of both f-TIGAR-GFP and γ -tubulin (**Figures 90, 91**), according to the fact that γ -tubulin is not only restricted to the centriole and indeed it is found in the cytoplasm of many cells (192). In iCT cells, treatment with H₂O₂ caused a dramatic enlargement of their surface and TIGAR showed a nuclear and perinuclear localisation under these conditions. Localisation of TIGAR was different between cells and experiments, but it was clear that those cells with higher surface showed highly increased levels of TIGAR in the nucleus (**Figure 90**). In other experiments, TIGAR was detected in both the cytoplasm and the nucleus of cells, as it will be shown in further figures. Interestingly, in the cells more enlarged, γ -tubulin formed a ring around the nuclei, its fluorescence overlapping to that of f-TIG-GFP (**Figure 90**). Centrosome disorganization was detected after treatment with H₂O₂, with many cells with separated centriole despite not showing signs of division (**Figure 90**, white arrows). The overall phenotype exhibited by H₂O₂-treated PDAC cells was consistent with a senescent phenotype.

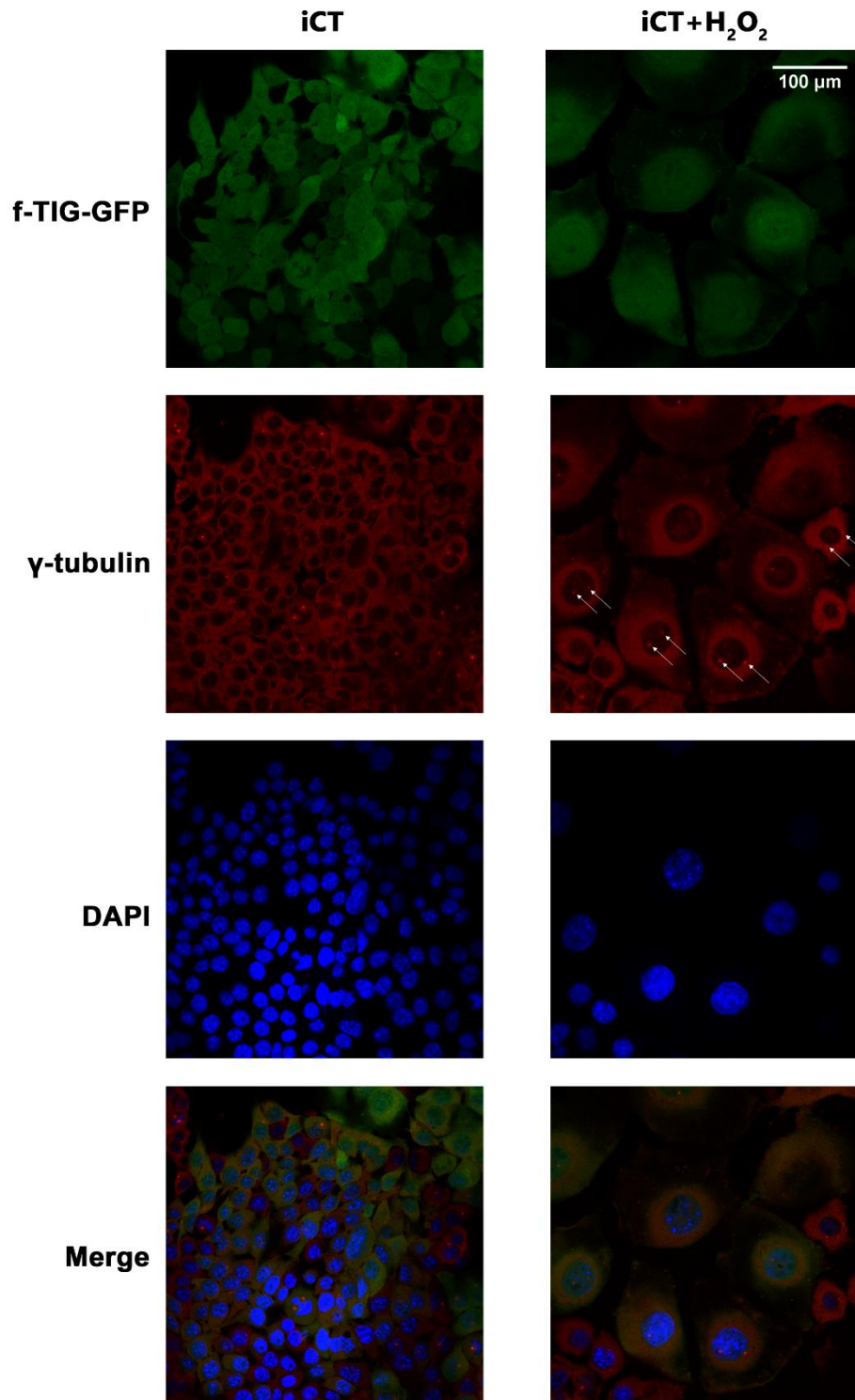


Figure 90. Localisation of TIGAR under oxidative stress in iCT cells. WT *Tigar* PDAC cells were infected with flag-TIGAR-GFP (f-TIG-GFP) (iCT cells) and treated with 0,5 mM H₂O₂ for 24 h. The construct f-TIG-GFP is shown in green, γ -tubulin was detected with an Alexa 594-conjugated secondary antibody (red) and nuclei were stained with DAPI (blue). Colocalisation between TIGAR and γ -tubulin can be observed in the Merge channel as yellowish areas. White arrows indicate centrioles.

A similar response was observed in iKO cells treated with H_2O_2 . Although in these cells the nuclear localisation of TIGAR and the γ -tubulin rings around the nuclei were less clear than in H_2O_2 -treated iCT, enlarged shape and centrosome disorganization were also appreciated (**Figure 91**).

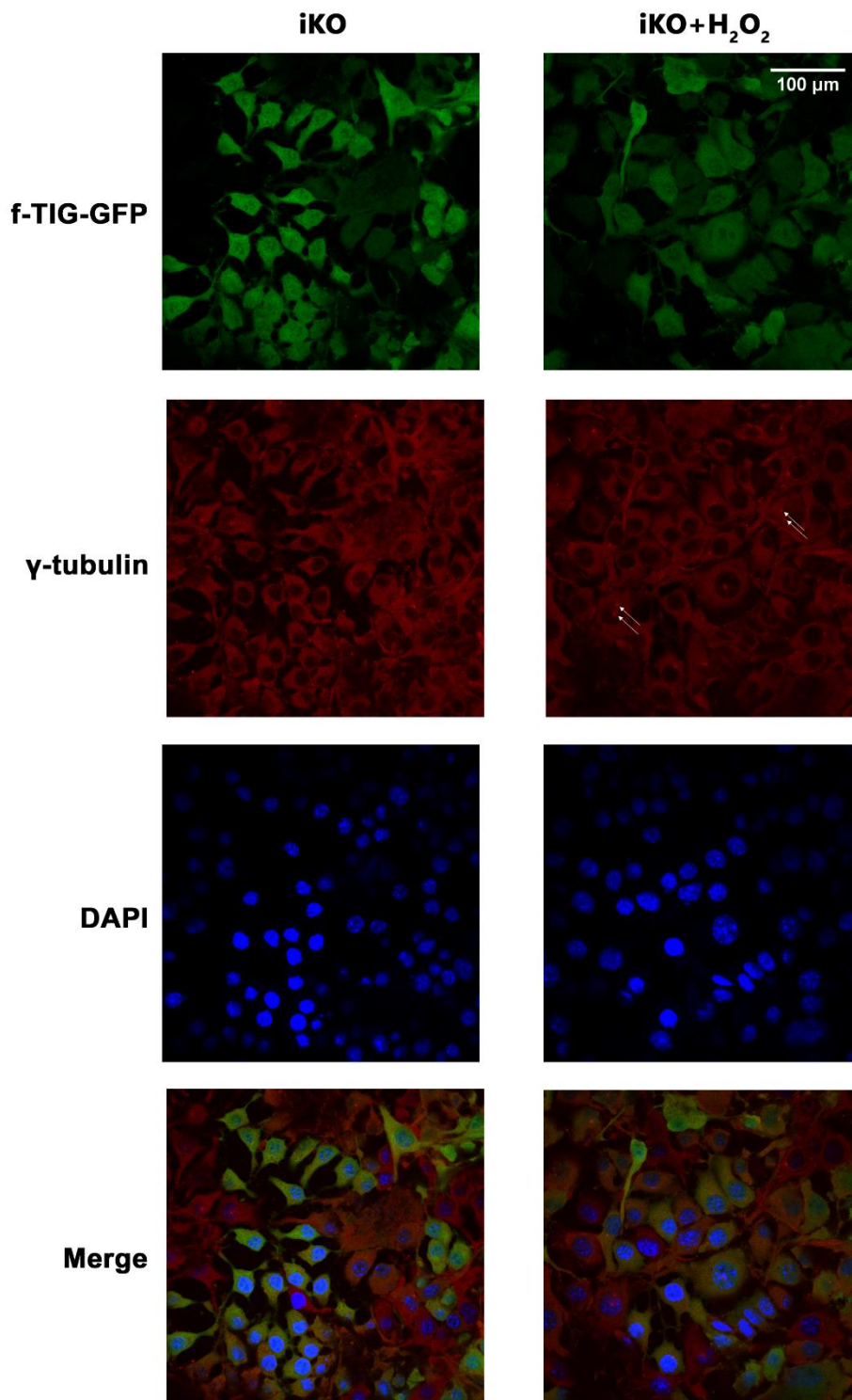


Figure 91. Localisation of TIGAR under oxidative stress in iKO cells. *Tigar* KO PDAC cells were infected with flag-TIGAR-GFP (f-TIG-GFP) (iKO cells) and treated with 0,5 mM H_2O_2 for 24 h. The construct f-TIG-GFP is shown in green, γ -tubulin was detected with an Alexa 594-conjugated secondary antibody (red) and nuclei were stained with DAPI (blue). Colocalisation between TIGAR and γ -tubulin can be observed in the Merge channel as yellowish areas. White arrows indicate centrosomes.

In order to determine the potential TIGAR contribution to the enlargement phenotype evidenced after H_2O_2 treatment, non-infected KO TIGAR cells were treated with at the same conditions and γ -tubulin immunofluorescence was performed. H_2O_2 -treated *Tigar* KO cells also showed enlarged nucleus and cytoplasm, indicating that TIGAR is not essential for PDAC cells response to H_2O_2 (Figure 92).

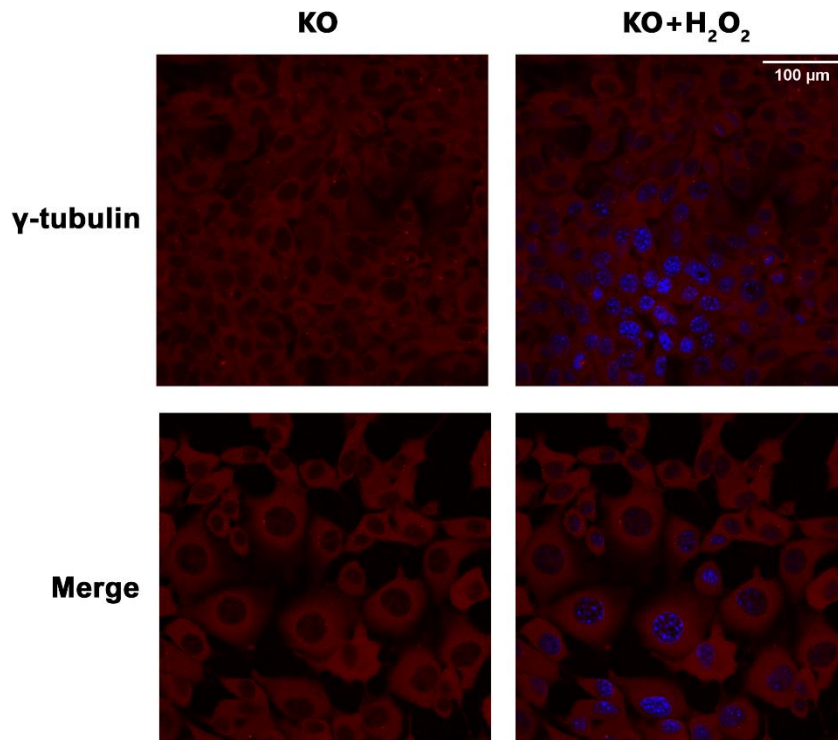


Figure 92. γ -tubulin distribution under oxidative stress. *Tigar* KO PDAC cells were treated with 0,5 mM H_2O_2 for 24 h and immunofluorescence against γ -tubulin was performed using an Alexa 594-conjugated secondary antibody (red). Nuclei were stained with DAPI (blue).

The dependency of ROS to induce this phenotype of cytoplasmic and nuclear enlargement with centrosome disorganization was assessed by treating iCT and iKO PDAC cells with 0,5 mM H_2O_2 in combination with 1 mM NAC, which increases the synthesis of glutathione and, thus, reduces ROS levels. In Figure 93 an additional image of H_2O_2 -treated iCT cells is shown, in which the cellular enlargement is not as dramatic as in Figure 90 and, moreover, TIGAR is localized both in the cytoplasm and the nucleus of cells, with increased signal in the nuclear and perinuclear area (Figure 93, second row). NAC treatment alone did not induce any detectable changes in cells (Figure 93, second row), but in combination with H_2O_2 it was able to prevent the phenotype induced by H_2O_2 in iCT (Figure 93, third row). However, H_2O_2 effects were only partially avoided by NAC in iKO cells, which showed decreased cellular size but still maintained centrosome disorganization (Figure 94).

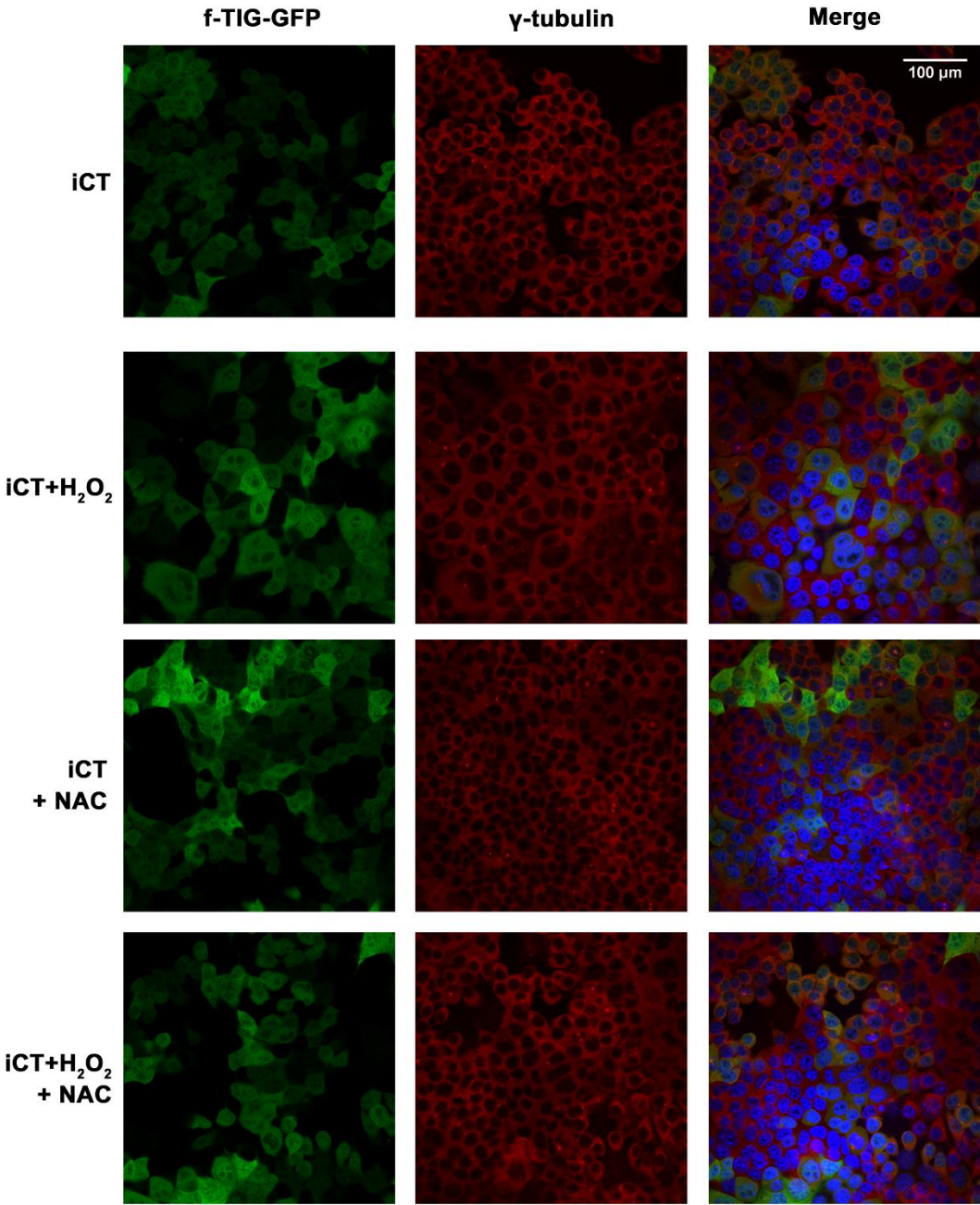


Figure 93. ROS-dependent effect of the phenotype induced by H₂O₂ in iCT cells. WT *Tigar* PDAC cells were infected with flag-TIGAR-GFP (f-TIG-GFP) (iCT cells) and treated with 0,5 mM H₂O₂ and/or 1 mM NAC for 24 h. The construct f-TIG-GFP is shown in green, γ-tubulin was detected with an Alexa 594-conjugated secondary antibody (shown in red) and nuclei were stained with DAPI (shown in blue).

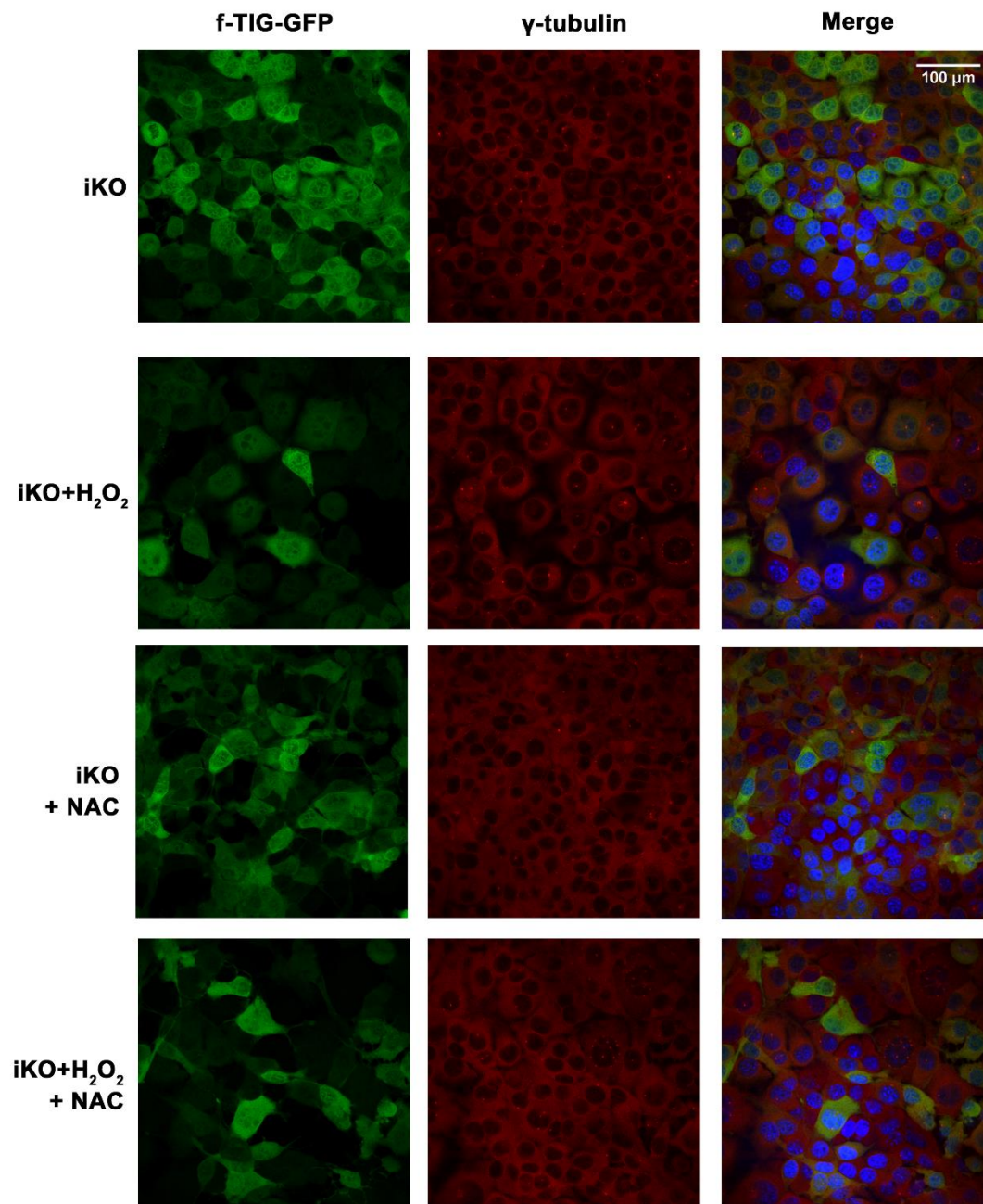


Figure 94. ROS-dependent effect of the phenotype induced by H₂O₂ in iKO cells. *Tigar* KO PDAC cells were infected with flag-TIGAR-GFP (f-TIG-GFP) (iKO cells) and treated with 0,5 mM H₂O₂ and/or 1 mM NAC for 24 h. The construct f-TIG-GFP is shown in green, γ -tubulin was detected with an Alexa 594-conjugated secondary antibody (shown in red) and nuclei were stained with DAPI (shown in blue).

Finally, we aimed to determine if the mobilization of TIGAR to the nucleus that we observed in several experiments with H₂O₂-treated PDAC cells through the fluorescence of the recombinant protein f-TIG-GFP was also detected in endogenous Tigar. With this aim, we treated non-infected WT *Tigar* PDAC cells with 0,5 mM H₂O₂ for 24 h and performed immunofluorescence of Tigar with an Alexa 488-conjugated secondary antibody. Non-infected *Tigar* KO cells were used as negative control. The images evidenced the translocation of endogenous Tigar to the nucleus of H₂O₂-treated cells (**Figure 95**). These results were clearer than some of the experiments performed with the f-TIG-GFP-overexpressing cells given that basal Tigar levels were reduced and slight changes in the distribution could be detected.

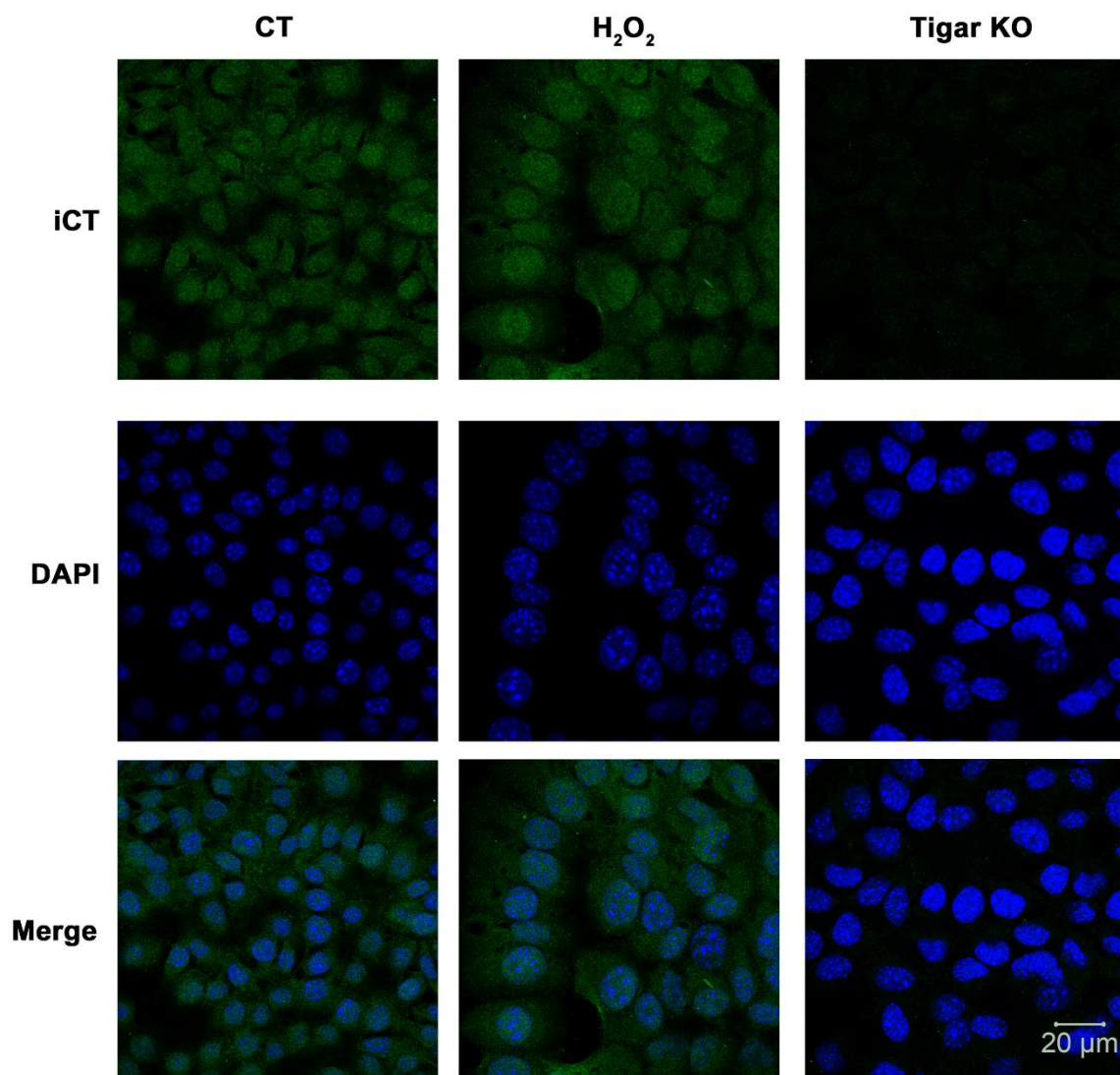


Figure 95. Tigar localisation under oxidative stress in PDAC cells. WT *Tigar* PDAC cells were treated with 0,5 mM H₂O₂ for 24 h and immunofluorescence against Tigar was performed with sc-67273 primary antibody and an Alexa 488-conjugated secondary antibody (shown in green). Nuclei were stained with DAPI (shown in blue). *Tigar* KO PDAC cells were used as negative control.

3. Contribution of TIGAR to cell survival in stress conditions

The potential of working with wild type *Tigar* and *Tigar* KO mouse cells was to determine the contribution of this enzyme to the survival of PDAC cells. We analysed that by exposing cells to oxidative stress and mitotic arrest, induced by H₂O₂ and nocodazole (Noco), respectively. Non-infected and infected *Tigar* KO PDAC cells were treated with 0,5mM H₂O₂ or 100 ng/mL Noco for 24 h. Cells were seeded at 0,5x10⁵ cells/mL and treatments were applied 10 h after the seeding. Cell number was determined at 10, 20 and 34 h post-seeding, the latter time corresponding to 24 h post-treatment. Growth curves were calculated during the 24 h of treatment. Results indicated that cells in which *Tigar* expression had been rescued by infection with f-TIG-GFP showed significantly increased proliferation in untreated conditions (**Figure 96A**). Importantly, *Tigar* KO cells showed decreased growth rates under H₂O₂ and nocodazole compared to PDAC cells with *TIGAR* overexpression (**Figure 96B,C**). Cells treated with H₂O₂ in combination with nocodazole showed similar growth rates regardless of *TIGAR* expression (**Figure 96D**).

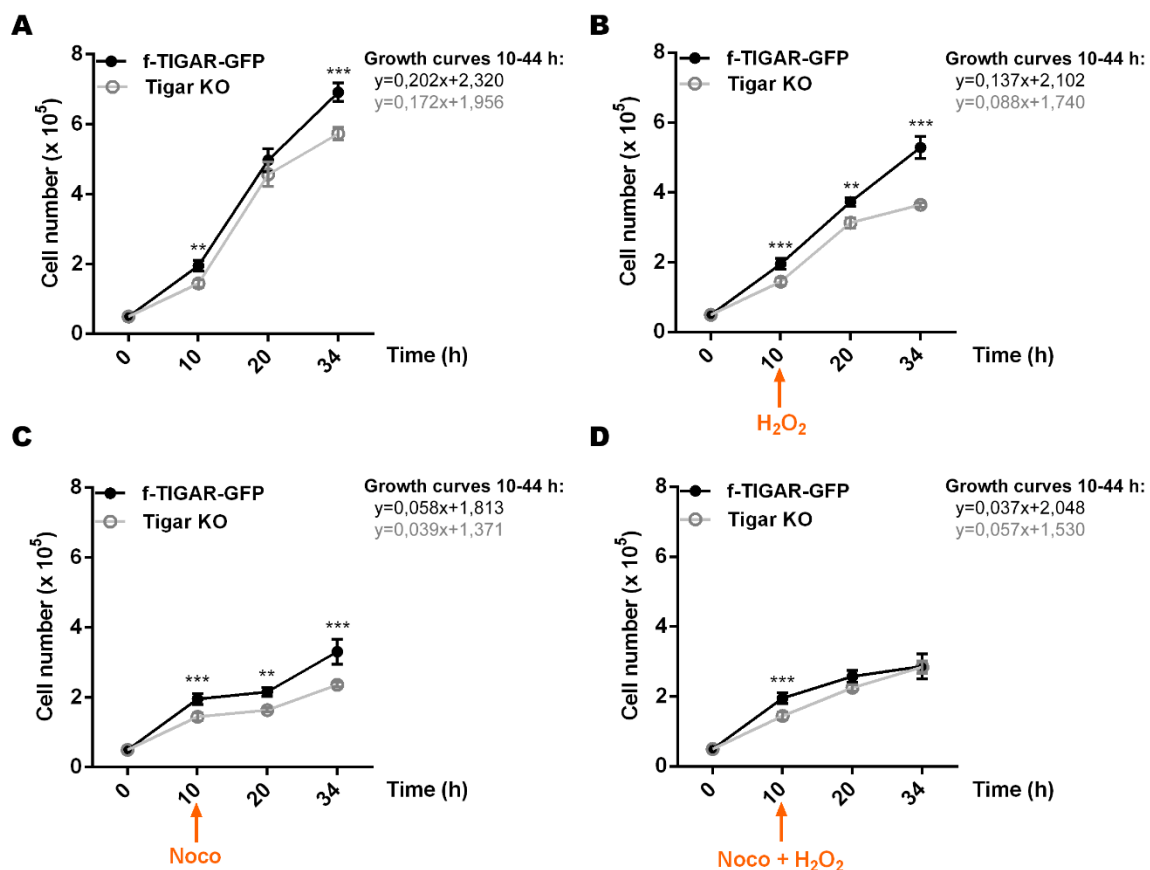


Figure 96. Evaluation of TIGAR contribution to the proliferation of PDAC cells. The capacity of TIGAR to affect the proliferation of PDAC cells was assessed at basal conditions and in response to stress stimuli. Parental and flag-TIGAR-GFP-infected *Tigar* KO cells (*Tigar* KO and f-TIGAR-GFP, respectively) were seeded at 0,5 x 10⁵ cells/mL and cellular counting were performed at different time points. **(A)** Cell number was evaluated at 10, 20 and 34 h post-seeding in both cell lines (f-TIGAR-GFP in black, *Tigar* KO in grey) in untreated conditions. At 10 h post-seeding, cells were treated with **(B)** 0,5 mM H₂O₂, **(C)** 100 ng/mL nocodazole (Noco) or **(D)** the combination of 0,5 mM H₂O₂ and 100 ng/mL nocodazole (Noco) for 24 h. Mean cell number ± SD is represented (n=3, **P < 0,01, ***P < 0,001) and the equations corresponding to the linear growth curves during the 24 h of treatment are provided.

4. Discussion

During the stay in the laboratory of Dr. Karen Vousden a very useful tool for the study of TIGAR localisation was generated, consisting in a viral vector expressing the human TIGAR protein fused with flag and EGFP (f-TIG-GFP). We generated PDAC cells stably expressing f-TIG-GFP in which we could determine that oxidative stress induced by H₂O₂ increased the presence of TIGAR in the perinuclear and nuclear areas. The analysis of TIGAR localisation was performed in parallel to the immunodetection of γ -tubulin, a protein involved in the nucleation and anchoring of microtubules to the centrosome, a structure that participates in the DNA damage response. PDAC cells responded to oxidative stress with an important enlargement of their cellular surface and showing signs of centrosome disorganization, as it was suggested by the detection of multiple centrioles and the separation of the two centrioles in cells that were not dividing. In those cells more enlarged, TIGAR was almost uniquely located in the perinuclear and nuclear areas and γ -tubulin formed a ring around the nucleus, indicating that these two proteins could colocalize under certain stress conditions. This phenotype has been demonstrated to be specific of the oxidative stress generated by H₂O₂ given that it was attenuated, and in some cases completely reverted, by NAC. Previous studies described that H₂O₂ can induce centrosome amplification and cellular senescence, characterized by enlarged cell shape (193), which is consistent with our results. The relevance of senescence in cancer is controverted, as it can function as a growth-arrest program and, therefore, have a tumour suppressor effect, or it can reflect a resting state of tumour development in which cancer cells can re-enter the cell cycle and keep multiplying. Besides, the secretory phenotype of senescent cells can cause both tumour-promoting and tumour-suppressing responses (194). A preliminary analysis of expression data available in Geoprofiles (accession number GSE11954) revealed increased expression of TIGAR in senescent activated hepatic stellate cells in response to etoposide, a DNA-damaging agent, which also supports our results (195). Additionally, a previous publication from Dr. Bartrons' Lab suggested that TIGAR disbalance can trigger senescence, both when the levels of this protein are too high or too low in stressed cells (79).

The functions attributed to cytoplasmic TIGAR seem to differ from those carried out in specific organelles such as mitochondria (87) and the nucleus (88). Nuclear localisation of proteins classically attributed to other cellular compartments has been described in response to H₂O₂, as it is the case of the hepatocyte growth factor receptor c-MET (196). This supports that moonlighting effects of proteins can be as determinant for the response to oxidative stress as their classically described functions.

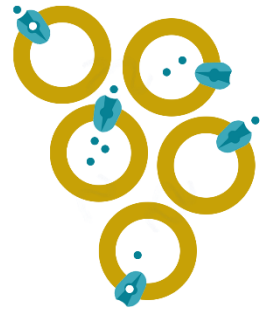
The interesting observation of potential colocalisation between TIGAR and γ -tubulin was in accordance with the finding that TIGAR participates in the DNA damage response induced by genotoxic drugs and hypoxia through its translocation to the nucleus (88). Besides, data obtained from a study that characterised the centrosome-cilium interface indicated that TIGAR interacts with Oral-Facial-Digital

Syndrome 1 protein, which is a centriolar satellite protein that at the same time interacts with γ -tubulin. This study used an *in vivo* proximity-dependent biotinylation approach with 58 known centrosome proteins fused with a biotin conjugating enzyme, which were used as baits. The proteins interacting with these baits, one of which was TIGAR, were biotinylated and could be detected (197). TIGAR was detected in the centrosomes, but not in cilia, and these results support the possibility of an interaction between TIGAR and γ -tubulin in response to oxidative stress. However, co-immunoprecipitation experiments should be performed to prove this hypothesis.

Regarding the basal localisation of TIGAR, we have been able to show that it is globally distributed along the cell, with a higher presence in the cytoplasm in unstressed conditions. Interestingly, the f-TIG-GFP construct was found to colocalize with Tom20 in some areas, indicating that TIGAR can also be located in mitochondria. As it has been previously mentioned, Dr. Karen Vousden's group described that TIGAR interaction with HK-II in the outer mitochondrial membrane is essential to activate HK-II in response to hypoxia and contributes to tumour cell survival in these conditions (167). Binding of HK-I and II to the outer mitochondrial membrane has been described to occur more frequently in transformed cells than in non-malignant cells, coupling ATP production to the phosphorylation of glucose and increasing glycolysis (198). Therefore, TIGAR binding to HK-II in the mitochondria would contribute to glycolysis, carrying out the opposite effect that has been attributed to cytoplasmatic TIGAR.

Overall, the mobilisation of TIGAR to the nucleus in response to oxidative stress, as well as the changes in the localisation of this protein reported in response to different damaging stimuli, indicate that other regulatory mechanisms rather than transcriptional control are involved in the role of this enzyme in cancer cells. The results presented here can help to understand the generalised observation that *TIGAR* inhibition sensitizes cells to different kinds of stress, at the same time that TIGAR protein levels remain unaltered in stress conditions.

GENERAL DISCUSSION



Cellular metabolism is not a static picture of the fuels and products that sustain cellular functioning. Instead, it can be depicted as a network of connections, some of which usually involve same players at same places, and some others changing so briefly that their detection is challenging even to the most advanced technologies. In this context, metabolic transformation emerges as a concept that is used to refer to the collection of metabolic alterations that cells accumulate to become tumorigenic. However, this list is not written anywhere, and each type of cancer displays deregulation of different metabolic pathways, not to mention the adaptations that cancer cells develop to adapt to the changing and challenging tumour microenvironment.

TIGAR is only a piece in this unattainable network. This gene was described for the first time thirteen years ago as a p53 target induced by ionizing radiation (3) and, because it takes time to consolidate new knowledge, it is still considered a novel gene. Maybe this is the reason why, although TIGAR was described as a Fru-2,6-P₂ phosphatase able to increase the flux through the PPP, its function and relevance in cancer development is still in discuss. This thesis has been focused on two main objectives, both of them addressed to the clarification of the role of TIGAR in cancer: to understand how *TIGAR* is induced in transformed cells, and to define the metabolic changes induced by TIGAR. Although a definitive answer to these questions is still far away, here we summarise the main findings of this thesis trying to give light to the understanding of how TIGAR contributes to the metabolic reprogramming of cancer cells.

In the first chapter of this thesis, we have approached the relevance of *TIGAR* expression in conditions of glycolytic blockage. We have described that *TIGAR* is induced by PFKFB3 inhibition, both through siRNA or long-term exposure to 3PO. However, glucose deprivation, which causes a strong inhibition of glycolysis and subsequent cell death, does not induce *TIGAR*. PFKFB3 inhibition, both by siRNA and 3PO, decreases Fru-2,6-P₂ levels and, thus, partially impairs glycolysis by inhibiting PFK-1. The impact of PFKFB3 inhibition on cell viability is exacerbated when TIGAR is inhibited at the same time, evidencing that both genes exert protective roles in cancer cells. Nevertheless, the fact that cells respond to decreased Fru-2,6-P₂ by increasing TIGAR is the first evidence that this enzyme plays other roles beyond its phosphatase activity on Fru-2,6-P₂.

Inhibition of PFK-1 causes accumulation of Fru-6-P, which is converted to Glu-6-P through GPI, increasing the flux through the PPP (170). By the same rationale, suppression of PFKFB2 activity by PP2A confers proliferative advantage in B cell malignancies. PFKFB2 inhibition increases the flux through the PPP, which is determinant for the survival of these cells in conditions of high oxidative stress (99). According to that, metabolomic abundance analyses performed during this thesis suggested increased Fru-6-P, Glu-6-P and 6-P-gluconate in *PFKFB3*-inhibited HeLa cells. TIGAR, by catalysing the opposite reaction of PFK-2, has been proposed to be essential to accomplish the purpose of increasing the PPP

by inhibiting glycolysis, at least in some cellular types (3,170). However, why should TIGAR be increased in a situation in which the PPP is already enhanced by PFKFB3 inhibition?

During this thesis, *TIGAR* overexpression has been proved to decrease Fru-2,6-P₂ concentration, but the metabolomic abundance and fluxomic analyses did not report changes in 6-phosphogluconate or ribose-5-P, metabolites of the PPP, after *TIGAR* overexpression or inhibition. These results, together with the unaltered ratio NADP⁺/NADPH measured in *TIGAR*-inhibited and *TIGAR* overexpressing cells, question the activity of TIGAR as an activator of the PPP, at least in HeLa cells. However, the capacity of TIGAR to increase NADPH has been proved in other cell lines (83,91–93), evidencing that TIGAR contribution to the PPP may vary depending on the cellular context. Nevertheless, complementary determinations such as quantification of GSH/GSSG ratio in our experimental conditions would be informative of changes in the antioxidant capacity of HeLa cells. In situations of high ROS levels, changes in NADPH might be masked by the rapid oxidation of this molecule to regenerate GSH.

Another variable that needs to be considered when comparing the effects of TIGAR modulation between cells is the activity of PFKFBs. PFKFB1 has not been found expressed in cancer cells, but PFKFB2–4 are expressed across different cancer types, displaying specificities according to tissue origin (36). HeLa cells express the three PFKFB2–4 isoenzymes, but their contribution to cell survival is different depending on cellular conditions. For example, PFKFB2 is involved in the response to amino acid deprivation in this cell line (51) whereas PFKFB3 is important when cells are exposed to stress stimuli that trigger the p38/MK2 such as NaCl, H₂O₂, UV radiation or anisomycin (41). In a previous thesis of the group, it was shown that PFKFB3 inhibition is not compensated by any other PFKFB isoenzyme in these cells (63), which explains the decreased Fru-2,6-P₂ and lactate concentrations detected in our experiments. In terms of balancing Fru-2,6-P₂ concentration, PFK-2 activity is much more potent than TIGAR bisphosphatase activity, providing an explanation for the mild effect of the single inhibition of TIGAR on the several parameters analysed, such as ROS or apoptosis. Interestingly, MTT signal was the only parameter significantly affected by *TIGAR* inhibition. The decreased MTT signal in *TIGAR*-inhibited cells reflects lower mitochondrial reduction capacity, which is in accordance with the findings by the group of Martínez-Outschoorn (82). This group has shown that *TIGAR* overexpression increases oxygen consumption and ATP production, as well as some mitochondrial markers such as TOM20, when glutamine or lactate are supplied (82).

TIGAR contribution to cell survival is evidenced when cells are facing some kind of stress. This has been analysed in several contexts along this thesis. One of the most studied scenarios has been the inhibition of glycolysis in HeLa cells. In our experiments, PFKFB3 blockage increased ROS levels, which we propose as the cause of increased DNA damage and cell death, according to previous publications (199,200).

When *PFKFB3* and *TIGAR* were inhibited at the same time, the damaging effects were exacerbated. The same occurred when cells were treated with 3PO or glucose deprivation in combination to *TIGAR* inhibition. The other context in which *TIGAR* contribution to cell survival has been analysed is the response of mouse PDAC cells to H₂O₂ or nocodazole, which revealed that *Tigar* KO cells are more susceptible to damaging agents. Interestingly, the nuclear localisation of *Tigar* under oxidative stress detected in PDAC indicates that the protective action of this enzyme is also supported by mechanisms independent of the modulation of its protein levels. These results point out that both *TIGAR* and *PFKFB3* carry on pro-survival roles in cells and, thus, that *TIGAR* promotes, rather than inhibits, cancer development. Similar observations have been described in cancer cells in response to hypoxia, where *TIGAR* interaction with HK-II in the outer mitochondrial membrane limits cell death independently of its Fru-2,6-P₂ bisphosphatase activity. These findings are in accordance with the evidence that *TIGAR* is overexpressed in many types of tumours in which *PFKFB3* is also increased, as it has been exposed in the Introduction of this thesis. Therefore, the simplification of *TIGAR* as an enzyme opposed to *PFKFB3* needs to be replaced by the growing evidence that *TIGAR* activation can represent a metabolic advantage in cells when the glycolytic flux is compromised.

One of the questions that arose during the characterisation of *TIGAR* induction by decreased glycolytic flux was the mechanism beyond this response. Western blot analyses from a previous thesis of the group revealed increased phosphorylation of several proteins of the PI3K/mTOR signalling pathway after *PFKFB3* suppression (161). During the present thesis these results have been confirmed and the phosphorylation of Akt at S473 has been demonstrated to be crucial for *TIGAR* upregulation in response to *PFKFB3* inhibition. In most cases of failing energy status, AMPK α is responsible for reorganizing the metabolic network to increase ATP production and decrease biosynthesis (174). However, the role of Akt under metabolic stress is in dispute because it is mainly considered a driver of energy production in conditions of nutrient abundance. Despite that, a growing number of studies are evidencing the contribution of Akt in the response to glycolytic inhibition, sometimes through a cross-talk with AMPK α (201). Short-term glucose deprivation has been described to induce AMPK α and Akt signalling and inhibit mTORC1, whereas prolonged culture in glucose-free media inhibits AMPK α , favouring mTORC1/Akt signalling (202). Akt phosphorylation has also been observed to initiate a pro-survival response in 2-DG-treated cells (203). Thus, our results support the role of Akt as a stress-response gene. Importantly, the Akt signalling pathway is known to activate Nrf2 in proliferating cells, oppositely to what occurs in quiescent cells, where Nrf2 is only activated by oxidants or electrophiles (142). The constitutive activation of Nrf2 in cancer cells confers chemo- and radio-resistance, especially to those drugs whose mechanism of action is based on ROS generation (139). We have shown that *PFKFB3* inhibition increases

Nrf2 total protein amounts and triggers its translocation to the nucleus. However, the question of whether the Akt-Nrf2 axis is responsible for *TIGAR* induction after *PFKFB3* inhibition remains open.

During this thesis we have shown that Nrf2 activation controls *TIGAR* mRNA and protein levels in HeLa cells, both through the physiological induction of the transcription factor with DMF and through direct overexpression of the factor. Accordingly, inhibition of Nrf2 decreases *TIGAR* expression, evidencing a direct relationship between the transcription factor and *TIGAR*. Thus, Nrf2 emerges as a new transcriptional regulator of *TIGAR*, which might be of special relevance in conditions of oxidative or metabolic stress in cells lacking p53. HeLa cells are considered p53-inactive given that they express the E6 oncoprotein, which triggers ubiquitin-dependent proteolysis of p53 (164). However, reactivation of p53 has been described in HeLa (165) and, thus, the participation of this transcription factor in the modulation of *TIGAR* cannot be excluded in these cells. However, *TIGAR* basal expression does not seem to depend on neither p53 or Nrf2 in these cells. The SP1 transcription factor, common in the promoter of most eukaryotic genes, has been described to control *TIGAR* expression through direct interaction with a region located at -177 bp before the translation start codon, in what has been described as the minimal promoter of *TIGAR* (76). Given the close proximity of the SP1 binding site to the transcription start site of *TIGAR*, with only 43 bp in-between, and the ubiquitous expression of this transcription factor, SP1 seems to be a good candidate to maintain basal *TIGAR* levels.

In a region upstream of *TIGAR* minimal promoter, we have identified two AREs. These AREs have been cloned in luciferase-reporter vectors, the activity of which is increased in cells overexpressing Nrf2 compared to cells with basal levels of Nrf2. More experiments are being performed to identify which of the AREs is responsible for the binding of Nrf2 to *TIGAR* promoter. Moreover, ChIP experiments will be also carried out. What can be concluded so far is that *TIGAR* expression is controlled by this transcription factor, either directly or indirectly, in HeLa cells. Besides, the results obtained in mouse cells support this hypothesis. In collaboration with Dr. Ventura's Lab, we have shown that the Nrf2 inducer DMF increases mouse *Tigar* expression, and so it does the overexpression of Nrf2. Moreover, we have proved that Nrf2 binds to an ARE located at -5762 bp in *Tigar* promoter by ChIP assays. The involvement of Nrf2 in the regulation of *Tigar* expression in mouse is of importance given that previous publications claim that neither *TP53* or *TAp73* control the expression of *Tigar* in this specie (75). *Tigar* expression is clearly induced in the intestine of mice following DNA-damaging stress such as ionising radiation (75,90) and therefore alternative transcription factors must be involved in this regulation. Nrf2 emerges as a potential candidate to regulate mouse *Tigar* in response to damaging stimuli. In this regard, it is important to mention that c-Myc was found to control *Tigar* expression in a mouse model of colon cancer induced by the loss of adenomatous polyposis coli gene, independently of Wnt/ β -catenin signalling (126). However, the direct transcriptional control of *Tigar* by c-Myc was not proved. Considering that Nrf2 can

be activated by c-Myc (143), it would be interesting to determine the potential role of Nrf2 as mediator of c-Myc-induced *Tigar* transcriptional regulation in this model.

Regarding human *TIGAR* gene, the role of Nrf2 as a transcriptional regulator has also been evaluated in three different NSCLC cells, A549, H460 and H1299, with inconclusive results. The analysis of microarray data from a previous study reported that *TIGAR* mRNA levels were not decreased after Nrf2 inhibition in A549 cells (142). In our experiments, *TIGAR* expression was indeed slightly increased after Nrf2 suppression in these cells. However, TIGAR protein levels were downregulated in this cell line at the same conditions, indicating a differential effect of Nrf2 suppression on *TIGAR* mRNA and protein. The results obtained with H460 cells suggested a link between Nrf2 and TIGAR given that Nrf2 inhibition downregulated *TIGAR* expression. p53-null H1299 cells, which are a clear example of the independent expression of *TIGAR* from p53, responded to Nrf2 inhibition by upregulating *TIGAR* expression without altering TIGAR protein levels. These results suggested an indirect effect of Nrf2 on TIGAR modulation in NSCLC which probably involves other transcriptional regulators. Importantly, the different results obtained in the three cell lines indicate that both mRNA and protein levels must be checked when analysing the consequences of the blockage of an important transcription factor, as it is Nrf2, and defining its potential target genes. Strategies based on the inhibition of Nrf2 or the activation of KEAP1 have been proposed in NSCLC to fight chemo- and radio-resistance (186). Besides, stratification of patients with lung cancer according to mutations in KEAP1 and Nrf2 has been proposed as a clinical strategy to predict the response to drugs such as glutaminase inhibitors (160). However, the potential implications of the deregulation of Nrf2 targets in response to therapies based on Nrf2 inhibition should be evaluated in advance. Whether Nrf2 target genes will be downregulated when Nrf2 is inhibited or will be compensated by alternative mechanisms in cancer cells, as it occurs with *TIGAR* in NSCLC, is something that only further research will be able to answer.

Linking the first and third chapters of this thesis, the question of what is TIGAR doing in cancer cells emerges. In one side, we have described that this gene is induced in response to decreased glycolytic flux and, on the other side, one of the most important antioxidant orchestrators in cells, Nrf2, controls *TIGAR* expression under certain conditions. Thus, it seems reasonable to think that the pro-survival role of TIGAR is attributed to its antioxidant potential. However, the results presented in the second chapter of this thesis question the role of TIGAR as a PPP enhancer.

It has already been discussed that *TIGAR* overexpression clearly decreases Fru-2,6-P₂ concentration without affecting the levels of PPP intermediates in HeLa cells. However, *TIGAR* inhibition only increases Fru-2,6-P₂ concentration. Accordingly, metabolomic analyses suggested that *TIGAR*-inhibited cells have increased levels of glycolytic intermediates, which is consistent with the idea of TIGAR as a glycolytic inhibitor (3). However, the question is whether these changes can be attributed to Fru-2,6-P₂. The answer

seems to be 'no', or at least 'not only', especially considering that *TIGAR* overexpression, which has a higher impact on Fru-2,6-P₂ than *TIGAR* inhibition, does not affect the levels of any of the glycolytic intermediates analysed.

What can be concluded from the metabolic studies performed is that *TIGAR* inhibition impacts cellular metabolism beyond its capacity to increase Fru-2,6-P₂ concentration. Two important metabolic alterations have been detected after *TIGAR* suppression, both of them related to the last reactions in glycolysis and the entrance of pyruvate to the mitochondria.

Both 3PG and pyruvate were found significantly increased in *TIGAR*-inhibited cells in metabolomic and spectrophotometric analyses, respectively. These results suggest a role for this enzyme in dephosphorylating 3PG, or even 2PG, which would be in accordance with the finding that the Km of *TIGAR* for 2,3-BPG, 2-PG and PEP is much lower than that for Fru-2,6-P₂ (73). In this previous publication, *TIGAR* was proposed as the phosphoglycolate-independent 2,3-BPG phosphatase. However, we could not determine 2,3-BPG by our experimental approaches and, thus, we cannot confirm this finding in HeLa cells. What can be concluded from sequence and structural alignments is that *TIGAR* and *PGAM* are closer than *TIGAR* and *FBPase-2*, and thus the increased concentration of 3-PG found after *TIGAR* inhibition should be further explored.

On the other hand, it does not seem plausible that *TIGAR* effect on pyruvate is based on its phosphatase activity given that it is not a phosphorylated metabolite. Thus, either *TIGAR* acts on a different metabolite, the increase of which is reflected by increased pyruvate, or *TIGAR* exerts bisphosphatase-independent effects on pyruvate. Interestingly, *TIGAR* was proposed to catalyse the dephosphorylation of PEP into pyruvate uncoupled from ATP production, which would allow cells to maintain high glycolytic flux for biosynthesis (73). According to that, *TIGAR* inhibition would increase PEP concentration, which might be reflected in increased pyruvate concentration through PK activity. However, our results do not show significantly increased PEP, questioning this hypothesis.

The most important metabolic change reported after *TIGAR* suppression involves mitochondrial metabolism. Increased m+2 citrate and decreased m+3 aspartate were found in *TIGAR*-inhibited cells, indicating increased flux through PDH and decreased oxidation of pyruvate through PCB. These results, together with the findings of increased NAD⁺/NADH ratio and decreased MTT signal in *TIGAR*-inhibited cells, reflect decreased functioning of the TCA cycle in these cells. Previous publications have reported that *TIGAR* overexpression increases lactate uptake and oxygen consumption, suggesting increased production of NADH and increased OXPHOS. These effects are observed when cells are cultured in glutamine and/or lactate-rich media and not when cells are cultured only with glucose, highlighting the contribution of extracellular lactate in TCA fuelling in *TIGAR* overexpressing cells (82). Accordingly, we

have shown that *TIGAR* overexpressing cells have higher levels of the lactate importer MCT1. These cells maintain high glycolytic flux, which is stimulated by PFK-2. In these conditions, OAA in the TCA cycle is regenerated by pyruvate through PCB and also by alternative substrates such as glutamine. Given that *TIGAR* overexpression could partially inhibit glycolysis in some cells, these cells have increased lactate uptake through MCT1, which represents an additional source of pyruvate to the TCA cycle, and show high oxygen consumption and ATP production, as it was reported by Ko, *et al.* (82).

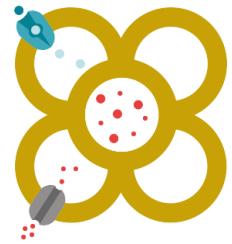
On the contrary, *TIGAR*-inhibited cells have lower levels of MCT1, increased PCB levels and decreased MTT mitochondrial reduction capacity. Thus, it could be interpreted that in a situation of decreased *TIGAR* levels, NADH production is reduced due to decreased mitochondrial metabolism, and restricted lactate import contributes to increase the NAD^+/NADH ratio. Considering the activity of *TIGAR* on Fru-2,6-P₂, glycolysis might be slightly enhanced in *TIGAR*-inhibited cells, as evidenced by increased glycolytic intermediates in the metabolomic analyses. In these conditions, pyruvate enters the mitochondria through PDH, in a reaction that generates NADH. *TIGAR*-inhibited cells rely on glycolysis to generate pyruvate. Due to decreased PCB activity in these cells, OAA needs to be regenerated by anaplerotic substrates such as glutamine to maintain the TCA cycle.

The contribution of glutamine to mitochondrial metabolism in *TIGAR*-inhibited and *TIGAR* overexpressing cells needs to be further analysed. We have observed decreased intracellular glutamine in *TIGAR* overexpressing cells, whereas the opposite occurs when *TIGAR* is inhibited. However, GLS1 is increased in *TIGAR* overexpressing cells and decreased in *TIGAR*-inhibited cells, suggesting that glutamine levels reflect the consumption of this metabolite. This means that glutamine anaplerosis is higher in *TIGAR* overexpressing cells, which is consistent to what Ko, *et al.* described (82). In *TIGAR*-inhibited cells, thus, decreased glutamine anaplerosis might account for decreased mitochondrial metabolism. However, additional experiments should be performed to confirm these results in our model.

In the light of the results discussed, *TIGAR* induction in response to *PFKFB3* inhibition can be interpreted as a compensatory mechanism by which cells increase mitochondrial metabolism to compensate the decreased ATP production in glycolysis. This might explain why MTT signal is not decreased in *PFKFB3*-inhibited cells despite these cells show decreased viability. As consequence of *TIGAR* induction, MCT1 might be enhanced in *PFKFB3*-inhibited cells, providing lactate for the obtention of pyruvate and acetyl-CoA to maintain mitochondrial activity. Suppression of *TIGAR* in *PFKFB3*-inhibited cells results in increased cell death, which might be attributed to decreased lactate import, which renders cells dependent on the pyruvate produced in glycolysis, a pathway that is inhibited by *PFKFB3* siRNA.

Possibly, the diverse functions of TIGAR –as a classical PPP promoter, as an enzyme that can potentially link glycolytic and mitochondrial metabolism by conditioning lactate import, and also as a nuclear effector in conditions of oxidative stress– are not excluding and, indeed, coexist in cells. It is also possible that none of them is more important than the others, but each one prevails depending on the cellular circumstances. Although more data are required to define the consequences of *TIGAR* modulation by Nrf2 and the contribution of TIGAR to mitochondrial metabolism and nuclear functions, here we have described several mechanisms that can contribute to explain how *TIGAR* inhibition impairs tumour development. What is important from these studies, as well as from the studies by Cheung, *et al.* (87) and Ko, *et al.* (82), is that alternative explanations are provided to the role of TIGAR as a Fru-2,6-P₂ bisphosphatase.

CONCLUSIONS



Chapter I. TIGAR and glycolysis inhibition: is that redundant?

1. *TIGAR* expression and protein levels are induced after siRNA-mediated *PFKFB3* inhibition and the phosphorylation of Akt at Ser473 is required for this modulation.
2. Oxidative stress, DNA damage and apoptosis are enhanced in *PFKFB3*-inhibited cells, whereas the inhibition of *TIGAR* decreases the mitochondrial reduction capacity. These effects are exacerbated by the combined inhibition of *PFKFB3* and *TIGAR*.
3. The PFK-2 inhibitor 3PO increases the expression of *TIGAR* and the phosphorylation of Akt at Ser473 without affecting cellular viability. A more severe blockage of glycolysis induced by glucose deprivation does not induce *TIGAR*.
4. The avidity of cells for glucose and the production of lactate are decreased by the inhibition of either *TIGAR* or *PFKFB3*.

Chapter II. Role of TIGAR in the metabolism of cancer cells: is it all about Fru-2,6-P₂?

5. *TIGAR* protein sequence and structure are closer to PGAM than to the bisphosphatase domain of *PFKFBs*, as revealed by *in silico* studies.
6. *TIGAR* overexpression significantly decreases Fru-2,6-P₂ concentration, whereas *TIGAR* inhibition increases the concentration of this metabolite and that of 3-PG and pyruvate. The modulation of *TIGAR* levels does not affect the abundance of intermediates of the pentose phosphate pathway in HeLa cells.
7. Inhibition of *TIGAR* affects mitochondrial metabolism by enhancing PDH activity at the expense of PCB and increasing the anaplerosis of other fuels rather than glucose to the TCA cycle.
8. The ratio NAD⁺/NADH is increased after *TIGAR* suppression and remains unaltered after *TIGAR* overexpression. The ratio NADP⁺/NADPH is not affected by *TIGAR* modulation in HeLa cells.
9. The levels of the lactate importer MCT1 are increased in *TIGAR* overexpressing HeLa cells.

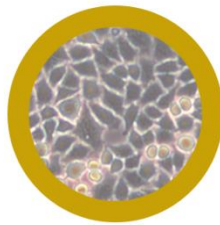
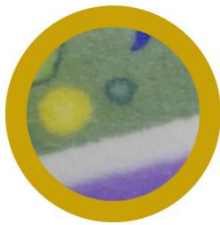
Chapter III. Control of *TIGAR* expression by Nrf2

10. Nrf2 activation by either Nrf2 overexpression or treatment with the Nrf2 inducer DMF increases *TIGAR* expression in human and mouse cells.
11. Inhibition of Nrf2 in HeLa cells decreases *TIGAR* expression. However, NSCLC cell lines showed heterogeneous responses to Nrf2 suppression, suggesting an indirect relationship between these two proteins in this subset of cancers.
12. Two antioxidant response elements located in the promoter of human *TIGAR* gene show functional activity after the overexpression of Nrf2 in luciferase assays. The direct binding of Nrf2 to an antioxidant response element in the promoter of mouse *Tigar* gene has been proved by ChIP assays.

Chapter IV. Looking at *TIGAR* in response to oxidative stress: location also matters

13. Hydrogen peroxide induces cellular enlargement and disorganization of centrioles in mouse pancreatic ductal adenocarcinoma cells. These effects are consistent with a senescent phenotype and are prevented by N-acetyl-cysteine.
14. *Tigar* is mobilized to the nucleus of mouse pancreatic ductal adenocarcinoma cells in response to hydrogen peroxide, and the flag-*TIGAR*-GFP fusion protein colocalizes with γ -tubulin in the perinuclear area at these conditions.
15. Overexpression of flag-*TIGAR*-GFP increases the proliferation of *Tigar* KO mouse pancreatic ductal adenocarcinoma cells treated with hydrogen peroxide and nocodazole.

MATERIALS AND METHODS



MATERIALS AND METHODS INDEX

1. Cell culture.....	195
1.1. Cell lines.....	195
1.2. Cell culture.....	195
1.3. Cell culture in low glucose conditions.....	195
1.4. Thawing cells.....	196
1.5. Freezing cells.....	196
1.6. Mycoplasma detection tests and treatment.....	196
2. Transfections.....	197
2.1. siRNA transfection with Oligofectamine.....	197
2.2. Plasmid transfection with Lipofectamine LTX.....	198
3. Protein analysis by western blot.....	199
3.1. Protein extraction.....	199
3.2. Protein quantification.....	202
3.3. Electrophoresis and western blot.....	203
4. Immunofluorescence.....	206
5. Gene expression analysis by RT-qPCR.....	209
5.1. mRNA extraction.....	209
5.2. RNA quantification.....	210
5.3. Retrotranscription.....	210
5.4. Real-time quantitative PCR.....	211
6. RT-MLPA.....	212
7. Flow cytometry analyses.....	212
7.1. Oxidative stress measurements by flow cytometry.....	212
7.2. Analysis of cell death by flow cytometry.....	213
8. Absorbance-based viability assessments.....	214
8.1. Crystal violet assay.....	214
8.2. MTT assay.....	214
9. Metabolic assays.....	215
9.1. Determination of glucose consumption.....	215
9.2. Determination of extracellular lactate.....	215
9.3. Determination of intracellular Fru-2,6-P2 concentration.....	216
9.4. Determination of intracellular Pyr, PEP, 2PG and 3PG.....	220
10. NAD(P) ⁺ /NAD(P)H assay.....	222

11. Metabolomics and fluxomics	223
11.1. Culture conditions	223
11.2. Obtention of cellular extracts.....	223
11.3. Sample processing and analysis	223
12. Molecular biology techniques	224
12.1. DNA purification from bacterial stabs.....	224
12.2. Obtention of DNA fragments by PCR	224
12.3. DNA electrophoresis in agarose gels and purification of bands	225
12.4. TOPO TA cloning.....	225
12.5. Restriction enzyme digestion.....	226
12.6. Dephosphorylation of vector 5'-P termini.....	229
12.7. Ligation.....	229
12.8. Transformation of Competent cells and selection of clones.....	230
12.9. Bacterial culture and plasmid purification.....	230
12.10. Preparation of glycerol stocks.....	231
12.11. Preparation of samples for sequencing	231
13. Generation of PDAC cells stably expressing flag-TIGAR-EGFP.....	232
13.1. Primer design for the amplification of the cDNA of interest.....	232
13.2. PCR amplification.....	233
13.3. Plasmid digestion and purification.....	233
13.4. Cloning and bacterial transformation	233
13.5. Production of viral particles and transduction	234
14. Luciferase assays	234
14.1. Luciferase Assay System.....	235
14.2. Luminescent β -galactosidase Detection Kit II	235
15. Chromatin Immunoprecipitation assay	235
16. Statistical analysis	235
17. General Buffers.....	236

1. Cell culture

1.1. Cell lines

The cell lines used for the experiments presented in this thesis are summarised in **Table M-I**. Additionally, human primary lymphocytes were used for the study presented in the Annex at the end of this thesis.

Cell line	Tumour origin	Reference
HeLa	Cervix adenocarcinoma	American Type Culture Collection
A549	Lung adenocarcinoma	These cells were kindly provided by the laboratory of Dr. Ricardo Enrique Pérez (Departament de Patologia i Terapèutica Experimental, Universitat de Barcelona)
H460	Lung adenocarcinoma	
H1299	Lung squamous cell carcinoma	These cells were kindly provided by the laboratory of Dr. Jose Luis Rosa (Departament de Ciències Fisiològiques, Universitat de Barcelona)
PDAC <i>Tigar</i> ^{+/+}	Mouse pancreatic ductal adenocarcinoma	These cells were kindly provided by the laboratory of Dr. Karen Vousden (The Beatson Institute for Cancer Research)
PDAC <i>Tigar</i> ^{-/-}	Mouse pancreatic ductal adenocarcinoma	

Table M-I. Cell lines used in this thesis and origin.

1.2. Cell culture

Cells were cultured in high glucose Dulbecco's Modified Eagle's Medium (DMEM; Biological Industries) supplemented with 10% Foetal Bovine Serum (FBS) (Biological Industries), 2 mM L-glutamine, 100U/mL penicillin and 100 ng/mL streptomycin (referred to as 'Complete DMEM', or 'Complete medium'). The culture conditions were 37 °C, 5% CO₂ and a relative humidity of 70–80%.

All cell lines were re-seeded in new plates every two days at a confluence of 25%. After two months of maintenance, cells were replaced by a fresh vial to reduce the number of mutations accumulated due to high number of cellular divisions.

1.3. Cell culture in low glucose conditions

HeLa cells were washed twice with PBS and complete DMEM was replaced by glucose-free DMEM (Biological Industries) supplemented with 5 mM glucose previously filtered, 10% dialyzed FBS (Biological Industries), 2 mM L-glutamine, 100U/mL penicillin and 100 ng/mL streptomycin. These culture conditions are referred to as 'Glucose deprivation'.

1.4. Thawing cells

For cells highly resistant to dimethyl sulfoxide (DMSO), the whole content of the frozen vial can be thawed and poured into a 10 cm Ø culture plate with 10 mL of complete DMEM. To avoid toxicity, it is recommended to eliminate DMSO. For that, thaw the cryopreservation vial in a water bath at 37°C and, just before it completely thaws, pour the whole content of the vial into a tube containing 10 mL of complete DMEM. Centrifuge at 1200 rpm for 5 min and discard the supernatant. Resuspend the cellular pellet in 10 mL complete DMEM and pour into a 10 cm Ø culture plate.

1.5. Freezing cells

Confluent plates are trypsinized and collected in 5 mL complete DMEM. Cells are centrifuged at 1200 rpm, 5 min, and the cellular pellet is resuspended in 800 µL complete DMEM, 100 µL FBS and 100 µL DMSO on ice. The volume is introduced in a cryopreservation vial and immediately frozen. Percentage of FBS can be increased depending on the cell line.

📌 It is important to immediately freeze cells at -80°C after addition of DMSO given that it is toxic for living cells.

1.6. Mycoplasma detection tests and treatment

1.6.1. Immunofluorescence-based detection of mycoplasma

Mycoplasma are a class of bacteria characterised by the absence of a cell wall, what makes them naturally resistant to many common antibiotics such as penicillin or other beta-lactam antibiotics that target the synthesis of the cell wall. Mycoplasma infect the cytoplasm of cells and can induce cellular changes. Detection can be performed by immunofluorescence or PCR. For immunofluorescence:

- Discard media from cultured cells and wash twice with non-sterile PBS. This protocol is for 24-well plates, the volumes can be adjusted according to the size of the plate.
- Fixation: add 300 µL PFA 4% (see Immunofluorescence section for the preparation) and leave the plate closed at room temperature for 20 minutes.
- Incubate cells with DAPI (Thermo Fisher Scientific) at 1/5000 in PBS for 10 minutes.
- Wash cells twice with PBS and directly observe in an inverted fluorescence microscope or mount coverslips over slips, as indicated in the Immunofluorescence protocol of this section.

1.6.2. PCR-based detection of mycoplasma

Culture cells for 5-7 days in a 30 mm plate in antibiotic-free medium. Isolate mycoplasma DNA by following the protocol:

- Take 1.5 mL of the medium and centrifuge at 4°C, 300 x g, 10 min.
- Transfer the supernatant to a new sterile tube and centrifuge at 4°C, 13,000 x g, 10 min.
- Remove the supernatant, resuspend the pellet with 50 µL of sterile water and heat at 95°C for 10 min. Samples can be immediately used or frozen for later analysis.
- Perform PCR with specific primers (Primer A: 5'-GGCGAATGGGTGAGTAACACG-3', Primer B: 5'-CGGATAACGCTTGCGACCTATG-3') in a thermocycler at the following conditions:
95°C, 5 min. [94°C, 1 min. 60°C, 1 min. 72°C, 1 min.] 30-35 cycles. 72°C, 7 min. 4°C, ∞.

1.6.3. Mycoplasma elimination treatment

Plasmocin Treatment (Invivogene) was used following manufacturer's recommendations:

- Remove medium from contaminated cells and wash twice with PBS.
 - Split an actively dividing culture of cells into medium containing 25 µg/mL Plasmocin.
 - Remove and replace with fresh Plasmocin-containing medium every 3-4 days for 2 weeks.
 - Confirm the elimination of mycoplasma by immunofluorescence/PCR.
- 📌 It is recommended to keep a cell plate with Plasmocin and repeat the test after one additional week.

2. Transfections

Two types of transfections were performed during this thesis, according to the nature of the genetic material to be transfected. Small-interfering RNAs (siRNAs) were transfected using Oligofectamine (Invitrogen) whereas plasmids were transfected with Lipofectamine LTX (Invitrogen). All experiments were performed in 6-well plates. The transfection medium used was Opti-MEM, which lacks FBS and antibiotics to avoid interference with the transfection.

2.1. siRNA transfection with Oligofectamine

- Prepare siRNAs: for each transfection sample, dilute the adequate volume of 20 µM stock siRNA in 350 µL Opti-MEM (Thermo Fisher Scientific) to the final siRNA concentration desired. Details of the siRNAs and concentrations used in this thesis are reported in **Table M-II**.
- Prepare Oligofectamine: mix 350 µL Opti-MEM with the same volume of Oligofectamine than that of siRNA. Vortex. Incubate for 5 min at room temperature.
- Prepare complexes: pour 350 µL of Oligofectamine mix inside the tube containing 350 µL of siRNA while slowly vortexing. Incubate the complexes for 20 min at room temperature.

- Wash cells twice with PBS and add the 700 μ L of siRNA complexes to each well.
- After 4h, add 1,3 mL of complete DMEM to each well. Alternatively, complete DMEM can be added the day after. The introduction of genetic material is accomplished within 4 h and complete medium is added to avoid cell dead due to FBS and Gln deprivation.

Gene	Sequence	Company	Concentration (nM)
TIGAR T1	5'-GAAGUUAACCAACGGUUCAGUGUA-3'	Stealth siRNA (Thermo Fisher Scientific)	75
TIGAR T2	5'-CAGGAUCAUCUAAAUGGACUGACUG-3'	Stealth siRNA (Thermo Fisher Scientific)	75
TIGAR T3	5'-CAAGCAGCAGCUGCUGGUUAUUUUC-3'	Stealth siRNA (Thermo Fisher Scientific)	75
PFKFB3	5'-AGCUGCCUGGACAAAACAUG-3'	Thermo Fisher Scientific	75
<i>NFE2L2</i>	5'-CCAACCAGUUGACAGUGAACUCAUU-3'	Thermo Fisher Scientific	100
Scrambled	5'-UAAAUGUACUGCGGUGGAGAGGAA-3'	Stealth siRNA (Thermo Fisher Scientific)	75/100

Table M-II. Small interfering RNAs (siRNAs) used in this thesis.

2.2. Plasmid transfection with Lipofectamine LTX

- Prepare plasmids: for each transfection sample, dilute the adequate volume of plasmid in 150 μ L Opti-MEM (Thermo Fisher Scientific) for a total amount of plasmid of 1 μ g. Add the same volume of Plus Reagent. The final volume in each well will be 300 μ L. Vortex. The plasmids for gene overexpression used in this thesis are reported in **Table M-III**.
- Prepare Lipofectamine: for each transfection sample, dilute 10 μ L of Lipofectamine in 150 μ L Opti-MEM. Vortex.
- Prepare complexes: pour 150 μ L of Lipofectamine mix inside the tube containing 150 μ L of plasmids.
- Incubate the complexes for 20 min at room temperature.
- Wash cells twice with PBS, put 400 μ L of Opti-MEM and add the 300 μ L of plasmid complexes to each well.
- After 4h, add 1,3 mL of complete DMEM to each well. Alternatively, complete DMEM can be added the day after. The introduction of genetic material is accomplished within 4 h and complete medium is added to avoid cell dead.

Gene	Plasmid name	Origin/Company
<i>TP53</i>	pcDNA3-p53	Addgene
SP1	CMV-SP1	Addgene
ATF4	pRK-ATF4	Addgene
CREB1	pFETCH_CREB1	Addgene
<i>NFE2L2</i>	NC16 pcDNA3.1 Flag Nrf2	Addgene (kindly provided by Dr. Ventura's Lab)
TIGAR	pcDNA3.1-Flag-tagged-TIGAR	(3) (kindly provided by Dr. Vousden's Lab)
Negative control	pcDNA3.1	Addgene

Table M-III. Overexpression plasmids used in this thesis.

3. Protein analysis by western blot

3.1. Protein extraction

Two approaches were performed to extract protein from cells, depending on whether we were interested in total amounts of protein or on the distribution of proteins within the different cellular organelles.

3.1.1. Extraction of whole protein amounts

📌 This protocol needs to be performed on ice if phosphorylated proteins are analysed. If we are not interested in phosphorylated proteins, the extraction can be performed at room temperature.

- Analysis of non-phosphorylated proteins:

Cells were washed twice in non-sterile PBS 1X and 70 μ l of **Whole cell lysis buffer*** were added to each well of 6-well plates. The volume of lysis buffer needs to be adapted to the cellular confluence. 70-100 μ l are usually enough to lyse a confluent well of a 6-well plate of HeLa cells. Cells were scrapped and the lysates were transferred to *ependorf* tubes for the quantification of protein concentration. Lysates can be frozen at -20°C before quantification.

- Analysis of phosphorylated proteins:

The procedure was the same as described for non-phosphorylated proteins, but cold PBS 1X was used for washing cells and the extraction buffer used was **RIPA**. RIPA is a softer lysis buffer due to its lower percentage of SDS. Protease and phosphatase inhibitors need to be added to RIPA buffer immediately before the extraction (**Table M-IV**).

Protease Inhibitor	Solvent	[Stock]	[Use]	Dilution
Leupeptin	Water	5 mg/ml	5 μ g/ml	1:1000
Benzamidine	Water	10 mg/ml	100 μ g/ml	1:100
Pepstatin	Acetic acid 10% Methanol 90%	1 mg/ml	1 μ g/ml	1:1000
PMSF	Isopropanol	100 mM	1 mM	1:100
Phosphatase Inhibitor	Solvent	[Stock]	[Use]	Dilution
NaF	Water	1 M	1 mM	1:1000
Sodium Orthovanadate	Water	0,2 M	0,2 mM	1:1000
β -glycerophosphate	Water	1 M	1 mM	1:100

Table M-IV. Protease and phosphatase inhibitors used for RIPA buffer.

Lysates were collected in *ependorf* tubes and maintained on ice or frozen at -20°C before protein quantification by BCA assay.

* The recipes for the buffers in blue can be found at the end of this Materials and Methods Section.

3.1.2. Subcellular fractionation

This protocol can be used to analyse phosphorylated and non-phosphorylated proteins from different cellular compartments. It is recommended to use confluent 10 cm Ø plates to have good protein yield. Two different buffers are suitable for this protocol, one based on Tris-HCl and the other on HEPES (**Subcellular Fractioning Buffer I and II**, respectively). In the tune up of this technique, the two buffers showed similar efficiency (**Figure M-1**). Buffer II was used for further experiments in this thesis.

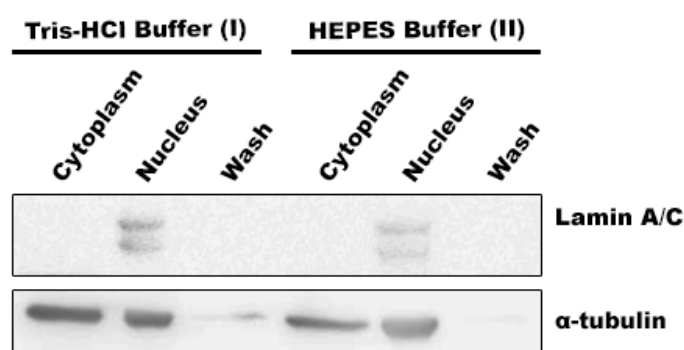


Figure M-1. Western blot analysis of cellular extracts obtained with Subcellular Fractioning Buffers I and II. α -tubulin, a cytoplasmatic marker, and Lamin A/C, a nuclear specific protein, were analysed in cytoplasmic and nuclear fractions. The cytoplasmic fractions obtained with both buffers did not contain nuclear proteins (absence of Lamin A/C). However, some cytoplasmatic proteins remained in the nuclear extracts. The efficiency of the separation varied between experiments.

Prepare the Subcellular Fractioning buffer by adding the following protease and phosphatase inhibitors just before use (**Table M-V**).

Protease Inhibitor	Solvent	[Stock]	[Use]	Dilution
Leupeptin	Water	5 mg/ml	10 μ g/ml	1:500
Benzamidine	Water	10 mg/ml	100 μ g/ml	1:100
Pepstatin	Acetic acid 10%	1 mg/ml	5 μ g/ml	1:500
	Methanol 90%			
PMSF	Isopropanol	100 mM	0,5 mM	1:200
Phosphatase Inhibitor	Solvent	[Stock]	[Use]	Dilution
NaF	Water	1 M	1 mM	1:1000
Sodium Orthovanadate	Water	0,2 M	0,1 mM	1:2000

Table M-V. Protease and phosphatase inhibitors used for subcellular fractioning.

Perform the protocol as follows:

- Wash cells twice with 10 mL of cold PBS 1X
- Add 1 ml of **Subcellular Fractioning Buffer**.
- Scrap cells and transfer the lysate to a cold *ependorf* tube.
- Pass the whole volume through a 27G syringe 4 or 5 times. The rupture of the cellular membrane can be checked by trypan blue staining. It is recommendable to perform this staining the first time that the protocol is performed to adapt the number of times to pass the volume through the syringe to each cell type. The optimal is to break as much cells as possible without breaking the nuclei (cells with integral membrane are refringent and nuclei from broken cells are stained in blue).
- Centrifuge at 4°C, 1000 x g, 10 min. Collect the supernatant (membranes and cytoplasmic fraction) and transfer it to a new tube*¹. Add 1 mL of buffer to the pellet (nuclear fraction) to wash it and centrifuge again at 4°C, 1000 x g, 10 min.
- Eliminate the supernatant and resuspend the pellet with 250 µl of buffer and store.
- With the tube containing the cytoplasmic fraction*¹, protocol can be stopped here or continue to separate the cytosol from membranes. To obtain the cytosolic fraction, centrifuge the cytoplasmic extract at 4°C, 10000 x g, 1 h (alternatively, centrifuge at 4°C, 13000, 30 min) and transfer the supernatant (cytosol) to a new tube and store. Add 1 mL of buffer to the pellet to wash it and centrifuge at 4°C, 10000 x g, 10 min. Eliminate the supernatant and resuspend the pellet (membranes) with 250 µl of buffer and store.
- At least two samples are obtained from each original protein extract: cytoplasmic and nuclear fractions (**Figure M-1**). Alternatively, three samples (cytosol, membranes and nuclei) are obtained. Proceed to the quantification of protein by BCA assay.

3.2. Protein quantification

Two assays, BCA and Bradford, were used according to the lysis buffer in which the samples were extracted (**Table M-VI**). BCA assay is compatible with all the protein lysis buffers used in this thesis except for the Fructose-2,6-P₂ extraction buffer, for which the Bradford assay was performed.

BCA-compatible lysis buffers	Bradford-compatible lysis buffers
Whole cell lysis buffer	Fru-2,6-P ₂ extraction buffer
RIPA	NaOH 1M
Subcellular fractioning buffer I	Luciferase assay lysis buffer
Subcellular fractioning buffer II	

Table M-VI. Compatibility between protein assays and lysis buffers

Both assays are based on the generation of coloured products the intensity of which is proportional to protein concentration. Thus, a standard curve is needed. Samples to perform the standard curves were prepared by diluting bovine serum albumin (BSA) in the corresponding buffer in which cells were lysed at concentrations from 10 to 0 µg/µL.

3.2.1. BCA assay

The Pierce™ BCA Protein Assay Kit (Thermo Fischer) was used, which is based on the reduction of Cu²⁺ to Cu¹⁺ by proteins in an alkaline medium (biuret reaction), coupled to the reaction of bicinchoninic acid (BCA) with Cu¹⁺, which produces an intense purple product. An advantage of BCA compared to Bradford is that, although cysteine, tyrosine and tryptophan are the amino acids that more strongly reduce Cu²⁺, the peptide backbone also contributes to colour formation, helping to minimize variability caused by protein compositional differences. 2 µL triplicates of each sample or standard curve, were dispensed in 96 well plates and 150 µL of the reaction mix was added to each well. The reaction mix was prepared by diluting 1 part of Reagent B in 50 parts of Reagent A. The plate was incubated at 37°C for 30 min and absorbance was read at 540 nm in a SunriseTecan plate reader. The absorbance is proportional to protein concentration, which can be extrapolated from the standard curve.

3.2.2. Bradford assay

The Bio-Rad Protein Assay was used, which is based on the binding of basic and aromatic amino acids to the Coomassie reagent, causing a shift from the reddish/brown form of the dye (maximum absorbance at 465 nm) to the blue form of the dye (maximum absorbance at 610 nm). 2 µL triplicates of each sample or standard curve were dispensed in 96 well plates and 150 µL of the reaction mix was added to each well. The reaction mix was prepared by diluting the Bio-Rad Protein Assay reagent with water 1:5 and the absorbance at 595 nm was read in a SunriseTecan plate reader. The absorbance is proportional to protein concentration, which can be extrapolated from the standard curve.

3.3. Electrophoresis and western blot

This technique is based on the separation of proteins by their molecular weight through electrophoresis in an acrylamide gel and the transference of proteins to a membrane where they can be detected by specific antibodies. For that, proteins need to be denatured to ensure that their migration through the gel will only be affected by their mass.

3.3.1. Sample preparation

After quantification, **Sample Buffer 4X** was added to protein extracts. This buffer contains SDS, which denatures and negatively charges proteins to be moved to the positive pole, dithiothreitol, which breaks disulphide bonds, and bromophenol blue, that allows to visualize samples during electrophoresis. Samples were heated for 10 min at 95°C to completely denature proteins.

Electrophoresis gels were prepared as indicated in **Table M-VII**:

Stacking gel (upper)		Separating gel (lower) 12,5%*	
Acrylamide	3,75 mL	Acrylamide	0,6 mL
Upper buffer	4,65 mL	Upper buffer	2,00 mL
Water	6,6 mL	Water	5,40 mL
APS 10%	75 µL	APS 10%	40 µL
TEMED	25 µL	TEMED	10 µL

Table M-VII. Recipe for two electrophoresis gels. * Percentage of acrylamide can vary according to the molecular weight of the proteins to be detected. ⓘ Acrylamide is toxic, handle with gloves!

All proteins analysed in this thesis were separated in 12,5% acrylamide gels except for the autophagic protein LC3, which was analysed in 17% acrylamide gels due to its low molecular weight.

3.3.2. Sodium Dodecyl Sulfate Polyacrylamide Gel Electrophoresis (SDS-PAGE)

Mini Protean II (Bio-Rad) was used to perform the SDS-PAGE. Samples were loaded in the gels and PageRuler™ Plus Prestained Protein Ladder (Thermo Fisher Scientific) was used as the protein marker. Buckets were filled with **Electrophoresis Buffer** and run for at least 1 h at 125 V until the bromophenol blue is at the lower part of the gel.

3.3.3. Transference to nitrocellulose membranes:

After the electrophoresis, two types of transference can be performed. In both procedures nitrocellulose membrane needs to be activated. This is achieved by incubating the membrane in methanol for 1 minute and subsequently submerging it into water until it completely sinks.

- In the Wet Mini Trans-Blot Transfer System (Bio-Rad), proteins are transferred from the gel to the nitrocellulose membrane due to the difference of potential created in a tank filled with **Electrophoresis Buffer**. The whole transference is completed after 90 min at 350 mA.
- In the Trans-Blot Semi-Dry Transfer System (Bio-Rad) the transference of proteins from the gel to the nitrocellulose membrane occurs in a cassette in which only the Whatman filter papers are soaked in the corresponding **anode** (in the membrane side) and **cathode** (in the gel side) **buffers**. In this system, the transference is completed after 30 min at 25 V.

After electrophoresis, it is recommended to wash the membrane in **TBS-T 1X** for 5 minutes, especially after the Semi-Dry system.

3.3.4. Immunodetection of proteins with specific antibodies:

The membrane is incubated with TBS-T 1X with 5% non-fat dry milk to avoid non-specific binding of the primary or secondary antibodies to the membrane, and subsequently incubated with the primary antibodies of interest at 4°C overnight. Usually the membrane needs to be cut for the incubation with different primary antibodies. The antibodies used in this thesis were prepared with TBS-T with 5% BSA and are reported in **Table M-VIII**.

The day after, the primary antibody is collected (it can be recycled) and membrane is rinsed in TBS-T 1X. Secondary antibody is prepared in TBS-T 1X with 5% non-fat dry milk and membranes are incubated within it for 1 h at room temperature. The secondary antibodies used in this thesis are reported in **Table M-IX**. After the incubation, the membrane needs to be washed twice in TBS-T for 5 minutes, plus an additional wash of 5 min in **TBS** prior to precede with the detection of the secondary antibody signal. The secondary antibodies used are conjugated with Horseradish Peroxidase, an enzyme that converts H_2O_2 to a luminescent product. EZ-ECL Chemiluminescence detection kit (Biological Industries), which contains H_2O_2 , was used and chemiluminescence was acquired with a Las-3000 detection system (Fujifilm).

① If primary antibodies display high signal, incubation can be performed for 2 h at room temperature.

Protein targeted	Dilution	Species of origin	Company	Mw of the protein (kDa)
P-Akt (S473)	1/1000	Rabbit	Cell Signalling	60
Akt	1/1000	Goat	Cell Signalling	60
ATF4	1/1000	Rabbit	Cell Signalling	39
CREB1	1/1000	Rabbit	Cell Signalling	37
G6PD	1/500	Rabbit	Abcam	59
GLS1	1/1000	Rabbit	Cell Signalling	65
HK-II	1/500	Mouse	Santa Cruz Biotechnology	102
HO-1	1/1000	Goat	Abcam	28
KEAP1	1/1000	Mouse	Santa Cruz Biotechnology	62
Lamin A/C	1/1000	Mouse	Cell Signalling	74 (Lamin A), 63 (Lamin C)
LC3-I/III	1/1000	Rabbit	MBL	16 (LC3-I), 14 (LC3-II)
MCT1	1/1000	Mouse	Santa Cruz Biotechnology	42
mTOR	1/1000	Mouse	Cell Signalling	289
P-mTOR (S2448)	1/1000	Rabbit	Cell Signalling	289
Nrf2	1/1000	Rabbit	Santa Cruz Biotechnology	95-110
P-p70S6K1 (T389)	1/1000	Rabbit	Cell Signalling	70
p53	1/1000	Mouse	Santa Cruz Biotechnology	53
p62	1/1000	Mouse	Abnova	62
PCB	1/1000	Mouse	Santa Cruz Biotechnology	126
PCK-2	1/1000	Rabbit	Abcam	71
PDH	1/1000	Rabbit	Merck	43
PFKFB3	1/1000	Rabbit	Homemade (serum 94) (33)	59
S6	1/1000	Mouse	Cell Signalling	32
P-S6 (S235/236)	1/1000	Rabbit	Cell Signalling	32
SP1	1/1000	Mouse	Santa Cruz Biotechnology	90
TIGAR	1/1000	Rabbit	LifeSpan	30
TIGAR	1/1000	Rabbit	Santa Cruz Biotechnology	30
TKT	1/1000	Mouse	Santa Cruz Biotechnology	68
TSC2	1/1000	Rabbit	Cell Signalling	200
α -tubulin	1/4000	Mouse	Sigma-Aldrich	50

Table M-VIII. Primary antibodies used for western blot.

Secondary antibody	Dilution	Species of origin	Company
α -Mouse	1/20000	Donkey	Amersham
α -Rabbit	1/20000	Donkey	Amersham
α -Mouse	1/10000	Goat	Advansta
α -Rabbit	1/10000	Goat	Advansta
α -Goat	1/10000	Donkey	Sigma-Aldrich

Table M-IX. Secondary antibodies used for western blot.

3.3.5. Stripping

The membrane can be reblotted several times with different primary antibodies. It is recommended to incubate first with the antibodies that emit less signal, such as those detecting phosphorylated proteins. If the antibody for the second incubation is specific for a protein with a molecular weight similar to that previously detected, stripping of the membrane is recommended. Stripping eliminates the first primary antibody and avoids steric impairment for the second primary antibody to bind. This protocol should be performed in a covered bucket to avoid the smell of the **Stripping Solution**:

- Incubate the membrane in Stripping Solution at 54°C in a water bath with agitation for 15-20 minutes. The time of incubation depends on the stripping astringency desired.
- Wash twice in TBT-T 1X for 10 min in agitation.
- Block again the membrane with TBS-T 1X with 5% non-fat dry milk and incubate with primary antibody.

4. Immunofluorescence

This technique is used to analyse protein localisation by confocal fluorescence microscopy, as well as to assess the presence of mycoplasma in the different cell lines cultured. Proceed as follows:

- Discard media from cultured cells and wash twice with non-sterile PBS. This protocol is for 24-well plates, the volumes can be adjusted according to the size of the plate.
- Fixation: add 300 µL **PFA 4%** (see preparation below) and leave the plate closed at room temperature for 20 minutes. Extended fixation time can damage cells.
 - ① PFA is toxic and needs to be handled with gloves and mask in a fume hood.
- Discard PFA in the appropriate residue container and wash cells twice with PBS. The protocol can be stopped at this point and plates can be stored at 4°C with 1 mL of PBS in each well. For extended storage, add sodium azide to a final concentration of 0,02% and seal the plate.
- If cells have been stored at 4°C, leave the plate at room temperature for 10-15 min before performing the immunofluorescence.
- Permeabilization: wash twice with **PBS/0,1% Triton-X100** for 5 minutes.
- Blocking: add 10% horse serum (HS) diluted in 200-300 µL of **PBS/0,1% Tween20** and incubate 2 h at room temperature.
- Primary antibody incubation: prepare the antibodies with 1% HS PBS/0,1% Tween20 and either add them to the plate (150-200 µL verifying that the whole coverslip is covered) or prepare a humid chamber with a drop of 30 µL of primary antibody for each coverslip as it is detailed in **Figure M-2**. Store the 24-well plate sealed with parafilm/humid chamber at 4°C overnight in a place protected from movement. The primary antibodies used in this thesis are reported in **Table M-X**.

① One coverslip for each cell type needs to be used as negative control: this coverslip will not be incubated with primary antibody and, thus, the fluorescence will reflect the inespecificities of secondary antibody. It can be stored in the original 24-well plate in PBS/0,1% Tween20 overnight.

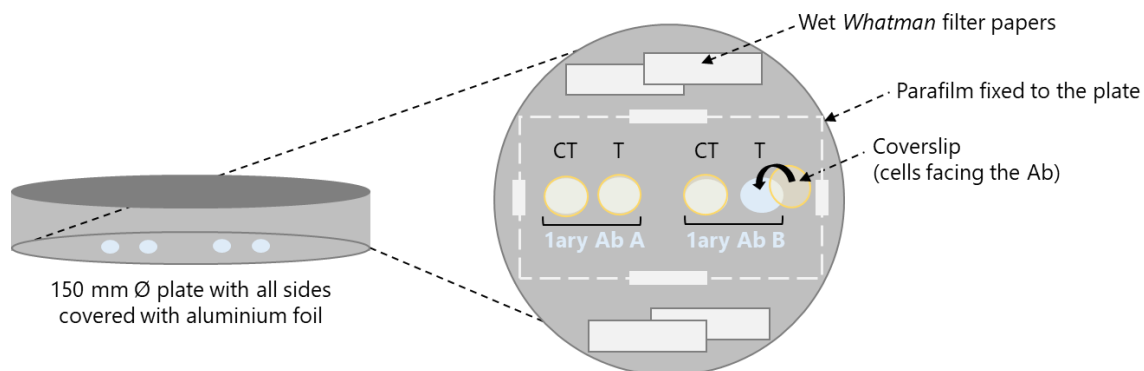


Figure M-2. Schematic representation of a humid chamber for immunofluorescence. 150 mm Ø plate with all sides covered with aluminium foil were used to create the humid chamber. Attach parafilm to the plate surface and dispense drops of 30 µL of each antibody on it. It is important to identify each antibody (A, B) and condition (control: CT, treated: T) on the parafilm. Take coverslips from the 24-well plate and place them above the antibody drops, with the cells facing down towards the antibody. The antibody spreads through the whole coverslip by capillarity. Dip *Whatman* filter papers on water and put them on two sides of the plate to maintain enough humidity inside to avoid coverslips to dry.

Continue the protocol protecting the samples from light:

- Secondary antibody incubation: the following day, transfer the coverslips into a new 24-well plate. Wash twice with PBS/0,1% Tween20 for 10 min and incubate with 150 µL of the secondary antibody prepared in 1% HS PBS/0,1% Tween20 for 1 hour at room temperature protected from light. The secondary antibodies used in this thesis are reported in **Table M-XI**.
- Nuclear staining: wash four times with PBS for 5 min and incubate with 150 µL of the nuclear marker desired. In this thesis, TO-PRO-3 iodide and DAPI were used. The incubation conditions are reported in **Table M-XII**.
- Mounting: wash three times in PBS and proceed to mount the coverslips on the slides. Put 5-10 µL of Fluoroshield mounting medium (Sigma-Aldrich) on the slide and cover it with a coverslip with cells facing down towards the slide.
- Leave at room temperature protected from light for the Fluoroshield to harden. After that, store at 4°C until observed at the confocal microscope.

Protein targeted	Dilution	Species of origin	Company
Nrf2	1/300	Rabbit	Santa Cruz Biotechnologies
p53	1/200	Mouse	Santa Cruz Biotechnologies
P- γ -H2AX (S139)	1/250	Rabbit	EMD Millipore
TIGAR	1/300	Rabbit	Santa Cruz Biotechnologies
γ -tubulin	1/200	Mouse	Abcam

Table M-X. Primary antibodies used for immunofluorescence.

Secondary antibody	Dilution	Species of origin	Company
Alexa488-conjugated α -Rabbit	1/400	Chicken	Thermo Fisher Scientific
Cy3-conjugated α -Mouse	1/400	Donkey	Thermo Fisher Scientific
Alexa594-conjugated α -Mouse	1/400	Donkey	Thermo Fisher Scientific

Table M-XI. Secondary antibodies used for immunofluorescence.

Nuclear staining	Dilution	Incubation time	Company
DAPI	1/5000	10 min	Thermo Fisher Scientific
TO-PRO-3 iodide	1/1000	2 h	Thermo Fisher Scientific

Table M-XII. Nuclear markers used for immunofluorescence.

Preparation of **16% and 4% PFA**

- 16% PFA is prepared in a fume hood by adding 16 g PFA (weighted in the fume hood) to 75 mL of autoclaved **Phosphate Buffer 0,4M** in continuous stirring at 40°C until it gets transparent (2-4 hours). Then, 25 mL Phosphate Buffer 0,4 M are added and the mix is left overnight with the fume hood closed. The day after, it is filtered with paper and aliquots are stored at -20°C.
- 4% PFA is prepared by diluting $\frac{1}{4}$ with water and can be stored at 4°C.

5. Gene expression analysis by RT-qPCR

5.1. mRNA extraction

mRNA was extracted from cells cultured in 6-well plates (it is not recommended to use smaller plates to ensure a good mRNA yield) by TRIre (Bioline) following manufacturer's procedure with some modifications. Perform the protocol on ice and with sterile material.

DAY 1

- Lyse cells directly in the culture dish by adding 0,5 mL of TRIre per well and ensure that the whole cell surface is covered. Scrap cells with a twisted 200 μ L tip and collect the lysate, pass three times the volume through the well surface and put the lysate into *eppendorf* tubes. At this stage, samples can be stored at -80°C .

- Phase separation: incubate samples for 5 min at room temperature. Add 100 μ L of chloroform per 0,5 mL of TRIre used. Cap tubes securely and shake vigorously by hand for 15 seconds. Incubate samples for 3 min at room temperature. Centrifuge samples at $12,000 \times g$ for 15 min at 4°C . The sample will separate into a pale green organic phase, an interphase, and a colourless upper aqueous phase.

- RNA precipitation I: transfer the aqueous phase carefully to a new tube previously set on ice. Add 500 μ L of cold isopropanol and incubate samples for 10 min at room temperature without shaking. Store at -20°C overnight to increase RNA yield.

DAY 2

- RNA precipitation II: thaw the tubes and centrifuge at $12,000 \times g$ for 10 min at 4°C .

RNA wash: decant the supernatant and add 500 μ L of cold 75% ethanol to wash the pellet. Vortex samples and centrifuge at $13000 \times g$ for 5 min at 4°C . Repeat this step for an additional wash.

- After the second wash, decant the supernatant and spin the *eppendorf* at $12000 \times g$. With a 20 μ L tip on the top of a 200 μ L tip, aspirate the remaining ethanol from the *eppendorf*. Be careful not to touch the pellet and, if the pellet is not visible, do not take the remaining ethanol the *eppendorf*.

- Air-dry the pellet at 50°C in a block heater and, once the remaining ethanol is evaporated, resuspend the pellet in 10 μ L PCR water or DEPC-treated water by pipetting the solution up and down. Leave at 4°C overnight for a complete resuspension.

DAY 3

- Incubate for 10 min at 65°C and proceed to quantification. At this point samples can be stored at -80°C .

5.2. RNA quantification

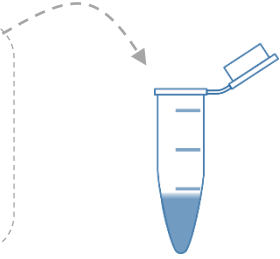
RNA concentration was determined by measuring the absorbance at 260 nm with NanoDrop (Thermo Fischer Scientific) and usually it was between 200-1000 ng/ μ L. RNA purity is determined by these two ratios:

- Absorbance 260 nm/Absorbance 280 nm \geq 1,8 indicates absence of contamination by proteins.
- Absorbance 260 nm/Absorbance 230 \geq 2 indicates absence of contamination by phenolic reagents such as TRIsure.

5.3. Retrotranscription

mRNA needs to be converted to cDNA to perform RT-qPCR. For that, High Capacity cDNA Reverse Transcription Kit (Thermo Fisher Scientific) was used. For each sample, 2 μ g of mRNA are retrotranscribed. The volume required from each sample is calculated and DEPC water is added until a final volume of 10 μ L. If the RNA concentration was lower than 200 ng/ μ L, the whole sample was retrotranscribed.

DEPC H ₂ O	4,2 μ L
10X Buffer	2 μ L
25X dNTPs mix	0,8 μ L
10 X Random Primers	2 μ L
Reverse Transcriptase	1 μ L
Final volume	10 μ L



Prepare reaction mix as follows and add 10 μ L to each sample.

Perform the PCR reaction at the following conditions:

10 min 25°C, 120 min 37°C, 5 sec 85°C, ∞ 4°C.

Store at -20°C until RT-qPCR.

5.4. Real-time quantitative PCR (RT-qPCR)

Quantification of gene expression by RT-qPCR is based on the fluorescence emitted by TaqMan Assays (Thermo Fisher Scientific), which is proportional to the number of cDNA copies of a given gene (**Figure M-3**). The reaction is performed in 388-well plates as follows:

- Dilute the cDNA obtained by retrotranscription at 1/20 with DEPC water and pipette 5 μ L triplicates to the 348-well plate. Add water in triplicates for each of the genes to be interrogated to perform the negative controls.
- Prepare TaqMan Assays by mixing 0,5 μ L of TaqMan Assay with 5,5 μ L of SensiFAST and add 6 μ L of the prepared TaqMan Assays to the corresponding wells.
- Cover the plate with the film and run RT-qPCR in the ABI PRISM 7700 Sequence Detection System (Applied Biosystems).

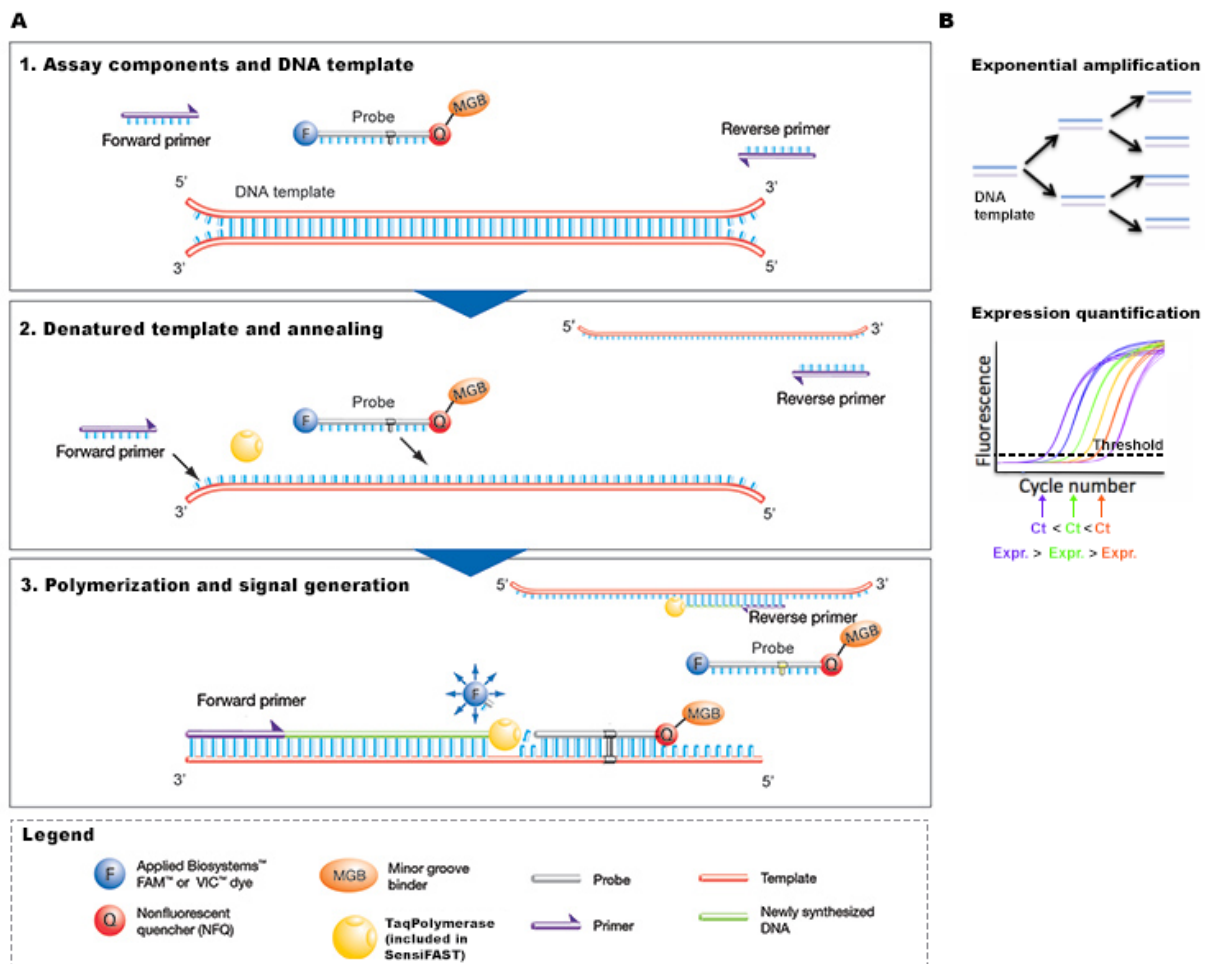


Figure M-3. RT-qPCR with TaqMan Assays. (A) RT-qPCR requires three components: a probe specific for the gene with a 5' fluorescent reporter dye, a 3' quencher of fluorescence and a minor groove binder (MGB), a pair of primers, one forward and one reverse, and the TaqPolymerase. Each TaqMan Assay (Thermo Fisher Scientific) contains one probe and a pair of primers specific to a given gene, and the TaqPolymerase is included in the Sensifast reagent (Bioline). Primers bind to the gene and when the polymerase reaches the TaqMan probe, its endogenous 5' nuclease activity cleaves it, separating the dye from the quencher. In each PCR cycle, the fluorescence is increased proportionally to the cDNA copies. (B) The number of cycles at which the fluorescence specific for a given gene reaches the threshold and starts the exponential phase is called the cycle threshold, Ct. A lower Ct value indicates higher expression of that gene. Adapted from Thermo Fisher Scientific.

RT-qPCR data are acquired with the Sequence Detection Software (SDS version 3.0; Applied Biosystems) and analysed with Expression Suite Software (Applied Biosystems). The normalization procedure is commonly called the $\Delta\Delta C_t$ -method and allows to compare the expression of a particular gene among different samples, relative to the C_t values of a housekeeping gene in that same sample.

The TaqMan Assays used in this thesis are reported in **Table M-XIII**.

Gene	TaqMan Assay reference
<i>TIGAR</i>	Hs00608644_m1
<i>PFKFB3</i>	Hs0019079_m1
<i>CDKN1A</i>	Hs00355782_m1
<i>G6PD</i>	Hs00166169_m1
<i>NQO1</i>	Hs01045993-g1
<i>NFE2L2</i>	Hs00975961_g1
<i>SLC2A1</i>	Hs01374610_m1
<i>HK2</i>	Hs00606086_m1
<i>TKT</i>	Hs01115545_m1
<i>LDHA</i>	Hs01378790_g1
<i>PHGDH</i>	Hs01106329_m1
<i>GAPDH</i>	Hs99999905_m1
<i>TBP</i>	Hs99999910_m1

Table M-XIII. TaqMan Assays (Thermo Fisher Scientific) used in this thesis.

6. RT-MLPA

Reverse transcriptase multiplex ligation-dependent probe amplification (RT-MLPA) were performed by the group of Dr. Joan Gil (Departament de Ciències Fisiològiques, Universitat de Barcelona) using the SALSA MLPA KIT R011 (MRC-Holland) as described in (204).

7. Flow cytometry analyses

7.1. Oxidative stress measurements by flow cytometry

Two probes were used to detect oxidative stress: CellROX Green (Life Technologies) and DCFDA (Sigma-Aldrich). The oxygen and nitrogen radicals detected by each probe are summarised in **Table M-XIV**.

Reactive specie	DCFDA	CellROX Green
H ₂ O ₂	✓	✗
ROO [•]	✓	✗
HO [•]	✓	✓
NOO [•]	✓	✗
O ₂ ^{•-}	✗	✓
NO	✗	✗

Table M-XIV. Reactive species detected by DCFDA and CellROX Green.

The protocol is similar for both probes and was adjusted to 12-well plates:

- Wash the cells three times with PBS in sterility conditions and incubate with 10 μ M DCFDA in Hank's Balanced Salt Solution or 5 μ M CellROX Green in complete DMEM for 30 min in a cell incubator at 37 °C with 5% CO₂.
- Add 50 μ L of trypsin, allow for trypsinization in the incubator and collect cells with 0,5 mL PBS supplemented with 10% of FBS. Protect from light.
- Analyse by flow cytometry. In this thesis, FACSCanto flow cytometer (Becton Dickinson) equipped with a 488 nm laser and a 530/30 nm filter was used. A minimum of 10000 events were analysed per sample using the FACSDIVA Software (BD Biosciences).

7.2. Analysis of cell death by flow cytometry

The presence of apoptotic or necrotic cells was determined with the Annexin V-FITC Apoptosis Detection Kit (eBioscience Bender MedSystems). Cells were seeded into six-well plates and allowed to grow for 72 h after siRNA transfection. Floating cells and attached cells freshly trypsinized were resuspended in PBS, washed twice in binding buffer and processed following manufacturer's instructions. All measurements were made with a FACSCalibur flow cytometer (Becton Dickinson) equipped with an air-cooled argon ion laser emitting at 488 nm. The barrier filters were 530/30 nm for annexin-FITC, and 670/LP for propidium iodide (PI) fluorescence. A minimum of 10000 events per sample were analysed using the CELL QUEST PRO software (BD Biosciences). A schematic representation of how apoptotic cells are detected is provided in **Figure M-4**.

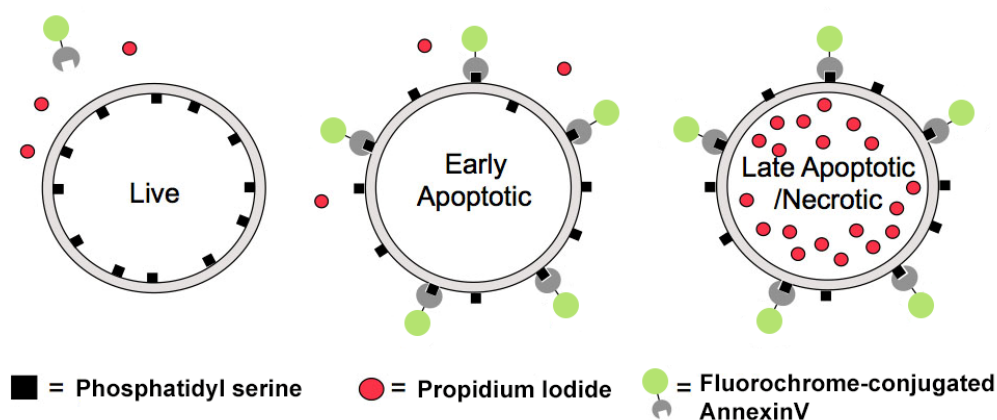


Figure M-4. Annexin/PI staining to measure cell death. A well-established feature of apoptosis is the externalisation of the lipid phosphatidyl serine from the inner to the outer plasma membrane. Annexin-V is a protein that specifically binds phosphatidyl serine and fluorescent labelling of annexin-V enables its flow cytometric detection. As a cell dies, plasma membrane becomes permeable allowing fluorescent dyes present outside the cell such as propidium iodide to enter it and emit fluorescence. Adapted from University of Dundee.

8. Absorbance-based viability assessments

Apart from the analysis of AnnexinV/PI by flow cytometry, viability can be assessed by more rudimentary methods that give an overall idea of cellular affectation. In this thesis, the crystal violet assay was used to determine the number of living cells after glycolysis inhibition. On the other hand, the MTT assay was used to determine the oxidative capacity of mitochondria, which is an indirect indicator of cellular wellness. The corresponding protocols are as follows:

8.1. Crystal violet assay

- Wash cells twice with PBS and stain with **Crystal Violet solution** for 30 min at 37°C. Adjust the volume according to plate surface (150 µL is enough for 96-well plates).
- After staining, remove the dye and recycle it. ⓘ The colour is very powerful and can stain any surface, so avoid direct contact with the dye.
- Rinse the cells in water. If possible, dry the plates and perform the quantification the day after.
- Dissolve the cell-attached dry with 1% SDS and read the absorbance by triplicates at 550. SunriseTecan plate reader was used.

8.2. MTT assay

The assay is based on the reduction of MTT by NAD(P)H-dependent cellular oxidoreductases, which convert the yellow tetrazolium MTT (3-(4, 5-dimethylthiazolyl-2)-2,5-diphenyltetrazolium bromide) to its reduced form, purple formazan. The activity of these enzymes is increased by the ratio NAD(P)H/NAD(P)⁺, which is higher in cells with a high mitochondrial metabolism, where most NADH is produced. Cells were seeded into 24-well plates and allowed to grow for 24, 48 or 72 h after siRNA transfection. After that, the subsequent protocol was performed:

- Wash cells twice with PBS, add 0,5 mg/mL MTT in PBS and incubate for 2 h at 37 °C.
- Carefully remove the MTT solution and dissolve the formazan crystals that have been formed in 200 µL Isopropanol:HCl 40 mM per well.
- Transfer 50 µL triplicates of each well to a 96-well plate and read the absorbance at 570 nm. SunriseTecan plate reader was used.

9. Metabolic assays

9.1. Determination of glucose consumption

Experiments were carried out in 6-well plates in triplicates and two approaches were performed. In a set of plates, medium was collected at the end of the experiment (24 h post-transfection for overexpressing experiments and 72 h post-transfection for siRNAs). In the other set of plates, cells were washed twice in PBS at the end of the experiment and medium was replaced by complete DMEM. After 6 hours of incubation, medium was collected. The concentration of glucose was determined using a method based on the coupling of glucose oxidase and peroxidase (PGO) activities (Sigma-Aldrich) according to manufacturer's instructions:

- Dilute medium samples 1/20 in distilled water.
- Prepare a 96-well plate with 200 μ L of the **PGO Enzymes Reaction Solution** and add 15 μ L of each sample per well.
- Incubate at 37°C for 30 min and read the absorbance at 450 nm. SunriseTecan plate reader was used.

9.2. Determination of extracellular lactate

Lactate determination is based on the reaction catalysed by LDH, which converts lactate to pyruvate coupled with the reduction of NAD⁺ to NADH. In this thesis, lactate measurements were performed from extracellular media collected at the end of experiments.

- Prepare the **Lactate Assay Buffer** to be used by adding NAD⁺ and EDTA to a final concentration of 2,5 mM and 0,19 mM, respectively.
- Prepare diluted LDH as follows: for each well, mix 2,5 μ L LDH (Roche) with 17,5 μ L of water and add 20 μ L of Lactate Assay Buffer.
- Prepare a standard curve of lactate from 10 to 0 mM in water.
- Pipette 10 μ L of media samples or standard curve samples in duplicates in a black bottom 96 well plate.
- Add 150 μ L of Lactate Assay Buffer to each well and protect the plate from light.
- Add 40 μ L of diluted LDH to each well using a multichannel pipette to minimize time between samples and immediately read absorbance at 340 nm. FluoStar Optima plate reader was used.
- Repeat the lecture after 20 minutes. Lactate concentration is proportional to the difference in absorbance between 0 and 20 minutes. The relation is determined by the standard curve.
- Determine protein concentration of the cells from which media was collected and perform relative quantification of μ mol of lactate per mg of protein.

9.3. Determination of intracellular Fru-2,6-P₂ concentration

The determination of Fru-2,6-P₂ is based on the capacity of this metabolite to regulate PFK-1, being the most potent allosteric regulator of this enzyme. However, instead of using PFK-1, this assay is based on the stimulation of the potato PPI-PFK. PPI-PFK catalyses the phosphorylation of Fru-6-P to Fru-1,6-P₂ but, unlike animal PFK-1, it uses PPI as phosphoryl donor instead of ATP.

The reactions of three enzymes, aldolase (ALDO), triose phosphate isomerase (TPI) and glycerol phosphate dehydrogenase (GPDH), are needed to couple Fru-2,6-P₂ stimulation of PPI-PFK to NADH formation by GPDH (**Figure M-5**).

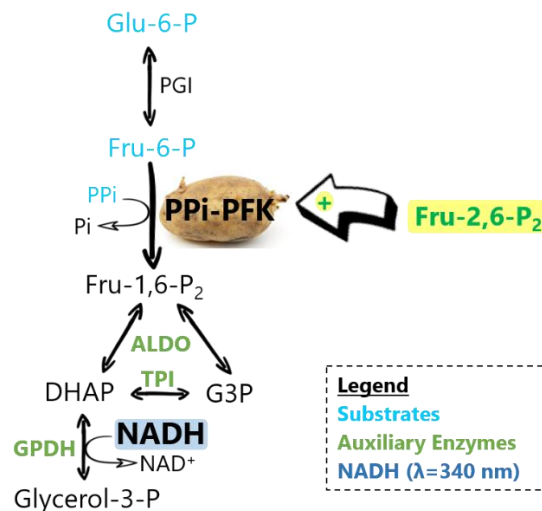


Figure M-5. Reactions involved in the Fru-2,6-P₂ assay. The capacity of Fru-2,6-P₂ to allosterically activate PPI-PFK is indirectly measured by the consumption of NADH by GPDH. This assay requires the reactions catalysed by ALDO and TPI. Substrates and enzymes implicated in these reactions are depicted blue and green, respectively.

9.3.1. Purification of PPI-PFK from potato tubers

This protocol was described by Van Schaftingen, Lederer, Bartrons and Hers in 1982 (38). Bartrons' Lab is one of the few laboratories that performs it due to the complexity to purify PPI-PFK. Utilisation of slightly germinated potatoes increases the purification yield. The protocol is as follows:

- Prepare **Hepes/CH₃COOK/DTT buffer** by adding 1M DTT to a final concentration of 2 mM just before use.
- Weight 165 g of peeled potato. Adjust the subsequent volumes according to the weight.
- Immediately after, grind the potato using a blender. Collect the liquid and pulp in a beaker on ice. Immediately add two volumes (330 mL) of **Hepes/CH₃COOK/DTT buffer** in the breaker on ice.
- Filter the mix through a funnel covered with gauzes into a graduated cylinder and stir with a spatula. Finally, make a sack with the gauzes and squeeze them inside the cylinder. **Annotate the collected volume ①.**

- Pour into a cold beaker and add PPI (solid) and 1M MgCl₂ until a final concentration of 2 mM each. The weight of PPI and volume of 1M MgCl₂ will depend on the collected volume.
- Dissolve with the help of a magnetic agitator with the beaker on ice. Measure pH until it stabilizes. It takes about 10 min to get to $\approx 7,6$.
- Once stabilized, adjust the pH to 8,2 with 1M KOH. **Annotate the volume of KOH added ②.**
- Put the beaker on a water bath at 70°C and continuously stir until it gets to 59°C. A thermometer inside the beaker is needed to properly control the temperature. Increased temperature could degrade PPI-PFK. Maintain at **59°C** for 5 min by taking the beaker in and out of the bath. Changes in temperature during these 5 min could also degrade PPI-PFK.
- Quickly put on ice.
- Adjust the pH to 7 by adding 1M HCl (or 5M HCl) with the beaker on ice. **Annotate the volume of HCl added ③.** At this point, an aliquot of 200 μ L can be stored at -80°C as a control of the first steps of the protocol.
- Add 6 g/100 mL of solid polyethylene glycol-600 (PEG-600) according to the total volume (**① + ② + ③**). [PEG-600] = 6%.
- Softly agitate for 15 min at 4°C in a cold room with a magnetic agitator.
- Leave 10 min without agitation at 4°C.
- Put into centrifuge tubes, equilibrate and centrifuge at 4°C, 4000 x g, 10 min in a swinging-bucket rotor. Do not centrifuge at lower velocity, the PPI-PFK yield would be drastically reduced. The precipitate obtained has two colours: blank at the end of the tube and yellow above.
- Collect the supernatant and the yellow precipitate with the help of a spatula or a spoon without taking the blank precipitate. **Annotate the volume collected ④.**
- Add 10 g/100 mL of solid polyethylene glycol-600 (PEG-600) **④**. [PEG-600]_{final} = 16%.
- Softly agitate for 15 min at 4°C in a cold room with a magnetic agitator.
- Leave 10 min without agitation at 4°C.
- Put again into centrifuge tubes, equilibrate and centrifuge at 4°C, 4000 x g, 10 min in a swinging-bucket rotor. Do not centrifuge at lower velocity, the PPI-PFK yield would be drastically reduced. Discard the supernatant (an aliquot of 200 μ L can be collected as a control of these steps).
- Collect the yellow precipitate with the help of a spatula or a spoon without touching the blank precipitate.
- Add 20 mL of **Tris/KCl/DTT buffer**. **1M DTT** needs to be added at the moment to a final concentration of 2 mM. Resuspend on ice.
- Add 1 volume of glycerol 100% (≈ 20 mL) slowly and mix. Aliquot on 1 mL *ependorf* tubes on ice and store at -80°C until de Fru-2,6-P₂ assay is performed.

9.3.2. Desalting auxiliary enzymes for Fru-2,6-P₂ determination

Commercial ALDO (10 mg/ mL, 9 U/mg) and TPI/GPDH (10 mg/mL, 4500 U/mg and 10 mg/mL, 1550 U/mg, respectively) (Sigma-Aldrich) are (NH₄)₂SO₄ solutions and desalting is required to avoid inhibition of PPI-PFK-2 activity. This protocol was described by (205).

- Insert glass wool at the end of 1 mL syringes and place syringes inside 15 mL tubes.
- Add 1 mL of Sephadex G-25 fine, previously swollen in **Tris/Acetate buffer**, to each syringe.
- Centrifuge at 4°C, 2500 rpm, 5 min in a swinging-bucket rotor. After centrifugation, glass wool should be compacted forming a column. Put the syringes on new 15 mL tubes.
- Prepare an *eppendorf* tube with 217 µL Aldo and 200 µL TPI/PGDH.
- Centrifuge the *eppendorf* tube at 4°C, 1300 rpm, 5 min and discard the supernatant.
- Resuspend the pellet in an equal volume of (417 µL) of **Tris/Acetate buffer** (this mix is referred to as the 'Desalted auxiliary enzymes').
- Add 41,7 µL of auxiliary enzymes mix into each syringe and centrifuge at 4°C, 2500 rpm, 5 minutes. Do not overload syringes to avoid column collapse.
- Collect the eluted volumes and transfer them to a unique 15 mL tube. Add 273,5 µL of **Tris/Acetate buffer** per each of the eluates added.
- Use fresh desalted auxiliary enzymes for the Fru-2-6-P₂ assay. Alternatively, store at -20°C.

9.3.3. Preparation of substrates for Fru-2,6-P₂ determination

Prepare a 20X stock of Fru-6-P and Glu-6-P in relation 1:3,5 in water. For 10 mL, mix 0,304 g Fru-6-P (Na₂ salt) with 1,07 g Glu-6-P (Na₂ salt) in water. Store at -20°C until the Fru-2-6-P₂ assay is performed.

9.3.4. Sample preparation and determination of Fru-2,6-P₂


- Keep plates (usually 6-well plates) on ice, remove medium and wash twice with cold PBS.
- Add 70 µL of **Fru-2-6-P₂ extraction buffer**, scrap and transfer the lysates into *eppendorf* tubes.
- Heat at 85°C for 20 min and centrifuge at 4°C, 1400 rpm, 15 minutes.
- Transfer equal volumes of each **supernatant** to new tubes. Annotate the **initial sample volume**. Make sure that there are at least 10 µL of supernatant remaining in the original tube, which will be used for **protein quantification**. Store all tubes on ice before setting up the assay with a standard curve.
- (Optional) Centrifuge the **supernatant** again at 4°C, 1400 rpm, 2 min to clarify the sample.
- Prepare the samples for the standard curve as described in **Table M-XV**.

Fru-2,6-P ₂ in the cuvette (pmols)	Water (μL)	Fru-2,6-P ₂ preparation from stock
30	495	5 μL of stock solution (3,5 mM)
8	982	18 μL of 30 pmol solution
6	0	250 μL 8 pmol solution + 250 μL 4 pmol solution
4	250	250 μL 8 pmol solution
2	250	250 μL 4 pmol solution
1	250	250 μL 2 pmol solution
0	250	-

Table M-XV. Preparation of a standard curve of Fru-2,6-P₂.

- Put 1 mL of Tris/Mg(CH₃COO)₂ Buffer to the spectrophotometer to set the Blank.
- Prepare the Tris/Mg(CH₃COO)₂ Buffer + NADH buffer (Assay buffer) by adding NADH to Tris/Mg(CH₃COO)₂ until the absorbance in the spectrophotometer is close to 1,8-2.
- Given the heterogeneous activity of PPI-PFK aliquots, do not neutralize the samples of interest until the assay is working with the standard curve.
- Prepare the six spectrophotometer cuvettes for the standard curve. For each cuvette, add:

Tris/Acetate Buffer	730 μL
Desalted Auxiliary enzymes	40 μL
Glu-6-P+Fru-6-P 20X	40 μL
H ₂ O	85 μL*
Sample/Standard	15 μL*
PPI-PFK	40 μL*
PPI (50 mM)	50 μL
Final Volume	1000 μL



* The volumes of PPI-PFK and sample can be adjusted according to the activity of the enzyme in each aliquot and the cell confluence in the samples. Water is compensated accordingly.

- Cup the cuvettes with parafilm and invert them. Immediately read in the spectrophotometer in the Programme: Fru-2,6-P₂ (λ=340 nm), Mode: Kinetics. Annotate the Rate Values from 0 to 6 min and from 2 to 6 minutes. Perform a standard curve with these values.
- If the standard curve has a R² value between 0,8-1, proceed to assay the samples.
- Neutralize the **supernatant** previously obtained from the samples of interest with **Acetic/Acetate buffer** to pH 7,0-7,5. Use pH strips to determine the pH. **Annotate the volume added.**
- Prepare spectrophotometer *cuvettes* with the samples in series of six as previously described and perform the lecture and annotation of the Rate Values.
- Perform **Bradford Assay** from non-neutralized samples to normalize Fru-2,6-P₂ to protein levels.

Absolute pmols of Fru-2-6-P₂ in each sample are obtained by extrapolating the Rate values in the standard curve. Determine the concentration of Fru-2,6-P₂ in the samples of interest as follows:

$$\text{pmols Fru-2,6-P}_2/\mu\text{L sample} = \frac{\text{pmols Fru}_{2,6}\text{P}_2}{\text{Sample volume in the cuvette} \cdot \text{Dilution}}$$

$$\text{where Dilution} = \frac{\text{Initial sample volume} + \text{Acetic/Acetate}}{\text{Initial sample volume}}$$

$$\text{pmols Fru-2,6-P}_2/\text{mg protein} = \frac{\text{pmols Fru}_{2,6}\text{P}_2/\mu\text{L sample}}{\mu\text{g protein}/\mu\text{L sample}} \cdot 1000$$

where $\mu\text{g protein}/\mu\text{L sample}$ is determined the Bradford Assay.

9.4. Determination of intracellular Pyr, PEP, 2PG and 3PG

This assay is based on the reaction catalysed by LDH, which converts Pyr to lactate in the presence of NADH, which is oxidized to NAD⁺, and the reactions catalysed by PK, ENO and PGAM (Figure M-6).

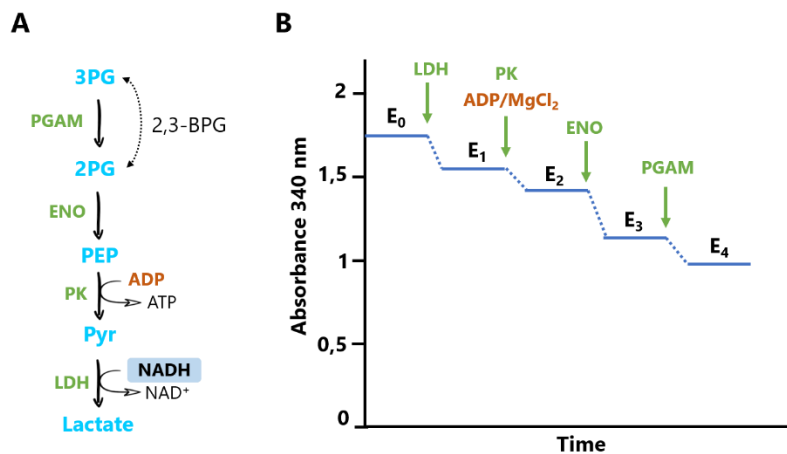


Figure M-6. Reactions involved in the assay for the determination of Pyr, PEP, 2PG and 3PG. (A) NADH consumption is the readout of LDH activity. **(B)** To initiate the assay, the absorbance of the sample needs to be stable. LDH is added to the spectrophotometer *cuvette* and the decrease in NADH absorbance (E₀-E₁) is proportional to the concentration of pyruvate in the sample. When absorbance is again stable, PK is added to the sample and the decrease in NADH absorbance (E₁-E₂) is proportional to the concentration of PEP. After addition of ENO, the readout (E₂-E₃) corresponds to the 2PG and, finally, the last decrease of NADH absorbance (E₃-E₄) is observed after the addition of PGAM and correspond to 3PG.

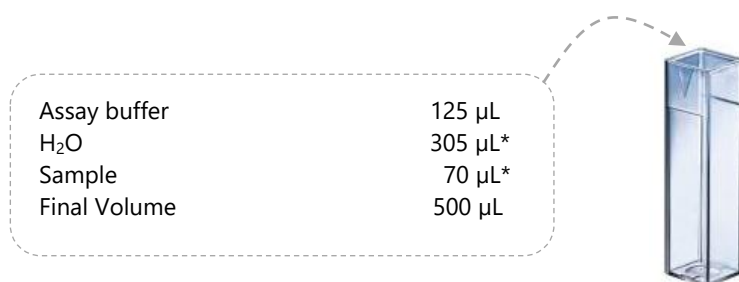
9.4.1. Sample preparation

- Keep plates (usually 6-well plates) on ice, remove medium and wash twice with cold PBS.
- Add 70 μL of 1M HClO_4 , scrap and transfer the lysates into *eppendorf* tubes.
- Centrifuge at 4°C, 15000 x g, 5 minutes.
- Transfer the supernatant to a new tube. A solid pellet will be formed at the bottom of the tube. Keep the **pellets*** for **protein quantification**.

9.4.2. Determination of Pyr, PEP, 2PG and 3PG

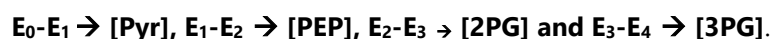
- Prepare LDH, PK and PGAM by diluting the solution stocks (Roche) at 1/20 in water. Weight the appropriate amount of ENO (Roche) to a final concentration of 100 U/mL.
- Prepare 50 mM ADP in 50 mM MgCl_2 .
- Add NADH to **PEP assay buffer** until the absorbance is close to 1,8-2.
- Neutralize samples with 3M KHCO_3 to pH 7,0-7,5.
- Prepare series of six *cuvettes* as follows:

Assay buffer	125 μL
H_2O	305 μL^*
Sample	70 μL^*
Final Volume	500 μL



- Add 20 μL of the enzymes and ADP- MgCl_2 at the corresponding time according to **Figure M-6**.
- Annotate the values (E0 to E4) at each step when absorbance is stabilized.
- Dissolve the **pellets*** with 30 μL 1M NaOH, vortex, heat at 95°C for 5 min for a complete dissolution and determine protein concentration by **Bradford Assay**.

The concentration of Pyr, PEP, 2PG and 3PG are calculated considering that:



The Beer-Lambert Law relates the Δ_{Abs} and the concentration of each metabolite as follows:

$$\Delta_{\text{Abs}} = \epsilon \cdot c \cdot d$$

where ϵ is the extinction coefficient of NADH at 340 nm ($6,22 \cdot 10^3 \text{ cm}^{-1} \text{ M}^{-1}$), c is the concentration of the metabolite in the cuvette (M) and d is the length of the cuvette (1 cm).

To compare between samples, concentration of metabolites is normalized to protein concentration.

10. NAD(P)⁺/NAD(P)H assay

Determination of NAD⁺ and NADH, and NADP⁺ and NADPH were measured individually using de NAD/NADH-Glo and the NADP/NADPH-Glo Assays (Promega), respectively (Figure M-7).

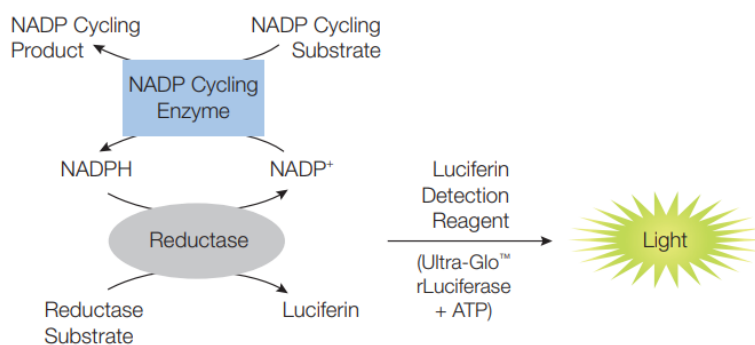
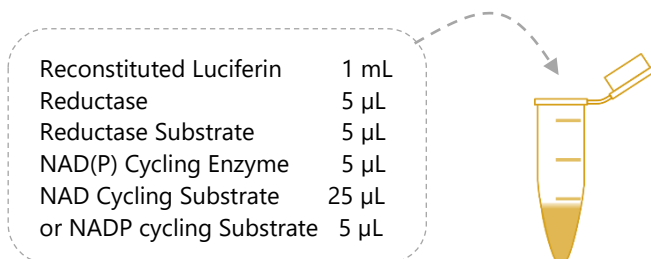


Figure M-7. Basis of the NAD(P)/NAD(P)H assays. These assays are based on a reduction reaction catalysed by Reductase, which couples NAD(P)H oxidation with the reduction of a specific substrate that becomes luminescent, luciferin. NAD(P) cycle enzyme is responsible for the conversion of NAD(P)⁺ to NAD(P)H coupled with the oxidation of NAD(P)⁺ cycling substrate. From Promega.

The day before the experiment, cells were plated at 20.000 cells/well in a 96-well plate in triplicates. An identical plate was prepared in parallel to perform crystal violet assay and normalize the results.

The assay was performed following manufacturer's indications. Luciferin reagent needs to be reconstituted and NAD(P)/NAD(P)H detection reagent is prepared as follows:



- Process cells: remove culture media and add 50 µL of PBS to each well and lyse cells by adding 50 µL of 0,2M NaOH with 1% DTAB. Transfer 50 µL of the lysate to another well.
 - Detection of NAD(P)⁺ → Add 25 µL of 0,4 N HCl. Heat at 60°C, 15 min. Incubate at room temperature for 10 min. Add 25 µL 0,5 M Tris Base.
 - Detection of NAD(P)H → Heat at 60°C, 15 min. Incubate at room temperature for 10 min. Add 50 µL 0,5 M Tris/HCl.
- Transfer 50 µL of each lysate to a well of a 96-well white-walled plate. Add 50 µL of NAD(P)/NAD(P)H detection reagent. Shake the plate and incubate for 60 min at room temperature. Record luminescence in a luminometer. FluoStar Optima plate reader was used.
- Perform crystal violet assay from the plate prepared the day before and normalize the concentration of NAD⁺, NADH, NADP⁺ and NADPH to cell number. This normalization is not required when calculation the ratio NAD⁺/NADH and NADP⁺/NADPH.

11. Metabolomics and fluxomics

11.1. Culture conditions

For abundance analyses, cells were transfected with either a *TIGAR*-pcDNA3-expressing vector or *PFKFB3* or *TIGAR*-targeting siRNAs. Cellular extracts were collected 24 h and 72 h after transfection for the overexpression and siRNA experiments, respectively. For fluxomic analyses, cells were transfected as described before and, at 24 or 72 h after transfection, media was replaced by glucose-free DMEM supplemented with 25 mM fully labelled ^{13}C -glucose (Cambridge Isotope Laboratories), 10% dialyzed FBS, 2 mM L-glutamine, 100U/mL penicillin and 100 ng/mL streptomycin. Cells were incubated at 37 °C and 5% CO_2 in these conditions for 6 hours and extracts were obtained.

11.2. Obtention of cellular extracts

All experiments were performed in 6-well plates that reached 90% confluence at the end of the experiments. Media was removed and cells were washed once with cold PBS with the plates on ice. Cells were scrapped with 50 μL of DEPC water, transferred to cold *ependorf* tubes and directly frozen in liquid nitrogen and stored at -80°C .

11.3. Sample processing and analysis

The processing and analysis of the samples was performed by Dr. Yanes Lab (Universitat Rovira i Virgili, Reus). Metabolites were extracted by adding 300 μL of cold methanol/water (8:1, v:v). Samples were vortexed for 30 seconds and immersed in liquid N_2 to disrupt cell membranes followed by 10 seconds of bath-sonication. These two steps were repeated 3 times. Cell lysates were incubated for 20 min on ice before centrifugation (4°C, 5000 g, 15 minutes). 10 μL of $^{13}\text{C}_3$ -glycerol (150 ppm) was added to the supernatant as internal standard. Next, 250 μL of each sample were dried under a stream of N_2 gas. Lyophilized polar extracts were incubated with 50 μL methoxyamine in pyridine (40 $\mu\text{g}/\mu\text{L}$) for 45 min at 60 °C. To increase volatility of the compounds, the samples were silylated using 25 μL N-methyl-N-trimethylsilyltrifluoroacetamide with 1% trimethylchlorosilane (Thermo Fisher Scientific) for 30 min at 60 °C. A 7890 A GC system coupled to a 7000 QqQ mass spectrometer (Agilent Technologies) was used for isotopologue determination. Derivatized samples were injected (1 μL) in the gas chromatograph system with a split inlet equipped with a J&W Scientific DB5-MS+DG stationary phase column (30 mm \times 0.25 mm i.d., 0.1 μm film, Agilent Technologies). Helium was used as carrier gas at a flow rate of 1 mL/minute in constant flow mode. The injector split ratio was adjusted to 1:5 and oven temperature was programmed at 70 °C for 1 minute and increased at 10 °C/minute to 325 °C. The ionization performed was positive chemical ionization (CI) with isobutene as reagent gas. Mass spectral data on the 7000 QqQ were acquired in scan mode monitoring selected ion clusters of the different metabolites.

12. Molecular biology techniques

12.1. DNA purification from bacterial stabs

Two BACs from chromosome 12 were provided by the BACPAC Service of the Children's Hospital Oakland Research Institute, RP11-177D20 and RP11-74J21, of 156,587 and 164,227 Kbp, respectively (**Figure M-8**). The BACs were supplied as bacterial stab cultures. Bacteria were cultured and DNA was purified. Given that each BAC's DNA is more than 150 Kbp, MaxiPrep Kits were not suitable for the purification and phenol/chloroform DNA extraction protocol was performed.

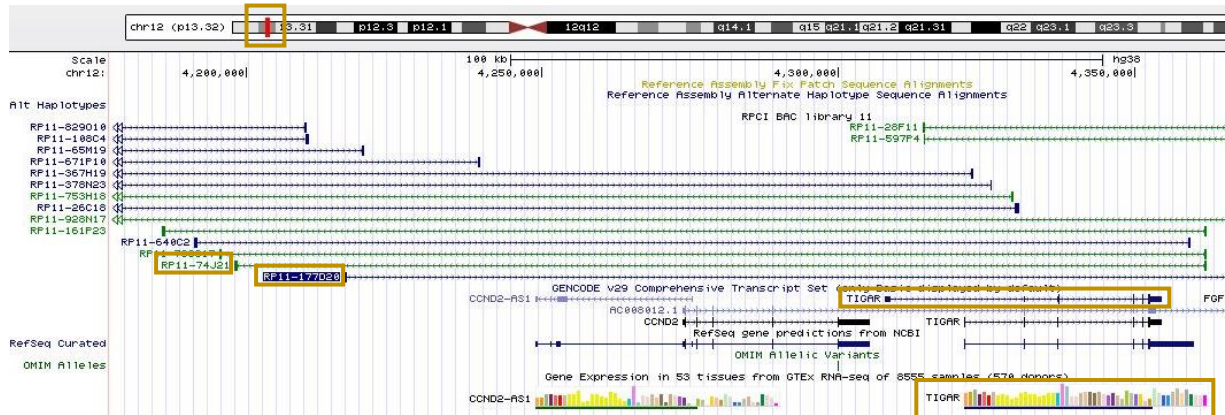


Figure M-8. Location of BACs RP11-177D20 and RP11-74J21 in human chromosome 12. The BACs used for the amplification of *TIGAR* promoter and the coding sequence of *TIGAR* gene are highlighted in squares. Adapted from UCSC Genome Browser.

12.2. Obtention of DNA fragments by PCR

In order to obtain the region of *TIGAR* promoter of interest, we performed PCR of the DNA purified from BACs using several primers specific to the fragments of interest. A schematic representation of the plasmids used is provided in Results Chapter III. MyFi™ DNA Polymerase (Bioline) was used according to manufacturer's instructions:

5x MyFi Reaction Buffer (contains dNTPs)	5 μ L
Template	100 ng (x μ L)
Primers (20 μ M)	1 μ L
MyFi DNA Polymerase	1 μ L
Water	up to 25 μ L1

The table lists the components and volumes for a PCR reaction. To the right, an illustration shows a blue pipette tip dispensing liquid into a multi-well plate.

PCR conditions were adapted to each pair of primers:

95°C, 5 min. [95°C, 15 sec. **T_m**, 30 sec. 72°C, **1 min.**] 30-35 cycles. 72°C, 2 min. 4°C, ∞ .

Melting temperature (T_m) depends on the composition of the primers.

Elongation time depends on the size of the DNA product. 1 min/Kbp.

The sequences for the primers used for the generation of the constructs that were successfully cloned into pGL3 vectors (D, J, 8 and 15, see Results Chapter III for nomenclature) are reported in **Table M-XVI**.

Primer name	Sequence	T _m (°C)	Construction
FW 4.1	5'-GCGTCCTTACAGATCTAGCATGG-3'	57,2	D, 15
FW 4.2	5'-GTGAACCCGGGAGGCGGAG-3'	63,3	J
FW 4.3	5'-GATCACACCACTGCACTCCA-3'	65,1	8
RV 2	5'-GCAAGCTTCCCCACACCAC-3'	59,4	8, 15
RV 3	5'-GCCCTTGATAGCTAGCAAAGTTC-3'	57,9	J, D

Table M-XVI. Primers used for the obtention of fragments D, J, 8 and 15 (see Results Chapter III).

12.3. DNA electrophoresis in agarose gels and purification of bands

1% agarose gels with ethidium bromide (EtBr) were prepared, and samples were loaded with 6X loading dye (Thermo Fisher Scientific) and run at 85 V for 30 min in **TAE buffer**. GeneRuler 100 bp Plus and GeneRuler Express (Thermo Fisher Scientific) DNA ladders were used. EtBr emits an orange light when excited by UV light and was used to visualize DNA bands in a UV transilluminator.

ⓘ EtBr is a DNA intercalating agent with mutagenic potential. Always handle with double glove and discard all residues in the appropriate container.

DNA bands were cut using a transilluminator with UV light and purified with QIAquick Gel Extraction Kit (Qiagen).

12.4. TOPO TA cloning

In order to clone the DNA fragments of interest into a plasmid for their amplification in bacterial cultures, the TOPO TA Cloning Kit (Thermo Fisher Scientific) was used (**Figure M-9**).

Some thermostable polymerases have 3' to 5' exonuclease activity and eliminate 3' A-overhangs from PCR products. MyFi™ DNA Polymerase (Bioline), which was used in our PCRs, preserves them.

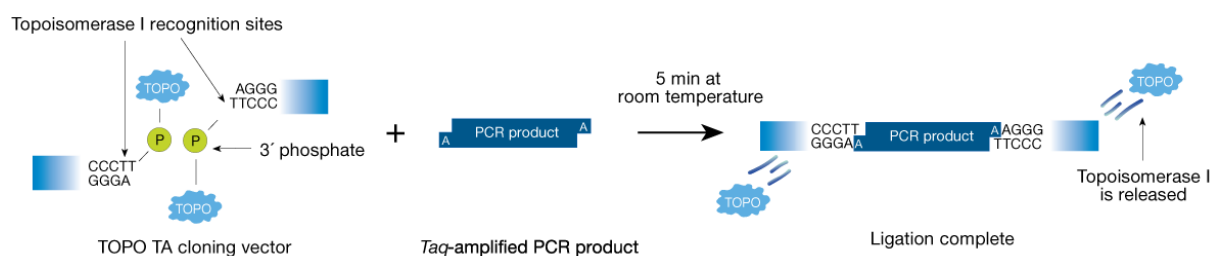
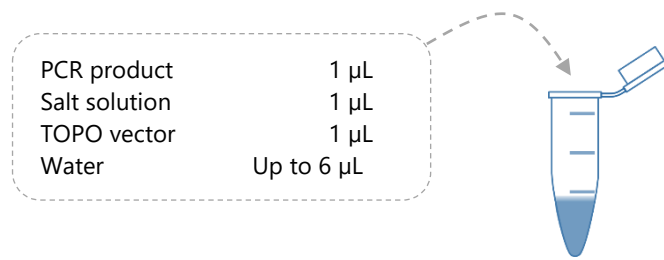


Figure M-9. TOPO TA cloning system. This cloning system is based on the recombination of 3' A-overhangs from PCR products with the TOPO vector, which has T-overhangs linked to Topoisomerase-I, which catalyses the reaction. From Thermo Fisher Scientific.

TOPO TA reactions were performed following manufacturer's indications:



Mix gently and incubate for 5 min at room temperature. Place the reaction on ice before transforming competent cells.

12.5. Restriction enzyme digestion

The digestion of DNA fragments was used to analyse the products of PCR and ligations, and to linearize vectors for subcloning. The incubation conditions were usually 5U enzyme/ μ g DNA in the appropriate buffer for 1 h at 37°C. Recently, FastDigest Restriction Enzymes have emerged as an alternative to save time (restriction takes only 15 minutes) and perform double digestions in a universal buffer.

The maps of the plasmids used in the cloning process can be checked in **Figures M10-M12**.

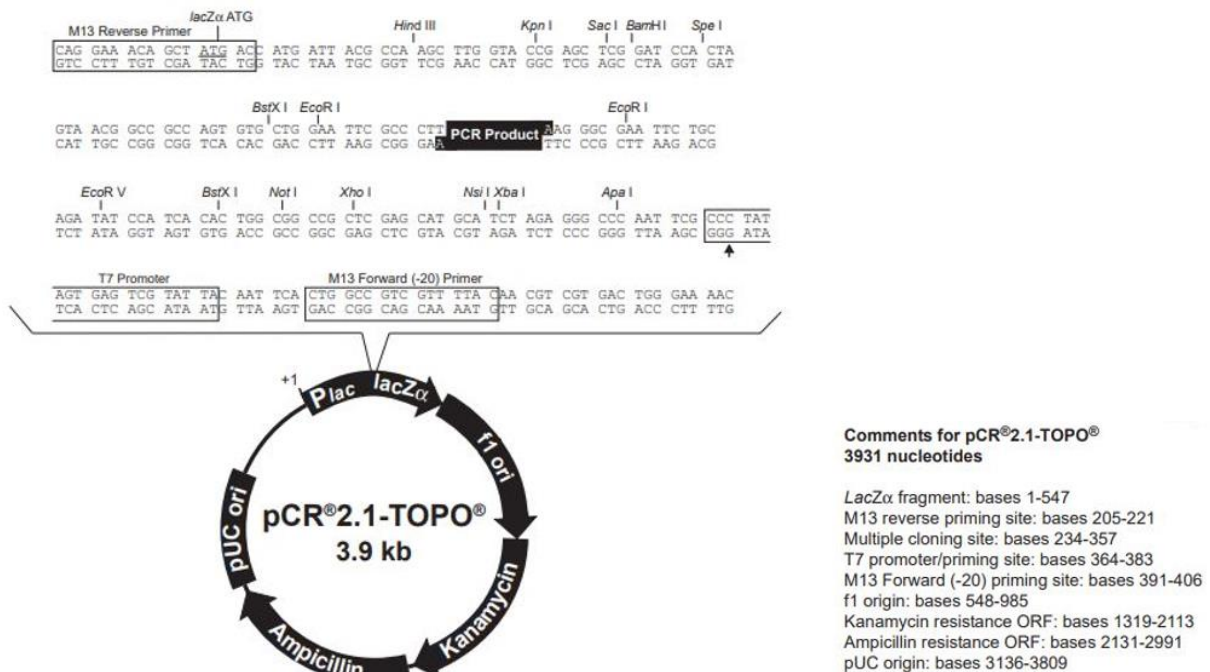


Figure M-10. Map of pCR-2.1-TOPO vector (Thermo Fisher Scientific)

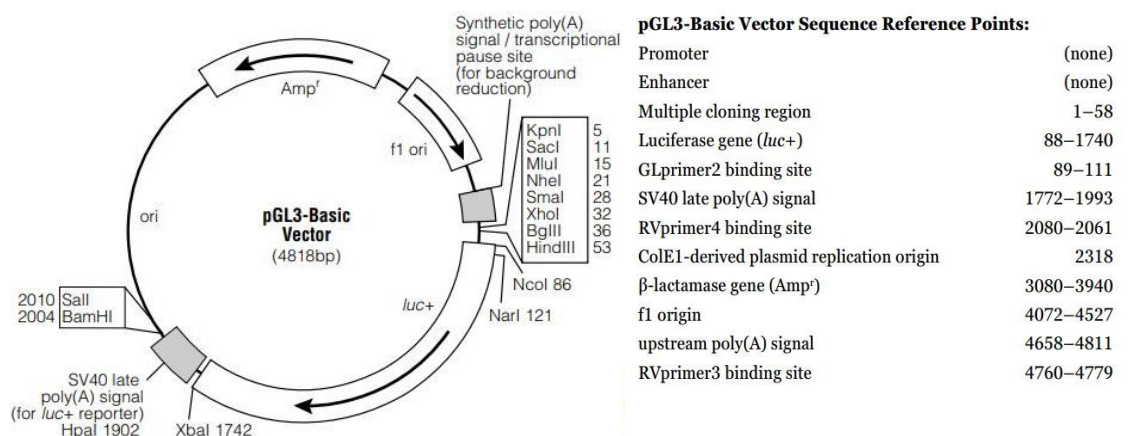


Figure M-11. Map of pGL3 Basic vector (Promega)

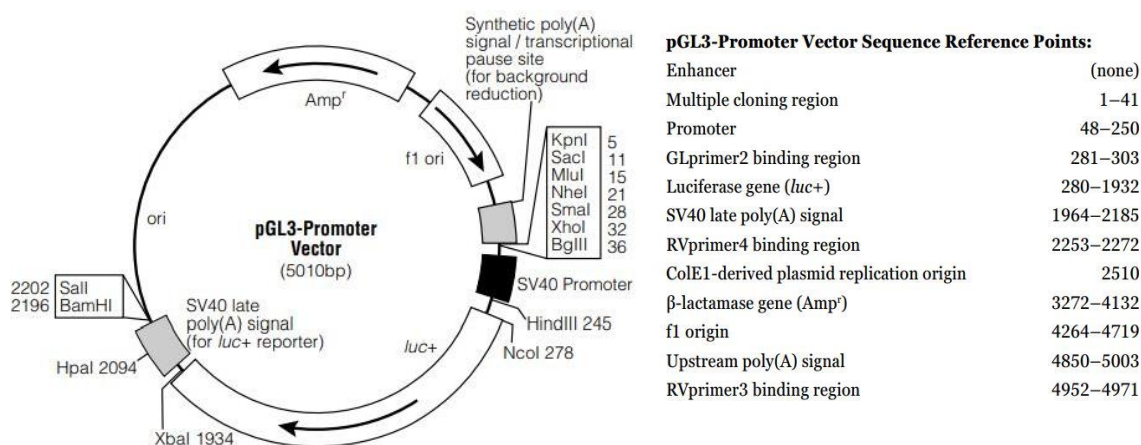


Figure M-12. Map of pGL3 Promoter vector (Promega)

The cloning strategies performed for the subcloning of PCR fragments of interest from TOPO TA to pGL3 vectors is detailed in **Figure M-13**.

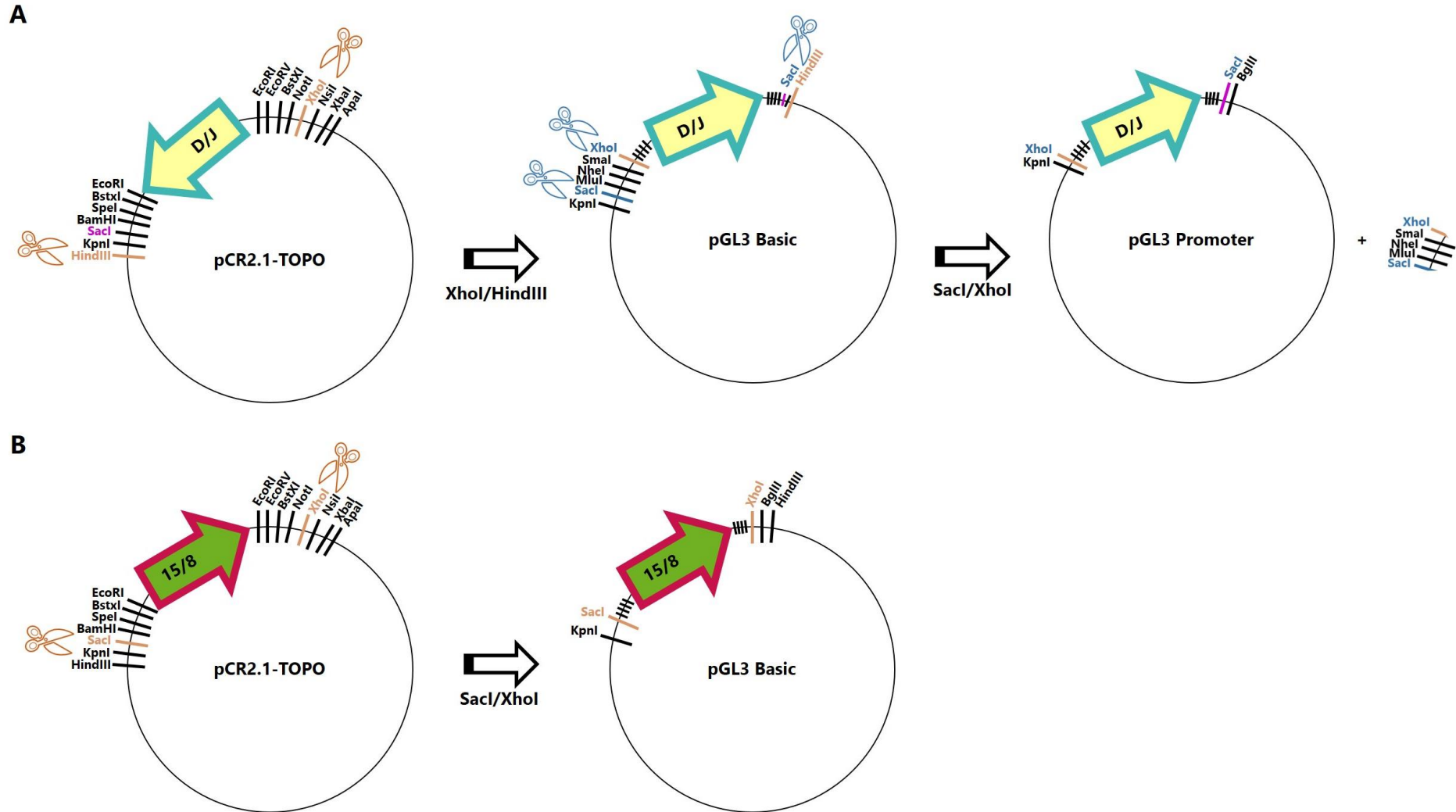


Figure M-13. Restriction enzyme strategies performed. The four PCR fragments (D, J, 8 and 15) were firstly cloned into TOPO vectors and then subcloned with different restriction strategies. **(A)** Constructs D and J were firstly cloned in pGL3 Basic vectors using HindIII/XhoI double digestion but given that they lack the transcription start site of TIGAR, we had to subclone these fragments again into pGL3 Promoter vectors, using SacI/XhoI. **(B)** Constructs D and J were directly subcloned from TOPO to pGL3 basic vectors with SacI/XhoI double digestion.

12.6. Dephosphorylation of vector 5'-P termini

5'-phosphorylated termini of vector DNA need to be dephosphorylated after digestion before a ligation reaction is performed to prevent self-ligation. With that purpose, Phosphatase FastAP (Thermo Fisher Scientific) was used following manufacturer's recommendations. 1 μ L of FastAP is added to 20 μ L digestion product and the mix is incubated for 10 min at 37°C. Reaction is stopped by heating at 65°C for 15 min.

12.7. Ligation

T4 DNA Ligase (Thermo Fisher Scientific) catalyses the formation of a phosphodiester bond between juxtaposed 5'-phosphate and 3'-hydroxyl termini in duplex DNA (**Figure M-14**).

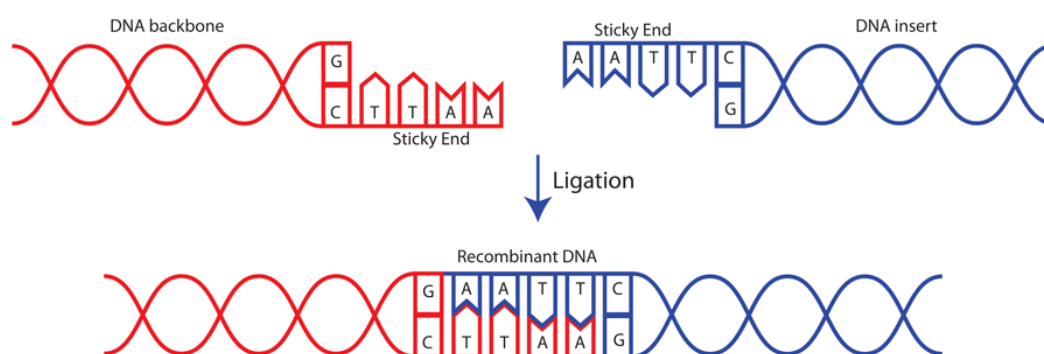


Figure M-14. Basis of the T4 DNA ligase reaction. T4 DNA ligase catalyses the recombination of two DNA strands that have been digested with the same restriction enzyme and, therefore, have sticky ends. In this example, DNA insert and backbone have been digested with EcoRI, which recognises the sequence GTTAAC. From Addgene.

T4DNA ligase reaction was performed according to manufacturer's recommendations:

Linear vector DNA	20-100 ng
Insert DNA	3:1 molar ratio insert:vector
10x T4 DNA Ligase buffer	2 μ L
T4 DNA Ligase	1 U
Water	up to 20 μ L



Incubate 10 min at 22°C. It is recommended to allow the reaction to continue overnight in a water bath at 16°C.

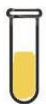
12.8. Transformation of Competent cells and selection of clones

JM109 *E. coli* or DH5 α competent cells (Promega) were used. DH5 α competent cells have a transformation efficiency greater than 10⁸cfu/ μ g and were used for subcloning.

- Thaw frozen competent cells on ice and aliquot 50 μ l for each transformation.
- Add 1–50ng of DNA (in this thesis, 6 μ l of TOPO reaction or 10 μ l of T4 DNA ligase were transformed) to each tube. Flick the tube several times. Perform a control of untransformed cells.
- Immediately return the tubes to ice for 30 minutes.
- Heat-shock the cells for 45 seconds in a water bath at 42°C (or 1 minute at 37°C).
- Immediately place the tubes on ice for 2 minutes.
- Add 900 μ l of warmed LB or SOC medium to each transformation reaction.
- Incubate for 45 min at 37°C with shaking.
- Centrifuge 10 min at 4000 rpm at room temperature. Discard 800 μ l of supernatant and use the remaining supernatant to softly resuspend the bacterial pellet.
- Plate cells in agar plates with the antibiotic of interest (given that all the plasmids used in this thesis confer resistance to Ampicillin, this antibiotic was used in all transformations).

12.9. Bacterial culture and plasmid purification

Liquid bacterial cultures were maintained in agitation (220 rpm) in Luria Bertani (LB) medium at 37°C overnight (14-16 h). Specific antibiotic (50 μ g/mL Ampicillin) was added according to the plasmid resistance genes. Avoid closing the recipients tight to facilitate oxygen diffusion within them and allow bacterial growth. Two types of liquid cultures were performed:



Minicultures: 5 mL LB culture from a bacterial colony as a first step for DNA amplification. The DNA from these cultures was isolated using GeneElute Plasmid Miniprep Kit (Sigma-Aldrich), digested with restriction enzymes and confirmed by agarose electrophoresis.



Maxicultures: 250 mL LB culture from a miniculture bacterial already confirmed to be the DNA of interest. The DNA from these cultures was isolated using GeneElute Plasmid Maxiprep Kit (Sigma-Aldrich) and used for subcloning or for the transfection of eukaryotic cells.

Solid bacterial cultures were performed in LB-Agar plates containing the antibiotic of interest (50 µg/mL Ampicillin) in an incubator at 37°C.

The following recipes were used to prepare LB and LB-Agar.

Reagent	LB	LB-Agar
Tryptone	10 g	10 g
NaCl	5 g	5 g
Yeast extract	5 g	5 g
Bacto agar	-	15 g
Water	Up to 1L	Up to 1L

Table M-XVII. LB and LB-Agar recipes.

LB and LB-Agar need to be autoclaved before using. In the case of LB-Agar, antibiotic is added when the temperature is about 30°C to avoid its degradation.

12.10. Preparation of glycerol stocks

Glycerol stocks are used to store bacterial cultures at -80°C and are prepared as follows:

- Transfer 810 µL of a mini/maxi bacterial culture grown at 37°C overnight to a cryopreservation vial and add 190 µL of glycerol 80%. The final concentration of glycerol will be 15%. Gently mix, put on ice and immediately freeze at -80°C.

12.11. Preparation of samples for sequencing

Premixed samples were prepared as follows and sequenced by Serveis Científicotècnics (Universitat de Barcelona).

- Mix 100 ng/Kb of DNA with 5 pmols of primer in a PCR tube. The primers used in this thesis were M13Forward and RVprimer3 for the sequencing of TOPO-TA and pGL3 vectors, respectively. Name samples in an easy way.
- Heat samples with the cap open in a thermocycler at 80°C for 15 minutes. Store at 4°C or -20°C until delivery.
- Generate an order at the WebLIMS service choosing the 'Premixed' mode and deliver the tubes with the printed order to Serveis Científicotècnics.
- Sequences can be downloaded from WebLIMS within 5 days. Analysis was performed with ApE plasmid editor.

13. Generation of PDAC cells stably expressing flag-TIGAR-EGFP

13.1. Primer design for the amplification of the cDNA of interest

The cDNA of interest was flag-TIGAR-GFP (f-TIG-GFP). Specific PCR primers were designed to amplify this sequence from another plasmid with the Primer Design Tool from Clontech. This tool designs primers specific to the DNA insert with 5' extensions of 15 bp complementary to the linearized vector of election with specific restriction sites. Our cloning strategy was based on the digestion of the retroviral vector pBABE-puro with BamHI and EcoRI (**Figure M-15**). The primers used where:

- Forward: 5' GGC GCC GGC CGG ATC CAT GGA CTA CAA AGA CGA CG
- Reverse: 5' CTG TGC TGG CGA ATT CTT ACT TGT ACA GCT CGT CCA TG

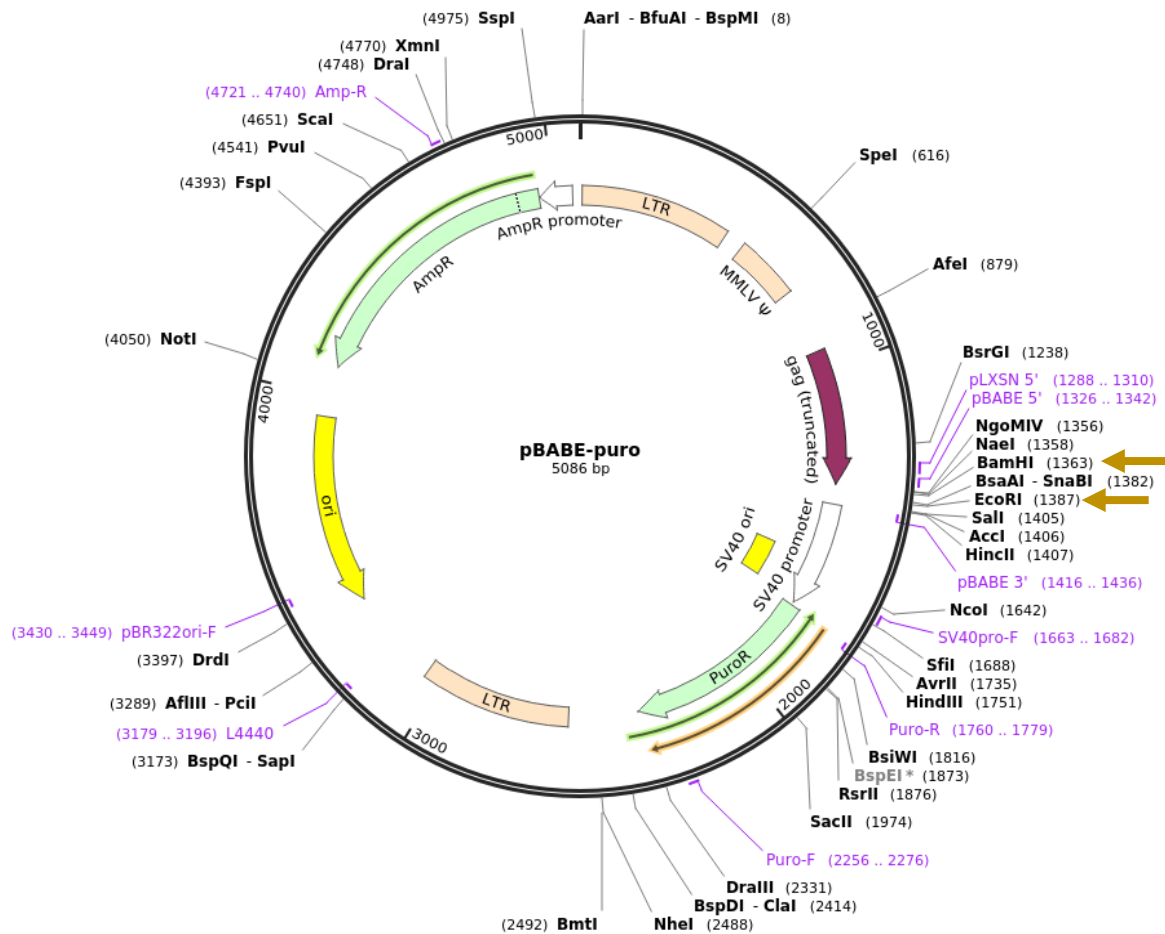
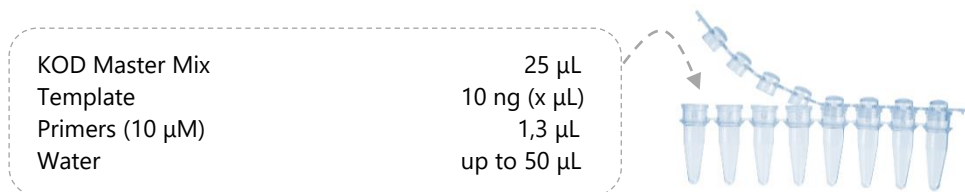


Figure M-15. Map of pBABE-puro vector. The restriction sites used for the cloning of f-TIG-GFP are indicated by arrows.

13.2. PCR amplification

PCR was performed using the KOD Hot Start Master Mix (Merck) as follows:



The PCR conditions were:

95°C, 2 min. [95°C, 20 sec. 66,7°C, 10 sec. 70°C, 32 sec] x 20 cycles. 70°C, 2 min. 4°C, ∞ .

PCR product was treated with DpnI to eliminate methylated DNA corresponding to the template bacterial plasmid and purified with NucleoSpin columns (Clontech).

13.3. Plasmid digestion and purification

1 μ g of pBABE-puro was digested with BamHI and EcoRI with 1 μ l of each restriction enzyme as previously described. The linearized plasmid was purified with NucleoSpin columns (Clontech).

13.4. Cloning and bacterial transformation

In Fusion HD-EcoDry System (Clontech) was used to perform the ligation (**Figure M-16**).

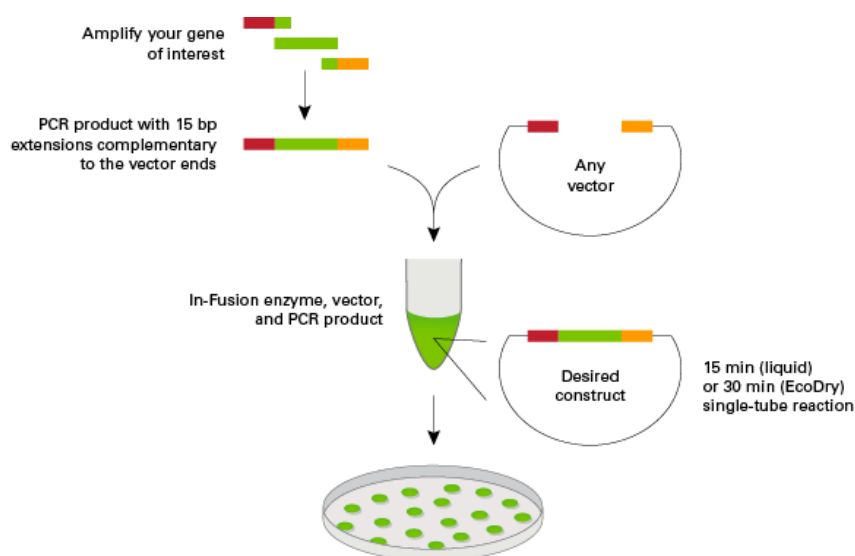


Figure M-16. InFusion cloning. The system is based on the recombination of the linearized vector and the insert. The insert has been previously generated by PCR with primers containing 15 bp overhangs complementary to the linearized vector. From Clontech.

Stellar competent cells were transformed with 1 μ L of InFusion product and plated on agar plates with 100 μ g/mL Ampicillin. Colonies were selected and DNA purification was performed by the Molecular Technology and Reagent Services (Beatson Institute for Cancer Research). The primers used for sequencing were pBABE 5' (5'-CTTTATCCAGCCCTCAC) and pBABE 3' (5'- ACCCTAACTGACACACATTCC).

13.5. Production of viral particles and transduction

The pBABE construct containing f-TIG-GFP was transfected into packaging Phoenix Eco cells using Lipofectamine 2000 following the same protocol as described for Lipofectamine LTX. Phoenix Eco cells generated viral particles which were excreted to the extracellular media. The supernatant from Phoenix cells was harvested after 48 hours of culture, filtered through a 0,45 μm syringe and used for the transduction of PDAC cells in Polybrene-containing media (**Figure M-17**). After 2 days, cells were split in selection media containing 1 $\mu\text{g}/\text{ml}$ puromycin. Transduction efficiency was assessed by fluorescence microscopy and after 5-day selection most cells displayed GFP fluorescence and were used to perform the experiments reported in Results Chapter IV.

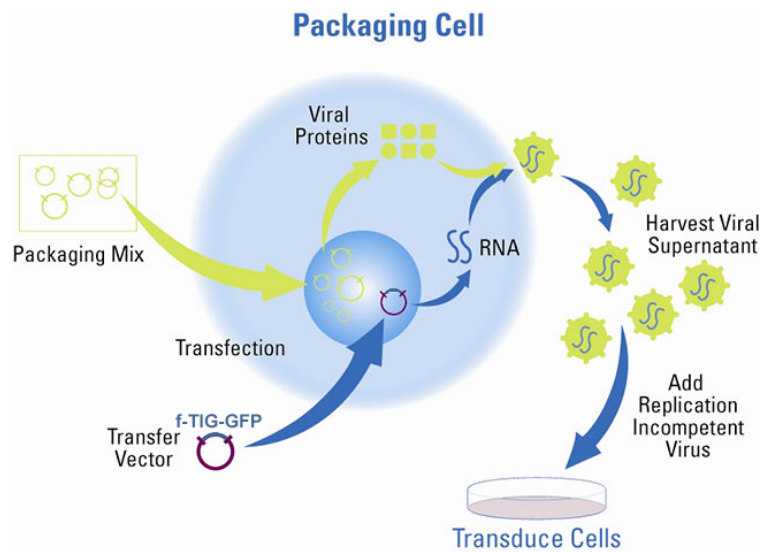


Figure M-17. Processes involved in the transduction of eukaryotic cells. Packaging cells, in this case Stellar Cells, were transfected with the retroviral vector pBABE-puro containing f-TIG-GFP coding sequence. Stellar cells produced replication incompetent viral particles, which were harvested from used for the transduction of PDAC cells. Adapted from Dharmacon.

14. Luciferase assays

Cells were transfected in 6-well plates with the luciferase reporter plasmid and a β -galactosidase plasmid to assess the efficiency of the transfection. In this thesis, RSV- β -galactosidase and SV40- β -galactosidase reporter vectors were assayed but only RSV- β -galactosidase was effectively expressed by HeLa cells. When the effect of a transcription factor on the luciferase activity was evaluated, transfection of the expression vector was performed together with luciferase and β -galactosidase reporter plasmids.

The day before to the luciferase assay, cells were splitted into 12-well plates by dividing each well of a 6-well plate into 3 wells of a 12-well plate.

The following day, cells were washed twice in cold PBS and the protocols of Luciferase Assay System (Promega) and Luminescent β -galactosidase Detection Kit II (Clontech) were performed.

14.1. Luciferase Assay System

- Maintain plates on ice and wash twice with PBS. Add 100 μ L lysis buffer to each well and agitate for 20 min at maximum potency on ice.
- During agitation, prepare eppendorf tubes with 50 μ L luciferin and switch on the luminometer.
- Add 50 μ L of cell lysate into the eppendorf tubes with luciferin and immediately read on a luminometer in an acquisition interval of 10 seconds. It is preferred to prepare and read sample by sample.

14.2. Luminescent β -galactosidase Detection Kit II

- Prepare eppendorf tubes with 100 μ L β -galactosidase Reagent (98 μ L Reaction Buffer + 2 μ L β -galactosidase) and add 30 μ L of the cell lysate obtained at the first step of Luciferase Assay System protocol.
- Incubate for 1 h protected from light without agitation.
- Read on a luminometer in an acquisition interval of 10 seconds.

15. Chromatin Immunoprecipitation assay

ChIP assay was performed by Cristina Sánchez from Dr. Ventura's Lab (Departament de Ciències Fisiològiques, Universitat de Barcelona) as previously described in (206). After treatments, cells were fixed in 1% formaldehyde for 10 minutes. ChIP was carried out using 1 μ g of anti-Nrf2 (Santa Cruz Biotechnology) or anti-IgG (Upstate) and purified with 20 μ L Magna ChIP Protein A+G Magnetic Beads (Merck). Purified DNA fragments were analysed by qPCR with SYBR Green. The primers used for the analysis *Tigar* gene promoter and first intron are detailed in Figure 84.

16. Statistical analysis

Data were analysed according to the comparisons performed. Student's t-test was used to compare a single variable in two independent groups, and was the statistical test used in most of the analyses. Two-way ANOVA with Tukey's *post-hoc* test was used to analyse differences between more than two groups in which multiple parameters were analysed at the same time such as fluxomic analyses, and to analyse differences between two groups with two independent variables, such as the combinations of siRNA transfections with Akt inhibitors.

17. General Buffers

Protein extraction and Western blot	Protein extraction and Western blot	Fru-2,6-P ₂ determination
Whole cell lysis buffer 50 mM Tris-HCl (pH 6,8) 2% SDS 10% Glycerol	Semidry Transference Cathode Buffer 40 mM 6-aminocaproic acid 10% Metanol	Tris/KCl/DTT Buffer 20 mM Tris 20 mM KCl 2 mM DTT (added at the moment) pH 8,2
RIPA 25 mM Tris-Cl 0,1% SDS 1% NP-40 1% Sodium deoxycholate pH 7,5 Protease and phosphatase inhibitors	Semidry Transference Anode Buffer 0,3M Tris-base 1,92 M Glycine pH 8,3	Tris/Acetate Buffer 50 mM Tris pH 7,8 (with acetic acid)
Subcellular fractioning Buffer I 10 mM Tris-HCl 10 mM KCl 10 mM MgCl ₂ 250 mM Sacarose pH 7,5 Protease and phosphatase inhibitors	Stripping Solution 67,5 mM Tris-HCl pH 7,5 2% SDS 0,1 M β-mercaptoethanol	Acetic/Acetate Buffer 250 mM CH ₃ COOH 250 mM CH ₃ COO ⁻ (Na ⁺) pH 4,7
Subcellular fractioning Buffer II 10 mM HEPES 10 mM KCl 1,5 mM MgCl ₂ 10% Glycerol 0,34 M Sacarose pH 7,5 Protease and phosphatase inhibitors	TBS 20X 200 mM Tris-HCl 3M NaCl pH 7,5	Other metabolic determinations
Sample Buffer 4X 200 mM Tris-HCl (pH 6,8) 40% Glycerol 8% SDS 20% β-mercaptoethanol 0,8% Bromophenol blue	TBS-Tween TBS 20X 2% Tween-20	Lactate Assay Buffer 0,3125 M Hydrazinium sulphate 0,875 M Glycine pH 9 (with NaOH)
Lower buffer 1,5 M Tris-HCl (pH 8,8) 0,4% SDS	Immunofluorescence	PGO enzyme reaction solution 1 PGO capsule 100 mL Water 1,6 mL o-Dianisidine solution
Upper buffer 0,5 M Tris-HCl (pH 6,8) 0,4% SDS	Phosphate Buffer 0,4 M (for PFA) 0,32 M NaH ₂ PO ₄ ·H ₂ O 0,08M K ₂ HPO ₄ pH 7,3-7,4 (with HCl)	o-Dianisidine solution 50 mg o-Dianisidine hydrochloride 20 mL Water
Electrophoresis buffer 250 mM Tris-HCl 1,92 M Glycine pH 8,3 10% SDS	Immunofluorescence blocking solution PBS 1X 0,1% Triton-X100	PEP assay buffer 0,2 M GlyGly 0,4 M KCl 40 mM MgCl ₂ pH 7,4
Wet Transference Buffer 250 mM Tris-HCl 1,92 M Glycine pH 8,3 10% Methanol	Immunofluorescence solution for antibodies preparation PBS 1X 0,1% Tween-20	Other general buffers
	Fru-2,6-P₂ determination	TAE 50X 40 mM Tris 1 mM EDTA 20 mM Acetic Acid
	Fructose-2,6-P₂ extraction buffer 0,1M NaOH 0,1% Triton-X100	Crystal Violet Solution 0,5% Crystal violet 20% Methanol
	Hepes/CH₃COOK/DTT Buffer 20 mM Hepes 20 mM CH ₃ COOK 2 mM DTT (added at the moment)	PBS 10X 1,37 M NaCl 27 mM KCl 100 mM Na ₂ HPO ₄ 18 mM KH ₂ PO ₄

REFERENCES



1. Hanahan D, Weinberg RA. The hallmarks of cancer. *Cell*. (2000) 100(1):57–70.
2. Hanahan D, Weinberg RA. Hallmarks of cancer: the next generation. *Cell*. (2011) 144(5):646–74. doi:10.1016/j.cell.2011.02.013
3. Bensaad K, Tsuruta A, Selak M a, Vidal MNC, Nakano K, Bartrons R, Gottlieb E, Vousden KH. TIGAR, a p53-inducible regulator of glycolysis and apoptosis. *Cell*. (2006) 126(1):107–20. doi:10.1016/j.cell.2006.05.036
4. Jen K-Y, Cheung VG. Identification of novel p53 target genes in ionizing radiation response. *Cancer Res*. (2005) 65(17):7666–73. doi:10.1158/0008-5472.CAN-05-1039
5. Cantor JR, Sabatini DM. Cancer Cell Metabolism: One Hallmark, Many Faces. *Cancer Discov*. (2012) 2(10):881–98. doi:10.1158/2159-8290.CD-12-0345
6. Lyssiotis CA, Cantley LC. Acetate fuels the cancer engine. *Cell*. (2014) 159(7):1492–4. doi:10.1016/j.cell.2014.12.009
7. DeNicola GM, Cantley LC. Cancer's Fuel Choice: New Flavors for a Picky Eater. *Mol Cell*. (2015) 60(4):514–23. doi:10.1016/j.molcel.2015.10.018
8. Röhrig F, Schulze A. The multifaceted roles of fatty acid synthesis in cancer. *Nat Rev Cancer*. (2016) 16(11):732–49. doi:10.1038/nrc.2016.89
9. Shah US, Dhir R, Gollin SM, Chandran UR, Lewis D, Acquafondata M, Pflug BR. Fatty acid synthase gene overexpression and copy number gain in prostate adenocarcinoma. *Hum Pathol*. (2006) 37(4):401–9. doi:10.1016/j.humpath.2005.11.022
10. Caro P, Kishan AU, Norberg E, Stanley IA, Chapuy B, Ficarro SB, Polak K, Tondera D, Gounarides J, Yin H, Zhou F, Green MR, Chen L, Monti S, Marto JA, Shipp MA, Danial NN. Metabolic signatures uncover distinct targets in molecular subsets of diffuse large B cell lymphoma. *Cancer Cell*. (2012) 22(4):547–60. doi:10.1016/j.ccr.2012.08.014
11. Warburg O, Wind F, Negelein E. The metabolism of tumors in the body. *J Gen Physiol*. (1927) 8(6):519–30. doi:10.1085/jgp.8.6.519
12. Gauthé M, Richard-Molard M, Cacheux W, Michel P, Jouve J-L, Mitry E, Alberini J-L, Lièvre A, Fédération Francophone de Cancérologie Digestive (FFCD). Role of fluorine 18 fluorodeoxyglucose positron emission tomography/computed tomography in gastrointestinal cancers. *Dig Liver Dis*. (2015) 47(6):443–54. doi:10.1016/j.dld.2015.02.005
13. Gatenby RA, Gillies RJ. Why do cancers have high aerobic glycolysis? *Nat Rev Cancer*. (2004) 4(11):891–9.
14. Szablewski L. Expression of glucose transporters in cancers. *Biochim Biophys Acta - Rev Cancer*. (2013) 1835(2):164–9. doi:10.1016/j.bbcan.2012.12.004
15. Smallbone K, Gatenby RA, Gillies RJ, Maini PK, Gavaghan DJ. Metabolic changes during carcinogenesis: Potential impact on invasiveness. *J Theor Biol*. (2007) 244(4):703–13. doi:10.1016/j.jtbi.2006.09.010
16. Brindle KM. Imaging metabolism with hyperpolarized (13)C-labeled cell substrates. *J Am Chem Soc*. (2015) 137(20):6418–27. doi:10.1021/jacs.5b03300
17. Hue L, Rider MH. Role of fructose 2,6-bisphosphate in the control of glycolysis in mammalian tissues. *Biochem J*. (1987) 245(2):313–24.
18. Newsholme E, Start C. Regulation in Metabolism. Chichester: Wiley; 1973. p. 88-145.
19. Rempel A, Mathupala SP, Griffin CA, Hawkins AL, Pedersen PL. Glucose catabolism in cancer cells: amplification of the gene encoding type II hexokinase. *Cancer Res*. (1996) 56(11):2468–71.
20. Vora S, Halper JP, Knowles DM. Alterations in the activity and isozymic profile of human phosphofructokinase during malignant transformation in vivo and in vitro: transformation- and progression-linked discriminants of malignancy. *Cancer Res*. (1985) 45(7):2993–3001.

21. Zancan P, Sola-Penna M, Furtado CM, Da Silva D. Differential expression of phosphofructokinase-1 isoforms correlates with the glycolytic efficiency of breast cancer cells. *Mol Genet Metab.* (2010) 100(4):372–8. doi:10.1016/j.ymgme.2010.04.006
22. Dai J, Ji Y, Wang W, Kim D, Fai LY, Wang L, Luo J, Zhang Z. Loss of fructose-1,6-bisphosphatase induces glycolysis and promotes apoptosis resistance of cancer stem-like cells: an important role in hexavalent chromium-induced carcinogenesis. *Toxicol Appl Pharmacol.* (2017) 331:164–73. doi:10.1016/j.taap.2017.06.014
23. Li B, Qiu B, Lee DSM, Walton ZE, Ochocki JD, Mathew LK, Mancuso A, Gade TPF, Keith B, Nissim I, Simon MC. Fructose-1,6-bisphosphatase opposes renal carcinoma progression. *Nature.* (2014) 513(7517):251–5. doi:10.1038/nature13557
24. Bartrons R, Simon-Molas H, Rodríguez-García A, Castaño E, Navarro-Sabaté À, Manzano A, Martínez-Outschoorn UE. Fructose 2,6-Bisphosphate in Cancer Cell Metabolism. *Front Oncol.* (2018) 8:331. doi:10.3389/fonc.2018.00331
25. Van Schaftingen E. Fructose 2,6-bisphosphate. *Adv Enzymol Relat Areas Mol Biol.* (1987) 59:315–95.
26. Pilkis SJ, Claus TH, Kurland IJ, Lange AJ. 6-Phosphofructo-2-Kinase/Fructose-2,6-Bisphosphatase: A Metabolic Signaling Enzyme. *Annu Rev Biochem.* (1995) 64(1):799–835. doi:10.1146/annurev.bi.64.070195.004055
27. Rider MH, Bartrons R. Fructose 2,6-bisphosphate: the last milestone of the 20th century in metabolic control? *Biochem J.* (2010) 32(2):1–5. doi:10.1042/BJ20091921
28. Okar DA, Manzano A, Navarro-Sabaté A, Riera L, Bartrons R, Lange AJ. PFK-2/FBPase-2: maker and breaker of the essential biofactor fructose-2,6-bisphosphate. *Trends Biochem Sci.* (2001) 26(1):30–5.
29. Bertrand L, Vertommen D, Freeman PM, Wouters J, Depiereux E, Di Pietro A, Hue L, Rider MH. Mutagenesis of the fructose-6-phosphate-binding site in the 2-kinase domain of 6-phosphofructo-2-kinase/fructose-2,6-bisphosphatase. *Eur J Biochem.* (1998) 254(3):490–6.
30. Hers HG, Van Schaftingen E. Fructose 2,6-bisphosphate 2 years after its discovery. *Biochem J.* (1982) 206(1):1–12.
31. Rider MH, Bertrand L, Vertommen D, Michels PA, Rousseau GG, Hue L. 6-Phosphofructo-2-kinase/fructose-2,6-bisphosphatase: head-to-head with a bifunctional enzyme that controls glycolysis. *Biochem J.* (2004) 381(3):561–79. doi:10.1042/BJ20040752
32. Colomer D, Vives-Corrons JL, Pujades A, Bartrons R. Control of phosphofructokinase by fructose 2,6-bisphosphate in B-lymphocytes and B-chronic lymphocytic leukemia cells. *Cancer Res.* (1987) 47(7):1859–62.
33. Riera L, Manzano A, Navarro-Sabaté A, Perales JC, Bartrons R. Insulin induces PFKFB3 gene expression in HT29 human colon adenocarcinoma cells. *Biochim Biophys Acta.* (2002) 1589(2):89–92.
34. Darville MI, Crepin KM, Hue L, Rousseau GG. 5' flanking sequence and structure of a gene encoding rat 6-phosphofructo-2-kinase/fructose-2,6-bisphosphatase. *Proc Natl Acad Sci U S A.* (1989) 86(17):6543–7.
35. Goren N, Manzano A, Riera L, Ambrosio S, Ventura F, Bartrons R. 6-Phosphofructo-2-kinase/fructose-2,6-bisphosphatase expression in rat brain during development. *Brain Res Mol Brain Res.* (2000) 75(1):138–42.
36. Bartrons R, Rodríguez-García A, Simon-Molas H, Castaño E, Manzano A, Navarro-Sabaté À. The potential utility of PFKFB3 as a therapeutic target. *Expert Opin Ther Targets.* (2018) 22(8):659–74. doi:10.1080/14728222.2018.1498082
37. Cavalier MC, Kim S-G, Neau D, Lee Y-H. Molecular basis of the fructose-2,6-bisphosphatase reaction of PFKFB3: transition state and the C-terminal function. *Proteins.* (2012) 80(4):1143–53.
38. Bartrons R, Hue L, Van Schaftingen E, Hers HG. Hormonal control of fructose 2,6-bisphosphate concentration in isolated rat hepatocytes. *Biochem J.* (1983) 214(3):829–37.
39. Minchenko O, Opentanova I, Caro J. Hypoxic regulation of the 6-phosphofructo-2-kinase/fructose-2,6-bisphosphatase gene family (PFKFB-1-4) expression in vivo. *FEBS Lett.* (2003) 554(3):264–70.

40. Bobarykina AY, Minchenko DO, Opentanova IL, Moenner M, Caro J, Esumi H, Minchenko OH. Hypoxic regulation of PFKFB-3 and PFKFB-4 gene expression in gastric and pancreatic cancer cell lines and expression of PFKFB genes in gastric cancers. *Acta Biochim Pol.* (2006) 53(4):789–99.
41. Novellasdemunt L, Bultot L, Manzano A, Ventura F, Rosa JL, Vertommen D, Rider MH, Navarro-Sabate À, Bartrons R. PFKFB3 activation in cancer cells by the p38/MK2 pathway in response to stress stimuli. *Biochem J.* (2013) 452(3):531–43. doi:10.1042/BJ20121886
42. Ventura F, Ambrosio S, Bartrons R, El-Maghrabi MR, Lange AJ, Pilkis SJ. Cloning and expression of a catalytic core bovine brain 6-phosphofructo-2-kinase/fructose-2,6-bisphosphatase. *Biochem Biophys Res Commun.* (1995) 209(3):1140–8.
43. Hamilton JA, Callaghan MJ, Sutherland RL, Watts CK. Identification of PRG1, a novel progestin-responsive gene with sequence homology to 6-phosphofructo-2-kinase/fructose-2,6-bisphosphatase. *Mol Endocrinol.* (1997) 11(4):490–502.
44. Manzano A, Rosa JL, Ventura F, Pérez JX, Nadal M, Estivill X, Ambrosio S, Gil J, Bartrons R. Molecular cloning, expression, and chromosomal localization of a ubiquitously expressed human 6-phosphofructo-2-kinase/fructose-2,6-bisphosphatase gene (PFKFB3). *Cytogenet Cell Genet.* (1998) 83(3–4):214–7.
45. Chesney J, Mitchell R, Benigni F, Bacher M, Spiegel L, Al-Abed Y, Han JH, Metz C, Bucala R. An inducible gene product for 6-phosphofructo-2-kinase with an AU-rich instability element: role in tumor cell glycolysis and the Warburg effect. *Proc Natl Acad Sci U S A.* (1999) 96(6):3047–52.
46. Navarro-Sabaté A, Manzano A, Riera L, Rosa JL, Ventura F, Bartrons R. The human ubiquitous 6-phosphofructo-2-kinase/fructose-2,6-bisphosphatase gene (PFKFB3): promoter characterization and genomic structure. *Gene.* (2001) 264(1):131–8.
47. Kessler R, Bleichert F, Warnke J-P, Eschrich K. 6-Phosphofructo-2-kinase/fructose-2,6-bisphosphatase (PFKFB3) is up-regulated in high-grade astrocytomas. *J Neurooncol.* (2008) 86(3):257–64.
48. Bartrons R, Caro J. Hypoxia, glucose metabolism and the Warburg's effect. *J Bioenerg Biomembr.* (2007) 39(3):223–9. doi:10.1007/s10863-007-9080-3
49. Obach M, Navarro-Sabaté A, Caro J, Kong X, Duran J, Gómez M, Perales JC, Ventura F, Rosa JL, Bartrons R. 6-Phosphofructo-2-kinase (pfkfb3) gene promoter contains hypoxia-inducible factor-1 binding sites necessary for transactivation in response to hypoxia. *J Biol Chem.* (2004) 279(51):53562–70. doi:10.1074/jbc.M406096200
50. Minchenko A, Leshchinsky I, Opentanova I, Sang N, Srinivas V, Armstead V, Caro J. Hypoxia-inducible factor-1-mediated expression of the 6-phosphofructo-2-kinase/fructose-2,6-bisphosphatase-3 (PFKFB3) gene. Its possible role in the Warburg effect. *J Biol Chem.* (2002) 277(8):6183–7.
51. Novellasdemunt L, Obach M, Millán-Ariño L, Manzano A, Ventura F, Rosa JL, Jordan A, Navarro-Sabate A, Bartrons R. Progestins activate 6-phosphofructo-2-kinase/fructose-2,6-bisphosphatase 3 (PFKFB3) in breast cancer cells. *Biochem J.* (2012) 442(2):345–56. doi:10.1042/BJ20111418
52. Imbert-Fernandez Y, Clem BF, O'Neal J, Kerr DA, Spaulding R, Lanceta L, Clem AL, Telang S, Chesney J. Estradiol stimulates glucose metabolism via 6-phosphofructo-2-kinase (PFKFB3). *J Biol Chem.* (2014) 289(13):9440–8. doi:10.1074/jbc.M113.529990
53. Ando M, Uehara I, Kogure K, Asano Y, Nakajima W, Abe Y, Kawauchi K, Tanaka N. Interleukin 6 enhances glycolysis through expression of the glycolytic enzymes hexokinase 2 and 6-phosphofructo-2-kinase/fructose-2,6-bisphosphatase-3. *J Nippon Med Sch.* (2010) 77(2):97–105.
54. Han J, Alvarez-Breckenridge CA, Wang Q-E, Yu J. TGF- β signaling and its targeting for glioma treatment. *Am J Cancer Res.* (2015) 5(3):945–55.
55. Ruiz-García A, Monsalve E, Novellasdemunt L, Navarro-Sabate A, Manzano A, Rivero S, Castrillo A, Casado M, Laborda J, Bartrons R, Diaz-Guerra MJM. Cooperation of Adenosine with Macrophage Toll-4 Receptor Agonists Leads to Increased Glycolytic Flux through the Enhanced Expression of PFKFB3 Gene. *J Biol Chem.* (2011) 286(22):19247–58. doi:10.1074/jbc.M110.190298

56. Rodríguez-García A, Samsó P, Fontova P, Simon-Molas H, Manzano A, Castaño E, Rosa JL, Martínez-Outshoorn U, Ventura F, Navarro-Sabaté À, Bartrons R. TGF- β 1 targets Smad, p38 MAPK, and PI3K/Akt signaling pathways to induce PFKFB3 gene expression and glycolysis in glioblastoma cells. *FEBS J.* (2017) 284(20):3437–54. doi:10.1111/febs.14201
57. Houddane A, Bultot L, Novellasdemunt L, Johanns M, Gueuning M-A, Vertommen D, Coulie PG, Bartrons R, Hue L, Rider MH. Role of Akt/PKB and PFKFB isoenzymes in the control of glycolysis, cell proliferation and protein synthesis in mitogen-stimulated thymocytes. *Cell Signal.* (2017) 34:23–37. doi:10.1016/j.cellsig.2017.02.019
58. Simon-Molas H, Arnedo-Pac C, Fontova P, Vidal-Alabró A, Castaño E, Rodríguez-García A, Navarro-Sabaté À, Lloberas N, Manzano A, Bartrons R. PI3K–Akt signaling controls PFKFB3 expression during human T-lymphocyte activation. *Mol Cell Biochem.* (2018) 448(1–2):187–97. doi:10.1007/s11010-018-3325-9
59. Sakakibara R, Uemura M, Hirata T, Okamura N, Kato M. Human placental fructose-6-phosphate,2-kinase/fructose-2,6-bisphosphatase: its isozymic form, expression and characterization. *Biosci Biotechnol Biochem.* (1997) 61(11):1949–52.
60. Duran J, Obach M, Navarro-Sabate A, Manzano A, Gómez M, Rosa JL, Ventura F, Perales JC, Bartrons R. Pfkfb3 is transcriptionally upregulated in diabetic mouse liver through proliferative signals. *FEBS J.* (2009) 276(16):4555–68. doi:10.1111/j.1742-4658.2009.07161.x
61. Garcia-Cao I, Song MS, Hobbs RM, Laurent G, Giorgi C, de Boer VCJ, Anastasiou D, Ito K, Sasaki AT, Rameh L, Carracedo A, Vander Heiden MG, Cantley LC, Pinton P, Haigis MC, Pandolfi PP. Systemic elevation of PTEN induces a tumor-suppressive metabolic state. *Cell.* (2012) 149(1):49–62.
62. Trefely S, Khoo P-S, Krycer JR, Chaudhuri R, Fazakerley DJ, Parker BL, Sultani G, Lee J, Stephan J-P, Torres E, Jung K, Kuijl C, James DE, Junutula JR, Stöckli J. Kinome Screen Identifies PFKFB3 and Glucose Metabolism as Important Regulators of the Insulin/Insulin-like Growth Factor (IGF)-1 Signaling Pathway. *J Biol Chem.* (2015) 290(43):25834–46. doi:10.1074/jbc.M115.658815
63. Calvo MN, Bartrons R, Castaño E, Perales JC, Navarro-Sabaté À, Manzano A. PFKFB3 gene silencing decreases glycolysis, induces cell-cycle delay and inhibits anchorage-independent growth in HeLa cells. *FEBS Lett.* (2006) 580(13):3308–14. doi:10.1016/j.febslet.2006.04.093
64. Clem B, Telang S, Clem A, Yalcin A, Meier J, Simmons A, Rasku MA, Arumugam S, Dean WL, Eaton J, Lane A, Trent JO, Chesney J. Small-molecule inhibition of 6-phosphofructo-2-kinase activity suppresses glycolytic flux and tumor growth. *Mol Cancer Ther.* (2008) 7(1):110–20.
65. Redman R, Pohlmann P, Kurman M, Tapolsky GH, Chesney J. PFK-158, first-in-man and first-in-class inhibitor of PFKFB3/ glycolysis: A phase I, dose escalation, multi-center study in patients with advanced solid malignancies. Proceedings of the AACR 106th Annual Meeting. In: Cancer Research. 2015. p. CT206 LP-CT206.
66. Mondal S, Roy D, Sarkar Bhattacharya S, Jin L, Jung D, Zhang S, Kalogera E, Staub J, Wang Y, Xuyang W, Khurana A, Chien J, Telang S, Chesney J, Tapolsky G, Petras D, Shridhar V. Therapeutic targeting of PFKFB3 with a novel glycolytic inhibitor PFK158 promotes lipophagy and chemosensitivity in gynecologic cancers. *Int J cancer.* (2019) 144(1):178–89. doi:10.1002/ijc.31868
67. Seo M, Lee Y-H. PFKFB3 Regulates Oxidative Stress Homeostasis via Its S-Glutathionylation in Cancer. *J Mol Biol.* (2014) 426(4):830–42.
68. Yamamoto T, Takano N, Ishiwata K, Ohmura M, Nagahata Y, Matsuura T, Kamata A, Sakamoto K, Nakanishi T, Kubo A, Hishiki T, Suematsu M. Reduced methylation of PFKFB3 in cancer cells shunts glucose towards the pentose phosphate pathway. *Nat Commun.* (2014) 5:3480. doi:10.1038/ncomms4480
69. Franklin DA, He Y, Leslie PL, Tikunov AP, Fenger N, Macdonald JM, Zhang Y. p53 coordinates DNA repair with nucleotide synthesis by suppressing PFKFB3 expression and promoting the pentose phosphate pathway. *Sci Rep.* (2016) 6(1):38067.
70. Gómez M, Manzano A, Navarro-Sabaté A, Duran J, Obach M, Perales JC, Bartrons R. Specific expression of pfkfb4 gene in spermatogonia germ cells and analysis of its 5'-flanking region. *FEBS Lett.* (2005) 579(2):357–62. doi:10.1016/j.febslet.2004.11.096

71. Ros S, Santos CR, Moco S, Baenke F, Kelly G, Howell M, Zamboni N, Schulze A. Functional Metabolic Screen Identifies 6-Phosphofructo-2-Kinase/Fructose-2,6-Biphosphatase 4 as an Important Regulator of Prostate Cancer Cell Survival. *Cancer Discov.* (2012) 2(4):328–43. doi:10.1158/2159-8290.CD-11-0234
72. Simon-Molas H, Rodríguez-García A, Navarro-Sabaté À, Fontova P, Bartrons R, Manzano A. C12orf5 (chromosome 12 open reading frame 5). *Atlas Genet Cytogenet Oncol Haematol.* (2014) 18(7):500–10.
73. Gerin I, Noël G, Bolsée J, Haumont O, Van Schaftingen E, Bommer GT. Identification of TP53-induced glycolysis and apoptosis regulator (TIGAR) as the phosphoglycolate-independent 2,3-bisphosphoglycerate phosphatase. *Biochem J.* (2014) 458(3):439–48. doi:10.1042/BJ20130841
74. Kasthuber ER, Lowe SW. Putting p53 in Context. *Cell.* (2017) 170(6):1062–78. doi:10.1016/j.cell.2017.08.028
75. Lee P, Hock AK, Vousden KH, Cheung EC. p53- and p73-independent activation of TIGAR expression in vivo. *Cell Death Dis.* (2015) 6(8):e1842–e1842. doi:10.1038/cddis.2015.205
76. Zou S, Gu Z, Ni P, Liu X, Wang J, Fan Q. SP1 plays a pivotal role for basal activity of TIGAR promoter in liver cancer cell lines. *Mol Cell Biochem.* (2012) 359(1–2):17–23. doi:10.1007/s11010-011-0993-0
77. Zou S, Wang X, Deng L, Wang Y, Huang B, Zhang N, Fan Q, Luo J. CREB, another culprit for TIGAR promoter activity and expression. *Biochem Biophys Res Commun.* (2013) 439(4):481–6. doi:10.1016/j.bbrc.2013.08.098
78. Hasegawa H, Yamada Y, Iha H, Tsukasaki K, Nagai K, Atogami S, Sugahara K, Tsuruda K, Ishizaki A, Kamihira S. Activation of p53 by Nutlin-3a, an antagonist of MDM2, induces apoptosis and cellular senescence in adult T-cell leukemia cells. *Leukemia.* (2009) 23(11):2090–101. doi:10.1038/leu.2009.171
79. Peña-Rico MA, Calvo-Vidal MN, Villalonga-Planells R, Martínez-Soler F, Giménez-Bonafé P, Navarro-Sabaté À, Tortosa A, Bartrons R, Manzano A. TP53 induced glycolysis and apoptosis regulator (TIGAR) knockdown results in radiosensitization of glioma cells. *Radiother Oncol.* (2011) 101(1):132–9. doi:10.1016/j.radonc.2011.07.002
80. Kimata M, Matoba S, Iwai-Kanai E, Nakamura H, Hoshino A, Nakaoka M, Katamura M, Okawa Y, Mita Y, Okigaki M, Ikeda K, Tatsumi T, Matsubara H. p53 and TIGAR regulate cardiac myocyte energy homeostasis under hypoxic stress. *Am J Physiol Heart Circ Physiol.* (2010) 299(6):H1908–16. doi:10.1152/ajpheart.00250.2010
81. Rajendran R, Garva R, Ashour H, Leung T, Stratford I, Krstic-Demonacos M, Demonacos C. Acetylation mediated by the p300/CBP-associated factor determines cellular energy metabolic pathways in cancer. *Int J Oncol.* (2013) 42(6):1961–72. doi:10.3892/ijo.2013.1907
82. Ko Y-H, Domingo-Vidal M, Roche M, Lin Z, Whitaker-Menezes D, Seifert E, Capparelli C, Tuluc M, Birbe RC, Tassone P, Curry JM, Navarro-Sabate A, Manzano A, Bartrons R, Caro J, Martinez-Outschoorn U. TIGAR Metabolically Reprograms Carcinoma and Stromal Cells in Breast Cancer. *J Biol Chem.* (2016) 291(51):26291–303. doi:10.1074/jbc.M116.740209
83. Sinha S, Ghildiyal R, Mehta VS, Sen E. ATM-NFκB axis-driven TIGAR regulates sensitivity of glioma cells to radiomimetics in the presence of TNFα. *Cell Death Dis.* (2013) 4(5):e615–e615. doi:10.1038/cddis.2013.128
84. Simon-Molas H, Calvo-Vidal MN, Castaño E, Rodríguez-García A, Navarro-Sabaté À, Bartrons R, Manzano A. Akt mediates TIGAR induction in HeLa cells following PFKFB3 inhibition. *FEBS Lett.* (2016) 590(17):2915–26. doi:10.1002/1873-3468.12338
85. Rigden DJ. The histidine phosphatase superfamily: structure and function. *Biochem J.* (2008) 409(2):333–48. doi:10.1042/BJ20071097
86. Li H, Jogl G. Structural and biochemical studies of TIGAR (TP53-induced glycolysis and apoptosis regulator). *J Biol Chem.* (2009) 284(3):1748–54. doi:10.1074/jbc.M807821200
87. Cheung EC, Ludwig RL, Vousden KH. Mitochondrial localization of TIGAR under hypoxia stimulates HK2 and lowers ROS and cell death. *Proc Natl Acad Sci U S A.* (2012) 109(50):20491–6. doi:10.1073/pnas.1206530109
88. Yu H-P, Xie J-M, Li B, Sun Y-H, Gao Q-G, Ding Z-H, Wu H-R, Qin Z-H. TIGAR regulates DNA damage and repair through pentosephosphate pathway and Cdk5-ATM pathway. *Sci Rep.* (2015) 5(1):9853. doi:10.1038/srep09853

89. Uhlen M, Fagerberg L, Hallstrom BM, Lindskog C, Oksvold P, Mardinoglu A, Sivertsson A, Kampf C, Sjostedt E, Asplund A, Olsson I, Edlund K, Lundberg E, Navani S, Szigartyo CA-K, Odeberg J, Djureinovic D, Takanen JO, Hober S, Alm T, Edqvist P-H, Berling H, Tegel H, Mulder J, Rockberg J, Nilsson P, Schwenk JM, Hamsten M, von Feilitzen K, Forsberg M, Persson L, Johansson F, Zwahlen M, von Heijne G, Nielsen J, Ponten F. Tissue-based map of the human proteome. *Science* (80-). (2015) 347(6220):1260419–1260419. doi:10.1126/science.1260419
90. Cheung EC, Athineos D, Lee P, Ridgway R a, Lambie W, Nixon C, Strathdee D, Blyth K, Sansom OJ, Vousden KH. TIGAR is required for efficient intestinal regeneration and tumorigenesis. *Dev Cell*. (2013) 25(5):463–77. doi:10.1016/j.devcel.2013.05.001
91. Lui VWY, Wong EYL, Ho K, Ng PKS, Lau CPY, Tsui SKW, Tsang C-M, Tsao S-W, Cheng SH, Ng MHL, Ng YK, Lam EKY, Hong B, Lo KW, Mok TSK, Chan a TC, Mills GB. Inhibition of c-Met downregulates TIGAR expression and reduces NADPH production leading to cell death. *Oncogene*. (2011) 30(9):1127–34. doi:10.1038/onc.2010.490
92. Yin L, Kosugi M, Kufe D. Inhibition of the MUC1-C oncoprotein induces multiple myeloma cell death by down-regulating TIGAR expression and depleting NADPH. *Blood*. (2012) 119(3):810–6. doi:10.1182/blood-2011-07-369686
93. Canaparo R, Varchi G, Ballestri M, Foglietta F, Sotgiu G, Guerrini A, Francovich A, Civera P, Frairia R, Serpe L. Polymeric nanoparticles enhance the sonodynamic activity of meso-tetrakis (4-sulfonatophenyl) porphyrin in an in vitro neuroblastoma model. *Int J Nanomedicine*. (2013) 8:4247–63. doi:10.2147/IJN.S51070
94. Madan E, Gogna R, Bhatt M, Pati U, Kuppusamy P, Mahdi AA. Regulation of glucose metabolism by p53: emerging new roles for the tumor suppressor. *Oncotarget*. (2011) 2(12):948–57. doi:10.18632/oncotarget.389
95. Madan E, Gogna R, Kuppusamy P, Bhatt M, Pati U, Mahdi AA. TIGAR induces p53-mediated cell-cycle arrest by regulation of RB-E2F1 complex. *Br J Cancer*. (2012) 107(3):516–26. doi:10.1038/bjc.2012.260
96. Christofk HR, Vander Heiden MG, Harris MH, Ramanathan A, Gerszten RE, Wei R, Fleming MD, Schreiber SL, Cantley LC. The M2 splice isoform of pyruvate kinase is important for cancer metabolism and tumour growth. *Nature*. (2008) 452(7184):230–3. doi:10.1038/nature06734
97. Ying H, Kimmelman AC, Lyssiotis CA, Hua S, Chu GC, Fletcher-Sananikone E, Locasale JW, Son J, Zhang H, Coloff JL, Yan H, Wang W, Chen S, Viale A, Zheng H, Paik J, Lim C, Guimaraes AR, Martin ES, Chang J, Hezel AF, Perry SR, Hu J, Gan B, Xiao Y, Asara JM, Weissleder R, Wang YA, Chin L, Cantley LC, DePinho RA. Oncogenic Kras maintains pancreatic tumors through regulation of anabolic glucose metabolism. *Cell*. (2012) 149(3):656–70. doi:10.1016/j.cell.2012.01.058
98. Patra KC, Hay N. The pentose phosphate pathway and cancer. *Trends Biochem Sci*. (2014) 39(8):347–54. doi:10.1016/j.tibs.2014.06.005
99. Xiao G, Chan LN, Klemm L, Weinstock DM, Graeber TG, Mü M, Braas D, Chen Z, Geng H, Zhang QC, Aghajani-refah A, Cosgun KN, Sadras T, Lee J, Mirzapioazova T, Salgia R, Ernst T, Hochhaus A, Jumaa H, Jiang X, Mü Schen M. B-Cell-Specific Diversion of Glucose Carbon Utilization Reveals a Unique Vulnerability in B Cell Malignancies Article B-Cell-Specific Diversion of Glucose Carbon Utilization Reveals a Unique Vulnerability in B Cell Malignancies. *Cell*. (2018) 173:470-484.e18. doi:10.1016/j.cell.2018.02.048
100. Kuehne A, Emmert H, Soehle J, Winnefeld M, Fischer F, Wenck H, Gallinat S, Terstegen L, Lucius R, Hildebrand J, Zamboni N. Acute Activation of Oxidative Pentose Phosphate Pathway as First-Line Response to Oxidative Stress in Human Skin Cells. *Mol Cell*. (2015) 59(3):359–71. doi:10.1016/j.molcel.2015.06.017
101. Snell K. Enzymes of serine metabolism in normal, developing and neoplastic rat tissues. *Adv Enzyme Regul*. (1984) 22:325–400.
102. Possemato R, Marks KM, Shaul YD, Pacold ME, Kim D, Birsoy K, Sethumadhavan S, Woo H-K, Jang HG, Jha AK, Chen WW, Barrett FG, Stransky N, Tsun Z-Y, Cowley GS, Barretina J, Kalaany NY, Hsu PP, Ottina K, Chan AM, Yuan B, Garraway LA, Root DE, Mino-Kenudson M, Brachtel EF, Driggers EM, Sabatini DM. Functional genomics reveal that the serine synthesis pathway is essential in breast cancer. *Nature*. (2011) 476(7360):346–50. doi:10.1038/nature10350
103. Mullarky E, Mattaini KR, Vander Heiden MG, Cantley LC, Locasale JW. PHGDH amplification and altered glucose metabolism in human melanoma. *Pigment Cell Melanoma Res*. (2011) 24(6):1112–5. doi:10.1111/j.1755-148X.2011.00919.x

104. Amelio I, Cutruzzolá F, Antonov A, Agostini M, Melino G. Serine and glycine metabolism in cancer. *Trends Biochem Sci.* (2014) 39(4):191–8. doi:10.1016/j.tibs.2014.02.004
105. Yang M, Vousden KH. Serine and one-carbon metabolism in cancer. *Nat Rev Cancer.* (2016) 16(10):650–62. doi:10.1038/nrc.2016.81
106. Fan J, Ye J, Kamphorst JJ, Shlomi T, Thompson CB, Rabinowitz JD. Quantitative flux analysis reveals folate-dependent NADPH production. *Nature.* (2014) 510(7504):298–302. doi:10.1038/nature13236
107. Maddocks ODK, Athineos D, Cheung EC, Lee P, Zhang T, van den Broek NJF, Mackay GM, Labuschagne CF, Gay D, Kruiswijk F, Blagih J, Vincent DF, Campbell KJ, Ceteci F, Sansom OJ, Blyth K, Vousden KH. Modulating the therapeutic response of tumours to dietary serine and glycine starvation. *Nature.* (2017) 544(7650):372–6. doi:10.1038/nature22056
108. Thompson CB, Bauer DE, Lum JJ, Hatzivassiliou G, Zong W-X, Zhao F, Ditsworth D, Buzzai M, Lindsten T. How do cancer cells acquire the fuel needed to support cell growth? *Cold Spring Harb Symp Quant Biol.* (2005) 70(0):357–62. doi:10.1101/sqb.2005.70.011
109. Menendez JA, Vellon L, Mehmi I, Oza BP, Ropero S, Colomer R, Lupu R. Inhibition of fatty acid synthase (FAS) suppresses HER2/neu (erbB-2) oncogene overexpression in cancer cells. *Proc Natl Acad Sci U S A.* (2004) 101(29):10715–20. doi:10.1073/pnas.0403390101
110. Valvona CJ, Fillmore HL, Nunn PB, Pilkington GJ. The Regulation and Function of Lactate Dehydrogenase A: Therapeutic Potential in Brain Tumor. *Brain Pathol.* (2016) 26(1):3–17. doi:10.1111/bpa.12299
111. Newell K, Franchi A, Pouyssegur J, Tannock I. Studies with glycolysis-deficient cells suggest that production of lactic acid is not the only cause of tumor acidity. *Proc Natl Acad Sci U S A.* (1993) 90(3):1127–31.
112. San-Millán I, Brooks GA. Reexamining cancer metabolism: lactate production for carcinogenesis could be the purpose and explanation of the Warburg Effect. *Carcinogenesis.* (2017) 38(2):119–33. doi:10.1093/carcin/bgw127
113. Vander Heiden MG, Locasale JW, Swanson KD, Sharfi H, Heffron GJ, Amador-Noguez D, Christofk HR, Wagner G, Rabinowitz JD, Asara JM, Cantley LC. Evidence for an alternative glycolytic pathway in rapidly proliferating cells. *Science.* (2010) 329(5998):1492–9. doi:10.1126/science.1188015
114. DeBerardinis RJ, Lum JJ, Hatzivassiliou G, Thompson CB. The Biology of Cancer: Metabolic Reprogramming Fuels Cell Growth and Proliferation. *Cell Metab.* (2008) 7(1):11–20. doi:10.1016/j.cmet.2007.10.002
115. Warburg O. On the origin of cancer cells. *Science.* (1956) 123(3191):309–14.
116. Koppenol WH, Bounds PL, Dang C V. Otto Warburg's contributions to current concepts of cancer metabolism. *Nat Rev Cancer.* (2011) 11(5):325–37. doi:10.1038/nrc3038
117. Crabtree HG. Observations on the carbohydrate metabolism of tumours. *Biochem J.* (1929) 23(3):536–45. doi:10.1042/bj0230536
118. Deberardinis RJ, Sayed N, Ditsworth D, Thompson CB. Brick by brick: metabolism and tumor cell growth. *Curr Opin Genet Dev.* (2008) 18(1):54–61.
119. Cardaci S, Zheng L, MacKay G, van den Broek NJF, MacKenzie ED, Nixon C, Stevenson D, Tumanov S, Bulusu V, Kamphorst JJ, Vazquez A, Fleming S, Schiavi F, Kalna G, Blyth K, Strathdee D, Gottlieb E. Pyruvate carboxylation enables growth of SDH-deficient cells by supporting aspartate biosynthesis. *Nat Cell Biol.* (2015) 17(10):1317–26. doi:10.1038/ncb3233
120. Wilde L, Roche M, Domingo-Vidal M, Tanson K, Philp N, Curry J, Martinez-Outschoorn U. Metabolic coupling and the Reverse Warburg Effect in cancer: Implications for novel biomarker and anticancer agent development. *Semin Oncol.* (2017) 44(3):198–203. doi:10.1053/j.seminoncol.2017.10.004
121. Ward PS, Thompson CB. Metabolic reprogramming: a cancer hallmark even warburg did not anticipate. *Cancer Cell.* (2012) 21(3):297–308. doi:10.1016/j.ccr.2012.02.014

122. Trefely S, Khoo P-S, Krycer JR, Chaudhuri R, Fazakerley DJ, Parker BL, Sultani G, Lee J, Stephan J-P, Torres E, Jung K, Kuijl C, James DE, Junutula JR, Stöckli J. Kinome Screen Identifies PFKFB3 and Glucose Metabolism as Important Regulators of the Insulin/Insulin-like Growth Factor (IGF)-1 Signaling Pathway. *J Biol Chem.* (2015) 290(43):25834–46. doi:10.1074/jbc.M115.658815
123. Hardie DG. New roles for the LKB1→AMPK pathway. *Curr Opin Cell Biol.* (2005) 17(2):167–73. doi:10.1016/j.ceb.2005.01.006
124. Semenza GL. Hypoxia-inducible factors: coupling glucose metabolism and redox regulation with induction of the breast cancer stem cell phenotype. *EMBO J.* (2017) 36(3):252–9. doi:10.15252/embj.201695204
125. Minchenko O, Opentanova I, Minchenko D, Ogura T, Esumi H. Hypoxia induces transcription of 6-phosphofructo-2-kinase/fructose-2,6-biphosphatase-4 gene via hypoxia-inducible factor-1 α activation. *FEBS Lett.* (2004) 576(1–2):14–20. doi:10.1016/j.febslet.2004.08.053
126. Cheung EC, Lee P, Ceteci F, Nixon C, Blyth K, Sansom OJ, Vousden KH. Opposing effects of TIGAR- and RAC1-derived ROS on Wnt-driven proliferation in the mouse intestine. *Genes Dev.* (2016) 30(1):52–63. doi:10.1101/gad.271130.115
127. Vousden KH. Outcomes of p53 activation--spoilt for choice. *J Cell Sci.* (2006) 119(Pt 24):5015–20. doi:10.1242/jcs.03293
128. Ryan KM, Vousden KH. Cancer: pinning a change on p53. *Nature.* (2002) 419(6909):795, 797. doi:10.1038/419795a
129. Vousden KH, Prives C. Blinded by the Light: The Growing Complexity of p53. *Cell.* (2009) 137(3):413–31. doi:10.1016/j.cell.2009.04.037
130. Gottlieb E, Vousden KH. p53 Regulation of Metabolic Pathways. *Cold Spring Harb Perspect Biol.* (2010) 2(4):a001040–a001040. doi:10.1101/cshperspect.a001040
131. Jiang P, Du W, Wang X, Mancuso A, Gao X, Wu M, Yang X. p53 regulates biosynthesis through direct inactivation of glucose-6-phosphate dehydrogenase. *Nat Cell Biol.* (2011) 13(3):310–6. doi:10.1038/ncb2172
132. Vousden KH, Ryan KM. p53 and metabolism. *Nat Rev Cancer.* (2009) 9(10):691–700. doi:10.1038/nrc2715
133. Won KY, Lim S-J, Kim GY, Kim YW, Han S-A, Song JY, Lee D-K. Regulatory role of p53 in cancer metabolism via SCO2 and TIGAR in human breast cancer. *Hum Pathol.* (2012) 43(2):221–8. doi:10.1016/j.humpath.2011.04.021
134. Gorrini C, Harris IS, Mak TW. Modulation of oxidative stress as an anticancer strategy. *Nat Rev Drug Discov.* (2013) 12(12):931–47. doi:10.1038/nrd4002
135. Rieber EE, Kosower NS, Jaffé ER. Reduced nicotinamide adenine dinucleotide and the reduction of oxidized glutathione in human erythrocytes. *J Clin Invest.* (1968) 47(1):66–71. doi:10.1172/JCI105715
136. Coussens LM, Werb Z. Inflammation and cancer. *Nature.* (2002) 420(6917):860–7. doi:10.1038/nature01322
137. Rani V, Deep G, Singh RK, Palle K, Yadav UCS. Oxidative stress and metabolic disorders: Pathogenesis and therapeutic strategies. *Life Sci.* (2016) 148:183–93. doi:10.1016/j.lfs.2016.02.002
138. Moi P, Chant K, Asunis I, Cao A, Kant YW, Kan YW. Isolation of NF-E2-related factor 2 (Nrf2), a NF-E2-like basic leucine zipper transcriptional activator that binds to the tandem NF-E2/AP1 repeat of the β -globin locus control region. *Genetics.* (1994) 91:9926–30.
139. Schafer H, Geismann C, Arlt A, Sebens S. Cytoprotection “gone astray’’: Nrf2 and its role in cancer. *Onco Targets Ther.* (2014) 7:1497. doi:10.2147/OTT.S36624
140. Kuosmanen SM, Kansanen E, Kaikkonen MU, Sihvola V, Pulkkinen K, Jyrkkänen H-K, Tuoresmäki P, Hartikainen J, Hippeläinen M, Kokki H, Tavi P, Heikkinen S, Levonen A-L. NRF2 regulates endothelial glycolysis and proliferation with miR-93 and mediates the effects of oxidized phospholipids on endothelial activation. *Nucleic Acids Res.* (2018) 46(3):1124–38. doi:10.1093/nar/gkx1155
141. Uruno A, Motohashi H. The Keap1–Nrf2 system as an in vivo sensor for electrophiles. *Nitric Oxide.* (2011) 25(2):153–60. doi:10.1016/j.niox.2011.02.007

142. Mitsuishi Y, Taguchi K, Kawatani Y, Shibata T, Nukiwa T, Aburatani H, Yamamoto M, Motohashi H. Nrf2 redirects glucose and glutamine into anabolic pathways in metabolic reprogramming. *Cancer Cell*. (2012) 22(1):66–79. doi:10.1016/j.ccr.2012.05.016
143. DeNicola GM, Karreth FA, Humpton TJ, Gopinathan A, Wei C, Frese K, Mangal D, Yu KH, Yeo CJ, Calhoun ES, Scrimieri F, Winter JM, Hruban RH, Iacobuzio-Donahue C, Kern SE, Blair IA, Tuveson DA. Oncogene-induced Nrf2 transcription promotes ROS detoxification and tumorigenesis. *Nature*. (2011) 475(7354):106–9. doi:10.1038/nature10189
144. Suzuki T, Yamamoto M. Molecular basis of the Keap1–Nrf2 system. *Free Radic Biol Med*. (2015) 88(Pt B):93–100. doi:10.1016/j.freeradbiomed.2015.06.006
145. Mitsuishi Y, Motohashi H, Yamamoto M. The Keap1–Nrf2 system in cancers: stress response and anabolic metabolism. *Front Oncol*. (2012) 2(December):200. doi:10.3389/fonc.2012.00200
146. Krajka-Kuźniak V, Paluszczak J, Baer-Dubowska W. The Nrf2–ARE signaling pathway: An update on its regulation and possible role in cancer prevention and treatment. *Pharmacol Rep*. (2017) 69(3):393–402. doi:10.1016/j.pharep.2016.12.011
147. Rushmore TH, Morton MR, Pickett CB. The antioxidant responsive element. Activation by oxidative stress and identification of the DNA consensus sequence required for functional activity. *J Biol Chem*. (1991) 266(18):11632–9.
148. Wang L, Chen Y, Sternberg P, Cai J. Essential Roles of the PI3 Kinase/Akt Pathway in Regulating Nrf2-Dependent Antioxidant Functions in the RPE. *Investig Ophthalmology Vis Sci*. (2008) 49(4):1671. doi:10.1167/iovs.07-1099
149. Dinkova-Kostova AT, Abramov AY. The emerging role of Nrf2 in mitochondrial function. *Free Radic Biol Med*. (2015) 88:179–88. doi:10.1016/j.freeradbiomed.2015.04.036
150. Sayin VI, LeBoeuf SE, Singh SX, Davidson SM, Biancur D, Guzelhan BS, Alvarez SW, Wu WL, Karakousi TR, Zavitsanou AM, Ubriaco J, Muir A, Karagiannis D, Morris PJ, Thomas CJ, Possemato R, Vander Heiden MG, Papagiannakopoulos T. Activation of the NRF2 antioxidant program generates an imbalance in central carbon metabolism in cancer. *Elife*. (2017) 6. doi:10.7554/eLife.28083
151. Thimmulappa RK, Mai KH, Srisuma S, Kensler TW, Yamamoto M, Biswal S. Identification of Nrf2-regulated genes induced by the chemopreventive agent sulforaphane by oligonucleotide microarray. *Cancer Res*. (2002) 62(18):5196–203.
152. Rojo de la Vega M, Chapman E, Zhang DD. NRF2 and the Hallmarks of Cancer. *Cancer Cell*. (2018) 34(1):21–43. doi:10.1016/j.ccell.2018.03.022
153. Chen W, Sun Z, Wang X-J, Jiang T, Huang Z, Fang D, Zhang DD. Direct Interaction between Nrf2 and p21Cip1/WAF1 Upregulates the Nrf2-Mediated Antioxidant Response. *Mol Cell*. (2009) 34(6):663–73. doi:10.1016/j.molcel.2009.04.029
154. Toledano MB. The Guardian Recruits Cops: The p53–p21 Axis Delegates Prosurvival Duties to the Keap1–Nrf2 Stress Pathway. *Mol Cell*. (2009) 34(6):637–9. doi:10.1016/j.molcel.2009.06.005
155. Pavlides S, Whitaker-Menezes D, Castello-Cros R, Flomenberg N, Witkiewicz AK, Frank PG, Casimiro MC, Wang C, Fortina P, Addya S, Pestell RG, Martinez-Outschoorn UE, Sotgia F, Lisanti MP. The reverse Warburg effect: aerobic glycolysis in cancer associated fibroblasts and the tumor stroma. *Cell Cycle*. (2009) 8(23):3984–4001. doi:10.4161/cc.8.23.10238
156. Koukourakis MI, Giatromanolaki A, Harris AL, Sivridis E. Comparison of metabolic pathways between cancer cells and stromal cells in colorectal carcinomas: a metabolic survival role for tumor-associated stroma. *Cancer Res*. (2006) 66(2):632–7. doi:10.1158/0008-5472.CAN-05-3260
157. Martinez-Outschoorn UE, Sotgia F, Lisanti MP. Power Surge: Supporting Cells “Fuel” Cancer Cell Mitochondria. *Cell Metab*. (2012) 15(1):4–5. doi:10.1016/j.cmet.2011.12.011
158. Sonveaux P, Végran F, Schroeder T, Wergin MC, Verrax J, Rabbani ZN, De Saedeleer CJ, Kennedy KM, Diepart C, Jordan BF, Kelley MJ, Gallez B, Wahl ML, Feron O, Dewhirst MW. Targeting lactate-fueled respiration selectively kills hypoxic tumor cells in mice. *J Clin Invest*. (2008) 118(12):3930–42. doi:10.1172/JCI36843

159. Gillies RJ, Robey I, Gatenby RA. Causes and consequences of increased glucose metabolism of cancers. *J Nucl Med.* (2008) 49 Suppl 2(Suppl_2):24S-42S. doi:10.2967/jnumed.107.047258
160. Romero IL, Mukherjee A, Kenny HA, Litchfield LM, Lengyel E. Molecular Pathways: Trafficking of Metabolic Resources in the Tumor Microenvironment. *Clin Cancer Res.* (2015) 21(4):680–6. doi:10.1158/1078-0432.CCR-14-2198
161. Calvo-Vidal MN. Fenotipo glucolítico en células tumorales: papel de la isoenzima ubicua de la 6-fosfofructo-2-quinasa/fructosa-2,6-bifosfatasa (uPFK-2) y del regulador de la glucólisis y la apoptosis inducido por TP53 (TIGAR). Doctoral thesis. University of Barcelona; 2008.
162. Cerami E, Gao J, Dogrusoz U, Gross BE, Sumer SO, Aksoy BA, Jacobsen A, Byrne CJ, Heuer ML, Larsson E, Antipin Y, Reva B, Goldberg AP, Sander C, Schultz N. The cBio Cancer Genomics Portal: An Open Platform for Exploring Multidimensional Cancer Genomics Data: Figure 1. *Cancer Discov.* (2012) 2(5):401–4. doi:10.1158/2159-8290.CD-12-0095
163. Gao J, Aksoy BA, Dogrusoz U, Dresdner G, Gross B, Sumer SO, Sun Y, Jacobsen A, Sinha R, Larsson E, Cerami E, Sander C, Schultz N. Integrative Analysis of Complex Cancer Genomics and Clinical Profiles Using the cBioPortal. *Sci Signal.* (2013) 6(269):pl1–pl1. doi:10.1126/scisignal.2004088
164. Hoppe-Seyler F, Butz K. Repression of endogenous p53 transactivation function in HeLa cervical carcinoma cells by human papillomavirus type 16 E6, human mdm-2, and mutant p53. *J Virol.* (1993) 67(6):3111–7.
165. Wsierska-Gadek J, Horky M. How the nucleolar sequestration of p53 protein or its interplayers contributes to its (re)-activation. *Ann N Y Acad Sci.* (2003) 1010:266–72.
166. Schindelin J, Arganda-Carreras I, Frise E, Kaynig V, Longair M, Pietzsch T, Preibisch S, Rueden C, Saalfeld S, Schmid B, Tinevez J-Y, White DJ, Hartenstein V, Eliceiri K, Tomancak P, Cardona A. Fiji: an open-source platform for biological-image analysis. *Nat Methods.* (2012) 9(7):676–82. doi:10.1038/nmeth.2019
167. Bensaad K, Cheung EC, Vousden KH. Modulation of intracellular ROS levels by TIGAR controls autophagy. *EMBO J.* (2009) 28(19):3015–26. doi:10.1038/emboj.2009.242
168. Jena NR. DNA damage by reactive species: Mechanisms, mutation and repair. *J Biosci.* (2012) 37(3):503–17.
169. Ye L, Zhao X, Lu J, Qian G, Zheng JC, Ge S. Knockdown of TIGAR by RNA interference induces apoptosis and autophagy in HepG2 hepatocellular carcinoma cells. *Biochem Biophys Res Commun.* (2013) 437(2):300–6. doi:10.1016/j.bbrc.2013.06.072
170. Lee P, Vousden KH, Cheung EC. TIGAR, TIGAR, burning bright. *Cancer Metab.* (2014) 2(1):1. doi:10.1186/2049-3002-2-1
171. Filomeni G, De Zio D, Cecconi F. Oxidative stress and autophagy: the clash between damage and metabolic needs. *Cell Death Differ.* (2015) 22(3):377–88. doi:10.1038/cdd.2014.150
172. Telang S, Clem BF, Klarer AC, Clem AL, Trent JO, Bucala R, Chesney J. Small molecule inhibition of 6-phosphofructo-2-kinase suppresses t cell activation. *J Transl Med.* (2012) 10(1):95. doi:10.1186/1479-5876-10-95
173. Boukouris AE, Zervopoulos SD, Michelakis ED. Metabolic Enzymes Moonlighting in the Nucleus: Metabolic Regulation of Gene Transcription. *Trends Biochem Sci.* (2016) 41(8):712–30. doi:10.1016/j.tibs.2016.05.013
174. Hardie DG, Ross FA, Hawley SA. AMPK: a nutrient and energy sensor that maintains energy homeostasis. *Nat Rev Mol Cell Biol.* (2012) 13(4):251–62. doi:10.1038/nrm3311
175. Li B, Wang Z, Xie J, Wang G, Qian L, Guan X, Shen X, Qin Z, Shen G, Li X, Gao Q. TIGAR knockdown enhanced the anticancer effect of aescin via regulating autophagy and apoptosis in colorectal cancer cells. *Acta Pharmacol Sin.* (2019) 40(1):111–21. doi:10.1038/s41401-018-0001-2
176. Calvo MN, Bartrons R, Castaño E, Perales JC, Navarro-Sabaté a, Manzano a. PFKFB3 gene silencing decreases glycolysis, induces cell-cycle delay and inhibits anchorage-independent growth in HeLa cells. *FEBS Lett.* (2006) 580(13):3308–14. doi:10.1016/j.febslet.2006.04.093

177. Derdak Z, Lang CH, Villegas KA, Tong M, Mark NM, de la Monte SM, Wands JR. Activation of p53 enhances apoptosis and insulin resistance in a rat model of alcoholic liver disease. *J Hepatol.* (2011) 54(1):164–72. doi:10.1016/j.jhep.2010.08.007
178. Huang S, Yang Z, Ma Y, Yang Y, Wang S. miR-101 Enhances Cisplatin-Induced DNA Damage Through Decreasing Nicotinamide Adenine Dinucleotide Phosphate Levels by Directly Repressing Tp53-Induced Glycolysis and Apoptosis Regulator Expression in Prostate Cancer Cells. *DNA Cell Biol.* (2017) 36(4):303–10. doi:10.1089/dna.2016.3612
179. Needleman SB, Wunsch CD. A general method applicable to the search for similarities in the amino acid sequence of two proteins. *J Mol Biol.* (1970) 48(3):443–53.
180. Ye Y, Godzik A. FATCAT: a web server for flexible structure comparison and structure similarity searching. *Nucleic Acids Res.* (2004) 32(Web Server issue):W582–5. doi:10.1093/nar/gkh430
181. Pons G, Carreras J. Functional characterization of the enzymes with 2,3-bisphosphoglycerate phosphatase activity from pig skeletal muscle. *Comp Biochem Physiol B.* (1986) 85(4):879–85.
182. Ovcharenko I, Nobrega MA, Loots GG, Stubbs L. ECR Browser: a tool for visualizing and accessing data from comparisons of multiple vertebrate genomes. *Nucleic Acids Res.* (2004) 32(Web Server issue):W280–6. doi:10.1093/nar/gkh355
183. Chorley BN, Campbell MR, Wang X, Karaca M, Sambandan D, Bangura F, Xue P, Pi J, Kleeberger SR, Bell DA. Identification of novel NRF2-regulated genes by ChIP-Seq: influence on retinoid X receptor alpha. *Nucleic Acids Res.* (2012) 40(15):7416–29. doi:10.1093/nar/gks409
184. Peña-Rico MA. Caracterización del gen TIGAR. Doctoral thesis. University of Barcelona; 2012.
185. Sarkar S, Payne CK, Kemp ML. Conditioned Media Downregulates Nuclear Expression of Nrf2. *Cell Mol Bioeng.* (2013) 6(2):130–7. doi:10.1007/s12195-013-0272-0
186. Best SA, De Souza DP, Kersbergen A, Policheni AN, Dayalan S, Tull D, Rathi V, Gray DH, Ritchie ME, McConville MJ, Sutherland KD. Synergy between the KEAP1/NRF2 and PI3K Pathways Drives Non-Small-Cell Lung Cancer with an Altered Immune Microenvironment. *Cell Metab.* (2018) 27(4):935–943.e4. doi:10.1016/j.cmet.2018.02.006
187. Taguchi K, Yamamoto M. The KEAP1–NRF2 System in Cancer. *Front Oncol.* (2017) 7:85. doi:10.3389/fonc.2017.00085
188. Wakabayashi N, Slocum SL, Skoko JJ, Shin S, Kensler TW. When NRF2 talks, who's listening? *Antioxid Redox Signal.* (2010) 13(11):1649–63. doi:10.1089/ars.2010.3216
189. He CH, Gong P, Hu B, Stewart D, Choi ME, Choi AMK, Alam J. Identification of Activating Transcription Factor 4 (ATF4) as an Nrf2-interacting Protein. *J Biol Chem.* (2001) 276(24):20858–65. doi:10.1074/jbc.M101198200
190. Jiang L-B, Cao L, Ma Y-Q, Chen Q, Liang Y, Yuan F-L, Li X-L, Dong J, Chen N. TIGAR mediates the inhibitory role of hypoxia on ROS production and apoptosis in rat nucleus pulposus cells. (2018) . doi:10.1016/j.joca.2017.10.007
191. Chumová J, Kourová H, Trögelová L, Halada P, Binarová P. Microtubular and Nuclear Functions of γ -Tubulin: Are They LINced? *Cells.* (2019) 8(3):259. doi:10.3390/cells8030259
192. Patel U, Stearns T. Quick Guide γ -Tubulin [Internet].
193. Chae S, Yun C, Um H, Lee J-H, Cho H. Centrosome amplification and multinuclear phenotypes are induced by hydrogen peroxide. *Exp Mol Med.* (2005) 37(5):482–7. doi:10.1038/emm.2005.59
194. Pérez-Mancera PA, Young ARJ, Narita M. Inside and out: the activities of senescence in cancer. *Nat Rev Cancer.* (2014) 14(8):547–58. doi:10.1038/nrc3773
195. Krizhanovsky V, Yon M, Dickins RA, Hearn S, Simon J, Miething C, Yee H, Zender L, Lowe SW. Senescence of Activated Stellate Cells Limits Liver Fibrosis. *Cell.* (2008) 134(4):657–67. doi:10.1016/j.cell.2008.06.049

196. Chen M-K, Du Y, Sun L, Hsu JL, Wang Y-H, Gao Y, Huang J, Hung M-C. H₂O₂ induces nuclear transport of the receptor tyrosine kinase c-MET in breast cancer cells via a membrane-bound retrograde trafficking mechanism. *J Biol Chem.* (2019) 294(21):8516–28. doi:10.1074/jbc.RA118.005953
197. Gupta GD, Coyaud É, Gonçalves J, Mojarad BA, Liu Y, Wu Q, Gheiratmand L, Comartin D, Tkach JM, Cheung SWT, Bashkurov M, Hasegan M, Knight JD, Lin Z-Y, Schueler M, Hildebrandt F, Moffat J, Gingras A-C, Raught B, Pelletier L. A Dynamic Protein Interaction Landscape of the Human Centrosome-Cilium Interface. *Cell.* (2015) 163(6):1484–99. doi:10.1016/j.cell.2015.10.065
198. Pedersen PL. Warburg, me and Hexokinase 2: Multiple discoveries of key molecular events underlying one of cancers' most common phenotypes, the "Warburg Effect", i.e., elevated glycolysis in the presence of oxygen. *J Bioenerg Biomembr.* (2007) 39(3):211–22. doi:10.1007/s10863-007-9094-x
199. Klarer AC, O'Neal J, Imbert-Fernandez Y, Clem A, Ellis SR, Clark J, Clem B, Chesney J, Telang S. Inhibition of 6-phosphofructo-2-kinase (PFKFB3) induces autophagy as a survival mechanism. *Cancer Metab.* (2014) 2(1):2. doi:10.1186/2049-3002-2-2
200. Liu Y, Song X-D, Liu W, Zhang T-Y, Zuo J. Glucose deprivation induces mitochondrial dysfunction and oxidative stress in PC12 cell line. *J Cell Mol Med.* (2003) 7(1):49–56. doi:10.1111/j.1582-4934.2003.tb00202.x
201. Zhao Y, Hu X, Liu Y, Dong S, Wen Z, He W, Zhang S, Huang Q, Shi M. ROS signaling under metabolic stress: cross-talk between AMPK and AKT pathway. *Mol Cancer.* (2017) 16(1):79. doi:10.1186/s12943-017-0648-1
202. Gao M, Liang J, Lu Y, Guo H, German P, Bai S, Jonasch E, Yang X, Mills GB, Ding Z. Site-specific activation of AKT protects cells from death induced by glucose deprivation. *Oncogene.* (2014) 33(6):745–55. doi:10.1038/onc.2013.2
203. Zhong D, Xiong L, Liu T, Liu X, Liu X, Chen J, Sun S-Y, Khuri FR, Zong Y, Zhou Q, Zhou W. The glycolytic inhibitor 2-deoxyglucose activates multiple prosurvival pathways through IGF1R. *J Biol Chem.* (2009) 284(35):23225–33. doi:10.1074/jbc.M109.005280
204. Iglesias-Serret D, de Frias M, Santidrián AF, Coll-Mulet L, Cosials AM, Barragán M, Domingo A, Gil J, Pons G. Regulation of the proapoptotic BH3-only protein BIM by glucocorticoids, survival signals and proteasome in chronic lymphocytic leukemia cells. *Leukemia.* (2007) 21(2):281–7. doi:10.1038/sj.leu.2404483
205. Panefsky H. Reversible binding of Pi by beef heart mitochondrial adenosine triphosphatase. - PubMed - NCBI. *J Biol Chem.* (1977) 252(9):2891–9.
206. Artigas N, Ureña C, Rodríguez-Carballo E, Rosa JL, Ventura F. Mitogen-activated protein kinase (MAPK)-regulated interactions between Osterix and Runx2 are critical for the transcriptional osteogenic program. *J Biol Chem.* (2014) 289(39):27105–17. doi:10.1074/jbc.M114.576793
207. Waterhouse AM, Procter JB, Martin DMA, Clamp M, Barton GJ. Jalview Version 2--a multiple sequence alignment editor and analysis workbench. *Bioinformatics.* (2009) 25(9):1189–91. doi:10.1093/bioinformatics/btp033
208. Chojnacki S, Cowley A, Lee J, Foix A, Lopez R. Programmatic access to bioinformatics tools from EMBL-EBI update: 2017. *Nucleic Acids Res.* (2017) 45(W1):W550–3. doi:10.1093/nar/gkx273
209. Altschul SF, Gish W, Miller W, Myers EW, Lipman DJ. Basic local alignment search tool. *J Mol Biol.* (1990) 215(3):403–10. doi:10.1016/S0022-2836(05)80360-2

ANNEX
PUBLICATIONS



Publications related to the topic of this thesis

Bartrons R, **Simon-Molas H**, Rodríguez-García A, Castaño E, Navarro-Sabaté A, Manzano A, Martínez-Outschoorn U. The glycolytic phenotype in the tumor ecosystem. *Front Oncology*. 2018;8:331. doi: 10.3389/fonc.2018.00331. IF JCR 2017: 4,416. **Review**.

Simon-Molas H, Calvo-Vidal MN, Castaño E, Rodríguez-García A, Navarro-Sabaté À, Bartrons R, Manzano A. Akt mediates TIGAR induction in HeLa cells following PFKFB3 inhibition. *FEBS Lett*. 2016;590(17):2915-26. doi: 10.1002/1873-3468.12338. IF JCR 2016: 3,62. ► **Full text included**.

Simon-Molas H, Rodríguez-García A, Navarro-Sabaté A; Fontova P, Bartrons R, Manzano A. TIGAR (TP53-inducible glycolysis and apoptosis regulator). *Atlas Genet Cytogenet Oncol Haematol*. 2014; 18(7):500-510. **Review**.

Publications related to other projects

Simon-Molas H, Arnedo-Pac C, Fontova P, Vidal-Alabró A, Castaño E, Rodríguez-García A, Navarro-Sabaté A, Lloberas N, Manzano A, Bartrons R. PI3K–Akt signaling controls PFKFB3 expression during human T-lymphocyte activation. *Mol Cell Biochem*. 2018;448(1-2):187-197. doi: 10.1007/s11010-018-3325-9. IF JCR 2017: 2,561. ► **Full text included and expanded with additional results**.

Publications in collaboration with other members of the group

Bartrons R, Rodríguez-García A, **Simon-Molas H**, Castaño E, Manzano A, Navarro-Sabaté A. The potential utility of PFKFB3 as a therapeutic target. *Expert Opin Ther Tar*. 2018;22(8):659-674. doi: 10.1080/14728222.2018.1498082. IF JCR 2017: 4,598. **Review**.

Rodríguez-García A, Samsó P, Fontova P, **Simon-Molas H**, Manzano A, Castaño E, Rosa JL, Martínez-Outschoorn U, Ventura F, Navarro-Sabaté À, Bartrons R. TGF- β 1 targets Smad, p38 MAPK, and PI3K/Akt signaling pathways to induce PFKFB3 gene expression and glycolysis in glioblastoma cells. *FEBS J*. 2017;284(20):3437-3454. doi: 10.1111/febs.14201. IF JCR 2017: 4,530.

Rodríguez-García A, Fontova P, **Simon-Molas H**, Manzano A, Bartrons R, Navarro-Sabaté A. PFKFB2 (6-phosphofructo-2-kinase/fructose-2,6-biphosphatase 2). *Atlas Genet Cytogenet Oncol Haematol*. 2014; 18(11):838-848. **Review**.

Akt mediates TIGAR induction in HeLa cells following PFKFB3 inhibition

Helga Simon-Molas^{1,*}, María Nieves Calvo-Vidal^{2,*}, Esther Castaño³, Ana Rodríguez-García¹, Àurea Navarro-Sabaté¹, Ramon Bartrons¹ and Anna Manzano¹

1 Unitat de Bioquímica, Departament de Ciències Fisiològiques, IDIBELL-Universitat de Barcelona, Spain

2 Department of Medicine, Weill Cornell Medical College, New York, NY, USA

3 Centres Científics i Tecnològics, IDIBELL-Universitat de Barcelona, Spain

Correspondence

R. Bartrons, Unitat de Bioquímica i Biologia Molecular, Departament de Ciències Fisiològiques, Universitat de Barcelona, Feixa Llarga s/n, E-08907 L'Hospitalet de Llobregat, Barcelona, Spain
Fax: (34)934024268
Tel: (34)934024252
E-mail: rbartrons@ub.edu

*These authors contributed equally to this work.

(Received 16 May 2016, revised 22 July 2016, available online 24 August 2016)

doi:10.1002/1873-3468.12338

Edited by Bé Wieringa

Neoplastic cells metabolize higher amounts of glucose relative to normal cells in order to cover increased energetic and anabolic needs. Inhibition of the glycolytic enzyme 6-phosphofructo-2-kinase/fructose-2,6-bisphosphatase 3 (PFKFB3) diminishes cancer cell proliferation and tumour growth in animals. In this work, we investigate the crosstalk between PFKFB3 and TIGAR (TP53-Induced Glycolysis and Apoptosis Regulator), a protein known to protect cells from oxidative stress. Our results show consistent TIGAR induction in HeLa cells in response to PFKFB3 knockdown. Upon PFKFB3 silencing, cells undergo oxidative stress and trigger Akt phosphorylation. This leads to induction of a TIGAR-mediated prosurvival pathway that reduces both oxidative stress and cell death. As TIGAR is known to have a role in DNA repair, it could serve as a potential target for the development of effective antineoplastic therapies.

Keywords: glycolysis; PFKFB3; TIGAR; Akt; tumour cell metabolism

Glycolysis is the most ancient pathway involved in carbohydrate oxidation and its regulation is crucial for cells to balance energy production and the synthesis of biomolecules for their proliferation and growth. Phosphofructokinase-1 (PFK-1), which converts fructose 6-phosphate into fructose 1,6-bisphosphate, is a key player in this regulation. PFK-1 is activated by the allosteric factor fructose 2,6-bisphosphate (Fru-2,6-P₂), a metabolite that can override the inhibitory effect of ATP, synergistically with AMP [1,2]. Fru-2,6-P₂ concentration has been found increased in proliferative and transformed cells [3–6]. Synthesis and degradation

of Fru-2,6-P₂ depend on the relative activities of 6-phosphofructo-2-kinase/fructose-2,6-bisphosphatase (PFK-2/FBPase-2) isoenzymes, coded by four genes (PFKFB1-4) [7], the expression of which is tissue and developmental stage-dependent [2,8]. Importantly, tissue-specific isoenzymes are not totally exclusive and cells and tissues can express more than one to respond to different physiological conditions or stimuli [6,9]. The PFKFB3 isoenzyme has a high kinase/bisphosphatase activity ratio, which makes it a net producer of Fru-2,6-P₂, and it is overexpressed in proliferative cells [10–12] and tumours [13–18].

Abbreviations

2,3-BPG, 2,3-bisphosphoglycerate; BHA, butylated hydroxyanisole; DCFDA, 2',7'-dichlorofluorescein diacetate; DMEM, Dulbecco's modified eagle's medium; FACS, fluorescence-activated cell sorting; Fru-2,6-P₂, fructose 2,6-bisphosphate; HBSS, Hank's balanced salt solution; PFK-1, phosphofructokinase-1; PFK-2/FBPase-2, 6-phosphofructo-2-kinase/fructose-2,6-bisphosphatase; PFKFB3, 6-phosphofructo-2-kinase/fructose-2,6-bisphosphatase 3; PI, propidium iodide; ROS, reactive oxygen species; siRNA, small interfering RNA; TIGAR, TP53-induced glycolysis and apoptosis regulator; PPP, pentose phosphate pathway.

PFKFB3 suppression decreases Fru-2,6-P₂ and lactate production, apoptosis, inhibition of anchorage-independent colony formation [6] and impaired vessel sprouting [19] and tumour growth [20,21].

TP53-Induced Glycolysis and Apoptosis Regulator (TIGAR) was first cloned as a TP53 target gene whose protein product has an active site similar to that of fructose-2,6-bisphosphatase and phosphoglycerate mutase, that reduces the concentration of Fru-2,6-P₂ [22] and 2,3-bisphosphoglycerate (2,3-BPG) [23]. The main function attributed to TIGAR is based on its activity of inhibiting glycolysis and triggering glucose-6-phosphate to the pentose phosphate pathway (PPP), which increases the synthesis of ribose-5-phosphate and NADPH and lowers intracellular reactive oxygen species (ROS) levels. These functions of TIGAR correlate with an ability to protect cells from ROS-associated apoptosis [22,24]. TIGAR overexpression has been described in invasive breast cancer [25], glioblastoma [26] and colorectal cancer [27–29]. Overexpression of TIGAR reduces ROS production, inhibiting apoptosis and promoting cell proliferation [24], and its inhibition sensitizes cells to radiotherapy by increasing ROS-mediated cell death [30]. Moreover, besides the widely studied antioxidant function of TIGAR, its recently described 2,3-BPG phosphatase activity could be crucial in understanding the role of this enzyme in cancer metabolism.

In this paper we aimed to investigate the crosstalk between PFKFB3 and TIGAR, and how the inhibition of these metabolically related enzymes impairs cancer cells survival. The results presented show that PFKFB3 silencing induces an Akt-dependent increase in TIGAR protein levels, which protects cells from DNA damage and cell death. Inhibiting both PFKFB3 and TIGAR genes increases oxidative stress and P- γ -H2AX foci formation, and causes more severe cell death.

Materials and methods

Cell culture

HeLa cells, obtained from the American Type Culture Collection (Manassas, VA, USA), were cultured in high-glucose Dulbecco's Modified Eagle's medium (DMEM; Biological Industries, Kibbutz Beit-Haemek, Israel) supplemented with 10% FBS (Biological Industries) and penicillin/streptomycin (100 U·mL⁻¹ and 100 μ g·mL⁻¹; Biological Industries), at 37 °C, in a 5% CO₂ atmosphere and a relative humidity of 70–80%.

Reagents: Akt inhibitor VIII, Isozyme-Selective, Akti-1/2 (Cat#124018; Calbiochem, San Diego, CA, USA) was used at 10 μ M to inhibit phosphorylation of Akt-1 and Akt-2 proteins.

siRNA transfection

Small interfering RNA (siRNA) targeting PFKFB3 were designed and synthesized as described [6]. For TIGAR silencing, three Stealth siRNA (Invitrogen) were used as described [30]. A scrambled siRNA was used as negative control and referred to as 'Scr.' (Invitrogen, Carlsbad, CA, USA). Cells were seeded at 15% confluence in the corresponding plates for each experiment and allowed to attach overnight. Then, siRNA transfection was performed using Oligofectamine (Invitrogen) in FBS and antibiotics-free DMEM. The final siRNA concentration was 75 nM. After 4 h, complete media was added to each well.

Antioxidant treatment

Transfected cells were treated with 1.5 mM *N*-acetyl *N*-acetylcystein (NAC) or 1 μ M butylated hydroxyanisole (BHA) 4 h after transfection and to the end of the experiments (72 h).

Protein extraction and western blot

Protein was extracted from cells using SDS buffer (50 mM Tris-Cl, 1% SDS, 10% glycerol) and concentration was determined by bicinchoninic acid protein assay (Thermo Fisher Scientific, Waltham, MA, USA). Equal amounts of total protein extracts were analysed in 12.5% (w/v) SDS/PAGE. Western blot was performed using the following antibodies: in-house rabbit polyclonal antibody against PFKFB3 [5], TIGAR (LifeSpan), P-Akt (S473), Akt, P-S6 (S235/S236), S6, P-p70S6K1 (T389), P-mTOR (S2448), mTOR and TSC2 (Cell Signaling Technology, Danvers, MA, USA), LC3-I/III (MBL), Bcl-2 (Dako, Sant Just Desvern, Spain), NOXA (Abgent, San Diego, CA, USA), p62 (Abnova, Taipei City, Taiwan) and α -tubulin (Sigma Aldrich, St. Louis, MO, USA). Peroxidase-conjugated secondary antibodies goat α -mouse and goat α -rabbit (Advantsta, Menlo Park, CA, USA) were used. Immunostaining was carried out using the ECL technique (Bio-Rad). Densitometric analysis was performed using MULTI-GAUGE v3.0 (FujiFilm Corporation, Tokyo, Japan) software. Protein levels were normalized to α -tubulin in all experiments.

Fru-2,6-P₂ determination

Fru-2,6-P₂ was determined following the method described by Van Schaftingen *et al.* [31]. Protein concentration was determined by the Bradford-based Bio-Rad assay.

Total cellular ROS levels

Cells were seeded into 12-well plates and allowed to grow for 72 h after siRNA transfection. After three washes with PBS, cells were loaded with the oxidative-sensitive dye 2',7'-dichlorofluorescein diacetate (DCFDA) at 10 μ M in Hank's Balanced

Salt Solution (HBSS). After 30 min in a cell incubator at 37 °C with 5% CO₂, cells were trypsinized, collected in 500 µL of PBS containing 10% of FBS and immediately analysed. All measurements were made with a FACSCanto flow cytometer (Becton Dickinson, Mountain View, CA, USA) equipped with a 488-nm laser. DCFDA fluorescence was collected by use of a 530/30-nm filter. A minimum of 10 000 events per sample was analysed using the BD FACSDIVA software.

Immunofluorescent phospho- γ -H2AX staining

Cells were seeded in coverslips inside 24-well plates and allowed to grow for 72 h after siRNA transfection. Then, cells were fixed with 4% paraformaldehyde and immunostained with primary antibody against phospho- γ -H2AX (S139) (EMD Millipore, Darmstadt, Germany) and secondary Cy3-conjugated anti-mouse IgG (Jackson ImmunoResearch, West Grove, PA, USA). Nuclei were stained with TO-PRO-3 Iodide (1 : 1000; Invitrogen). Images were acquired with a Spectral Confocal Microscope (TCS-SL; Leica Microsystems, Wetzlar, Germany) using a Plan-Apochromat 63 \times /1.4 N.A. immersion oil objective (Leica Microsystems). We used excitation He/Ne laser beams (Lasos, Jena, Germany) at 633 nm for TO-PRO-3 and 456 nm for Cy3, and a pinhole of 115 µm. Images were captured using LEICA CONFOCAL Software (Leica Microsystems, Wetzlar, Germany). Images of γ -H2AX foci and nuclei were exported separately as .tif files and processed using IMAGE J software (NIH, Maryland, USA). Images shown were obtained with the Merge Channels command. Total nuclei number was determined by manual counting and γ -H2AX foci were counted with the Find Maxima command. At least 150 cells from five randomly chosen fields of view were counted in each condition, and the average number of P- γ -H2AX foci per cell nucleus was calculated.

mRNA expression

RNA was analysed by reverse transcriptase multiplex ligation-dependent probe amplification (RT-MLPA) using SALSA MLPA KIT R011 Apoptosis mRNA from MRC-Holland (Amsterdam, The Netherlands).

MTT assay

MTT (3-(4,5-dimethylthiazolyl)-2,5-diphenyltetrazolium bromide) was used to determine cell viability. Cells were seeded into 24-well plates and allowed to grow for 24, 48 or 72 h after siRNA transfection. MTT dissolved in PBS was added to the cultures at a final concentration of 0.5 mg·mL⁻¹. After incubation at 37 °C for 2 h, the medium was carefully removed and formazan crystals were dissolved in 200 µL Isopropanol:HCl 40 mM per well. Triplicates of 50 µL were transferred to a 96-well plate and the absorbance was measured at 570 nm (SunriseTecan plaque reader).

Staining by Annexin V and propidium iodide

The appearance of apoptotic or necrotic cells was determined with the Annexin V-FITC Apoptosis Detection Kit (eBioscience Bender MedSystems, eBioscience (San Diego, CA, USA). Cells were seeded into six-well plates and allowed to grow for 72 h after siRNA transfection. Floating and freshly trypsinized cells were pooled, washed twice in binding buffer and processed following manufacturer's instructions. All measurements were made with a FACSCalibur flow cytometer (Becton Dickinson) equipped with an air-cooled argon ion laser emitting at 488 nm. The barrier filters were 530/30 nm for annexin-FITC, and 670/LP for propidium iodide (PI) fluorescence. A minimum of 10 000 events per sample were analysed using the CELL QUEST PRO software (BD Biosciences, San Jose, CA, USA).

Data analysis

Results are expressed as the mean \pm standard error of the mean (SEM) of the values obtained from the indicated number of independent experiments. Differences between samples were analysed with the Student's *t* test. Significant differences at *P* < 0.05, 0.01, and 0.001 between conditions are indicated by *, ** and *** respectively. All calculations were performed using the GRAPHPAD PRISM version 4.00 for Windows (GraphPad Software, La Jolla, CA, USA).

Results

PFKFB3 inhibition enhances TIGAR protein expression and decreases Fru-2,6-P₂

We transfected HeLa cells with PFKFB3 and TIGAR-targeted siRNA. siRNA concentration (75 nM) effectively suppressed PFKFB3 and TIGAR protein levels at 72 h after transfection. Interestingly, we observed a significant upregulation of TIGAR protein amount in response to PFKFB3 inhibition (Fig. 1A,B). To further investigate this effect, we performed western blot analysis of HeLa protein extracts from 24 to 72 h after PFKFB3-targeted siRNA transfection. The results obtained showed a significant decrease in PFKFB3 protein from 24 h after siRNA transfection, being abrogated at 72 h. Oppositely, TIGAR protein levels were significantly increased at 48 h after PFKFB3-targeted siRNA transfection, being even higher at 72 h post-transfection, showing a time-dependent induction of TIGAR in response to PFKFB3 removal (Fig. 1C, D). TIGAR silencing does not modify PFKFB3 protein levels (Fig. 1A–D). Fru-2,6-P₂ levels were significantly decreased with PFKFB3-targeted siRNA and this effect was reverted by the inhibition of TIGAR (Fig. 1E).

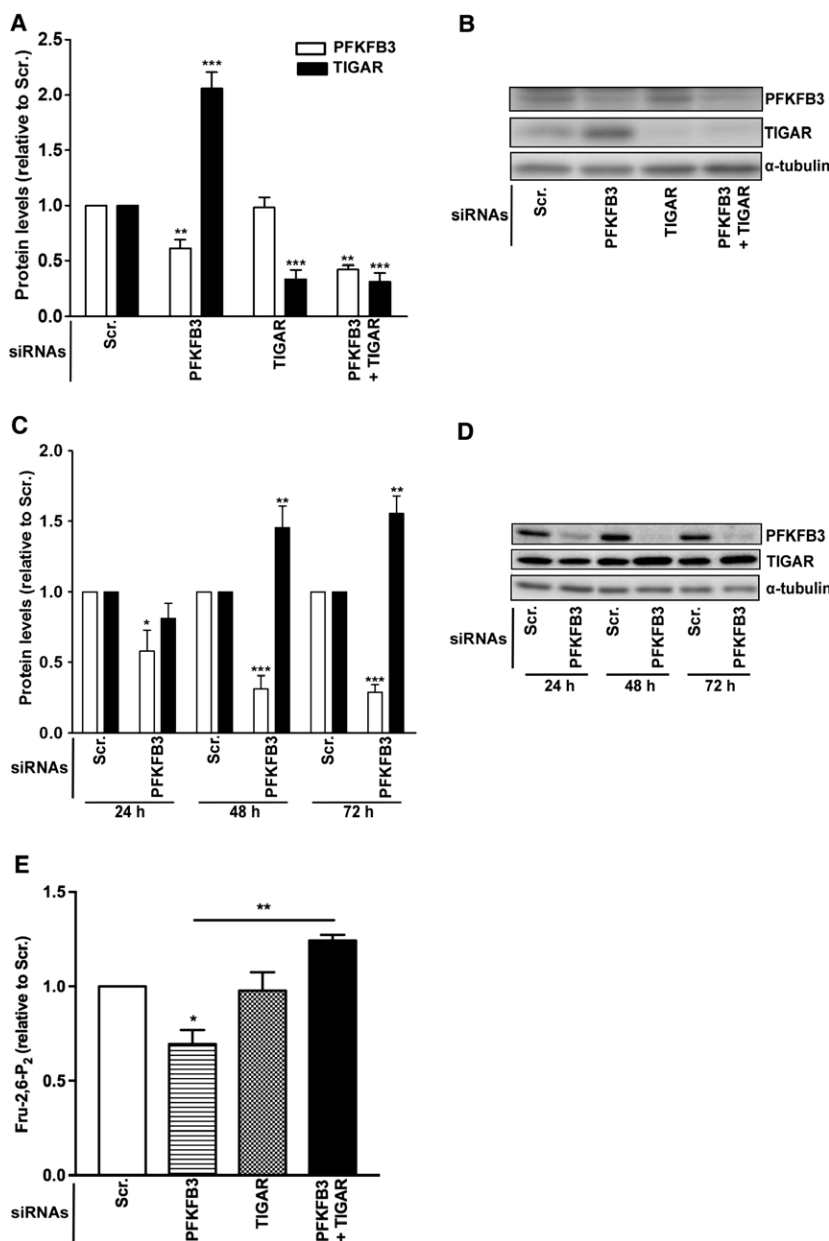


Fig. 1. Analysis of the effects of PFKFB3 and TIGAR inhibition on HeLa cells by western blotting and Fru-2,6-P₂ quantification. (A) Western blot analysis quantification of PFKFB3 (white bars) and TIGAR (black bars) after 72 h of siRNA transfection from three independent experiments. (B) Western blot images representative of three independent blots are shown. (C) Quantification of PFKFB3 (white bars) and TIGAR (black bars) after 24 to 72 h of siRNA transfection from five independent experiments. (D) Western blot images, representative of five independent blots are shown. (E) Quantification of Fru-2,6-P₂ after 72 h of siRNA transfection. All data are presented as the mean fold change relative to the scrambled siRNA (Scr.) of the corresponding time \pm SEM (* P < 0.05, ** P < 0.01, *** P < 0.001).

TIGAR limits ROS production in PFKFB3-inhibited cells

It has been described that glycolysis impairment raises oxidative stress production [32,33]. In order to assess if the same response occurred after PFKFB3 inhibition in our model, we transfected HeLa cells with PFKFB3 and TIGAR-targeted siRNA and quantified ROS levels with the fluorescent probe DCFDA by Fluorescence-Activated Cell Sorting (FACS). The inhibition of PFKFB3 alone significantly increased oxidative stress, whereas cells lacking TIGAR did not show any changes in ROS levels. However, TIGAR

silencing in cells lacking PFKFB3 caused a significant increase in oxidative stress (Fig. 2A,B). The antioxidants NAC and BHA significantly reduced basal ROS levels, but the increase in ROS after PFKFB3 and TIGAR inhibition was not prevented by any of them (Fig. 2C,D).

Akt signalling pathway drives TIGAR induction in response to PFKFB3 silencing

The results obtained described a crosstalk between PFKFB3 and TIGAR (Fig. 1), and thus we wondered which signalling pathway could be orchestrating it.

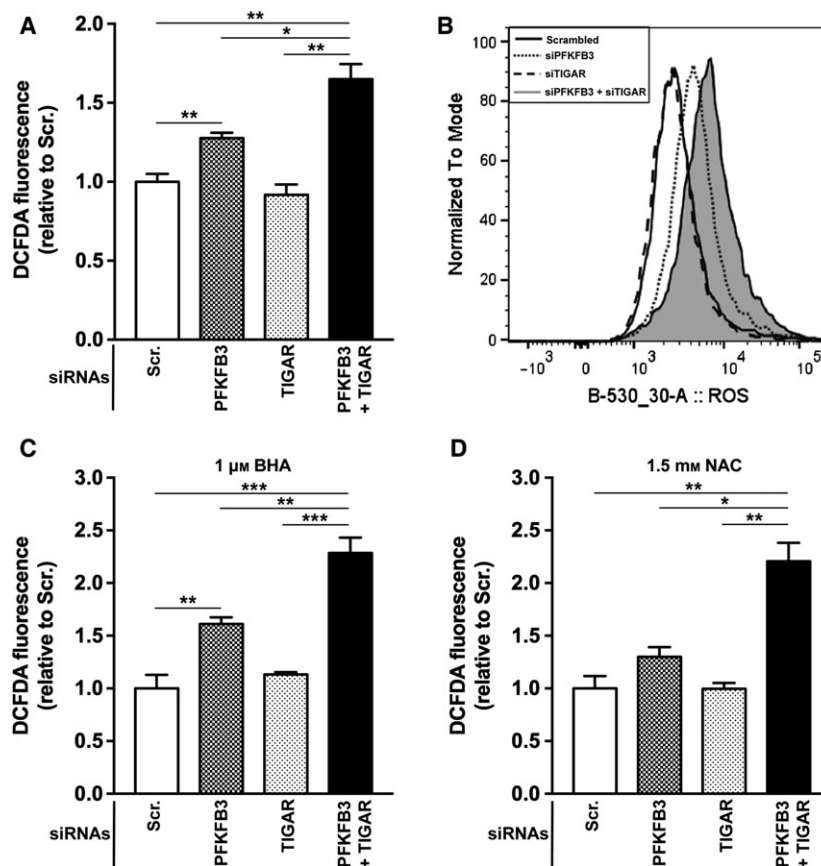


Fig. 2. Reactive oxygen species analysis in HeLa cells 72 h after PFKFB3 and/or TIGAR-targeted siRNA transfection. (A) Quantification of DCFDA fluorescence. (B) Raw data of DCFDA fluorescence peaks of a representative experiment. Quantification of ROS levels after cotreatment with the antioxidant molecules BHA (C) and NAC (D). Data are presented as the mean fold change with respect to scrambled siRNA (Scr.) \pm SEM of three independent experiments with duplicates, and comparison between conditions is indicated by horizontal bars (* P < 0.05, ** P < 0.01, *** P < 0.001).

The mTORC2-Akt-mTORC1 axis has been described to control PFKFB3 levels [34,35] and, moreover, this pathway has been found activated in cancer cells under glucose deprivation conditions and oxidants exposure [36,37]. As we have shown, TIGAR limits ROS production after PFKFB3 inhibition (Fig. 2). Thus, we decided to analyse the phosphorylation status of several proteins of the Akt cascade after 72 h of PFKFB3 silencing and found increased amounts of P-Akt (S473), P-mTOR (S2448), P-p70 S6K1 (T389) and P-S6 (S235/236) (Fig. 3A,B). We sought to determine if P-Akt was upstream of TIGAR induction. We found increased phosphorylated Akt levels 72 h after siRNA transfection in both single PFKFB3 and in PFKFB3 and TIGAR-suppressed cells, with no modulation of the total amounts of Akt in any of the assayed conditions (Fig. 3C,D). Next, we treated cells with the Akt inhibitor Akti-1/2, which targets all forms of Akt, and we transfected these cells with scrambled or PFKFB3-targeted siRNA. TIGAR induction in response to PFKFB3 suppression was abolished by this inhibitor, which indicates that Akt Ser-473 phosphorylation is necessary for TIGAR modulation under these conditions (Fig. 3E,F). Akt

phosphorylation and TIGAR induction in response to PFKFB3 inhibition were not prevented by NAC or BHA (data not shown).

PFKFB3 inhibition does not affect autophagy in HeLa cells

Overexpression of TIGAR has been related with the inhibition of autophagy [24]. In contrast, PFKFB3 inhibition has been described to activate autophagy in the HCT116 cell line [32]. In order to investigate whether autophagy was triggered as a survival mechanism in our model of PFKFB3 and TIGAR inhibition, we analysed LC3 cleavage and p62 protein levels by western blot after 72 h of siRNA transfection. No significant changes were observed in the LC3-II/LC3-I ratio nor in p62 total amounts in any of the analysed conditions (Fig. 4).

TIGAR deficiency increases DNA damage and cell death

We aimed to investigate the functional relevance of TIGAR upregulation after PFKFB3 inhibition. First, we analysed the effect of TIGAR deficiency on DNA

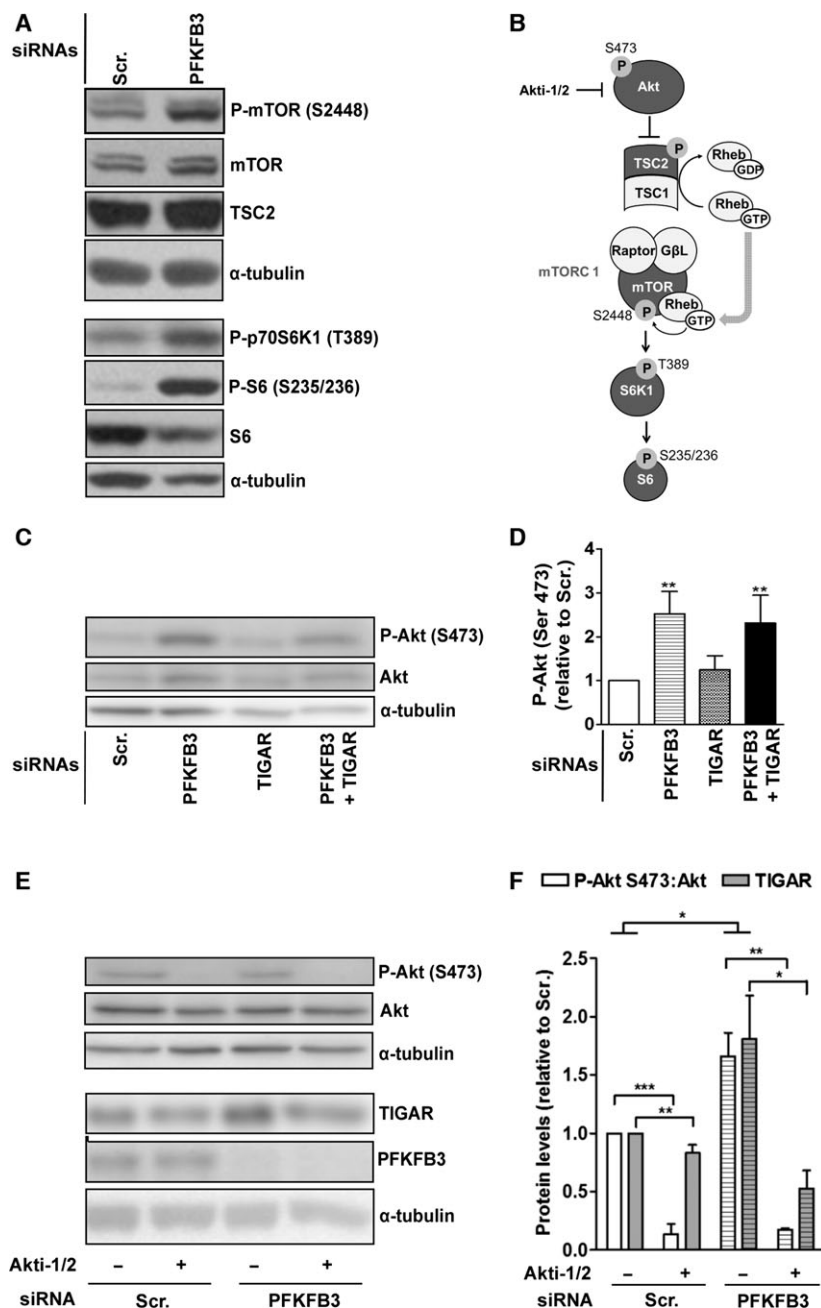


Fig. 3. Western Blot analysis of Akt signaling pathway in protein extracts of HeLa cells obtained 72 h after PFKFB3 and/or TIGAR-targeted siRNA transfection. (A) Representative images of phosphorylated targets in the Akt signaling cascade. (B) Scheme of the Akt/mTORC1 signaling pathway. The proteins analysed by western blot are coloured in dark grey. (C) Western blot analysis of Akt phosphorylation at S473 after PFKFB3 and TIGAR-targeted siRNA transfection, representative of four independent blots. (D) Quantification of Akt phosphorylation, calculated as the ratio between phosphorylated Akt at S473 and total amounts of Akt in four independent experiments. Data are presented as the mean fold change relative to the scrambled siRNA (Scr.) \pm SEM (** $P < 0.01$). (E) Western blot analysis of Akt phosphorylation at S473 and TIGAR after PFKFB3-targeted siRNA transfection, in the presence or absence of Akti-1/2, representative of three independent blots. (F) Quantification of Akti-1/2 effects in the mentioned proteins in three independent experiments. Data are presented as the mean fold change relative to scrambled siRNA (Scr.) \pm SEM, and comparison between conditions is indicated by horizontal bars (* $P < 0.05$, ** $P < 0.01$, *** $P < 0.001$).

damage. For this, we performed immunostaining of phospho- γ -H2AX (Ser 139) foci formation in PFKFB3 and TIGAR-silenced cells. Single inhibition of PFKFB3 or TIGAR was sufficient to increase DNA damage, but the phenotype was even more severe in cells lacking both proteins, with the number of phospho- γ -H2AX foci being significantly higher compared to each siRNA alone (Fig. 5).

Furthermore, we wanted to assess if the increased DNA damage observed after TIGAR suppression

occurred in parallel with exacerbated cell death. Firstly, we analysed the effects of PFKFB3 and TIGAR simultaneous inhibition on cell proliferation and viability through an MTT assay. Remarkably, cells in which both PFKFB3 and TIGAR were silenced had significant 40% decreased growth rate compared to controls (Fig. 6A). However, we did not see any significant reduction in MTT signal in cells transfected with either single PFKFB3 or TIGAR-targeted siRNA. To further assess if apoptosis and

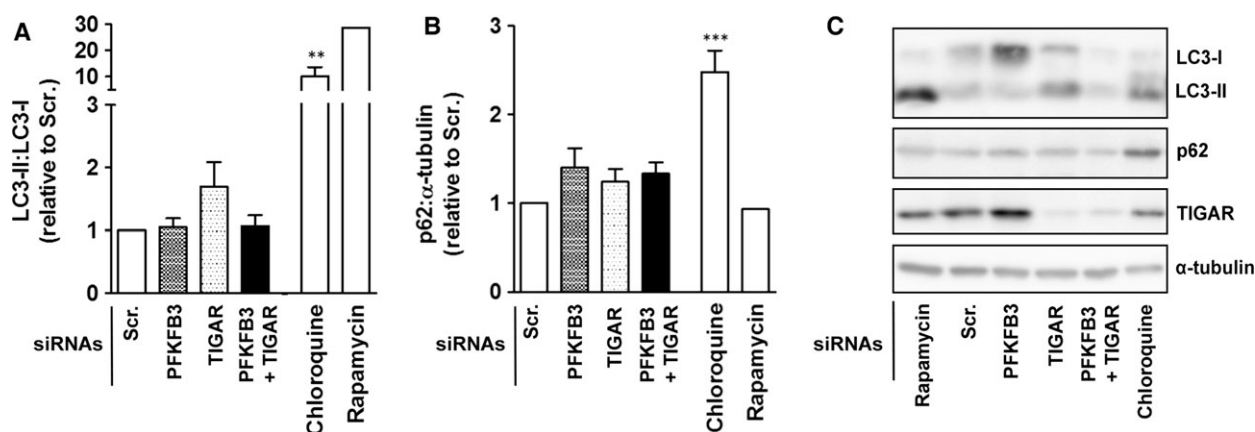


Fig. 4. Western Blot analysis of LC3 cleavage (LC3-II) and p62 protein levels in HeLa cell extracts 72 h after PFKFB3 and TIGAR-targeted siRNA transfection. Quantification of LC3-II:LC3-I ratio (A) and p62 (B) of four independent blots. Data are presented as the mean fold change relative to scrambled siRNA (Scr.) \pm SEM (** $P < 0.01$, *** $P < 0.001$). (C) Western blot images of a representative experiment are shown.

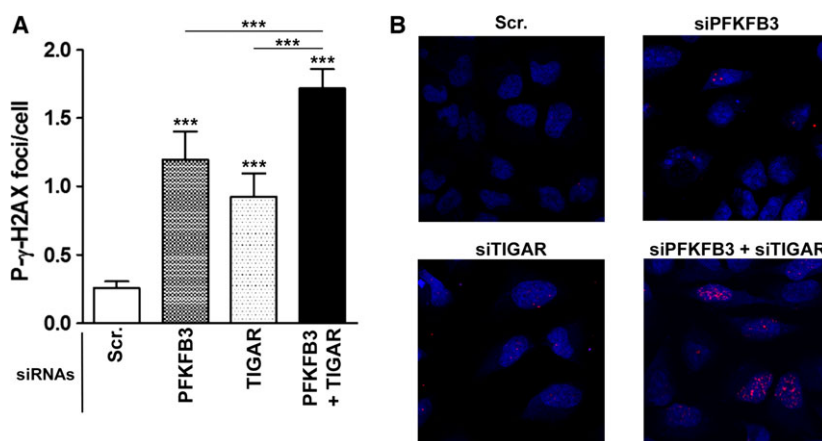


Fig. 5. Effect of PFKFB3 and TIGAR silencing on P-H2AX S139 foci in HeLa cells after 72 h of PFKFB3 and/or TIGAR-targeted siRNA transfection. (A) Quantification of the average number of foci/cell determined with IMAGEJ software from at least 150 cells counted from five randomly chosen fields of view in each condition. Data are presented as mean \pm SEM, and comparison between conditions is indicated by horizontal bars (*** $P < 0.001$). (B) Images of a representative experiment showing merged channels of P-H2AX S139 (Cy3, in red) and nuclei (TO-PRO-3, in blue).

necrosis were triggered in the experimental conditions analysed, an Annexin V/PI assay was performed, showing increased early and late apoptotic and necrotic populations (Annexin V+/PI−, Annexin V+/PI+ and Annexin V−/PI+ cells respectively) after PFKFB3 silencing. TIGAR inhibition alone did not affect viability. However, the combination of PFKFB3 and TIGAR silencing exacerbated the effects of PFKFB3 inhibition alone, causing 15% decreased cell viability compared to PFKFB3-inhibited cells, and leading to double number of apoptotic and necrotic cells (Fig. 6B).

To investigate the mechanism behind these results, the expression of a panel of apoptosis-related genes was analysed by RT-MLPA confirming that apoptosis was

triggered after PFKFB3 inhibition: NOXA was overexpressed at 72 h after PFKFB3-targeted siRNA transfection, whereas Bcl-2 was significantly decreased at the same time point. These results were confirmed at the protein level by western blot (Fig. 7A). On the other hand, there were no significant changes in any of the analysed apoptotic-related genes after TIGAR silencing (Fig. 7B).

Discussion

It was nearly a century ago when Warburg described that cancer cells show characteristic metabolic alterations which make them highly dependent on glycolysis for survival and spreading [38]. PFKFB3 gene is overexpressed in tumours and codes for the PFKFB3

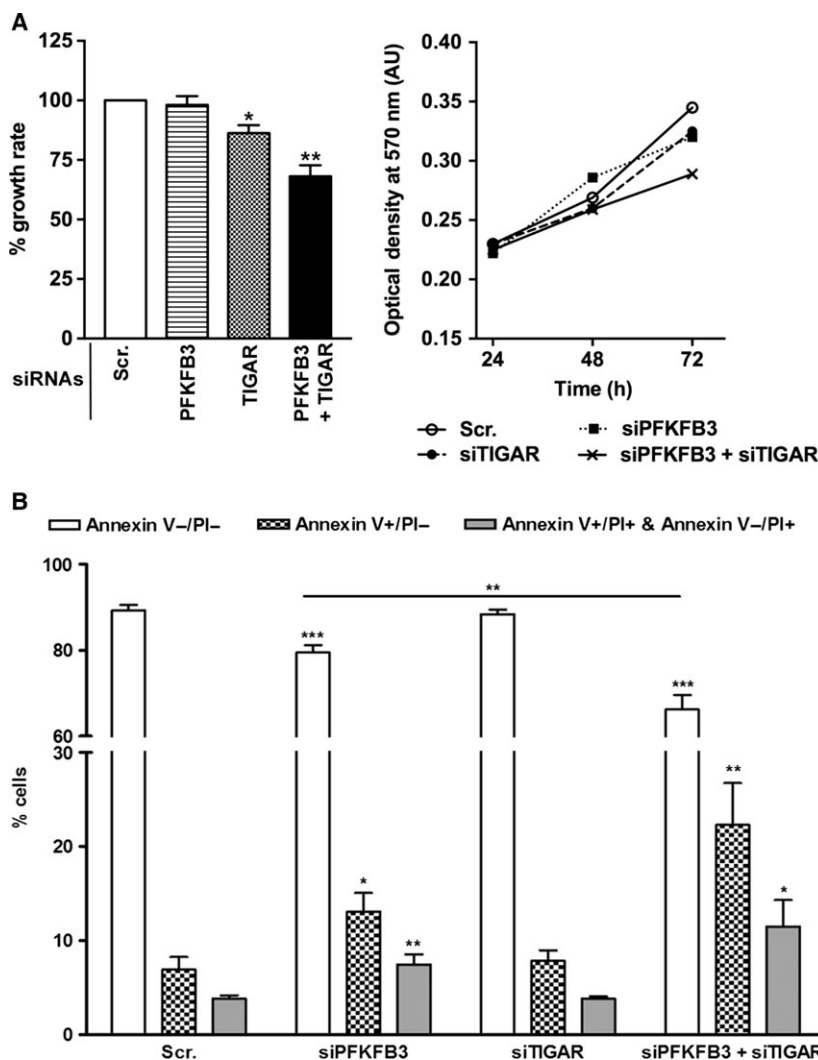


Fig. 6. Effect of PFKFB3 and TIGAR silencing on HeLa cells viability. (A) MTT assay was performed 72 h after PFKFB3 and/or TIGAR-targeted siRNA transfection. Data are presented as the mean fold change in growth rate relative to the scrambled siRNA (Scr.) \pm SEM (* $P < 0.05$) (left panel). Raw data of a single experiment is shown (right panel). (B) Annexin V-FITC/PI staining was performed 72 h after siRNA transfection. Cells AnnexinV-/PI- were considered as viable cells, cells AnnexinV+/PI- were considered as early apoptotic cells, cells AnnexinV+/PI+ were considered as late apoptotic or necrotic cells, and cells AnnexinV-/PI+ were considered as necrotic cells. AnnexinV+/PI+ and AnnexinV-/PI+ populations are represented in a single column. Data are presented as % of cells in each population \pm SEM of six independent experiments, and comparison between conditions is indicated by horizontal bars (* $P < 0.05$, ** $P < 0.01$, *** $P < 0.001$).

isoenzyme of PFK-2/FBPase-2, which has the highest kinase/bisphosphatase ratio [10] and maintains a high Fru-2,6-P₂ concentration in tumour cells [14,17]. The inhibition of PFKFB3 causes a glycolytic blockage that results in impaired vessel sprouting [19], cell cycle arrest and cell death, and reduction of anchorage-independent growth of tumour cell colonies [6] and animal tumour burden [20,21]. Since much of the effects of glycolysis inhibition have been attributed to increased oxidative stress [32,33], the study of proteins which contribute to the antioxidant potential of cells under these conditions can elucidate pro-survival mechanisms triggered by cancer cells in response to glycolysis inhibition.

TIGAR, which catalyses the opposite reaction of PFKFB3, limits cellular oxidative stress. This gene is also overexpressed in tumours [22,25–27,29], in which it reduces ROS production, inhibits apoptosis and promotes cell proliferation. Downregulation of the gene

decreases the ratio between reduced and oxidized glutathione levels, which results in increased ROS and apoptosis [24]. Moreover, the inhibition of this gene in combination with radiotherapy has been shown to improve the anticancer effect of this therapy [30]. Additionally, TIGAR has been identified as 2,3-bisphosphoglycerate phosphatase and this recently described activity points out that this enzyme can have other key effects on cancer cells metabolism beyond PPP enhancement [23].

In this study, we have focused on the potential value of inhibiting both PFKFB3 and TIGAR in HeLa, a cell line in which PFKFB3 inhibition alone has already been shown to impair tumour growth by decreasing Fru-2,6-P₂ [6], as we have confirmed in our model. We demonstrate here that TIGAR is upregulated after PFKFB3 removal in a time-dependent manner, protecting cells from apoptosis and necrosis caused by PFKFB3 inhibition (Fig. 8). Opposite to what was

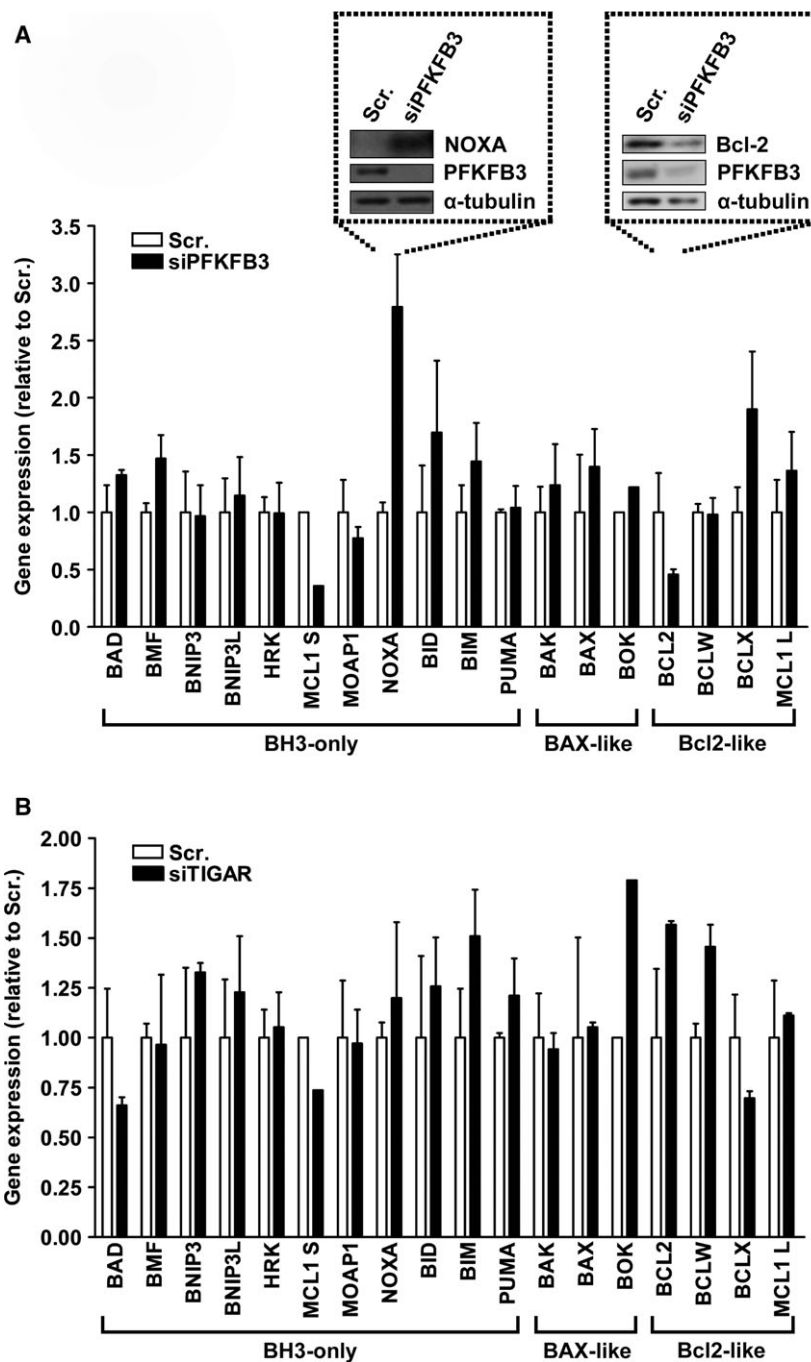


Fig. 7. RT-MLPA analysis of apoptotic-related genes in HeLa cells after 72 h of siRNA transfection targeting PFKFB3 (A) or TIGAR (B). Data are presented as the expression of each gene relative to the expression of that gene in the scrambled condition (Scr.) ± SEM. Western blot analysis of NOXA and Bcl-2 protein levels after 72 h of PFKFB3-targeted siRNA transfection was performed to confirm the mRNA expression results (dotted boxes).

shown in other cell lines, PFKFB3 inhibition in HeLa does not trigger autophagy [32]. In fact, TIGAR overexpression has been previously found to inhibit autophagy, which is consistent with the results presented here [39]. The removal of both PFKFB3 and TIGAR increases ROS production and DNA damage measured by phospho-γ-H2AX foci formation. Consequently, it significantly impairs HeLa cancer cell survival compared to PFKFB3 inhibition alone, as we

have proven both by MTT and Annexin V/PI assays. TIGAR direct contribution to DNA repair mechanisms has been described in other models [40].

According to previous publications describing that the mTORC2-Akt-mTORC1 axis links glycolytic metabolism to ROS homeostasis [36,41], here we show that levels of phosphorylated Akt, mTORC, p70S6K and S6 are increased after PFKFB3 silencing. Moreover, Akt inhibition with Akti-1/2 prevents TIGAR induction in

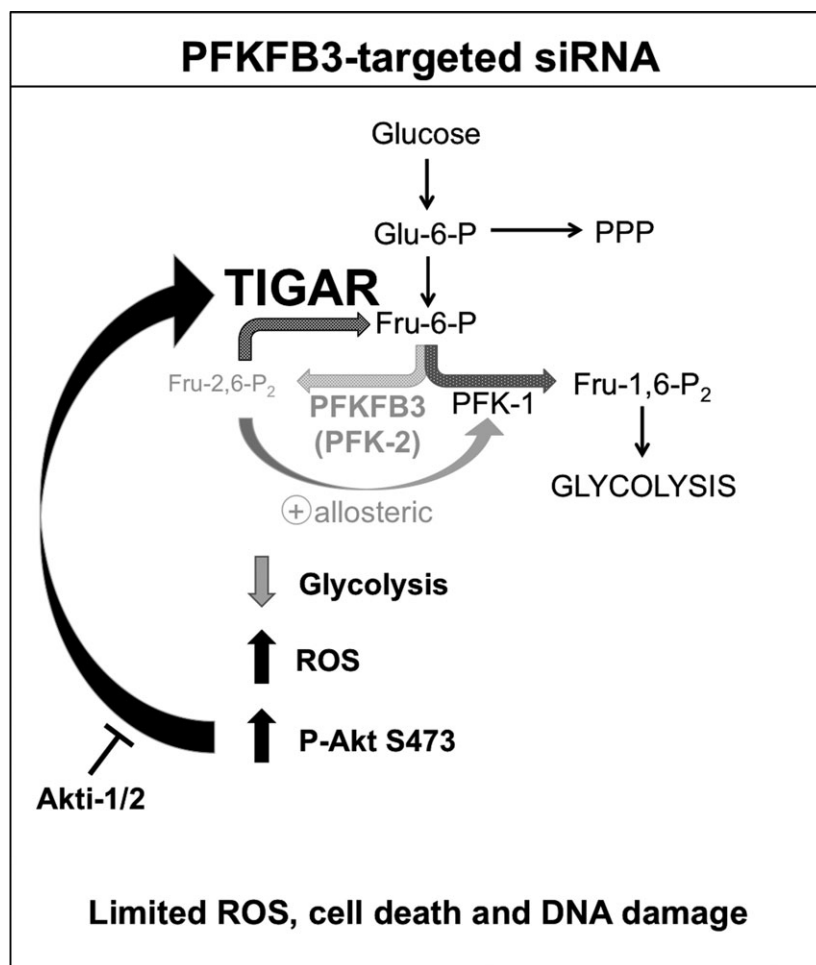


Fig. 8. Summary of the main findings of this work. Abbreviations: Glu-6-P, glucose-6-phosphate; PPP, pentose phosphate pathway; Fru-6-P, fructose-6-phosphate; Fru-1,6-P₂, fructose-1,6-bisphosphate; Fru-2,6-P₂, fructose-2,6-bisphosphate; PFKFB3, 6-phosphofructo-2-kinase/fructose-2,6-bisphosphatase 3; PFK-1, phosphofructokinase-1; PFK-2/FBPase-2, 6-phosphofructo-2-kinase/fructose-2,6-bisphosphatase.

response to PFKFB3 suppression. Thus, we report that Akt activation is necessary for TIGAR modulation in the experimental conditions analysed. These results point out that HeLa cells lacking PFKFB3 trigger the mTORC2-Akt-mTORC1 prosurvival axis in an attempt to rescue glycolysis, since Akt has been widely described to activate GLUT1, Hexokinase, PFK-1 and PFKFB3 [34,35], and be essential for tumour growth [42]. On the contrary, Akt inhibition has been proven to decrease early metabolites in glycolysis and the pentose phosphate pathway [43], which is consistent with the inhibition of TIGAR that we have observed with Akti-1/2. It seems reasonable to hypothesize that the increase in ROS observed after PFKFB3 inhibition is responsible for the induction of the pathway, as it has been described in HeLa cells under glucose deprivation conditions [37]. This is the first time to describe that Akt is necessary for TIGAR modulation, and therefore here we set the basis for considering this gene as part of the Akt-driven prosurvival and growth response of cancer cells, which has been widely described to be one of the

most important pathways for cancer development and progression. It is not clear yet whether TIGAR effects are mainly due to its bisphosphatase activity on Fru-2,6-P₂, as it has been reported in many other models [22], or to its action on other metabolites such as 2,3-BPG [23]. However, what is clear is that when a stressful stimulus such as PFKFB3 inhibition threatens cells, TIGAR is required to redirect glycolytic intermediates to other pathways for the synthesis of biomolecules, which maintain ROS homeostasis and favour tumour growth. On the other hand, when TIGAR is lacking, both glycolysis and alternative metabolic pathways are blocked, so cells fail to overpass the stress and undergo necrosis. Therefore, strategies based on blocking both PFKFB3 and TIGAR could be more effective in impairing tumour growth than PFKFB3 inhibition alone.

Acknowledgements

We are grateful to J. Gil and A. Fernandez Santidrian for helping in RT-MLPA analysis; B. Torrejón from

the Microscopy Unit of *Centres Científics i Tecnològics* of the *Universitat de Barcelona* (CCiT-UB) for excellent technical assistance and advice; E. Adanero for skilful technical assistance; and P. Samsó and C. Arnedo for suggestions and helpful comments. This work was supported by Instituto de Salud Carlos III – FIS (PI13/0096) and Fondo Europeo de Desarrollo Regional (FEDER). With the support of Secretaria d'Universitats i Recerca del Departament d'Economia i Coneixement de la Generalitat de Catalunya.

Author contributions

AM and RB conceived and designed the experiments; MC and HS performed the experiments; EC contributed reagents and materials; AM, HS and EC analysed the data; AR, AN and MC critically commented and revised the work; and RB, AM and HS wrote the manuscript.

References

- 1 Van Schaftingen E (1987) Fructose 2,6-bisphosphate. *Adv Enzymol Relat Areas Mol Biol* **59**, 315–395.
- 2 Rider MH, Bertrand L, Vertommen D, Michels PA, Rousseau GG and Hue L (2004) 6-phosphofructo-2-kinase/fructose-2,6-bisphosphatase: head-to-head with a bifunctional enzyme that controls glycolysis. *Biochem J* **381**, 561–579.
- 3 Colomer D, Vives-Corrons JL, Pujades A and Bartrons R (1987) Control of phosphofructokinase by fructose 2,6-bisphosphate in B-lymphocytes and B-chronic lymphocytic leukemia cells. *Cancer Res* **47**, 1859–1862.
- 4 Hue L and Rousseau GG (1993) Fructose 2,6-bisphosphate and the control of glycolysis by growth factors, tumor promoters and oncogenes. *Adv Enzyme Regul* **33**, 97–110.
- 5 Riera L, Manzano A, Navarro-Sabate A, Perales JC and Bartrons R (2002) Insulin induces PFKFB3 gene expression in HT29 human colon adenocarcinoma cells. *Biochim Biophys Acta* **1589**, 89–92.
- 6 Calvo MN, Bartrons R, Castano E, Perales JC, Navarro-Sabate A and Manzano A (2006) PFKFB3 gene silencing decreases glycolysis, induces cell-cycle delay and inhibits anchorage-independent growth in HeLa cells. *FEBS Lett* **580**, 3308–3314.
- 7 Okar DA, Manzano A, Navarro-Sabate A, Riera L, Bartrons R and Lange AJ (2001) PFK-2/FBPase-2: maker and breaker of the essential biofactor fructose-2,6-bisphosphate. *Trends Biochem Sci* **26**, 30–35.
- 8 Goren N, Manzano A, Riera L, Ambrosio S, Ventura F and Bartrons R (2000) 6-Phosphofructo-2-kinase/fructose-2,6-bisphosphatase expression in rat brain during development. *Brain Res Mol Brain Res* **75**, 138–142.
- 9 Telang S, Yalcin A, Clem AL, Bucala R, Lane AN, Eaton JW and Chesney J (2006) Ras transformation requires metabolic control by 6-phosphofructo-2-kinase. *Oncogene* **25**, 7225–7234.
- 10 Sakakibara R, Uemura M, Hirata T, Okamura N and Kato M (1997) Human placental fructose-6-phosphate,2-kinase/fructose-2,6-bisphosphatase: its isozymic form, expression and characterization. *Biosci Biotechnol Biochem* **61**, 1949–1952.
- 11 Manzano A, Rosa JL, Ventura F, Perez JX, Nadal M, Estivill X, Ambrosio S, Gil J and Bartrons R (1998) Molecular cloning, expression, and chromosomal localization of a ubiquitously expressed human 6-phosphofructo-2-kinase/fructose-2,6-bisphosphatase gene (PFKFB3). *Cytogenet Cell Genet* **83**, 214–217.
- 12 Navarro-Sabate A, Manzano A, Riera L, Rosa JL, Ventura F and Bartrons R (2001) The human ubiquitous 6-phosphofructo-2-kinase/fructose-2,6-bisphosphatase gene (PFKFB3): promoter characterization and genomic structure. *Gene* **264**, 131–138.
- 13 Bartrons R and Caro J (2007) Hypoxia, glucose metabolism and the Warburg's effect. *J Bioenerg Biomembr* **39**, 223–229.
- 14 Atsumi T, Chesney J, Metz C, Leng L, Donnelly S, Makita Z, Mitchell R and Bucala R (2002) High expression of inducible 6-phosphofructo-2-kinase/fructose-2,6-bisphosphatase (iPFK-2; PFKFB3) in human cancers. *Cancer Res* **62**, 5881–5887.
- 15 Chesney J (2006) 6-phosphofructo-2-kinase/fructose-2,6-bisphosphatase and tumor cell glycolysis. *Curr Opin Clin Nutr Metab Care* **9**, 535–539.
- 16 Novellademunt L, Navarro-Sabate A, Manzano A, Rodríguez-García A and Bartrons R (2013) PFKFB3 (6-phosphofructo-2-kinase/fructose-2,6-bisphosphatase 3). *Atlas Genet Cytogenet Oncol Haematol* **17**, 609–622.
- 17 Obach M, Navarro-Sabate A, Caro J, Kong X, Duran J, Gomez M, Perales JC, Ventura F, Rosa JL and Bartrons R (2004) 6-Phosphofructo-2-kinase (pfkfb3) gene promoter contains hypoxia-inducible factor-1 binding sites necessary for transactivation in response to hypoxia. *J Biol Chem* **279**, 53562–53570.
- 18 Minchenko OH, Ochiai A, Opentanova IL, Ogura T, Minchenko DO, Caro J, Komisarenko SV and Esumi H (2005) Overexpression of 6-phosphofructo-2-kinase/fructose-2,6-bisphosphatase-4 in the human breast and colon malignant tumors. *Biochimie* **87**, 1005–1010.
- 19 De Bock K, Georgiadou M, Schoors S, Kuchnio A, Wong BW, Cantelmo AR, Quaegebeur A, Ghesquiere B, Cauwenberghs S, Eelen G *et al.* (2013) Role of PFKFB3-driven glycolysis in vessel sprouting. *Cell* **154**, 651–663.
- 20 Clem B, Telang S, Clem A, Yalcin A, Meier J, Simmons A, Rasku MA, Arumugam S, Dean WL,

- Eaton J *et al.* (2008) Small-molecule inhibition of 6-phosphofructo-2-kinase activity suppresses glycolytic flux and tumor growth. *Mol Cancer Ther* **7**, 110–120.
- 21 Domenech E, Maestre C, Esteban-Martinez L, Partida D, Pascual R, Fernandez-Miranda G, Seco E, Campos-Olivas R, Perez M, Megias D *et al.* (2015) AMPK and PFKFB3 mediate glycolysis and survival in response to mitophagy during mitotic arrest. *Nat Cell Biol* **17**, 1304–1316.
- 22 Bensaad K, Tsuruta A, Selak MA, Vidal MN, Nakano K, Bartrons R, Gottlieb E and Vousden KH (2006) TIGAR, a p53-inducible regulator of glycolysis and apoptosis. *Cell* **126**, 107–120.
- 23 Gerin I, Noel G, Bolsee J, Haumont O, Van Schaftingen E and Bommer GT (2014) Identification of TP53-induced glycolysis and apoptosis regulator (TIGAR) as the phosphoglycolate-independent 2,3-bisphosphoglycerate phosphatase. *Biochem J* **458**, 439–448.
- 24 Lee P, Vousden KH and Cheung EC (2014) TIGAR, TIGAR, burning bright. *Cancer Metab* **2**, 1.
- 25 Won KY, Lim SJ, Kim GY, Kim YW, Han SA, Song JY and Lee DK (2012) Regulatory role of p53 in cancer metabolism via SCO2 and TIGAR in human breast cancer. *Hum Pathol* **43**, 221–228.
- 26 Wanka C, Steinbach JP and Rieger J (2012) Tp53-induced glycolysis and apoptosis regulator (TIGAR) protects glioma cells from starvation-induced cell death by up-regulating respiration and improving cellular redox homeostasis. *J Biol Chem* **287**, 33436–33446.
- 27 Cheung EC, Athineos D, Lee P, Ridgway RA, Lambie W, Nixon C, Strathdee D, Blyth K, Sansom OJ and Vousden KH (2013) TIGAR is required for efficient intestinal regeneration and tumorigenesis. *Dev Cell* **25**, 463–477.
- 28 Simon H, Rodríguez-García A, Navarro-Sabate A, Fontova P, Bartrons R and Manzano A (2014) C12orf5 (chromosome 12 open reading frame 5). *Atlas Genet Cytogenet Oncol Haematol* **18**, 500–510.
- 29 Al-Khayal K, Abdulla M, Al-Obeed O, Al Kattan W, Zubaidi A, Vaali-Mohammed MA, Alsheikh A and Ahmad R (2016) Identification of the TP53-induced glycolysis and apoptosis regulator in various stages of colorectal cancer patients. *Oncol Rep* **35**, 1281–1286.
- 30 Pena-Rico MA, Calvo-Vidal MN, Villalonga-Planells R, Martinez-Soler F, Gimenez-Bonafe P, Navarro-Sabate A, Tortosa A, Bartrons R and Manzano A (2011) TP53 induced glycolysis and apoptosis regulator (TIGAR) knockdown results in radiosensitization of glioma cells. *Radiother Oncol* **101**, 132–139.
- 31 Van Schaftingen E, Lederer B, Bartrons R and Hers HG (1981) A kinetic study of pyrophosphate: fructose-6-phosphate phosphotransferase from potato tubers. Application to a microassay of fructose 2,6-bisphosphate. *Eur J Biochem* **129**, 191–195.
- 32 Klarer AC, O'Neal J, Imbert-Fernandez Y, Clem A, Ellis SR, Clark J, Clem B, Chesney J and Telang S (2014) Inhibition of 6-phosphofructo-2-kinase (PFKFB3) induces autophagy as a survival mechanism. *Cancer Metab* **2**, 2.
- 33 Liu Y, Song XD, Liu W, Zhang TY and Zuo J (2003) Glucose deprivation induces mitochondrial dysfunction and oxidative stress in PC12 cell line. *J Cell Mol Med* **7**, 49–56.
- 34 Duran J, Obach M, Navarro-Sabate A, Manzano A, Gomez M, Rosa JL, Ventura F, Perales JC and Bartrons R (2009) Pfkfb3 is transcriptionally upregulated in diabetic mouse liver through proliferative signals. *FEBS J* **276**, 4555–4568.
- 35 Trefely S, Khoo PS, Krycer JR, Chaudhuri R, Fazakerley DJ, Parker BL, Sultani G, Lee J, Stephan JP, Torres E *et al.* (2015) Kinome screen identifies PFKFB3 and glucose metabolism as important regulators of the insulin/insulin-like growth factor (IGF)-1 signaling pathway. *J Biol Chem* **290**, 25834–25846.
- 36 Dong-Yun S, Yu-Ru D, Shan-Lin L, Ya-Dong Z and Lian W (2003) Redox stress regulates cell proliferation and apoptosis of human hepatoma through Akt protein phosphorylation. *FEBS Lett* **542**, 60–64.
- 37 Gao M, Liang J, Lu Y, Guo H, German P, Bai S, Jonasch E, Yang X, Mills GB and Ding Z (2014) Site-specific activation of AKT protects cells from death induced by glucose deprivation. *Oncogene* **33**, 745–755.
- 38 Warburg O (1956) On the origin of cancer cells. *Science* **123**, 309–314.
- 39 Bensaad K, Cheung EC and Vousden KH (2009) Modulation of intracellular ROS levels by TIGAR controls autophagy. *EMBO J* **28**, 3015–3026.
- 40 Yu HP, Xie JM, Li B, Sun YH, Gao QG, Ding ZH, Wu HR and Qin ZH (2015) TIGAR regulates DNA damage and repair through pentosephosphate pathway and Cdk5-ATM pathway. *Sci Rep* **5**, 9853.
- 41 Kodiha M, Banski P and Stochaj U (2009) Interplay between MEK and PI3 kinase signaling regulates the subcellular localization of protein kinases ERK1/2 and Akt upon oxidative stress. *FEBS Lett* **583**, 1987–1993.
- 42 Garcia-Cao I, Song MS, Hobbs RM, Laurent G, Giorgi C, de Boer VC, Anastasiou D, Ito K, Sasaki AT, Rameh L *et al.* (2012) Systemic elevation of PTEN induces a tumor-suppressive metabolic state. *Cell* **149**, 49–62.
- 43 Makinoshima H, Takita M, Saruwatari K, Umemura S, Obata Y, Ishii G, Matsumoto S, Sugiyama E, Ochiai A, Abe R *et al.* (2015) Signaling through the phosphatidylinositol 3-kinase (PI3K)/mammalian target of rapamycin (mTOR) axis is responsible for aerobic glycolysis mediated by glucose transporter in epidermal growth factor receptor (EGFR)-mutated lung adenocarcinoma. *J Biol Chem* **290**, 17495–17504.



PI3K–Akt signaling controls PFKFB3 expression during human T-lymphocyte activation

Helga Simon-Molas¹ · Claudia Arnedo-Pac¹ · Pere Fontova² · Anna Vidal-Alabró² · Esther Castaño³ · Ana Rodríguez-García¹ · Àurea Navarro-Sabaté¹ · Núria Lloberas² · Anna Manzano¹ · Ramon Bartrons¹

Received: 13 September 2017 / Accepted: 7 February 2018 / Published online: 12 February 2018
© Springer Science+Business Media, LLC, part of Springer Nature 2018

Abstract

Lymphocyte activation is associated with rapid increase of both the glycolytic activator fructose 2,6-bisphosphate (Fru-2,6-P₂) and the enzyme responsible for its synthesis, 6-phosphofructo-2-kinase/fructose-2,6-bisphosphatase (PFK-2/FBPase-2). PFKFB3 gene, which encodes for the most abundant PFK-2 isoenzyme in proliferating tissues, has been found overexpressed during cell activation in several models, including immune cells. However, there is limited knowledge on the pathways underlying PFKFB3 regulation in human T-lymphocytes, and the role of this gene in human immune response. The aim of this work is to elucidate the molecular mechanisms of PFKFB3 induction during human T-lymphocyte activation by mitotic agents. The results obtained showed PFKFB3 induction during human T-lymphocyte activation by mitogens such as phytohemagglutinin (PHA). PFKFB3 increase occurred concomitantly with GLUT-1, HK-II, and PCNA upregulation, showing that mitotic agents induce a metabolic reprogramming process that is required for T-cell proliferation. PI3K–Akt pathway inhibitors, Akti-1/2 and LY294002, reduced PFKFB3 gene induction by PHA, as well as Fru-2,6-P₂ and lactate production. Moreover, both inhibitors blocked activation and proliferation in response to PHA, showing the importance of PI3K/Akt signaling pathway in the antigen response of T-lymphocytes. These results provide a link between metabolism and T-cell antigen receptor signaling in human lymphocyte biology that can help to better understand the importance of modulating both pathways to target complex diseases involving the activation of the immune system.

Keywords PFKFB3 · PI3K–Akt · Mitogens · Lymphocytes · Glycolysis · Metabolism

Helga Simon-Molas and Claudia Arnedo-Pac have contributed equally to this work.

Anna Manzano and Ramon Bartrons share senior co-authorship.

Electronic supplementary material The online version of this article (<https://doi.org/10.1007/s11010-018-3325-9>) contains supplementary material, which is available to authorized users.

✉ Ramon Bartrons
rbartrons@ub.edu

¹ Departament de Ciències Fisiològiques, Facultat de Medicina i Ciències de la Salut, Universitat de Barcelona, C/Feixa Llarga, s/n 08907 L'Hospitalet de Llobregat, Barcelona, Spain

² Departament de Nefrologia, Hospital Universitari de Bellvitge, IDIBELL, Barcelona, Spain

³ Centres Científics i Tecnològics, Universitat de Barcelona, Barcelona, Spain

Abbreviations

3PO	3-(3-pyridinyl)-1-(4-pyridinyl)-2-propen-1-one
7-AAD	7-Aminoactinomycin D
AICD	Activation-induced cell death
CFSE	Carboxyfluorescein succinimidyl ester
ConA	Concanavalin A
FBS	Fetal bovine serum
Fru-2,6-P ₂	Fructose 2,6-bisphosphate
GLUT-1	Glucose transporter 1
HIF	Hypoxia-inducible factor
HK-II	Hexokinase-II
IL2RA	Interleukin-2 receptor alpha chain
LPS	Lipopolysaccharide
MFI	Mean fluorescence intensity
mTORC1	Mammalian target of rapamycin
mTORC1	Mammalian target of rapamycin complex 1
OXPHOS	Oxidative phosphorylation
PBMCs	Peripheral blood mononuclear cells

PCNA	Proliferating cell nuclear antigen
PFK-1	Phosphofructokinase-1
PFK-2/FBPase-2	6-Phosphofructo-2-Kinase/ Fructose-2,6-Bisphosphatase
PFKFB3	6-Phosphofructo-2-Kinase/Fructose- 2,6-Bisphosphatase 3
PHA	Phytohemagglutinin
P-S6	S6 ribosomal protein
TCR	T-cell antigen receptor

Introduction

An adequate immune system response relies on a rapid activation and proliferation of several tissues. Upon encountering pathogens, T-lymphocytes undergo massive clonal expansion and differentiation, which requires the coordination of cellular signaling cascades and metabolic enzymes to express and secrete inflammatory molecules. These processes are dependent on high amounts of energy [1]. Circulating naive T-lymphocytes are quiescent, have low metabolic demands, and use predominantly oxidative phosphorylation (OXPHOS) to generate ATP. After T-cell antigen receptor (TCR)-mediated recognition of antigens and costimulatory signals, T-lymphocytes become activated and initiate a growth phase adopting anabolic metabolism. In this context, nutrients are not only exclusively used for survival and homeostasis but also for the generation of building blocks for clonal expansion and for effector functions, such as secretion of cytokines [2]. Activated T-lymphocytes show induced expression of glucose transporter 1 (GLUT-1) [3] and several rate-limiting glycolytic enzymes such as hexokinase-II (HK-II) [1, 4, 5]. Moreover, most of the pyruvate synthesized in proliferating T-lymphocytes is converted to lactate instead of entering the tricarboxylic acid cycle, which means that ATP production in these cells is completely dependent on glycolysis [3].

Lymphocyte activation is associated with a rapid increase in intracellular fructose 2,6-bisphosphate (Fru-2,6-P₂) [6–9], the most potent allosteric activator of phosphofructokinase-1 (PFK-1) [10]. The steady-state concentration of Fru-2,6-P₂ in cells is dependent on the expression of 6-Phosphofructo-2-Kinase/Fructose-2,6-Bisphosphatase (PFK-2/FBPase-2), the activity of which is increased by T-cell activators [7]. This enzyme is encoded by four different genes (PFKFB1–4) that differ in their kinase/phosphatase activity ratio, their response to protein kinases, and their tissue expression profiles [11]. 6-Phosphofructo-2-Kinase/Fructose-2,6-Bisphosphatase 3 (PFKFB3) isoenzyme has the highest PFK-2/FBPase-2 activity ratio, promoting net synthesis of Fru-2,6-P₂ [12–14]. It is ubiquitously expressed and it is present in proliferating tissues [14, 15], transformed cells [16–18], and in various solid tumors [19, 20]. PFKFB3 expression

has been widely studied in cancer research, describing different stimuli that can modulate this gene including hypoxia [21], progestins [13, 22], growth factors (e.g., insulin [17] and TGF-β1 [23]), proinflammatory molecules (e.g., interleukin-6 [24], lipopolysaccharide (LPS), and adenosine [25]), and stress stimuli [26]. Along with its role in cancer, PFKFB3 is becoming more relevant in the context of inflammatory responses. Its expression has been described in atherosclerotic macrophages, in which Hypoxia-Inducible Factor (HIF) has a key role [27], rheumatoid arthritis [28], and during macrophages antiviral defence [29]. Recently, our group has collaborated to describe that mitogen stimulation of rat thymocytes with concanavalin A (ConA) increases Fru-2,6-P₂ concentration and PFKFB3 expression in an Akt-dependent manner [30].

However, despite the important role of this isoenzyme in the glycolytic control of proliferating cells, there is limited knowledge about PFKFB3 role during the physiological responses of human immune cells. Therefore, the aim of the present work is to elucidate the molecular mechanism underlying PFKFB3 control during primary human T-lymphocyte activation and proliferation induced by the mitotic agents phytohemagglutinin (PHA), ConA, and LPS.

Materials and methods

Lymphocyte purification and cell culture

Human peripheral blood mononuclear cells (PBMCs) were isolated from buffy coats from healthy volunteers by Ficoll density gradient (GE Healthcare, Uppsala, Sweden). Human cells were obtained from healthy volunteers in accordance with protocols approved by the Ethics Committee of the Bellvitge University Hospital (Barcelona, Spain) and in accordance with the principles of the 1964 Helsinki Declaration and its later amendments or comparable ethical standards. Informed consent was obtained from all individual participants included in the study.

PBMCs (10 × 10⁶ cells/ml) were cultured in X-VIVO™ (Lonza, Basel, Switzerland) with 2% Human Serum (Sigma-Aldrich, Madrid, Spain) for 2–3 h (37 °C, 5% CO₂, 70–80% humidity) in 175 cm² adherent flasks (Sarstedt, Nümbrecht, Germany). The purification efficiency of two different adhesion protocols was compared, and the double-sided approach was chosen for further experiments. Technical procedures and purification results are detailed in Extended Methods. Non-adherent cells were re-suspended in complete RPMI with 10% heat-inactivated fetal bovine serum, 1% L-glutamine, and 1% penicillin–streptomycin (Biological Industries, Israel). Lymphocytes were cultured at 2–2.3 × 10⁶ cells/ml (37 °C, 5% CO₂, 70–80% humidity) for the indicated times in non-adherent 75 cm² flasks (Sarstedt).

Lymphocyte activation

Doses of 1, 5, and 15 $\mu\text{g/ml}$ of PHA (Sigma-Aldrich) were tested and 5 $\mu\text{g/ml}$ was set as the optimal PHA concentration. ConA from *Canavalia ensiformis* and LPS from *Escherichia coli* (Sigma-Aldrich) were used at 10 and 1 $\mu\text{g/ml}$, respectively. A fraction of the isolated lymphocytes remained untreated for each donor sample (untreated cells, CT).

Inhibition of PI3K–Akt signaling pathway

LY294002 and Akti-1/2 (Catalog Numbers #440202 and #124018, respectively, Calbiochem, San Diego, CA, USA) were added to T-lymphocyte cultures 30 min before PHA treatment at doses of 20 and 10 μM , respectively.

Cell phenotype, activation, and viability analysis by flow cytometry

In order to characterize different subpopulations in PBMCs samples, cells (2×10^5) were stained with fluorochrome-conjugated antibodies anti-CD3-APC, anti-CD20-PE, and anti-CD14-FITC (Becton Dickinson Pharmingen, San Diego, CA, USA) for the identification of T-lymphocytes, B-lymphocytes, and monocytes, respectively. Anti-CD25-FITC (BD Biosciences, San Jose, CA) was used to assess T-cell activation at the indicated times. T-cell viability was assessed by the staining of 7-AAD (BD Biosciences) at 120 h after treatment. A BD FACSCanto II Cytometer with FACSDIVA software (BD Biosciences) was used.

Cell proliferation assay by flow cytometry

PBMCs were labeled with CellTrace CFSE proliferation kit (Invitrogen, Molecular Probes, Madrid, Spain). CFSE-labeled PBMCs (2×10^6) were cultured in 25 cm^2 flasks. After 120 h of culture, 2×10^5 cells were labeled with anti-CD3-APC (Becton Dickinson Pharmingen) as previously described [31] and BD FACSCanto II Cytometer with FACSDIVA software (BD Biosciences) was used to analyze CD3⁺ cells proliferation.

Western blot analysis

Protein extraction and western blot were performed as previously described [32]. For the analysis of phosphorylated proteins, protein pellets were kept on ice and lysed with RIPA buffer (25 mM Tris–HCl pH 7, 5, 150 mM NaCl, 1% Triton-X-100, 1% sodium deoxycholate, 0,1% SDS) containing protease and phosphatase inhibitors. The following primary antibodies were used: GLUT-1 (1:2000; Abcam, Cambridge, UK), HK-II and PCNA (1:500; Santa

Cruz Biotechnology, Dallas, TX, USA), PFKFB3 (1:1000; [17]), P-Akt (S473) (1:500; Cell Signaling Technology, Danvers, MA, USA), and P-S6 (S235/S236) (1:1000; Cell Signaling Technology). All proteins were normalized to β -actin (1:4000; Abcam) and analyses were performed with Multi-Gauge v3.0 (FujiFilm Corporation, Tokyo, Japan).

Immunofluorescence

Lymphocytes were collected at different times after treatment with PHA, re-suspended in PBS, and incubated at room temperature for 30–60 min over poly-L-lysine-coated coverslips (0.01% solution; Sigma-Aldrich). Then, cells were fixed with 4% paraformaldehyde and immunostained with primary antibodies against PCNA and PFKFB3 (1:100, Santa Cruz Biotechnology). Secondary antibodies Cy3-conjugated donkey anti-mouse IgG antibody (1:500; Jackson Immunoresearch, West Grove, PA, USA) and Alexa-555-conjugated donkey anti-goat (1:400, Invitrogen) were used for the detection of PCNA and PFKFB3, respectively. Nuclei were stained with TO-PRO-3 Iodide (1:1000; Invitrogen), when detecting PCNA and DRAQ5 (1:1000; BioStatus, Loughborough, UK), when detecting PFKFB3. Images were acquired with a Spectral Confocal Microscope (TCS-SL; Leica Microsystems), using a Plan-Apochromat 63X/1.4 N.A. immersion oil objective (Leica Microsystems). Excitation He/Ne laser beams (Lasos, Jena, Germany) at 543 nm for Cy3 and Alexa-555, and 633 nm for TO-PRO-3 and DRAQ5, and a pinhole aperture of 1 AU were used. Images were captured using Leica confocal software (Leica Microsystems) and merged using ImageJ software (Wayne Rasband, National Institutes of Health, Bethesda, MD, USA).

RNA isolation and RT-PCR analysis

Total RNA was extracted using TRIsure (Bioline, Ewelligh, Australia), according to the manufacturer's protocol. RNA was reverse transcribed using High-Capacity cDNA Reverse Transcription Kit (Applied Biosystems, Foster City, CA, USA). PFKFB3 was specifically amplified using the probe and primer set for human PFKFB3 (Hs0019079_m1) (Applied Biosystems). TBP (housekeeping control gene, TATA-box binding protein) (Hs Hs99999910_m1) (Applied Biosystems) was used for normalization. PCR data were captured using an ABI PRISM 7700 Sequence Detection System (Applied Biosystems) with Sequence Detection Software (SDS version 3.0; Applied Biosystems). Data were analyzed with Expression Suite Software (version 1.1; Applied Biosystems).

Metabolic determinations

Fru-2,6-P₂ was determined as previously described [33]. Extracellular lactate was measured spectrophotometrically in 1 mL of supernatants from cultured cells under the corresponding treatments using standard enzymatic methods [34]. Fru-2,6-P₂ and lactate measurements were normalized to protein concentration, determined by the Bradford assay (Bio-Rad, Hercules, CA, USA).

Data analysis

GraphPad for Windows (version 6.0; GraphPad Software, La Jolla, CA, USA) was used for analysis. Results are expressed as the mean \pm Standard Error of the Mean (SEM) from at least three independent experiments. The statistical test used for each analysis is specified in each figure legend, according to the nature of the data, and the compared conditions are indicated with a line above the columns. Differences were considered statistically significant at *p* values below 0.05 (*, #*p* < 0.05; **, ##*p* < 0.01; ***, ###*p* < 0.001; *****p* < 0.0001).

Results and discussion

Mitotic agents trigger activation and proliferation of human T-lymphocytes

In order to set the experimental model to study metabolic changes occurring during T-lymphocyte antigen response, several markers of activation and proliferation were analyzed in the presence of mitogens.

PHA has been widely used as a T-lymphocyte activator [35]. However, high doses of this lectin lead to activation-induced cell death (AICD) [36]. To avoid mortality, T-lymphocytes viability in response to several doses of PHA was analyzed with the 7-aminoactinomycin D (7-AAD) assay. Results showed an increase in 7-AAD fluorescence upon PHA concentration (Fig. 1a), describing a dose-dependent effect of PHA on lymphocyte viability. Percentage of 7-AAD-negative cells (viable cells) in the untreated condition was set as reference. Doses of 1 and 5 μ g/ml did not significantly affect cell viability, whereas the dose of 15 μ g/ml decreased viability. Based on these results, the dose of 5 μ g/ml was used for further experiments.

To analyze the effects of mitotic agents on human T-lymphocytes, we assessed the presence of the early activation marker CD25 (interleukin-2 receptor alpha chain, IL2RA) in lymphocyte membranes by flow cytometry [37]. CD25 mean fluorescence intensity (MFI) was found significantly increased in a time-dependent manner after 48 and 120 h of PHA treatment, compared to control lymphocytes (Fig. 1b).

Considering that cell activation usually triggers cell proliferation, a carboxyfluorescein succinimidyl ester (CFSE) staining assay was performed after 120 h of PHA treatment. According to CD25 results, untreated cells showed higher CFSE fluorescence compared to PHA-treated cells (Fig. 1c), which is consistent with increased number of cell divisions and consequent loss of CFSE staining in the membrane of PHA-stimulated cells. Similar results were obtained with other mitogenic stimuli such as ConA and LPS, which also increased CD25 expression and decreased CFSE fluorescence in human T-lymphocytes (Supplementary Figure S2A, B).

As an alternative measure of proliferation, total protein levels of proliferating cell nuclear antigen (PCNA) were analyzed by western blot. Results showed that PCNA was significantly induced in a time-dependent manner from 24 to 120 h of PHA treatment (Fig. 1d), confirming that PHA triggers proliferation in this model. Immunofluorescence analysis of PCNA revealed increased localization of this protein, which is a processivity factor for DNA polymerase δ , in the nucleus over time (Fig. 1e). These results are in agreement with previous studies proving that PHA is sufficient to initiate mitosis by itself [38]. ConA and LPS-triggered PCNA overexpression along time as well (Supplementary Figure S2C).

Mitogens increase glycolytic metabolism in human T-lymphocytes

Western blot analyses of HK-II and GLUT-1 were used to determine the effect of PHA on human T-lymphocyte glycolysis. The levels of these proteins were increased from 24 h after PHA treatment compared to untreated cells. In the case of HK-II, the maximum level of expression was reached at 120 h after treatment (Fig. 2a), whereas GLUT-1 maximum expression was at 48 h and it was maintained at 120 h (Fig. 2b). PHA effects on PFKFB3 expression were analyzed both at the mRNA and protein level. PFKFB3 mRNA levels were significantly increased in PHA-treated lymphocytes from 24 to 120 h, being slightly lower at the latter time point (Fig. 3a). PFKFB3 protein levels significantly increased from 24 to 48 h, when the maximum expression was reached (Fig. 3b), which is consistent with mRNA results. PFKFB3 protein returned to control levels at 120 h. The decreased PFKFB3 protein induction in response to PHA at 120 h suggests that PFKFB3 upregulation could be especially important in early T-cell activation, as it has been demonstrated in other activation models [9]. Immunofluorescence analysis of PFKFB3 confirmed the existence of high levels of this protein after 48 h of PHA treatment and revealed that it was exclusively located in the cytoplasm (Fig. 3c). The expression of other PFKFB isoenzymes

Fig. 1 PHA activates human T-lymphocytes and triggers their proliferation. **a** 7-AAD viability assay showing the dose-dependent response of T-lymphocytes treated with 1–15 $\mu\text{g/ml}$ PHA and stained 120 h after treatment. **b** Time course of relative CD25 mean fluorescence intensity (MFI) in 5 $\mu\text{g/ml}$ PHA-treated T-lymphocytes. Data are presented as the mean fold change relative to untreated cells (CT) at 24 h \pm SEM. **c** CFSE MFI on 5 $\mu\text{g/ml}$ PHA-treated and untreated T-lymphocytes after 120 h. **d** Western blot analysis of PCNA normalized to β -actin in 5 $\mu\text{g/ml}$ PHA-treated and untreated T-lymphocytes at several times. Data are presented as the mean fold change relative to untreated cells at 24 h \pm SEM. Representative images are shown. Differences were calculated with two-tailed unpaired (a) or paired (b–d) Student’s t test with normal-based 95% confidence interval (CI). Significant p values are indicated: * $p \leq 0.05$; ** $p \leq 0.01$, *** $p < 0.001$; **** $p < 0.0001$. **e** Images of a representative immunofluorescence analysis of PCNA in PHA-treated and untreated cells along time. Single PCNA detected with a Cy5-conjugated secondary antibody (shown in red) and nuclei stained with TO-PRO-3 (shown in blue) are displayed, together with the resulting merged channel image. (Color figure online)

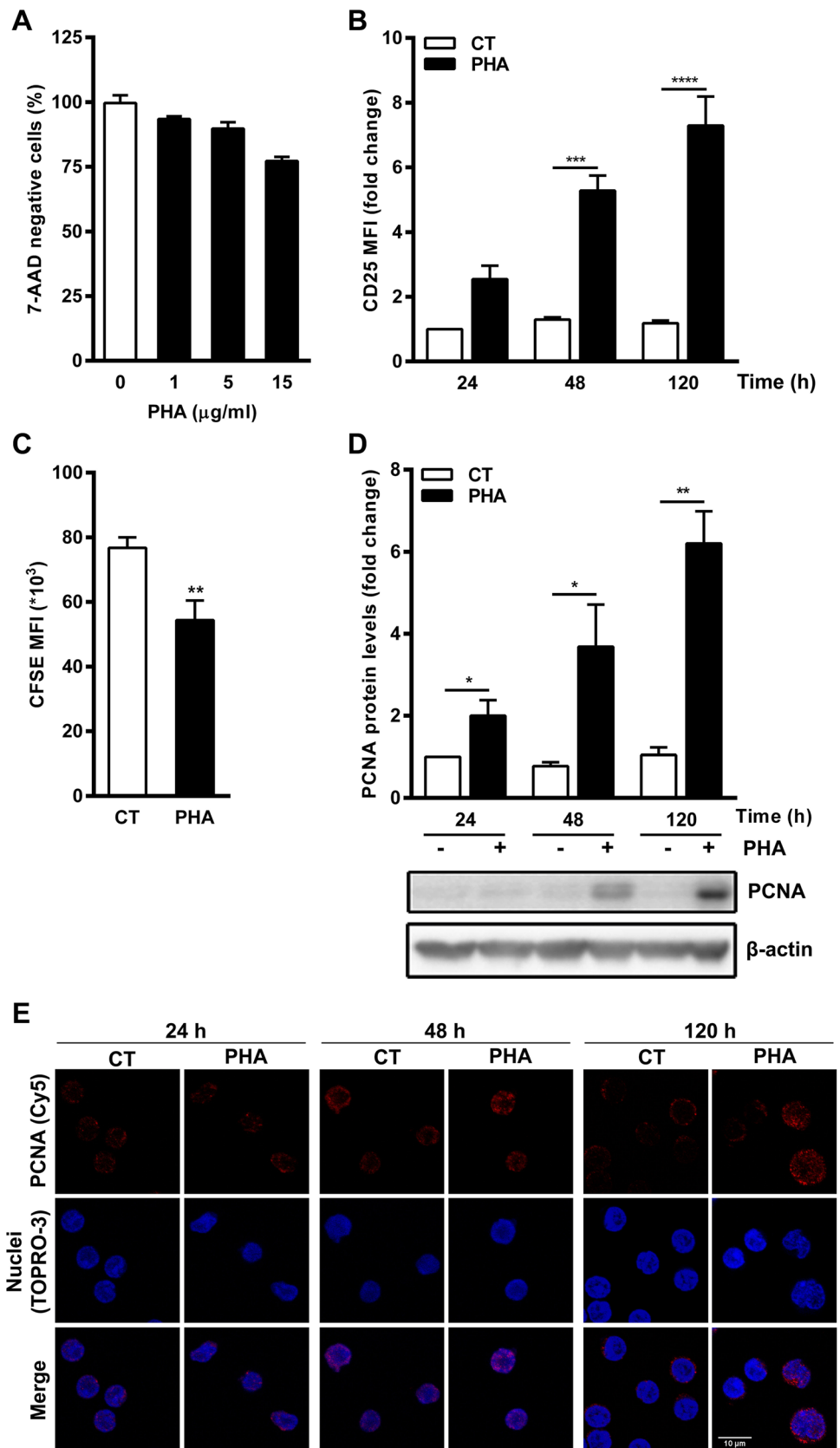
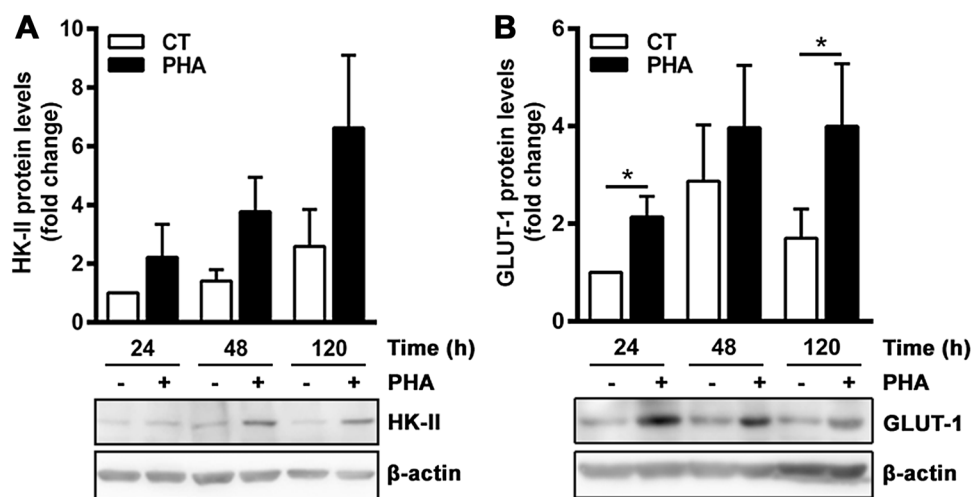


Fig. 2 PHA increases the expression of HK-II and GLUT-1. Western blot analysis of HK-II (a) and GLUT-1 (b) at several time points after 5 $\mu\text{g}/\text{ml}$ PHA treatment. Quantification of each protein level was normalized to β -actin levels. Data are presented as the mean fold change relative to untreated cells (CT) at 24 \pm SEM. Differences were calculated with two-tailed paired Student's *t* test with normal-based 95% CI. Significant *p* values are indicated: **p* \leq 0.05. Representative western blot images are shown in the lower panel



was not affected or could not be detected in this model (data not shown), which is consistent with previous studies showing that PFKFB3 is the isoenzyme preferentially expressed in proliferating cells [9, 14, 15, 39] and also in mitogen-stimulated thymocytes [30].

In order to study PFKFB3 activity, Fru-2,6-P₂ concentration was assessed. The results obtained showed a significant raise of this metabolite at 24 and 48 h after PHA treatment (Fig. 3d). Fru-2,6-P₂ concentration decreased at 120 h, although it was maintained higher in PHA-treated cells compared to controls, which is consistent with PFKFB3 protein levels. These results were complemented with the measurement of the final product of glycolysis, lactate. Extracellular lactate quantification indicated that glycolysis was significantly increased after PHA treatment along time (Fig. 3e). Other mitotic agents, such as ConA and LPS, likewise increased PFKFB3 protein levels and Fru-2,6-P₂ concentration along time (Supplementary Figure S2C-E).

These results confirm that mitotic agents drive lymphocytes to a glycolytic phenotype by increasing the expression of key enzymes such as HK-II, GLUT-1, and PFKFB3. Given the regulatory role of the PFKFB3 product, Fru-2,6-P₂, on PFK-1 activity, the induction of this gene plays a key role in the metabolic adaptation of T-lymphocytes and contributes to overcome the energetic and anabolic demands of the early activation response in front of an antigen.

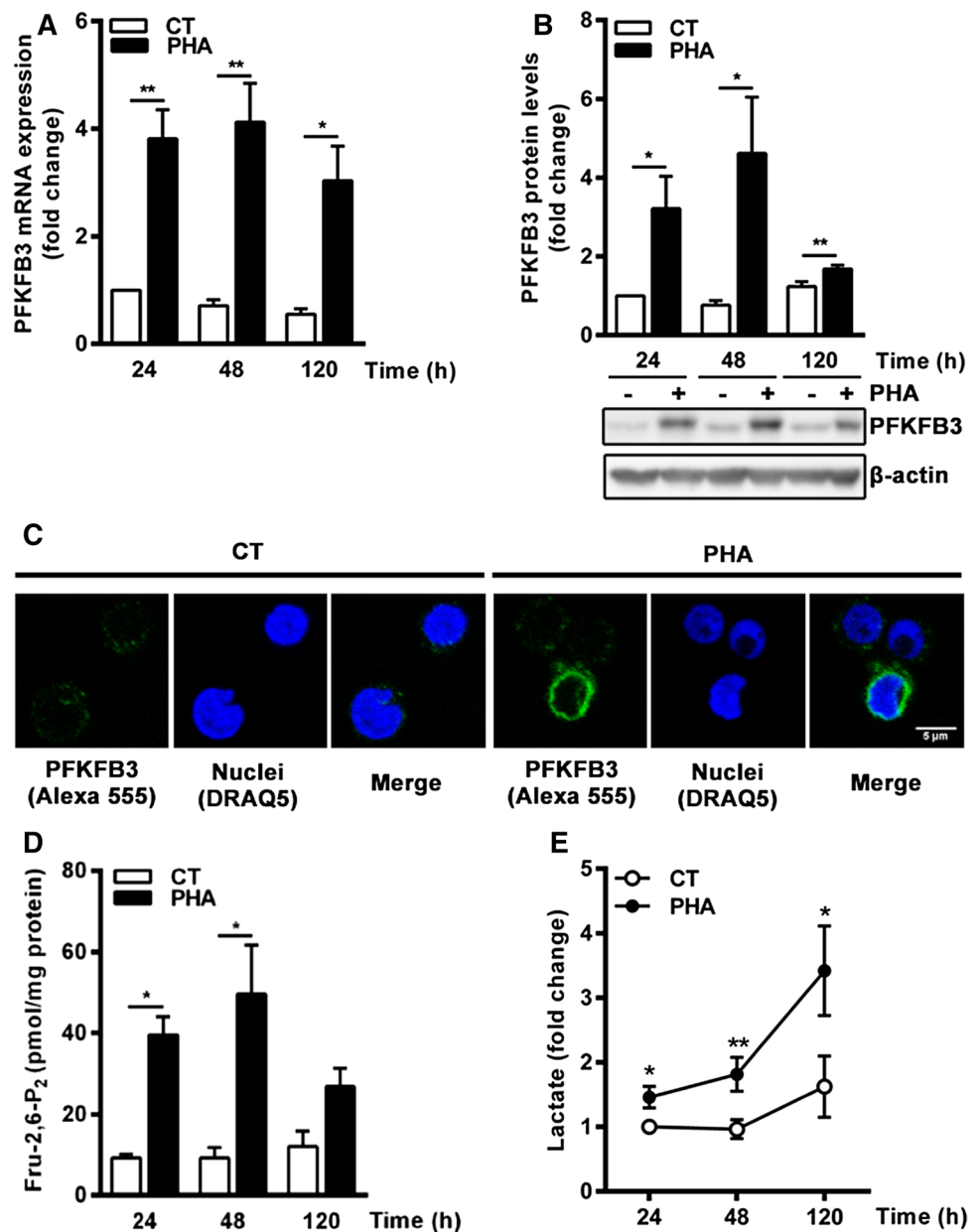
These data are consistent with previous studies, showing glycolysis upregulation with increased GLUT-1 and HK-II levels in response to PHA [4, 40]. PFKFB3 overexpression has also been described in a model of T-cell activation with anti-CD3/anti-CD28-conjugated microbeads in which pharmacological inhibition of the enzyme attenuates T-lymphocyte activation in vitro and suppresses T-cell-dependent immunity in vivo [9].

PFKFB3 is regulated by the PI3K–Akt signaling pathway in activated T-lymphocytes

An important regulator of T-cell biology is the mammalian target of rapamycin (mTOR), which integrates immune and metabolic cues, such as antigens and nutrients. Under certain stimuli, TCR, CD28, and IL-2R signaling through the PI3K–Akt pathway can activate the mammalian target of rapamycin complex 1 (mTORC1), which positively regulates helper and effector T-lymphocytes [41]. The same PI3K–Akt–mTORC1 axis has been described to be involved in GLUT-1-mediated glucose transport in lymphocytes [3, 42] and in HK-II expression [43]. Moreover, this axis has been previously described to regulate PFKFB3 in cancer cells and rat thymocytes [15, 30, 44]. With the aim of studying whether PI3K–Akt–mTORC1 links PHA signaling to PFKFB3 induction in human lymphocytes, the phosphorylation levels of Akt and the target of mTORC1 pathway, S6 ribosomal protein (P-S6), were analyzed after 48 h of PHA treatment, when PFKFB3 expression reached the highest levels, as it has been shown before (Fig. 3a, b). Significantly increased levels of P-Akt (S473) and P-S6 (S235/236) were detected in PHA-treated cells compared to untreated cells. Co-treatment of PHA with the Akt inhibitor Akti-1/2 significantly reduced Akt and S6 phosphorylation. The same effect was observed when inhibiting the signaling cascade upstream Akt with the PI3K inhibitor LY294902. Both Akti-1/2 and LY294902 significantly impaired PFKFB3 induction in response to PHA. Furthermore, PHA-induced PCNA overexpression was also prevented by both inhibitors (Fig. 4a, b).

In terms of lactate production, the combination of PHA with Akti-1/2 or LY294902 avoided the extracellular lactate increase observed in T-lymphocytes treated with PHA alone (Fig. 4c). Moreover, cell activation and proliferation was also prevented by both inhibitors, as it was evidenced

Fig. 3 PFKFB3 expression, Fru-2,6-P₂ and lactate production are increased by PHA. **a** RT-PCR analysis of PFKFB3 expression in 5 µg/ml PHA-treated and untreated T-lymphocytes (CT) at several times. **b** Western blot analysis of PFKFB3 normalized to β-actin in 5 µg/ml PHA-treated and untreated T-lymphocytes (CT) at several times. Representative western blot images are shown. **c** Images of a representative immunofluorescence analysis of PFKFB3 in PHA-treated and untreated cells at 48 h. Single PFKFB3 detected with an Alexa-555-conjugated secondary antibody (shown in green) and nuclei stained with DRAQ5 (shown in blue) are displayed together with the resulting merged channel image. **d** Fru-2,6-P₂ concentration in T-lymphocytes at several times after 5 µg/ml PHA treatment. **e** Relative extracellular lactate production at several times after 5 µg/ml PHA treatment. All data are presented as the mean fold change relative to untreated cells at 24 h ± SEM. Differences were calculated with two-tailed paired Student's *t* test with normal-based 95% CI. Significant *p* values are indicated: **p* ≤ 0.05; ***p* ≤ 0.01. (Color figure online)



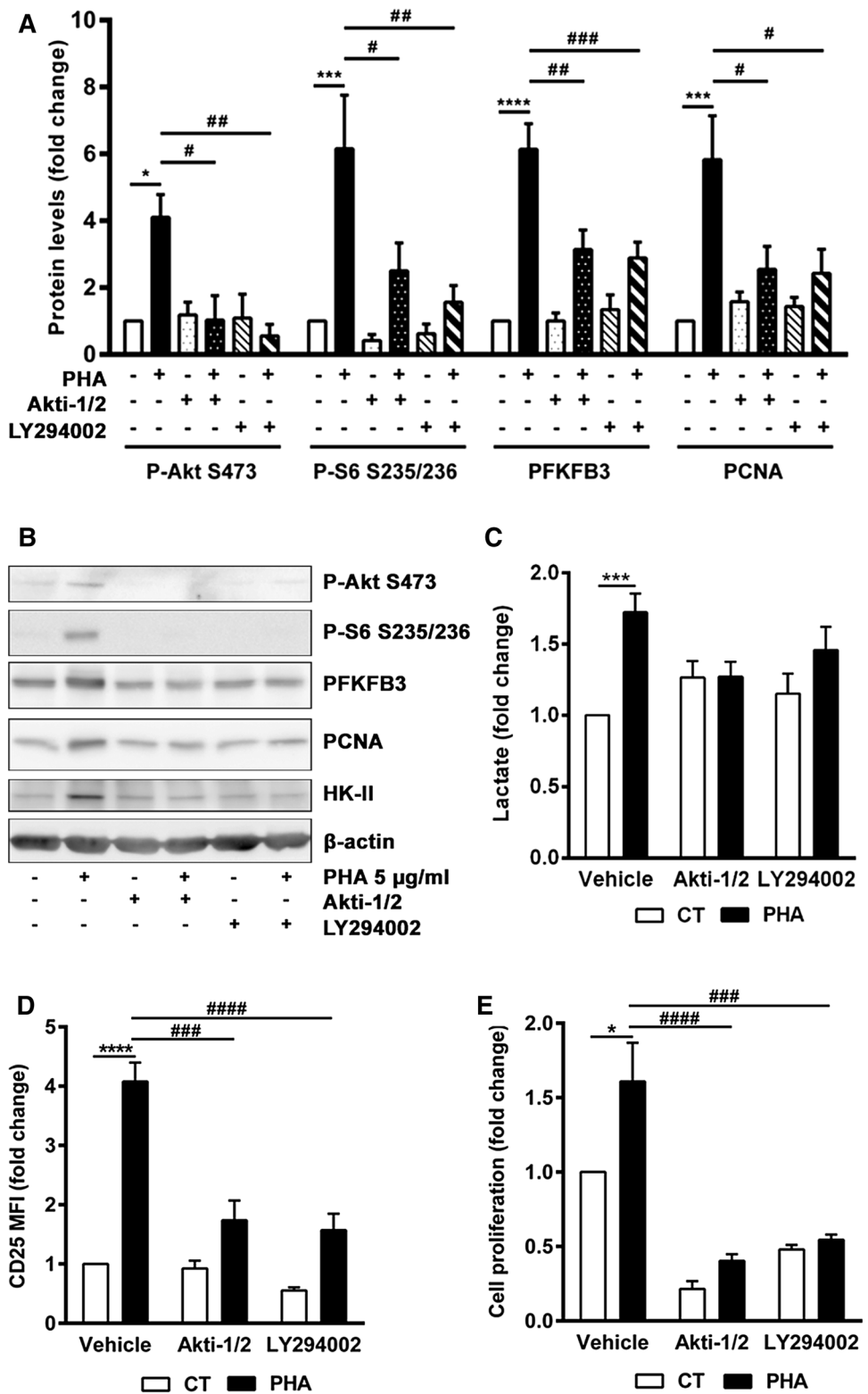
by significantly decreased CD25 expression in PHA-treated cells in combination with the inhibitors, compared to PHA treatment alone (Fig. 4d). Accordingly, PHA-induced decrease in CFSE fluorescence was significantly prevented by both inhibitors (Fig. 4e). This corroborates that PI3K and the glycolytic pathway are part of the activation and proliferation processes in human T-lymphocytes.

These results demonstrate that PI3K–Akt signaling pathway activation is required for PFKFB3 upregulation in response to PHA in human lymphocytes. Moreover, the data presented here confirm that inhibiting the PI3K/Akt signaling cascade impairs lymphocyte activation and proliferation, establishing a link between cellular signaling, metabolic reprogramming, and proliferation in human T-lymphocytes.

This finding will contribute to broaden the network of metabolic effectors involved in mitogen-mediated lymphocyte activation and proliferation.

TCR signaling and metabolic reprogramming are fundamental processes in T-lymphocyte biology. The inhibition of key players in these events can be used to target autoimmune diseases in which there is an overactivation of cellular signaling. For example, co-administration of rapamycin or other mTOR inhibitors has been proposed as a therapy to improve T regulatory cells differentiation and promote transplant tolerance in organ rejects [41]. Moreover, glycolysis inhibition with either 2-deoxy-glucose [45] or pharmacological inhibition of PFKFB3 isoenzyme with 3-(3-pyridinyl)-1-(4-pyridinyl)-2-propen-1-one (3PO) [9] has recently been

Fig. 4 PI3K and Akt inhibition prevents PHA-induced PFKFB3 and glycolysis induction, decreasing lymphocyte activation and proliferation. Analysis of the effects of 5 µg/ml PHA treatment in combination with the Akt inhibitor (Akti-1/2) or the PI3K inhibitor (LY294002) for 48 h. **a** Relative quantification of western blot analysis of P-Akt (S473), P-S6 (S235/236), PFKFB3, and PCNA normalized to β-actin. **b** Western blot images from a representative experiment. **c** Relative extracellular lactate production by T-lymphocytes at the mentioned conditions. **d** Relative CD25 MFI in T-lymphocytes at the mentioned conditions. **e** Proliferation measured by CFSE staining in 5 µg/ml PHA-treated or untreated T-lymphocytes after 120 h. Data in **a**, **d**, and **e** are represented as the mean fold change relative to the untreated vehicle condition ± SEM. Differences were calculated with two-way ANOVA and Tukey’s multiple comparisons test with normal-based 95% CI. Significant p values are indicated: **p* < 0.05; ****p* < 0.001; *****p* < 0.0001 and #*p* < 0.05; ##*p* < 0.01; ###*p* < 0.001 when comparing to the untreated vehicle condition or the PHA-treated vehicle condition, respectively



proposed as a possible strategy for autoimmune diseases such as graft versus host disease [46] or in inflammatory processes such as atherogenesis [27] and angiogenesis [47]. In contrast, strategies based on PFKFB3 overexpression

have been proposed in rheumatoid arthritis, in which PFKFB3 deficiency is the cause of the energy-deprived and autophagy-deficient, apoptosis-sensitive T-lymphocytes that are characteristic of this autoimmune disease [28].

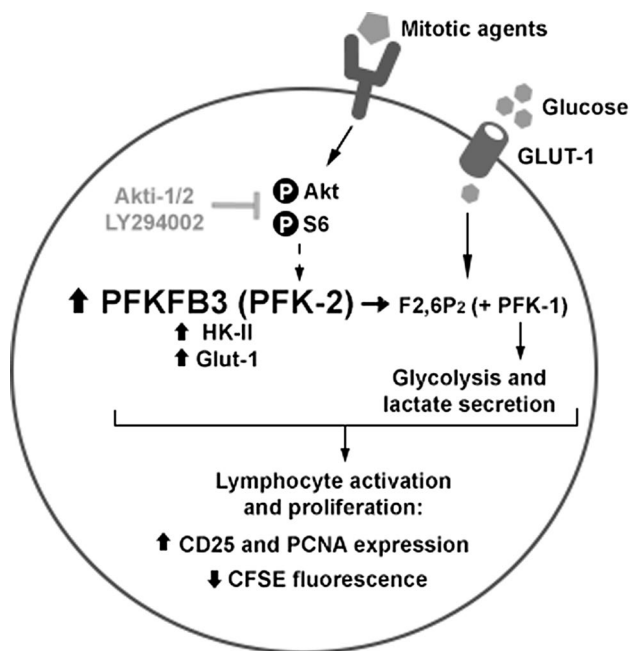


Fig. 5 Graphical summary of the main findings of this work. Mitotic agents induce PFKFB3 in a PI3K/Akt-dependent manner. Inhibition of this pathway prevents metabolic reprogramming, activation, and proliferation of T-lymphocytes

In conclusion (summarized in Fig. 5), this study demonstrates a tight interconnection between PI3K signaling and induction of PFKFB3 and Fru-2,6-P₂ synthesis during T-lymphocyte activation and proliferation. Results provide evidence for the role of PFKFB3 in T-lymphocyte early activation and show how metabolic adaptations that take place after exposure to a mitogen contribute to a time-dependent activation and proliferation process in these cells. These results provide a link between metabolism and mitogen-activated TCR signaling in human lymphocyte biology that can help to better understand the importance of modulating both pathways to target complex diseases that affect immune system activation and proliferation.

Acknowledgements We are grateful to B. Torrejón from the Microscopy Unit of Centres Científics i Tecnològics of the Universitat de Barcelona (CCiT-UB) for excellent technical assistance and advice; A. M. Cosials for technical advice in blood cells cultures; J. L. Rosa and F. Viñals for providing reagents; P. Giménez-Bonafé for English revision and E. Adanero for technical assistance.

Author contributions RB and AM conceived and designed the experiments; HS, CA, PF, and AV performed the experiments; HS, CA, AM, PF, AV, and EC analyzed the data; NLL, AR, and AN critically commented and revised the work; and HS, RB, and AM wrote the manuscript.

Funding This work was supported by Instituto de Salud Carlos III—FIS [PI13/0096] and FIS [PI17/00412]—and Fondo Europeo de

Desarrollo Regional (FEDER), and by Astellas European Foundation Award (13th European Society of Transplantation). HS was recipient of a fellowship from Secretaria d'Universitats i Recerca del Departament d'Economia i Coneixement de la Generalitat de Catalunya and AR was recipient of a fellowship from the University of Barcelona.

Compliance with ethical standards

Conflict of interest The authors declare no conflict of interest.

References

1. Maciolek JA, Pasternak JA, Wilson HL (2014) Metabolism of activated T lymphocytes. *Curr Opin Immunol* 27:60–74. <https://doi.org/10.1016/j.coi.2014.01.006>
2. Chang CH, Pearce EL (2016) Emerging concepts of T cell metabolism as a target of immunotherapy. *Nat Immunol* 17(4):364–368. <https://doi.org/10.1038/ni.3415>
3. Frauwirth KA, Riley JL, Harris MH et al (2002) The CD28 signaling pathway regulates glucose metabolism. *Immunity* 16(6):769–777. [https://doi.org/10.1016/S1074-7613\(02\)00323-0](https://doi.org/10.1016/S1074-7613(02)00323-0)
4. Marko AJ, Miller RA, Kelman A, Frauwirth KA (2010) Induction of glucose metabolism in stimulated T lymphocytes is regulated by mitogen-activated protein kinase signaling. *PLoS ONE* 5(11):e15425. <https://doi.org/10.1371/journal.pone.0015425>
5. Wang R, Dillon CP, Shi LZ et al (2011) The transcription factor Myc controls metabolic reprogramming upon T lymphocyte activation. *Immunity* 35(6):871–882. <https://doi.org/10.1016/j.immuni.2011.09.021>
6. Colomer D, Vives-Corrons JL, Pujades A, Bartrons R (1987) Control of phosphofructokinase by fructose 2,6-bisphosphate in B-lymphocytes and B-chronic lymphocytic leukemia cells. *Cancer Res* 47(7):1859–1862
7. Colomer D, Vives-Corrons JL, Bartrons R (1991) Effect of TPA on fructose 2,6-bisphosphate levels and protein kinase C activity in B-chronic lymphocytic leukemia (B-CLL). *Biochim Biophys Acta* 1097(4):270–274
8. Hue L, Rousseau GG (1993) Fructose 2,6-bisphosphate and the control of glycolysis by growth factors, tumor promoters and oncogenes. *Adv Enzyme Regul* 33:97–110
9. Telang S, Clem BF, Klarer AC, Clem AL, Trent JO, Bucala R et al (2012) Small molecule inhibition of 6-phosphofructose-2-kinase suppresses T cell activation. *J Transl Med* 10:95. <https://doi.org/10.1186/1479-5876-10-95>
10. Van Schaftingen E (1987) Fructose 2,6-bisphosphate. *Adv Enzymol Relat Areas Mol Biol* 59:315–395
11. Okar DA, Manzano A, Navarro-Sabatè A, Riera L, Bartrons R, Lange AJ (2001) PFK-2/FBPase-2: maker and breaker of the essential biofactor fructose-2,6-bisphosphate. *Trends Biochem Sci* 26(1):30–35. [https://doi.org/10.1016/S0968-0004\(00\)01699-6](https://doi.org/10.1016/S0968-0004(00)01699-6)
12. Sakakibara R, Uemura M, Hirata T, Okamura N, Kato M (1997) Human placental fructose-6-phosphate,2-kinase/fructose-2,6-bisphosphatase: its isozymic form, expression and characterization. *Biosci Biotechnol Biochem* 61(11):1949–1952. <https://doi.org/10.1271/bbb.61.1949>
13. Hamilton JA, Callaghan MJ, Sutherland RL, Watts CK (1997) Identification of PRG1, a novel progesterin-responsive gene with sequence homology to 6-phosphofructose-2-kinase/fructose-2,6-bisphosphatase. *Mol Endocrinol* 11(4):490–502. <https://doi.org/10.1210/mend.11.4.9909>
14. Manzano A, Rosa JL, Ventura F et al (1998) Molecular cloning, expression, and chromosomal localization of a ubiquitously expressed human 6-phosphofructose-2-kinase/fructose-2,

- 6-bisphosphatase gene (PFKFB3). *Cytogenet Cell Genet* 83(3–4):214–217. <https://doi.org/10.1159/000015181>
15. Duran J, Obach M, Navarro-Sabate A et al (2009) Pfkfb3 is transcriptionally upregulated in diabetic mouse liver through proliferative signals. *FEBS J* 276(16):4555–4568. <https://doi.org/10.1111/j.1742-4658.2009.07161.x>
 16. Chesney J, Mitchell R, Benigni F et al (1999) An inducible gene product for 6-phosphofructo-2-kinase with an AU-rich instability element: role in tumor cell glycolysis and the Warburg effect. *Proc Natl Acad Sci USA* 96(6):3047–3052. <https://doi.org/10.1073/pnas.96.6.3047>
 17. Riera L, Manzano A, Navarro-Sabaté A, Perales JC, Bartrons R (2002) Insulin induces PFKFB3 gene expression in HT29 human colon adenocarcinoma cells. *Biochim Biophys Acta* 1589(2):89–92. [https://doi.org/10.1016/S0167-4889\(02\)00169-6](https://doi.org/10.1016/S0167-4889(02)00169-6)
 18. Calvo MN, Bartrons R, Castaño E, Perales JC, Navarro-Sabaté A, Manzano A (2006) PFKFB3 gene silencing decreases glycolysis, induces cell-cycle delay and inhibits anchorage-independent growth in HeLa cells. *FEBS Lett* 580(13):3308–3314. <https://doi.org/10.1016/j.febslet.2006.04.093>
 19. Atsumi T, Chesney J, Metz C et al (2002) High expression of inducible 6-phosphofructo-2-kinase/fructose-2,6-bisphosphatase (iPFK-2; PFKFB3) in human cancers. *Cancer Res* 62(20):5881–5887
 20. Kessler R, Bleichert F, Warnke JP, Eschrich K (2008) 6-Phosphofructo-2-kinase/fructose-2,6-bisphosphatase (PFKFB3) is up-regulated in high-grade astrocytomas. *J Neurooncol* 86(3):257–264. <https://doi.org/10.1007/s11060-007-9471-7>
 21. Obach M, Navarro-Sabaté A, Caro J et al (2004) 6-Phosphofructo-2-kinase (pfkfb3) gene promoter contains hypoxia-inducible factor-1 binding sites necessary for transactivation in response to hypoxia. *J Biol Chem* 279(51):53562–53570. <https://doi.org/10.1074/jbc.M406096200>
 22. Novellasedemunt L, Obach M, Millán-Ariño L et al (2012) Progestins activate 6-phosphofructo-2-kinase/fructose-2,6-bisphosphatase 3 (PFKFB3) in breast cancer cells. *Biochem J* 442(2):345–356. <https://doi.org/10.1042/BJ20111418>
 23. Rodríguez-García A, Samsó P, Fontova P et al (2017) TGF- β 1 targets Smad, p38 MAPK, and PI3K/Akt signaling pathways to induce PFKFB3 gene expression and glycolysis in glioblastoma cells. *FEBS J* 284(20):3437–3454. <https://doi.org/10.1111/febs.14201>
 24. Ando M, Uehara I, Kogure K et al (2010) Interleukin 6 enhances glycolysis through expression of the glycolytic enzymes hexokinase 2 and 6-phosphofructo-2-kinase/fructose-2,6-bisphosphatase-3. *J Nippon Med Sch* 77(2):97–105. <https://doi.org/10.1272/jnms.77.97>
 25. Ruiz-García A, Monsalve E, Novellasedemunt L et al (2011) Cooperation of adenosine with macrophage Toll-4 receptor agonists leads to increased glycolytic flux through the enhanced expression of PFKFB3 gene. *J Biol Chem* 286(22):19247–19258. <https://doi.org/10.1074/jbc.M110.190298>
 26. Novellasedemunt L, Bultot L, Manzano A et al (2013) PFKFB3 activation in cancer cells by the p38/MK2 pathway in response to stress stimuli. *Biochem J* 452(3):531–543. <https://doi.org/10.1042/BJ20121886>
 27. Tawakol A, Singh P, Mojena M et al (2015) HIF-1 α and PFKFB3 mediate a tight relationship between proinflammatory activation and anerobic metabolism in atherosclerotic macrophages. *Arterioscler Thromb Vasc Biol* 35(6):1463–1471. <https://doi.org/10.1161/ATVBAHA.115.305551>
 28. Yang Z, Fujii H, Mohan SV, Goronzy JJ, Weyand CM (2013) Phosphofructokinase deficiency impairs ATP generation, autophagy, and redox balance in rheumatoid arthritis T cells. *J Exp Med* 210(10):2119–2134. <https://doi.org/10.1084/jem.20130252>
 29. Jiang H, Shi H, Sun M et al (2016) PFKFB3-driven macrophage glycolytic metabolism is a crucial component of innate antiviral defense. *J Immunol* 197(7):2880–2890. <https://doi.org/10.4049/jimmunol.1600474>
 30. Houddane A, Bultot L, Novellasedemunt L et al (2017) Role of Akt/PKB and PFKFB isoenzymes in the control of glycolysis, cell proliferation and protein synthesis in mitogen-stimulated thymocytes. *Cell Signal* 34:23–37. <https://doi.org/10.1016/j.cellsig.2017.02.019>
 31. Lloberas N, Rama I, Llaudó I et al (2013) Dendritic cells phenotype fitting under hypoxia or lipopolysaccharide; adenosine 5'-triphosphate-binding cassette transporters far beyond an efflux pump. *Clin Exp Immunol* 172(3):444–454. <https://doi.org/10.1111/cei.12067>
 32. Simon-Molas H, Calvo-Vidal MN, Castaño E et al (2016) Akt mediates TIGAR induction in HeLa cells following PFKFB3 inhibition. *FEBS Lett* 590(17):2915–2926. <https://doi.org/10.1002/1873-3468.12338>
 33. Van Schaftingen E, Lederer B, Bartrons R, Hers HG (1982) A kinetic study of pyrophosphate: fructose-6-phosphate phosphotransferase from potato tubers. Application to a microassay of fructose 2,6-bisphosphate. *Eur J Biochem* 129(1):191–195. <https://doi.org/10.1111/j.1432-1033.1982.tb07039.x>
 34. Gutmann I, Wahlefeld A (1974) L-(+)-lactate determination with lactate dehydrogenase and NAD. In: Bergmeyer H (ed) *Methods of enzymatic analysis*, 2nd edn. Academic Press, New York, pp 1464–1468
 35. Nowell PC (1960) Phytohemagglutinin: an initiator of mitosis in cultures of normal human leukocytes. *Cancer Res* 20(4):462–466
 36. Green DR, Droin N, Pinkoski M (2003) Activation-induced cell death in T cells. *Immunol Rev* 193:70–81. <https://doi.org/10.1034/j.1600-065X.2003.00051.x>
 37. Wieland E, Shipkova M (2016) Lymphocyte surface molecules as immune activation biomarkers. *Clin Biochem* 49(4–5):347–354. <https://doi.org/10.1016/j.clinbiochem.2015.07.099>
 38. Mire-Sluis AR, Wickremasinghe RG, Hoffbrand AV, Timms AM, Francis GE (1987) Human T lymphocytes stimulated by phytohaemagglutinin undergo a single round of cell division without a requirement for interleukin-2 or accessory cells. *Immunology* 60(1):7–12
 39. Moreno-Aurioles VR, Montaña R, Conde M, Bustos R, Sobrino F (1996) Streptozotocin-induced diabetes increases fructose 2,6-bisphosphate levels and glucose metabolism in thymus lymphocytes. *Life Sci* 58(6):477–484. [https://doi.org/10.1016/0024-3205\(95\)02312-7](https://doi.org/10.1016/0024-3205(95)02312-7)
 40. Chakrabarti R, Jung CY, Lee TP, Liu H, Mookerjee BK (1994) Changes in glucose transport and transporter isoforms during the activation of human peripheral blood lymphocytes by phytohemagglutinin. *J Immunol* 152(6):2660–2668
 41. Liu C, Chapman NM, Karmaus PW, Zeng H, Chi H (2015) mTOR and metabolic regulation of conventional and regulatory T cells. *J Leukoc Biol* 97(5):837–847. <https://doi.org/10.1189/jlb.2RI0814-408R>
 42. Basu S, Hubbard B, Shevach EM (2015) Foxp3-mediated inhibition of Akt inhibits Glut1 (glucose transporter 1) expression in human T regulatory cells. *J Leukoc Biol* 97(2):279–283. <https://doi.org/10.1189/jlb.2AB0514-273RR>
 43. Siska PJ, van der Windt GJ, Kishton RJ et al (2016) Suppression of Glut1 and glucose metabolism by decreased Akt/mTORC1 signaling drives T cell impairment in B cell leukemia. *J Immunol* 197(6):2532–2540. <https://doi.org/10.4049/jimmunol.1502464>
 44. Trefely S, Khoo PS, Krycer JR et al (2015) Kinome screen identifies PFKFB3 and glucose metabolism as important regulators of the insulin/insulin-like growth factor (IGF)-1 signaling pathway. *J Biol Chem* 290(43):25834–25846. <https://doi.org/10.1074/jbc.M115.658815>

45. Renner K, Geiselhöringer AL, Fante M et al (2015) Metabolic plasticity of human T cells: preserved cytokine production under glucose deprivation or mitochondrial restriction, but 2-deoxy-glucose affects effector functions. *Eur J Immunol* 45(9):2504–2516. <https://doi.org/10.1002/eji.201545473>
46. Nguyen HD, Chatterjee S, Haarberg KM et al (2016) Metabolic reprogramming of alloantigen-activated T cells after hematopoietic cell transplantation. *J Clin Invest* 126(4):1337–1352. <https://doi.org/10.1172/JCI82587>
47. De Bock K, Georgiadou M, Schoors S et al (2013) Role of PFKFB3-driven glycolysis in vessel sprouting. *Cell* 154(3):651–663. <https://doi.org/10.1016/j.cell.2013.06.037>

Supplementary Material

Extended Methods – Lymphocyte purification

Two lymphocyte purification protocols were compared. In the classical protocol - referred as one-sided adhesion protocol - 175 cm² adherent flasks were kept in horizontal position for 2 hours and supernatant was collected. In the newly developed method - referred as double-sided adhesion protocol - flasks were inverted after 2 hours of incubation and kept in horizontal position for an additional hour to foster monocytes adhesion to the other side of the flask.

To test the purification efficacy of each protocol, the percentages of CD3⁺, CD20⁺ and CD14⁺ cell populations were assessed by flow cytometry. The CD3⁺ T lymphocytes population was significantly increased with the double-sided adhesion protocol. CD14⁺ monocytes population was found significantly reduced in the new protocol compared to the original protocol. The population of CD20⁺ B lymphocytes was similar between the one-sided and two-sided adhesion protocols. Overall, the double-sided adhesion protocol resulted in better T lymphocyte purification and was used for further experiments (Supplementary Figure S1A, C).

T lymphocytes remained the main population at the end of the experiment and their number significantly increased at 120 h in the PHA-treated condition compared to untreated cells (Supplementary Figure S1B, D).

In LPS-mediated activation experiments, the experiment was performed in the presence of monocytes, given that these cells are required as antigen presenting cells to lymphocytes. In this case, PBMCs were cultured in 175 cm² adherent flasks in the presence or absence of LPS. At the time of sample

collection, supernatants containing lymphocytes were collected, leaving adhesion cells (monocytes, dendritic cells) attached to the flask.

Supplementary figures' legends

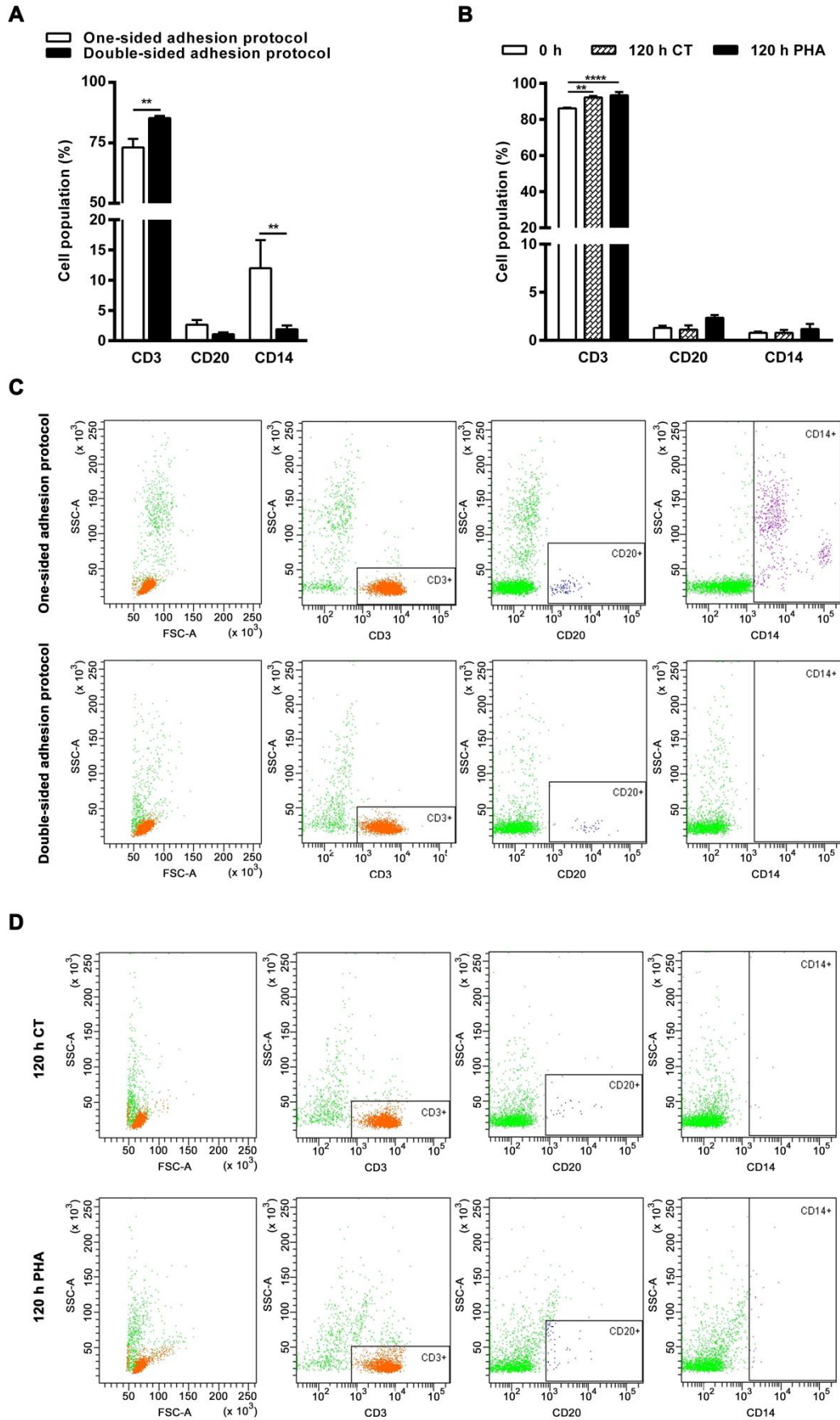
Supplementary Figure S1. Characterization of cell populations.

(A) Populations obtained with the one-sided and the double-sided adhesion protocols at the beginning of the experiment. Percentages of CD3+ (T lymphocytes), CD20+ (B lymphocytes) and CD14+ (monocytes) cells are represented. (B) FSC-SSC plots and each CD-SSC plot from a one-sided (upper panel) and a double-sided (lower panel) representative experiment are shown. (C) Characterization of cell populations obtained with the double-sided adhesion protocol after 120 h of culture. PHA-treated and untreated cells are represented. (D) FSC-SSC plots and each CD-SSC plot from untreated (upper panel) and PHA-treated cells (lower panel) from a representative experiment are shown. Data are presented as % of total cells analyzed. Differences were calculated with two-tailed unpaired (A) or paired (B) Student's t test with normal-based 95% CI and significant p values are indicated: **p ≤ 0.01; ****p ≤ 0.0001.

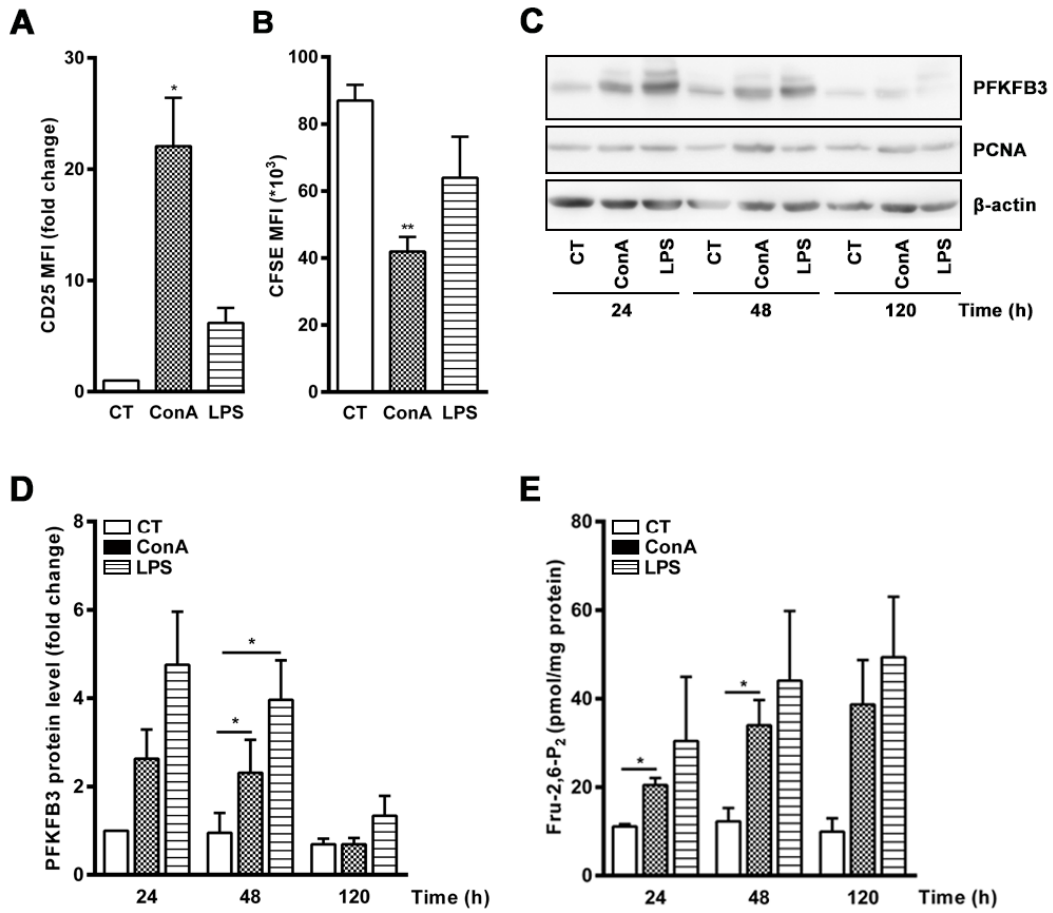
Supplementary Figure S2. ConA and LPS trigger lymphocyte activation and proliferation and increase PFKFB3 protein levels and Fru-2,6-P2 synthesis. Analysis of the effects of 10 µg/ml ConA and 1µg/ml LPS in T lymphocytes. (A) Relative CD25 MFI in ConA or LPS-treated T lymphocytes at 120 h. Data are presented as the mean fold change relative to untreated cells ± SEM. (B) CFSE MFI in ConA or LPS-treated T lymphocytes at 120 h. Data are presented as the mean fold change relative to untreated cells ± SEM. (C) Representative western blot images of PCNA and β-actin in ConA and LPS-treated T lymphocytes at several times. (D) Western blot quantification of PFKFB3 normalized to β-actin in ConA or LPS-treated and untreated T lymphocytes (CT) at several times. Data are presented as the mean fold change relative to untreated cells at 24 h ± SEM. (E) Fru-2,6-P2 concentration in ConA and LPS-treated T lymphocytes at several times. Data are presented as the mean fold change relative to untreated cells at 24 h ± SEM.

Differences were calculated with paired Student's t test with normal-based 95% CI. Significant p values are indicated: *p ≤ 0.05; **p ≤ 0.01.

Supplementary Figure S1



Supplementary Figure S2



TIGAR involvement in the activation of human T lymphocytes

The study of TIGAR in human lymphocytes emerged as an interesting project after analysing the expression of this gene across tissues in the Genotype-Tissue Expression (GTEx) database. GTEx project aim is to build a comprehensive public resource to study tissue-specific gene expression and regulation. The analysis presented here was performed with the GTEx release V6p (2016), when 8555 samples from 552 donors had been processed, analysing the expression of all human genes in 53 different tissues. TIGAR expression was found significantly increased in transformed lymphocytes and fibroblasts compared to the mean expression across tissues (**Figure A1**).

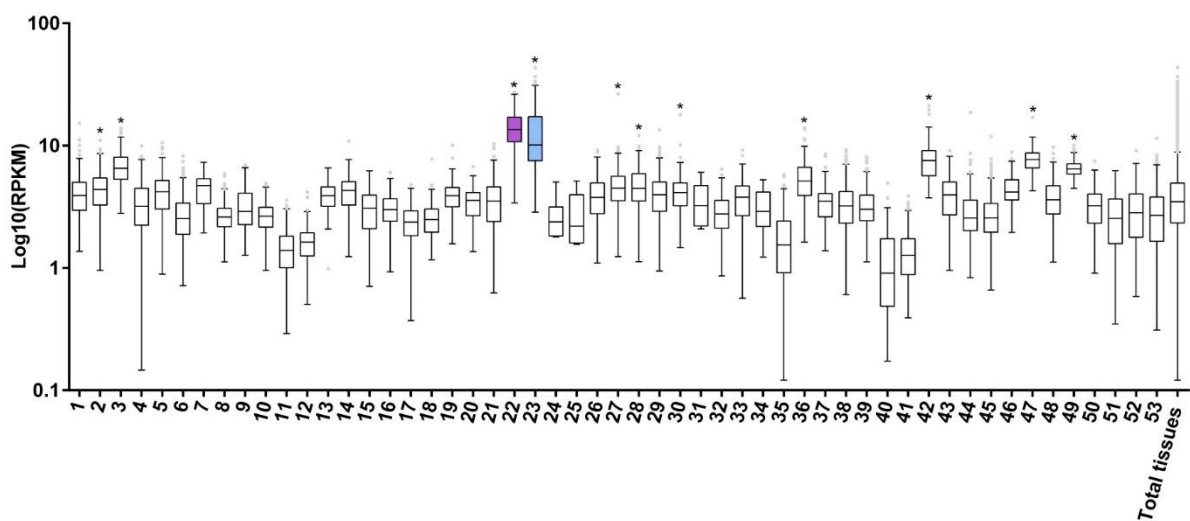


Figure A1. GTEx analysis of TIGAR expression across 53 human tissues. EBV-transformed lymphocytes and fibroblasts are colored in purple and blue, respectively, and the mean expression across all tissues is indicated in the last box.

Following the procedures described in (58), human T-lymphocytes were purified and treated with 10 $\mu\text{g}/\text{mL}$ ConA or 1 $\mu\text{g}/\text{mL}$ LPS for 120 h. TIGAR protein levels were determined by western blot. Results showed significantly increased TIGAR protein levels in ConA-treated lymphocytes compared to untreated lymphocytes at 24 and 48 h (**Figure A2**). LPS enhanced TIGAR levels to a lesser extent than ConA at 24 h and did not modulate TIGAR at any other time point (**Figure A2**). These results indicate that TIGAR is increased in parallel to PFKFB3 in lymphocytes activated with ConA. Moreover, the upregulation of these two proteins occurs in parallel to increased Fru-2,6-P₂ concentration and proliferation, as it was previously described (58). Activated lymphocytes induce metabolic reprogramming to accomplish the requirements of cell proliferation. In this context, it becomes clear that TIGAR is required for proliferation, resembling what occurs in tumour cells. The increase in Fru-2,6-P₂ in parallel to increased TIGAR protein levels supports the results presented in this thesis, which point out other pro-survival functions of TIGAR besides its role as a Fru-2,6-P₂ phosphatase.

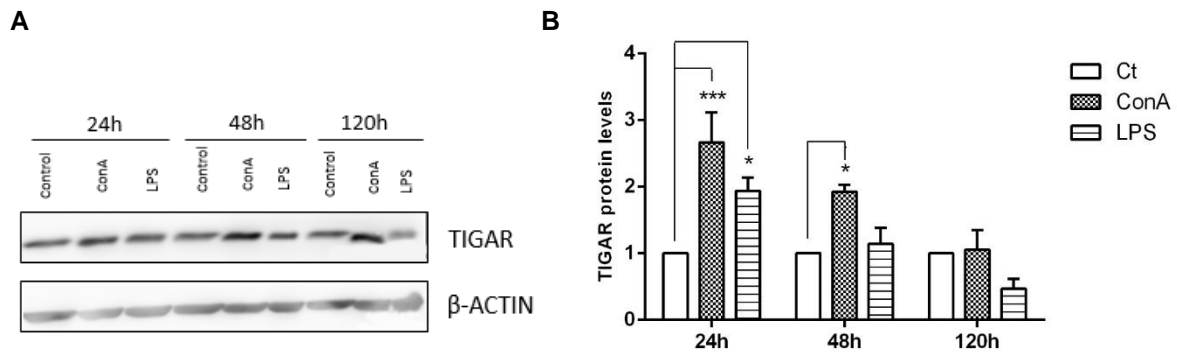


Figure A2. Time-course analysis of TIGAR protein levels in lymphocytes treated with ConA and LPS. T-lymphocytes were treated with ConA or LPS for the times indicated and TIGAR protein levels were determined by western blot. Data are represented as the mean fold change compared to untreated cells \pm SEM, n=3 (* p <0,05; *** p <0,001).

In order to determine the contribution of the PI3K/Akt signalling pathway in the upregulation of TIGAR during lymphocytes activation, we analysed TIGAR protein levels in lymphocytes treated with ConA and LPS in combination with 20 μ M LY294002 or 10 μ M Akti-1/2, as previously described (58). The results obtained indicated that the inhibition of any of these two kinases prevented TIGAR induction in response to ConA and LPS. P-S6 was used as control of the signalling through the pathway (**Figure A3**).

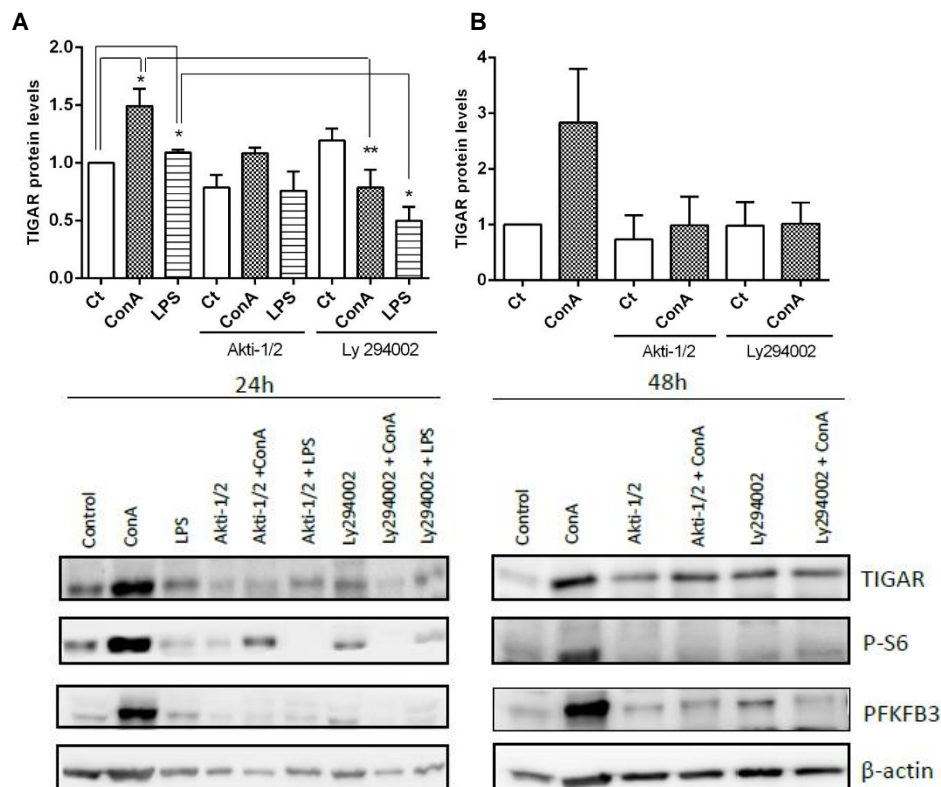


Figure A3. Western blot analysis of the involvement of the PI3K/Akt signaling pathway in the activation of T-lymphocytes. T-lymphocytes were pre-treated with the inhibitors LY294002 or Akti-1/2 and then treated with ConA or LPS for (A) 24 h and (B) 48 h. Western blot analysis of TIGAR, P-S6 and PFKFB3 were determined by western blot. B-actin was used as endogenous control. Data are represented as the mean fold change compared to untreated cells \pm SEM, n=3 (* p <0,05; ** p <0,01).

In conclusion, these results indicate that the same molecular mechanisms that we described to be involved in the activation of PFKFB3 during T-lymphocyte activation (58) are involved in the upregulation of TIGAR. PI3K and Akt are two kinases involved in signalling pathways that sustain proliferation and, thus, the inhibition of any of them results deregulation of metabolic transformation, which prevents adequate activation of lymphocytes.

The experiments summarised in these pages were part of the Final Degree Projects of Claudia Arnedo and Irene Caldera, students in our lab. This project is being continued by other students who are contributing to the determination of the link between Nrf2 and TIGAR in lymphocytes.



Fructose 2,6-Bisphosphate in Cancer Cell Metabolism

Ramon Bartrons^{1*}, Helga Simon-Molas¹, Ana Rodríguez-García¹, Esther Castaño²,
Àurea Navarro-Sabaté¹, Anna Manzano¹ and Ubaldo E. Martínez-Outschoorn³

¹ Unitat de Bioquímica, Departament de Ciències Fisiològiques, Universitat de Barcelona, Institut d'Investigació Biomèdica de Bellvitge (IDIBELL), Catalunya, Spain, ² Centres Científics i Tecnològics, Universitat de Barcelona, Catalunya, Spain,

³ Department of Medical Oncology, Thomas Jefferson University, Philadelphia, PA, United States

OPEN ACCESS

Edited by:

Michael Breitenbach,
University of Salzburg, Austria

Reviewed by:

Markus Schösserer,
Universität für Bodenkultur Wien,
Austria

Johannes A. Mayr,
Paracelsus Medical University
Salzburg, Austria

*Correspondence:

Ramon Bartrons
rbartrons@ub.edu

Specialty section:

This article was submitted to
Molecular and Cellular Oncology,
a section of the journal
Frontiers in Oncology

Received: 07 June 2018

Accepted: 01 August 2018

Published: 04 September 2018

Citation:

Bartrons R, Simon-Molas H,
Rodríguez-García A, Castaño E,
Navarro-Sabaté À, Manzano A and
Martínez-Outschoorn UE (2018)
Fructose 2,6-Bisphosphate in Cancer
Cell Metabolism. *Front. Oncol.* 8:331.
doi: 10.3389/fonc.2018.00331

For a long time, pioneers in the field of cancer cell metabolism, such as Otto Warburg, have focused on the idea that tumor cells maintain high glycolytic rates even with adequate oxygen supply, in what is known as aerobic glycolysis or the Warburg effect. Recent studies have reported a more complex situation, where the tumor ecosystem plays a more critical role in cancer progression. Cancer cells display extraordinary plasticity in adapting to changes in their tumor microenvironment, developing strategies to survive and proliferate. The proliferation of cancer cells needs a high rate of energy and metabolic substrates for biosynthesis of biomolecules. These requirements are met by the metabolic reprogramming of cancer cells and others present in the tumor microenvironment, which is essential for tumor survival and spread. Metabolic reprogramming involves a complex interplay between oncogenes, tumor suppressors, growth factors and local factors in the tumor microenvironment. These factors can induce overexpression and increased activity of glycolytic isoenzymes and proteins in stromal and cancer cells which are different from those expressed in normal cells. The fructose-6-phosphate/fructose-1,6-bisphosphate cycle, catalyzed by 6-phosphofructo-1-kinase/fructose 1,6-bisphosphatase (PFK1/FBPase1) isoenzymes, plays a key role in controlling glycolytic rates. PFK1/FBPase1 activities are allosterically regulated by fructose-2,6-bisphosphate, the product of the enzymatic activity of the dual kinase/phosphatase family of enzymes: 6-phosphofructo-2-kinase/fructose 2,6-bisphosphatase (PFKFB1-4) and TP53-induced glycolysis and apoptosis regulator (TIGAR), which show increased expression in a significant number of tumor types. In this review, the function of these isoenzymes in the regulation of metabolism, as well as the regulatory factors modulating their expression and activity in the tumor ecosystem are discussed. Targeting these isoenzymes, either directly or by inhibiting their activating factors, could be a promising approach for treating cancers.

Keywords: fructose 2,6-bisphosphate, cancer metabolism, glycolysis, PFKFB isoenzymes, TIGAR, tumor microenvironment

INTRODUCTION

Otto Warburg, using the Warburg manometer to measure the oxygen consumption in cells, demonstrated that tumor cells showed rapid and intense glycolysis, in which glucose was oxidized into lactate, despite the presence of abundant oxygen (1). This “Warburg effect” is characteristic of proliferating and transformed cells. Warburg postulated that cancer was a result of defects in mitochondrial respiration, which forced the cell to adopt an anaerobic form of energy generation,

Gene Section

Review

C12orf5 (chromosome 12 open reading frame 5)

Helga Simon, Ana Rodríguez-García, Àurea Navarro-Sabaté, Pere Fontova, Ramon Bartrons, Anna Manzano

Departament de Ciències Fisiològiques II, Campus de Bellvitge, Universitat de Barcelona, Feixa Llarga s/n, 08907, L'Hospitalet de Llobregat, Barcelona, Spain (HS, ARG, ÀNS, PF, RB, AM)

Published in Atlas Database: December 2013

Online updated version : <http://AtlasGeneticsOncology.org/Genes/C12orf5ID50684ch12p13.html>
DOI: 10.4267/2042/53971

This work is licensed under a Creative Commons Attribution-Noncommercial-No Derivative Works 2.0 France Licence.
© 2014 Atlas of Genetics and Cytogenetics in Oncology and Haematology

Abstract

Review on C12orf5, with data on DNA/RNA, on the protein encoded and where the gene is implicated.

Identity

Other names: FR2BP, TIGAR

HGNC (Hugo): C12orf5

Location: 12p13.32

DNA/RNA

Description

The human TIGAR gene is composed of 6 exons spanning genomic region about 50,4 kb (GenBank

NC_000012.11). The transcript mRNA is 8,2 kb (GenBank NM_020375.2) and it is composed by the exon regions 5827..5937, 15914..15951, 21673..21794, 34453..34530, 35901..36011 and 36894..44662.

Transcription

The human TIGAR coding sequence consists of 813 bp from the start codon to the stop codon. There are no splicing variants reported.

Pseudogene

A pseudogene of the ribosomal protein S15 has been located in the region 8981..9473 by computational analysis using a gene prediction method, but there is not experimental data proving it.

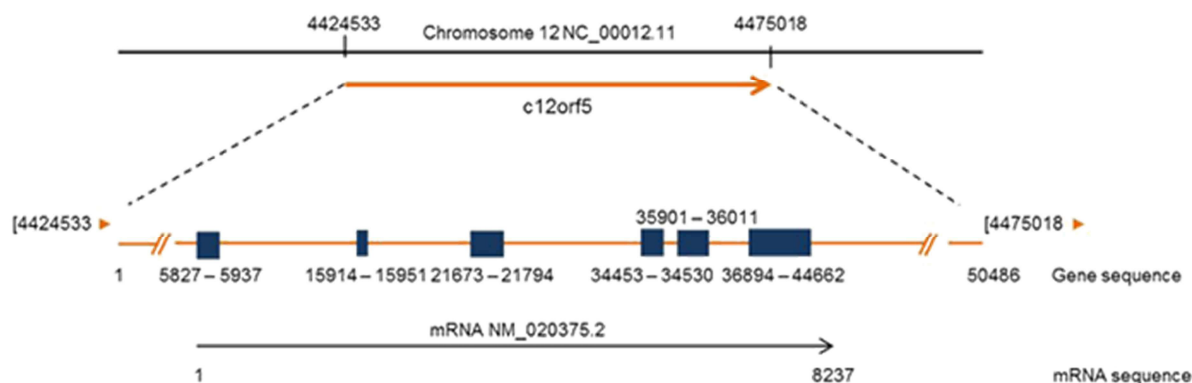


Figure 1. Schematic representation of TIGAR location in chromosome 12, gene structure and transcript mRNA. Different numbering has been used considering chromosomal, gene or mRNA sequence.

REVIEW



The potential utility of PFKFB3 as a therapeutic target

Ramon Bartrons, Ana Rodríguez-García, Helga Simon-Molas, Esther Castaño, Anna Manzano and Àurea Navarro-Sabaté

Unitat de Bioquímica, Departament de Ciències Fisiològiques, Universitat de Barcelona, IDIBELL, Catalunya, Spain

ABSTRACT

Introduction: It has been known for over half a century that tumors exhibit an increased demand for nutrients to fuel their rapid proliferation. Interest in targeting cancer metabolism to treat the disease has been renewed in recent years with the discovery that many cancer-related pathways have a profound effect on metabolism. Considering the recent increase in our understanding of cancer metabolism and the enzymes and pathways involved, the question arises as to whether metabolism is cancer's Achilles heel.

Areas covered: This review summarizes the role of 6-Phosphofructo-2-kinase/fructose-2,6-bisphosphatase 3 (PFKFB3) in glycolysis, cell proliferation, and tumor growth, discussing PFKFB3 gene and isoenzyme regulation and the changes that occur in cancer and inflammatory diseases. Pharmacological options currently available for selective PFKFB3 inhibition are also reviewed.

Expert opinion: PFKFB3 plays an important role in sustaining the development and progression of cancer and might represent an attractive target for therapeutic strategies. Nevertheless, clinical trials are needed to follow up on the promising results from preclinical studies with PFKFB3 inhibitors. Combination therapies with PFKFB3 inhibitors, chemotherapeutic drugs, or radiotherapy might improve the efficacy of cancer treatments targeting PFKFB3.

ARTICLE HISTORY

Received 9 January 2018
Accepted 4 July 2018

KEYWORDS

Cancer; glycolysis; metabolism; PFKFB3; PFKFB3 inhibitors

1. Introduction

Some of the earliest modern studies on cancer observed abnormalities in tumor metabolism. In the pioneering studies of the 1920s, Otto Warburg observed that cancers possessed a remarkable ability to sustain high rates of anaerobic glycolysis even in the presence of oxygen [1]. Anaerobic glycolysis uses glucose to produce lactate, while aerobic glycolysis (respiration) produces pyruvate for the tricarboxylic acid cycle and generates energy via oxidative phosphorylation. An essential thermodynamic trade-off exists between these two pathways with respect to the rate (moles of adenosine triphosphate (ATP) per unit of time) and yield (moles of ATP per mole of substrate), with fermentation occurring approximately 100 times faster than respiration, although yielding roughly 18-fold less ATP per mole of glucose. Population biology modeling has demonstrated how organisms use the intrinsic trade-off between these two pathways to maximal effect. Cells with a higher rate, but lower yield of ATP production, may gain a selective advantage when competing for shared energy resources [2].

There are numerous molecular modulators of glycolytic flux, the most well-known of which was discovered in 1860 by Louis Pasteur [3]. Pasteur showed that oxygen inhibits fermentation and that glucose consumption is inversely proportional to oxygen availability (the Pasteur effect). It is now clear that the allosteric properties of 6-Phosphofructo-1-kinase (PFK-1) can account for most aspects of the Pasteur's effect [4]. Many tumors have high rates of glycolysis

regardless of oxygen availability (the Warburg effect). These tumors depend largely on the glycolytic pathway for the generation of ATP and biomolecules to meet most of their energy demand. Warburg attributed this metabolic alteration to mitochondrial 'respiration injury' and considered this the most fundamental metabolic change in malignant transformation or 'the origin of cancer cells' [1]. However, this hypothesis was neglected because some tumors do not have defects in respiration; besides, respiration also exerts a regulatory effect on glycolysis [5]. Although some cancer cells do not show high glycolytic activity [6], the Warburg effect has been consistently observed in a wide range of human cancers and forms the physiological basis for the use of positron emission tomography (PET) scans in clinical oncology [7]. There are likely to be several biochemical and molecular mechanisms underlying the Warburg effect, including mitochondrial dysfunction [8,9], oncogenic alterations, leading to increased glycolysis [10,11], as well as adaptive responses to the tumor microenvironment [12,13].

2. Fructose 2,6-bisphosphate: a regulator of the glycolytic pathway

Studies on glycolysis regulation in the 1960s, involving thermodynamic assessments and measurements of intracellular metabolite concentrations, led to the identification of non-equilibrium reactions catalyzed by Hexokinase, PFK-1, and Pyruvate kinase [14]. In 1980, fructose-2,6-bisphosphate (Fru-2,6-P₂), a potent allosteric stimulator of PFK-1, was discovered

TGF- β 1 targets Smad, p38 MAPK, and PI3K/Akt signaling pathways to induce PFKFB3 gene expression and glycolysis in glioblastoma cells

Ana Rodríguez-García¹, Paula Samsó¹, Pere Fontova¹, Helga Simon-Molas¹, Anna Manzano¹, Esther Castaño², Jose Luis Rosa¹, Ubaldo Martinez-Outshoorn³, Francesc Ventura¹, Àurea Navarro-Sabaté^{1,2,*} and Ramon Bartrons^{1*}

¹ Unitat de Bioquímica, Departament de Ciències Fisiològiques, IDIBELL, Universitat de Barcelona, Spain

² Centres Científics i Tecnològics, Universitat de Barcelona, Spain

³ Department of Medical Oncology, Sidney Kimmel Cancer Center, Thomas Jefferson University, Philadelphia, PA, USA

Keywords

gene regulation; glycolysis and glioblastoma; PFKFB3; transforming growth factor- β 1

Correspondence

R. Bartrons, Unitat de Bioquímica, Departament de Ciències Fisiològiques, IDIBELL, Universitat de Barcelona, Feixa Llarga s/n, E-08907 L'Hospitalet, Barcelona, Spain

Fax: (+34)934024268

Tel: (+34)934024252

E-mail: rbartrons@ub.edu

*These authors share senior co-authorship.

(Received 9 May 2017, revised 25 July 2017, accepted 16 August 2017)

doi:10.1111/febs.14201

In human cancers, transforming growth factor- β 1 (TGF- β 1) plays a dual role by acting as both a tumor suppressor and a promoter of tumor metastasis. Although TGF- β 1 contributes to the metabolic reprogramming of cancer cells and tumor-associated stromal cells, little is known of the molecular mechanisms connecting this cytokine with enhanced glycolysis. PFKFB3 is a homodimeric bifunctional enzyme, belonging to the family of 6-phosphofructo-2-kinase/fructose-2,6-bisphosphatases, that controls the conversion of fructose-6-phosphate (Fru-6-P) to fructose-2,6-bisphosphate (Fru-2,6-P₂). This metabolite is important for the dynamic regulation of glycolytic flux by allosterically activating phosphofructokinase-1, a rate-limiting enzyme in glycolysis. The PFKFB3 gene is involved in cell proliferation via its role in carbohydrate metabolism. Here, we studied the mechanisms connecting TGF- β 1, glucose metabolism, and PFKFB3 in glioblastoma cell lines. We demonstrate that TGF- β 1 upregulates PFKFB3 mRNA and protein expression resulting in an increase in fructose 2,6-bisphosphate concentration, glucose uptake, glycolytic flux and lactate production. Moreover, these increases in PFKFB3 mRNA and protein expression and Fru-2,6-P₂ concentration were reduced when the Smad3, p38 mitogen-activated protein kinase (MAPK), and phosphoinositide 3-kinase (PI3K)/Akt signaling pathways were inhibited. We demonstrate that inhibition of PFKFB3 activity with 3PO or siRNA-mediated knockdown of PFKFB3 significantly eliminated the capacity of the T98G cells to form colonies by TGF- β 1, one of the hallmarks of transformation. Taken together, these results show that TGF- β 1 induces PFKFB3 expression through activation of the p38 MAPK and PI3K/Akt signaling pathways that complement and converge with early activation of Smad signaling. This suggests that PFKFB3 induction by TGF- β 1 can be one of the main mechanisms mediating the reprogramming of glioma cells.

Abbreviations

3PO, 3-(3-pyridinyl)-1-(4-pyridinyl)-2-propen-1-one; Erk, extracellular signal-regulated kinase; Fru-2,6-P₂, fructose 2,6-bisphosphate; GLUT1, glucose transporter 1; HK-II, hexokinase-II; Hsp25, heat shock protein 25; JNK, c-Jun N-terminal kinase; LDH-A, lactate dehydrogenase-A; MAPK, mitogen-activated protein kinase; PFK-1, phosphofructokinase-1; PFKFB1-4, phosphofructo-2-kinase/fructose-2,6-bisphosphatase 1-4; PI3K, phosphoinositide 3-kinase; S6, S6 ribosomal protein; TGF- β 1, transforming growth factor- β 1; T β R1, TGF- β type I serine/threonine kinase receptor; T β R2, TGF- β type II serine/threonine kinase receptor.

Gene Section

Review

PFKFB2 (6-phosphofructo-2-kinase/fructose-2,6-biphosphatase 2)

Ana Rodríguez-García, Pere Fontova, Helga Simon, Anna Manzano, Ramon Bartrons, Àurea Navarro-Sabaté

Departament de Ciències Fisiològiques II, Campus de Bellvitge, Universitat de Barcelona, Feixa Llarga s/n, 08907, L'Hospitalet de Llobregat, Barcelona, Spain (ARG, PF, HS, AM, RB, ÀNS)

Published in Atlas Database: March 2014

Online updated version : <http://AtlasGeneticsOncology.org/Genes/PFKFB2ID52100ch1q32.html>
DOI: 10.4267/2042/54168

This work is licensed under a Creative Commons Attribution-Noncommercial-No Derivative Works 2.0 France Licence.
© 2014 Atlas of Genetics and Cytogenetics in Oncology and Haematology

Abstract

Review on PFKFB2, with data on DNA/RNA, on the protein encoded and where the gene is implicated.

Identity

Other names: PFK-2/FBPase-2

HGNC (Hugo): PFKFB2

Location: 1q32.2

Local order

The human PFKFB2 gene is located on the chromosome 1 at position 1q31-q32.2 (GeneCards) (Fig. 1).

DNA/RNA

Description

The human PFKFB2 is composed of 15 exons

spanning 22617 bp (GenBank: AJ005577.1). This gene has 9 transcripts; two of them have been reported to codify a protein and three contain an open reading frame, but no protein has been identified. The transcripts are derived from different promoters and vary only in non-coding sequences at the 5' end. Therefore, the resulting proteins differ in their C-terminal amino acid sequence (Heine-Suñer et al., 1998).

The main products of the gene correspond to mRNAs of 7073 bp and 3529 bp for the variant 1 (isoform a; NM_006212.2) and variant 2 (isoform b; NM_001018053.1), respectively (Fig. 2). The isoform b differs in the 3' UTR and the coding region compared to isoform a. The resulting isoform b is shorter and has a distinct C-terminus compared to isoform a. However, it is not known how these different 5' ends are related to the three mRNAs (H1, H2 and H4) that encode the isoform a or the H3 mRNA that encodes the isoform b. None of these mRNAs are strictly heart-specific.

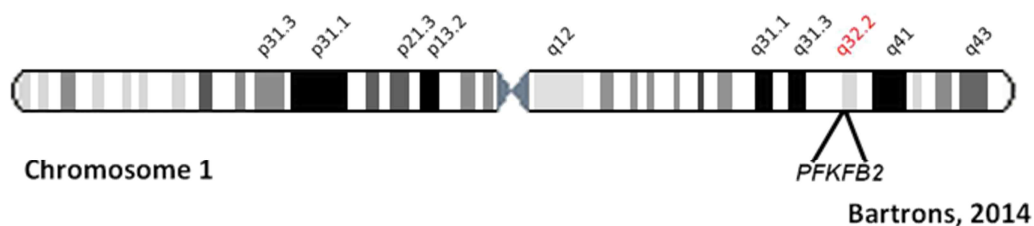


Figure 1. Localization of human PFKFB2 gene.



L'iniciat no és el que serà, però ha deixat d'ésser el que era anteriorment.

JOAN FRIGOLÉ REIXACH